

**CONSOLIDATION THEORIES FOR SATURATED-UNSATURATED SOILS
AND NUMERICAL SIMULATION OF
RESIDENTIAL BUILDINGS ON EXPANSIVE SOILS**

A Dissertation

by

XIONG ZHANG

Submitted to the Office of Graduate Studies of
Texas A&M University
in partial fulfillment of the requirements for the degree of

DOCTOR OF PHILOSOPHY

August 2004

Major Subject: Civil Engineering

**CONSOLIDATION THEORIES FOR SATURATED-UNSATURATED SOILS
AND NUMERICAL SIMULATION OF
RESIDENTIAL BUILDINGS ON EXPANSIVE SOILS**

A Dissertation

by

XIONG ZHANG

Submitted to Texas A&M University
in partial fulfillment of the requirements
for the degree of

DOCTOR OF PHILOSOPHY

Approved as to style and content by:

Jean-Louis Briaud
(Chair of Committee)

Robert L. Lytton
(Member)

Charles Aubeny
(Member)

Alan Palazzolo
(Member)

Paul Roschke
(Head of Department)

August 2004

Major Subject: Civil Engineering

ABSTRACT

Consolidation Theories for Saturated-Unsaturated Soils and
Numerical Simulation of Residential Buildings on Expansive Soils.
(August 2004)

Xiong Zhang, B.S., Tongji University, P.R. China;
M.S., China Institute of Water Resources & Hydropower Research
(IWHR), Beijing, China

Chair of Advisory Committee: Dr. Jean-Louis Briaud

The coupled and uncoupled consolidation theories for saturated-unsaturated soils have been discussed. A new method for constructing the constitutive surfaces for saturated-unsaturated soils has been proposed. The consolidation processes for saturated-unsaturated soils have been explained by thermodynamic analogue. One dimensional consolidation theory for saturated-unsaturated soils is presented and a new method is proposed to calculate the immediate settlement, total settlement and the time history of the consolidation settlement manually in the same way as what we have done for saturated soils with a higher accuracy. It makes the consolidation theory of unsaturated soils as applicable as that of saturated soils. This method can also be used to perform uncoupled two or three dimensional consolidation calculation for both expansive soils and collapsible soils. From the analysis, the equivalent effective stress and excessive pore water pressure can be easily calculated. At the same time, the physical meanings for the parameters in the constitutive laws for saturated-unsaturated are illustrated. A new set of the differential equations for the coupled two or three dimensional consolidation of saturated-unsaturated soils are proposed, together with the corresponding method to solve the differential equations. It is also proved numerically and analytically that during the consolidation process the Mandel-Cryer effect exists for unsaturated expansive soils and there is a “reverse” Mandel-Cryer effect for unsaturated

collapsible soils. A new method is proposed to estimate the volume change of expansive soils.

A complete system is proposed for the numerical simulation of residential buildings on expansive soils. The strength of this method lies in its use of simple and readily available historic weather data such as daily temperature, solar radiation, relative humidity, wind speed and rainfall as input. Accurate three dimensional predictions are obtained by integrating a number of different analytical and numerical techniques: different simulation methods for different boundary conditions such as tree, grass, and bare soils, coupled hydro-mechanical stress analysis to describe deformation of saturated-unsaturated soils, jointed elements simulation of soil-structure interaction, analysis of structure stress moment by general shell elements, and to assess structural damage by the smeared cracking model. The real-time and dynamic simulation results are consistent with field measurements.

ACKNOWLEDGEMENTS

I would like to thank my Ph.D committee chairman, Dr. Jean-Louis Briaud, for his invaluable guidance and inspiration, immense help and support, and constant trust and acceptance throughout my doctoral studies. This research and dissertation would not have been possible were it not for his invaluable guidance and inspiration, caring, coaching, patience, kindness and encouragement. I am greatly indebted to Dr. Jean-Louis Briaud for giving me the opportunity to work on this excellent research project and assisting me to achieve my goals.

I am indebted to Dr. Robert L. Lytton, not only for his invaluable suggestion and inspiration, but also for the assistance, the encouragement, the patience and the kindness he offered me in the past three years. I am deeply moved by his keen and enthusiastic pursuit of science. Many of his ideas form the basis of this dissertation.

My special sincere appreciation goes to Dr. Charles Aubeny and Dr. Giovanna Biscontin for their invaluable advice, creative ideas, care, encouragement and constructive discussions during this study. Whenever I had a question, no matter whether academically related or not, their answers were always timely and extremely helpful.

I am also indebted to Dr. Jose M. Roesset, Dr. James D. Murff, Dr. Alan Palazzolo, Dr. Hamn-Ching Chen, Dr. J.N. Reddy, Dr. Paul Roschke, Dr. Luciana Barroso, Dr. Joseph Bracci in addition to others who have taught me whatever I have contributed to this dissertation for their kind help, encouragement, and inspiration.

Words can fail in expressing my love and gratitude to my parents and my family. Through turbulent times and calm, through creative periods and fallow, there is always home and family to give me encouragement and comfort. Special thanks are given to my girlfriend, Juanyu Liu, for her continuous support, help and care during this study.

I would like to express my sincere gratitude for all the support and assistance from many individuals who made this work possible. I want to thank sincerely Remon Melek, Elizabeth Hungerford, Sanghoo Moon and Mike Linger for helping me in accomplishing the laboratory and field tests. I want to thank Dr. Ya Li, Dr. Yanfeng Li, Wei Wang,

Junying Pan, Xiaoyan Long, Hongrui Hu and Xinlian Chen for the sharing of their wisdom and knowledge with me.

Finally, I want to thank especially the Spencer J. Buchanan Chair for its sponsorship and continuous support. I would like also to thank Dr. Peter Keating for providing me with the teaching assistantship.

TABLE OF CONTENTS

	Page
ABSTRACT	iii
ACKNOWLEDGEMENTS	v
TABLE OF CONTENTS	vii
LIST OF FIGURES	xi
LIST OF TABLES	xxv
CHAPTER	
I INTRODUCTION	1
1.1 Definition	1
1.2 Problems Caused by Expansive Soils	2
1.3 Significance of the Research	6
1.4 Objective of Study	6
1.5 Outline of This Dissertation	7
II FACTORS INFLUENCING DAMAGE TO RESIDENTIAL BUILDINGS	11
2.1 Introduction	11
2.2 Soil Structure and Factors Influencing the Mechanical Behaviors of Soils	11
2.3 Factors Influencing the Soil Water Balance	29
2.4 Problems Associated with the Soil Structure Interaction	33
2.5 Convention of This Dissertation	36
III MODELS NEEDED FOR NUMERICAL SIMULATIONS OF RESIDENTIAL BUILDINGS ON EXPANSIVE SOILS	39
3.1 Introduction	39
3.2 Evaluating of the Weather's Influence	40
3.3 Modeling of Moisture Movements	46
3.4 Volume Change of Soil due to Moisture Variations	48
3.5 Soil Volume Change due to Mechanical Stress Variations	50
3.6 The Coupled Hydro-Mechanical Stress Analysis (or the Coupled Consolidation Theory) for Saturated- Unsaturated Soils	51
3.7 The Finite Element Method of the Plate Theory	57

CHAPTER	Page
3.8 Model of Soil-Structure Interaction	59
3.9 The Smearred Cracking Model for Concrete	63
3.10 Research Methodology.....	64
IV FIELD OBSERVATION, LABORATORY TESTS AND DATA	
REDUCTION.....	73
4.1 Introduction	73
4.2 Field Observations	74
4.3 Laboratory Tests	82
4.4 Methods to Obtain the Needed Curves	93
4.5 Variation of Degree of Saturation in the Free Shrink Test	103
V CONSTITUTIVE SURFACES FOR SATURATED- UNSATURATED SOILS.....	104
5.1 Introduction	104
5.2 Sign Conventions for State Variables	104
5.3 Constitutive Surfaces for Saturated Soils.....	106
5.4 The Constitutive Surfaces for Unsaturated Soils	111
5.5 Constructing the Void Ratio Constitutive Surfaces for Saturated-Unsaturated Soils	121
5.6 Degree of Saturation Constitutive Surface and Water Content Constitutive Surface	123
VI CONSOLIDATION THEORY FOR SATURATED- UNSATURATED SOILS	129
6.1 Scope of the Research, Assumptions and Some Basic Definitions.....	129
6.2 Review of the Coupled Thermal Stress Problem	134
6.3 Constitutive Laws for Volume Changes of Unsaturated Soils.....	154
6.4 Similarity between the Coupled Thermal Stress Problem and the Couple Hydro-Mechanical Stress (Consolidation) Problem for Saturated-Unsaturated Soils.....	186
6.5 Uncoupled Consolidation Theory for Saturated- Unsaturated Soils1.....	195

CHAPTER	Page
6.6 Coupled Consolidation Theory for Saturated- Unsaturated Soils.....	253
6.7 Some Discussions on the Consolidation Theory for Unsaturated Soils.....	289
VII EVAPOTRANSPIRATION, INFILTRATION AND BOUNDARY CONDITIONS.....	303
7.1 Introduction.....	303
7.2 Boundary Conditions and Evapotranspiration	306
7.3 Potential Evapotranspiration	307
7.4 Crop Evapotranspiration under Standard Conditions.....	324
7.5 Crop Evapotranspiration under Non-Standard Conditions	326
7.6 Soil Water Balance and Net Water Loss.....	331
7.7 Boundary Conditions for Different Surface Conditions	337
7.8 Discussion	342
VIII VERIFICATION OF THE PROPOSED METHOD.....	343
8.1 Introduction.....	343
8.2 Model Used in the Simulation.....	343
8.3 Material Properties Used in the Analysis	345
8.4 Modifying the Coupled Thermal Stress Problem to Include the Influence of Gravity	363
8.5 Initial Conditions, Boundary Conditions and Loadings.....	367
8.6 Programming.....	373
8.7 Results and Discussion.....	382
IX CURRENT DESIGN METHODS AND NUMERICAL SIMULATIONS OF RESIDENTIAL BUILDINGS ON EXPANSIVE SOILS.....	384
9.1 Introduction.....	384
9.2 Review of Current Design Methods for Foundations on Expansive Soils	385
9.3 Theory of Contact Elements.....	394
9.4 Theory of General Shell Elements	406

CHAPTER	Page
9.5 Pseudo Moisture Variation Simulations	414
9.6 Two Examples	419
9.7 Design Criterion and Crack Model for Concrete	480
9.8 Discussion	486
X PREDICTING THE VOLUME CHANGE OF EXPANSIVE SOILS.....	489
10.1 Introduction	489
10.2 Current Methods for Predicting the Movements of Expansive Soils	489
10.3 Variables Needed to Determine the Soil Status.....	498
10.4 A Simplified Method to Obtain the $e-w-\sigma$ Surface	502
10.5 An Example of the Proposed Method	506
10.6 Discussion	509
10.7 Conclusion.....	514
XI CONCLUSIONS AND FUTURE RESEARCH.....	515
11.1 Conclusions	516
11.2 Future Research Needed.....	525
REFERENCES.....	527
APPENDIX A	545
APPENDIX B	557
APPENDIX C	607
APPENDIX D.....	617
APPENDIX E	644
VITA	664

LIST OF FIGURES

FIGURE	Page
1.1 Factors Influencing the Soil Volume	3
1.2 Damages Cause by Expansive Soils at Different Seasons	5
2.1 Diffuse Double Layers	13
2.2 The Relative Sizes of Absorbed Water Layers on Sodium Montmorillonite and Sodium Kaolinite	14
2.3 Schematic Diagram of the Soil Microfabric and Macrofabric System	15
2.4 Simplified Bimodal Structure of the Clay Soil	16
2.5 Drying Process of a Sand	22
2.6 Drying Process of a Clay.....	22
2.7 Mechanical Stress and Matric Suction's Influence on Macrostructure	24
2.8 Mechanical Stress and Matric Suction's Influence on Microstructure.....	25
2.9 Mechanical Stress and Matric Suction's Influence on Micropores and Macropores.....	26
2.10 Mechanical Stress and Matric Suction's Influence on Soil Water Characteristic Curve	27
2.11 Typical Relationships for Evaporation from Soil as a Function of Time	31
2.12 Typical Relationships for Infiltration into Soil as a Function of Time	33
2.13 Two Typical Damage Modes of Slab on Grade.....	35

FIGURE	Page
2.14 Slab on Grade When the Load Is Not Symmetric	36
3.1 Comparison between Results Obtained from Winkler Foundation and the Actual Deflections	60
3.2 Deformations of the Elastic Half Space Foundation under Concentrated and Uniform Load.....	62
3.3 Typical Environments around a House	64
4.1 Map of the Site Location.....	73
4.2 Soil Stratigraphy, the Average Soil Properties and the Parameters for Each Soil Layer for the Site	74
4.3 Plan View of the Site.....	75
4.4 Footing Movements over Two Years.....	76
4.5 The Water Content and Total Suction versus Depth at Footing RF1.....	78
4.6 Daily Weather Data over Two Years of a Site at Arlington, Texas	79
4.7 Comparisons between the Net Water Input and the Mean Footing Movements over a Period of Two Years for the Site	81
4.8 The Free Shrink Tests for the Three Soils: SW145, SW189 and Sporc.....	86
4.9 KAROL.WARBER Soil Testing Systems for the One Dimensional Swell-Consolidation Test and the LSCT Transducer	87
4.10 Schematic Plot of the Pressure Plate Extractor	89
4.11 Schematic Plot of the Salt Concentration Test	91

FIGURE	Page
4.12 The e-log (σ_v) Relationship for the Soil Specimen SW145 Obtained from the Swell-Consolidation Test	93
4.13 The e-log (σ_m) Relationship for the Soil Specimen SW145 Obtained from the Swell - Consolidation Test	95
4.14 The w-log (σ_v) Relationship for the Soil Specimen SW145 Obtained from the Swell - Consolidation Test	97
4.15 The w-log (σ_m) Relationship for the Soil Specimen SW145 Obtained from the Swell - Consolidation Test	97
4.16 The Soil Water Characteristic Curve Obtained from the Suction Tests.....	99
4.17 The Void Ratio and the Degree of Saturation versus Water Content Curves Obtained from the Swell Test and the Free Shrink Test.....	100
4.18 The Void Ratio versus Matric Suction Curve.....	102
4.19 The Degree of Saturation versus Matric Suction Curve	103
5.1 Nonlinear Void Ratio versus Stress State Variables Curve.....	106
5.2 The e- σ_m' Relationship for Soil Specimen SW145 Obtained from the Consolidation Test.....	107
5.3 Void Ratio Constitutive Surface in the Effective Stress σ' versus Pore Water Pressure - u_w Space.....	108
5.4 Void Ratio Constitutive Surface for a Saturated Soil	109
5.5 Water Content Constitutive Surface for the Saturated Soil Shown in Figure 5.2.....	110
5.6 Curves Needed for Constructing the Constitutive Surfaces of an Unsaturated Soil	113

FIGURE	Page
5.7 Method Proposed by Fredlund and Rahardjo.....	112
5.8 Three Planes Have One Convergent Point If Any Two of Them Are Not Parallel	115
5.9 Possible Styles for Two Small Portions of Lines with the Same Void Ratio	116
5.10 Constant Void Ratio Curves for Some Unsaturated Soils	117
5.11 Assumptions for Constant Void Ratio Curves.....	119
5.12 Constructed Void Ratio Constitutive Surface for the Soil Sample SW145.....	122
5.13 The Water Content Constitutive Surface for the Soil Sample SW145	126
5.14 The Degree of Saturation Constitutive Surface for the Soil Sample SW145...	127
5.15 Water Content versus Matric Suction Curve at Different Net Normal Stress Levels	128
5.16 Void Ratios versus Matric Suction Curve at Different Net Normal Stress Levels	128
6.1 Different Influences of Temperature and Mechanical Stress on the Volume Change of Material	138
6.2 A Coupled Thermal Stress Problem	138
6.3 Volume Change for a Material in the Coupled Thermal Stress Problem	139
6.4 Energy Constitutive Surface for a Coupled Thermal Stress Problem.....	147
6.5 Energy Constitutive Surface When the Mechanical Stress Has No Influence in Energy Variation	149
6.6 Mechanical Stress and Matric Suction's Influence in Soil Deformation	156

FIGURE	Page
6.7 Schematic Void Ratio Constitutive Surface for Unsaturated Soils.....	161
6.8 Water Content Constitutive Surface for a Coupled Hydro-Mechanical Stress Problem.....	169
6.9 A Unit Volume of Soil Element.....	179
6.10 Void Ratio Constitutive Surface for a Saturated Soil.....	203
6.11 Water Content Constitutive Surface for a Saturated Soil	203
6.12 Consolidation Stress Path on the Water Content Constitutive Surface for Unsaturated Soils	209
6.13 Consolidation Stress Path on the Void Ratio Constitutive Surface for Unsaturated Soils.....	210
6.14 Model for an Expansive Soil Example.....	219
6.15 Soil Water Characteristic Curves at Different Mechanical Stress Levels.....	223
6.16 Void Ratio versus Matric Suction at Different Mechanical Stress Levels.....	223
6.17 Permeability Function for the Soil	224
6.18 Suction Distribution Profiles at Different Times.....	224
6.19 Void Ratio Distribution Profiles at Different Times.....	225
6.20 The Consolidation Settlements and Total Settlements at Different Times.....	225
6.21 Water Content Variations during the Consolidation Process of a Soil	228
6.22 Void Ratio Variations during the Consolidation Process of a Soil	228

FIGURE	Page
6.23	Explanation of the Excess Pore Water Pressure by the Bimodal Structure of Soils230
6.24	Compression Curves of a Saturated Soil and Settlement Calculations235
6.25	Water Content and Void Ratio Constitutive Surfaces for a Collapsible Unsaturated Soil238
6.26	Degree of Saturation Constitutive Surface for a Collapsible Unsaturated Soil239
6.27	Consolidation for a Collapsible Soil239
6.28	Schematic Plot of the Consolidation Process for the Collapsible Soil242
6.29	Permeability Function of the Collapsible Soil When the Mechanical Stress Is Equal to 300kpa243
6.30	Soil Water Characteristic Curve of the Collapsible Soil When the Mechanical Stress Is Equal to 300kpa244
6.31	Matric Suction Profiles for the Collapsible Soil at Different Times245
6.32	The Void Ratio versus Matric Suction Curve for the Collapsible Soil at $\sigma - u_a = 300 \text{ kPa}$245
6.33	The Void Ratio Profiles for the Collapsible Soil at Different Times.....246
6.34	Settlements of a Collapsible Soil at Different Times246
6.35	Cooling Down of a Ring Attached on a Solid Cylinder253
6.36	Mandel-Cryer Effect.....259
6.37	Total Stress Variations during the Consolidation Process of a Soil Cylinder259

FIGURE	Page
6.38 Explanation of the Mandel-Cryer Effect.....	260
6.39 Consolidation of a Soil Cylinder.....	265
6.40 Pore Water Pressure Variations at Different Times for a Cylinder during the Consolidation Process	266
6.41a Simulation of $2m_1^s = m_2^s = m_1^w = m_2^w = -1.2 \times 10^{-4}$	269
6.41b Simulation of $\frac{1}{2}m_1^s = m_2^s = m_1^w = m_2^w = -1.2 \times 10^{-4}$	270
6.41c Simulation of $m_1^s = 2m_2^s = m_1^w = m_2^w = -1.2 \times 10^{-4}$	271
6.41d Simulation of $m_1^s = \frac{1}{2}m_2^s = m_1^w = m_2^w = -1.2 \times 10^{-4}$	271
6.41e Simulation of $m_1^s = m_2^s = 2m_1^w = m_2^w = -1.2 \times 10^{-4}$	272
6.41f Simulation of $m_1^s = m_2^s = \frac{1}{2}m_1^w = m_2^w = -1.2 \times 10^{-4}$	273
6.41g Simulation of $m_1^s = m_2^s = m_1^w = 2m_2^w = -1.2 \times 10^{-4}$	273
6.41h Simulation of $m_1^s = m_2^s = m_1^w = \frac{1}{2}m_2^w = -1.2 \times 10^{-4}$	274
6.42 Summary of the Simulation for Expansive Soils	274
6.43a Simulation of $2m_1^s = -m_2^s = m_1^w = m_2^w = -1.2 \times 10^{-4}$	279
6.43b Simulation of $\frac{1}{2}m_1^s = -m_2^s = m_1^w = m_2^w = -1.2 \times 10^{-4}$	279
6.43c Simulation of $m_1^s = -2m_2^s = m_1^w = m_2^w = -1.2 \times 10^{-4}$	280
6.43d Simulation of $m_1^s = -\frac{1}{2}m_2^s = m_1^w = m_2^w = -1.2 \times 10^{-4}$	280
6.43e Simulation of $m_1^s = -m_2^s = 2m_1^w = m_2^w = -1.2 \times 10^{-4}$	281
6.43 Simulation of $m_1^s = -m_2^s = \frac{1}{2}m_1^w = m_2^w = -1.2 \times 10^{-4}$	281
6.43g Simulation of $m_1^s = -m_2^s = m_1^w = 2m_2^w = -1.2 \times 10^{-4}$	282

FIGURE	Page
6.43h Simulation of $m_1^s = -m_2^s = m_1^w = \frac{1}{2}m_2^w = -1.2 \times 10^{-4}$	282
6.44 Summary of Simulation for Collapsible Soils.....	284
6.45 Comparison between the Coupled and Uncoupled Solutions for Expansive Soils and Collapsible Soils.....	285
6.46 The Air and Water Coefficients of Permeability for a Westwater Soil	298
6.47 Compressibility of Water, Free Air and Air-water Mixture.....	300
7.1 Schematic Representation of an Unsaturated Porous Material	304
7.2 Two Bases for the FAO 56 Penman-Monteith Method	308
7.3 The Air Relative Humidity and Total Suction at Different Times in a Day	309
7.4 Calculation Procedures of the FAO 56 Penman-Montieth Method	315
7.5 Daily Values of R_a , R_{s0} and R_s between 08/01/1999 and 05/30/2003 for the Site at Arlington, Texas	318
7.6 Daily Values of R_{ns} between 08/01/1999 and 05/30/2003 for the Site at Arlington, Texas.....	321
7.7 Daily Evapotranspiration and Rainfall of the Site between 08/01/1999 and 05/30/2003.....	324
7.8 Water Stress Coefficient, K_s	329
7.9 Water Stress Coefficient, K_s for the Site at Arlington, Texas.....	330
7.10 Cumulative Evapotranspiration, Rainfall and Net Water Loss over a Period of Two Years for a Site at Arlington, Texas	331
7.11 Water Balance of the Grass Root Zone	332
7.12 Water Loss in the Grass Root Zone.....	339
7.13 Water Losses in the Tree Root Zone	341

FIGURE	Page
8.1 Model Used for the Simulation	344
8.2 Mesh Generation of the Model.....	345
8.3 The Permeability Coefficient Surface for the Soil SW145	362
8.4 The Permeability Coefficient Surface for the Soil SW189	362
8.5 Comparison between the Heat Flow and the Water Flow under Equilibrium	366
8.6 Interpolation of the Water Content Profile for 08/01/1999	368
8.7 Mechanical Stresses versus Water Content at Different Soil Layers	369
8.8 Calculated Matric Suction Profiles for 08/01/1999.....	369
8.9 Boundary Conditions for the Simulation Domain.....	370
8.10 Grass at the Site at Arlington, Texas	372
8.11 Flowchart of the Main Program	375
8.12 Flow Chart for the User Subroutine USDFLD.....	377
8.13 Flow Chart for the User Subroutine UMTHT	380
8.14 Comparisons between the Observation and Simulation Results	383
9.1 Assumption of the BRAB Method	385
9.2 Assumed Support Conditions and Locations of Maximum Moment.....	386
9.3 Supporting Index, C, Based on Criterion for Soils Sensitivity and Climatic Rating.....	387
9.4 The Soil-Climate Support Index	389
9.5 Beam Spacing Determination.....	390
9.6 Length Modification Factors for Long and Short Directions.....	390
9.7 A Contact Element	395
9.8 Hard Contact	402
9.9 Slip Regions for the Basic Coulomb Friction Model	405

FIGURE	Page
9.10 A General Shell Element	407
9.11 Soil-Structure Interactions and Contact Elements.....	416
9.12 Simulation Domain	420
9.13 Exponential Decay Friction Model	424
9.14 Mechanical Boundary Conditions for the Simulations	425
9.15 Flow Chart for the User Subroutine USDFLD.....	428
9.16 Loads Applied in the Simulations	430
9.17 Mesh Generation of the Example Problems.....	432
9.18 An Example When There Is a Tree at the Corner of Wall 3 and Wall 6.....	435
9.19 Top View and Profiles of the Simulation Domain for an Center Lift Case.....	436
9.20 Suction Distributions at the 301 st Day for a Center Lift Case.....	438
9.21 Deformations at the 301 st Day for a Center Lift Case.....	439
9.22 Openings between the Soils and the Slab at the 301 st Day for a Center Lift Case	440
9.23 Contact Pressure between the Soils and the Slab at the 301 st Day for a Center Lift Case	441
9.24 Slips between the Soils and the Slab at the 301 st Day for a Center Lift Case.....	442
9.25 Shear Stresses between the Soils and the Slab at the 301 st Day for a Center Lift Case	443
9.26 Shapes of the Ground Soil Surface and the Slab at Different Times	444
9.27 Displacements of the Ground Soils and the Slab at Two Locations for a Center Lift Case	446
9.28 Moments at Three Different Locations at Different Times	448

FIGURE	Page
9.29 A Slab on the Ground Losing Support from Soils at the Left Side	449
9.30 Locations Where the Moments Are Presented	450
9.31 Slab Moments along the x Direction at the 1 st Day (08/01/1999) for a Center Lift Case	451
9.32 Slab Moments along the x Direction at the 101 st Day (11/09/1999) for a Center Lift Case	452
9.33 Slab Moments along the x Direction at the 201 st Day (02/17/2000) for a Center Lift Case	453
9.34 Slab Moments along the x Direction at the 301 st Day (05/27/2000) for a Center Lift Case	454
9.35 Slab Moments along the x Direction at the Different Locations and Times for a Center Lift Case	455
9.36 Maximum and Minimum Slab Moments along the x Direction in 300 Days for a Center Lift Case	457
9.37 Slab Moments along the y Direction at the 1 st Day for a Center Lift Case	458
9.38 Slab Moments along the y Direction at the 101 st Day for a Center Lift Case	460
9.39 Slab Moments along the y Direction at the 201 st Day for a Center Lift Case	461
9.40 Slab Moments along the y Direction at the 301 st Day for a Center Lift Case	462
9.41 Maximum and Minimum Slab Moments along the y Direction in 300 days for a Center Lift Case	463

FIGURE	Page
9.42 Shear Stresses between the Soils and the Slab at the 301 st Day for an Edge Lift Case	464
9.42 An Example When There Is a Tree at the Corner of the House	465
9.43 An Example When There Is a Tree at the Edge of the House	466
9.44 Suction Distributions at the 301 st Day for an Edge Lift Case	468
9.45 Deformations at the 3001st Day for an Edge Lift Case	469
9.46 Openings between the Soils and the Slab at the 301 st Day for an Edge Lift Case	469
9.47 Contact Pressure between the Soils and the Slab at the 301 st Day for an Edge Lift Case	470
9.48 Slips between the Soils and the Slab at the 301 st Day for an Edge Lift Case	471
9.49 Shear Stresses between the Soils and the Slab at the 301 st Day for an Edge Lift Case	472
9.50 Displacements of the Ground Soils and the Slab along the B-B' at Different Times for an Edge Lift Case	473
9.51 Slab Moments along the x Direction at the 1 st Day for an Edge Lift Case	474
9.52 Slab Moments along the x Direction at the 101 st Day for an Edge Lift Case	474
9.53 Slab Moments along the x Direction at the 201 st Day for an Edge Lift Case	475
9.54 Slab Moments along the x Direction at the 301 st Day for an Edge Lift Case	475

FIGURE	Page
9.55	Maximum and Minimum Slab Moments along the x Direction in 350 Days for an Edge Lift Case476
9.56	Slab Moments along the y Direction at the 1 st Day for an Edge Lift Case477
9.57	Slab Moments along the y Direction at the 101 st Day for an Edge Lift Case477
9.58	Slab Moments along the y Direction at the 201 st Day for an Edge Lift Case478
9.59	Slab Moments along the y Direction at the 301 st Day for an Edge Lift Case478
9.60	Maximum and Minimum Slab Moments along the y Direction in 350 Days for an Edge Lift Case479
9.61	Von Mises Stresses in the Structure at the 301 st Day for an Edge Lift Case480
9.62	The Smeared Cracking Model.....482
9.63	Yield and Failure Surfaces in the $(p-q)$ Plane.....484
9.64	“Tension Stiffening” Model485
9.65	Fracture Energy Cracking Model486
10.1	The Void Ratio versus Suction Curve for Soil Sample SW145492
10.2	The Void Ratio versus Water Content Curve for Soil Sample SW145493
10.3	Soil Water Characteristic Curve for Soil Sample SW145495
10.4	Actual Stress Path and Analysis Stress Path.....497
10.5	Method for Correcting the Swell Pressure498
10.6	Void Ratio versus Mechanical Stress and Water Content Surface for Soil Sample SW145500

FIGURE	Page
10.7 Plots for Simplified Coupled Water Content Method	505
10.8 Water Content Profiles of the Site over a Period of Two Years	507
10.9 The Obtained Void Ratio Profile of the Site.....	508
10.10 The Calculated PVR Values for the Site over a Period of Two Years	510

LIST OF TABLES

Table	Page
1.1	Classification of Shrinkage Potential by BRE 2
1.2	Shrink-Swell Index I_{ss} for Shrink-Swell Potential..... 2
2.1	Characteristics of the Three Clay Minerals..... 12
2.2	Typical Suction Values at Different Relative Humidity 17
3.1	The Representative Equations for These Three Methods..... 40
4.1	Type and Number of Soil Tests Performed 77
4.2	The Osmotic Coefficients for Different Salt Solutions 92
6.1	Thermodynamic Analogues to the Process of Consolidation.....187
6.2	The Comparisons in Symbols between the Coupled Consolidation Theory and the Coupled Thermal Stress Problem.....194
6.3	The Comparisons in Units between the Coupled Consolidation Theory and the Coupled Thermal Stress Problem.....195
6.4	Summary of the Results for the Consolidation of an Unsaturated Soil220
6.5	Calculation Results for the Consolidation of a Collapsible Soil.....237
6.6	Summary of the Signs of Parameters in the Constitutive Laws248
6.7	Parameter Studies for an Expansive Soil269
6.8	Parameter Studies for a Collapsible Soil.....278
7.1	Equations and Variables Summary304
7.2	Constitutive Equations and Equilibrium Restrictions305
8.1	Regression Parameters for Boundary Curves for Soil Sample SW145357
8.2	Regression Parameters for Boundary Curves for Soil Sample SW189357

CHAPTER I

INTRODUCTION

1.1 Definition

By definition, “expanse” means “great extent of something spread out”, “expansive” means “having a capacity or a tendency to expand”. So “expansive soil” means “soil with great capacity to spread out”. Expansive soils are also known as “swelling soils”, “heaving soils”, and “volume change” soils. In the United Kingdom, these soils are known as “shrinkable” soils. A new name defined by Dr. Briaud at Texas A&M University is “swell-shrink” soils. By whatever name they are called, expansive soils are clay soils. Sometimes highly compressed shale can also be expansive. The characteristic of expansive soils is that they expand when they get wetter and shrink when they get drier. Actually all clayey soils have a volume change when their water content changes, only those soils that shrink and swell to extremes are called “expansive soils”.

The potential for a clay soil to cause damage by shrinking or swelling is called its shrinkage potential. For convenience, the shrinkage potential is assumed to be proportional to the difference between the liquid limit and the plastic limit, i.e., plasticity index of the soil. Three classifications of shrinkage potential are suggested by the National House-Building Council (NHBC), and the Building Research Establishment (BRE) have more recently proposed the classifications as shown in Table 1.1.

However, the plasticity index is only a rough indicator of the potential of the soil to change volume. Usually the soil in the field will change the volume from swell limit to shrinkage limit. Based on experience with the shrink test and the swell test, Briaud et al (2003) proposed that the shrinkage potential of soil can be determined by the shrink-swell index which is defined as the difference between the swell limit and shrinkage limit. Table 1.2 shows the proposed classifications.

The style and format of this dissertation follow the *Journal of Geotechnical and Geoenvironmental Engineering, ASCE*.

It is important to appreciate, however, that all these classifications are based only the soils' ability when there is no load application. When loads are applied to the soils, soil volumes will also change due to compression. The final properties of the soils will depend on the combination of two factors. Therefore, the classifications depending on the single plasticity index or "shrink-swell index" is not good enough for determining the shrinkage potential of the soil. An example is the shale, which have low plasticity index, but have high shrinkage potential. Further discussions please see Chapter X.

Table 1.1. Classification of Shrinkage Potential by BRE

Classification	Plasticity Index: %
low	less than 20
medium	20 to 40
high	40 to 60
very high	over 60

Table 1.2. Shrink-Swell Index I_{ss} for Shrink-Swell Potential

Potential	Shrink-Swell Index I_{ss}
Very High	> 60%
High	40% - 60%
Moderate	20% - 40%
Low	< 20%

1.2 Problems Caused by Expansive Soils

The characteristic of expansive soils is that when expansive soils absorb water from the environment, they will increase volume. If the increase in volume is not restrained and the soil has the opportunity to swell in all the direction, the soil increases its volume in all the direction with the same amount (Fig.1.1a). But for the soil in the field on which we build our house, when it gets wetter the lateral expansion is prevented by the soil adjacent to it. In this case, there is no lateral expansion, instead all the expansion or swell occurs in the vertical direction and the expansive soil near the ground surface move upward, or "heave" (Fig. 1.1b).

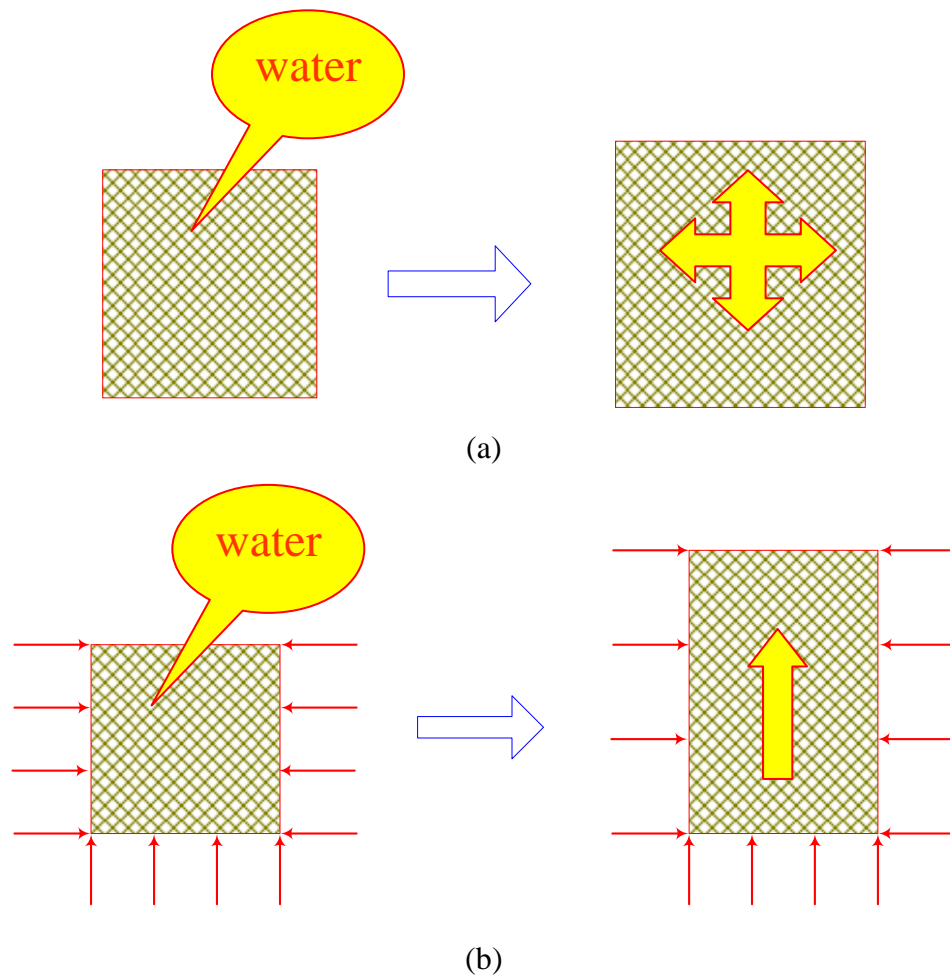


Fig. 1.1. Factors influencing the soil volume. (a) soil expands in three directions when there is no restriction; (b) soil heaves when the horizontal deformation is restricted

Conversely, if the soil is drying out, the soil decreases its volume in all the directions. In both lateral and vertical direction, soil decreases volume. The volume decrease in vertical direction causes the soil surface to “go down” or “recede”, the lateral decrease in volume causes soil to crack, if it is large enough.

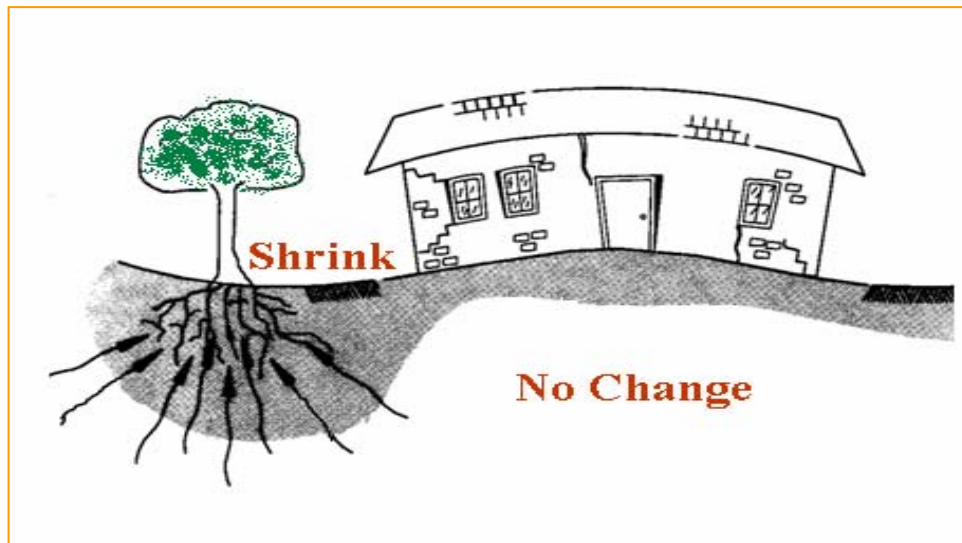
Generally, weather changes cyclically every year, precipitations such as rainfall, snow and ice lead to increases in soil water content by water infiltration. Evaporation from the soil surface or transpiration from vegetation or tree leads to decreases in soil

water content. The water content variations in the soil caused by environment lead to the soil surface heave or recede cyclically.

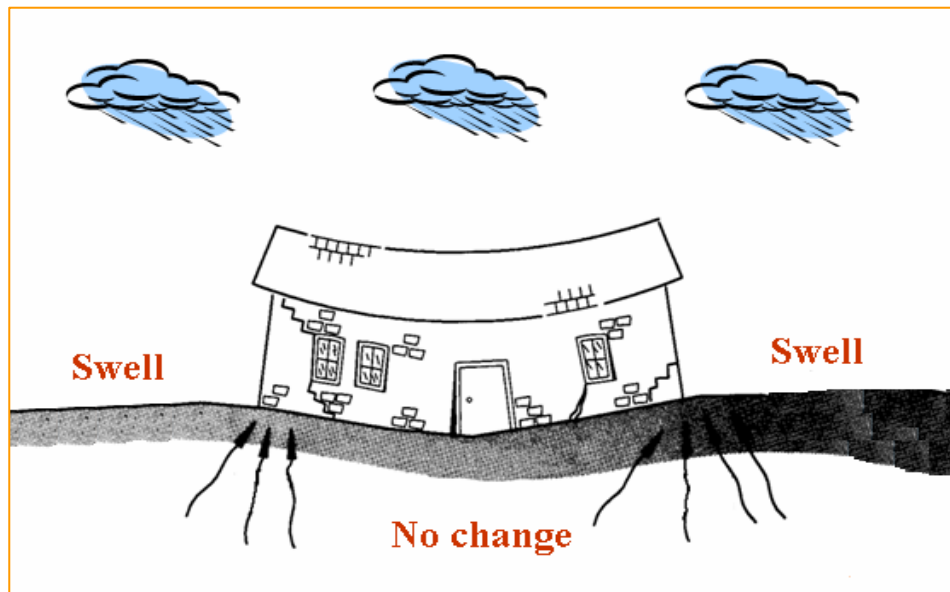
If a building is built on expansive soil and the building going upward or downward uniformly, there will be no damage to the building. Most damage happens when there are differential movements caused by expansive soils, that is, when different parts of the building have different amount of vertical movements. In these cases, the differential movements cause stress concentration in the structure because of the differential movements. If the structure is strong enough or the stress concentration is small, there is still no damage. Otherwise, damage will occur and usually crack will appear in the structure.

Fig.1.2 illustrates the damage caused by the expansive soils at different seasons. Usually during summer, the weather is dry and the dominant influence of weather on soils is evaporation or evapotranspiration if there is vegetation. Under this condition, the soils underneath the edge of the house shrink due to water loss. Correspondingly, the ground surface recedes. At the same time, the soils underneath the center of the house remain unchanged or change very little because the foundation covers the soil surface and evaporation from the soil is prevented. As a consequence there are differential movements and the differential movements will cause damage to house if the differential movements are large enough.

Fig.1.2b illustrates the condition during winter. The weather is wet and the dominant influence of weather on expansive soils is to wet the soils. Under this condition, the soils underneath the edge of the house will swell and the ground surface will heave correspondingly. At the same time, the soil underneath the center of the house remains unchanged. There are also differential movements, and if they are large enough, damage appears.



(a)



(b)

Fig.1.2. Damages cause by expansive soils at different seasons. (a) in summer; (b) in winter (Modified from Wray 1995)

1.3. Significance of the Research

Expansive soils are found through out the United States and in almost all parts of the world. The influence of expansive soil damage on a local, regional, or national scale is considerable. Jones and Holtz (1973) estimated that the annual cost of expansive soil damage in the U.S. is \$2.2 billion, which exceeds that caused by earthquakes, hurricanes, and flood combined in an average year. Krohn and Slosson (1980) estimated that the annual cost of expansive soil damage in the US to be \$7.billion in 1980. Krohn and Slosson further estimated that damages to single-family and commercial buildings accounted for nearly one-third of the total amount of damage resulting from expansive soils. A damage survey conducted solely in Dallas County, Texas, identified 8,470 residential foundation failures in only one year, 98% of which occurred in expansive soils (Wray 1995). Huge loss caused by expansive soils and the awareness of the public to the damage caused by expansive soils pose great requirement for the research in the foundation on expansive soils.

1.4. Objective of Study

Most of the volume change of expansive soils occurs when there is water content variation and when the soils are unsaturated soils. It is noted that the unsaturated soils here are referred as either the soils with negative pore water pressure or the soils with degree of saturation less than 100%. The research on expansive soils belongs to the scope of unsaturated soil mechanics. In the past three decades, especially in the past 10 years, there is great progress in the unsaturated soil mechanics. The most representative is the textbook by Fredlund and Rahardjo (1993). They use two stress state variables concept to explain the phenomenon for unsaturated soils such as shear strength of the soils, bear capacity of foundation and the volume change of expansive soils. However, the practice of expansive soil in the industry is still highly empirical. There are still great needs for further research in this field. The objectives of my research are as follows:

1) Study the mechanism of volume change of expansive soils, and their influence on the structure,

2) Numerically simulate the behavior of building on expansive soils by using climatologic data directly, to explain some typical phenomenon of building on expansive soils, and

3) Provide some guidelines for the practical design and develop a simple technology to be used in the future which is practical, economical and has a sound theoretical basis.

1.5. Outline of This Dissertation

Chapter II presents the factors influencing the damage caused by the expansive soils. Firstly the soil structure is discussed. Literature reviews indicate that soils have two levels of structure: a microstructure level and a macrostructure level. Evidence tends to indicate that the mechanical stress mainly influences the soil's macrostructure and the matric suction influences both the microstructure and macrostructure. The possible reason why the maximum suction in the soil is 1,000,000kPa is also presented. Factors influencing the soil water balance are mainly weather factors such as temperature, solar radiation, relative humidity, wind speed and rainfall. Vegetations also have great influences on water balance in soils. Some problems associated with soil structure interaction are also discussed. Finally, the conventions of this dissertation are also presented.

Chapter III presents the models needed for the simulation of the residential buildings on expansive soils. The models include the coupled consolidation theory for saturated-unsaturated soils, potential and actual evapotranspiration estimation by using daily weather data, theories for the simulation of the soil-structure interaction at the soil-slab interface, the finite element method of plate simulation, the smeared cracking model for house cracking simulation. The methodology of the research is also presented.

Chapter IV presents the laboratory tests needed for the construction of the constitutive surfaces for saturated-unsaturated soils. At minimum four lab tests are needed: the swell test-one dimensional consolidation test, the free shrink test, soil water

characteristic curve (the pressure plate test and salt concentration test), and the specific gravity test. The methods to use these tests to obtain the six curves needed for the construction of the constitutive surfaces are presented and the tests results for three soils are presented.

Chapter V proposes a new method to construct the constitutive surfaces for saturated-unsaturated soils. Straight line assumption is used to construct the constitutive surfaces for three soils. The method and the program used to obtain the derivatives (the parameters for the coupled consolidation for saturated unsaturated soils) of the constitutive surfaces are introduced.

Chapter VI compares the coupled thermal stress problem and the coupled hydro-mechanical stress problem. It is found that there are close similarity between them. The thermodynamic analogue to the consolidation process is used to illustrate the two stress state variable concept, essentiality of the equivalent effective stress principle and the excess pore water pressure parameters. The differential equations for the coupled hydro-mechanical stress analysis are derived and a simple method is proposed to solve them by modifying the current available programs for the coupled thermal stress problem. The thermodynamic analogue to the consolidation process is also used to explain the numerical analysis results for the coupled and uncoupled consolidation theory. The physical meanings of the parameters in the constitutive laws for unsaturated soils are explained. Literature reviews and discussions for the consolidation theory are also presented.

Terzaghi's consolidation theory for saturated soils is explained by considering saturated soils as a special case of unsaturated soils. The void ratio and water content constitutive surfaces are used to describe the Terzaghi's consolidation theory and the essentiality of the method is discussed. Based on the discussion, the Terzaghi's consolidation theory is extended to the unsaturated soils. For the first time, the immediate settlement, consolidation settlement, total settlement, time rate of consolidation for unsaturated soils and excessive pore water pressure can be calculated manually in the same way as what we have done for saturated soils with a higher

accuracy. It makes the consolidation theory of unsaturated soils as applicable as that of saturated soils. This method can also be used to perform uncoupled two or three dimensional consolidation calculation for both expansive soils and collapsible soils. From the analysis, the equivalent effective stress and excessive pore water pressure can be easily calculated.

The proposed method is also used for the calculation of the consolidation of collapsible soils. Based on the discussion of the consolidation of expansive soils and collapsible soils, parameter studies are performed to investigate the coupled consolidation theory for expansive and collapsible soils. Finally, some basic topics for the consolidation theory of unsaturated soils are discussed.

Chapter VII introduces the FAO 56 Penman-Monteith method for the estimation of the evapotranspiration by using daily or hourly weather data. A site at Arlington, Texas is used to show the calculation procedure. The method to estimate the soil water balance proposed by the FAO 56 Penman-Monteith method is discussed and the corresponding method to determine the boundary conditions for different environmental conditions such as tree, grass and bare soils are proposed.

Chapter VIII performs a simulation by using the proposed theory and the method for estimating the evapotranspiration. The simulation result is compared with the observation data and it is found that they match reasonably well. Contact element is also used in the simulation.

Chapter IX proposes a complete system for the simulations of residential buildings on expansive soils. The coupled consolidation theory is used to simulate the volume change behavior for saturated-unsaturated soils. Contact (jointed) elements are used to simulate the slab-soil interaction at the interface while general purpose shell elements are used to simulate the behavior of slabs and walls. A pseudo moisture variation simulation is proposed to solve the problem during the conversion from the coupled mechanical stress and matric suction analysis and the mechanical stress analysis. Some tentative results as well as recommendations for future research are presented. The smeared crack model is proposed for the simulation of house cracking.

Chapter X reviews current methods and tests for movement predictions and their limitations. Based on the theory of unsaturated soil mechanics, a void ratio versus mechanical stress and water content surface is constructed, which can potentially be used to predict the potential vertical swell and potential vertical shrink of shrink-swell soils at the same time. A simplified method is proposed to construct the surface and a procedure is proposed to calculate the volume change due to moisture variations. Based on the constructed surface, the existing methods are discussed and their limitations are eliminated. A new method which couples the influence of both mechanical stress and suction is provided for practical estimates of the volume change of shrink-swell soils.

Chapter XI summarizes the conclusions reached by this study and some recommendations for the future research are presented.

CHAPTER II

FACTORS INFLUENCING DAMAGE TO RESIDENTIAL BUILDINGS

2.1 Introduction

As we discussed in Chapter I, the factors influencing the damage to the house will be soil behavior, weather (or environmental) condition, soil-structure interaction and the behavior of the structure. To better understand the problem, this chapter discusses in detail the soil structure and behavior, weather factors, possible soil-structure interactions and damage to the structure.

2.2 Soil Structure and Factors Influencing the Mechanical Behaviors of Soils

2.2.1 Introduction

To understand the soil behaviors, first we need understand the soil structures. The soil fabric has been studied by using a variety of techniques in the past, revealing two distinct structural levels: a micro-structural one and a macro-structural one. Pusch (1982) observed a double structure made up of clay aggregates and large macro-structural pores for compacted expansive soils. Other evidences were provided by Gens and Alonso (1992), Atabek et al. (1991), Romero et al. (1999), Pusch and Moreno (2001), and Cui et al. (2002). The engineering behaviors of these deposits are strongly influenced by both macro- and microstructure. At present, no quantitative connection exists between the microstructure and the engineering properties of the soils, but a qualitative knowledge is helpful to understand their relation to engineering behavior.

2.2.2 Microstructure of Soils

Clay minerals are very tiny crystalline substances consisting of two fundamental crystal sheets: (1) the tetrahedron or silica, and (2) the octahedron or alumina, sheets. These sheets are stacked together in particular ways, together with different bonding and different metallic ions in the crystal lattice, constituting the different clay minerals:

Kaolinite, illite and montmorillonite. Clay particles are very small. Table 2.1 shows the characteristic of the three clay minerals. Montmorillonite has the smallest dimension and the biggest specific area. The bigger the specific area, the greater the ability of clay particle to absorb water.

Table 2.1. Characteristics of the Three Clay Minerals (Yong and Warkentin 1975)

Clay Minerals Character	Kaolinite	Illite	Montmorillonite
Length and width (nm)	0.3-3.0	0.1-2.0	0.1-1.0
Thickness	0.03-1.0	0.01-0.02	0.001-0.01
Specific area (m ² /g)	20-80	80-100	800
Liquid limit (%)	30-110	60-120	100-900
Plastic limit (%)	25-40	35-60	50-100
Shrink- swell potential	Low	Medium	High

Research indicates there are usually some imbalanced charges at the clay particles surface (Mitchell 1976). The surface charges on the clay soils are negative (anions). The source of the negative charge results from both isomorphous substitution and imperfections in the crystal lattice, especially at the surface. "Broken" edges contribute greatly to unsatisfied valence charges at the edges of the crystal. It is well known that where the smaller the particle, the larger the specific surface. Clay minerals, being relatively small particles, have large specific surfaces. At the same time, large negative charges are derived from large specific surfaces.

Clay particles are almost always hydrated in nature for the following three reasons: Firstly, water molecules have a dipole. Consequently, a water molecule acts like a small rod with a positive charge at one end and a negative charge at the other end. The clay particles carry a net negative charge on their surfaces. Therefore, the water molecule is electro-statically attracted to the surface of the clay crystal. Secondly, water is held to the clay crystal by hydrogen bonding (hydrogen of the water is attracted to the oxygen or

hydroxyls on the surface of the clay). The third factor is that the negatively charged clay surface also attracts cations present in the water. Since all cations are hydrated to some extent, depending on the ion, cations also contribute to the attraction of water to the clay surface.

Due to the negative charge at the surface of the soil particles, an electric field is formed around the soil particles. The ions in the water will be attracted to the surrounding of the soil particles. The water will also be attracted to arrange in an oriented direction. The negative charge at the soil surface forms the inner layer of electric field and the attracted ions and the orientally arranged water molecules form the outer layer of the electric field, these two layers are called “double diffusion layer”(Fig. 2.1). All of the water held to clay particles by force of attraction is known as double-layer water. The innermost layer of double-layer water, which is held very strongly by clay, is known as adsorbed water. This water is more viscous than free water. The orientation of water around the clay particles gives clay soils their plastic properties. The largest concentration of cations occurs at the mineral surface, which can reach 1,000,000kPa, and decreases exponentially with distance away from the surface. Fig. 2.2 shows the relative sizes of absorbed water layers on sodium montmorillonite and sodium kaolinite.

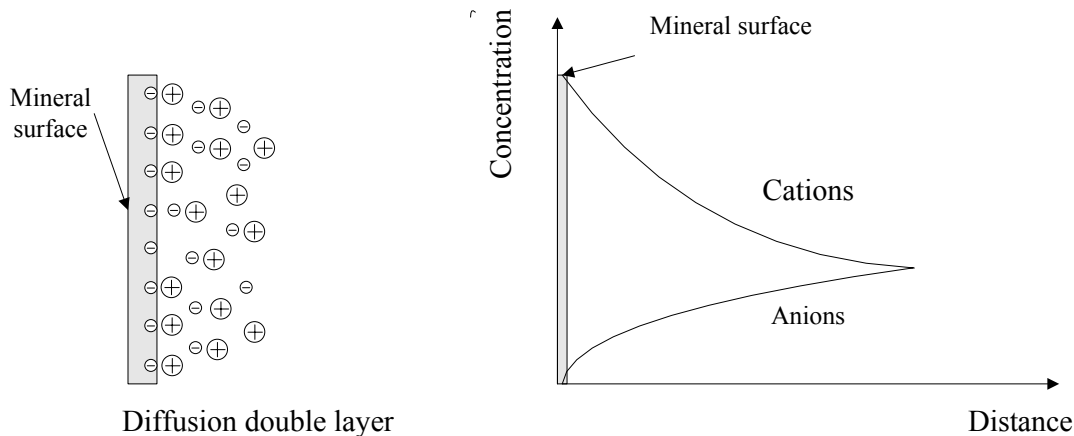


Fig. 2.1. Diffuse double layers (after Mitchell 1976)

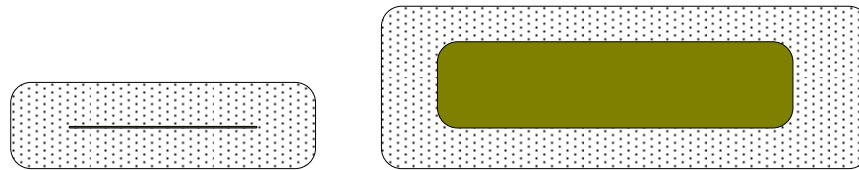


Fig. 2.2. The relative sizes of absorbed water layers on sodium montmorillonite and sodium kaolinite (adapted from Lambe and Whitman 1969)

2.2.3 Macrostructure of Soils

From the studies of real clay soils with the scanning electron microscope (SEM), the individual clay particles seem to always be aggregated or flocculated together in submicroscopic fabric units called domains. Domains then in turn group together to form cluster which large enough to be seen with a visible light microscope. Clusters group together to form peds and even groups of peds. Peds can be seen without a microscope, and they and other macrostructural features such as joints and fissures constitute the macrofabric system. A schematic sketch of this system proposed by Yong and Sheeran (1973) is shown in Fig. 2.3. A microscopic view of a marine clay is also included (Pusch 1973). Collins and McGown (1974) show microphotographs of several natural soils which illustrate the similar classification.

As can be seen for sand, different sizes of particles form different sizes of pore size. The bigger the particles sizes, the bigger the pore sizes in the soil. It is easy to image that there are two levels of pore size in the clay corresponding to the microstructure and the macro structural level. Because the clay particles are very small, the diameter of the pore between clay particles will be much smaller than that of the pore between the peds.

The soil behavior will be easier to understand if we use a simplified model as following: the clay aggregates such as domain, clusters and peds are corresponding to different sizes of sand particles and these particles form different macropore sizes. The bigger the clay aggregates, the greater the pore sizes they forms. There are also a lot of small pores interior to the clay aggregates, they are much smaller than that formed by the

clay aggregates. Fig. 2.4 shows the simplified bimodal structure for clay soils. The strength of the clay aggregate will depend on the water it hold, the more water it holds, the softer the clay aggregate.

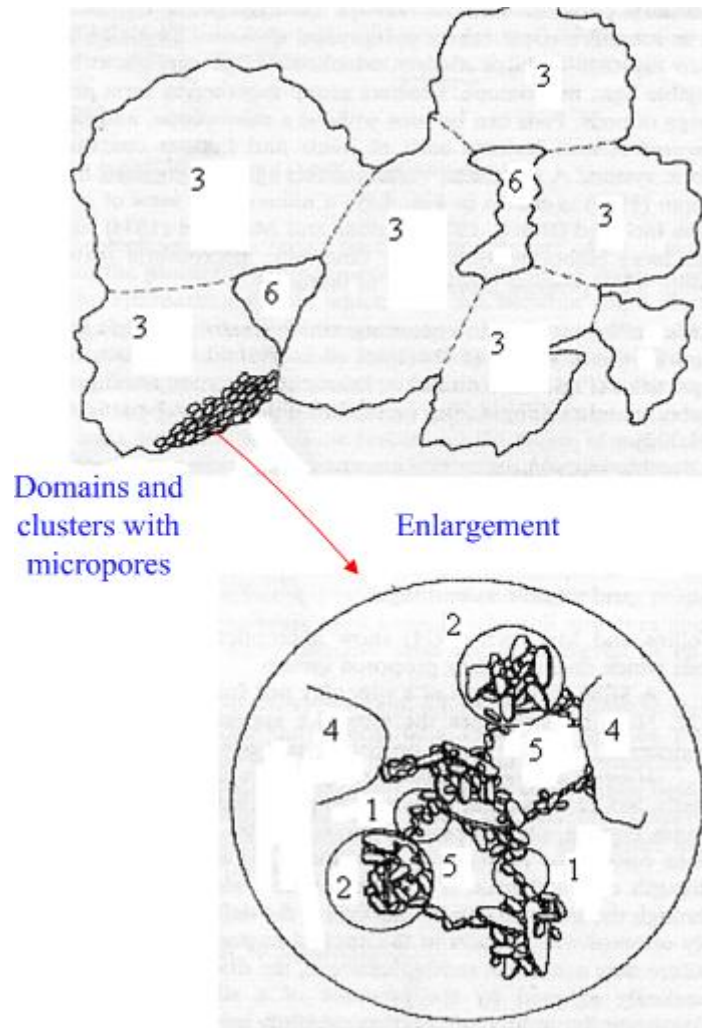


Fig. 2.3. Schematic diagram of the soil microfabric and macrofabric system (Yong and Sheeran 1973; Pusch 1973): 1, domain; 2, cluster; 3, ped; 4, silt grain; 5, micropores; and 6, macropore

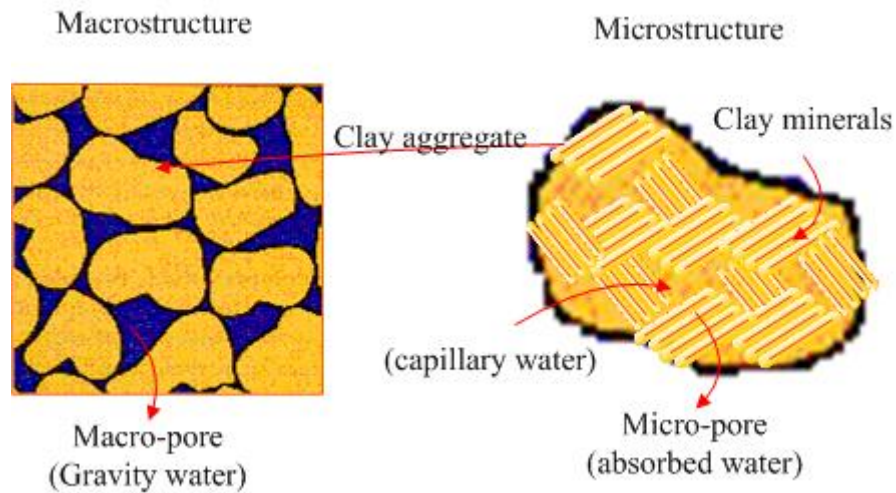


Fig. 2.4. Simplified bimodal structure of the clay soil (adapted from Biddle 1998)

2.2.4 Two Stress State Variables

Fredlund and Rahardjo (1993) proposed two stress state variables for unsaturated soils: mechanical stress and matric suction.

2.2.4.1 Suction

Soil suction referred as the free energy state of soil water, which is related to the relative humidity. The total suction of a soil can be calculated by the Kelvin's Equation as followings:

$$\psi = -\frac{RT}{v_{w0}w_v} \ln\left(\frac{P}{P_0}\right) \quad (2.1)$$

where ψ =total suction (kPa); R =universal gas constant, equal to 8.31432 J/(mol•K); T =absolute temperature (K); v_{w0} = specific volume of water (m^3/kg); w_v =molecular mass of water vapor (kg/kmol); P = partial pressure of pore-water vapor (kPa); and P_0 =

saturation pore water pressure at the same temperature; and $RH = \frac{P}{P_0}$ is also called relative humidity.

Table 2.2. Typical Suction Values at Different Relative Humidities

RH	(%)	100	99.999	99.99	99.9	99	93	80	70	60	50	1	0
suction	kPa	0	1.4	14	135	1357	9799	30129	48159	68973	93590	621799	∞
suction	(pF)		1.1	2.1	3.1	4.1	5.0	5.5	5.7	5.8	6.0	6.8	∞

Table 2.2 shows some typical suction values at different relative humidity values. As can be seen, for the normal relative humidity range, 50%-100%, the suction varies from 0 to 100,000kPa. Therefore, the range of suctions of interest in geotechnical engineering will respond to huge suction range.

Suction calculated by Eq. 2.1 is called total suction. It has two components, namely, matric suction and osmotic suction.

$$\psi = (u_a - u_w) + \pi \quad (2.2)$$

where $(u_a - u_w)$ = matric suction (kPa); u_a = pore-air pressure(kPa); u_w =pore-water pressure(kPa); and π = osmotic suction (kPa).

Matric suction is related to capillary phenomenon and osmotic suction is related to solution salt concentration. Under this condition when the pore air pressure is zero (engineering atmospheric pressure), matric suction actually is the absolute value of the negative pore water pressure.

It has been observed for many soils that the soil-water characteristic curve extrapolates to a suction value of 1,000,000 kPa at zero percentage water content. An explanation for this is that the suction actually represents the potential of soil to hold water. As has been discussed before, the ability of the soil to hold water depends on the soil electricity at the soil particle surfaces. The maximum suction value by Eq. 2.1 could

be infinite when the relative humidity is zero. However, the ability of soil particle to hold water is limited. The suction which is required to remove the water from the soil is in balance with the soil water potential. This soil water potential will depend on the electric force that the soil particle has to hold the water molecules. Research indicates that the maximum force the electric field can applied to water molecules is 1,000,000kPa (Chen et al. 1994). Consequently, the maximum suction value should also be 1,000,000 kPa. This fact will be helpful in estimating the position of soil water characteristic curves at high suction.

Osmotic suction is also important for the soil properties. The dilute concentration in the soil will directly influence the thickness of the double diffusion layer. In this dissertation, to make the problem simple, the osmotic suction is considered as constant and the water content variation will not lead to variations in osmotic suction. Another assumption is that at high suction range, the total suction is equal to matric suction.

Matric suction is related to pore size of a soil. The relationship is expressed by the Kelvin's Equation:

$$(u_a - u_w) = \frac{2T_s}{R_s} \quad (2.3)$$

where T_s = surface tension of the water, and R_s = pore size.

2.2.4.2. Air-Entry Value of the Soil

The air-entry value of the soil, $(u_a - u_w)_b$, is defined as the matric suction value that must be exceeded before air recedes into the soil pores. From the definition of the air-entry value, we can see that before the soil suction reaches the air-entry value, the soil is actually saturated. The air-entry value depends on the soil pore size, the smaller the soil pore size, the bigger the air entry value. As can be seen in Table 2.1, the clay particles are very small, it is expected that the soil pore sizes are also very small and the air entry values for the clay soil are always very high and for the same soil classification, the air

entry value will be the same because the soil mineral is the same. However, it is not the truth. As we discussed before, the clay soil have two levels of structure, a microstructure and a macrostructure level. Because the clay aggregates have different sizes and they arrange in different ways, for soils with the same soil mineral, the macro structures of the soils will be different, and the corresponding macro pore sizes are different. Usually the pore sizes in a soil are not uniform but vary greatly. Different pore sizes have corresponding different air-entry values. For a real soil, the pore sizes vary in a very large range. The corresponding air-entry values will also be different. The traditional meaning of “air-entry value” for a soil seems to be associated with the maximum macropores rather than the micropores. Therefore, even for the soils with the same soil minerals, the air entry values could be different.

2.2.4.3. Soil Water Characteristic Curve

The soil water characteristic curve is referred to the relationship between the water content and the matric suction of the soil. It reflects the matric suction variation when there is water content variation. Because matric suction is related to the pore size, the soil water characteristic curve is also related to the soils pore size. Generally speaking, the soil water characteristic curve reflects the pore size distributions of the soil.

2.2.5. Water in the Soils

The water in the soil can be divided into two main categories: absorbed water and free water.

2.2.5.1. Absorbed Water

According to the distance to the surface of the soil particle and the attraction force, the absorbed water can be divided into strongly absorbed water and weakly absorbed water.

2.2.5.1.1. Strongly Absorbed Water

The strongly absorbed water refers to the water molecules innermost to the surface of the soil particles, which are strongly attracted to the soil particles. It has a crystalline structure and the water molecules are fixed at the soil particle surface. Its melting point is much less than 0°C and the density is bigger than natural water. Temperature must be higher than 100°C to remove all the water from the soil.

2.2.5.1.2. Weakly Absorbed Water

Weakly absorbed water refers to the water molecules in the influence scope of the electric field except the strongly absorbed water. The water is attracted to the soil particles but the attraction force decreases with the distance to the soil particle. It is not crystalline any more but a water membrane with viscosity higher than the normal viscosity and should exhibit non-Newtonian flow. The water molecules can move slowly from one soil particles to another due to the load application and the electric field force, that is, the weakly absorbed water can deform but can not flow under the influence of gravity. The existence of the weakly absorbed water is also considered as the cause of the soil plasticity.

The absorbed water is the water at innermost part of the double diffusion layer and it is in the influence range of electric field. Generally speaking, Darcy's law will not be applicable anymore for absorbed water because it is non-Newtonian flow. In this dissertation, the problem is neglected. Further research is needed in this direction.

2.2.5.2. Free Water

Free water refers to the water under the influence of the gravity. Free water can be divided into capillary water and gravity water.

2.2.5.2.1. Capillary Water

Capillary water is related to the capillary phenomenon. It is caused by the surface tension force between the clay mineral and the water molecules. It can be visualized as the water interior to the clay aggregates.

2.2.5.2.2. Gravity Water

Gravity water is referred as the water in the macropore of the soil. Gravity water is the water below the ground water level; it will not be influenced by soil particle electric field, and can move under the influence of gravity. The water will be drained when the soil is at position higher than the ground water level. The definition of the field capacity is that a soil above the ground water table level which has been allowed to drain naturally is described as being at field capacity. At field capacity those structural voids larger than about 60 μm will be drained (Biddle 1998). So the Gravity water corresponds to the water in the soil structural voids greater than 60 μm . Both capillary water and gravity water are Newtonian flow.

2.2.5.3. Drying Procedure for Clays

As sand particles are not compressible, the changes in moisture content will not produce any volumetric change. Fig. 2.5 shows this relationship; with this non-compressible sandy soil it is of limited interest, but as we discussed before, the clay soils have bimodal structure, the macrostructure is similar to sand. Therefore, it is included to allow comparisons with the situation in clay soils. Fig. 2.5a shows a fully saturated sand, and all the voids are filled with water, in this case, the suction is zero or positive. Fig. 2.5b shows the when the sand is at field capacity, voids larger than 60 μm have a lower air-entry value and are drained. Fig. 2.5c shows sand at a little bit higher suction, the sand can only holds water in the finest voids due to capillarity.

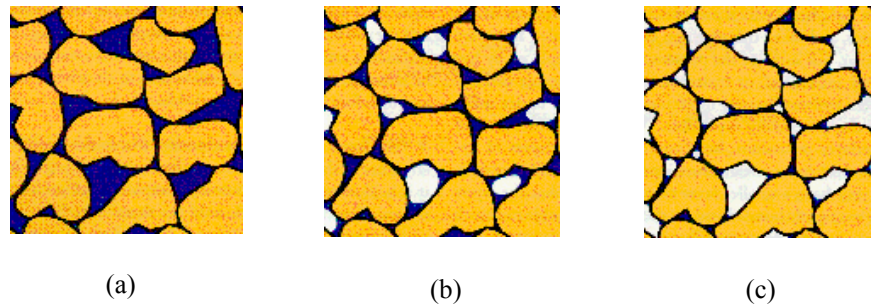


Fig. 2.5. Drying process of a sand (adapted from Biddle 1998)

Biddle (1998) proposed that four stages can be recognized in the clay soil drying:

a) Structural shrinkage, large water-filled pores will be drained firstly and fill with air because the air-entry value is low. No volume change occurs in this range when the soil water content decreases (Fig. 2.6a). This is a process which is similar to the drying process of sand. The soil will be at field capacity and the corresponding suction value is about 5-10kPa, depending on the pore size of the structural void. The lost water is the gravity water.

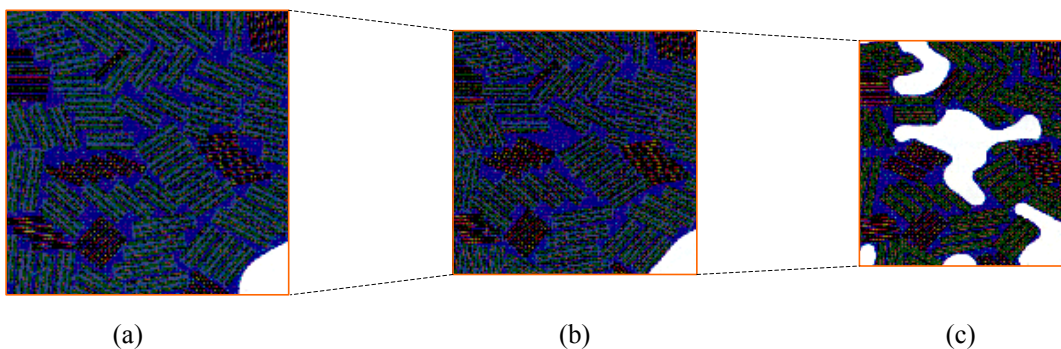


Fig. 2.6. Drying process of a clay (adapted from Biddle 1998)

b) Normal shrinkage, as suction increases, the water in the soil continues losing by evaporation. The suction value at this stage is lower than the air-entry value of microstructure pores. No air enters into the clay aggregates and the clay aggregates are

still “saturated” and the effective stress principle holds internally. The volume of the aggregate will decrease. The structural void will also decrease too. Whether the degree of saturation will decrease or not will depend on the relative ratio of the reduction in water volume and structural void volume, the volume change of the soil will be equal to the volume of water loss approximately. The water is capillary water (Fig. 2.6b).

c) Residual shrinkage –As suction further increases, the soil continuously dries, air starts to enter the relative large micropores which have a relative low air-entry value with respect to the smallest micro pores. Consequently, although there is further reduction in volume, the rate of water loss exceeds the volume loss of soil, and the degree of saturation will decrease continuously. The water is partially capillary water and partially weakly absorbed water (Fig. 2.6c).

d) Zero shrinkage, Water content is between the 0 and the shrinkage limit and the soil particles have reached their densest configuration, and there is no further volume loss. Further loss of water produces a corresponding increase in the air volume within the soil aggregates. The lost water is absorbed water. The total suction value at the zero water content will depend on the ability of the soil to hold water, and the maximum electric field force at the soil surface is 1,000,000 for most soil. Therefore, the maximum suction value in the soil is 1,000,000kPa.

2.2.6 Mechanical Stress and Matric Suction’s Influence on Soil Structure

Both mechanical stress and matric suction will influence the macrostructure of the soil. When there is load application, the structural void of the clay soil is much easier to be compressed than the soil particle(The compressibility of the water and the clay particles is less than 10^{-7} kPa⁻¹, the compressibility of air is about 10^{-3} kPa⁻¹, and the compressibility the soil structure is about 10^{-4} kPa⁻¹ to 10^{-6} kPa⁻¹). At the same time, water in the macro-pore is easy to move. Consequently, when there is mechanical load application, the macropore will be compressed firstly. Fig. 2.7a shows the conceptual bimodal structure of the clay, the three balls represent the clay aggregates consisting of a lot of clay particles, the pore size of the ball depends on the clay particles and the ball is

saturated. Three balls (clay aggregates) form a macropore. Fig. 2.7b shows the condition when there is a mechanical load application, the shapes of the clay aggregate change without volume change due to undrained compression. The clay aggregates deforms and the macro-pore is compressed and the void decrease due to air drainage (or air compression). At the instant of load application, there is no water drainage. The water between the soil particles is squeezed out and the radius of curvature of the meniscus increases, which causes a decrease in matric suction (an increase in pore water pressure).

Increase in matric suction will also cause soil volume change. Fig.2.7c shows the influence of matric suction on the macropore. When there is an increase in matric suction, the water in the soil aggregate is evaporated and the volumes of the aggregates decrease. Due to the decrease in volume of the aggregates, the macropore between aggregates also decreases somewhat.

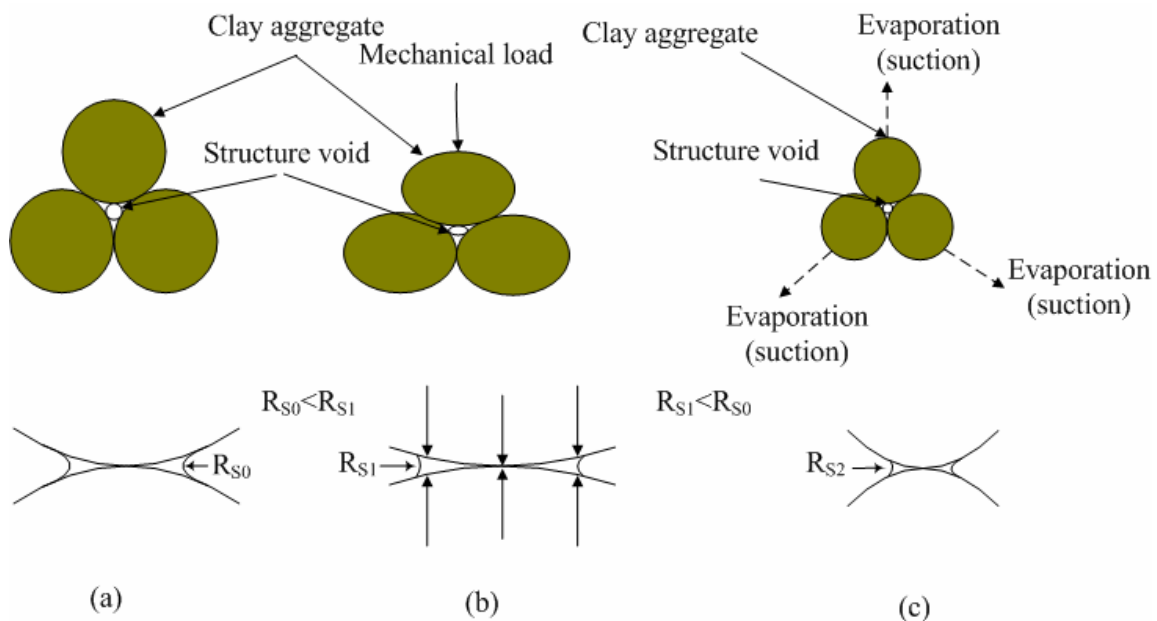


Fig. 2.7. Mechanical stress and matric suction's influence on macrostructure

Mechanical stress and matric suction will also influence the microstructure of the soil. Fig. 2.8 shows the mechanical stress and matric suction's influence on the micropore of clays. When there is mechanical load application, the applied load will be

transferred to the clay particles, the radius of curvature of the meniscus tends to increase because the compression tends to squeeze the water out (Fig. 2.8a). The matric suction will decrease according to Eq. 2.3.

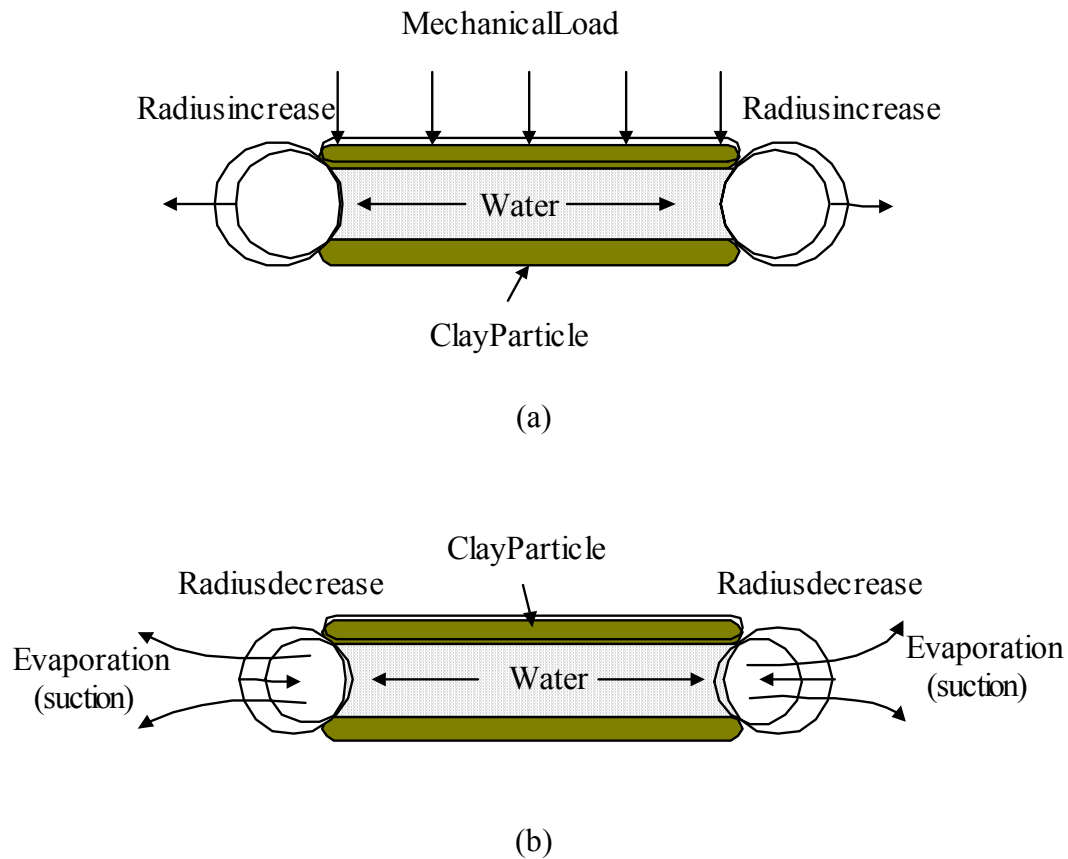


Fig. 2.8. Mechanical stress and matric suction's influence on microstructure

Fig. 2.8b shows the influence of drying (increase in matric suction) on the micropore. When soil is drying, the water between the soil particles tends to lose due to evaporation, the water will recede between the particles, which cause the radius of curvature of the meniscus decreases, consequently, the matric suction will increase. The micropore between the particles is usually very small, which corresponds to a high air entry value. Under the condition that the air can not enter into the soil, lose in water will cause decreases in the thickness of the double diffusion layer.

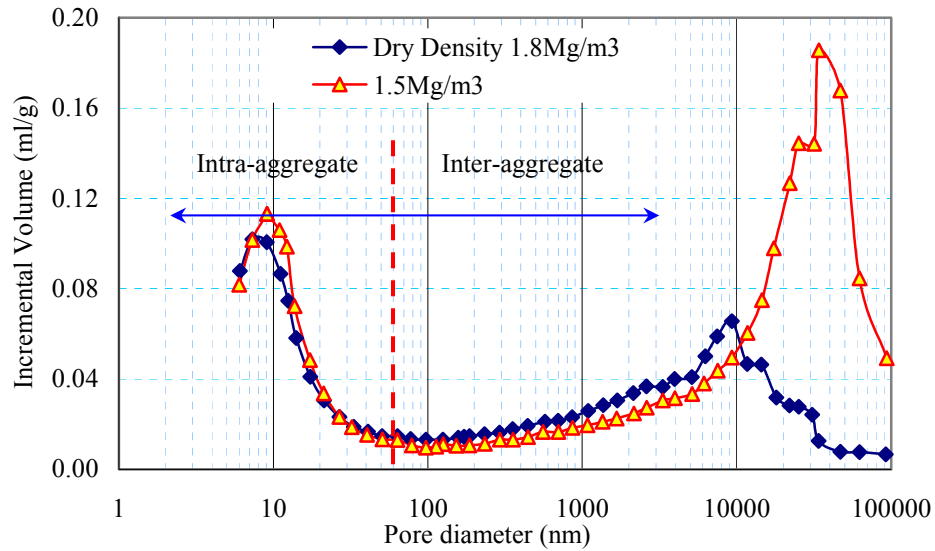


Fig. 2.9. Mechanical stress and matric suction's influence on micropores and macropores (Lloret et al. 2003)

Lloret et al. (2003) used the mercury intrusion porosimetry (MIT) tests to examine the pore size distribution of the statically compacted bentonite. Fig. 2.9 shows the measured incremental pore volume for two samples compacted to very different values of dry density (ρ_d), 1.5 Mg/m^3 and 1.8 Mg/m^3 . It can be observed that the pore size distribution is clearly bimodal. The dominant values corresponding to the micropores in the clay aggregates are 10 nm. A larger pore size corresponding to the inter-aggregate pores ranges from $10 \text{ }\mu\text{m}$ (for $\rho_d = 1.8 \text{ Mg/m}^3$) to $40 \text{ }\mu\text{m}$ (for $\rho_d = 1.5 \text{ Mg/m}^3$), depending on the compaction dry density. The distinctions between the two pore size families can be seen to be around 130 nm, and pores smaller than this magnitude do not appear to be affected by the compaction load. It can be visualized that the different dry density represents different mechanical stress where high dry density corresponds to high mechanical load and low dry density corresponds to low mechanical stress. Consequently, Fig. 2.9 indicates that mechanical stress affects mainly the pore structure

of the macropore between aggregates, namely the mechanism in Fig. 2.8a is not dominant. In other words, when an unsaturated soil is compressed, the deformation is due to the decrease in the volume of the macropore instead of the micropore.

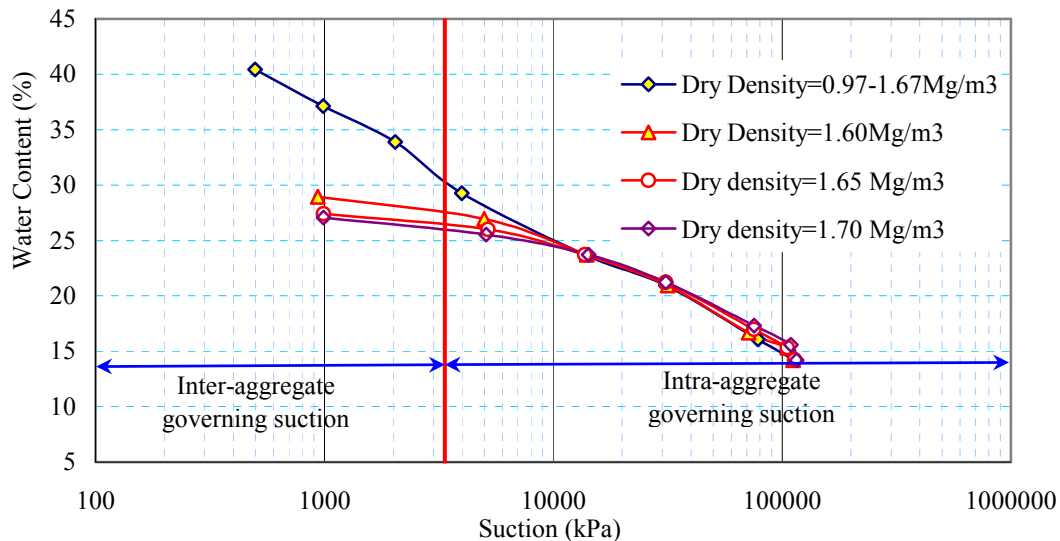


Fig. 2.10. Mechanical stress and matric suction's influence on soil water characteristic curve (Lloret et al. 2003)

The same conclusion can be obtained from the soil water characteristic curves. Fig. 2.10 shows the results of the soil water characteristic curves for the same kind of soil from free swelling and constant-volume tests. As has been discussed previously, soil water characteristic curve is actually a reflection of the pore size distribution of the soil. Different dry densities are visualized as different levels of mechanical stress applied on the soil. It can be observed that the mechanical stress has no influence on the soil water characteristic curve at suction range higher than about 15,000 kPa, which represents the micropore size of the soil, that is, the mechanical stress has little influence on the microstructure of the soil. At the range that suction is less than 15,000 kPa, the soil water characteristic curves are different for different dry densities. For the same water content level, it is observed that the higher the dry density, the lower the suction.

Because lower suction value reflects the macropore size distribution, the observations leads to a conclusion that the mechanical stress mainly reduces the macropore size. The reason for this is as explained previously that the macropore is much easier to be compressed.

Fig. 2.7c and 2.8b also show the relationship between water content and matric suction. Fig. 2.7c shows the meniscus of the capillary phenomenon when the soil water content is high and Fig. 2.8b shows the condition when the soil water content is very low. It can be seen that under either condition adding water to the soil will cause an increase in the radius of curvature of the meniscus, resulting in a decrease in matric suction. Conversely, water loss will always result in a decrease in the radius of curvature of the meniscus, which leading to an increase in matric suction. As a consequence, the soil water characteristic curve will always has a negative slope as shown in Fig. 2.10, which means when the soil water content increases, the matric suction of the soil will decrease and when the soil water content decreases the matric suction of the soil will increase. The slope of the soil water characteristic curve is the b_t or m_2^w / ρ_d defined by Fredlund and Rahardjo (1993). Fredlund and Rahardjo considered that m_2^w is positive for collapsible soils. The statement means that when adding water to a collapsible soil, the matric suction of the soil will increase. It conflicts with the above discussion and numerous experiment data (Pereira and Fredlund 1997). More discussions will be presented in the Chapter VI.

In a summary, all the observational data concerning the fabric of compacted soils indicate a clear presence of two structural levels in the material: a microstructure inside the aggregates and a macrostructure consisting of the ensemble of aggregates and inter-aggregate pores. Microstructure features appear to be largely influenced by compaction effort.

The macrostructure of a soil is similar to granular structure. The clay aggregates work as granular particles and are deformable. The microstructure is related to the soil minerals and their spatial arrangement. Both the mechanical stress and matric suction will influence the soil structure. At microstructure level, increase in mechanical stress

(load application) will lead to decrease in matric suction. Conversely, evaporation of soil water (suction application) will increase matric suction in the soil. At macrostructure level, increase in mechanical stress (load application) will lead to decrease in structural void mainly. Evaporation of soil water (suction application) will lead to decrease in sizes of both structural void and micropore. Current evidence tends to indicate that the mechanical stress influences the macrostructure while the matric suction mainly affects both the microstructure and the macrostructure, that is, the influence of the mechanical stress on the microstructure as shown in Fig. 2.8 a is small, the mechanical stress's influence on matric suction is mainly due to the mechanism as shown in Fig. 2.8b.

The bimodal concept was proposed by Lloret et al. (2003) and it is a very useful concept. In this dissertation, it will extensively be used to explain soil behaviors, especially the volume change of soils.

2.3 Factors Influencing the Soil Water Balance

2.3.1 Introduction

Soil in the field loses water from the soil surface by evaporation and from the vegetation by transpiration. Soil gains water by infiltration from precipitation such as rainfall etc. When there is water loss or water gain, the volume of expansive soil will change, which in turn influence the foundation or structure built on it. So all the factors influencing the evaporation, transpiration and infiltration will finally influence the foundation and structure.

2.3.2 Evapotranspiration

Evaporation refers to the process that water is converted to water vapor and removed from the soil surface. Vegetation absorbs the water in the soil and then the water contained in plant tissues is converted to water vapor at its leaf and the vapor is removed to the atmosphere, this process is called transpiration. The combination of two separate processes, evaporation and transpiration, is referred to as evapotranspiration (ET) (Allen

et al. 1998). Two procedures are involved in the evaporation, the first step is water vaporization and the second step is vapor removal.

Energy is required to change the state of the molecules of water from liquid to vapor. Direct solar radiation and the ambient temperature of the air provide this energy. The driving force to remove water vapor from the evaporating surface is the difference between the water vapor pressure at the evaporating surface and that of the surrounding atmosphere. As evaporation proceeds, the surrounding air becomes gradually saturated and the process will slow down and might stop if the wet air is not transferred to the atmosphere. The replacement of the saturated air with drier air depends greatly on wind speed.

Where the evaporating surface is the soil surface, the amount of water available at the evaporating surface is another factor that affects the evaporation process. Frequent rains, irrigation and water transported upwards in a soil from a shallow water table wet the soil surface. Where the soil is able to supply water fast enough to satisfy the evaporation demand, the evaporation from the soil is determined only by the meteorological conditions. However, where the interval between rains and irrigation becomes large and the ability of the soil to conduct moisture to near the surface is small, the water content in the topsoil drops and the soil surface dries out. Under these circumstances the limited availability of water exerts a controlling influence on soil evaporation. In the absence of any supply of water to the soil surface, evaporation decreases rapidly and may cease almost completely within a few days. Fig. 2.11 shows the typical functional relationships for evaporation from soil with respect to various values of potential evaporation (Hillel 1980). Curve A represents a high evaporation rate at the soil surface, and Curves B, C, D represent decreasing evaporation rates with similar tendency.

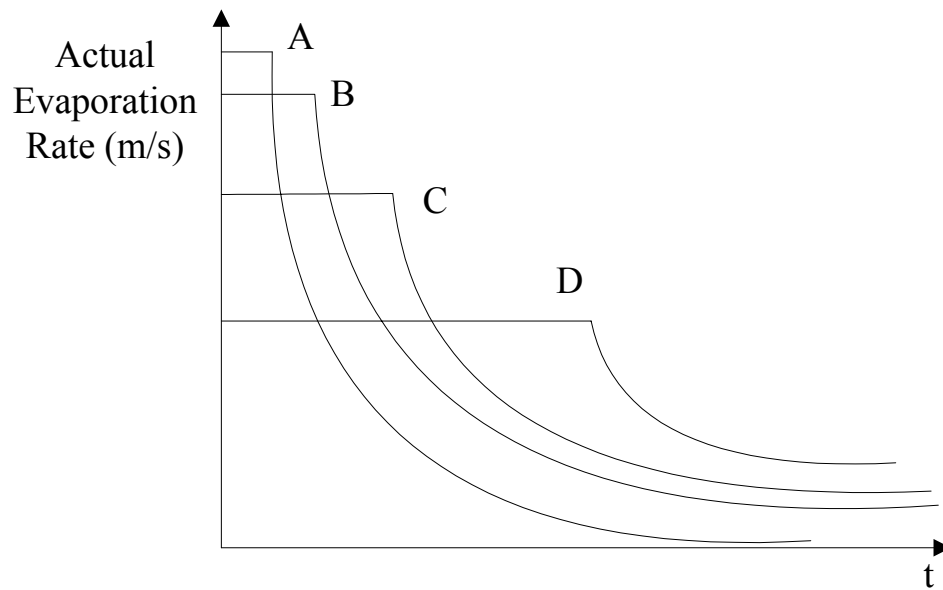


Fig. 2.11. Typical relationships for evaporation from soil as a function of time (Hillel 1980)

Transpiration consists of the vaporization of liquid water contained in plant tissues and the vapor removal to the atmosphere. Unlike the evaporation from soil surface which water is lost from the soil surface, the water loss due to transpiration occurs locally in the soils. The water, together with some nutrients, is taken up by the roots from the surrounding soils locally and transported through the plant. Plants lose their water through stomata. These are small openings on the plant leaf through which gases and water vapor pass. The vaporization occurs within the leaf and the vapor exchange with the atmosphere. Nearly all water taken up is lost by transpiration and only a tiny fraction is used within the plant.

Transpiration, like direct evaporation, depends on the energy supply, vapor pressure gradient and wind. Hence, radiation, air temperature, air humidity and wind terms should be considered when assessing transpiration. The soil water content and the ability of the soil to conduct water to the roots also determine the transpiration rate, as do water-logging and soil water salinity. The transpiration rate is also influenced by crop

characteristics, environmental aspects and cultivation practices. Different kinds of plants may have different transpiration rates.

Hence, solar radiation, air temperature, air humidity and wind speed are climatological parameters to consider when assessing the potential (maximum) evaporation. Soil properties such as the storage ability of the soil and the soil permeability are the factors influence the actual evapotranspiration (Allen et al. 1998).

2.3.3 Infiltration

Soils gain water from precipitations. Mein and Larson (1973) showed the infiltration rate into an unsaturated soil surface to be a function of time. Fig. 2.12 shows typical functional relationships for infiltration rates into unsaturated soil. Various boundary conditions are imposed on an initially dry soil surface. The infiltration rate shown as line A corresponds to a constant applied flux or rainfall intensity less than the saturated hydraulic conductivity of the soil. The infiltration rate equals the rainfall intensity since the minimum infiltration capacity of the soil is equal to the saturated hydraulic conductivity under a hydraulic gradient of one.

Curve B shows the infiltration rate into the same unsaturated soil profile under a ponding condition or with the pressure head set equal to zero at the surface. The initial infiltration rate greatly exceeds the saturated hydraulic conductivity. This occurs as a result of the strong downward hydraulic gradient associated with the high value of matric suction at the soil surface being suddenly set equal to zero. The infiltration rate decreases with time as water continues to infiltrate into the soil profile, which dissipates the initially large values of matric suction. In other words, the advancing wetting front results in the progressive reduction of matric suction values and associated pressure head gradients. The downward vertical hydraulic gradient continues to decrease with time, together with the resulting infiltration rate. The infiltration rate continues to decay with time until it reaches the minimum value equal to the saturated hydraulic conductivity of the soil.

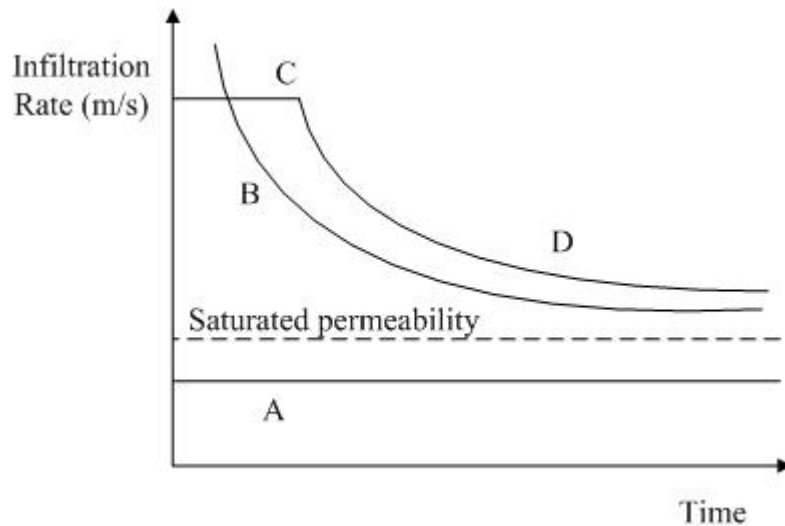


Fig. 2.12. Typical relationships for infiltration into soil as a function of time (Mein and Larson 1973)

The curve shown as segments C and D in Fig. 2.12 show the case for a constant rainfall event in which the rainfall intensity exceeds the saturated hydraulic conductivity of the soil. The infiltration rate is equal to the rainfall intensity during the earlier stages of the event, resulting in all rainfall entering the soil surface. As water continues to enter, the soil suction and hydraulic gradients continue to decline, the infiltration rate begins to decay at some time. The time required for the decline in infiltration from line C to curve D corresponds to ponding at the surface. Runoff develops at this point in time if free topographic drainage is provided and the quantity of runoff is simply computed as the difference between rainfall intensity and infiltration rate.

In summary, the actual infiltration rate into the soil is a function of the climatic fluxes, soil properties, initial conditions such as matric suction values and soil water content, and the surface topography.

2.4 Problems Associated with the Soil Structure Interaction

The amount of swell expected beneath a slab is important to the design problem. However, if the soil beneath the slab were to swell uniformly, then no distortion would be caused in the slab and the superstructure it supports. Distortion occurs when the

supporting soil swells non-uniformly or differentially. Thus, the differential swell is more important than the total expected swell.

2.4.1 Modes of Soil-Structure Interaction

Post Tensioning Institute (1996) proposed two possible distortion modes for the slab on expansive soils: a center lift (or edge drop) mode (Fig. 2.13a) or an edge lift (center lift) mode (Fig. 2.13b). Center lift is considered as a condition which occurs when the moisture content of the soil around the perimeter of the slab gradually decreases and the soil shrinks relative to the soil beneath the center of the slab, or when the moisture content of the soil beneath the center of the slab increasing, which is a general condition after the initial construction of the building. Conversely, edge lift is a condition and occurs when the soil beneath the perimeter becomes wetter than the soil beneath the center of the slab, for example, when there is rainfall. The center lift case is considered as long term condition while the edge lift case is considered as a short term condition.

As shown in Fig. 2.13, not all the slab is supported on the foundation due to the differential movements at the ground surface. The support area will depend on the shape of the ground surface, which in turn depends on the severity of environmental condition soil properties such as permeability and stiffness, and the slab properties such as the stiffness. The problem is actually a contact problem. As can be seen, the weather varies cyclically every year, which causes the soil water content at edge to vary cyclically. The water content variations cause the shape of the ground surface to change and finally the support area and the load distribution in the structure will change too.

If both the building structure and the applied load are symmetric, there is approximately no shear force between the slab and the soil underneath it as shown in Fig. 2.13. If either the structure or the load are asymmetric or there is relative movements between the slab and the ground soil such as post-tensioning slab. There is friction between the soil and the slab as shown in Fig. 2.14. Both the normal force and the friction force are functions of two stress state variables: mechanical stress and matric suction because the soil's properties are function of the two stress state variable. The

model for the soil structure interaction should have the ability to simulate both the normal force and the friction force.

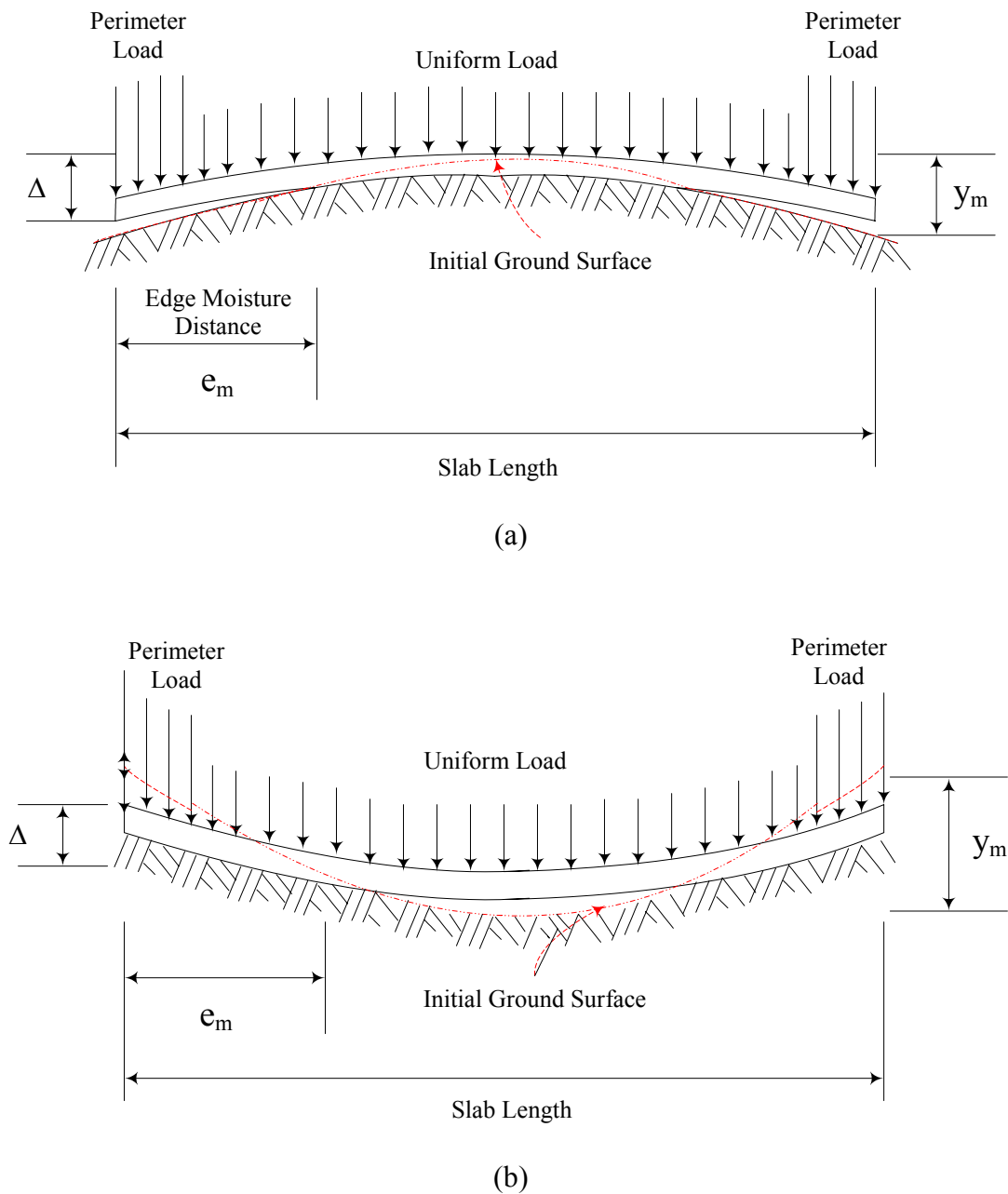


Fig. 2.13. Two typical damage modes of slab on grade (Post Tensioning Institute 1996)
 (a) center lift (edge drop) case; (b) edge lift (center drop) case

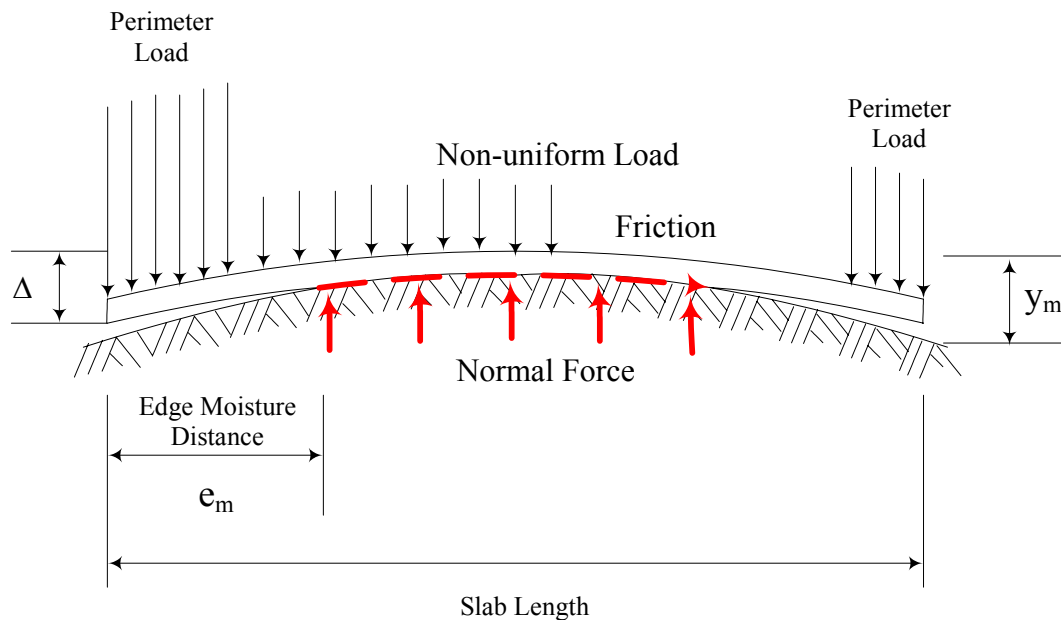


Fig. 2.14. Slab on grade when the load is not symmetric

2.5 Convention of This Dissertation

Foundation on expansive soils is a very complicated problem. In this dissertation, to make the problem a little simpler, some assumptions are made. At the same time, some conventions are made to make the descriptions simple and consistent. Some of the assumptions and convention are presented as followings.

1. Only two stress state variables are considered, i.e. the mechanical stress and the matric suction.

2. The pore air phase, if there is, is always considered as continuous and connected to the atmosphere, that is the pore air pressure is always zero $u_a=0$. For the case when the degree of saturation is higher than 85%, the air is occluded in the soil as air bubble. Under this condition, water phase can be “visualized” behaving similarly to the solid phase, and the soil can be treated as a “saturated” soil having a reduced water content and increased compressibility. The lump value of u_a-u_w is referred as matric suction without distinguish the pore air pressure and the pore water pressure, which is similar to the concept used in the axis translation technique. In other words, the assumption will

influence the shape of the constitutive surfaces for saturated-unsaturated soils, but will not influence the consolidation theory developed in the later chapters. More discussions will be presented in the Chapter VI.

Under this assumption, mechanical stress is total stress extensively used in the soil mechanics for saturated soils and matric suction is the same as negative pore water pressure. As we can see in the later chapters, all the theories are applicable for both saturated soils and unsaturated soils, and saturated soils are special case of unsaturated soil. If not specified, all the comments will be applicable for both saturated soils and unsaturated soils.

The conventions about pore water pressure and matric suction are defined as followings: Pore water pressure could be either positive or negative. When it is positive, it means the soil is saturated soil. Conversely, when the pore water pressure is negative, it is matric suction, it means the soil is an unsaturated soil even if the degree of saturation of the soil is 100%. $u_a - u_w$ is a positive value because $u_a = 0$ and u_w is negative pore water pressure. We can also say, it is the absolute value of the negative pore water pressure for unsaturated soils. In this way, we can avoid the difficulty in taking the log for negative pore water pressure. For saturated soils, $u_a - u_w$ is actually a negative value.

To be consistent with the tradition of unsaturated soil mechanics, net normal stress $\sigma - u_a$ is used to stand for the total net normal mechanical stress for both saturated soils and unsaturated soils, when it is used for saturated soils, it means total stress σ only because no air phase exists. Because the $u_a = 0$ for all the condition, $\sigma - u_a$ has the same meaning as σ . To avoid the difficulty for taking log for zero, 1 kPa is always used to represent the condition when zero mechanical stress or matric suction is encountered for log scale.

3. Darcy's law is applicable for the flow of water through an unsaturated soil (Buckingham 1907; Richards 1931; Childs and Collis-George 1950) in the whole range of 0-1,000,000 kPa. Water can be visualized as flowing only through the pore space filled with water. The air-filled pores in an unsaturated soil can be considered as behaving similarly to the solid phase, and the soil can be treated as a saturated soil

having reduced water content (Childs 1969) and increased compressibility. It is not true for the absorbed water, especially strong absorbed water, because it non-Newtonian flow while Darcy's law only holds for Newtonian flow. However, the coefficient of permeability used in this dissertation is a variable which is predominantly a function of water content of the matric suction of the unsaturated soils. Under this condition, Darcy's law holds for any small range of pore water pressure change.

CHAPTER III

MODELS NEEDED FOR NUMERICAL SIMULATIONS OF RESIDENTIAL BUILDINGS ON EXPANSIVE SOILS

3.1 Introduction

The design of residential buildings on expansive soils is a very complicated problem. The climate greatly affects the volume change of expansive soils. On the one hand, water is lost either by evaporation from the soil surfaces or by transpiration from vegetations, which is referred as evapotranspiration, on the other hand, rainfall and other forms of precipitations provide water infiltration into the soil. Usually the moisture content in the soil changes frequently with the climate and the expansive soil ground surface heaves or recedes cyclically. When a house is built on expansive soils, the soils underneath the center of the foundation are covered by the building and experience less or no influence of the weather, while the soils under the edge of the house are influenced by the weather significantly. The differential movements between the center and the edge of the house cause non-uniform stresses in the structure, and then damages to house, if large enough. Hence, a model to completely simulate the damage of the building on expansive soils should consider the following factors:

- 1) Evaluating of the influence of the weather,
- 2) Modeling of the coupled mechanical stress and moisture variations,
- 3) Modeling of the soil-structure interactions at the soil-slab interface,
- 4) Modeling of the behaviors of slabs and walls, and
- 5) Modeling of structure damage.

In this chapter, all these factors and their applications for foundations on expansive soils are introduced.

3.2 Evaluating the Weather's Influence

Weather conditions determine the boundary conditions for the soil analysis. Soil gains through rainfall infiltration and loses water by evapotranspiration. As discussed in Chapter II, the factors influencing the evapotranspiration are solar radiation, temperature, relative humidity, wind speed, etc. When evaluating the evaporation and the transpiration, all these factors should be included. In this dissertation, an empirical method is used to calculate the evapotranspiration by using daily or hourly weather data such as solar radiation, temperature, relative humidity, and wind speed.

Evapotranspiration have been studied in the agriculture engineering for a long time. Three general approaches are used extensively to estimate evapotranspiration: the temperature methods, the radiation methods and the combination methods. Table 3.1 listed the representative equations for these three methods.

Table 3.1. The Representative Equations for These Three Methods (Jacobs and Satti 2001)

Abbreviation	Approach	Source and Description
McCloud	Temperature	IFAS golf course and turf publications
Thornthwaite	Temperature	Thornthwaite and Mather (1955)
MBC	Temperature	Modified Blaney-Criddle
SFWMD	Temperature	Modified Blaney-Criddle with SFWMD crop coefficients
MMBC	Radiation	SFWMD Modified-Modified Blaney-Criddle (Shih, 1981)
Harg	Radiation	1985, Hargreaves (Hargreaves et al., 1985)
Turc	Radiation	1961, (Turc, 1961)
Pen48	Combination	1948 Original Version of Penman (Penman, 1948)
Pen63	Combination	1963 Version of Penman (Penman, 1963)
Pen77	Combination	FAO24 Modified Penman (Doorenbos and Pruitt, 1977)
IFAS Pen	Combination	IFAS Florida Modified Penman (Jones et al, 1984)
ASCE PM-90	Combination	ASCE-Penman Monteith, Jensen et al. (1990) w/Rn56, G56, r_a & $r_s = F(ht)$, $\lambda = F(T)$
Pen, FAO	Combination	ASCE-PM w/ $ht = 0.12$ m, $r_s = 70$ s/m and albedo = 0.23, R_n 56, $G = 0$, $\lambda = 2.45$ MJ kg^{-1} (Allen et al., 1998)
ASCE00	Combination	ASCE-PM, $r_a = f(ht)$, albedo=0.23, daily ET_o $r_s = 70$ s/m, hourly ET_o $r_s = 50$ & 200 s m^{-1} ; daily ET_r $r_s = 45$ s m^{-1} , hourly ET_r $r_s = 30$ s/m & 200 s m^{-1} (Walter et al., 2000)

3.2.1 The Temperature Methods

The temperature methods are empirical equations that rely on air temperature as a surrogate for the amount of energy available to the reference crop (vegetation) for evapotranspiration. The main advantage of the temperature methods is its simplicity. It uses the air temperature only to estimate the evapotranspiration. The McCloud method (McCloud 1955), the Thornthwaite method (Thornthwaite 1948), the Soil Conservation Service (SCS), the Modified Blaney-Criddle method and the SFWMD model are typical temperature methods (Jacobs and Satti 2001) while the Thornthwaite method has been used most frequently in the geotechnical engineering. The Thornthwaite moisture index has been used in PTI manual (PTI 1996) as a parameter to determine the edge moisture distance. Gay (1994) also used it to estimate the evapotranspiration in his dissertation. The Thornthwaite method estimates potential evapotranspiration (PET) by making use of air temperature solely. PET estimates are based upon a 12-hour day (amount of daylight) and 30-day month. The Thornthwaite method was developed for the potential evapotranspiration estimation for the east-central U.S. The method requires a constant ratio of reflected radiation to incident radiation (albedo), no advection of wet or dry air, and a constant ratio of the energy used in evaporation to the energy used to heat the air. The formulae are based on the catchment-area data and controlled experiments. The equation of the Thornthwaite method is

$$PET = 1.6x \frac{(10T_{mean})^a}{I} \quad (3.1)$$

where PET =potential evapotranspiration(cm/mon.); x =adjustment factor related to hours of daylight and latitude; T_{mean} =mean monthly air temperature($^{\circ}C$); I =heat index where

$$I = \sum_{i=1}^{12} \frac{(T_{mean})_i^{1.5}}{5}; \text{ and } a = \text{a function of the Heat Index given by}$$

$$a = 0.49 + 0.0179I - 7.71 \times 10^{-5} I^2 + 6.75 \times 10^{-7} I^3 \quad (3.2)$$

However, there is no direct, unique relationship between temperature and energy. This limits the generality of the temperature methods. At the same time, it can just estimate potential evapotranspiration for a relative long period and local calibration of the methods is needed to provide some measure of accuracy, particularly for averaging periods on a monthly or seasonal basis.

3.2.2 The Radiation Methods

As discussed in Chapter II, energy is required to change the state of the molecules of water from liquid to vapor in the process of evaporation or transpiration. The radiation methods use a measure of solar radiation coupled with air temperature to predict evapotranspiration. Priestley and Taylor (1972) demonstrated that for a well water surface that extends over a large surface area, the potential evapotranspiration process is well described by net radiation, air temperature and pressure. The Hargreaves (Hargreaves and Samani 1985) and SWFWMD Modified–Modified Blaney-Criddle (Shih et al. 1981) methods are typical radiation methods. The Hargreaves method is an empirical equation developed in Davis, California from a lysimeter study on Alta fescue grass. The original Hargreaves formula calculates reference potential evapotranspiration from solar radiation and temperature

$$ET_0 = 0.0135 \frac{R_s}{\lambda} (T_{mean} + 17.8) \quad (3.3)$$

where ET_0 =reference evapotranspiration(mm/day); λ =latent heat of vaporization,2.45 MJ/kg; R_s =solar radiation, MJ/(m² d); and T_{mean} =mean air temperature (°C).

When the solar radiation data are not available, an alternate approach is proposed that only measurements of maximum and minimum temperature, with extraterrestrial radiation (R_a), are needed to estimate the solar radiation. The relationship between R_s and R_a is given by

$$R_s = k_{R_s} R_a \sqrt{T_{\max} - T_{\min}} \quad (3.4)$$

where k_{R_s} =Adjustment coefficient based on mean monthly relative humidity; k_{R_s} =0.16 for interior regions not influenced by a large water body; k_{R_s} =0.19 for coastal locations; T_{\max} =Mean monthly maximum temperature, °C; T_{\min} =Mean monthly minimum temperature, °C; and R_a is determined from the latitude and the day of the year.

With this estimate, the method becomes a temperature-based method. However, Jensen et al. (1990) found that the radiation methods considerably underestimated ET for rates greater than 4mm/day. The reason for this is that the aerodynamic effect (wind speed) doesn't be included. The radiation method is rarely used in the geotechnical engineering.

3.2.3 The Combination Methods

All combination methods consist of two terms: the radiation term and the aerodynamic term. The aerodynamic term considers the evaporation is due to turbulent transport of vapor by a process of eddy diffusion. The radiation term considers the evaporation is one of the ways of degrading incoming radiation. The combination proposed by Penman (1948) eliminated the surface temperature and provided an opportunity to theoretically estimate the evaporation rates. All the factors influencing evaporation or transpiration including net radiation, air temperature, wind speed and relative humidity are considered. The combination type of equations gives the best results for a variety of vegetated surfaces and climates. For those locations where measured data on temperature, wind and sunshine duration or radiation are available, their applications are the most suitable. There are about seven version of combination methods: 1948 original Penman method (Penman 1948), 1963 Penman method (Penman 1963), FAO 24 modified Penman method (Doorenbos and Pruitt 1977), IFAS Florida Modified Penman method, ASCE- Penman Montieth method (Jensen et al.1990), ASCE Penman-Montieth method (Aellen et al. 1998), ASCE- Penman Montieth method (Walter et al. 2000), and FAO 56 Penman-Montieth method (Allen et al. 1998). The FAO 56 Penman –Montieth

method is well established as the most accurate and robust method to estimate reference ET, and the past decade of research has solidified its status as the international standard.

The FAO 56-PM method is an hourly or daily grass reference ET equation derived from the ASCE PM-90 by assigning certain parameter values based on a specific reference surface. This surface has an assumed height of 0.12 m, a fixed surface resistance of 70 s/ m, and an albedo of 0.23. The zero plane displacement height and roughness lengths are estimated as a function of the assumed crop height, so that r_a becomes a function of only the measured wind speed. The height for the temperature, humidity, and wind measurements is assumed to be 2 m. The latent heat of vaporization (λ) is assigned a constant value of 2.45 MJ/kg. The FAO 56 Penman-Monteith form of the combination equation is:

$$ET_0 = \frac{0.408\Delta(R_n - G) + \gamma \frac{900}{T + 273} u_2 (e_s - e_a)}{\Delta + \gamma(1 + 0.34u_2)} \quad (3.5)$$

where ET_0 =reference evapotranspiration (mm day^{-1}); R_n =net radiation at the crop surface ($\text{MJ m}^{-2} \text{day}^{-1}$); G =soil heat flux density ($\text{MJ m}^{-2} \text{day}^{-1}$); T = air temperature at 2 m height ($^{\circ}\text{C}$); u_2 =wind speed at 2 m height (m s^{-1}); e_s =saturation vapor pressure (kPa); e_a =actual vapor pressure (kPa); $e_s - e_a$ =saturation vapor pressure deficit (kPa); Δ =slope vapor pressure curve ($\text{kPa } ^{\circ}\text{C}^{-1}$); and γ =psychrometric constant ($\text{kPa } ^{\circ}\text{C}^{-1}$).

The combination methods have never been used in the geotechnical engineering. In this dissertation, the FAO 56 Penman-Monteith method is used for the first time in the simulation of foundation on expansive soils. Detailed discussions about the FAO 56 Penman-Monteith method are presented in Chapter VII.

3.2.4. Infiltration

The precipitation or irrigation provides the water for infiltration. Generally the infiltration is calculated by assuming the suction at the infiltration surface is zero, and by defining different initial conditions, the Richard's equation is solved and the infiltration

rates are computed. The typical methods for infiltration are: 1) The Green and Ampt Approach (Green and Ampt 1911); 2) Kostiakov equation; 3) Horton (1940) equation; 4) Phillip (1957); 5) Holtan (1961); 6) Mein and Larson (1973).

The program used for the coupled hydro-mechanical stress analysis includes solving the stress equilibrium and the water mass balance at the same time. It is an advanced version for the Richards equation. Hence, it can be used to predict infiltration rate.

3.2.5 Actual Evapotranspiration and Infiltration

Basically speaking, the potential evapotranspiration and the actual rainfall provide the upper limits of the evapotranspiration and the infiltration. The actual infiltration and evapotranspiration depend on the ability of soil to deliver water, which is a function of the content and potential of water in the soil, as well as upon its conductive properties. These two factors together determine the maximal rate at which the soil can transmit water to evaporation site or water can infiltrate. Accordingly the actual evapotranspiration rate is determined either by external evaporability or by the ability of soil to deliver water, whichever is the lesser and hence the limiting factor. Similarly, the infiltration depends on the infiltration ability and rainfall intensity, whichever is the lesser and hence the limiting factor. Currently, no well-accepted method has been proposed to estimate the actual evapotranspiration and infiltration. A general method for actual evapotranspiration is to multiply some empirical factors with potential evapotranspiration to estimate the actual evapotranspiration. Some limitations can be added to the ability for soil to deliver water to estimate the actual evapotranspiration. By using the recommendations from the FAO 56 Penman –Montieth method, a simple function can be used to determine the actual evapotranspiration by considering the soil water content. A detailed discussion about the actual evapotranspiration and infiltration will be discussed in Chapter VII.

3.3 Modeling of Moisture Movements

3.3.1. Darcy's Law

The movement of the water in the saturated soils is described by Darcy's law, which is, the flow of the water in the soil is proportional to the hydraulic gradient. Darcy's law is written as follows:

$$q_i = ki_i = k \frac{dh}{dx_i} \quad (3.6)$$

where q_i = Darcy's flux in i -direction; k = hydraulic conductivity, which is a function of matric suction; h = hydraulic head; and x_i = the i - direction coordinate.

For unsaturated soils, Childs and Collis -George (1950) proposed that water can be visualized as flowing only through the pore space filled with water. The air-filled pores in an unsaturated soil can be considered as behaving similarly to the solid phase, and the soil can be treated as a saturated soil having reduced water content (Childs 1969). Subsequently, the validity of Darcy's law can be verified in the unsaturated soil in the similar manner to its verification for a saturated soil. Darcy's law holds only when the water flow is Newton's flow. For the soil with very low water content, the water in the soils is absorbed water and it is non-Newtonian flow. Therefore, Darcy's law is not applicable. However, the coefficient of permeability used in this dissertation is a function of both the mechanical stress and matric suction of the unsaturated soils and the analysis is nonlinear. Under this condition, Darcy's law holds for any small range of pore water pressure change.

3.3.2 Richard's Equation

The water continuity equation in an unsaturated soil is actually the equation of soil water mass conversation where the water is considered to be incompressible, which can be written as follows:

$$\text{net water flow in} + \text{water source (if any)} = \text{rate of change of stored water}$$

By applying the continuity equation to Darcy' law, together with the Bernoulli's equation (relationship between the hydraulic head and pore water pressure), the Richard's equation for the water movements in unsaturated soils can be obtained. There are three versions of differential equation for the moisture movements in unsaturated soils, which are listed as follows:

$$\frac{\partial}{\partial z} \left(K \frac{\partial u_w}{\partial z} \right) + \frac{\partial K}{\partial z} = C_w \frac{\partial u_w}{\partial t} \quad (3.7a)$$

$$-\frac{\partial}{\partial z} \left(K \frac{\partial u_w}{\partial z} \right) - \frac{\partial K}{\partial z} = \frac{\partial \theta}{\partial t} \quad (3.7b)$$

$$\frac{\partial}{\partial z} \left(\frac{K}{C_w} \frac{\partial \theta}{\partial z} \right) - \frac{\partial K}{\partial z} = \frac{\partial \theta}{\partial t} \quad (3.7c)$$

where K = the permeability of unsaturated soils, which is a function of negative pore water pressure (matric suction); u_w = pore water pressure, (or matric suction); θ = volumetric water content; C_w = slope of the soil water characteristic curve; z = Coordinate in z direction; and t = time.

All these three equations are considered as forms of Richard's equation (Swartzendruber 1969). As can be seen, Eq. 3.7a derives the differential equation for water continuity in terms of pore water pressure; Eq. 3.7c derives the differential equation in terms of volumetric water content, while Eq. 3.7b uses a combination of pore water pressure and volumetric water content. The transformations are performed by assuming a single-valued soil water characteristic curve, that is, hysteresis is neglected. Both Eq. 3.7a and 3.7b have been used in the geotechnical engineering extensively while Eq. 3.7c is only used in the soil physics. Some people also use differential equation for heat transfer to describe the moisture movements of water in soils because the Richard's equation is the same as the heat transfer equation when the influence of gravity is neglected. However, based on our research, the simplification will cause errors for simulation of unsaturated water flow, which will be discussed in the future.

Considering that the permeability for unsaturated soils decreases rapidly with increase in the suction, Mitchell (1980) assumed: (1) the unsaturated permeability is linearly proportional to the reciprocal of suction and (2) the water content is linearly related to the suction in terms of pF unit. In this way, Mitchell transformed the differential equation into a linear equation as following:

$$\alpha \frac{\partial^2 U}{\partial z^2} = \frac{dU}{dt} \quad (3.8)$$

where U is the matric suction in pF units; α = diffusion coefficient for the soil;

$$\alpha = \frac{k_0 u_0}{0.4343 \frac{G_s}{1+e_0} C_w}, \quad G_s = \text{specific gravity of the soil}; \quad e_0 = \text{initial void ratio}; \quad u_0 = \text{matric}$$

suction at the field capacity; and k_0 = saturated permeability coefficient.

Detailed derivation for Mitchell's equation is presented in Chapter VI. The advantage of Mitchell's equation is that it transforms the nonlinear equation into a linear equation and the close form solution for one dimensional case can be obtained. The disadvantage of the equation is that the permeability function and the soil water characteristic curve have fixed styles of mathematical expression and the influence of gravity on the suction isn't considered. Gay (1994) and VOFLO version II are based on Mitchell's equation.

3.4 Volume Change of Soil due to Moisture Variations

Soil volume will change due to matric suction variations. Matric suction is sort of hydrostatic pressure. When there are suction variations, the soil volume changes uniformly in all the directions if the soil is homogenous. Two kinds of constitutive laws have been proposed: one is based on matric suction, and the other is based on water content.

3.4.1 Suction Based Constitutive Law

The most famous representatives of suction based methods are Lytton (1977), Johnson (1977), Fredlund (1979), Mckeen (1981), and Fargher et al (1979) .The basic concept of suction based methods is that the volume change of an unsaturated soil due to moisture variations is linearly proportional to the suction variations in log scale, i.e.

$$\gamma_h = \frac{1}{1 + e_0} \frac{\Delta e}{\Delta \log(h)} \quad (3.9)$$

where h = matric suction; e = void ratio; e_0 = initial void ratio; and γ_h =the matrix suction compression index, equals to the slope of the void ratio versus the matric suction in log scale.

Suction based method uses suction as a stress state variable to describe the volume change of unsaturated soils. When it works together with solving Eq. 3.7a or 3.8, it forms a complete theoretical and practical frame for the volume change problems for unsaturated soils (VOLFLO 1978 and PTI manual 1980; 1996). Suction based methods are also most frequently used for numerical simulation. To obtain the constitutive law, the void ratio versus matric suction curve must be obtained.

3.4.2 Water Content-Based Constitutive Law

Water content-based constitutive law uses water content as a parameter to construct the relationship between volume change and moisture variation. The basic concept is that there is a linear relationship between volume change of an unsaturated soil and the water content variation (Briaud et al. 2003), i.e.

$$\frac{\Delta V}{V} = \frac{\Delta w}{E_w} \quad (3.10)$$

where V =soil volume; Δw =water content variation; and E_w = shrink-swell modulus.

The swell test-free shrink test is proposed to get the constitutive law for the water content method. It is simpler than that needed for the suction method (obtaining the void ratio versus matric suction curve). Eq. 3.10 can work with Eq. 3.7c to form a complete frame for the numerical analysis of soil volume change due to moisture variation. It is the same as that suction based method and the laboratory work is also the same. However, the tradition of the geotechnical engineering is to use matric suction as a stress state variable, and the boundary conditions are very easy to handle with matric suction. Water content is a state variable of soil, not a stress state variable. It is not easy to determine the boundary conditions for Eq. 3.7 c. Difficulties are also encountered at the interface of two different soil layers with different soil water characteristic curve because it is the hydraulic head (or approximately matric suction) instead of water content that dominates the flow of water. When water content based constitutive law is used as an empirical method, it has some advantages. For example, huge local databases have been established for water content.

Other empirical water content methods such as the Potential Vertical Rise (PVR) method and the Vijayvergiya-Ghazzaly method (O'Neill 1980), also used water content as a parameter to predict the volume change, the constitutive law is basically the same as Eq. 3.10 although it is not stated explicitly.

3.5. Soil Volume Change due to Mechanical Stress Variations

Soil volume also changes due to mechanical stress variations in this dissertation, the soils are considered as homogenous, elastic materials. The problem of soil deformations due to the mechanical stress variations is exactly the same as what described in the classical elasticity of mechanics, which is introduced in Chapter VI “Consolidation theory for saturated-unsaturated soils”.

3.6 The Coupled Hydro-Mechanical Stress Analysis (or the Coupled Consolidation Theory) for Saturated-Unsaturated Soils

Soil is a special kind of material. When a load is applied to it, the pore water pressure (if it is an unsaturated soil, it will be negative pore water pressure) will increase, which is called excess pore water pressure. If the surrounding conditions (pore water pressure or matric suction) keep unchanged and water is allowed to drain, the excess pore water pressure will dissipate with time and the volume of soil will change corresponding to the dissipation. This phenomenon is called consolidation. Consolidation exists for both saturated soils and unsaturated soils. When there are pore water pressure variations, the soil volume will also change. If the volume change due to the pore water pressure variation is restricted. Under this condition, mechanical stress will change to adjust the volume change. Therefore, the mechanical stress and pore water pressure are always coupled together, which is a coupled hydro-mechanical stress problem. The volume change problem for saturated-unsaturated soils is actually a consolidation problem. To investigate the volume change behaviors of an expansive soil and their resulting damages to structures, the consolidation of the soils must be studied firstly.

3.6.1 Consolidation Theory for Saturated Soils

3.6.1.1 Terzaghi's Consolidation Theory

The theory describing the dissipation of excess pore water pressure and associated deformation of a saturated soil is called consolidation theory, which was developed by Karl Terzaghi (1943). The discovery marked the beginning of modern soil mechanics. Currently the consolidation theory for saturated soils has been well developed and is used extensively in practice.

For saturated soils, Terzaghi assumed total stress is constant during the consolidation and proposed the effective stress principle for saturated soils. In this way, the consolidation theory is uncoupled into two stages: (1). at the instant of load application, there is no volume change, and the excess pore water pressure is equal to applied load. (2). at any time t , the excess pore water pressure will dissipated. The volume change of

the soil is equal to the volume of water flowing out. The problem has an initial condition as followings:

$$u_{w0}=p$$

where u_{w0} = the excess pore water pressure, and P = the applied load.

The differential equation for the one dimensional consolidation of saturated soils is

$$C_v \frac{\partial^2 u_w}{\partial z^2} = \frac{\partial u_w}{\partial t} \quad (3.11)$$

where u_w = pore water pressure; C_v = coefficient of consolidation; z = coordinate in the z direction; and t =time.

The initial excess pore water pressure is equal to the applied load. Eq. 3.11 is also called diffusion equation because it is the same as the differential equation for the heat transfer problem. For the two- or three- dimensional uncoupled theory, the same assumptions are made, and it is called pseudo two- or three- dimensional consolidation theory because the assumption that the mean total mechanical stress is constant during the consolidation process is not strictly true for two-or three- dimensional consolidation conditions. The three dimensional uncoupled consolidation theory is also called Terzaghi-Rendulic Theory. The corresponding differential equations are:

$$\begin{aligned} G\nabla^2 u + \frac{G}{1-2\mu} \frac{\partial \varepsilon_v}{\partial x} - \frac{\partial u_w}{\partial x} + X &= 0 \\ G\nabla^2 v + \frac{G}{1-2\mu} \frac{\partial \varepsilon_v}{\partial y} - \frac{\partial u_w}{\partial y} + Y &= 0 \end{aligned} \quad (3.12)$$

$$G\nabla^2 w + \frac{G}{1-2\mu} \frac{\partial \varepsilon_v}{\partial z} - \frac{\partial u_w}{\partial z} + Z = 0$$

$$C_{v3} \left[\left(\frac{\partial^2 u_w}{\partial x^2} \right) + \left(\frac{\partial^2 u_w}{\partial y^2} \right) + \left(\frac{\partial^2 u_w}{\partial z^2} \right) \right] = \frac{\partial u_w}{\partial t} \quad (3.13)$$

where u , v , and w = displacements in x -, y -, and z -directions, respectively; X , Y , and Z = Body force in x -, y -, and z -directions, respectively; G =shear modulus of the soil; μ =Poisson's ration; ε_v = volumetric strain; and C_{v3} = the consolidation coefficient for three dimensional case.

3.6.1.2 Biot's Consolidation Theory

Biot (1941) derived a three-dimensional consolidation theory for perfect ideal soils. The difference between the Biot's theory and the Terzaghi-Rendulic theory is that the former considers the mean mechanical stress (or the sum of the mechanical stress in three directions) is varied during the consolidation process while the latter considers it is a constant. For the Biot's consolidation theory, Eq. 3.13 is changed into:

$$\frac{k}{\rho_w g} \left[\left(\frac{\partial^2 u_x}{\partial x^2} \right) + \left(\frac{\partial^2 u_y}{\partial x^2} \right) + \left(\frac{\partial^2 u_z}{\partial x^2} \right) \right] = - \frac{\partial \varepsilon_v}{\partial t} \quad (3.14)$$

where, ε_v = volumetric strain; k =permeability coefficient; ρ_w = water density; and g =acceleration of gravity.

Biot's Consolidation theory is called true three- dimensional consolidation theory. When solving the differential equations, the initial condition for the Biot's consolidation theory is different form that for the Terzaghi-Rendulic Theory. The initial condition for the former is the applied load, and through the mass conversation (Eq. 3.14), the initial excess pore water pressure can be obtained. Since the stress distribution in the soils is varying during the consolidation process, the resulting excess pore water pressure is also changing. The initial condition for the latter (Eq. 3.13) is the excess pore water pressure and it is equal to the applied load. The solutions for the two theories are also different. For the Terzaghi-Rendulic theory, the excess pore water pressure reaches the maximum at the instant of load application and equal to the applied load everywhere. The excess pore water pressure then dissipates with time continuously. For the Biot's consolidation theory, the excess pore water pressure in some places in the soils will not dissipate at the

initial stage. Instead, it increases to some peak value which is greater than the applied load, and then dissipates gradually. This phenomenon is called Mandel-Cryer effect (Mandel 1953; Cryer 1963). The coupled and uncoupled consolidation theory for saturated-unsaturated soils and the Mandel-Cryer effect will be explained in Chapter VI.

3.6.2 Consolidation Theory for Unsaturated Soils

Biot (1941) proposed a general theory of consolidation by using two constitutive equations, one relating total stress σ and strain, and the other for the pore water pressure u_w . The theory was proposed for an unsaturated soil with occluded air bubbles. However, there was a minor mistake in deriving relationship between two material parameters. Only four material parameters were needed and their physical meanings were explained. Furthermore, no method was proposed to obtain the proposed material parameters.

By using two independent variables concept, Fredlund (1973) presented the following constitutive relationships for the soil structure and the water phase in compressibility forms and derived a coupled hydro-mechanical stress analysis analysis.

$$\frac{dV_v}{V_0} = m_1^s d(\sigma_m - u_a) + m_2^s d(u_a - u_w) \quad (3.15)$$

$$\frac{dV_w}{V_0} = m_1^w d(\sigma_m - u_a) + m_2^w d(u_a - u_w) \quad (3.16)$$

Where m_1^s =coefficient of total volume change with respect to net normal stress; m_2^s =coefficient of total volume change with respect to changes in matric suction; m_1^w = coefficient of the pore-water volume change with respect to changes in net normal stress; m_2^w = coefficient of the pore-water volume change with respect to changes in matric suction; and σ_{mean} = the mean net normal stress (i.e. $(\sigma_x + \sigma_y + \sigma_z)/3$).

3.6.2.1 Uncoupled Consolidation Theory for Unsaturated Soils

By using the above two constitutive laws, Fredlund and Hansan (1980) presented two partial differential equations which could be solved for the pore air pressure and the pore water pressure during the consolidation of an unsaturated soil. The air phase is assumed to be continuous. Darcy's law and Fick's laws were applied to the flow of the water and the air phases, respectively. The material parameters were assumed to be constants to perform the calculation. Similar consolidation equations have also been proposed by Lloret and Alonso (1981). Rahardjo and Fredlund (1990) conducted one-dimensional consolidation test on an unsaturated silty sand in a specially designed K_0 cylinder. The pore air and water pressure were measured simultaneously. The results indicated an essentially instantaneous dissipation of the excess pore-air pressure for the particular soil. To date most authors verify their results by Skempton's Equation, which concludes that the excess pore water pressure parameter is between 0 and 1. However, Skempton's Equation is not right because it used the effective stress principle for saturated soils to derive the excess pore water pressure parameter for unsaturated soils. Actually the excess pore water pressure parameters for unsaturated soils can be greater than 1, which will be explained in Chapter VI. The theories proposed by the above authors therefore should be reexamined.

3.6.2.2 The Coupled Consolidation Theory for Unsaturated Soils

For coupled consolidation theory for unsaturated soils, Fredlund & Rahardjo (1993) derived the following sets of differential equations by using a similar way to what Biot's theory had used.

$$\begin{aligned}
 (\lambda + G) \frac{\partial \varepsilon_v}{\partial x} + G \nabla^2 u - (3\lambda + 2G) \alpha \frac{\partial (u_a - u_w)}{\partial x} + X &= 0 \\
 (\lambda + G) \frac{\partial \varepsilon_v}{\partial y} + G \nabla^2 v - (3\lambda + 2G) \alpha \frac{\partial (u_a - u_w)}{\partial y} + Y &= 0 \\
 (\lambda + G) \frac{\partial \varepsilon_v}{\partial z} + G \nabla^2 w - (3\lambda + 2G) \alpha \frac{\partial (u_a - u_w)}{\partial z} + Z &= 0
 \end{aligned} \tag{3.17}$$

$$\frac{1}{\rho_w g} \left(\frac{\partial}{\partial x} \left(k \frac{\partial u_w}{\partial x} \right) + \frac{\partial}{\partial y} \left(k \frac{\partial u_w}{\partial y} \right) + \frac{\partial}{\partial z} \left(k \left(\frac{\partial u_w}{\partial z} + 1 \right) \right) \right) = \beta_{w1} \frac{\partial \varepsilon_v}{\partial t} + \beta_{w2} \frac{\partial (u_a - u_w)}{\partial t} \quad (3.18)$$

where $\beta_{w1} = \frac{m_1^w}{m_1^s}$; and $\beta_{w2} = (m_2^w - m_1^w \frac{m_2^s}{m_1^s})$.

However, the physical meaning of Eq. 3.15, 3.16 and the parameters in them have not been explained very clearly. The insufficiency leads to the condition that to solve the Eq. 3.17 and 3.18, a special program is needed to solve the coupled problem and some wrong conclusions are made. Hung et al. (2002) predicted the volume change of an expansive soil by using a program called COUPSO. Detailed discussion for coupled and uncoupled, one- dimensional, two- dimensional, and three- dimensional the consolidation theory for saturate-unsaturated soils will be presented in Chapter VI.

3.6.2.3 The Influence of Gravity

The gravity influences the suction distribution in soils. When there is no vertical flow, the hydrostatic distribution for suction is straight line with slope of -1 (VOLFLO 1978; PTI manual 1996). If the gravity term is neglected, the differential equation is the same as heat transfer, and the hydrostatic state has uniform suction distribution in the vertical direction, i.e. the capillary phenomenon can not be simulated. The Influence of the gravity will be explained in Chapter VIII.

3.6.3 Test Needed to Obtain the Parameters and Construction of Constitutive Surfaces for Unsaturated Soils

To perform coupled hydro-mechanical stress analysis analysis, some material parameters such as m_1^s , m_2^s , m_1^w , and m_2^w are needed. To obtain these parameters, the void ratio and water content constitutive surfaces are needed. They can be obtained by the consolidation test or triaxial test with suction control. However, such a test is usually very time-consuming and costive. Ho et al (1992) proposed a simple method to estimate the void ratio and water content constitutive surfaces for unsaturated soils under log-log

coordinates by using simple laboratory tests such as the specific gravity test, the swell test, the free shrink test, the one dimensional consolidation test, and the suction tests (the pressure plate test and the salt concentration test). Fredlund and Rahardjo (1993) also proposed a similar method by using natural coordinates. However, there are some problems associated with these methods. A new method is needed for estimating the constitutive surface for unsaturated soils. The method for constructing the constitutive surfaces for saturated-unsaturated soils will be presented in Chapter V.

3.7. The Finite Element Method of the Plate Theory

The slabs used for the foundation on expansive soils can be considered as plate or flat shell and the finite element method for plate or shell can be used for the analysis of slab behaviors. The Kirchhoff plate theory and the Mindlin plate theory are the most frequently used theory in the analysis of plate.

3.7.1 The Kirchhoff Plate Theory

The Kirchhoff plate theory is used extensively in thin plate simulation. The basic assumptions are: (1) the plate is thin and linearly elastic, (2) the plate undergoes small lateral deflections, (3) the transverse normals do not elongate and the normal stress along the thickness direction is neglected, (4) the straight line perpendicular to the mid surface before deformation, remain straight after deformation, and (5) The transverse normals rotate such that they remain perpendicular to the mid surface after deformation.

In the Kirchhoff plate theory, the deflection is dependent on the rotation. Only the interpolation of the deflection is performed, and the rotation is equal to the derivative of the deflection. The influences of both the shear deformation and in-plane stretching are neglected. The Kirchhoff plate theory is used to simulate pure bending only of a plate. The Kirchhoff plate theory uses the displacement method to solve the plate bending problem. It requires that the interpolation functions of both the deflection w and its first derivative be continuous at the common boundary of two adjacent elements, which is not

easy to satisfy.

3.7.2 The Mindlin Plate Theory

According to the Kirchhoff plate theory, both the deflection w and its first derivative are continuous at the common boundary of two adjacent elements, which is not true. Actually only the deflection is continuous. The Mindlin plate theory takes into account the shear deformations of the plate and interpolates the deflection and the rotation separately. The deflection and the rotation of the normals of the mid surface are independent of each other. By interpolating them separately, the continuity of the deflection and rotation of adjacent elements can be ascertained. The finite element method of the Mindlin plate theory is simple and more accuracy. Coordinate transformation can be used to adapt irregular shape, which is very valuable for practical use.

The Mindlin plate theory has same assumptions as those in the Kirchhoff plate theory except that the transverse normals to the mid-surface before deformation remain straight but not necessarily normal to the mid-surface after deformation.

When the plate is very thin, shear locking may occur in the plate problem when using the Mindlin theory. Reduced integration can be used to overcome the problem of the coefficients of the stiffness matrix being too stiff (Reddy 1993). Bulut (2000) used the Mindlin theory combining with Bussinsq's solution to simulate the slab on expansive soils.

3.7.3 The General Shell Theory

The thick shell theory is proposed by Ahmad et al (1970) by assuming the mid surface normal remain straight line after deformation and neglect the strain energy caused by the stress perpendicular to the mid surface. Every node has five degree of freedom, and shape functions are used to make coordinate transformations. The mid surface of the shell could be arbitrary curved surface. The calculation includes the influence of transverse stress and plate stretching, so it is more accurate than thin shell element

theory. Pawsey and Clough (1971) and Zienkiewicz et al (1971) found when the general shell theory is applied in thin shell or plate the results are not good because the applied displacement function generates faked shear deformation under pure bending condition, which increases the stiffness of the element stiffness matrix improperly for thin shell or plate. By using the reduced integration, this theory can be applicable for both thin and thick plates and shells. The general shell element theory is introduced in Chapter IX.

3.8 Model of Soil-Structure Interaction

Models to specify the stress-strain relationship at the interface between the soil and structure are needed in the analysis of soil structure interaction.

3.8.1 The Winkler Foundation

The Winkler foundation is the simplest and mostly widely used model in geotechnical engineering. The foundation is assumed to be composed of a number of closely spaced, vertical, independent, linear elastic springs providing vertical reaction only. The vertical reaction force is usually assumed to be proportional to the deflection of the slab. The relationship between the soil reaction force and the vertical displacement of the foundation is

$$p(x, y) = kw(x, y) \quad (3.19)$$

where P =the vertical reaction force; w = the vertical displacement of the slab; and k = the foundation soil modulus.

Eq. 3.19 indicates that the vertical reaction force at any point depends only on the vertical displacement of the slab at the same point and is independent of the displacements of any other points nearby. Such a foundation is equivalent to a liquid base and there is no shear strength between soil columns (Huang 1993). The deformation occurs only immediately under the applied load and displacement are zero outside the loaded area. According to the Winkler's model, the vertical displacement of the plate is

uniform as shown in Fig. 3.1a when it is subjected to a uniformly distributed load because the influence of the shear strength is neglected. Due to shear deformation, the deflections of a slab subjected to a uniformly distributed load are not uniform as shown in Fig. 3.1b. It is evident that the Winkler foundation is not realistic for most foundation. As we discussed in Chapter II, if the weather condition is too severe, it is possible to have a gap between the soil and the foundation. It is very hard to simulate the gap between the soil and the foundation by the Winkler foundation. Furthermore, it is also difficult to determine a single-valued k for the soil because the Young's modulus of soil is a function of both mechanical stress and matric suction (water content). When there are multiple soil layers, it is more difficult to determine a single-valued k for the Winkler Foundation.

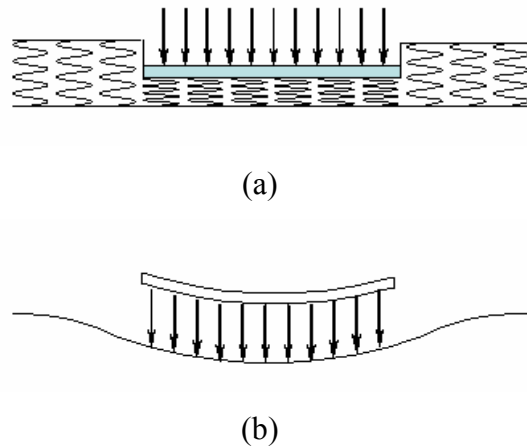


Fig. 3.1 Comparison between results obtained from Winkler foundation and the actual deflections

Similar methods include Pasternak foundation model, Hetenyi foundation model, Filionenko-Borodich Foundation model and Vlasov Foundation model.

3.8.2 The Elastic Half Space Foundation

The Elastic half space foundation considers ground soil as an elastic, isotropic, and homogenous semi-infinite continuum with modulus of elasticity E and Poisson's ratio μ , respectively. When a concentrated load P is applied on ground soil surface, the horizontal displacements produced in the semi-infinite elastic space is given by the Boussinesq's equation (Timoshenko and Goodier 1970):

$$u = \frac{P(1-2\mu)(1-2\mu)}{2\pi Er} \left[\frac{z}{\sqrt{r^2 + z^2}} + \frac{1}{1-2\mu} \frac{r^2 z}{\sqrt{(r^2 + z^2)^3}} - 1 \right] \quad (3.20)$$

Where u = the horizontal displacement; r and z are defined in Fig. 3.2a; P =applied concentrated load; E =Young's modulus; and μ = Poisson's ratio.

The vertical displacement w produced in the semi-infinite elastic space by the concentrated load P is:

$$w = \frac{P}{2\pi E} \left[\frac{2(1-\mu^2)}{\sqrt{r^2 + z^2}} + \frac{(1+\mu)z^2}{\sqrt{(r^2 + z^2)^3}} \right] \quad (3.21)$$

where w = the vertical displacement.

Eq. 3.20 and 3.21 indicate that the horizontal and vertical displacements at the ground surface depend not only on the force at the point but also on the forces at all other adjacent points. If there is a distributed external load applied on the ground soil surface as shown in Fig. 3.2b, the horizontal and vertical displacements can be obtained by numerical integration.

The results obtained by the elastic half space foundation are much closer to reality (Poulos 2000). Bulut (2001) uses the elastic half space foundation to simulate the soil-structure interaction of the foundations on expansive soils. The shape of the ground soil

surface is obtained by VOLFLO (1978) and an iteration scheme is used to calculate the contact area and the soil reaction force. A disadvantage for this method is that the Boussinesq's equation assumed that the load is applied on a semi-infinite continuum with modulus of elasticity E and Poisson's ratio μ . In practice, the semi-infinite half space assumption is not easy to satisfy. Usually slabs are built on ground with multiple soil layers. Their Young's moduli and Poisson's ratios are different from each other and are a function of both mechanical stress and matric suction. It will be very difficult to find an equivalent half space Young's Modulus for a real condition.



(a)



(b)

Fig. 3.2. Deformations of the elastic half space foundation under concentrated and uniform load

3.8.3 Contact Elements

When a residential building is built on expansive soils, the soil-structure interaction at the soil-slab interface influences the stresses and the displacements in the structure directly. The Winkler foundation and the elastic half space foundation can only handle very simple soil-structure interactions assumptions and the actual mechanical behaviors

at the soil-slab interface can not be reflected accurately, which make the simulation results different greatly from the actual conditions.

A contact element whose thickness is zero (Goodman 1968) has been used extensively in rock mechanics for the simulation of the jointed rocks. By setting up the stress strain relationship in the contact surfaces, virtual work principle is applied and the stiffness matrix is gotten for contact elements. Depending on the relative displacement of the corresponding nodes on both surfaces, separation, sliding and rotation of the surface can be simulated. Contact elements can handle very complicated stress-strain relationships for the soil-structure interaction easily and the calculation results matches the real conditions very well (Duncan and Clough 1971).

Contact elements can also be used in the simulation of foundation on expansive soil. At the soil-slab interface, soil is considered as solid continuum and the slab is considered as plate, which constitute the two sides of the contact elements. The gap between the slab and the ground soils when the weather conditions are very severe can be simulated easily by contact elements. Some slabs are built by post tensioning concrete and the slab-subgrade friction can also be simulated by contact element easily. Due to their adaptability and adjustability, contact elements are proposed to simulate the soil-structure interaction for the foundations on expansive soils in this dissertation. Detailed discussions about the theory of contact elements are presented in Chapter IX.

3.9 The Smeared Cracking Model for Concrete

When the deflection in the wall or slab is large enough, crack appears. There are many fracture mechanics models to simulate the cracking development of concrete, among which is smeared cracking model (Bazant et al. 1979). The difference between the smeared model and classic model lies that the smeared model doesn't use the stress strength factor, but depends on the energy variation between before and after the generation of the crack and its ratio with the crack length to determine whether the crack develops or not. In this dissertation, the smeared cracking model is proposed to simulate

the cracking in the slab and walls. Detailed discussions are presented in Chapter IX.

3.10 Research Methodology

The objective of this dissertation is to investigate the behaviors of residential buildings on expansive soils. Numerical methods are used to perform the simulation. Fig. 3.3 shows a typical environment around a residential building. As discussed above, the simulation of the behaviors of residential buildings on expansive soils is a very complicated problem. It requires knowledge ranging from a lot of fields. The volume change of the expansive soils is a topic for unsaturated soil mechanics while the evaluation of the evapotranspiration by using daily weather data is in the investigation scope of agriculture engineering. The simulation of the soil-structure interaction by using contact elements is discussed in the rock mechanics most frequently. The simulation of slabs and walls of residential buildings by using plate or general shell theory is covered by the structure engineering and the simulation of the damage to the building caused by expansive soils is a problem of fracture mechanics.

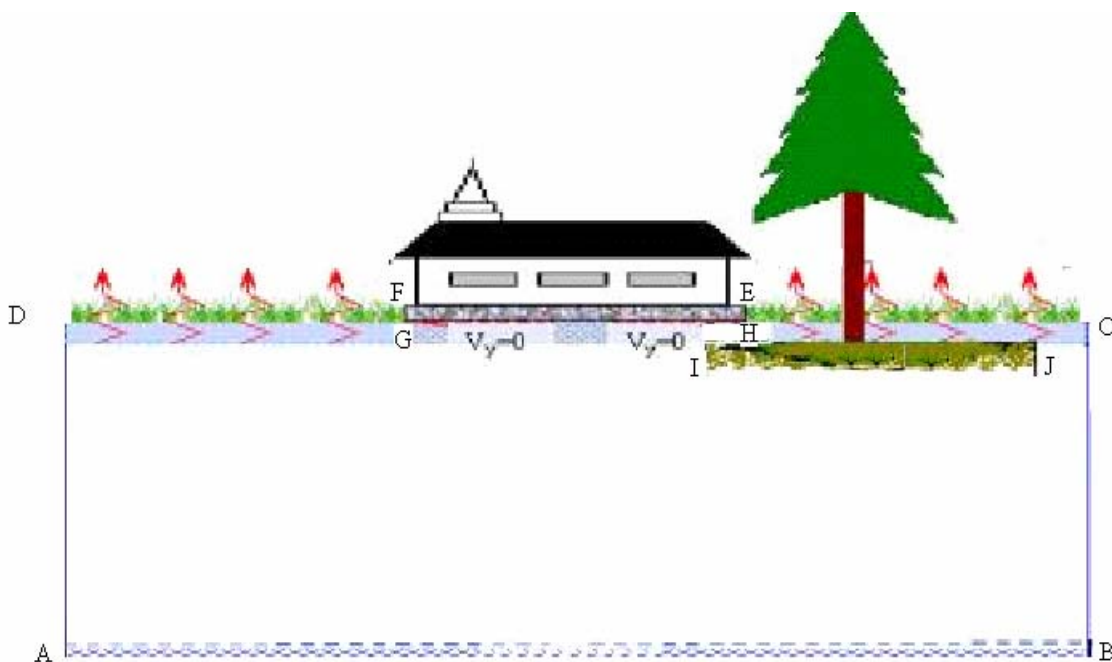


Fig. 3.3. Typical environments around a house

All those fields described as above have been investigated by lots of researchers in different fields in the past, and huge accomplishments have been achieved. However, they are always investigated the problems separately, and to the author's knowledge so far no attempt has been made to study the problem in a unified system. It is obvious that all the factors influencing the behaviors of residential buildings on expansive soils are interacting with each other. Variations in any one factor will finally lead to changes of the behaviors for the whole system. As a consequence, any attempt to investigate the factors separately will cause difference from the real conditions. In this dissertation, efforts have mainly been put to develop a complete system for the simulation of the behaviors of foundation on expansive soils. The research will mainly focus on the following aspects:

3.10.1 Simulation of the Volume Change and Discussions on the Consolidation Theory of Saturated-Unsaturated Soils

When a load is applied on an unsaturated soil externally, both the volume and the matric suction of the soil will decrease. When there is a suction variation, the volume of the soil will also change. If the volume change is restricted, the mechanical stress in the soil will change to adapt the restriction. In a summary, soil will deform due to both mechanical stress and matric suction variations. Mechanical stress variation can cause suction variation and the suction variations can cause mechanical stress variations, too. To investigate the volume change behaviors of saturated-unsaturated soils, we need consider the mechanical stress and matric suction variations and their influences on the soil volume at the same time. As a consequence, a coupled hydro-mechanical stress analysis for the soils is needed. The corresponding differential equations are as followings:

$$(\lambda + G) \frac{\partial \theta}{\partial x} + G \nabla^2 u - \frac{E}{H(1-2\mu)} \frac{\partial (u_a - u_w)}{\partial x} + X = 0$$

$$(\lambda + G) \frac{\partial \theta}{\partial y} + G \nabla^2 v - \frac{E}{H(1-2\mu)} \frac{\partial (u_a - u_w)}{\partial y} + Y = 0$$

$$(\lambda + G)\frac{\partial \theta}{\partial z} + G\nabla^2 w - \frac{E}{H(1-2\mu)}\frac{\partial(u_a - u_w)}{\partial z} + Z = 0 \quad (3.22)$$

$$\frac{\partial}{\partial x}\left(k\frac{\partial u_w}{\partial x}\right) + \frac{\partial}{\partial y}\left(k\frac{\partial u_w}{\partial y}\right) + \frac{\partial}{\partial z}\left(k\left(\frac{\partial u_w}{\partial z} + 1\right)\right) = m_1^w \frac{\partial(\sigma_m - u_a)}{\partial t} + m_2^w \frac{\partial(u_a - u_w)}{\partial t} + S' \quad (3.23)$$

Where E = Young's Modulus; G =shear modulus; ν = Poisson ratio; H = Elastic modulus for the soil structure with respect to matric suction; K = Permeability; m_1^w = Coefficient of the pore water volume change with respect to changes in net normal stress; m_2^w = Coefficient of the pore water volume change with respect to changes in matric suction; and S' = water source (if there is).

Eq. 3.23 is a little bit different from Eq. 3.18 while their physical meaning is the same. Eq. 3.23 has some advantages over Eq. 3.18. A detailed derivation for the above differential equations and the consolidation theory for saturated-unsaturated soils will be presented in Chapter VI.

To make the discussions of the coupled consolidation theory for saturated-unsaturated soils more clear and complete, some other topics related to the consolidation theory for saturated-unsaturated soils such as the two stress state variable concept, the effective stress principle, excess pore water pressure parameter and so forth are also discussed. Coupled as well as uncoupled one-dimensional, two dimensional and three dimensional consolidation theories are discussed even only the coupled three dimensional consolidation theory is used for the simulation of volume change of saturated-unsaturated soils. The purpose is to make it easier to understand the consolidation theory for unsaturated soils as well as to provide some useful tools for the practical application when numerical simulation is not available. Some discussions are also made for collapsible soils to make the discussions more complete even the main purpose of this research is to investigate the behaviors of unsaturated expansive soils. Literature reviews are also made to illustrate the developments of unsaturated soil

mechanics at different stages, their relationships and differences, and potential insufficiency. All the discussions are presented in Chapter VI.

3.10.2 Laboratory Tests and Methods to Determine the Needed Soil Parameters

To perform the coupled hydro-mechanical stress analysis, material properties should be determined. Material parameters such as Young's modulus, coefficient of expansion due to matric suction variations and so forth will be determined by laboratory tests. A site at Arlington, Texas is used as an experimental site. Soil behaviors are investigated in the whole range of possible suction (pore water pressure) and saturated soils are considered as a special case of unsaturated soils. The effective stress principle for saturated soils is reexamined by using the theory of unsaturated soils mechanics. Firstly the constitutive surfaces for saturated soils are plotted, and then the constitutive surfaces are extended to conditions when the soils are unsaturated. Laboratory tests and methods needed for the construction of the constitutive surfaces for saturated-unsaturated soils are discussed. One dimensional consolidation test is proposed for the construction of the constitutive surfaces when the soils are saturated and specific gravity test, free swell-consolidation test (suction is equal to zero), free shrink test (net normal stress is zero) and suction tests (pressure plate and salt concentration tests) are proposed for the construction of the constitutive surfaces when the soils are unsaturated. The laboratory tests results are presented in Chapter IV. Six curves are obtained by the above four laboratory tests, i.e. void ratio versus total mechanical stress curve $e = f(\sigma, u_a - u_w = 0)$, void ratio versus total mechanical stress curve $e = f(\sigma, u_a - u_w = 0)$, void ratio versus suction curve $e = f(\sigma = 0, u_a - u_w)$, water content versus mechanical stress curve $w = f(\sigma, u_a - u_w = 0)$, soil water characteristic curve $w = f(\sigma = 0, u_a - u_w)$, degree of saturation versus total mechanical stress curve $S = f(\sigma, u_a - u_w = 0)$, degree of saturation versus suction curve. $S = f(\sigma = 0, u_a - u_w)$. The corresponding procedures are presented in Chapter V.

Current methods for the measuring and the construction of the constitutive surfaces for unsaturated soils are reviewed. The advantages and disadvantages are discussed. A

possible inefficiency of current available method is discussed and a new method is proposed to construct the constitutive surfaces for unsaturated soils based on the laboratory tests results and some other available observations. The final objective is to define the soil properties in a unified frame when the soils are either saturated or unsaturated.

m_1^s, m_2^s, m_1^w and m_2^w in Eq. 3.15 and 3.16 are obtained by taking the derivatives of the void ratio constitutive surface and water content constitutive surface, which are used to calculate Young's modulus, coefficients of expansion and so forth.

The saturated permeability will be calculated from the consolidation test for different mechanical stress level. Using the water content constitutive surface, the permeability function surface will be estimated from current permeability functions for unsaturated soils such as Gardner's equation or Mitchell's equation.

It is known that the Poisson's ratio is a function of both net normal stress and matric suction. Lytton (1994) proposed a method to compute the Poisson's ratio function varying with matric suction. Duncan and Chang's model (1970) is a stress-based Poisson's ratio function. Research also indicates that Poisson's ratio does not change very much for the same soil. Poisson's ratios are therefore assumed as constants (0.4 for all the soils) in this dissertation.

3.10.3 Daily Historic Weather Data Used as Inputs to Calculate the Surface Boundary Conditions

To perform the coupled hydro-mechanical stress analysis, boundary conditions are needed. The boundary conditions for a planned residential building will be dominated by the future weather conditions. However, the future weather data are unknown until it really happens. The prediction of the future weather conditions is extremely difficult even some attempts have been made (Briaud et al. 2003). An alternative way is to assume the weather conditions are repeatable and the future weather can be represented by the historic weather conditions. It is reasonable and common sense that the weather on earth are changing seasonally and are cyclic yearly or longer. This assumption is also

the basis of the future weather prediction method mentioned above. It is proposed in this dissertation to use the historic daily weather data such as rainfall, solar radiation, relative humidity, temperature, wind speed and so forth to represent the future weather conditions and use it to determine boundary conditions for the simulation of the behaviors of residential buildings on expansive soils even though the real weather data are used to verify the proposed model for the movements prediction for a site at Arlington, Texas. The method is to use the historic weather data during a reasonable period, for example, the daily weather data during the past four years from January 1, 2000 to January 1, 2004 to represent the future four years weather conditions, say, from January 1, 2004 to January 1, 2008, and then a coupled hydro-mechanical stress transient analysis is performed by using a fixed time step (for example, one day per step) to simulate the behaviors of planned residential buildings on expansive soils for four years. The most dangerous conditions such as the biggest bending moment of the slab in the four years will be used as the design moment. Depending on the importance of the building, the simulation period can be longer or shorter. The advantage of this method is that the historic daily weather data are easily available from the local weather stations.

As we discussed previously, the FAO 56 Penman –Monteith method is well established as the most accurate and robust methods to estimate reference ET, and the past decade of research has solidified its status as the international standard. The FAO 56 Penman –Monteith method has extensively been used in the agriculture engineering but seldom used in geotechnical engineering. In this dissertation, the FAO 56 Penman –Monteith method will be used to evaluate the evapotranspiration at the ground soil surfaces. The daily historic data will be used for the evapotranspiration calculation.

The actual evapotranspiration and infiltration also depend on soil conditions and vegetation types. A lot of research has been performed in the agriculture engineering and recommendations for actual evapotranspiration and infiltration calculations have been provided. A soil water balance analysis is performed based on the recommendations provided by “the Crop evapotranspiration - Guidelines for computing crop water requirements - FAO Irrigation and drainage paper 56”. Combined with the

numerical simulation results (soil suction or water content) at the ground surfaces, the actual evapotranspiration and infiltration can be determined. Chapter VII introduces the FAO 56 Penman –Monteith method sketchily and analyze the soil water balance, the results are used in Chapter VIII to use numerical simulation to verify the field observation at a site at Arlington, Texas.

3.10.4 Simulation of the Soil-Structure Interaction by Contact Elements

Contact elements are used to simulate the soil-structure interaction at the slab-ground soil interface. The mechanical behaviors at the interface can be measured by special experiments. In this dissertation, due to the limited time, the mechanical behaviors of the contact element are assumed simply as followings to illustrate the applicability of the proposed unified system. Two behaviors are defined for the contact elements, one is normal behavior and the other is tangential behavior.

The normal behavior of the contact elements is defined as following: when surfaces are in contact, any contact pressure can be transmitted between them. The surfaces separate if the contact pressure reduces to zero.

For the tangential behavior, Coulomb friction model will be used to simulate the tangential behavior of the soil-structure interaction, i.e. two contacting surfaces can carry shear stresses up to a certain magnitude across their interface before they start sliding relative to each other. The Coulomb friction model defines this critical shear stress, $\tau_{critical}$, at which sliding of the surfaces starts as a fraction of the contact pressure, P , between the surfaces ($\tau_{critical} = \mu P$).

3.10.5 Simulation of the Behaviors of Slab and Wall by Using the General Shell Theory

The thicknesses of slabs and walls of residential buildings are usually much smaller than the other two dimensions. To simulate the behaviors of slabs and walls, the plate or shell theory is needed. General shell elements assume that the normals of the mid-surface keep straight after deformation and the strain energy caused by normal stress

perpendicular to the mid-surface is neglected, every node has five degree of freedoms. General shell elements can simulate the plate bending with shear deformation and plate stretching. In this dissertation, general shell theory is proposed for the simulation of the behaviors of slab and wall.

3.10.6 Pseudo Moisture Variation Simulation

In this dissertation, attempts are made to simulate the behaviors of residential buildings on expansive soils in a unified system. The coupled consolidation theory is used to simulate the volume change of saturated-unsaturated soils while for the simulation of the soil-structure interaction and behaviors of structure only mechanical stress analysis is of interest. A dilemma is therefore encountered due to the different types in the simulations for different parts. To solve the problem, a pseudo moisture variation simulation technique is proposed. In other words, a coupled consolidation analysis is performed for the simulation of the soil-structure interaction and behaviors of structure even when there is no water flow in them. The principle is to assign some special material properties to the contact elements and the general shell elements to make sure that the pseudo water flow in them has no influence on the stress analysis. The pseudo moisture variation simulation technique is discussed in Chapter IX.

3.10.7 Damage Simulation for the Slab and Walls by the Smeared Cracking Model

Due to the limited lime, the smeared crack model is proposed for the future research to simulate the damages to the slab and wall caused by the differential movements of the underground.

The intact concrete can be simulated with isotropic, linear elasticity. When there is cracking, the concrete is modeled with orthotropic material and the strains will be decomposed into elastic, intact concrete strain and cracking strains. Rankine criterion can be used to detect the crack initiation, which states that cracking forms when the maximum principal tensile stress exceeds the tensile strength of the brittle material.

3.10.8 Verification of the Proposed Models

A site at Arlington, Texas is chosen as an experiment site. Four footings are built on expansive soils and their movements over a two years period are monitored. The relationship between the weather conditions and the observations are discussed. Numerical simulations are performed by using the proposed methods and theory to calculate the movements of the four footings. The calculation results are compared with the actual observation to verify the proposed method.

3.10.9 A Simplified Method for the Movements Prediction of Saturated-Unsaturated Soils

Current available methods and tests for movement predictions, including suction based methods, water content based methods and consolidation test based methods, are reviewed and their relationships and differences are discussed. The Potential Vertical Rise (PVR) method and the Fredlund's total heave prediction method in fact estimates the potential vertical swell only. PVR method and Fredlund's method can only predict the potential vertical swell. As a consequence, the calculation results obtained by these methods are dependent of the timing of soil sampling. Soil in the field can experience both swell and shrinkage. Therefore both potential vertical swell and potential vertical shrink are needed for the design purpose. Based on the constitutive surfaces of expansive soils, a method is proposed to predict both potential vertical swell and potential vertical shrink with consideration of the influence of mechanical stress. Some Guidelines for foundation design are proposed.

CHAPTER IV

FIELD OBSERVATION, LABORATORY TESTS AND DATA REDUCTION

4.1. Introduction

To investigate the damage caused by expansive soils, the behavior of expansive soils should be investigated firstly. A site in Arlington, Texas was selected for the field experiment. Fig. 4.1 shows the site location. The predominant soil type at the site is classified as borderline between CL and CH according to the Unified Soil Classification System. The soil stratigraphy, the average soil properties and the parameters for each soil layers are shown in Fig. 4.2. The test program includes two parts: field observations of the footing movements with time and the laboratory tests to measure the soil properties.

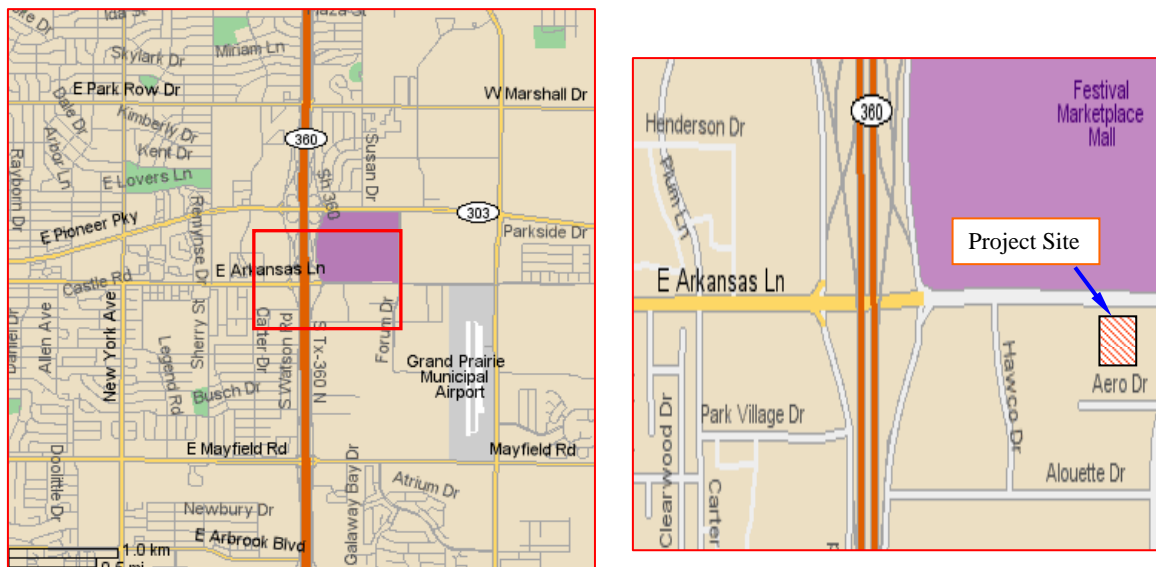


Fig. 4.1. Map of the site location

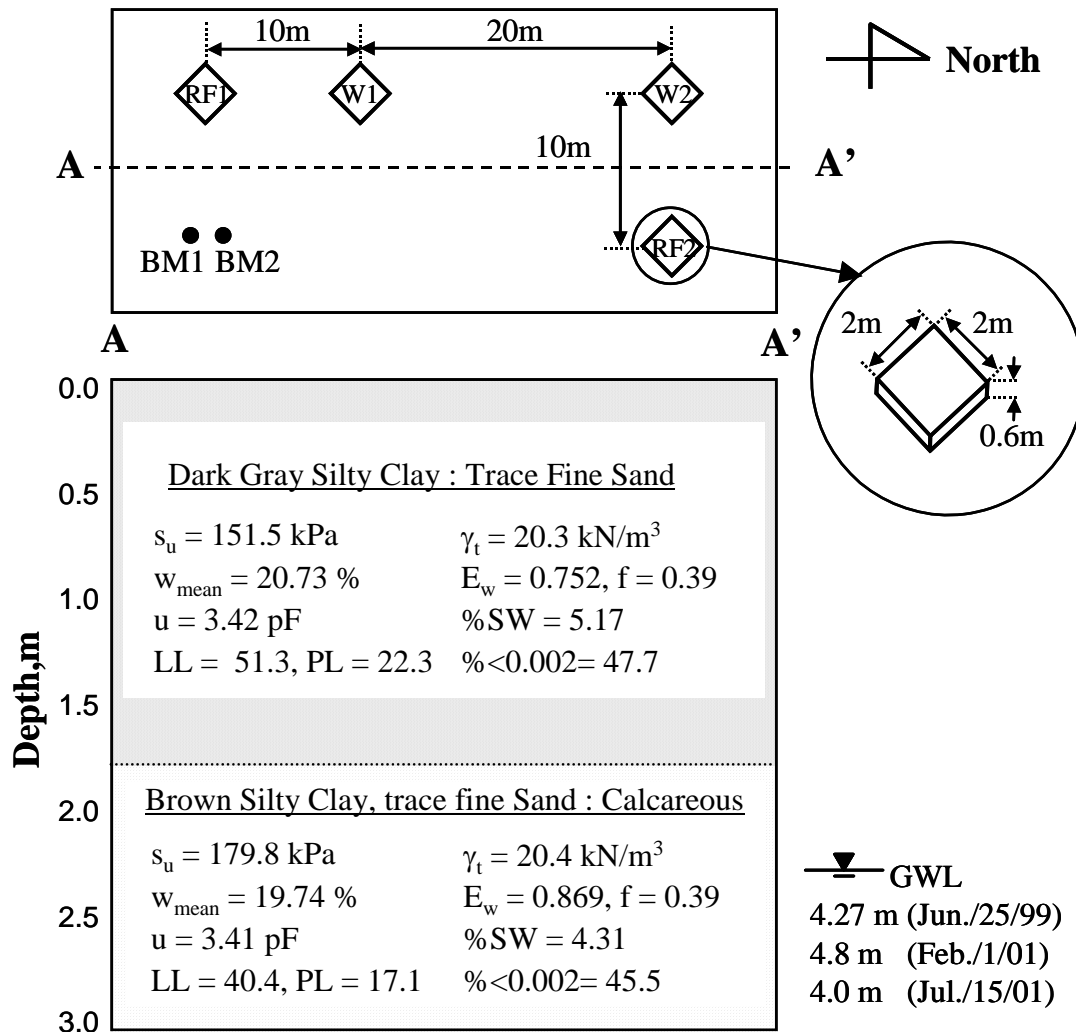


Fig. 4.2. Soil stratigraphy, the average soil properties and the parameters for each soil layer for the site (Briaud et al. 2003)

4.2 Field Observations

Four 10m × 10m areas were outlined at the site (Fig. 4.3). These areas are called RF1, RF2, W1, and W2. The areas RF1 and RF2 were left intact but each of the areas W1 and W2 was injected with 3600 gallons of water per day for three days (July 6, 7, and 8, 1999). The injection was done under pressure by pushing perforated rods to a depth of 3 meters on a 0.9 m grid covering an area 4.6m × 4.6m centered on the future location of

the footing. A $2\text{m} \times 2\text{m}$ square footing 0.6m thick was constructed at the center of each of the areas between July 15 and July 30, 1999. At each corner of the footings, a nail was secured and served as a monument for the surveying rod. A benchmark was installed to a depth of 10m following the standard procedure for Class A Rod Marks (NOAA Manual NOS-NGS 1, Floyd 1978).

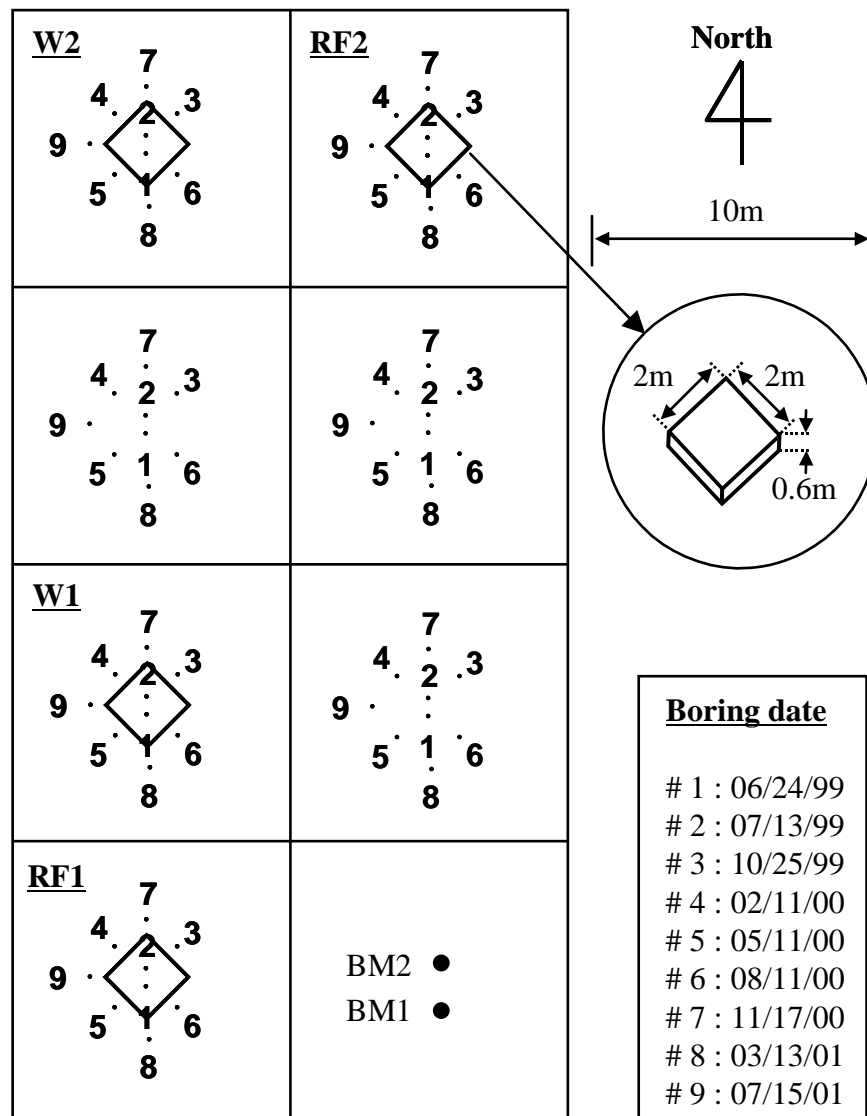


Fig. 4.3. Plan view of the site (Briaud et al. 2003)

Starting on August 11, 1999, the vertical movement of the footings with respect to the benchmark was recorded every month with a digital level until November 2001. The observed movements are shown in Fig. 4.4.

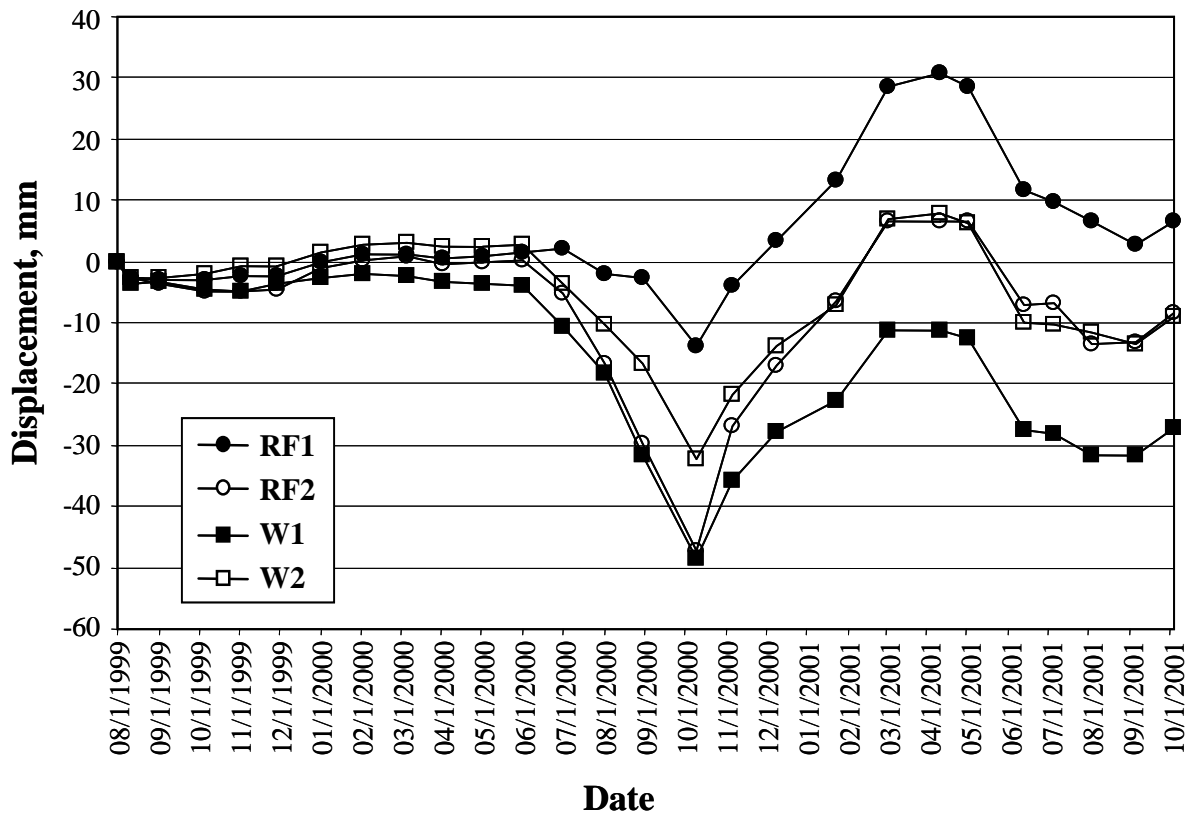


Fig. 4.4. Footing movements over two years (Briaud et al. 2003)

Every three months, one boring was done next to each footing. This process was repeated nine times over the period of two years. In each boring, samples were retrieved by pushing continuously 76mm diameter Shelby tubes at the bottom of the dry hole. Tests were performed on samples from depths typically equal to 0.6m, 1.5m, and 2.4m. The samples were extruded at the site, the pocket penetrometer test was performed, and the samples were sealed and brought back to the humidity room in the laboratory. In the laboratory, the tests listed on Table 4.1 were performed. Fig. 4.5 shows the water content and total suction versus depth at footing RF1.

Table 4.1. Type and Number of Soil Tests Performed (Briaud et al. 2003)

Test Type	Boring								
	# 1	# 2	# 3	# 4	# 5	# 6	# 7	#8	# 9
Pocket Penetrometer	66	49	70	21	21	43	75	0	0
Water Content	66	49	70	21	21	21	75	30	28
Atterberg Limits	21	6	0	0	0	0	21	0	0
Specific Gravity	0	0	0	0	0	4	0	0	0
Hydrometer	0	0	0	0	0	4	0	0	0
Unit Weight	21	15	21	21	21	21	33	0	0
Total Suction	28	20	28	21	20	21	75	30	28
Swell Test	18	5	19	0	21	21	0	0	0
Shrink Test	37	29	33	21	21	17	30	0	0
Chemical Evaluation Series	0	0	0	0	0	4	0	0	0

A total of 63 dry borings were performed at the site over a period of two years (Fig. 4.3); 61 borings were done to a depth of 3m and 2 to a depth of 7m. Each boring consisted of pushing Shelby tubes continuously without any drilling and without adding water or drilling mud. The water level in the 7m deep standpipes varied between 4m and 4.8m below the ground surface over a period of 2 years. More information can be found from Hungerford (2001).

The Southern Regional Climate Center at Louisiana State University provided hourly or daily weather data such as temperature, relative humidity, wind speed, and rainfall etc. (Fig. 4.6) taken at the Arlington Municipal Airport (Fig. 4.1) from August 1, 1999 until October 2001. Any further data requests can be made to Elizabeth Mons at emons@ mistral.srcc.isu.edu.

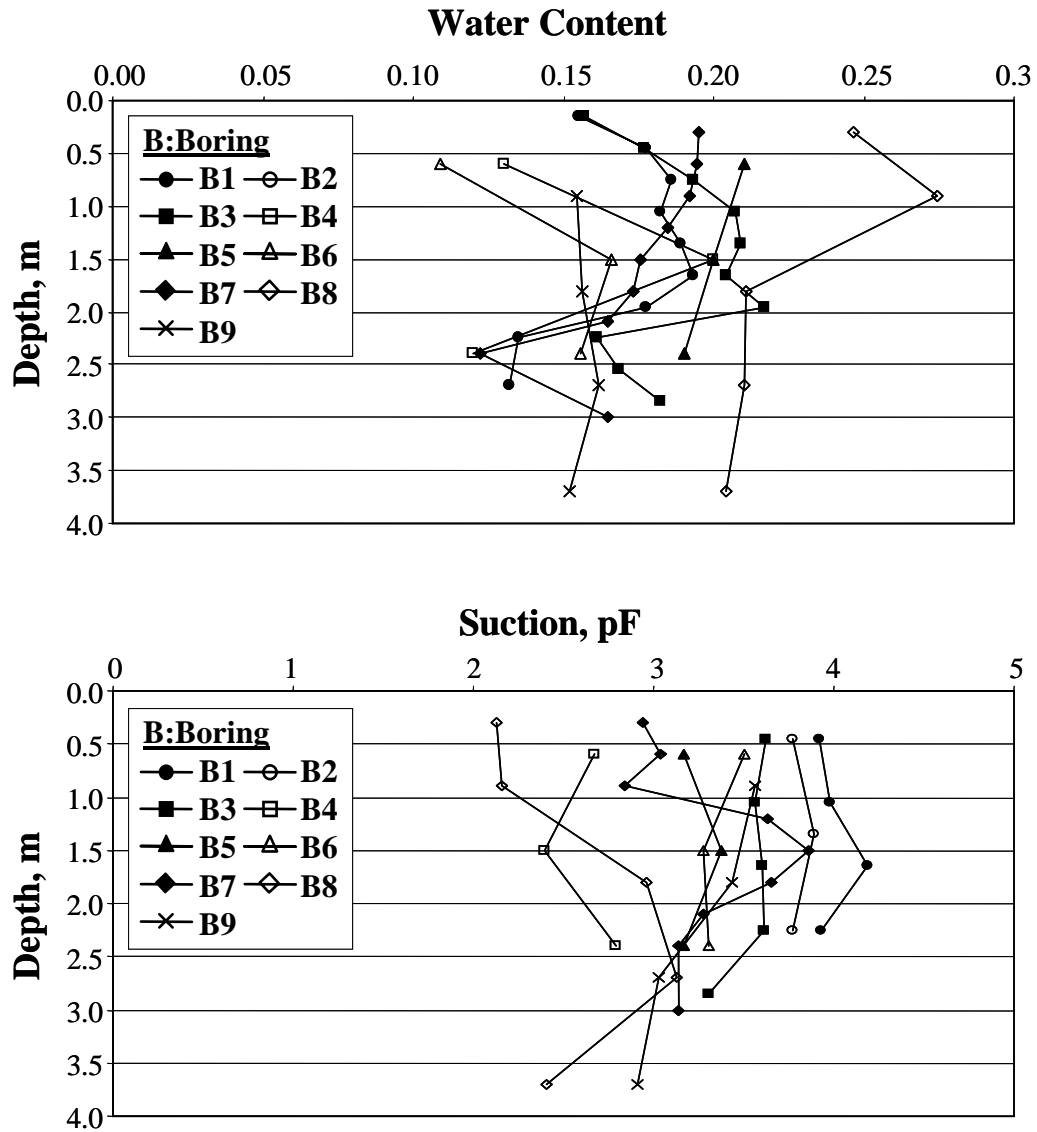
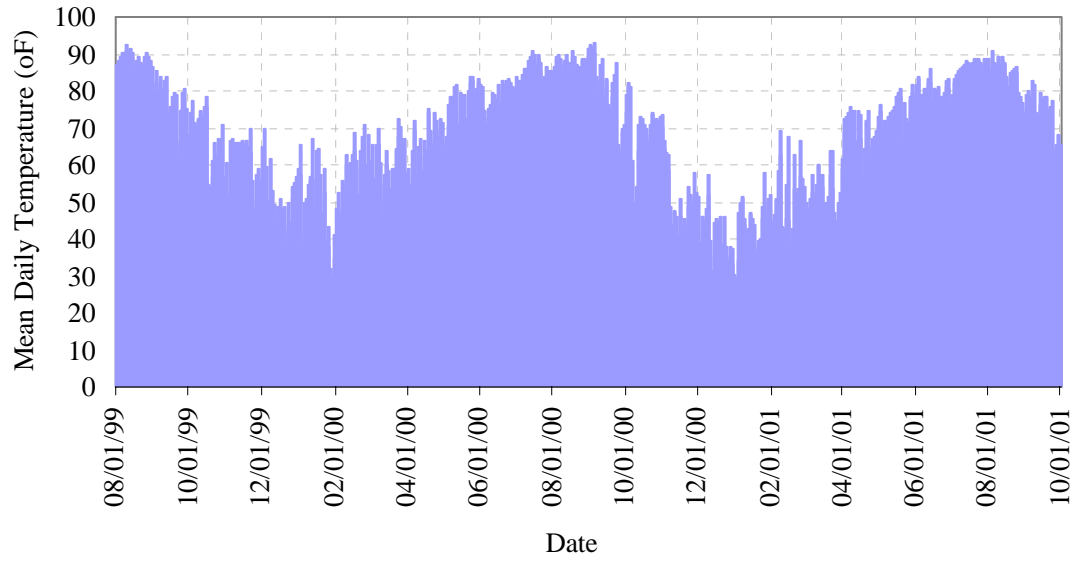
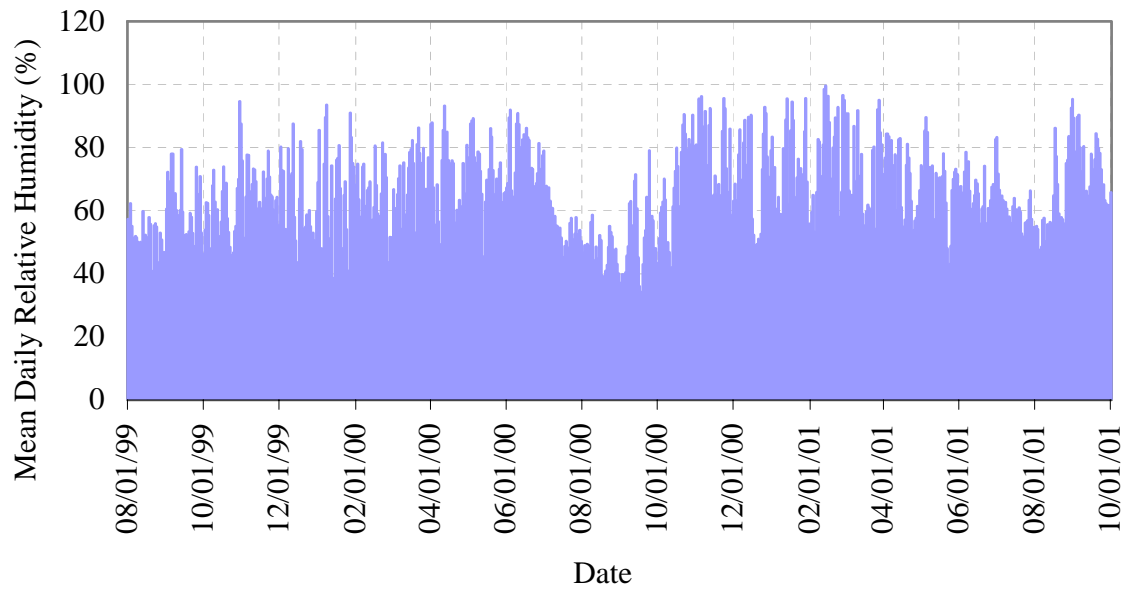


Fig. 4.5. The water content and total suction versus depth at footing RF1(Briaud et al. 2003)

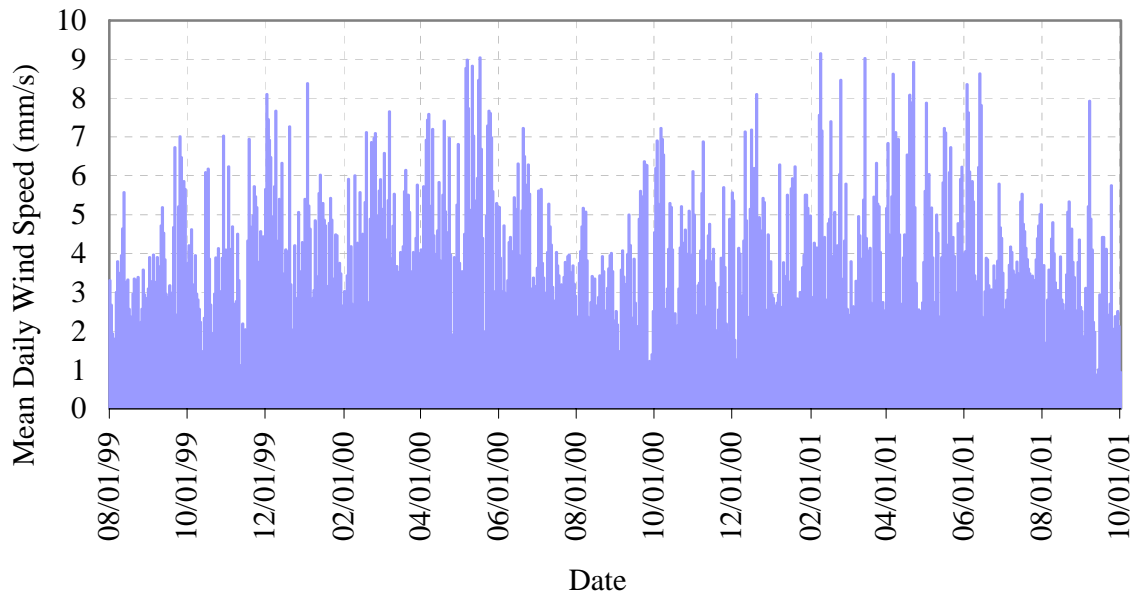


(a)

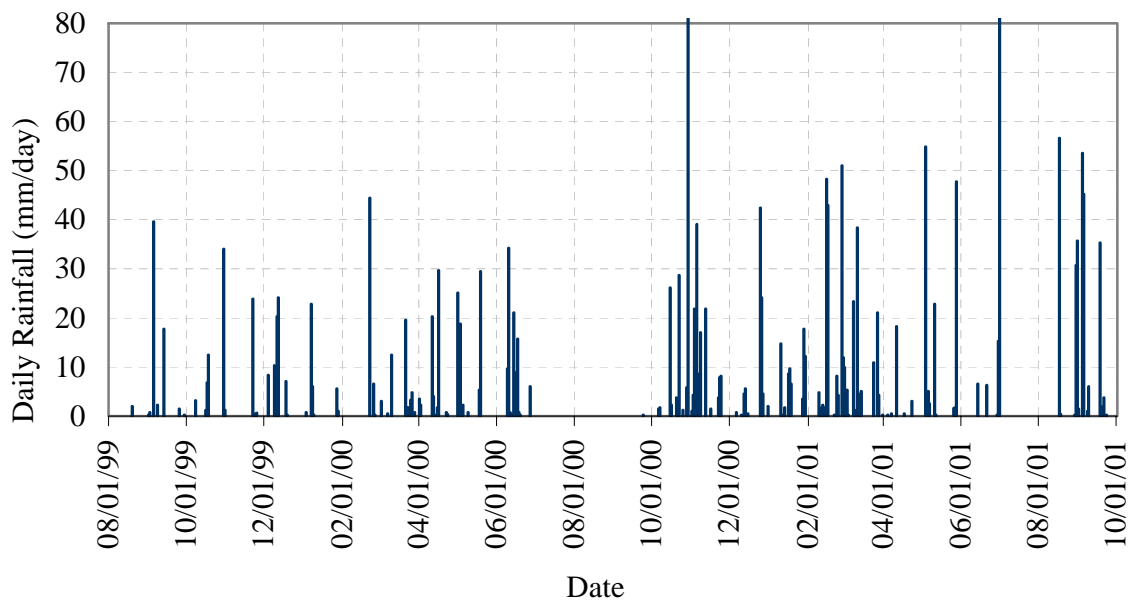


(b)

Fig. 4.6. Daily weather data over two years of a site at Arlington, Texas: (a) mean daily temperature; (b) mean daily relative humidity;



(c)



(d)

Fig. 4.6. (Continued): (c) mean daily wind speed; (d) daily accumulative rainfall

The cumulative evaporations are calculated by Thornthwaite method and the cumulative rainfalls are calculated by adding the daily rainfall data together. If there is no water supply to the ground water and there is no runoff, the difference between the cumulative rainfall and evaporation is actually the net water input into the soils. Fig. 4.7 shows the comparison between the mean footing movements in Fig. 4.4 and the calculated net water input. It can be seen that the measured movements has nearly the same tendency with the net water variation, except that there is two month's lag in movement variation. The time lag can be explained as followings. The clayey soil has low permeability, it takes time for the clayey soil to absorb water in or lose water.

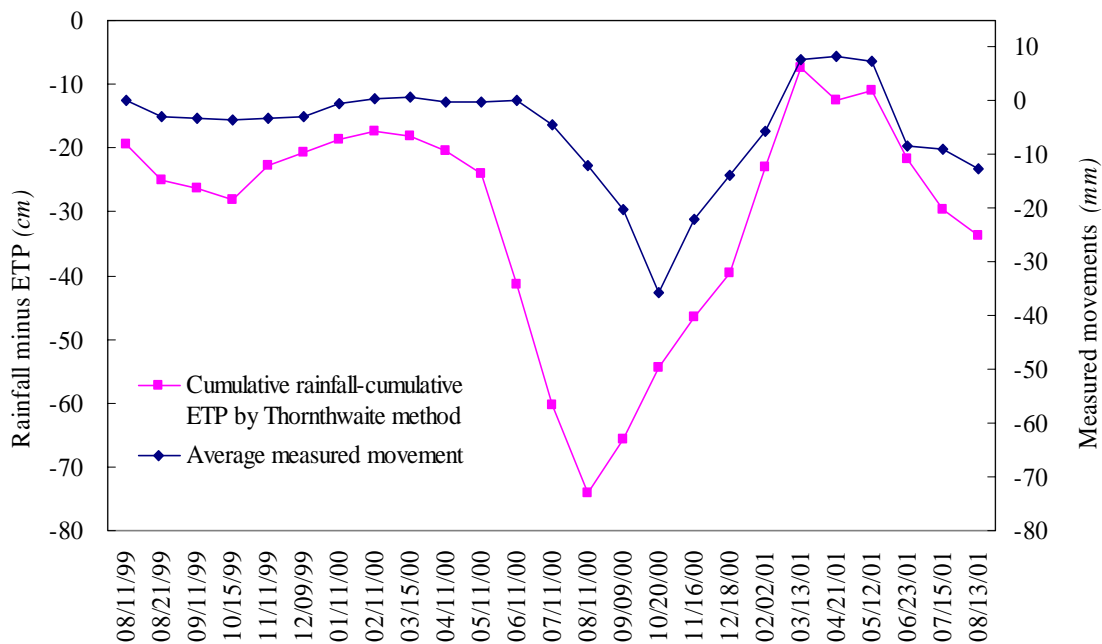


Fig. 4.7. Comparisons between the net water input and the mean footing movements over a period of two years for the site

From Fig. 4.7, it can be seen that the maximum shrinkage in fact occurs when the weather became wet, this means portion of the shrink had been eaten up by the following wet season. so the movements of footing on expansive soil will not only depend on net

water input or out put, but also depend on the time procedure (weather cycle period). It is in fact a transient problem. As we discussed in the previous chapters, Thornthwaite method is not the most accurate method for predicting the potential evapotranspiration because it just reflects partially the relationship between the evaporation and the weather factors. A better method, such as FAO56 PM Method, is expected to give a better understanding of the relationship between the movements and the weather. To predict the soil movements, firstly some lab tests are needed to measure the soil properties.

4.3 Laboratory Tests

The objectives of the laboratory tests are (1). to understand the volume change behaviors of tested materials under the influence of both mechanical stress and matric suction and (2). to obtain the necessary data for the numerical simulation.

4.3.1 Laboratory Tests Needed

Laboratory tests are performed to measure the soil properties needed for the research. To understand the soil properties, the constitutive surfaces for the soil such as void ratio, degree of saturation and water content constitutive surfaces are needed. Two methods can be used to get the constitutive surfaces for unsaturated soils. One is to use tri-axial or consolidation tests with suction control to measure them directly. Usually this kind of test requires advanced lab equipments and the testing is very time-consuming. So far it is not easy to get high quality data, especially in the high suction range. A second method is to use some boundary curves to interpolate the whole surfaces. A new method is proposed in the Chapter V to construct the constitutive surfaces for saturated-unsaturated soils. The following boundary curves are needed:

(1). The void ratio versus net normal stress curve when the matric suction is zero, i.e., $e=f(\sigma-u_a, u_a-u_w=0)$.

(2). The void ratio versus suction curve when the net normal stress is zero, i.e., $e=f(\sigma-u_a=0, u_a-u_w)$

(3). The water content versus net normal stress curve when the matric suction is zero, i.e., $w=f(\sigma-u_a, u_a-u_w=0)$.

(4). The soil water characteristic curve when net normal stress is zero, i.e., $e=f(\sigma-u_a=0, u_a-u_w)$.

(5). The degree of saturation versus mechanical stress curve when the matric suction is zero, i.e. $S=f(\sigma-u_a, u_a-u_w=0)$.

(6). The degree of saturation versus matric suction curve when net normal stress is zero, i.e. $S=f(\sigma-u_a=0, u_a-u_w)$.

The minimum laboratory tests needed for constructing the constitutive surfaces of unsaturated soils are: the swell test-consolidation test, the suction test (the plate pressure test and the salt concentration test), the free shrink test and the specific gravity test. The method is explained as follows: Curve (1) is obtained from the one dimensional swell test and consolidation test. For one dimensional swell test and consolidation test, matric suction is assumed to be zero and degree of saturation is equal to 1 ($S=100\%$). Hence, the degree of saturation versus mechanical stress curve when the matric suction is zero, i.e. curve (5), is $S=f(\sigma-u_a, u_a-u_w=0) = 1$. As a consequence curve (3) can be obtained by the equation $Se = wG_s$, which gives $w = e/G_s$. The soil water characteristic curve when the net normal stress is zero (curve (4)) can be obtained from the suction tests (the pressure plate tests, the salt concentration tests, and the swell test). From the free shrink tests, the void ratio versus water content curve and degree of saturation versus water content curve can be obtained. Combining these curves with curve (4), curve (2) and (6) can be obtained. In this way, there is no need to measure the void ratio versus matric suction curve and it is very time-saving. Because the free shrink test is very easy to perform, high quality data can be obtained easily. Examples will be given in the later sections.

4.3.2 Tested Materials

Three categories of soils were used for laboratory testing. As can be seen in Fig. 4.2, the soil between 0 and 1.8m is dark gray silty clay (which is called SW145) and the soil

deeper than 1.8m is brown silty clay (which is called SW189). Soil samples from these two layers were considered the same in each layer and are used as testing materials. The third soil was man-made bentonite clay which was obtained by mixing 30 % bentonite clay, 70% porcelain clay, and some water. The soil properties are as follows: Liquid limit, 60.6%; Plastic limit, 21.2% and specific gravity 2.725.

4.3.3 Descriptions of the Performed Lab Tests

Four types of the test were performed for the three soils: the specific gravity test, the free shrink test, the swell test-consolidation test and the soil water characteristic curve (the suction-water content test).

4.3.3.1 The Specific Gravity Test

The specific gravity tests for three soils described above were performed by following the ASTM D 5550. The original data and the data reduction please see the Hungerford (2001). The specific gravity for the bentonite clay is 2.725, the specific gravity for the dark gray silty clay SW145 (0-1.8m) is 2.65, and the specific gravity for the brown silty clay SW189 (>1.8m) is 2.79.

4.3.3.2 The Free Shrink Test

The purpose of the shrink test is to obtain the void ratio versus water content curve when there is no mechanical load. The test procedure was proposed by Briaud et al. (2003). A modification for the method is to use a smaller specimen. It is recommended that the free shrink test together with soil water characteristic curve is used to get the void ratio versus matric suction curve. Since both the soil water characteristic curve and the void ratio versus matric suction curve are relationships when the soil suction is in equilibrium, the void ratio versus water content curve must be obtained when the soil is in equilibrium, that is, the soil water content and the matric suction is uniform for the specimen. Under this requirement, it is better to use a smaller specimen to shorten the time needed for the soil to reach equilibrium. The specimen dimension is recommended

to be 63.6mm in diameter and 25.4 mm thick, which is exactly the same as what we used for one dimensional consolidation test. The consolidation ring is used to trim the specimen. Good-shaped specimen can be obtained to measure the initial soil volume accurately. Comparing the small-dimension specimen free shrink test with the bigger one, it is founded that the big dimension free shrink test will lead to a lower shrinkage limit. The reason for this is that for natural conditions, the shrinkage limit can be defined as the intersection of the two linear parts of the water content vs. volume change curve. If the soil is too big, the soil at the specimen surface will dry quickly and reach shrinkage limit but the soil at the inner part of the specimen is still wet. Consequently, the volume of the specimen will decrease continuously until the all the soil in the specimen reaches shrinkage limit. Therefore, the shrinkage limit for bigger size specimen will be lower than that obtained from the smaller size specimen.

The procedures for the free shrink test are recommended as follows:

(1). Trim the sample into a specimen by the consolidation ring, measure the dimension of the specimen and total weight of the specimen. A minimum of 4 heights and 2 diameters measurements per height at 90° intervals are recommended. These measurements are most easily taken with a digital caliper. Measure the initial water content by making use of the leftover.

(2). Let the sample to sit vertically and air dry on the laboratory table (Fig.4.8). Record the weight W , the height H , and the diameter D of the sample as a function of time t . Readings every hour for the first 8 hours are recommended. At each reading time a minimum of 4 heights and 2 diameter measurements per height at 120° intervals are recorded.

(3). Put the specimen in plastic bag and store it under the same condition for 10 hours, then take it out and continue the air dry process, take the readings every hour for the 8 hours. Repeat the same procedure until the soil stop losing weight. A week may be needed to complete the test.

(4). After the last reading is taken, dry the sample in the oven and measure its oven-dried weight W_d .

(5). It is desirable to monitor the temperature and the relative humidity although they will not affect the parameters used in the method.

Fig. 4.8 shows the free shrink tests for the three soils. Data reduction includes calculating the water content for each reading (time), and the corresponding void ratio and degree of saturation (Appendix A.1, Table A.1.1, Table A.1.2., and Table A.1.3.). The void ratio versus water content curve and degree of saturation versus water content curve can be obtained.



Fig. 4.8. The free shrink tests for the three soils (From left to right: SW145, SW189 and Spore)

4.3.3.3 The Swell-Consolidation Test

4.3.3.3.1 Equipment and Data Acquisition System

All the equipments are the same as the standard one dimensional consolidation test except the loading system and the data acquisition system. The load frame used is the KAROL.WARBER soil testing systems (Fig. 4.9). It is pneumatic load frame for use in consolidation and stress controlled testing. CONBELS are designated to apply loads instantaneously and maintain any set load regardless of sample compression occurring within the loading interval. The CONBEL is capable of applying light precision loads from 1/16 tsf up to 32 tsf on a 63.6 mm (2.5”) sample.

The data acquisition is accomplished by using the LSCT transducers. The LSCT transducer firstly switched the displacements of the soil into electric voltage output and a

Notebook is used to record the voltage output at different time continuously by making use of a Labview program called GGeotech written by Dr. Giovanna Biscontin. Each time three consolidation tests are performed at the same time. The Serial Numbers for the three transducers are TAMU, TAMU003 and TAMU 007. Before the tests, the transducers were calibrated. Please see the calibration curves for the three transducers in Appendix A.2.

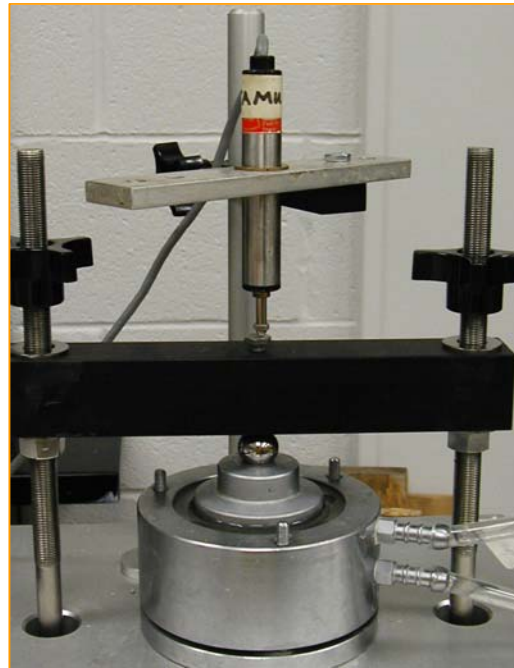


Fig. 4.9. KAROL.WARBER soil testing systems for the one dimensional swell-consolidation test and the LSCT transducer

4.3.3.3.2 Test Methods and Data Reduction

The swell test - consolidation test is performed by following the ASTM standard D4546-96 Standard Test Methods for One-Dimensional Swell or Settlement Potential of Cohesive Soils, Method A was used. The initial water content, total weight, diameters and heights of the soil were recorded to calculate the initial void ratio and the degree of saturation. The specimen is inundated and allowed to swell vertically at the seating

pressure. The seating pressure of at least 1kPa is applied by the weight of the top porous stone and load plate until primary swell is complete. Usually it will take 3 to 5 days. The specimen is loaded after primary swell has finished. Its initial void ratio and height are obtained. Nine load levels are used and the corresponding test results are shown in Appendix A.3. The tests strictly follow the ASTM D4546-96 Method A. At the first 5 minutes of the loading process, the program records the displacements every 1 second. Between 5 and 15 minutes, the program recorded the displacements every 10 seconds. After that the program recorded the displacements every 1 minute. Each load lasted at least 24 hours until the settlement reached equilibrium.

The data reduction includes calculate the water content, void ratio and degree of saturation at the initial condition, at the completion of swell test, and at the end of each loading levels. The void ratio at the completion of the swell test is calculated from the initial condition and the total heave, and then the water content is calculated out by assuming the degree of saturation is 100%. The void ratio versus vertical mechanical stress curves for three different soils are obtained.

4.3.3.4 The Suction Tests

Suction tests are performed to obtain the soils water characteristic curve. Two types of suction tests are performed: pressure plate test and salt concentration test. The pressure plate tests are used for measuring the lower matric suction values, while the salt concentration tests are performed to obtain the high total suction value. These two types of tests are performed for all the three types of soils. It is assumed that at high suction range, the matric suction is equal to total suction. Other two assumptions are the matric suction of the soil at the completion of swell test is 0 kPa, and the matric suction of the soil is 1,000,000kPa when the soil water content is zero.

4.3.3.4.1 The Pressure Plate Tests

The soil-water characteristic curve of a soil is obtained through the pressure plate test (ASTM D2325-68) by using a pressure plate extractor shown as in Fig. 4.10. The matric

suction can be applied to a soil specimen by controlling the difference in the pore air pressure u_a and the pore water pressure u_w with both pressures being positive. The pore water pressure is controlled at an atmospheric pressure while the pore air pressure is changed to obtain the specific matric suction value. This procedure is referred to as the axis-translation technique (Hilf 1956).

The main component of the pressure plate extractor is the high air entry disk that remains saturated for matric suction applications below the air entry value of the disk. The disk is always saturated and in contact with in a compartment below the compartment below the disk. The water pressure in the compartment is opened to the atmosphere to maintain at a positive pressure in the closed system. During the test soil specimen is placed on the high air entry disk. A good contact between the specimen and the disk results in the pore water pressure in the soil being controlled at the same pressure as the water pressure in the compartment. The air pressure is then applied to the specimen in order to impose the desire matric suction.

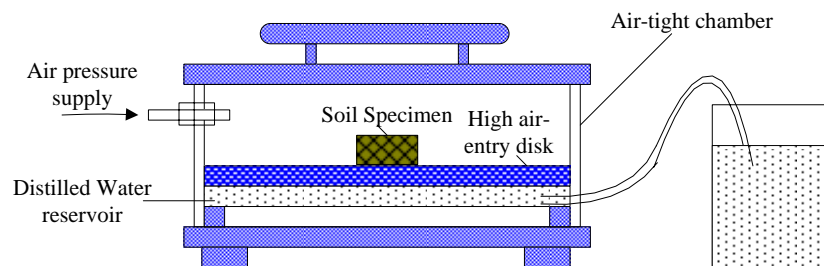


Fig. 4.10. Schematic plot of the pressure plate extractor

The equipments for the pressure plate suction test are the 1Bar, 15 Bar and 100Bar ceramic plate extractors (Soil moisture Equipment Corp., Santa Barbara, CA93105 U.S.A). Pressure gauge is the ASHCROFT Laboratory Test Gauge CAT. No. 1082A with 0-300psi range was used. The procedure of the pressure plate tests were:

- (1). Completely submerge the high air entry disk in the distilled water for three days.
- (2). Install the high air entry value disk into the pressure plate extractor.

(3). Fill enough distilled water into the pressure plate extractor until the high air entry value disk is submerged completely, install the pressure plate extractor and wait for one day.

(4). Applying about 10 kPa a air pressure to squeeze the water out.

(5). Uninstall the pressure plate extractor, keep the high air-entry value disk intact, and add a small amount of water to submerge the disk surface.

(6). Trim the soil sample to a shape fitting with the disk surface, the soil sample is the same size as that for consolidation test, put the tested soil sample on the high air entry disk, make sure the bottom of the soil is in good contact with the surface of the disk. The water should submerge part of the soil sample.

(7). Install the pressure plate extractor and apply an air pressure.

(8). Note that during the test, frequently observe the air pressure to avoid air leakage, and keep the air pressure constant. Keep the water level of the outlet to make sure that the whole pipe system is completely filled with water.

(9). After one week, record the matric suction and the soils were taken out to measure the water content. The water content tests were performed in a way as soon as possible to avoid the water evaporation.

It is a very time-consuming test, so three sets of equipments are used to perform the pressure plate test simultaneously. The same soils were used for all the tests.

4.3.3.4.2 The Salt Concentration Tests

For the higher level matric suction is usually assumed that the matric suction is equal to the total suction (Fredlund and Rahardjo 1993). The salt concentration tests can be used to measure the relationship between the water content and the total suction at high suction levels. The osmotic suction of electrolyte solution is usually used to calibrate the filter paper and psychrometers. Therefore, it is expected the results obtained from the salt concentration tests will be better than that obtained by the filter paper method. Table 4.2 gives the osmotic coefficients for different salt solutions (Goldberg and Nuttall 1978). Fig. 4.11 shows the schematic plot for the salt concentration tests. Six 250mm× 324mm

(diameter \times Overall Height) desiccators (Fruehling & Schultz Company) were used simultaneously with $MgCl_2$ concentration of 0.05M, 0.2M, 0.5M, 0.9M, 1.8M and 2.5 M, and the corresponding total suctions are 324kPa (3.51pF), 1302kPa (4.11pF), 3523kPa (4.55pF), 7187kPa (4.86pF), 19425kPa (5.29pF) and 32776kPa (5.52pF), respectively. To make sure the soil specimen reach the equilibrium suction with the salt dilution, all the soil specimens were stored in the desiccators for at least two weeks. It is a very time-consuming test. However, the drawback is overcome by using a lot of desiccators simultaneously. The efficiency is improved. All the expenses for purchasing desiccators and the chemicals are less than 1,000 dollars and the equipment can be used repeatedly in the future. The test procedure is also very simple: (1). put the soil specimens on the porcelain plate; (2). wait for two weeks and (3). measure the water contents of the soils. Each time one desiccators can accommodate six specimens. Combined with the pressure plate tests, actually the soil water characteristic curves for three types of soils can be obtained in two or three weeks.

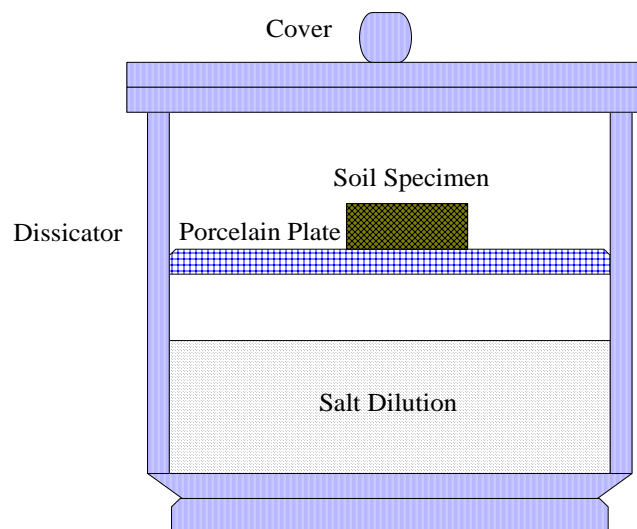


Fig. 4.11. Schematic plot of the salt concentration test

The oven dry suction value is assumed as 1,000,000 kPa (7 pF) and the corresponding water content and degree of saturation are 0%. To make sure the soil water characteristic curve reflects the whole possible range of the water content variation, some pre-swelled soil specimens are also used besides the use of undisturbed soil specimen. The pre-swelled soil specimens are the specimens after free swell tests were completed. The soil specimens are then taken out to perform the suction test, i.e. the pressure plate tests and the salt concentration tests. All the suction tests data are summarized in Appendix A.4.

Table 4.2. The Osmotic Coefficients for Different Salt Solutions

Concentration		Suction		MgCl ₂ .6H ₂ O	Weight of MgCl ₂ .6H ₂ O (g)			
		kPa	pF	g/M per1000ml	1000ml	1500ml	2000ml	2500ml
0.001	M	7	1.85	203.218	0.20322	0.30483	0.40644	0.50805
0.002	M	14	2.15	203.218	0.40644	0.60965	0.81287	1.01609
0.005	M	35	2.54	203.218	1.01609	1.52414	2.03218	2.54023
0.01	M	68	2.83	203.218	2.03218	3.04827	4.06436	5.08045
0.02	M	133	3.12	203.218	4.06436	6.09654	8.12872	10.1609
0.05	M	324	3.51	203.218	10.1609	15.2414	20.3218	25.4023
0.1	M	643	3.81	203.218	20.3218	30.4827	40.6436	50.8045
0.2	M	1303	4.11	203.218	40.6436	60.9654	81.2872	101.609
0.3	M	2000	4.30	203.218	60.9654	91.4481	121.931	152.414
0.4	M	2739	4.44	203.218	81.2872	121.931	162.574	203.218
0.5	M	3523	4.55	203.218	101.609	152.414	203.218	254.023
0.6	M	4357	4.64	203.218	121.931	182.896	243.862	304.827
0.7	M	5244	4.72	203.218	142.253	213.379	284.505	355.632
0.8	M	6186	4.79	203.218	162.574	243.862	325.149	406.436
0.9	M	7187	4.86	203.218	182.896	274.344	365.792	457.241
1	M	8249	4.92	203.218	203.218	304.827	406.436	508.045
1.5	M	14554	5.16	203.218	304.827	457.241	609.654	762.068
2	M	22682	5.36	203.218	406.436	609.654	812.872	1016.09
2.5	M	32776	5.52	203.218	508.045	762.068	1016.09	1270.11

4.4 Methods to Obtain the Needed Curves

As has been discussed before, six curves are needed for the construction of constitutive surfaces for unsaturated soils. This section will explain the procedure to obtain the needed curves. The soil sample called SW145 was used to explain the procedure. The soil specimen is from the w1 footing and the depth of the soil sample is 4-5 feet (1.2m to 1.5m). All the curves for the SW145, SW189 and Sporc were attached in the Appendix A.5.1, A.5.2, and A.5.3, respectively.

4.4.1. The Void Ratio versus the Net Mechanical Stress Curve When the Matric Suction Is Equal to Zero, i.e., $e = f(\sigma - u_a, u_a - u_w = 0)$

It is the consolidation test curve. The vertical mechanical stress can be calculated from the applied load. The void ratio is calculated from the initial water content, the applied load and the corresponding displacement at each load level. Fig. 4.12 shows the e - $\log(\sigma_v)$ relationship for soil specimen SW145 obtained from the swell test- consolidation test.

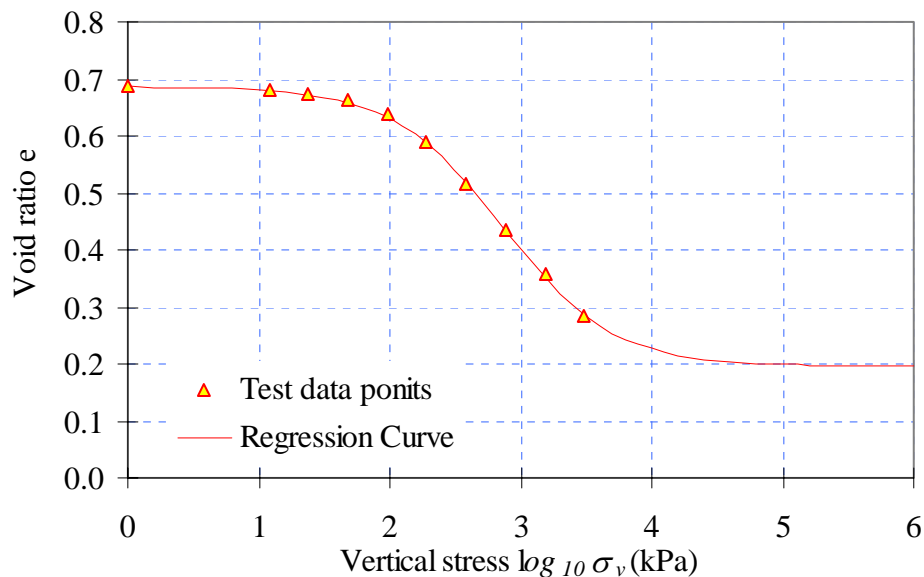


Fig. 4.12. The e - $\log(\sigma_v)$ relationship for the soil specimen SW145 obtained from the swell-consolidation test

The regression curve for the test data was obtained by a commercial software called SigmaPlot. The Mathematical expression for the best-fitted curve is

$$e = 0.1956125 + \frac{0.490945938}{1 + \exp\left(\frac{\log_{10}(\sigma_v) - 2.86157532}{0.421062101}\right)} \quad (4.1)$$

where e = void ratio, and σ_v = the vertical mechanical stress.

For two or three dimensional analysis, relationship between the void ratio and the mean mechanical stress is needed. The one dimensional consolidation test is K_0 loading. For K_0 loading, the load is applied vertically while the soil is not allowed to deform horizontally. From the Hooker's law,

$$\begin{aligned} \varepsilon_x &= \frac{\sigma_x}{E} - \frac{\mu}{E}(\sigma_y + \sigma_z) = 0, & \gamma_{yz} &= \frac{\tau_{yz}}{G} = 0 \\ \varepsilon_y &= \frac{\sigma_y}{E} - \frac{\mu}{E}(\sigma_z + \sigma_x) = 0, & \gamma_{zx} &= \frac{\tau_{zx}}{G} = 0 \\ \varepsilon_z &= \frac{\sigma_z}{E} - \frac{\mu}{E}(\sigma_x + \sigma_y), & \gamma_{xy} &= \frac{\tau_{xy}}{G} = 0 \end{aligned} \quad (4.2)$$

where, σ_x , σ_y , σ_z = the mechanical stresses in the x , y , and z directions, respectively; γ_{yz} , γ_{zx} , γ_{xy} = shear stresses; E = Young's Modulus; G = Shear Modulus; and μ = Poisson's ratio.

For clay soils, the Poisson's ratio are usually doesn't change very much. Here for all the soils, Poisson's ratios are assumed to 0.4 and maintain constant. Therefore,

$$\sigma_x = \sigma_y = \frac{\mu}{1 - \mu} \sigma_z = \frac{0.4}{1 - 0.4} \sigma_z = 0.6667 \sigma_z$$

and

$$\sigma_m = \frac{\sigma_x + \sigma_y + \sigma_z}{3} = 0.7778\sigma_z = 0.7778\sigma_v \quad (4.3)$$

where σ_m = the mean mechanical stress.

Fig. 4.13 shows the e - $\log(\sigma_m)$ relationship for soil specimen SW145 obtained from the swell - consolidation test. The regression curve for the test data was obtained by a commercial software called SigmaPlot. The Mathematical expression for the best-fitted curve is

$$e = 0.19544900 + \frac{0.49127602}{1 + \exp\left(\frac{\log_{10}(\sigma_m) - 2.75275012}{0.42147606}\right)} \quad (4.4)$$

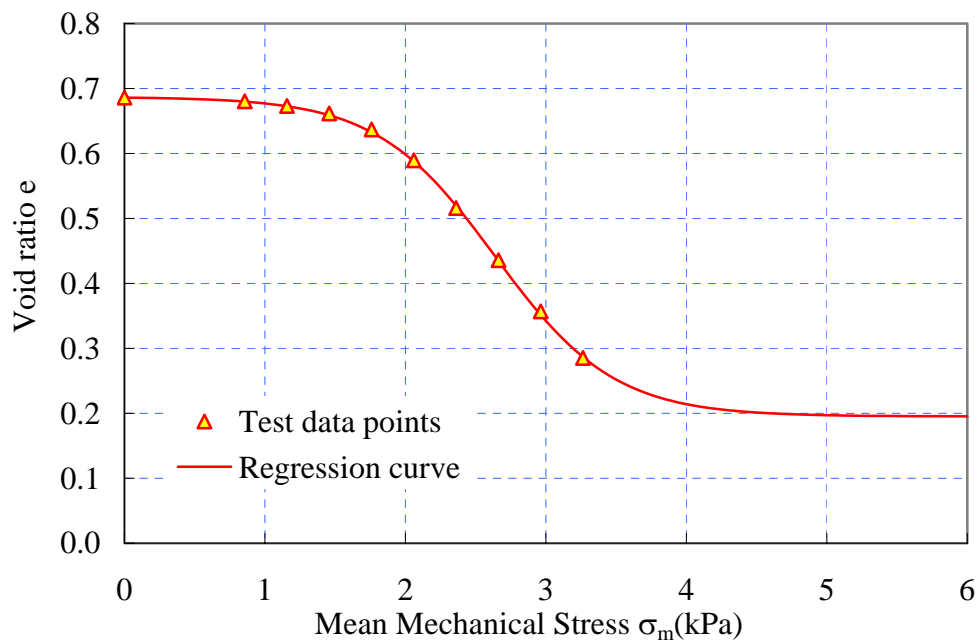


Fig. 4.13. The e - $\log(\sigma_m)$ relationship for the soil specimen SW145 obtained from the swell - consolidation test

4.4.2. The Degree of Saturation versus the Net Mechanical Stress Curve When the Matric Suction Is Equal to Zero, i.e. $S = f(\sigma - u_a, u_a - u_w = 0)$

The degree of saturation versus the net mechanical stress curve when the matric suction is zero is assumed to be 100% during the one dimensional consolidation test, i.e., for any vertical mechanical stress level and the corresponding mean mechanical stress level, $S = 1$.

4.4.3. The Water Content versus the Mechanical Stress Curve When the Matric Suction Is Equal to Zero, i.e., $w = f(\sigma - u_a, u_a - u_w = 0)$

The corresponding water content versus the vertical mechanical stress curve can be obtained by applying the relationship $Se = wG_s$. Because the degree of saturation curve for the one-dimensional consolidation test is $S = 1$, therefore, $w = Se/G_s$ where $G_s = 2.65$ for SW145.

Fig. 4.14 shows the w - $\log(\sigma_v)$ relationship for the soil specimen SW145 obtained from the swell - consolidation test. The Mathematical expression for the best-fitted curve is

$$w = \frac{e}{G_s} = 0.07381605 + \frac{0.18526262}{1 + \exp\left(\frac{\log_{10}(\sigma_v) - 2.86157532}{0.42106210}\right)} \quad (4.5)$$

In the same way, the corresponding water content versus the mean mechanical stress curve can be obtained by applying the relationship $Se = wG_s$. Assume $S = 1$, $w = Se/G_s$ where $G_s = 2.65$ for SW145. Fig. 4.15 shows the w - $\log(\sigma_m)$ relationship for soil specimen SW145 obtained. The Mathematical expression for the best-fitted curve is

$$w = \frac{e}{G_s} = 0.07375434 + \frac{0.18538718}{1 + \exp\left(\frac{\log_{10}(\sigma_m) - 2.75275012}{0.42147606}\right)} \quad (4.6)$$

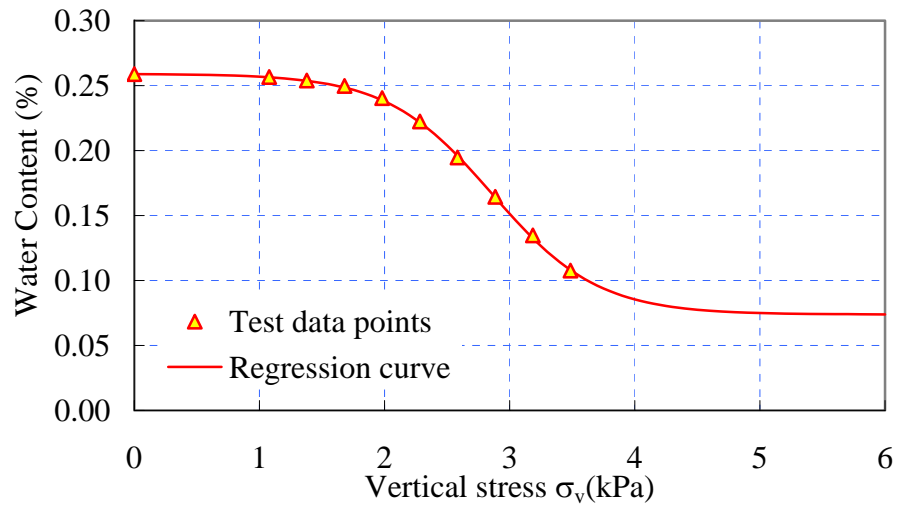


Fig. 4.14. The w - $\log(\sigma_v)$ relationship for the soil specimen SW145 obtained from the swell - consolidation test

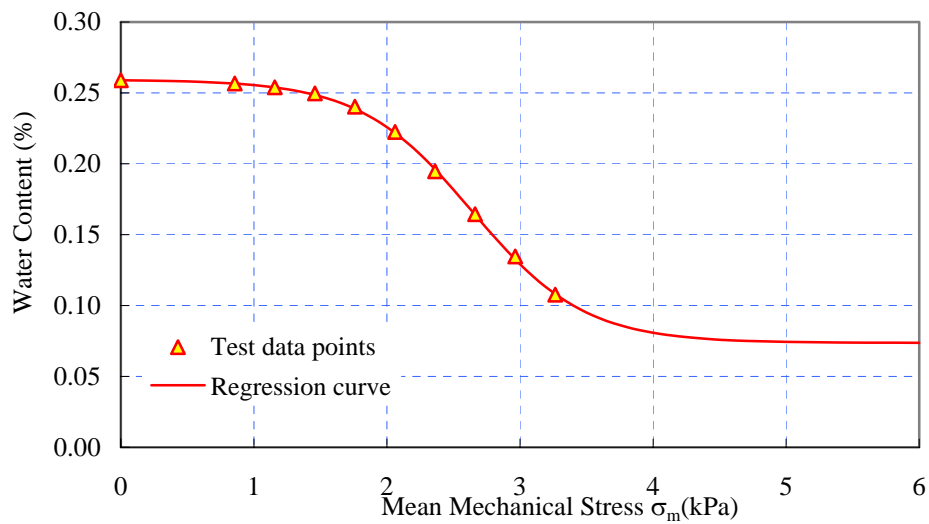


Fig. 4.15. The w - $\log(\sigma_m)$ relationship for the soil specimen SW145 obtained from the swell - consolidation test

4.4.4. The Water Content versus Matric Suction Curve When the Mechanical Stress Is Equal to Zero, i.e., $w = f(\sigma - u_a = 0, u_a - u_w)$

The curve is usually called the soil water characteristic curve. Usually the soil water characteristic curve is referred as the relationship between the volumetric water content and the matric suction. It is recommended that the gravimetric water content is used. The reason for this is that as we can see in Chapter VI, the slope of the gravimetric water content versus the matric suction curve can be defined as the “specific water capacity”, which is a parallel of the specific heat capacity in the thermodynamics.

The soil water characteristic curve is obtained from the results of the suction tests, that is, the pressure plate test and the slat concentration test. Two assumptions were made here. The first one is that the matric suction at the swell limit was assumed to be 1kPa and the second one is that the matric suction for the oven dry soil was assumed to be 1,000,000kPa. Fig. 4.16 shows the all the tests results from the suction tests and the imposed points. Detailed test data for each point please see the Appendix A.4.1. Sigmaplot is used to get the regression curve. The mathematical expression of the best fitted soil water characteristic curve for the soil specimen SW145 is:

$$w = -0.026264216 + \frac{0.285551272}{1 + \exp\left(\frac{\log_{10}(u_a - u_w) - 4.386436815}{0.671559558}\right)} \quad (4.7)$$

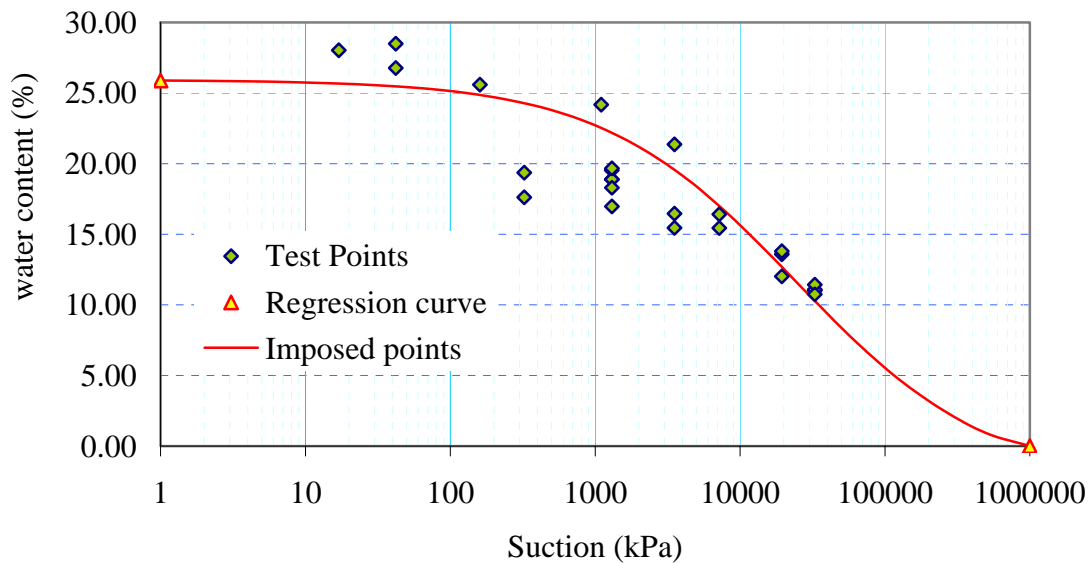


Fig. 4.16. The soil water characteristic curve obtained from the suction tests

4.4.5. The Void Ratio or Degree of Saturation versus Water Content Curve When the Mechanical Stress Is Equal to Zero, i.e., $e = f(w)_{\sigma-u_a=0}$ or $S = f(w)_{\sigma-u_a=0}$

The Free shrink test and the swell test are used together to obtain the void ratio versus water content curve. Fig. 4.17 shows the results obtained from the swell test and the free shrink test for the soil specimen SW145. The soil specimen is submerged into water for three days before the free shrink test. The two triangle points stand for result from the swell test, and it has just two points, the initial and the final void ratio e_0 , water content w and degree of saturation S . The final status (swell limit) is the start point of the consolidation test in Fig. 4.12 and Fig. 4.13. The other square points stand for the test points from the free shrink test for void ratios and the corresponding degree of saturations.

Usually there are some measurements errors for the constant void ratio range when the water content is below the shrinkage limit. The general way to get the constant void ratio is to take an average for the approximately horizontal part. Here a simple method is recommended to find the constant void ratio. Note that $Se=wGs$, for the constant void

ratio range, $S=wG_s/e=Kw$, where K is constant because the void ratio e is constant when the soil water content is below the shrinkage limit. Therefore, the degree of saturation versus water content curve at the range when water content is below the shrinkage limit is a straight line passing through the origin in the degree of saturation and the water content coordinate system. By using the regression, the relationship can be gotten $S=8.4996w$. The corresponding constant void ratio is $e=G_s/K=2.65/8.4996=0.312$. In this way, a better accuracy of the constant void ratio can be obtained. The mathematical expression of the regressive void ratio versus water content curve is:

$$e = -0.3159323 + \frac{0.429355664}{1 + \exp\left(-\frac{w - 0.192599516}{0.036185098}\right)} \quad (\text{For } w \geq 0.0944) \quad (4.8)$$

and

$$e = 0.3120 \quad (\text{For } w \leq 0.0944) \quad (4.9)$$

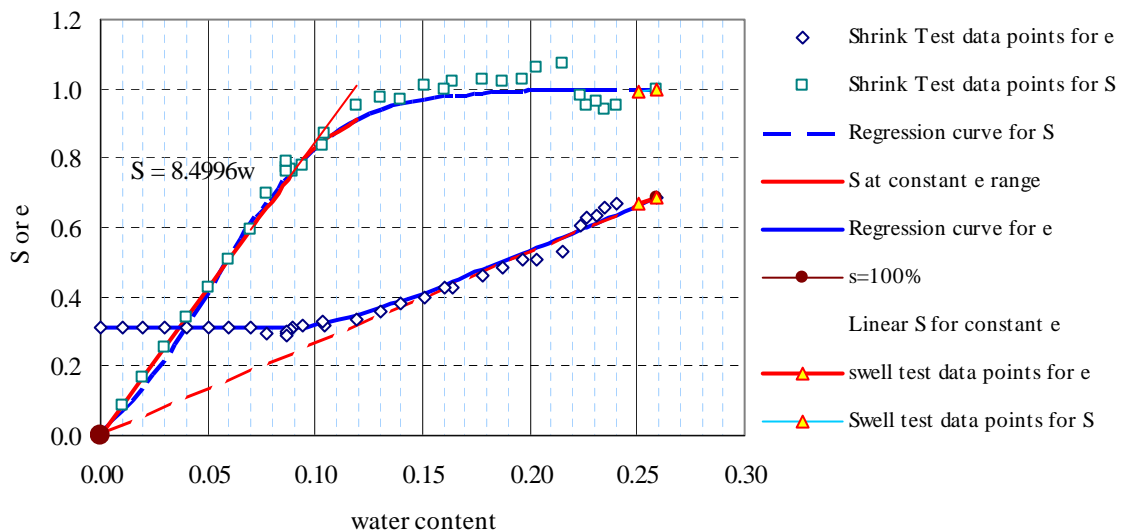


Fig. 4.17. The void ratio and the degree of saturation versus water content curves obtained from the swell test and the free shrink test

The corresponding mathematical expression of the degree of saturation versus water content curve is,

$$S = -0.127572688 + \frac{1.128166863}{1 + \exp\left(-\frac{w - 0.052044763}{0.027400096}\right)} \quad (\text{For } w \geq 0.0944) \quad (4.10)$$

and

$$S = 8.4996w \quad (\text{For } w \leq 0.0944) \quad (4.11)$$

4.4.6. The Void Ratio versus Matric Suction Curve When the Mechanical Stress Is Zero, i.e., $e = f(\sigma - u_a = 0, u_a - u_w)$

The soil water characteristic curve and the void ratio versus water content curve are combined together to obtain the void ratio versus matric suction curve. The procedure is, for a certain matric suction value, find its corresponding water content value from the soil water characteristic curve Fig. 4.16 (or from the mathematical expression Eq. 4.7 directly), and then the void ratio corresponding to this water content was found from the void ratio versus water content curve Fig. 4.17 (or Eq. 4.8 directly). Repeat this procedure for the whole suction range from 0 to 1,000,000kPa. The relationship between the void ratio and the matric suction is obtained as shown in Fig. 4.18. Its mathematical expression is obtained by Sigmaplot as followings:

$$e = 0.299088 + \frac{0.387060274}{1 + \exp\left(\frac{\log_{10}(u_a - u_w) - 3.624238826}{0.456383725}\right)} \quad (4.12)$$

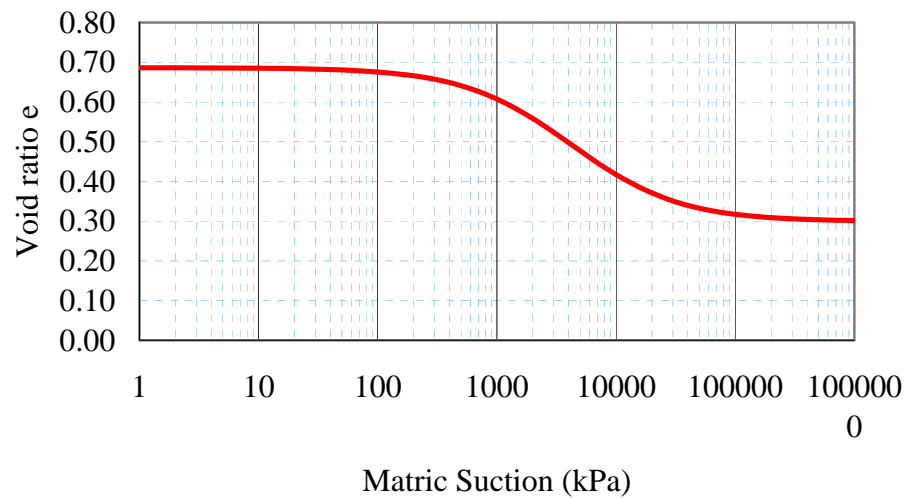


Fig. 4.18. The void ratio versus matric suction curve

4.4.7. The Void Ratio versus Matric Suction Curve When the Mechanical Stress Is Equal to Zero, i.e., $S = f(\sigma - u_a = 0, u_a - u_w)$

Once the void ratio versus matric suction curve is obtained, the relationship $Se = wG_s$, together with the soil water characteristic curve is used to obtain the degree of saturation versus matric suction curve (Fig. 4.19). Its mathematical expression can be obtained by SigmaPlot as following:

$$S = -0.0247898 + \frac{1.0247900}{1 + \exp\left(\frac{\log_{10}(u_a - u_w) - 4.9795434}{0.3240133}\right)} \quad (4.13)$$

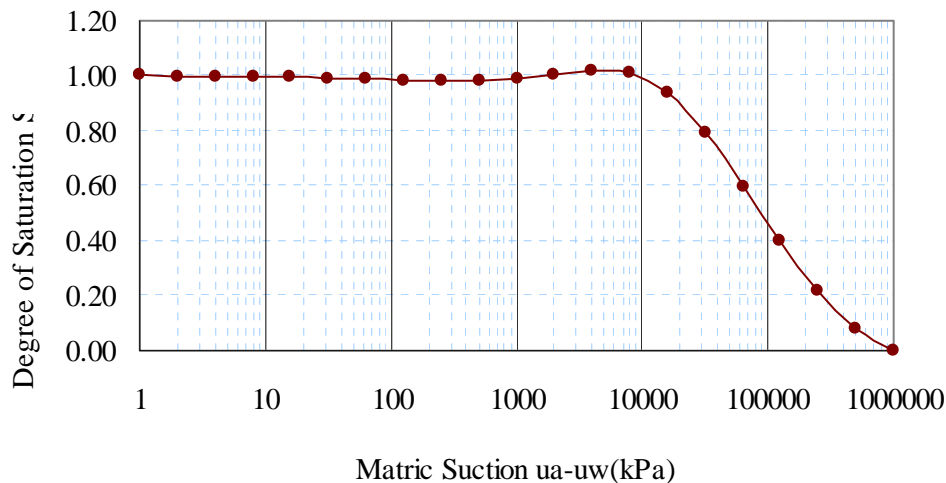


Fig. 4.19. The degree of saturation versus matric suction curve

4.5. Variation of Degree of Saturation in the Free Shrink Test

From Fig. 4.19, it can be seen that during the drying process, the degree of saturations experience an increasing process when the matric suctions are between 500kPa and 8000kPa instead of decreasing uniquely. This phenomenon can be also be explained by the bimodal structure of the soil. During the drying process, an increase in matric suction will cause soil to lose water. Air tends to enter into the soil, which will decrease the degree of saturation of the soil. In some matric suction range, the water loss is mainly from the clay aggregates and the “grain sizes” of the clay aggregates will decrease. Air will be unable to enter into the pores interior to the clay aggregates due to its high air entry value. The macropores formed by the clay aggregates will also decrease, causing the volume of the air to decrease. It is possible the air loss is bigger than the water loss. Under this condition, the degree of saturation of the soil will increase even when the matric suction of the soil increases.

CHAPTER V

CONSTITUTIVE SURFACES FOR SATURATED-UNSATURATED SOILS

5.1 Introduction

To investigate the behaviors of saturated and unsaturated soils, the constitutive relationships are needed. Soil volume will change due to two reasons, one is a change in mechanical stress and the other is a change in matric suction. Therefore, two constitutive relationships are needed for the two stress state variables, one is for the volume change of soil structure and the other is for the volume change of water phase, and the constitutive relationships are surfaces. A saturated soil can be visualized as a special case of an unsaturated soil. For saturated soils, because the effective stress principle is assumed, the constitutive relationship is the void ratio versus effective stress curve. In this chapter, a new method for constructing the constitutive surfaces for unsaturated soils is proposed. Before discussing the constitutive surfaces for saturated-unsaturated soils, the sign conventions for the stress state variables are discussed.

5.2 Sign Conventions for State Variables

In the classical soil mechanics, the sign for the compression stress is positive. When there is a load application (increase in stress), the soil volume decreases. The stress variation is positive (increase) and the strain variation is negative (decrease), which causes a negative Young's Modulus as shown in Fig. 5.1. As shown in Fig. 5.1, a positive or negative sign is associated with the deformation or stress state variable

change in order to indicate an increase or decrease. However, when there is an increase in pore water pressure, the effective stress actually decreases, which leads to an increase in volume. Consequently, the corresponding volumetric modulus with respect to the pore water pressure is positive. The increase in total mechanical stress and the increase in pore water pressure (positive or negative) have reverse signs in modulus. This is also true for the water phase modulus, which can be seen in the later. To avoid the possible mess caused by this phenomenon, it is suggested that the $-u_w$ as a whole to be stress state variable for saturated soils and $(u_a - u_w)$ as a whole to be the stress state variable for unsaturated soils when two stress state variables are used. In this way, All the parameters, m_1^s , m_2^s , m_1^w , and m_2^w defined by Fredlund and Rahardjo (1993) in the constitutive laws will be negative for stable-structured soils (for example, expansive soils). When calculating the modulus, a negative sign is taken for all the parameters to make them become positive.

For metastable-structured soils (such as collapsible soils), the m_2^s will be positive because the increase in matric suction will cause the decrease in volume for collapsible soils. m_1^s , m_1^w , and m_2^w will still be negative values. Fredlund and Rahardjo (1993) stated that m_2^w has a positive sign for collapsible soil, but it is wrong. The explanation will be presented in the Chapter VI.

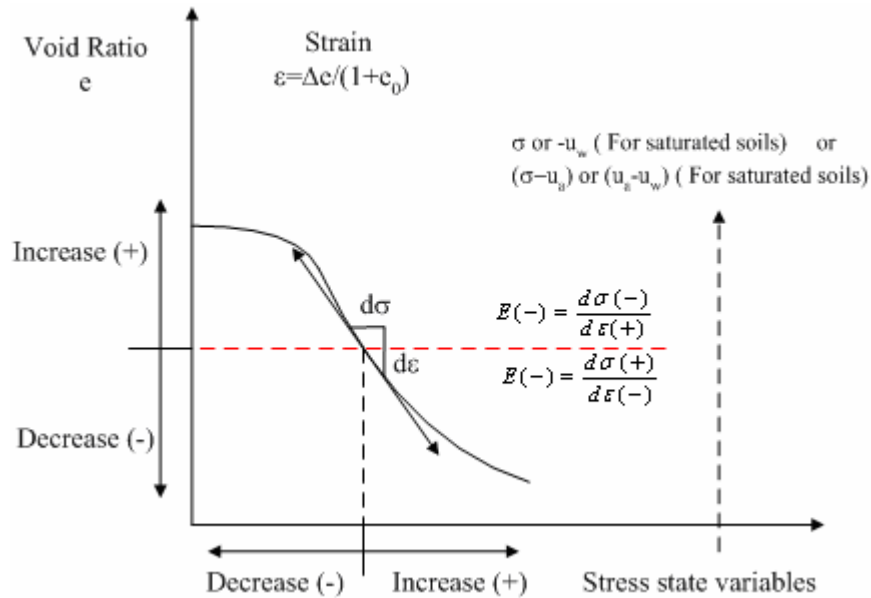


Fig. 5.1. Nonlinear void ratios versus stress state variables curve (after Fredlund and Rahardjo 1993)

5.3 Constitutive Surfaces for Saturated Soils

The effective stress principle was stated as follows by Terzaghi in 1936 :

(1). The effective stress is equal to the total stress minus the pore water pressure. In this way,

$$\sigma' = \sigma - u_w \quad (5.1)$$

where σ' = the effective stress; σ = the total stress; and u_w = pore water pressure.

(2). The effective stress controls certain aspects of the soil behavior, notably compression and strength. This means that the compression depends on the effective stress only. In this way,

$$e = f(\sigma') \quad (5.2)$$

Where e is the void ratio of soil and $f(\sigma')$ stands for the function for the consolidation curve obtained by the routine consolidation test.

Fig. 5.2 shows the consolidation curve for the specimen SW145, which is the same as Fig. 4.14, but the coordinates is Cartesian coordinates, and the mathematical expression for Eq. (5.2) is Eq. 4.4. When Fig. 5.2 is plotted in the effective stress σ' versus pore water pressure $-u_w$ space, it has a shape of surface ADGF as shown in Fig. 5.3. The void ratio surface ADGF is a surface parallel to the pore water press axis, indicating the void ratio constitutive surface is independent of pore water pressure and a function of effective stress only. The curve ACD is the same curve as shown in Fig. 5.2, representing the condition when the pore water pressure is zero.

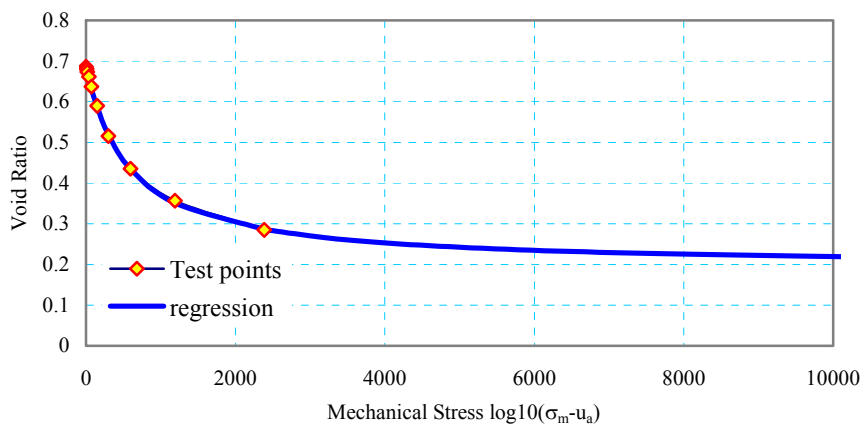


Fig. 5.2. The $e-\sigma_m'$ relationship for soil specimen SW145 obtained from the consolidation test

Saturated soils can be visualized as a special case of unsaturated soils. Substitute Eq. 5.1 into 5.2, hence,

$$e = f(\sigma') = f(\sigma - u_w) = f((\sigma - u_a) + (u_a - u_w)) \quad (5.3)$$

The water content constitutive surface for a saturated soil is $wG_s = e$ because $S=1$. G_s is 2.65 for the soil SW145. Therefore, for a saturated soil, the void ratio constitutive surface is the same as the wG_s constitutive surface, which is shown in Fig.5.5. However, the physical meanings for the two surfaces are totally different, void ratio surface (Fig. 5.4) stands for the constitutive relation between void ratio and net normal mechanical stress and matric suction, while water content constitutive surface (Fig. 5.5) shows the constitutive relationship between water content and net normal mechanical stress and matric suction. Similarly, Line OS stands for the positive pore water pressure axis, while line OI stands for negative pore water pressure (matric suction) axis. Line ED and AB have an angle of 45° with the axis OS and OI, respectively. ABG is a constant water content plane. Surface BNMC is a constant net normal stress plane and curve BC is a soil water characteristic curve at the same stress level.

The mathematical expression of the water content constitutive surface for the soil SW145 when the soil is saturated (Fig. 5.5) can be obtained either by substituting Eq. 5.5 into Eq. 5.4 or by substituting Eq. 4.6 into Eq. 5.1 as followings,

$$wG_s = 0.19523780 + \frac{0.49171347}{1 + \exp\left(\frac{\log_{10}\left((\sigma_m - u_a) + (u_a - u_w)\right) - 2.64046235}{0.42202433}\right)} \quad (5.6)$$

The right side of Eq. 5.6 is exactly the same as that of Eq. 5.4

5.4 The Constitutive Surfaces for Unsaturated Soils

If the soil is unsaturated and the effective stress principle still holds, the void ratio constitutive surface for unsaturated soils can be obtained by extending the void ratio constitutive surface ABED in Fig. 5.4 to negative pore water pressure (matric suction) direction, and a surface ADI is obtained, and the mathematical expression for the surfaces will be the same as that for the saturated soil. The only difference is the pore water pressure is negative (matric suction). Curve AI represents the void ratio versus

matric suction curve when there is no load (total mechanical stress is zero), and it can be obtained by rotating the curve AB 90° anti-clockwisely. However, it is known that the effective stress principle does not hold for unsaturated soils. That is, suction does not have the same influence as total stress in changing the volume of the soil any more. As a consequence, the void ratio versus matric suction curve when the total mechanical stress is zero is curve AP instead of AI. The void ratio constitutive surface has a shape of surface ADP instead of surface ADI. For the water content constitutive surface, it will have the similar problem. The water content constitutive surface for the soil SW145 has a shape like surface ADP' in Fig. 5.5. Surface ABEDP in Fig. 5.4 and Surface ABEDP' in Fig. 5.5 show the schematic plots of the void ratio and water content surfaces for the soil SW145 when the soil is either saturated or unsaturated, respectively. To understand the consolidation of unsaturated soils, the constitutive surfaces for unsaturated soils must be obtained firstly.

Two methods can be used to obtain the constitutive surfaces for unsaturated soils. One is to use tri-axial or consolidation tests with suction control to measure them directly. Usually this kind of test requires advanced lab equipments and the testing is very time-consuming. So far it is not easy to get high quality data, especially in the high suction range. The second method is proposed by Fredlund and Rahardjo (1993) to construct the constitutive surfaces approximately by interpolation. The method is summarized as follows:

(1). The following curves can be obtained:

a) The void ratio versus net normal stress curve when the matric suction is zero, i.e., $e = f(\sigma - u_a, u_a - u_w = 0)$. It is the consolidation test curve.

b) The void ratio versus suction curve when the net normal stress is zero, i.e., $e = f(\sigma - u_a = 0, u_a - u_w)$

c) The water content versus net normal stress curve when the matric suction is zero, i.e., $w = f(\sigma - u_a, u_a - u_w = 0)$.

d) The soil water characteristic curve when net normal stress is zero, i.e., $w = f(\sigma - u_a = 0, u_a - u_w)$.

e) The degree of saturation versus mechanical stress curve when the matric suction is zero, i.e., $S = f(\sigma - u_a, u_a - u_w = 0)$,

f) The degree of saturation versus matric suction curve when net normal stress is zero, i.e. $S = f(\sigma - u_a = 0, u_a - u_w)$.

The minimum laboratory tests needed for constructing the constitutive surfaces of unsaturated soils are: the swell test-consolidation test, the suction test (plate pressure test and salt concentration test), the free shrink test and the specific gravity test. The corresponding methods for obtaining all these curves have been presented in the Chapter IV.

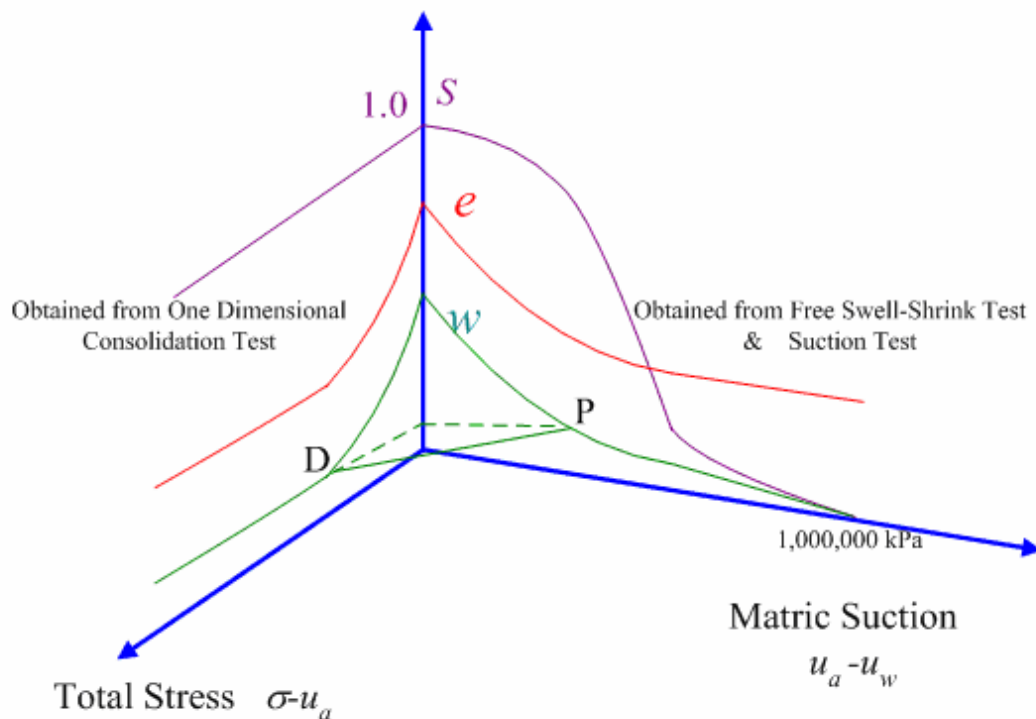


Fig. 5.6. Curves needed for constructing the constitutive surfaces of an unsaturated soil

All the curves are illustrated in Fig. 5.6, where curve (a) is obtained from one dimensional consolidation test. For consolidation test, curve (e) $S=100\%$, and then curve (c) can be obtained by the equation $Se = wG_s$. curve (d) can be obtained from suction test. From free shrink test, the void ratio versus water content curve and degree of

saturation versus water content curve can be obtained. Combining them with curve (d), curve (a) and (f) can be obtained.

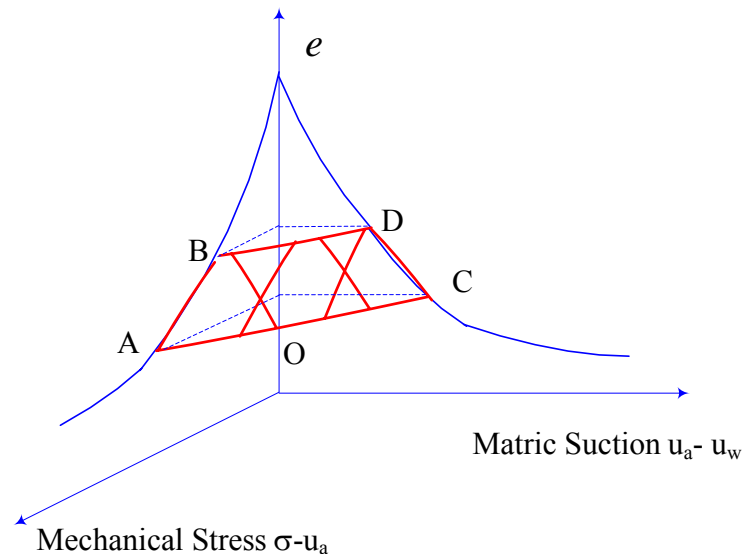


Fig. 5.7. Method proposed by Fredlund and Rahardjo (1993)

(2). It is assumed that the constitutive surface is planar at a particular void ratio or water content range. By making a lot of planes at different void ratio ranges, the whole constitutive surface is constructed. Fig. 5.7 shows the proposed methods for constructing the void ratio constitutive surface. In Fig. 5.7, straight line AB is a small segment on the void ratio versus net normal stress curve, and straight line CD is a small segment on the void ratio versus matric suction curve with the same void ratio range as that for line AB. A plane ABCD is made by using line AB and line CD. Repeating the same process for all the other void ratio ranges, a whole surface is obtained. For the water content constitutive surface, the same method is recommended.

Apparently this method works, however, a deep scrutiny indicates in most cases the planar assumption is not satisfied. For unsaturated soils, the net normal mechanical stress and matric suction are independent stress state variables. Therefore, the void ratio

versus net normal mechanical stress curve is independent of the void ratio versus matric suction curve. As a consequence the two curves could be two arbitrary curves in the net normal mechanical stress and matric suction space.

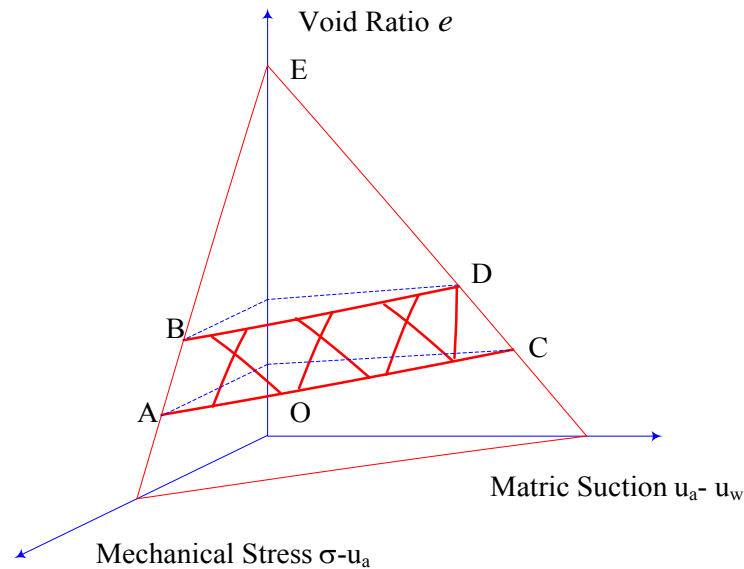


Fig. 5.8. Three planes must have one intersection point if any two of them are not parallel

However, to form a plane at the same void ratio level, the two small segment straight lines must be in the same plane, a dramatic character for this requirement is that they must converge at a certain point on the void ratio axis because three planes must have one intersection point if any two of them are not parallel (Fig. 5.8). As a result, the method proposed by Fredlund and Rahardjo (1993) requires that for any small portion of void ratio range, curve (a) and curve (b) in Fig. 5.6 (i.e., the void ratio versus net normal mechanical stress curve and the void ratio versus matric suction curve, respectively) are two straight lines in the same plane. If it is possible, it is very difficult to be satisfied. Even if the void ratio constitutive surface can be constructed by the method shown in Fig. 5.7, the surface constructed will be discontinuous in its first derivative. It is not

good for further applications because the discontinuity in the first derivative will cause the numerical calculation difficult to converge. For most unsaturated soils, the two curves are arbitrary. When the two curves are arbitrary curves in space, they can not form a plane. Fig. 5.9 shows that AB and CD are two arbitrary lines in space and ABCD are a surface in space instead of a plane.

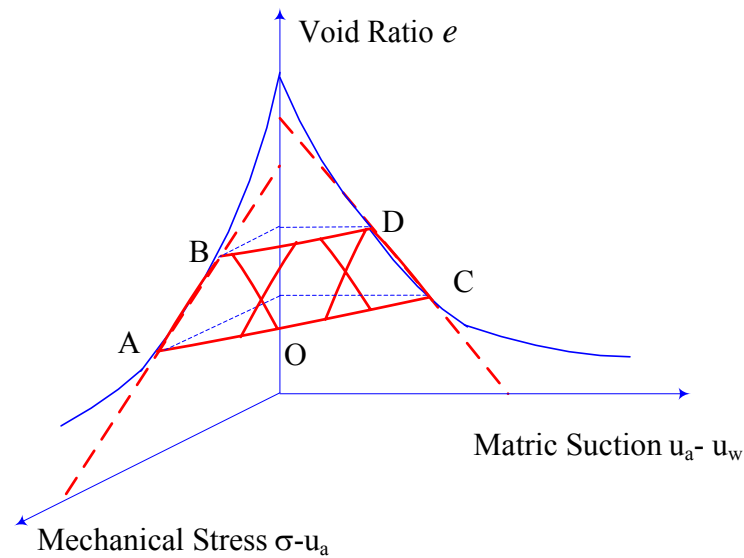
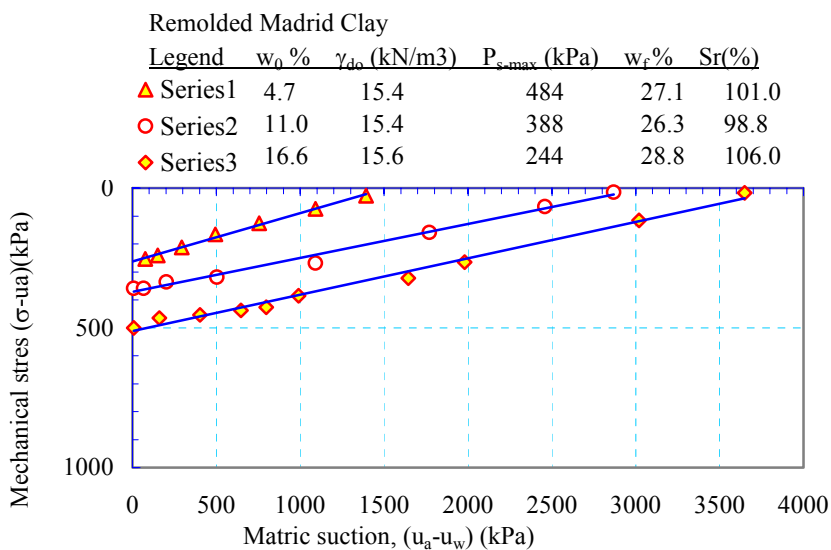
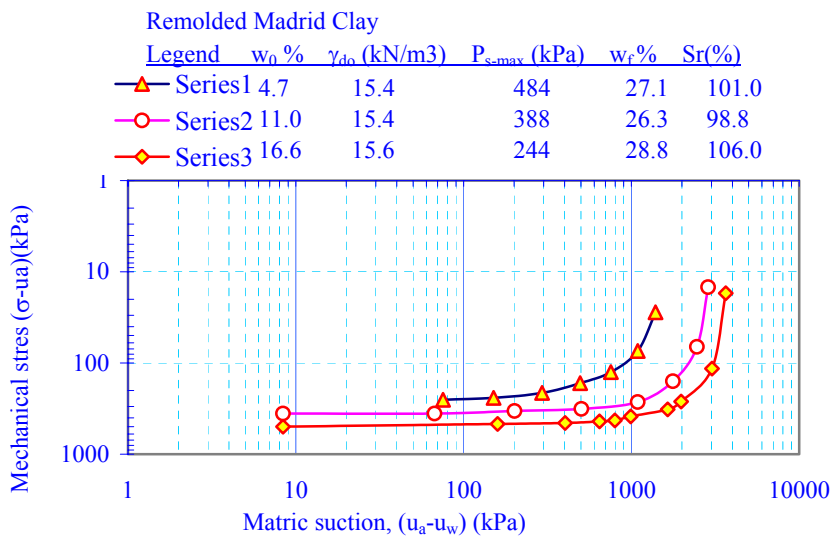


Fig. 5.9. Possible styles for two small portions of lines with the same void ratio

In this chapter, an alternative method is proposed. The method is to assume that the constant void ratio curve is a straight line for any void ratio level. Fig. 5.10a shows the constant volume test data for remolded Madrid clay by Escario (1969). It indicates the straight-line assumption is a good enough assumption. Fig. 5.10b shows the data points when they are plotted in the log-log coordinate system.



(a)



(b)

Fig. 5.10. Constant void ratio curves for some unsaturated soils (After Escario 1969). (a) Cartesian Coordinate; (b) Log-Log Coordinate

The detailed procedures are described as follows: (1). Find the corresponding two points for any void ratio from the void ratio versus net normal mechanical stress curve and the void ratio versus matric suction curve respectively; (2). Connect the two points

with a straight line, and (3). Repeat the procedure for all the void ratio levels, finally a surface will be obtained.

At the first glance, it seems this method is not applicable because there are infinite pairs of points for even a small portion of curve pairs. If it is finished by hand with finite sets of void ratio levels, it will end up with the same method proposed by Fredlund and Rahardjo (1993) as discussed above. The answer for this question is that it can be done mathematically and the close form expression of the surface can be obtained.

To make the discussion a little bit simpler, it is assumed that the void ratio versus net normal mechanical stress curve, i.e. the consolidation curve (a) in Fig. 5.6, has a mathematical expression of

$$e = a \times \log_{10}(\sigma - u_a) + b \quad (5.7)$$

and the void ratio versus matric suction curve has a mathematical expression of

$$e = c \times \log_{10}(u_a - u_w) + d \quad (5.8)$$

where a, b, c and d are best-fitted constants determined by laboratory test data.

The mathematical expression of a straight line DP in Fig. 5.11 (which is the same line DP as shown in Fig. 5.4) in the net normal stress and matric suction plane for a constant void ratio level is

$$\frac{\sigma_m - u_a}{OD} + \frac{u_a - u_w}{OP} = 1 \quad (5.9)$$

For a certain void ratio level $e = e_0$, the corresponding net normal stress and matric suction can be obtained from curve (a) as in Eq. 5.7 and Curve (b) as in Eq. 5.8, thus,

$$OD_{e=e_0} = (\sigma_m - u_a)_{(u_a - u_w = 0, e = e_0)} = 10^{\left(\frac{e_0 - b}{a}\right)} \quad (5.10)$$

$$OP_{e=e_0} = (u_a - u_w)_{((\sigma_m - u_a)=0, e=e_0)} = 10^{\left(\frac{e_0 - d}{c}\right)} \quad (5.11)$$

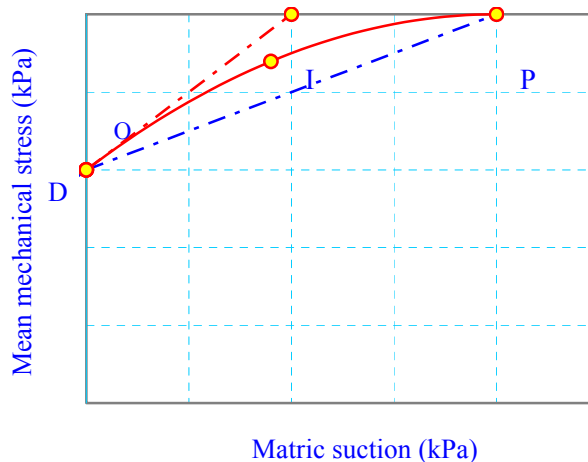


Fig. 5.11. Assumptions for constant void ratio curves

Combining Eq. 5.10, 5.11 and 5.9, and considering that for any arbitrary void ratio e , the similar approach can be applied, and the mathematical expression for the void ratio constitutive surface is as following:

$$\frac{\sigma_m - u_a}{10^{\left(\frac{e-b}{a}\right)}} + \frac{u_a - u_w}{10^{\left(\frac{e-d}{c}\right)}} = 1 \quad (5.12)$$

The only requirement for this method is that both net normal mechanical stress and matric suction can be expressed as a function of void explicitly, which is very easy to realize by regression.

Further research indicates that the constant void ratio curve for the void ratio constitutive surface does not necessarily have to be a straight line. If only the constant void ratio curve is a function of both the net normal mechanical stress and matric suction on the curve (a) and (b), this method is applicable. A further example can explain this

argument more clearly. Fig. 5.4 illustrates that the void ratio constitutive surface of saturated soils, and the constant void ratio line ED has an angle 45^0 with the total mechanical stress axis. With the straight line assumption, the line DP will have an angle different from 45^0 with the total mechanical stress axis at the point D. It indicates the soil properties will change abruptly when the soil pore water pressure changes from positive to negative. A better assumption is to assume that the constant void ratio curve is quadratic and the tangential line DI of the curve at point D is still 45^0 with the net normal mechanical stress axis (Fig. 5.11). This transition at the point D means the soil properties will change smoothly from saturated to unsaturated. The condition can be expressed as,

$$\left(\frac{d(\sigma - u_a)}{d(u_a - u_w)} \right)_{(u_a - u_w)=0} = -1 \quad (5.13)$$

The mathematical expression of the curve DP in Fig. 5.4 or Curve BCD in Fig. 5.11 is:

$$(\sigma - u_a) = \frac{OP - OD}{OP^2} (u_a - u_w)^2 - (u_a - u_w) + OD \quad (5.14)$$

where OP and OD are determined by Eq. 5.10 and Eq. 5.11. Combining Eq. 5.10 and 5.11 with Eq. 5.14, the void ratio constitutive surface of the soil can be obtained.

Furthermore, it can also be proven that if the mathematical expressions for the void ratio versus net normal mechanical stress curve and the void ratio versus matric suction curve and the constant void ratio are continuous and have continuous first derivatives, the obtained void ratio constitutive surface will be continuous and has continuous first derivative. It is very desirable for the actual application when the derivatives of the surface are needed. Any discontinuity for the first derivative of the constitutive surface will cause difficulties in converges when performing numerical simulation.

In addition, even the surface is measured by laboratory tests directly, this method is still useful. Because the measurements are always a lot of discrete points, to form a complete surface, numerical interpolation is needed, and this method is potentially a good method for the data reduction. For situations when higher accuracy is needed, it is recommended that some tests are performed to measure the shape of the constant void ratio curve, and then this proposed method is applied to obtain the whole constitutive surface. For general applications in practice, the straight line assumption or the quadratic curve assumption is considered as a good enough assumption.

5.5. Constructing the Void Ratio Constitutive Surfaces for Saturated-Unsaturated Soils

For the specimen SW145, SW189, and Sporc, all the required six curves have been obtained by the method presented in the Chapter IV. In this section, SW145 is used as an example to show the procedures to construct the constitutive surfaces for saturated-unsaturated soils. The same procedure had been used for the other two soils and the corresponding constitutive surfaces can be found in the Appendix B.1.2 and B.1.3, respectively. For the soil SW145, the regression curves for the void ratio versus net normal mechanical stress curve. Solving the mean mechanical stress form Eq. 4.4 in terms of void ratio, gives

$$(\sigma_m - u_a) = 10^{\left(0.42202433 \ln \left(\frac{0.49171347}{e^{-0.19523780}} - 1 \right) + 2.64046235 \right)} \quad (5.15)$$

The mathematical expression for the void ratio versus matric suction curve is Eq. 4.10. Solving the matric suction form Eq. 4.10 in terms of void ratio, gives

$$(u_a - u_w) = 10^{\left(0.456383725 \ln \left(\frac{0.387060274}{e^{-0.299088}} - 1 \right) + 3.624238826 \right)} \quad (5.16)$$

Substituting Eq. 5.15 and 5.16 into Eq. 5.9, gives,

$$\frac{(\sigma_m - u_a)}{10^{\left(0.42202433 \ln\left(\frac{0.49171347}{(e-0.19523780)} - 1\right) + 2.64046235\right)}} + \frac{(u_a - u_w)}{10^{\left(0.456383725 \ln\left(\frac{0.387060274}{e-0.299088} - 1\right) + 3.624238826\right)}} = 1 \quad (5.17)$$

For any net moral stress $(\sigma - u_a)$ and matric suction, the void ratio determined by Eq. 5.17 can be obtained by iteration. The solver in the Microsoft Excel or the bisection method can be used to perform the iteration, which will be explained in the later. Fig. 5.12 shows the corresponding void ratio constitutive surface of the real soil. The reason why Fig. 5.12 is different from Fig. 5.4 is that the coordinate system is double log scale instead of Cartesian system.

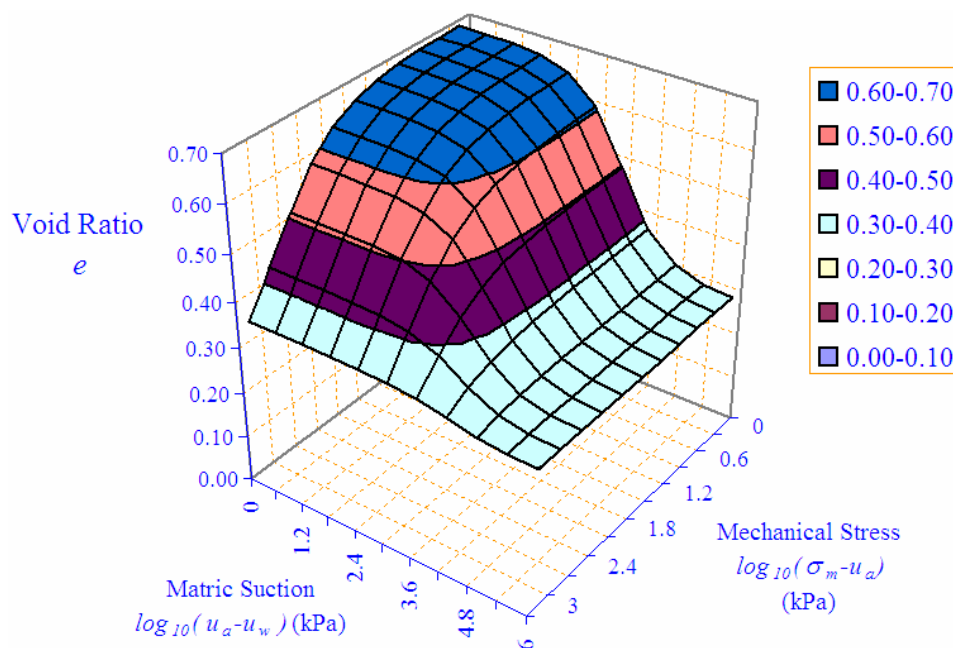


Fig. 5.12 Constructed void ratio constitutive surface for the soil sample SW145

In summary, mathematical expression for the void ratio constitutive surface for the soil SW145 is:

Eq. 5.4: under saturated conditions ($u_w \geq 0$ or $u_a - u_w \leq 0$)

Eq. 5.17: under unsaturated conditions ($u_w \leq 0$ or $u_a - u_w \geq 0$)

The void ratio constitutive surface has a shape similar to the surface ABEDP as shown in Fig. 5.4 under Cartesian's coordinate system. If plotted in a log-log coordinate system, the void ratio constitutive surface will have a shape as shown in Fig. 5.12 for unsaturated soil conditions.

5.6 Degree of Saturation Constitutive Surface and Water Content Constitutive Surface

The void ratio constitutive surface is obtained by the proposed the method (Fig. 5.12). If the water content constitutive surface is known, the degree of saturation constitutive surface can be obtained by the relationship $S_e = wG_s$. In the same way, if the degree of saturation constitutive surface is known, the water content constitutive surface can be obtained by the relationship $S_e = wG_s$.

The same approach can be used to construct the water content constitutive surface. When the straight line assumption is applied to construct the water content constitutive surface, the connected two points have different degree of saturation. For example, point P in Fig. 5.6 is a point on the soil water characteristic curve, matric suction at point P is not zero and the corresponding degree of saturation is less than 1. Point D in Fig. 5.6 is on the water content versus total stress curve obtained from the consolidation test. Matric suction at point D is zero and the degree of saturation is 100%. From Point P to point D, the net normal stress will increase, and the matric suction will decrease and the degree of saturation will increase. It is consistent with the soil behavior because the line DP in Fig. 5.6 represents the undrained loading process. The water content of the soil does not change because line DP is a constant water content line. As discussed previously, DP could also be a curve instead of straight line. It is recommended that some tests are performed to measure the shape of constant water content curve to get the better results. For general applications in practice, the straight line assumption or the quadratic curve assumption is considered as a good enough assumption. Further research is needed in this direction.

One problem associated with the construction of water content constitutive surface is that usually the consolidation test are performed in limited net normal stress range and the soil water can not be squeezed out of the soil completely. Hence, on the water content versus total stress curve, the water content can not reach zero, but for the soil water characteristic curve, when the matric suction is 1,000,000kPa, the water content is zero or close to zero (Fig. 5.6). As a consequence the proposed method can only construct part of the water content constitutive surface instead of the whole surface.

An additional technique is needed to solve the problem. It is assumed that for the water content range which the consolidation test can not reach, the degree of saturation for the soil will not be influence by the net normal mechanical stress. It is considered as a reasonable assumption because if the soil has already reached a status which the increase in net normal mechanical stress is unable to compress the soil, the soil can be considered to have the properties similar to sand, and the degree of saturation is dependent on matric suction only. As can be seen in Chapter II, the mechanical stress has no influence on the soil water characteristic curve when the suction is high. Thus the method for constructing the water content constitutive surface consists of two parts: (1). for high water content levels (that is, the water content range of consolidation test), the water content surface is constructed by the straight line assumption method, and then the degree of saturation surface is obtained form $S=wGs/e$; (2). for the lower water content level, the degree of saturation is assumed to be independent of net normal mechanical stress. The degree of saturation versus matric suction curve in the low water content range can be obtained from the free shrink test and soil water characteristic curve. The water content constitutive surface is then obtained form the relationship $w=Se/Gs$. The mathematical expressions for the two portions can be obtained, too.

The mathematical expression for the water content versus mean mechanical stress curve is Eq. 4.6. Solving the mean mechanical stress from Eq. 4.10 in terms of water content, gives

$$\sigma_m - u_a = 10^{\left(0.42202433 \ln \left(\frac{0.18555225}{(w-0.07367464)} - 1 \right) + 2.64046235 \right)} \quad (5.18)$$

The mathematical expression for the water content versus mean mechanical stress curve is Eq. 4.7. Solving the matric suction from Eq. 4.7 in terms of water content, gives

$$(u_a - u_w) = 10^{\left(0.671559558 \ln\left(\frac{0.285551272}{(w+0.026264216)} - 1\right) + 4.386436815\right)} \quad (5.19)$$

The obtained water content constitutive surface by making use of straight line assumption is:

$$\frac{\sigma_m - u_a}{10^{\left(0.42202433 \ln\left(\frac{0.18555225}{(w-0.07367464)} - 1\right) + 2.64046235\right)}} + \frac{u_a - u_w}{10^{\left(0.671559558 \ln\left(\frac{0.285551272}{(w+0.026264216)} - 1\right) + 4.386436815\right)}} = 1$$

$$\text{for } (\sigma_m - u_a) + (u_a - u_w) \leq 32637.8 \text{ kPa} \quad (5.20)$$

For the range $(\sigma_m - u_a) + (u_a - u_w) > 32637.8$ kPa, the degree of saturation is assumed to be independent of mechanical stress. Therefore the degree of saturation surface is the same as Eq. 4.13 in Chapter IV,

$$S = -0.024789788 + \frac{1.024790004}{1 + e^{\left(\frac{\log_{10}(u_a - u_w) - 4.979543423}{0.324013298}\right)}}$$

$$\text{for } (\sigma_m - u_a) + (u_a - u_w) > 32637.8 \text{ kPa} \quad (4.13)$$

The water content surface for the range $(\sigma_m - u_a) + (u_a - u_w) > 32637.8$ kPa can be obtained by making use of the relationship $wGs = Se$, Eq. 4.11 and 5.17 as following:

$$\frac{(\sigma_m - u_a)}{10^{\left(0.42202433 \ln \left(\frac{0.49171347}{(wG_s/S - 0.19523780)} - 1 \right) + 2.64046235 \right)}} + \frac{(u_a - u_w)}{10^{\left(0.456383725 \ln \left(\frac{0.387060274}{(wG_s/S - 0.299088)} - 1 \right) + 3.624238826 \right)}} = 1 \quad (5.21)$$

Since the void ratio, water content, and degree of saturation constitutive surfaces for the soil SW145 have been obtained, if the two stress state variables, i.e. total stress and matric suction, are known, all the other parameters such as void ratio e , water content w , and degree of saturation S can be calculated by inputting the two known stress state variables into the corresponding equations from the surfaces. It is noted that Eq. 5.17 and 5.20 are implicit for void ratio and water content, respectively. Consequently an iteration scheme is needed to calculate the void ratio and water content with the two knowing state variables. Once the void ratio and the water content constitutive surface are obtained, the degree of saturation surface can be obtained by the relationship $Se = wG_s$.

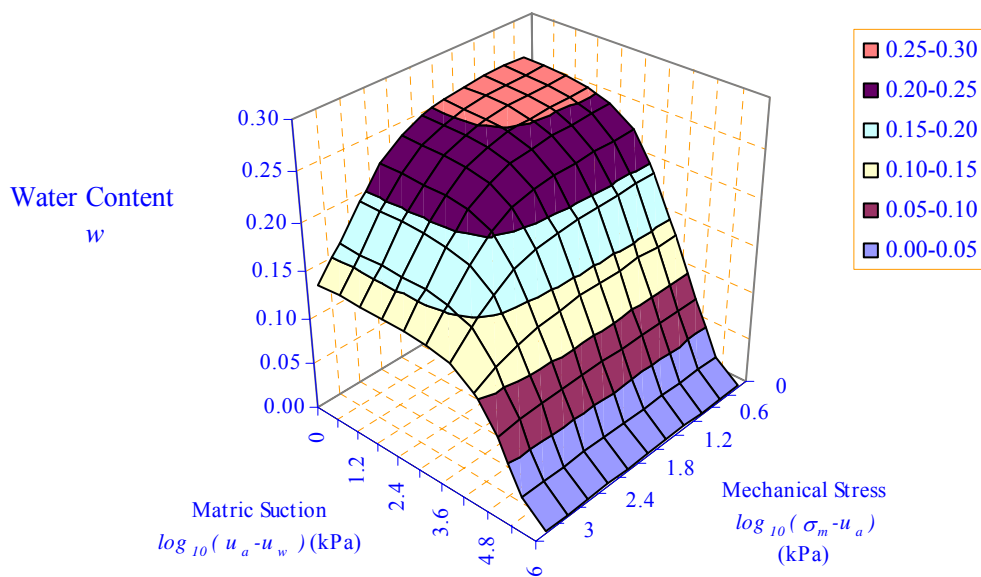


Fig. 5.13. The water content constitutive surface for the soil sample SW145

A program called SurfaceCalculation (Appendix B.2) is used to perform the iterations by using bisection method. The calculated constitutive surfaces for water content and degree of saturation are shown in Fig. 5.13 and 5.14, respectively.

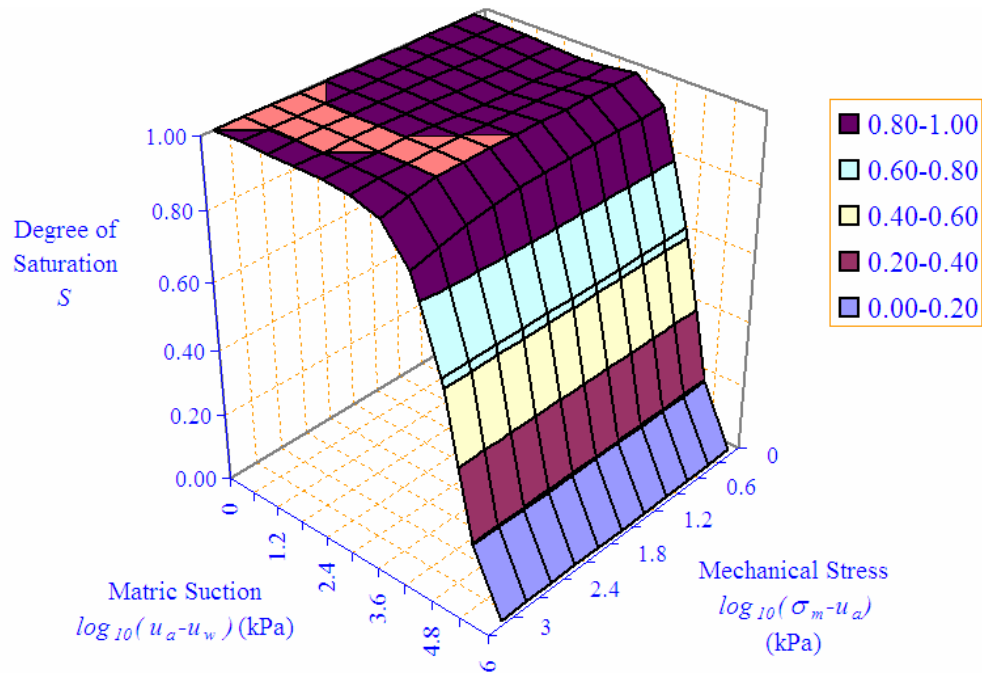


Fig. 5.14. The degree of saturation constitutive surface for the soil sample SW145

The water content constitutive surface as shown in Fig. 5.13 for the soil SW145 is actually a collection of soil water characteristic curves at different net normal stress level (Fig. 5.15). Similarly, the void ratio constitutive surface as shown in Fig. 5.12 for the soil SW145 is actually a collection of void ratio versus matric suction curves at different net normal stress level (Fig. 5.16). The physical meaning for the slopes of these curves will be explained in the Chapter VI. It can also be seen that Eq. 5.17 and 5.20 are continuous and have continuous first derivatives. Their first derivatives are related to the material properties and will be discussed in Chapter VI.

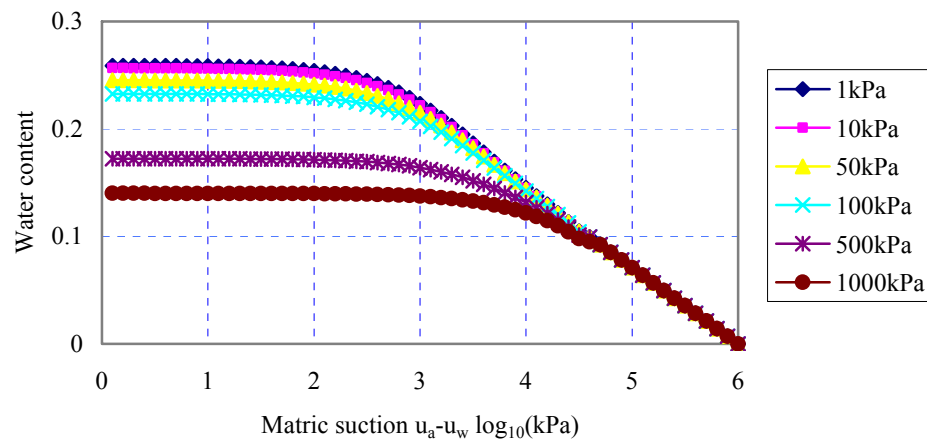


Fig. 5.15 Water content versus matric suction curve at different net normal stress levels

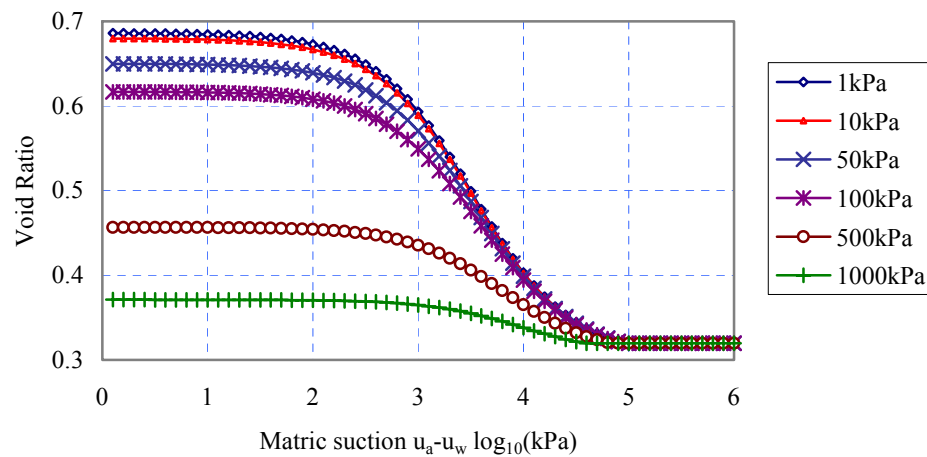


Fig. 5.16. Void ratios versus matric suction curve at different net normal stress levels

CHAPTER VI

CONSOLIDATION THEORY FOR SATURATED-UNSATURATED SOILS

6.1 Scope of the Research, Assumptions and Some Basic Definitions

6.1.1 Scope of the Research

To analyze the damages to structure caused by expansive soils, firstly we need understand the volume change behaviors of expansive soils. Two reasons can cause the volume change of expansive soils, the first one is the mechanical stress variations and the second is matric suction variations. Like that for saturated soils, the matric suction (pore water pressure) will change when an external load is applied to an unsaturated soil. The volume of the unsaturated soil will also change when the excess pore water pressure (matric suction) is dissipated.

The study of this dissertation is confined to the volume change or consolidation behaviors of unsaturated soils. Saturated soils are actually a special case of unsaturated soils. All the discussions therefore are applicable to both saturated soils and unsaturated soils.

The consolidation for an unsaturated soil is much more complicated than that for saturated soils. Thanks to the existence of air phase, the soil is compressed under an undrained loading condition at the instant of load application and the excess pore water pressure is not equal to the applied load any more. In the mean time, the pore air pressure also changes due to the external load. If the excess pore air and water pressure are allowed to dissipate, the excess pore water and air pressure will dissipate gradually and it is a time dependent process. Moreover, the volume change of the unsaturated soil is not equal to the water drainage any more. Available data reveals that the material properties for unsaturated soils are usually highly nonlinear and can not be considered constant any more.

For saturated soils, a true three dimensional consolidation theory of consolidation couples the equilibrium of total stresses and the continuity of the soil water mass. A

pseudo three-dimensional theory uncouples these two phenomena, under the assumption that the total stresses are constant. This condition is only strictly true in special cases. One dimensional consolidation is one such case. For unsaturated soils, the consolidation theory can also be discussed in the same way. Namely, both the coupled and uncoupled theories are needed. The uncoupled consolidation theory is not strictly true, but it is of great practical use.

The uncoupled consolidation theory for unsaturated soils need answer the following questions:

- (1). What are the excess pore water and air pressure at the instant of load application?
- (2). What is the immediate volume change due to an undrained loading?
- (3). What is the final volume change of the soils?
- (4). What is the relationship between the volume change, pore water and air pressure variation and time?

For the coupled consolidation theory, the influence of mechanical stress variations during the consolidation process should also be considered. For saturated soils, the difference between the coupled and uncoupled consolidation theory for two or three dimensional case is the Mandel-Cryer effect (Mandel 1961; Cryer 1963; Gibson et al. 1963). For unsaturated soils, no similar research has been done in the past.

How to calculate the excess pore water and air pressure is another problem. Currently the compressibility of air-water mixture is used to calculate the excess pore water and air pressure. More research is needed in this direction.

Some other issues also need be further understood. For example, what is the nature of the effective stress principle? How many stress state variables are needed to describe soil behaviors? Since Terzaghi (1943) first used the principle of effective stress for saturated soils, the validity of the principle is well established and proved to be invaluable for such soils. Numerous researchers attempted to extend the principle to the case of partly saturated soils (Bishop and Blight 1959; Aitchison 1961). However, Jennings and Burland (1962) questioned the validity of effective stresses in collapsible

soils. They concluded that the effective stress principle failed to explain the behaviors of collapsible soils. They further stated that collapsible behaviors existed extensively in nearly all the soils from silt to highly expansive soils, depending on the applied external load. The results finally lead to the appearance of two stress state variables concept (Matyas and Radhakrishna 1968; Fredlund and Morganstern 1973). That is, the mechanical stress and the matric suction should be considered separately. When studying the volume change behaviors of unsaturated soils, great efforts have been put recently to validate this statement. The questions are: What is the essence of the effective stress principle? Why did the effective stress principle fail to explain the behavior of collapsible soils? What causes the different behaviors between the expansive soils and collapsible soils? How many stress state variables do we need for describing the behavior of unsaturated soils?

6.1.2 Assumptions

The purpose of this chapter is to discuss the coupled and uncoupled consolidation theories for unsaturated-saturated soils with a view to investigating the above questions.

The investigation is confined to the following assumptions:

- (1). The soil is homogeneous and elastic,
- (2). The soil particles and the water are incompressible,
- (3). Darcy's law is valid,
- (4). The air phase is continuous and the excess pore air pressure is dissipated instantly so that the pore air pressure can be considered as a constant during the consolidation process, and
- (5). All the other material parameters are functions of both mechanical stress and matric suction and nonlinear.

Of the basic assumptions, (1) is most subject to criticism. However, we should keep in mind that it also constituted the basis of Terzaghi's theory, which has been found quite satisfactory for the practical requirements of engineering. Another excuse for this assumption is that the soils used in this investigation are expansive soils and the main

volume change is from water content variation. According to the bimodal structure discussed in the Chapter II, for expansive soils, the microstructure will dominate the deformation and the deformation behaviors of the soils can be considered fully reversible. Hence, for expansive soils, it should be a reasonable assumption. For collapsible soils, it is not the case and a clear discussion based on elastic assumption will provide a basis for the further discussion of plastic soil behaviors.

Assumption (4) is considered to be reasonable because the air coefficients of permeability are much greater than the water coefficients of permeability. As a consequence, the excess pore air pressure can be considered to be dissipated instantly compared with excess pore water pressure. When the air is occluded, the air phase can be considered as part of the soil structure and be compressible. It is considered that the method in this chapter will still be applicable under this condition because the influence has been included in the constitutive surfaces of soils. The conditions when the constant pore air pressure assumption is not valid will be discussed at the end of the Chapter. Under this assumption, the pore air pressure can be considered as zero. As a consequence, matric suction $u_a - u_w$ is the same as the negative pore water pressure $-u_w$ and the net normal mechanical stress $\sigma - u_a$ is the same as the mechanical stress σ .

Darcy's law will always hold when permeability is a function of both mechanical stress and matric suction and nonlinear.

In this chapter, first of all, the coupled thermal stress problem will be used as a parallel to illustrate the concept of two stress state variables. Second, the coupled consolidation theory for unsaturated soils is derived. The physical meanings of the parameters in the constitutive laws for the coupled consolidation theory for unsaturated soils are explained. Some basic concepts such as the effective stress and the excess pore water pressure are explained by the proposed constitutive laws. Third, a comparison is made between the coupled thermal stress problem and the coupled consolidation theory for unsaturated soils. Fourth, a method is developed to extend the Terzaghi's consolidation theory for saturated soils to unsaturated soils. Two examples, one for an expansive soil and the other for collapsible soils, are given to validate the proposed

method. Fifth, by using the thermodynamic analogue, the coupled consolidation theory for saturated-unsaturated soils is discussed. Finally some topics such as the stress state variables, constitutive laws and fundamental laws for multiphase flow and air in the soil are discussed.

A saturated soil is actually a special case of an unsaturated soil. All the following discussions are applicable for saturated soils even though they are especially stated for unsaturated soils. To be consistent with the convention in the soil mechanics, the compressive stresses and matric suction are assumed to be positive. Therefore, the Young's Modulus of a soil has a negative sign because when increasing compressive stresses, the volume of the material will decrease. The negative temperature is used as a whole to be a stress state variable, which is corresponding to the negative pore water pressure in the soil. Signs for the other parameters will be discussed in a later section for expansive soils and collapsible soils specially.

6.1.3 Some Basic Definitions

Fredlund (1973) proposed that two stress state variables should be used to describe the behavior of unsaturated soils. As can be seen in the further discussion, saturated soils can be considered as a special case of unsaturated soils. Therefore, two stress state variables are also needed for saturated soils, one is effective stress and the other is pore water pressure. Fredlund and Rahardjo (1993) stated that only one stress state variable (effective stress) is needed for saturated soils, which is questionable. Before the further discussion, some basic terminologies are reviewed. Fredlund and Rahardjo (1993) define the following terminologies for the investigation of unsaturated soils.

(1). Stress state variable: the nonmaterial variables required for the characterization of the stress condition.

(2). State variable: a limited set of dynamical variables of system, such as pressure, temperature, volume, etc., which are sufficient to describe or specify the state of the system completely for the considerations at hand.

(3). Constitutive relations: Single-value equations expressing the relationship between the state variables.

The two independent stress state variables needed for unsaturated soils are: the mechanical stress $\sigma-u_a$ and the matric suction u_a-u_w . The other state variables needed for describing the behavior of unsaturated soils are: the void ratio e , the water content w , and the degree of saturation S of the soil.

The constitutive relations needed for describing the volume change of unsaturated soils are: stress (mechanical stress and matric suction)-strain constitutive law and the water content-stress (mechanical stress and matric suction) constitutive law.

6.2 Review of the Coupled Thermal Stress Problem

6.2.1 Introduction

Terzaghi (1943) used the thermodynamic analogue to explain the one dimensional (or uncoupled) consolidation theory for saturated soils in his theoretic soil mechanics, where the pore water pressure is corresponding to temperature and the water content is corresponding heat energy per unit mass. A scrutiny will find that the thermodynamic analogue to the coupled consolidation theory of soils can also be used to illustrate problems associated with volume change, two stress state variables, equivalent effective stress and the excess pore water pressure for saturated-unsaturated soils.

6.2.2 Constitutive Laws for Deformation

6.2.2.1 Deformations due to Mechanical Stresses Variations

Let us consider the volume change of a coupled thermal stress problem of an ideal elastic, isotropic material. The volume of the material will change when a load is applied to it. The constitutive law of deformation due to mechanical stresses is described by the Hooker's law:

$$\begin{aligned}
(d\varepsilon_x)_\sigma &= \frac{d\sigma_x}{E} - \frac{\mu}{E}(d\sigma_y + d\sigma_z), & d\gamma_{yz} &= \frac{d\tau_{yz}}{G} \\
(d\varepsilon_y)_\sigma &= \frac{d\sigma_y}{E} - \frac{\mu}{E}(d\sigma_z + d\sigma_x), & d\gamma_{zx} &= \frac{d\tau_{zx}}{G} \\
(d\varepsilon_z)_\sigma &= \frac{d\sigma_z}{E} - \frac{\mu}{E}(d\sigma_x + d\sigma_y), & d\gamma_{xy} &= \frac{d\tau_{xy}}{G}
\end{aligned} \tag{6.1}$$

where E = the Young's modulus of the material; μ = Poisson's ratio; G = the shear modulus; $d\sigma_x$, $d\sigma_y$, $d\sigma_z$ = the applied incremental mechanical stress in the x , y , and z directions, respectively; and $d(\varepsilon_x)_\sigma$, $d(\varepsilon_y)_\sigma$, $d(\varepsilon_z)_\sigma$ = the corresponding strains in x , y , and z directions, respectively. The subscription σ stands for the strains caused by the mechanical stress.

Eq. 6.1 is the constitutive law for the deformation of the elastic material due to mechanical stress variations under isothermal conditions. By using small increments of stress and strain, the Hooker's law in the form of incremental procedure can be used to apply the linear elastic formulation to a nonlinear problem. The nonlinear stress versus strain curve is assumed to be linear within each small stress and strain increment. For all the other constitutive relations in the following discussions, the same principle is applied. The volumetric deformation of the material due to mechanical stress variations is:

$$\begin{aligned}
(d\varepsilon_v)_\sigma &= (d\varepsilon_x)_\sigma + (d\varepsilon_y)_\sigma + (d\varepsilon_z)_\sigma \\
&= \frac{3(1-2\mu)}{E} \frac{(d\sigma_x + d\sigma_y + d\sigma_z)}{3} = \frac{1}{B} d\sigma_m
\end{aligned} \tag{6.2}$$

where $(d\varepsilon_v)_\sigma$ is the volumetric strain due to mechanical stress; B is the bulk modulus of the material; and $\sigma_m = \frac{(\sigma_x + \sigma_y + \sigma_z)}{3}$ is the mean mechanical stress.

6.2.2.2 Deformation due to Temperature Variations

The volume of the material will also change due to temperature variations. When there are temperature variations, the material will swell or shrink in all the directions with the same magnitude. The deformations due to temperature variations can be defined as follows:

$$\begin{aligned} (d\varepsilon_x)_T &= (d\varepsilon_y)_T = (d\varepsilon_z)_T = \alpha d(-T_x) \\ &= \alpha d(-T_y) = \alpha d(-T_z) = \alpha d(-T) \end{aligned} \quad (6.3)$$

where α = the coefficient of heat expansion of the metal; and $(\varepsilon_x)_T$, $(\varepsilon_y)_T$, $(\varepsilon_z)_T$ = the corresponding strains in the x , y , and z directions, respectively. The subscription “T” stands for the deformation caused by the temperature variation.

Note that temperature is a scalar and is the same in all directions. Hence, $T_x = T_y = T_z = T$. No shear deformation is caused by temperature variations. Eq. 6.3 is the constitutive law for the deformation of the elastic material due to temperature variations under constant mechanical stress conditions and without mechanical restrictions. Negative temperature is used to be consistent with future discussions. The volumetric deformation due to temperature variation is:

$$\begin{aligned} (d\varepsilon_v)_T &= (d\varepsilon_x)_T + (d\varepsilon_y)_T + (d\varepsilon_z)_T \\ &= 3\alpha d(-T) \end{aligned} \quad (6.4)$$

where $(d\varepsilon_v)_T$ is the volumetric thermal strain.

6.2.2.3 Constitutive Laws for the Deformations in the Coupled Thermal Stress Problem

When there are both load applications and temperature variations, the volume change of the material will change due to both reasons. The final volume of the material depends on the combination effect of the two processes. It is a coupled thermal stress problem.

Under the assumption of small strains, the principle of superposition can be applied. Eq. 6.5 shows the constitutive laws for the coupled thermal stress problem.

$$\begin{aligned}
 d\varepsilon_x &= (d\varepsilon_x)_\sigma + (d\varepsilon_x)_T = \left[\frac{d\sigma_x}{E} - \frac{\mu}{E}(d\sigma_y + d\sigma_z) \right] + \alpha d(-T), & \gamma_{yz} &= \frac{d\tau_{yz}}{G} \\
 d\varepsilon_y &= (d\varepsilon_y)_\sigma + (d\varepsilon_y)_T = \left[\frac{d\sigma_y}{E} - \frac{\mu}{E}(d\sigma_z + d\sigma_x) \right] + \alpha d(-T), & \gamma_{zx} &= \frac{d\tau_{zx}}{G} \\
 d\varepsilon_z &= (d\varepsilon_z)_\sigma + (d\varepsilon_z)_T = \left[\frac{d\sigma_z}{E} - \frac{\mu}{E}(d\sigma_x + d\sigma_y) \right] + \alpha d(-T), & \gamma_{xy} &= \frac{d\tau_{xy}}{G}
 \end{aligned} \quad (6.5)$$

where $d\varepsilon_x$, $d\varepsilon_y$, $d\varepsilon_z$ = the corresponding strain in the x , y , and z directions, respectively. The subscription “ σ ” and “ T ” stand for the strains caused by the mechanical stress variations and the temperature variations, respectively.

The volumetric strain for the coupled thermal stress problem can be obtained as follows:

$$\begin{aligned}
 d\varepsilon_v &= d\varepsilon_x + d\varepsilon_y + d\varepsilon_z = \frac{3(1-2\mu)}{E} d(\sigma_m) + 3\alpha d(-T) \\
 &= \frac{1}{B} d(\sigma_m) + 3\alpha d(-T)
 \end{aligned} \quad (6.6)$$

where $d\varepsilon_v$ is the total volumetric strain.

As can be seen in Eq. 6.5, all the three normal strains in the x , y and z directions have two components: the strains caused by mechanical stress variations and the strain caused by the temperature changes. Only mechanical stresses cause shear deformation.

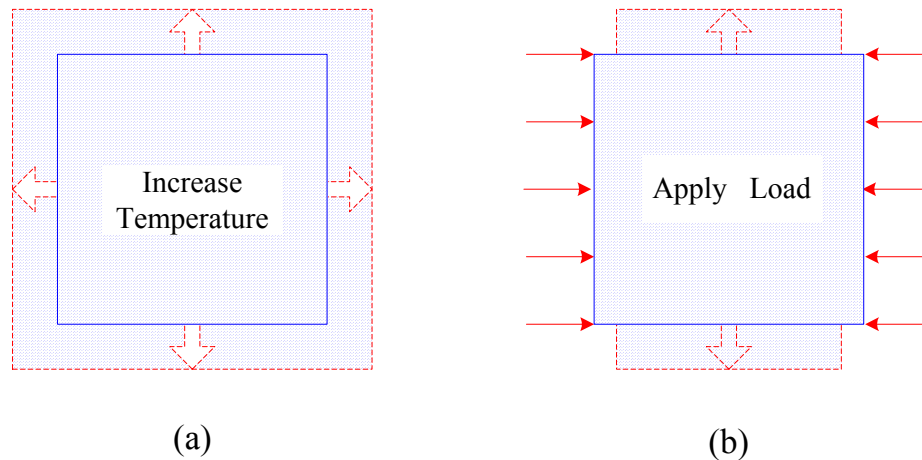


Fig. 6.1. Different influences of temperature and mechanical stress on the volume change of material

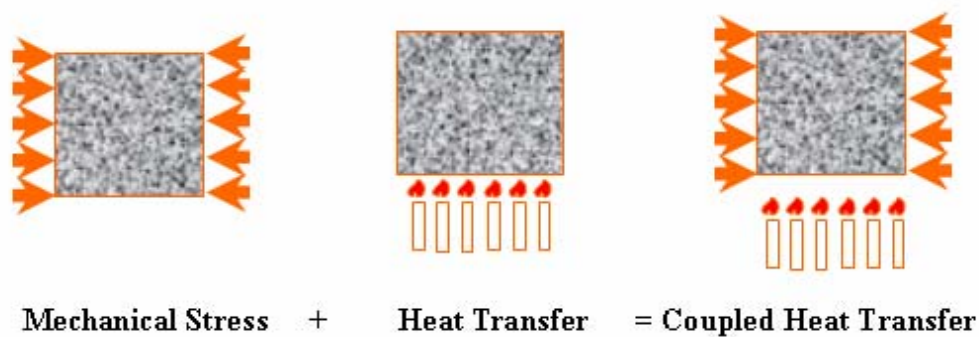


Fig. 6.2. A coupled thermal stress problem

In the coupled thermal stress problem, mechanical stress and temperature are two “independent stress state variables” because they represent different physical phenomena. Mechanical stress and temperature have different influences on the volume change behaviors of the material as shown in Eq. 6.1 and 6.3. When temperature increases, the volume of the material expands in all three directions in the same magnitude as shown in Fig. 6.1a. When an external load is applied on the material in one direction, the strains in different directions are different and are dependent on Poisson’s Ratio as shown in Fig. 6.1b. We can not use the mechanical stress replace the influence of temperature, neither can we use the temperature to replace the influence of mechanical stress. They work independently and have different constitutive laws. Therefore, when we describe the

volume change behavior of the material, two stress state variables, i.e. mechanical stress and temperature, are needed. Fig. 6.2 shows the coupled thermal stress problem.

6.2.2.4 Volume Constitutive Surface and Material Parameter Determination

For an ideal elastic material in the coupled thermal stress problem, the volume of the material depends on both the applied mechanical stress and its temperature, which can be plotted as Fig. 6.3. If the mean mechanical stress and the temperature are known, the volume of the material is known. Note that temperature is negative. The reasons for this are two-fold. Firstly, it makes the constitutive surface have a more clear perspective. Secondly, it is convenient for the further discussion because the negative temperature is corresponding to the negative pore water pressure.

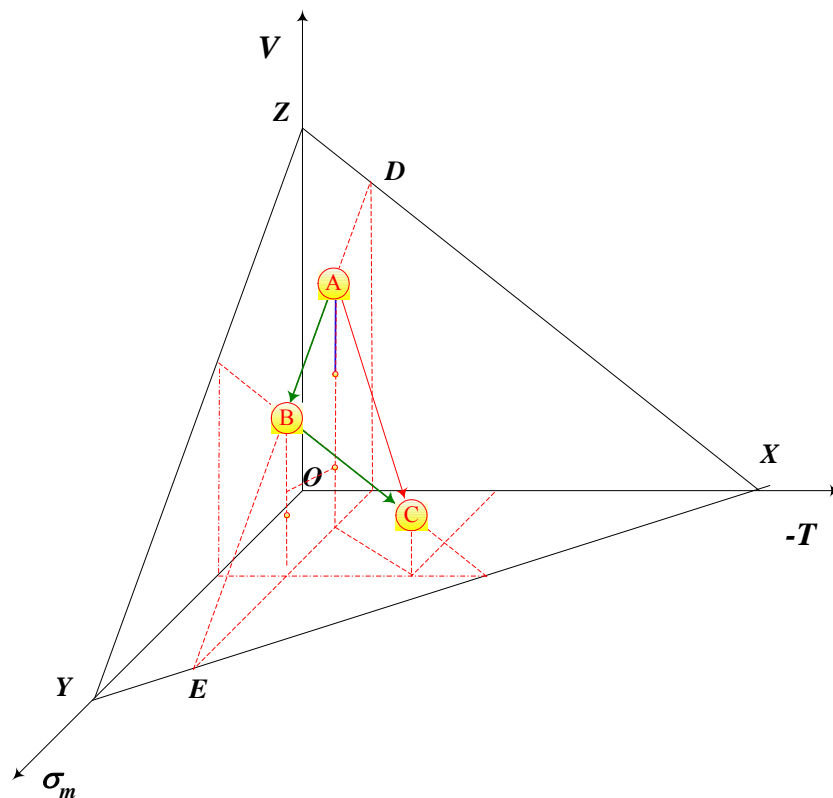


Fig. 6.3. Volume change for a material in the coupled thermal stress problem

The plane in Fig. 6.3 includes information about material properties in relation to volume change of the material. Straight line ZY reflects the relationship between the volume and the applied mean mechanical stress when temperature is zero, i.e. $T=0$. Surface XYZ can be viewed as a collection of volume versus mean mechanical stress curves at different temperature levels. The volume versus mean mechanical stress curve can be further converted into the stress-strain curve and used to determine the Young's Modulus of the material, if the Poisson's ratio of the material is known.

Similarly, straight line ZX reflects the relationship between the volume and temperature when the applied mechanical stress is zero, i.e. $\sigma_m=0$. Surface XYZ can be also visualized as a collection of volume versus temperature curves at different mean mechanical stress levels. The volume versus temperature curve includes the information about temperature-strain relationship, which can be used to determine the coefficient of expansion of the material.

These two material parameters, i.e. the Young's Modulus and the coefficient of expansion, can be determined by using the volume constitutive surface in the following way. The mathematical expression for the surface is:

$$V = f(\sigma_m, -T) \quad (6.7)$$

where V = material volume; σ_m = mean mechanical stress; $-T$ = negative temperature; and f = a function expressing the relationship between material volume and the mean mechanical stress and negative temperature.

Any small volume change of the material is equal to the total derivative of the volume function with respect to the mechanical stress and the negative temperature, that is,

$$\Delta V = \frac{\partial V}{\partial \sigma_m} \Delta \sigma_m + \frac{\partial V}{\partial (-T)} \Delta (-T) \quad (6.8)$$

and, the volumetric strain of the material is,

$$\Delta \varepsilon_v = \frac{\Delta V}{V_0} = \frac{\partial V}{V_0 \partial \sigma_m} \Delta \sigma_m + \frac{\partial V}{V_0 \partial (-T)} \Delta(-T) \quad (6.9)$$

where V_0 = the initial material volume, equal to V_A .

Taking the limit of Eq. 6.9 if the strain is infinitesimal small, gives,

$$d\varepsilon_v = \frac{\partial f}{V_0 \partial \sigma_m} d\sigma_m + \frac{\partial f}{V_0 \partial (-T)} d(-T) \quad (6.10)$$

Comparing Eq. 6.6 and 6.10, gives,

$$\begin{aligned} \frac{1}{B} &= \frac{3(1-2\mu)}{E} = \frac{1}{V_A} \frac{\partial V}{\partial \sigma_m} \\ 3\alpha &= \frac{1}{V_A} \frac{\partial V}{\partial (-T)} \end{aligned} \quad (6.11a)$$

or

$$\begin{aligned} E &= \frac{3(1-2\mu)V_0}{\frac{\partial V}{\partial \sigma_m}} \\ \alpha &= \frac{1}{3V_0} \frac{\partial V}{\partial (-T)} \end{aligned} \quad (6.11b)$$

Fig. 6.3 shows the components of the volume change of a coupled thermal stress problem. As shown in Fig. 6.3, from an arbitrary point A to an arbitrary point C, the volume change of the material is made up of two components:

(1). Volume change due to mean mechanical stress variations under isothermal condition, which is from A to B as shown in Fig.6.3;

(2). Volume change due to temperature variations under constant mean mechanical stress, which is from B to C as shown in Fig. 6.3;

Eq. 6.10 can also be derived by the following way,

$$\begin{aligned}
 d\varepsilon_v &= \frac{\Delta V}{V_A} = \frac{V_C - V_A}{V_A} = \frac{V_B - V_A}{V_A} + \frac{V_C - V_B}{V_A} \\
 &= \frac{\frac{\partial V}{\partial \sigma_m} d\sigma_m}{V_A} + \frac{\frac{\partial V}{\partial(-T)} d(-T)}{V_A} \\
 &= (d\varepsilon_v)_\sigma + (d\varepsilon_v)_T = \frac{1}{B} d\sigma_m + 3\alpha d(-T)
 \end{aligned} \tag{6.12}$$

6.2.2.5 Equivalent Effective Stress Concept

Equivalent effective stress is the corresponding “equivalent” stress to generate the same amount of volumetric strain $d\varepsilon_v$, caused by the combination of mechanical stress variation $d\sigma_m$ and the temperature variation $d(-T)$. Eq. 6.6 is the constitutive law of volumetric strain for the coupled thermal stress problem. The volume of the material changes due to both mechanical stress and temperature variations. From Eq. 6.6, the equivalent effective stress can be calculated. For any volumetric strain $d\varepsilon_v$ caused by the mechanical stress variation $d\sigma_m$ and the temperature variation $d(-T)$,

$$d\varepsilon_v = \frac{1}{B} d(\sigma_m) + 3\alpha d(-T) = \frac{1}{B} d(\sigma_m')$$
(6.13)

where σ_m' = the equivalent effective stress of the mechanical stress σ_m and temperature $-T$.

It is noted that the bulk modulus is the same as that for the total stress. Correspondingly, the equivalent effective stress is,

$$d(\sigma_m') = d(\sigma_m) + 3\alpha B d(-T) \quad (6.14a)$$

or

$$\sigma_m' = \sigma_m - (3\alpha B)T \quad (6.14b)$$

Correspondingly, the effective stresses for a three dimensional condition can be written as follows:

$$\begin{aligned} \sigma_x' &= \sigma_x - (3\alpha B)T & \tau_{xy}' &= \tau_{xy} \\ \sigma_y' &= \sigma_y - (3\alpha B)T & \tau_{xz}' &= \tau_{xz} \\ \sigma_z' &= \sigma_z - (3\alpha B)T & \tau_{yz}' &= \tau_{yz} \end{aligned} \quad (6.15)$$

It can be seen that the equivalent effective stresses are related to the material properties α and B . As a consequence, the equivalent effective stress can not be used as a stress state variable according to the definition of stress state variable.

If $3\alpha B$ is a constant, the effective stress concept can bring some kinds of convenience to the investigation of the volume change behavior of the material. As we can see in the further discussion, there is a similarity between the coupled thermal stress problem and the coupled hydro-mechanical stress problem. The matric suction (or negative pore water pressure) has the similar influence on soil deformation in the coupled hydro-mechanical stress problem as that temperature in the coupled thermal stress problem. Moreover, a saturated soil is a special case of an unsaturated soil. For saturated soils, $3\alpha B$ is equal to unity because of the effective stress principle. The effective stress principle brings great convenience to practical application and it is the basis for classical soil mechanics. However, for unsaturated soils, $3\alpha B$ is not a constant because the corresponding void ratio constitutive surface is highly nonlinear. Consequently, $3\alpha B$ is a function of both the mechanical stress and matric suction (pore

water pressure). It is not good to use the equivalent effective stress concept for unsaturated soils any more and we need use two independent stress state variables to describe the behavior of unsaturated soils, which will be discussed later.

6.2.3 Constitutive Law for Energy Variations

In the coupled thermal stress problem, temperature variations will cause volume change of the material. Because temperature is related to energy, it is necessary to find out the constitutive law for energy variations of the material. The constitutive law for energy variations of the material defines the relationship between the volumetric energy variations and the mechanical stress and temperature variations, respectively. As what we have done previously for the constitutive law for the material deformation, firstly we will discuss the influence of the mechanical stress and temperature variation separately, and then combine their influence together by applying the principle of superposition.

6.2.3.1 Constitutive Law for Energy Variations due to Temperature Variations

When energy is supplied to a material, the temperature of the material will increase. Recall that the specific heat capacity of a solid or liquid is defined as the heat required raising unit mass of substance by one degree of temperature. This can be stated by the following equation:

$$dQ_T = mC dT \quad (6.16a)$$

or

$$dE_T = \frac{dQ_T}{V} = \frac{m}{V} C_T dT = \rho C_T dT \quad (6.16b)$$

or

$$C_T = \frac{dQ_T}{m dT} \quad (6.16c)$$

where ΔQ = Heat supplied to substance; m = Mass of the substance; C_T = Specific heat capacity; ΔT = Temperature rise; and E is the volumetric heat energy. The subscription “T” stands for the deformation caused by the temperature variation.

Eq. 6.16a is the constitutive law for heat energy variation due to temperature variation under constant mechanical stress condition.

6.2.3.2 Constitutive Laws for Energy Variations due to Mechanical Stress Variations

When a load is applied to a material, the material will deform and the mechanical force is doing work. Part of the mechanical work can be converted to heat energy and cause the temperature increase in the material. A typical representation of this phenomenon is the temperature increase due to friction. To keep the material temperature constant, the energy in the material must be reduced. In some sense, energy can be “squeezed “out of the material by mechanical stress.

The constitutive law for energy variations due to mechanical stress variations can be expressed by using the semi-empirical method (Fredlund and Rahardjo 1993). It can be stated as that: the energy variations are linearly proportional to any small mechanical stress variations, which is as follows:

$$dE_\sigma = \frac{dQ_\sigma}{V} = m_1^w d\sigma \quad (6.17)$$

where Q = Heat supplied to substance; m_1^w =a material constant determining the temperature increase at the instant of load application; and E =the volumetric heat energy. The subscription “ σ ” stands for the deformation caused by the mechanical stress variation.

For some materials, if the heat energy variation caused by mechanical stress variation is not significant, $m_1^w = 0$.

6.2.3.3 Constitutive Laws for Energy Variations for the Coupled Thermal Stress Problem

For a coupled thermal stress problem, the energy in the material will change due to both the mechanical stress and the temperature variations. By applying the principle of superposition, the constitutive laws for the energy variation for a coupled thermal stress problem is as follows:

$$dE = dE_\sigma + dE_T = m_1^w d\sigma + \rho C_T d(T) \quad (6.18)$$

That is, the energy variations are composed of two components, one component is caused by the temperature variations, the other is caused by the mechanical stress variations. For a solid material that mechanical stresses cause no variation in energy variation, $m_1^w = 0$. Consequently, Eq. 6.18 changes into Eq. 6.16b.

If an increase in energy is taken as positive and the negative temperature is taken as stress state variable, the C_T will have a negative value.

6.2.3.4 Energy Constitutive Surface and Parameter Determination

Heat energy in the material in a coupled thermal stress problem is also a function of both mechanical stress and temperature. If plotted in the mean mechanical stress and negative temperature space, energy is a surface as shown in Fig. 6.4, which can be called as “energy constitutive surface” for the coupled thermal stress problem. Similar to what we have done for volume constitutive surface, the energy constitutive surface can also be used to determine the material parameters for the constitutive laws for the energy variations.

In Fig. 6.4 the straight line ZY reflects the relationship between the energy and the applied mean mechanical stress when temperature is equal to zero, i.e. $T=0$. Surface

XYZ can be viewed as a collection of energy versus mean mechanical stress curves at different temperature levels. The energy versus mean mechanical stress curve includes the information about energy-mechanical stress relationship, which in turn can be used to determine the m_1^w of the material.

Similarly, the straight line ZX reflects the relationship between the energy and temperature when the applied mechanical stress is equal to zero, i.e. $\sigma_m=0$. Surface XYZ can be also visualized as a collection of energy versus temperature curves at different mechanical stress levels. The energy versus temperature curve includes the information about temperature-energy relationship, which in turn can be used to determine the specific heat capacity of the material.

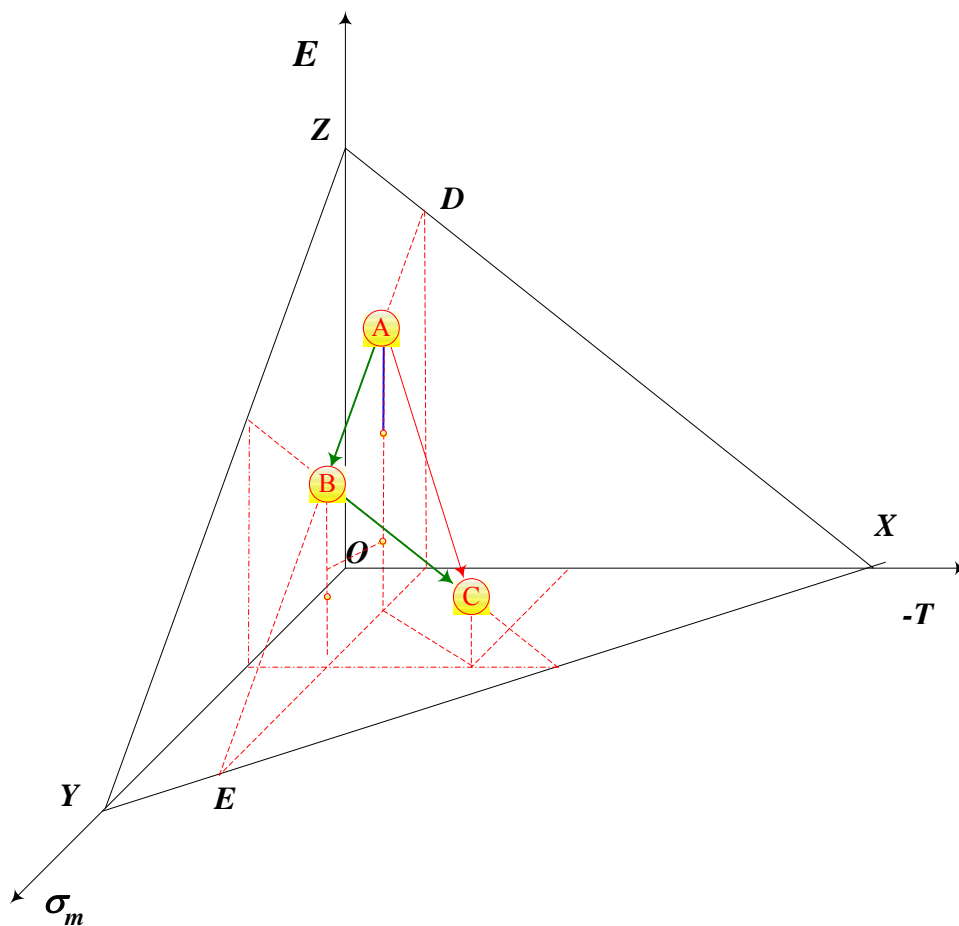


Fig. 6.4. Energy constitutive surface for a coupled thermal stress problem

The mathematical expression for the energy surface is:

$$Q = g(\sigma_m, -T) \quad (6.19)$$

where Q = material volume; σ_m = mean mechanical stress; $-T$ = negative temperature; and g = a function expressing the relationship between the energy in the material and the mean mechanical stress and negative temperature.

A small energy change of the material is equal to the total derivative of Eq. 6.19, that is

$$\Delta Q = \frac{\partial Q}{\partial \sigma_m} \Delta \sigma_m + \frac{\partial Q}{\partial (-T)} \Delta(-T) \quad (6.20)$$

The volumetric energy variation of the material is,

$$\Delta E = \frac{\Delta Q}{V_0} = \frac{\partial Q}{V_0 \partial \sigma_m} \Delta \sigma_m + \frac{\partial Q}{V_0 \partial (-T)} \Delta(-T) \quad (6.21)$$

where V_0 = the initial material volume.

Taking the limit of Eq. 6.21 if the energy variation is infinitesimal small, gives,

$$dE = \frac{\partial f}{V_0 \partial \sigma_m} d\sigma_m + \frac{\partial f}{V_0 \partial (-T)} d(-T) \quad (6.22)$$

Comparing Eq. 6.18 and 6.22, gives,

$$m_1^w = \frac{1}{V_0} \frac{\partial Q}{\partial \sigma_m}$$

$$\rho C_T = \frac{1}{V_0} \frac{\partial Q}{\partial (-T)} \quad (6.23)$$

For some materials, mechanical stress variations will not lead to energy variations. In this case, surface XYZ in Fig. 6.4 will become a surface parallel to the mechanical stress axis as shown in Fig. 6.5. Correspondingly, the mathematical expression for the surface becomes,

$$Q = g(-T)$$

and

$$m_1^w = \frac{1}{V_0} \frac{\partial Q}{\partial \sigma_m} d\sigma_m = 0$$

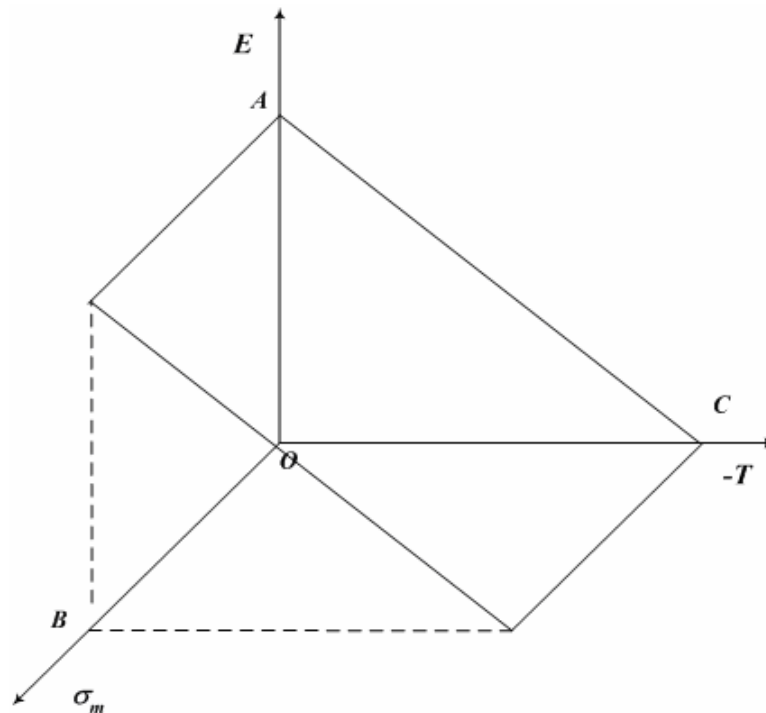


Fig. 6.5. Energy constitutive surface when the mechanical stress has no influence in energy variation

6.2.3.5 Load Application under Adiabatic Conditions

If a load is applied instantly to a material, there is no heat exchange between the material and its environment at the instant of load application, that is, the material is under adiabatic condition. The heat energy caused by the mechanical stress application will result in temperature increases. That is,

$$dE = dE_\sigma + dE_T = m_1^w d\sigma + \rho C_T d(-T) = 0$$

therefore,

$$d(-T) = -\frac{m_1^w d\sigma}{\rho C_T} \quad (6.24)$$

Eq. 6.24 shows the temperature increase is linearly related to the applied load. This phenomenon is very similar to the pore water pressure increase at the instant of load application for soils. It is the basis of using the coupled thermal stress analysis to simulate the coupled consolidation of saturated-unsaturated soils.

6.2.4 Derivation of the Differential Equations for the Coupled Thermal Stress Problem

The stress and strain tensor need satisfy the requirement of equilibrium and continuity equations. By applying the volume change constitutive law to the equilibrium equations and satisfying the continuity requirements, the differential equations for the coupled thermal stress problem can be derived.

6.2.4.1 Equilibrium Equations

Equations of equilibrium for the mechanical stresses are

$$\frac{\partial \sigma_x}{\partial x} + \frac{\partial \tau_{yx}}{\partial y} + \frac{\partial \tau_{zx}}{\partial z} + X = 0$$

$$\frac{\partial \tau_{xy}}{\partial x} + \frac{\partial \sigma_y}{\partial y} + \frac{\partial \tau_{zy}}{\partial z} + Y = 0 \quad (6.25a)$$

$$\frac{\partial \tau_{xz}}{\partial x} + \frac{\partial \tau_{yz}}{\partial y} + \frac{\partial \sigma_z}{\partial z} + Z = 0$$

or

$$\sigma_{ij,j} + b_j = 0 \quad (6.25b)$$

Where σ_{ij} = components of the net total stress tensor, and b_i = components of the body force vector.

6.2.4.2 Strain-Displacement Equations

Strain-displacement equations (Cauchy's Equation):

$$\begin{aligned} \varepsilon_x &= \frac{\partial u}{\partial x}, & \gamma_{yz} &= \frac{\partial w}{\partial y} + \frac{\partial v}{\partial z} \\ \varepsilon_y &= \frac{\partial v}{\partial y}, & \gamma_{xz} &= \frac{\partial w}{\partial x} + \frac{\partial u}{\partial z} \\ \varepsilon_z &= \frac{\partial w}{\partial z}, & \gamma_{xy} &= \frac{\partial v}{\partial x} + \frac{\partial u}{\partial y} \end{aligned} \quad (6.26a)$$

or

$$\varepsilon_{ij} = \frac{1}{2}(u_{i,j} + u_{j,i}) \quad (6.26b)$$

where ε_{ij} = components of the strain tensor; and u_i = components of displacement in i -direction.

6.2.4.3 Differential Equations for the Coupled Thermal Stress Problem

The derivation of the differential equation for coupled thermal stress problem is as follows. From Eq. 6.5 and 6.26, the stress can be expressed in terms of displacement as follows:

$$\begin{aligned}
 \sigma_x &= \lambda \varepsilon_v + 2G \varepsilon_x - (3\lambda + 2G)\alpha T, \quad \tau_{yz} = G \left(\frac{\partial w}{\partial y} + \frac{\partial v}{\partial z} \right) \\
 \sigma_y &= \lambda \varepsilon_v + 2G \varepsilon_y - (3\lambda + 2G)\alpha T, \quad \tau_{xz} = G \left(\frac{\partial u}{\partial z} + \frac{\partial w}{\partial x} \right) \\
 \sigma_z &= \lambda \varepsilon_v + 2G \varepsilon_z - (3\lambda + 2G)\alpha T, \quad \tau_{xy} = G \left(\frac{\partial v}{\partial x} + \frac{\partial u}{\partial y} \right)
 \end{aligned} \tag{6.27}$$

Substituting Eq. 6.27 into Eq. 6.25, gives

$$\begin{aligned}
 (\lambda + G) \frac{\partial \varepsilon_v}{\partial x} + G \nabla^2 u - \frac{E}{(1-2\nu)} \alpha \frac{\partial T}{\partial x} + X &= 0 \\
 (\lambda + G) \frac{\partial \varepsilon_v}{\partial y} + G \nabla^2 v - \frac{E}{(1-2\nu)} \alpha \frac{\partial T}{\partial y} + Y &= 0 \\
 (\lambda + G) \frac{\partial \varepsilon_v}{\partial z} + G \nabla^2 w - \frac{E}{(1-2\nu)} \alpha \frac{\partial T}{\partial z} + Z &= 0
 \end{aligned} \tag{6.28}$$

Eq. 6.28 is the equilibrium equations for the coupled thermal stress problem.

6.2.4.4 Heat Continuity Equation

The material also need satisfy the continuity equation for heat flow. Fourier's law is used to describe the heat flow in a continuous media. This law states that the rate of heat flow by conduction in a given direction is proportional to the area normal to the direction of heat flow and to the gradient of the temperature in that direction. Fourier's law is written as follows:

$$Q_i = -k_i A \frac{dT}{dx_i} \quad (6.29)$$

or

$$q_i = -k_i \frac{dT}{dx_i} \quad (6.30)$$

where k =heat conductivity of the material; and q = the heat flow in unit time.

The heat continuity equation is written as follows:

Net rate of heat gain by conduction +rate of energy generation =rate of increase of internal energy, or

$$\frac{\partial}{\partial x} \left(k \frac{\partial T}{\partial x} \right) + \frac{\partial}{\partial y} \left(k \frac{\partial T}{\partial y} \right) + \frac{\partial}{\partial z} \left(k \frac{\partial T}{\partial z} \right) = m_1^w \frac{\partial \sigma}{\partial t} + \rho C \frac{\partial T}{\partial t} - S \quad (6.31a)$$

For material that heat energy variation due to mechanical stress variations are negligible, i.e. $m_1^w = 0$, Eq. 6.31 becomes

$$\frac{\partial}{\partial x} \left(k \frac{\partial T}{\partial x} \right) + \frac{\partial}{\partial y} \left(k \frac{\partial T}{\partial y} \right) + \frac{\partial}{\partial z} \left(k \frac{\partial T}{\partial z} \right) = \rho C \frac{\partial T}{\partial t} - S \quad (6.31b)$$

Eq. 6.28 and Eq. 6.31 (or 6.31a) are the differential equations for a coupled thermal stress problem. When Eq. 6.31a is used, to apply a load to the material does not cause any temperature variations in the material. Gay (1994) used the Eq. 6.28 and Eq. 6.31a to simulate the volume change of unsaturated expansive soils. Consequently, the increase in pore water pressure at the instant of load application cannot be simulated.

6.3 Constitutive Laws for Volume Changes of Unsaturated Soils

6.3.1 Two Independent Stress State Variables for Unsaturated Soils

Great efforts have been put in the past to isolate the relevant stress variables concerning (saturated-unsaturated) soil behaviors. Adopting the matric suction $u_a - u_w$ and the excess of total stress over air pressure $\sigma - u_a$ as the relevant stress variables have been extensively accepted, which is called “two stress state variables” concept. In this dissertation, u_a is the atmospheric pressure. The air phase is assumed to be continuous and the excess pore air pressure will dissipate instantly (Rahardjo and Fredlund 1995). When the air is occluded, the air is considered to be part of the soil structure. Under these assumptions, the air pressure is constant and always zero. The occluded air will cause the constitutive surface of soil to change, while the proposed method for the consolidation theory for saturated-unsaturated soils is not affected. Consequently, $\sigma - u_a$ is the same as σ and $u_a - u_w$ is the same as $-u_w$. However, to keep consistent with the convention for unsaturated soil mechanics, $u_a - u_w$ and $\sigma - u_a$ are still used as stress state variables.

For saturated soils, there is no air in the soil. The air pressure is the atmospheric pressure and always zero. Therefore, by using the above assumptions, the two stress state variables can be used for both saturated and unsaturated soils. For unsaturated soils, matric suction is actually “negative pore water pressure”. In the following discussion, the pore water pressure and the matric suction can be considered to be one concept, that is, the pore water pressure can be either positive or negative. When it is negative, it represents the matric suction.

6.3.2 The Coupled Hydro-Mechanical Stress Problem or the Consolidation Theory for Saturated-Unsaturated Soils

As we discussed previously, soil will deform due to two reasons, one is mechanical stress (total stress) variations, the other is matric suction (or pore water pressure) variations. Their influences on soil deformations are different. A load application in one

direction will cause a soil to deform in all the three directions, and their magnitudes are different, depending on the Poisson's ratio. Matric suction (pore water pressure) variations will cause the soil to change volume in three directions with the same magnitudes. The final effect will depend on the combination of these two effects. For saturated soils, the final effect will depend on the effective stress. For unsaturated soils, the final effect will depend on the equivalent effective stress defined by Bishop's Equation (Bishop 1959).

When there is a load application, the pore water pressure in the soil will increase. If the soil is allowed to drain, the pore water pressure will dissipate gradually and the volume of the soil will also decrease gradually. It is a time-dependent process, which is also called the consolidation.

When there are pore water pressure variations, the soil tends to change its volume in three dimensions in the same magnitudes because the pore water pressure is neutral hydrostatic. If the volume change is restricted, mechanical stress will be generated to adjust the deformation of the soil. In other words, the mechanical stress variations are able to cause pore water pressure variations in the soil. In the mean time, the pore water pressure variations are also able to cause the mechanical stress variations in the soil. To describe the volume change behaviors of soils, both the water flow and the mechanical stress variations in the soils should be considered simultaneously. Therefore, the coupled consolidation problem for soils is also called the coupled hydro-mechanical stress problem.

Fig. 6.6 shows the different influences of the mechanical stress and matric suction variations in the soil deformations. To make the discussion simple, we will keep one stress state variable constant and change the other to see the influences.

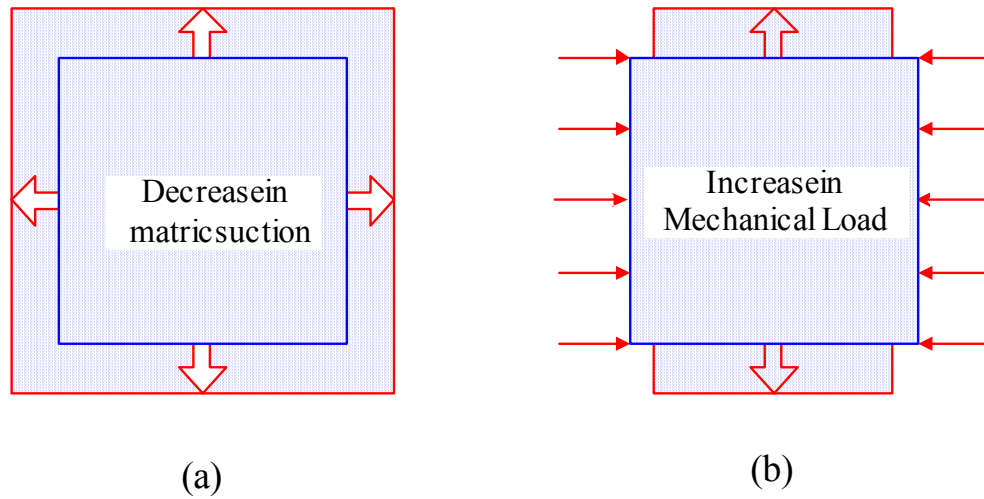


Fig. 6.6. Mechanical stress and matric suction's influence in soil deformation

6.3.2.1 Volume Change of a Soil due to Mechanical Stress Variations

The volume change of an unsaturated soil is very similar to the volume change of an elastic material in the coupled thermal stress problem as we discussed previously. If the unsaturated soil is assumed to be homogenous and elastic, and the matric suction in the soil keeps unchanged, the volume change of the soil will be:

$$\begin{aligned}
 d(\varepsilon_x)_\sigma &= \frac{d(\sigma_x - u_a)}{E} - \frac{\mu}{E} \left[d(\sigma_y - u_a) + d(\sigma_z - u_a) \right], & d\gamma_{yz} &= \frac{d\tau_{yz}}{G} \\
 d(\varepsilon_y)_\sigma &= \frac{d(\sigma_y - u_a)}{E} - \frac{\mu}{E} \left[d(\sigma_x - u_a) + d(\sigma_z - u_a) \right], & d\gamma_{zx} &= \frac{d\tau_{zx}}{G} \\
 d(\varepsilon_z)_\sigma &= \frac{d(\sigma_z - u_a)}{E} - \frac{\mu}{E} \left[d(\sigma_y - u_a) + d(\sigma_x - u_a) \right], & d\gamma_{xy} &= \frac{d\tau_{xy}}{G}
 \end{aligned} \tag{6.32}$$

where E = Young's modulus of the soil; μ = Poisson's ratio of the soil; G = shear modulus of the soil; $\sigma_x - u_a, \sigma_y - u_a, \sigma_z - u_a$ = the applied mechanical stresses in the x, y , and z direction, respectively; and $\varepsilon_x, \varepsilon_y, \varepsilon_z$ = the corresponding strain in the x, y , and z direction, respectively. The subscription " σ " stands for the deformation caused by the mechanical stress variation.

Eq. 6.32 is the constitutive law for the soil deformation due to mechanical stress variations only, which is actually the Hooker's law. It states that stress variations in one direction will cause deformations in other two directions as shown in Fig. 6.6b. The magnitudes depend on the Poisson's ratio of the soil.

The situations described by Eq. 6.32 represent the condition when the consolidation of the soil is accomplished, i.e. the final pore water pressure is the same as the initial pore water pressure (before the load application).

The volumetric deformation due to mechanical stress variations is:

$$\begin{aligned}
 (d\varepsilon_v)_\sigma &= (d\varepsilon_x)_\sigma + (d\varepsilon_y)_\sigma + (d\varepsilon_z)_\sigma \\
 &= \frac{3(1-2\mu)}{E} \left[\frac{d(\sigma_x - u_a) + d(\sigma_y - u_a) + d(\sigma_z - u_a)}{3} \right] \\
 &= \frac{1}{B} d(\sigma_m - u_a)
 \end{aligned} \tag{6.33}$$

where B = bulk modulus of the soil; and $\sigma_m = \frac{(\sigma_x + \sigma_y + \sigma_z)}{3} - u_a$, the mean mechanical stress.

6.3.2.2 Volume Change of an Unsaturated Soil due to Matric Suction Variations

The matric suction variations will also cause the volume change of unsaturated soils. If there is no mechanical stress variation, the constitutive law for the volume change of an unsaturated soil due to matric suction variation is:

$$\begin{aligned}
 d(\varepsilon_x)_{(u_a - u_w)} &= d(\varepsilon_y)_{(u_a - u_w)} = d(\varepsilon_z)_{(u_a - u_w)} \\
 &= \alpha d(u_a - u_w)_x = \alpha d(u_a - u_w)_y = \alpha d(u_a - u_w)_z = \alpha d(u_a - u_w)
 \end{aligned} \tag{6.34}$$

where α = coefficient of expansion of the soil due to matric suction variations; and $(\varepsilon_x)_{(u_a - u_w)}$, $(\varepsilon_y)_{(u_a - u_w)}$, $(\varepsilon_z)_{(u_a - u_w)}$ = the corresponding strains in the x , y , and z direction,

respectively. The subscription “ $(u_a - u_w)$ ” stands for the deformation caused by the matric suction variation.

It is noted the matric suction (or negative pore water pressure) is a neutral hydrostatic and is the same in all directions. No shear deformation is caused by matric suction variations.

Eq. 6.34 is the constitutive law for the volume change of soils due to matric suction variations. It illustrates that the matric suction variation will cause the soil to deform in three directions with the same magnitudes. The volumetric deformation due to matric suction variations is:

$$\begin{aligned} d(\varepsilon_v)_{(u_a - u_w)} &= d(\varepsilon_x)_{(u_a - u_w)} + d(\varepsilon_y)_{(u_a - u_w)} + d(\varepsilon_z)_{(u_a - u_w)} \\ &= 3\alpha d(u_a - u_w) \end{aligned} \quad (6.35)$$

Eq. 6.35 states that the volumetric strain caused by the matric suction variations is triple of the strains in any one direction.

6.3.2.3 Constitutive Laws for the Volume Change of the Coupled Hydro-Mechanical Stress (Consolidation) Problem

In the similar way, when there are both load applications and matric suction variations, the volume of an unsaturated soil will change due to both factors. The final volume of the soil will depend on the combination effect of the two processes. For any small increment of strains, stresses and matric suction (pore water pressure) variations, the principle of superposition can be applied. Eq. 6.6 shows the constitutive laws for coupled thermal stress problem.

$$\begin{aligned}
d\varepsilon_x &= \frac{d(\sigma_x - u_a)}{E} - \frac{\mu}{E} [d(\sigma_y - u_a) + d(\sigma_z - u_a)] + \alpha d(u_a - u_w), & d\gamma_{yz} &= \frac{d\tau_{yz}}{G} \\
d\varepsilon_y &= \frac{d(\sigma_y - u_a)}{E} - \frac{\mu}{E} [d(\sigma_x - u_a) + d(\sigma_z - u_a)] + \alpha d(u_a - u_w), & d\gamma_{zx} &= \frac{d\tau_{zx}}{G} \\
d\varepsilon_z &= \frac{d(\sigma_z - u_a)}{E} - \frac{\mu}{E} [d(\sigma_y - u_a) + d(\sigma_x - u_a)] + \alpha d(u_a - u_w), & d\gamma_{xy} &= \frac{d\tau_{xy}}{G}
\end{aligned} \tag{6.36}$$

where $d\varepsilon_x$, $d\varepsilon_y$, $d\varepsilon_z$ = the corresponding strain in the x , y , and z direction, respectively.

As can be seen in Eq. 6.36, all the three normal strains in the x , y and z direction have two components: the strains caused by mechanical stress variations and the strains caused by matric suction variations. Only mechanical stress variations result in shear deformations.

In the coupled hydro-mechanical stress problem, mechanical stress and matric suction are two independent stress state variables. They have completely different physical meanings. The constitutive relations for these two stress state variables are totally different and their influences on the volume change of the soil are also different as shown in Eq. 6.32 and 6.34. When the matric suction decreases, the soil swells in all three directions in the same magnitudes as shown in Fig. 6.6a. When there is a load application in one direction, the strains in different directions are different and dependent on Poisson's ratio as shown in Fig. 6.6b. Actually, their relationship is exactly the same as the relationship between the temperature and the mechanical stress in the coupled thermal stress problem. We can not use the mechanical stress to replace matric suction, neither can we use the matric suction to replace the mechanical stress. They work independently with different constitutive laws. Therefore, when we describe the volume change behavior of unsaturated soils, both mechanical stress and the matric suction are needed.

The volumetric strain for the coupled thermal stress problem can be obtained as follows:

$$\begin{aligned}
d\varepsilon_v &= d\varepsilon_x + d\varepsilon_y + d\varepsilon_z = \frac{3(1-2\mu)}{E} d(\sigma_m - u_a) + 3\alpha d(u_a - u_w) \\
&= \frac{1}{B} d(\sigma_m - u_a) + 3\alpha d(u_a - u_w)
\end{aligned} \tag{6.37}$$

In conclusion, two stress state variables are needed for describing the volume change behavior of unsaturated soils: mechanical stress and matric suction. The coupled thermal stress problem is very similar to the coupled hydro-mechanical stress problem. For saturated soils, the effective stress principle states that the pore water pressure will have the exactly same influence as the mechanical stress on the volume change of soils. Since that the degree of saturation for saturated soils is $S=1$, then the water content constitutive surface is the same as void ratio constitutive surface as discussed in Chapter V.

6.3.2.4 Void Ratio Constitutive Surface and Soil Parameter Determination

The soil volume in a coupled hydro-mechanical stress problem is a function of both mechanical stress and matric suction (pore water pressure). Fredlund and Morgenstern (1977) performed null tests in which the individual components of the stress state variables i.e. σ , $-u_w$ and u_a , were varied while the stress state variables, i.e. $(\sigma - u_a)$ and $(u_a - u_w)$ were maintained constant. Experimental data indicated that essentially no overall volume change or water content change during the null tests. The relationship between the soil volume and the mechanical stress and matric suction is a surface in the mechanical stress and matric suction space. The void ratio is used to represent the soil volume because the specific volume of the soil is $V=1+e$. This surface is called void ratio constitutive surface as shown in Fig. 6.7.

Similarly, straight line ZX reflects the relationship between the void ratio and matric suction $u_a - u_w$ when the applied mean mechanical stress is equal to zero $(\sigma - u_a) = 0$. Surface XYZ can be also viewed as a collection of void ratio versus matric suction $u_a - u_w$ curves at different mean mechanical stress levels. The void ratio versus matric suction $u_a - u_w$ curve includes the information about pore water pressure-strain relationship, which can be used to determine the coefficient of expansion due to matric suction variation of the soil.

These two parameters, Young's modulus and coefficient of expansion due to matric suction variation can be determined by using the void ratio constitutive surface in the following way. The mathematical expression for the void ratio constitutive surface is:

$$e = f(\sigma_m - u_a, u_a - u_w) \quad (6.38)$$

where e = void ratio; $\sigma_m - u_a$ = mean mechanical stress; $u_a - u_w$ = negative temperature; and f = arbitrary function.

The volume change of the material is,

$$\Delta e = \frac{\partial e}{\partial (\sigma_m - u_a)} \Delta (\sigma_m - u_a) + \frac{\partial e}{\partial (u_a - u_w)} \Delta (u_a - u_w) \quad (6.39)$$

The volumetric strain of the material is,

$$\begin{aligned} \Delta \varepsilon_v &= \frac{\Delta e}{1 + e_0} \\ &= \frac{\partial e}{(1 + e_0) \partial (\sigma_m - u_a)} \Delta (\sigma_m - u_a) + \frac{\partial e}{(1 + e_0) \partial (u_a - u_w)} \Delta (u_a - u_w) \end{aligned} \quad (6.40)$$

where e_0 = the initial void ratio of the soil.

Taking the limit of Eq. 6.40 if the strain is infinitesimal small, gives,

$$d\varepsilon_v = \frac{\partial e}{(1+e_0)\partial(\sigma_m - u_a)} d(\sigma_m - u_a) + \frac{\partial e}{(1+e_0)\partial(u_a - u_w)} d(u_a - u_w) \quad (6.41)$$

Comparing Eq. 6.37 and 6.41, gives,

$$\begin{aligned} \frac{1}{B} &= \frac{3(1-2\mu)}{E} = \frac{1}{(1+e_0)} \frac{\partial e}{\partial(\sigma_m - u_a)} \\ 3\alpha &= \frac{1}{(1+e_0)} \frac{\partial e}{\partial(u_a - u_w)} \end{aligned} \quad (6.42a)$$

or

$$\begin{aligned} E &= \frac{3(1-2\mu)(1+e_0)}{\frac{\partial e}{\partial(\sigma_m - u_a)}} \\ \alpha &= \frac{1}{3(1+e_0)} \frac{\partial e}{\partial(u_a - u_w)} \end{aligned} \quad (6.42b)$$

Eq. 6.42 and 6.42a express the relationship between the void ratio constitutive surface and the volume change parameters of a soil.

6.3.2.5 Equivalent Effective Stress Concept

For soil deformation, effective stress is the corresponding equivalent stress to generate the same volumetric strain $d\varepsilon_v$ caused by the mechanical stress variation $d\sigma_m$ together with the matric suction (or pore water pressure) variation $d(u_a - u_w)$. Eq. 6.37 is the constitutive law of volumetric strain for a coupled hydro-mechanical stress problem. From Eq. 6.37, the equivalent effective stress of soil can be calculated. The precise definition of the effective stress was given by Bishop and Blight (1963): “Effective stress is that function of total stress and pore water pressure which control the

mechanical effects of change in stress, and change in shear strength". Actually the effective stress for volume change is different from the effective stress for shear strength in unsaturated soils. For any volumetric strain $d\varepsilon_v$ caused by the mechanical stress variation $d\sigma_m$ and the matric suction (or pore water pressure) variation $d(u_a - u_w)$,

$$d\varepsilon_v = \frac{1}{B}d(\sigma_m - u_a) + 3\alpha d(u_a - u_w) = \frac{1}{B}d(\sigma_m' - u_a) \quad (6.43)$$

Correspondingly, the equivalent effective stress is,

$$d(\sigma_m' - u_a) = d(\sigma_m - u_a) + 3\alpha B d(u_a - u_w) \quad (6.44)$$

or

$$\sigma_m' - u_a = (\sigma_m - u_a) + (3\alpha B)(u_a - u_w) \quad (6.44a)$$

where $\sigma_m' - u_a$ = the equivalent effective stress for the combination effect of the mechanical stress and matric suction.

It is noted that the bulk modulus is the same as that for the total stress and effective stress. Correspondingly, the effective stresses for a three dimensional condition can be written as follows:

$$\begin{aligned} \sigma_x' - u_a &= (\sigma_x - u_a) + (3\alpha B)(u_a - u_w) & \tau_{xy}' &= \tau_{xy} \\ \sigma_y' - u_a &= (\sigma_y - u_a) + (3\alpha B)(u_a - u_w) & \tau_{xz}' &= \tau_{xz} \\ \sigma_z' - u_a &= (\sigma_z - u_a) + (3\alpha B)(u_a - u_w) & \tau_{yz}' &= \tau_{yz} \end{aligned} \quad (6.45)$$

Eq. 6.43a and 6.44 are actually Bishop's equation, that is,

$$\sigma_m' - u_a = (\sigma_m - u_a) + \chi(u_a - u_w) \quad (6.46)$$

Comparing Eq. 6.44a and 6.46, gives,

$$\chi = 3\alpha B \quad (6.47)$$

As we can see in the further discussion, a saturated soil is a special case of an unsaturated soil. For saturated soils, $3\alpha B$ is equal to unity because of the effective stress principle.

For unsaturated soils, the χ is not a constant. Because of the highly nonlinear properties of unsaturated soils, both α and B are functions of both mechanical stress and matric suction, depending on material properties.

Morgenstern (1979) stated that: “the effective stress is a stress variable and hence related to equilibrium considerations alone while Eq. 6.46 contains a parameter χ , that bears on constitutive behavior, this parameter is found by assuming that the behavior of a soil can be expressed uniquely by a single effective stress variable and by matching unsaturated soils behavior with saturated soil behavior in order to calculate χ . Normally, we link equilibrium consideration to deformations through constitutive behavior and do not introduce constitutive behavior directly into the stress variable”. In other words, it is not proper to include material properties in the stress state variable. For unsaturated soils, the χ parameter includes the material properties and is a function of both mechanical stress and matric suction. This is the reason why Bishop’s equation has limited success in practice. For saturated soils, the effective stress principle states that the effective stress is equal to the total stress minus pore water pressure for all the saturated soils. As a consequence, $3\alpha B$ is equal to unity and the effective stress can be used as a stress state variable. No material property is included in the effective stress any more.

In summary, it is not proper to include material properties in stress variable. However, it can bring some convenience under special conditions, for example, for

saturated soils when χ is a constant for all soils. For unsaturated soils, Bishop's equation is not applicable because of the highly nonlinear behaviors in volume change. Namely, both the bulk modulus and coefficient of expansion are functions of both mechanical stress and matric suction as expressed in Eq. 6.42.

6.3.3 Constitutive Law for the Volume Change of the Water Phase

The constitutive law for soil structure alone is not sufficient to completely describe the volume change behavior of an unsaturated soil. Rather, the constitutive relation for the volume change of the water phase must be formulated. The constitutive law for the soil structure defines the relationship between volumetric strains and the mechanical stress and matric suction variations. Consequently, the constitutive law for water phase defines the relationship between the volumetric water content variation and the mechanical stress and matric suction variation. Firstly we will discuss the influence of the matric suction and mechanical stress separately, and then combine their influences together by applying the principle of superposition.

6.3.3.1 Constitutive Law for Water Content Variations due to Matric Suction Variations

Under constant mechanical stress conditions, adding water to soil will cause matric suction to decrease as discussed in Chapter II. The relationship between the water content and the matric suction of a soil is called soil water characteristic curve, which is also known as water retention curve. It plays the same role as the energy versus temperature curve and its slope has the same role as the specific heat capacity in the coupled thermal stress problem, which can be defined as the specific water capacity. The constitutive law for water content variation due to matric suction variation can be expressed by using the semi-empirical method (Fredlund and Rahardjo 1993). It can be stated as that: the water content variation is linearly proportional to any small matric suction variation, which is as follows:

$$d\theta_{(u_a - u_w)} = m_2^w d(u_a - u_w) \quad (6.48a)$$

where θ = the volumetric water content, and m_2^w = material parameter for a given soil status, i.e. given mean mechanical stress ($\sigma_m - u_a$) and matric suction value ($u_a - u_w$). The subscription “ $(u_a - u_w)$ ” stands for that the water content variation is caused by the matric suction variation.

m_2^w illustrates the ability of matric suction to change soil water content. When water is added to the soil, the matric suction of the soil will change. The matric suction variation will depend on the reverse of the m_2^w value. For saturated soils, when there is water drainage in the consolidation test, the pore water pressure will decrease. Eq. 6.47 indicates that, when the volumetric water content of the soil changes the amount of m_2^w , the pore water pressure will decrease 1 kPa. By using Eq. 6.47, given a water content variation, the matric suction (pore water pressure) variation of the soil can be calculated. Similarly, given the matric suction (pore water pressure) variation, the water content variation of the soil can be calculated.

6.3.3.2 Constitutive Law for Water Content Variations due to Mechanical Stress Variations

When a load is applied to a soil, the pore water pressure in the soil will increase, or, the matric suction will decrease due to compression. To keep the matric suction constant, soil water content must be reduced. In a sense, mechanical stress can squeeze water out of the soil. It is true for both saturated and unsaturated soils.

Similarly, by using the semi-empirical method (Fredlund and Morgenstern 1976), the constitutive law for volumetric water content variations due to mechanical stress variations under constant matric suction condition can be stated as that: the water content variation is linearly proportional to any small mechanical stress variation, that is,

$$d\theta_{\sigma} = m_1^w d(\sigma_m - u_a) \quad (6.48b)$$

where θ =volumetric water content, and m_1^w =material parameter for a given soil status, i.e. given mean mechanical stress ($\sigma_m - u_a$) and matric suction value ($u_a - u_w$). The subscription “ σ ” stands for that the water content variation is caused by the mechanical stress variation.

m_1^w illustrates the ability of mechanical stress to squeeze water out of the soil. In other words, it reflects that the volumetric water content variation when there is a unit load application under a constant matric suction value.

When a unit load is applied to the soil, the soil pore water pressure will increase. If the soil is allowed to drain and the environment keeps unchanged, water will flow out of the soil due to compression. m_1^w expresses the quantity of water squeezed out of the soil at the accomplishment of consolidation process.

6.3.3.3 Constitutive Law for Water Content Variation for the Coupled Hydro-Mechanical Stress Problem

For the coupled hydro-mechanical stress (consolidation) problem for soils, water content will change due to both mechanical stress and pore water pressure (matric suction) variations. By applying the principle of superposition, the constitutive laws for volume change of the water phase is:

$$d\theta = \frac{dV_w}{V_0} = d\theta_{\sigma} + d\theta_{(u_a - u_w)} = m_1^w d(\sigma_m - u_a) + m_2^w d(u_a - u_w) \quad (6.49)$$

Eq. 6.49 indicates that the volumetric water content change of the soil have two components: the volumetric water content variations due to mechanical stress variations and that due to the matric suction variations. In other words, both mechanical stress and

In Fig. 6.8 straight line ZY reflects the relationship between the water content and the applied mean mechanical stress when the matric suction is zero, i.e. $(u_a - u_w) = 0$. Surface XYZ in Fig. 6.8 can be viewed as a collection of the water content versus the mean mechanical stress curves at different matric suction levels. The water content versus mean mechanical stress curve includes the information about water content-mechanical stress relationship, which can be used to determine the m_1^w of the material. As discussed previously, m_1^w represents the ability of the mechanical stress to squeeze the water out of the soil.

Similarly, straight line ZX reflects the relationship between the water content and the matric suction when the applied mean mechanical stress is equal to zero, i.e. $(\sigma_m - u_a) = 0$. It is also the soil water characteristic curve of the soil under the zero mean mechanical stress condition. Surface XYZ can be also viewed as a collection of soil water characteristic curves at different mean mechanical stress levels, which in turn can be used to determine the m_2^w of the material. As discussed previously, m_2^w represents the ability of the matric suction to force the water out of the soil.

The mathematical expression for the surface is:

$$wG_s = g(\sigma_m - u_a, u_a - u_w) \quad (6.50)$$

where w = water content; G_s = specific gravity of the soil; $\sigma_m - u_a$ = mean mechanical stress; $u_a - u_w$ = negative temperature; and g = arbitrary function.

The water content variation of the soil is,

$$\Delta wG_s = \frac{\partial wG_s}{\partial(\sigma_m - u_a)} \Delta(\sigma_m - u_a) + \frac{\partial wG_s}{\partial(u_a - u_w)} \Delta(u_a - u_w) \quad (6.51)$$

The volumetric water content variation is,

$$\Delta\theta = \frac{\Delta w G_s}{V_0} = \frac{\partial w G_s}{(1+e_0)\partial(\sigma_m - u_a)} \Delta(\sigma_m - u_a) + \frac{\partial w G_s}{(1+e_0)\partial(u_a - u_w)} \Delta(u_a - u_w) \quad (6.52)$$

where V_0 is the initial material volume.

Taking the limit of Eq. 6.52 if the energy variation is infinitesimal small, gives,

$$d\theta = \frac{\partial w G_s}{(1+e_0)\partial(\sigma_m - u_a)} d(\sigma_m - u_a) + \frac{\partial w G_s}{(1+e_0)\partial(u_a - u_w)} d(u_a - u_w) \quad (6.53)$$

Comparing Eq. 6.49 and 6.53, gives,

$$\begin{aligned} m_1^w &= \frac{G_s}{(1+e_0)} \frac{\partial w}{\partial(\sigma_m - u_a)} = \rho_d \frac{\partial w}{\partial(\sigma_m - u_a)} \\ m_2^w &= \frac{G_s}{(1+e_0)} \frac{\partial w}{\partial(u_a - u_w)} = \rho_d \frac{\partial w}{\partial(u_a - u_w)} \end{aligned} \quad (6.54)$$

6.3.3.5 Specific Water Capacity of the Soil

The specific heat capacity in the coupled thermal stress problem has been introduced previously. Similarly, “the specific water capacity of a soil” can be defined as: the volume of water required decreasing unit mass of soil by one kPa of matric suction.

$$\Delta V_w = m C_w \Delta(u_a - u_w) \quad (6.55)$$

where ΔV_w = volume of water supplied to substance; m = mass of the soil solid; C_w = the specific water capacity of the soil; and $\Delta(u_a - u_w)$ = matric suction variation.

Correspondingly, the volumetric water content of the soil is

$$d\theta_{(u_a - u_w)} = \frac{\Delta V_w}{V} = \frac{m C_w \Delta(u_a - u_w)}{V} = \frac{G_s C_w \Delta(u_a - u_w)}{1+e_0} \quad (6.56)$$

Combining Eq. 6.47, and 6.56 gives:

$$d\theta_{(u_a-u_w)} = \frac{d(V_w)_{(u_a-u_w)}}{V} = \frac{G_s}{1+e_0} \frac{dw}{d(u_a-u_w)} \Delta(u_a-u_w) \quad (6.57)$$

Combining Eq. 6.47, and 6.57 gives:

$$m_2^w = \frac{G_s}{1+e_0} \frac{dw}{d(u_a-u_w)} = \rho_d C_w \quad (6.58)$$

and,

$$C_w = \frac{dw}{d(u_a-u_w)} \quad (6.59)$$

Eq. 6.59 shows that the specific water capacity C_w is the slope of soil-water characteristic curve and m_2^w is the multiply of the dry unit weight of the soil and the specific water capacity.

6.3.3.6 Excess Pore Water Pressure

When a load is applied to an unsaturated soil, the pore water pressure in the soil will increase at the instant of load application because the soil is under undrained compression, i.e. the matric suction in the soil will decrease at the instant of load application. The variation in pore water pressure (matric suction) is called excess pore water pressure. The ratio between the excess pore water pressure and the applied load is called excess pore water pressure parameter. The excess pore water pressure can be calculated from the constitutive law for the water phase. At the instant of load application, the time is so short that there is no water drainage, i.e. the soil is under undrained compression. As a consequence, we have,

$$d\theta = \frac{dV_w}{V_0} = d\theta_\sigma + d\theta_{(u_a - u_w)} = m_1^w d(\sigma_m - u_a) + m_2^w d(u_a - u_w) = 0 \quad (6.60a)$$

Correspondingly, we have,

$$d(u_a - u_w) = -\frac{m_1^w}{m_2^w} d(\sigma_m - u_a) \quad (6.60b)$$

Eq. 6.60 is satisfied for small mechanical stress variations, and the excess pore water pressure parameter is

$$B_w = \frac{d(u_a - u_w)}{d(\sigma_m - u_a)} = -\frac{m_1^w}{m_2^w} \quad (6.61)$$

For saturated soils, m_1^w is equal to m_2^w under any condition because of the effective stress principle. Therefore, the excess pore water pressure parameter is always 1. In other words, any load application will cause a pore water pressure increase with the same magnitude. The m_1^w and m_2^w for saturated soils will be discussed later. For unsaturated soils, the constitutive relation for water phase is usually highly nonlinear because m_1^w and m_2^w are functions of both the mechanical stress and the matric suction. For any variation in mechanical stress, the excess pore water pressure is the integration of Eq. 6.60 under the constant water content condition, that is,

$$\begin{aligned} \Delta\theta &= \int_{\theta_0}^{\theta_f} d\theta = \theta_f - \theta_0 = \int_{V_{w0}}^{V_{wf}} \frac{dV_w}{V_0} \\ &= \int_{(\sigma_m - u_a)_0}^{(\sigma_m - u_a)_f} m_1^w d(\sigma_m - u_a) + \int_{(u_a - u_w)_0}^{(u_a - u_w)_f} m_2^w d(u_a - u_w) \\ &= 0 \end{aligned} \quad (6.62)$$

where the subscription “0” stands for the initial conditions and subscription “ f ” stands for the final conditions of the soil.

If the initial conditions, $(\sigma_m - u_a)_0$, $(u_a - u_w)_0$ are known and the applied load (or the final mechanical stress $(\sigma_m - u_a)_f$) is known, the excess pore water pressure (the final matric suction) can be calculated with the known material parameters m_1^w and m_2^w because there is only one unknown, which is the integration upper limit $(u_a - u_w)_f$, i.e. the final matric suction. Eq. 6.62 represents the undrained loading condition. It actually defines a constant water content curve on the water content constitutive surface because for any $(u_a - u_w)_f$, the equation must be satisfied and $\theta_f - \theta_0 = 0$.

From Eq. 6.62, we can see the excess pore water pressure parameter depends on not only soil properties m_1^w and m_2^w , but the initial and final status of the soil. By solving Eq. 6.62, the excess pore water pressure can be obtained.

6.3.4 Differential Equations for the Coupled Hydro-Mechanical Stress (Consolidation) Problem

In the following discussion, the air phase is assumed to be continuous, and the excess pore air pressure will dissipate instantly at the instant of load application (Rahardjo and Fredlund 1995). For the soil with degree of saturation greater than 85%, the air is occluded. For an unsaturated soil with degree of saturation greater than 85%, the pore water pressure and the pore air pressure is nearly the same, which corresponds to a low suction value. Under these conditions, the air phase can be considered as a part of the soil structure, that is, the air phase can not move, but is compressible. The occluded air will influence the shape of the constitutive surface. However, the proposed consolidation theory will not be influenced.

6.3.4.1 Differential Equations for Soil Structure for the Coupled Consolidation Problem

Similar to the coupled thermal stress problem, the stress and strain tensor need satisfy equilibrium and continuity equations. Equations of equilibrium for the soil structure of an unsaturated soil are

$$\begin{aligned}\frac{\partial(\sigma_x - u_a)}{\partial x} + \frac{\partial\tau_{yx}}{\partial y} + \frac{\partial\tau_{zx}}{\partial z} + X &= 0 \\ \frac{\partial\tau_{xy}}{\partial x} + \frac{\partial(\sigma_x - u_a)}{\partial y} + \frac{\partial\tau_{zy}}{\partial z} + Y &= 0 \\ \frac{\partial\tau_{xz}}{\partial x} + \frac{\partial\tau_{yz}}{\partial y} + \frac{\partial(\sigma_x - u_a)}{\partial z} + Z &= 0\end{aligned}\tag{6.63a}$$

or

$$\sigma_{ij,j} + b_j = 0\tag{6.63b}$$

where σ_{ij} = components of the net total stress tensor; and b_i = components of the body force vector.

Eq. 6.63a and 6.63b is the same as Eq. 6.25a and 6.25b except that the stress is mechanical stress, that is, the difference between the mechanical stress and the atmospheric pressure u_a , which is a constant in this dissertation.

The strain-displacement equations (Cauchy's Equation) for the soil structure of an unsaturated soil are given by Eq. 6.26a:

$$\begin{aligned}\varepsilon_x &= \frac{\partial u}{\partial x}, & \gamma_{yz} &= \frac{\partial w}{\partial y} + \frac{\partial v}{\partial z} \\ \varepsilon_y &= \frac{\partial v}{\partial y}, & \gamma_{xz} &= \frac{\partial w}{\partial x} + \frac{\partial u}{\partial z} \\ \varepsilon_z &= \frac{\partial w}{\partial z}, & \gamma_{xy} &= \frac{\partial v}{\partial x} + \frac{\partial u}{\partial y}\end{aligned}\tag{6.26a}$$

or

$$\varepsilon_{ij} = \frac{1}{2}(u_{i,j} + u_{j,i}) \quad (6.26b)$$

where ε_{ij} = components of the strain tensor; and u_i = components of displacement in i -direction.

Solve Eq. 6.36 to get the expressions of $\sigma_x - u_a$, $\sigma_y - u_a$, $\sigma_z - u_a$ in terms of ε_x , ε_y , ε_z , $u_a - u_w$, we have,

$$\begin{aligned} \sigma_x - u_a &= \lambda \varepsilon_v + 2G \varepsilon_x + (3\lambda + 2G)\alpha(u_a - u_w), \tau_{yz} = G \gamma_{yz} \\ \sigma_y - u_a &= \lambda \varepsilon_v + 2G \varepsilon_y + (3\lambda + 2G)\alpha(u_a - u_w), \tau_{xz} = G \gamma_{xz} \\ \sigma_z - u_a &= \lambda \varepsilon_v + 2G \varepsilon_z + (3\lambda + 2G)\alpha(u_a - u_w), \tau_{xy} = G \gamma_{xy} \end{aligned} \quad (6.64)$$

Combining Eq. 6.26, 6.63 and 6.64 gives differential equations for equilibrium in terms of displacement:

$$\begin{aligned} (\lambda + G) \frac{\partial \varepsilon_v}{\partial x} + G \nabla^2 u - (3\lambda + 2G)\alpha \frac{\partial (u_a - u_w)}{\partial x} + X &= 0 \\ (\lambda + G) \frac{\partial \varepsilon_v}{\partial y} + G \nabla^2 v - (3\lambda + 2G)\alpha \frac{\partial (u_a - u_w)}{\partial y} + Y &= 0 \\ (\lambda + G) \frac{\partial \varepsilon_v}{\partial z} + G \nabla^2 w - (3\lambda + 2G)\alpha \frac{\partial (u_a - u_w)}{\partial z} + Z &= 0 \end{aligned} \quad (6.65)$$

Eq. 6.65 is the differential equations for the soil structure equilibrium for the coupled hydro-mechanical stress problem.

6.3.4.2 Differential Equations for Water Flow for the Coupled Consolidation Problem

6.3.4.2.1 Darcy's Law

Darcy's law is used to describe water flow through soils in both saturated and unsaturated condition (Freeze and Cherry 1979). A non-linear relationship can be used to take into account the dependency between the hydraulic conductivity and the pore-water pressure in the unsaturated soil mass. Darcy's law is written as follows:

$$q_i = ki_i = k \frac{dh}{dx_i} \quad (6.66)$$

where q = Darcy's flux in i -direction; k = hydraulic conductivity; which is a function of matric suction; h = hydraulic head; and x_i = the i - direction coordinate.

6.3.4.2.2 Bernoulli's Equation

Water flow in the soil not only satisfies the continuity equation, but also satisfies the energy equation, that is, Bernoulli's equation. It is convenient to express energy in terms of head, which is energy per unit of mass. Bernoulli's equation states that the total head of water equals to the sum of the elevation head, pressure head and the velocity head, i.e.,

$$h = z + \frac{u_w}{\rho_w g} + \frac{v^2}{2g} \quad (6.67)$$

where h is the total hydraulic head; z is the elevation head; u_w is the pore water pressure, ρ_w = the density of water; g = the gravity acceleration; and v = the velocity of the water flow.

Usually the velocity head in soils is much too small to be of any consequence and thus can be neglected. Eq. 6.88 is converted to:

$$h \approx z + \frac{u_w}{\rho_w g} \quad (6.68a)$$

For unsaturated soils, the pore water pressure u_w is negative and it is called the matric suction. Note that usually $u_a - u_w$ is used for matric suction to make the matric suction a positive value because the log scale is always used for matric suction. In this dissertation, u_w is used to represent the pore water pressure, which can be either positive (saturated soils) or negative (unsaturated soils). $u_a - u_w$ is used to represent the matric suction, which is always positive or it is the absolute value for $-u_w$. When expressed in terms of matric suction, Eq. 6.68a is

$$h \approx z + \frac{u_w}{\rho_w g} = z + \left[-\frac{(u_a - u_w)}{\rho_w g} \right] \quad (6.68b)$$

Because the air pressure is always considered to be continuous to the atmosphere and equal to zero, Eq. 6.68b is the same as Eq. 6.68a in deriving the differential equation for water phase.

6.3.4.2.3 Continuity Equation

Because the water is considered to be incompressible, the equation of soil water mass conversation is the same as the water continuity equation in an unsaturated soil. It can be written as follows:

Net water flow in+ water source (if any) = rate of change of stored water.

Consider a unit volume of soil such as shown in Fig. 6.9. The water source term can be simply written as “S” times the unit soil volume $dx dy dz$. Rate of water storage is mass times specific water capacity times rate of change of matric suction (pore water pressure):

$$mC_w \frac{d(u_a - u_w)}{dt} \quad \text{or} \quad \rho_d (dxdydz) C_w \frac{d(u_a - u_w)}{dt} \quad (6.69)$$

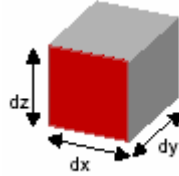


Fig. 6.9. A unit volume of soil element

The net rate of fluid mass flow in to the element is given by the sum of water flow rates over all 6 faces (remembering to multiply water flux by face area). Water fluxes on the high x,y,z faces are outward and therefore negative when water flux is positive. Combine all terms:

$$\begin{aligned} & \left[q_x - \left(q_x - \frac{\partial q_x}{\partial x} dx \right) \right] dydz + \left[q_y - \left(q_y - \frac{\partial q_y}{\partial y} dy \right) \right] dxdz \\ & + \left[q_z - \left(q_z - \frac{\partial q_z}{\partial z} dz \right) \right] dydx + S (dxdydz) = \rho_d (dxdydz) C_w \frac{d(u_a - u_w)}{dt} \end{aligned} \quad (6.70)$$

Cancel out water fluxes (q_x, q_y, q_z) and element volume ($dxdydz$), combine Eq. 6.66, 6.68a and 6.70 gives,

$$\begin{aligned} & \frac{1}{\rho_w g} \left(\frac{\partial}{\partial x} \left(k \frac{\partial(-u_w)}{\partial x} \right) + \frac{\partial}{\partial y} \left(k \frac{\partial(-u_w)}{\partial y} \right) + \frac{\partial}{\partial z} \left(k \left(\frac{\partial(-u_w)}{\partial z} + 1 \right) \right) \right) \\ & = \rho_d C_w \frac{\partial(u_a - u_w)}{\partial t} + S \end{aligned} \quad (6.71)$$

Eq. 6.71 is the differential equation for water phase in the soil. It reflects the water flow in the soil. The water squeezed out of the soil is not included. For the coupled consolidation of an unsaturated soil, undrained loading will cause the pore water

pressure to change instantaneously in the whole soil element. This phenomenon acts like the “water source term” because the pore water pressure at any point of the soil increases instantly. If this phenomenon is explained by the thermodynamic analogue, it means the temperature at any point of the soil is changed instantly, which also means the energy of the material is changed instantly and it is called energy generation. Similarly, at the instant of load application, there is “water generation” in the soil element. If there is no drainage at the instant of load application, the “water generation” will cause the pore water pressure increase. The water generation for the soil is linearly proportional to the applied external load as shown in Eq. 6.48. In a unit time period, the water source terms is:

$$S = m_1^w \frac{\partial(\sigma_m - u_a)}{\partial t} \quad (6.72)$$

Consequently, Eq. 6.72 is converted into

$$\begin{aligned} \frac{1}{\rho_w g} \left(\frac{\partial}{\partial x} \left(k \frac{\partial(-u_w)}{\partial x} \right) + \frac{\partial}{\partial y} \left(k \frac{\partial(-u_w)}{\partial y} \right) + \frac{\partial}{\partial z} \left(k \left(\frac{\partial(-u_w)}{\partial z} + 1 \right) \right) \right) \\ = \rho C_w \frac{\partial(\sigma_m - u_a)}{\partial t} + m_2^w \frac{\partial(u_a - u_w)}{\partial t} \end{aligned} \quad (6.73)$$

Eq. 6.65 and 6.73 together are the differential equations for the coupled hydro-mechanical stress (consolidation) problem for unsaturated soils. In the further discussion, we can find Eq. 6.65 and 6.73 can also be used for saturated soils as an extreme condition. For saturated soils, Eq. 6.65 and 6.73 are converted into the Biot’s consolidation theory, which will be discussed in a later section.

6.3.5 Constitutive Laws and Differential Equations for the Coupled Consolidation Theory for Unsaturated Soils by Fredlund and Rahardjo

Under the assumption that the air phase is continuous and the pore air pressure is always constant, the constitutive laws proposed by Fredlund (1973) is the same as the above discussion. The derivation of the differential equation is also similar to the coupled thermal stress problem. A simple introduction is made in this section.

6.3.5.1 Constitutive Relationships by Fredlund and Rahardjo and the Physical Meanings of Their Parameters

Fredlund (1973) used the principle of superimposition of coincident equilibrium stress fields to isolate the stress state variables associated with the soil particles and the contractile skin. A conclusion was reached that any two of three possible normal stress variables can be used to define the stress state. Possible combinations are:

- (1). $(\sigma - u_a)$ and $(u_a - u_w)$;
 - (2). $(\sigma - u_w)$ and $(u_a - u_w)$;
 - (3). $(\sigma - u_w)$ and $(\sigma - u_a)$;
- (6.74)

where σ = total mechanical stress; u_a = pore air pressure; and u_w = pore water pressure.

Fredlund and Morgenstern (1976) proposed the constitutive relations for volume change in unsaturated soils by using the stress state variables, that is, $(\sigma - u_a)$ and $(u_a - u_w)$ concept. The continuity requirement for an unsaturated soil can be stated as follows:

$$\frac{\Delta V_v}{V_0} = \frac{\Delta V_w}{V_0} + \frac{\Delta V_a}{V_0} \quad (6.75)$$

where V_0 = initial overall volume of the referential soil element; V_v = volume of soil voids; V_w = volume of water; and V_a = volume of air.

The constitutive relations for the total volume change and the volumetric water content variation in compressibility forms:

$$\frac{dV_v}{V_0} = m_1^s d(\sigma_m - u_a) + m_2^s d(u_a - u_w) \quad (6.76)$$

$$\frac{dV_w}{V_0} = m_1^w d(\sigma_m - u_a) + m_2^w d(u_a - u_w) \quad (6.77)$$

where m_1^s = coefficient of total volume change with respect to mechanical stress; m_2^s = coefficient of total volume change with respect to changes in matric suction; m_1^w = coefficient of the pore-water volume change with respect to changes in mechanical stress; m_2^w = coefficient of the pore-water volume change with respect to changes in matric suction; and σ_{mean} = the mean mechanical stress.

Combining Eq. 6.75, 6.76, and 6.77, the constitutive relationship for the air phase can be obtained:

$$\frac{dV_a}{V_0} = (m_1^s - m_1^w) d(\sigma_m - u_a) + (m_2^s - m_2^w) d(u_a - u_w) \quad (6.78)$$

Correspondingly, they concluded that only two constitutive relationships are needed for the soil volume change.

All these coefficients in Eq. 6.65 and 6.66 can be calculated from constitutive surfaces for void ratio and water content of the soil (Fredlund and Rahardjo 1993):

$$m_1^s = \frac{1}{1+e_0} \frac{de}{d(\sigma_m - u_a)} = \frac{1}{1+e_0} a_t \quad (6.79)$$

$$m_2^s = \frac{1}{1+e_0} \frac{de}{d(u_a - u_w)} = \frac{1}{1+e_0} a_m \quad (6.80)$$

$$m_1^w = \frac{G_s}{1+e_0} \frac{dw}{d(\sigma_m - u_a)} = \frac{G_s}{1+e_0} b_t \quad (6.81)$$

$$m_2^w = \frac{G_s}{1+e_0} \frac{dw}{d(u_a - u_w)} = \frac{G_s}{1+e_0} b_m \quad (6.82)$$

where a_t = coefficient of compressibility with respect to a change in mechanical stress; a_m = coefficient of compressibility with respect to a change in matric suction; b_t = coefficient of water content change with respect to a change in mechanical stress; and b_m = coefficient of water content change with respect to a change in matric suction.

Compare Eq. 6.41, 6.49 with Eq. 6.76 and 6.77, we can found that:

$$m_1^s = \frac{1}{B} = \frac{3(1-2\mu)}{E} \quad (6.83)$$

$$m_2^s = 3\alpha \quad (6.84)$$

$$m_2^w = \frac{G_s}{1+e_0} \frac{dw}{d(u_a - u_w)} = \rho_d C_w \quad (6.85)$$

where B = bulk modulus of the soil.

Eq. 6.85 indicates that m_1^s is the inverse of bulk modulus, m_2^s is the triple of coefficient of expansion due to matric suction variation, and m_2^w is the multiply of the dry unit weight of the soil and the specific water capacity. The physical meaning of m_1^w is related to “water generation” or “water source term”. Biot (1941) explained the physical meanings of m_2^s ($\frac{1}{H}$) and m_2^w ($\frac{1}{R}$) in a similar way for both saturated soils and unsaturated soils with occluded air bubbles. He defined that “ $\frac{1}{H}$ (m_2^s) is a measure of the

compressibility of the soils for a change in water pressure, while $\frac{1}{R}(m_2^w)$ measures the change in water content for a given change in water pressure". However, he proved that $m_2^s = m_1^w$ (that is, $3\alpha = m_1^w$) by assuming the existence of a potential energy of the soil, which is questionable because these two parameters have two different physical meanings. Only under the special case when the soil is saturated, it is right.

6.3.5.2 Differential Equations for the Coupled Consolidation Theory for Unsaturated Soils by Fredlund and Rahardjo

Fredlund and Rahardjo (1993) derived the water continuity equation in an unsaturated soil as follows:

$$\nabla \cdot q = \frac{\partial \left(\frac{V_w}{V} \right)}{\partial t} \quad (6.86)$$

where $\nabla = \frac{\partial}{\partial x}i + \frac{\partial}{\partial y}j + \frac{\partial}{\partial z}k$, the divergence operator; and $q = q_x i + q_y j + q_z k$, the Darcy's flux.

By performing the similar derivation and combining the constitutive relationship for water phase (Eq. 6.10), Fredlund and Rahardjo (1993) derived the water continuity equation as following:

$$-\left[\frac{\partial q_x}{\partial x} + \frac{\partial q_y}{\partial y} + \frac{\partial q_z}{\partial z} \right] = m_1^w \frac{\partial (\sigma_m - u_a)}{\partial t} + m_2^w \frac{\partial (u_a - u_w)}{\partial t} \quad (6.87)$$

Finally they get the same equation as Eq. 6.85. Comparing Eq. 6.58 with Eq. 6.87, we also can give Eq. 6.73

Fredlund and Rahardjo (1993) further derived Eq. 6.87 by following the derivation of the Biot's consolidation theory for saturated soils. The procedure is introduced simply as follows. Solve $d(\sigma_m - u_a)$ by Eq. 6.76 in terms of $d\varepsilon_v$, that is,

$$d(\sigma_m - u_a) = \frac{1}{m_1^s} d\varepsilon_v - \frac{m_2^s}{m_1^s} d(u_a - u_w) \quad (6.88)$$

Substitute Eq. 6.88 into Eq. 6.77, it gives,

$$\frac{dV_w}{V_0} = m_1^w \left\{ \frac{1}{m_1^s} d\varepsilon_v - \frac{m_2^s}{m_1^s} d(u_a - u_w) \right\} + m_2^w d(u_a - u_w) \quad (6.89a)$$

or

$$\frac{dV_w}{V_0} = \frac{m_1^w}{m_1^s} d\varepsilon_v + (m_2^w - m_1^w \frac{m_2^s}{m_1^s}) d(u_a - u_w) \quad (6.89b)$$

Denoting $\beta_{w1} = \frac{m_1^w}{m_1^s}$ and $\beta_{w2} = (m_2^w - m_1^w \frac{m_2^s}{m_1^s})$, substituting Eq. 6.89b into Eq. 6.86

gives,

$$\begin{aligned} \frac{1}{\rho_w g} \left(\frac{\partial}{\partial x} \left(k \frac{\partial(-u_w)}{\partial x} \right) + \frac{\partial}{\partial y} \left(k \frac{\partial(-u_w)}{\partial y} \right) + \frac{\partial}{\partial z} \left(k \left(\frac{\partial(-u_w)}{\partial z} + 1 \right) \right) \right) \\ = \beta_{w1} \frac{\partial \varepsilon_v}{\partial t} + \beta_{w2} \frac{\partial(u_a - u_w)}{\partial t} \end{aligned} \quad (6.90)$$

Eq. 6.65 and 6.90 together are the differential equations proposed by Fredlund and Rahardjo for the coupled consolidation for unsaturated soils. Eq. 6.73 and 6.90 are actually the same, the left sides of both equations represent the net water flow into the unit element and the right sides are the volumetric water content variation. However, the physical meaning of Equation 6.73 is much clearer than that of Eq. 6.90. As discussed previously, the coupled consolidation theory for unsaturated soils is similar to the coupled thermal stress problem. If Eq. 6.73 is used, the water generation can be easily simulated by the heat generation in the coupled thermal stress problem. Consequently, we can modify current programs for the coupled thermal stress problem, which are

readily available and well-developed, for the simulation of the coupled consolidation problem for saturated-unsaturated soil. Under the conditions that there is not much commercial software especially for the coupled consolidation theory for unsaturated soils, it is very convenient and cost-saving. More efforts will be needed in programming if Eq. 6.90 is used. A more detailed discussion about this will be presented in the following section.

6.4 Similarity between the Coupled Thermal Stress Problem and the Couple Hydro-Mechanical Stress (Consolidation) Problem for Saturated-Unsaturated Soils

As we can see, there are close similarities between the coupled thermal stress problem and the coupled hydro-mechanical stress (consolidation) problem for saturated-unsaturated soils. The thermodynamic analogue to process of consolidation was first proposed by K. Terzaghi to facilitate the visualization of the mechanics of consolidation and swelling. The continuity equation for the water phase is similar to that for heat transfer. Terzaghi (1943) stated that “If we assume $\gamma_w = 1$ ”, the differential equation of Terzaghi’s consolidation theory “becomes identical with the differential equation for the non-stationary, one-dimensional flow of heat through isotropic bodies, proved that we assign the symbols in the equation the following physical meanings (Table 6.1).

The loss of water (consolidation) corresponds to the loss of heat (cooling) and the absorption of water (swelling) to an increase of the heat content of a solid body. The existence of the thermodynamic analogue is useful in two different ways. First of all it eliminates in some cases the necessity of solving the differential equation because a great variety of solutions has already been obtained in connection with thermodynamic problems. Second, in contrast to the phenomenon of consolidation and swelling, the processes of cooling and heating are familiar to everybody from daily experience. Therefore, the knowledge of the existence of the analogue facilitates the visualization of the mechanics of consolidation and swelling.”

Table 6.1. Thermodynamic Analogues to the Process of Consolidation.

Theory of consolidation	Symbol	Thermodynamics
Excess hydraulic pressure	u	Temperature
Time	t	Time
Coefficient of permeability	k	Coefficient of heat conductivity
Coefficient of volume change	$\frac{\alpha_v}{(1+e_0)}$	Heat capacity times unit weight
Coefficient of consolidation or swelling	C_V	Diffusivity

Saturated soils are special cases for unsaturated soils. For the same reasons as what Terzaghi stated above, it is also meaningful to find the thermodynamic analogues to the coupled and uncoupled consolidation theory for saturated-unsaturated soils. In addition, the heat transfer problem and the coupled thermal stress problem have been studied in the mechanical engineering for decades. Some methods for solving those problems are already well-established and a lot of commercial software packages. For examples, ABAQUS, SUPER and ANSYS have provided options for solve the differential equations numerically. On the contrary, the research for the coupled hydro-mechanical stress (consolidation) problem for saturated-unsaturated soils is still not well-established and relatively new. Commercial programs for solving the coupled consolidation theory for unsaturated soils are still scarce. It is highly desirable to understand the similarity between the coupled thermal stress problem and the coupled consolidation theory and to implement current commercial soft ware packages to simulate the complicated problem for geotechnical engineering. The thermodynamic analogue also make it much easier to understand the tow stress state variable concept.

In this section, dimensional analysis is performed to make a comparison between the coupled thermal stress problem and the coupled hydro-mechanical stress (consolidation) problem. The discussion provides a possibility to modify the program especially for the coupled thermal stress problem into one for the coupled consolidation problem for saturated-unsaturated soils.

Eq. 6.65 and 6.73 are the differential equations for the coupled consolidation theory for saturated-unsaturated soils. If the gravity is the only body force and there is a water source term in the future analysis, Eq. 6.65 and 6.73 can be rewritten as follows:

$$(\lambda + G) \frac{\partial \varepsilon_v}{\partial x} + G \nabla^2 u - \frac{\alpha E}{1 - 2\mu} \frac{\partial (u_a - u_w)}{\partial x} = 0 \quad (6.91a)$$

$$(\lambda + G) \frac{\partial \varepsilon_v}{\partial y} + G \nabla^2 v - \frac{\alpha E}{1 - 2\mu} \frac{\partial (u_a - u_w)}{\partial y} = 0 \quad (6.91b)$$

$$(\lambda + G) \frac{\partial \varepsilon_v}{\partial z} + G \nabla^2 w - \frac{\alpha E}{1 - 2\mu} \frac{\partial (u_a - u_w)}{\partial z} + \rho g = 0 \quad (6.91c)$$

$$\begin{aligned} & \frac{1}{\rho_w g} \left(\frac{\partial}{\partial x} \left(k \frac{\partial (u_a - u_w)}{\partial x} \right) + \frac{\partial}{\partial y} \left(k \frac{\partial (u_a - u_w)}{\partial y} \right) + \frac{\partial}{\partial z} \left(k \left(\frac{\partial (u_a - u_w)}{\partial z} + \rho_w g \right) \right) \right) \\ & = m_1^w \frac{\partial (\sigma_m - u_a)}{\partial t} + m_2^w \frac{\partial (u_a - u_w)}{\partial t} + S \\ & = m_1^w \frac{\partial (\sigma_m - u_a)}{\partial t} + \rho_d C_w \frac{\partial (u_a - u_w)}{\partial t} + S \end{aligned} \quad (6.91d)$$

Eq. 6.91a, 6.91b, 6.91c and 6.91d indicate that the body forces in x and y directions are zero and the body force in z direction is the gravity. A water source term is included to make the further discussion more convenient.

The differential equations for the coupled thermal stress problem are expressed by Eq. 6.28 and 6.31a. In the mechanical engineering, usually the heat generation caused by load application is not significant and m_1^w is usually zero. If the gravity is the only body force, Eq. 6.28 and 6.31a can be rewritten as:

$$(\lambda + G) \frac{\partial \varepsilon_v}{\partial x} + G \nabla^2 u - \frac{\alpha E}{1 - 2\mu} \frac{\partial T}{\partial x} = 0 \quad (6.92a)$$

$$(\lambda + G) \frac{\partial \varepsilon_v}{\partial y} + G \nabla^2 v - \frac{\alpha E}{1 - 2\mu} \frac{\partial T}{\partial y} = 0 \quad (6.92b)$$

$$(\lambda + G) \frac{\partial \varepsilon_v}{\partial z} + G \nabla^2 w - \frac{\alpha E}{1 - 2\mu} \frac{\partial T}{\partial z} + \rho g = 0 \quad (6.92c)$$

$$\frac{\partial}{\partial x} \left(k \frac{\partial T}{\partial x} \right) + \frac{\partial}{\partial y} \left(k \frac{\partial T}{\partial y} \right) + \frac{\partial}{\partial z} \left(k \frac{\partial T}{\partial z} \right) = \rho C_T \frac{\partial T}{\partial t} + S \quad (6.92d)$$

For the equilibrium equations for the coupled consolidation theory for saturated-unsaturated soils (Eq. 6.91a, 6.91b and 6.91c), λ and G have the unit of Young's modulus E , which is kPa. The volumetric strain has no unit. The displacements in x , y and z direction u , v , and w have the unit of length, m. The coordinates in x , y and z directions have the unit of length, m. The coefficient of expansion due to matric suction has the unit of kPa^{-1} . The unit for pore water pressure is kPa. Eq. 6.91c is used as an example to show the dimension analysis, which is as follows,

$$(\text{kPa} + \text{kPa}) \left(\frac{1}{\text{m}} \right) + (\text{kPa}) \left(\frac{\text{m}}{\text{m}^2} \right) - \frac{\left(\frac{1}{\text{kPa}} \right) (\text{kPa})}{(1)} \left(\frac{\text{kPa}}{\text{m}} \right) + \left(\frac{1000\text{kg}}{\text{m}^3} \right) \left(\frac{10\text{m}}{\text{s}^2} \right) = \frac{\text{kPa}}{\text{m}} \quad (6.93)$$

$$\text{where } \rho g = \left(\frac{1000\text{kg}}{\text{m}^3} \right) \left(\frac{10\text{m}}{\text{s}^2} \right) = \frac{10000\text{kg} \cdot \text{m} \cdot \text{s}^{-2}}{\text{m}^2} \frac{1}{\text{m}} = \frac{10\text{kPa}}{\text{m}}$$

To keep unit consistent with each other in kPa, the mass density should have a unit of $1000\text{kg}/\text{m}^3$. For example, if the mass density for the soil is $2,000\text{kg}/\text{m}^3$, the input for the mass density is 2.0.

For the equilibrium equations for the coupled thermal stress problem (Eq. 6.92a, 6.92b and 6.92c), λ and G have the unit of Young's modulus E , which is kPa. The volumetric strain has no unit. The displacements in x , y and z direction u , v , and w have the unit of length, m. The coordinates in x , y and z directions have the unit of length, m.

The coefficient of expansion has the unit of K^{-1} (or $^{\circ}C^{-1}$). The unit for temperature is K (or $^{\circ}C$). Eq. 6.92c is used as an example to show the dimension analysis, which is as follows,

$$(kPa + kPa) \left(\frac{1}{m} \right) + (kPa) \left(\frac{m}{m^2} \right) - \frac{\left(\frac{1}{K} \right) (kPa)}{(1)} \left(\frac{K}{m} \right) + \left(\frac{1000kg}{m^3} \right) \left(\frac{10m}{s^2} \right) = \frac{kPa}{m} \quad (6.94)$$

$$\text{where } \rho g = \left(\frac{1000kg}{m^3} \right) \left(\frac{10m}{s^2} \right) = \frac{10000kg \cdot m \cdot s^{-2}}{m^2} \frac{1}{m} = \frac{10kPa}{m}.$$

In ABAQUS, when it is geostatic condition, the acceleration of gravity is required, which is $10m/s^2$, that is, the input is 10. Therefore, to keep unit consistent with each other, the mass density should have a unit of $1000kg/m^3$. For example, if the mass density for the concrete is $2,400kg/m^3$, the input for the mass density in ABAQUS is 2.4.

Comparing Eq. 6.93 with Eq. 6.94, it is found that the matric suction (unit: kPa) in the coupled consolidation theory is corresponding to temperature (unit: K) in the coupled thermal stress problem and the coefficient of expansion due to pore water pressure (matric suction, unit: kPa^{-1}) corresponds to the corresponding coefficient of expansion due to temperature (unit: K^{-1})

The water continuity equation (Eq. 6.91d) for the coupled consolidation problem can be rewritten as:

$$\begin{aligned} & \left(\frac{\partial}{\partial x} \left(\frac{k}{g} \frac{\partial(-u_w)}{\partial x} \right) + \frac{\partial}{\partial y} \left(\frac{k}{g} \frac{\partial(-u_w)}{\partial y} \right) + \frac{\partial}{\partial z} \left(\frac{k}{g} \left(\frac{\partial(-u_w)}{\partial z} + \rho_w g \right) \right) \right) \\ & = \rho_w \left(\frac{G_s}{1+e_0} \frac{dw}{d(\sigma_m - u_a)} \frac{\partial(\sigma_m - u_a)}{\partial t} + \frac{G_s}{1+e_0} \frac{dw}{d(\sigma_m - u_a)} \frac{\partial(u_a - u_w)}{\partial t} + S \right) \quad (6.91e) \\ & = \rho_d \frac{dw}{d(\sigma_m - u_a)} \frac{\partial(\sigma_m - u_a)}{\partial t} + \rho_d C_w \frac{\partial(u_a - u_w)}{\partial t} + S' \end{aligned}$$

The dimensional analysis of Eq. 6.91e is

$$\begin{aligned} \text{Left side: } & \frac{1}{m} \frac{m}{s} \frac{s^2}{m} \frac{kPa}{m} + \frac{1}{m} \frac{m}{s} \frac{s^2}{m} \frac{kPa}{m} + \frac{1}{m} \frac{m}{s} \frac{s^2}{m} \left(\frac{kPa}{m} + \frac{1000kg}{m^3} \frac{10m}{s^2} \right) = \frac{kg}{m^3 s} \\ \text{Right side: } & \frac{kg}{m^3} \frac{1}{kPa} \frac{kPa}{s} + \frac{kg}{m^3} \frac{1}{kPa} \frac{kPa}{s} + \frac{kg}{m^3} \frac{1}{s} = \frac{kg}{m^3 s} \end{aligned} \quad (6.95)$$

Where S has a unit of s^{-1} and S' has a unit of $\frac{kg}{m^3 s}$.

For the heat continuity equation (Eq. 6.92d) for the coupled thermal stress problem, the heat conductivity has a unit of $\frac{J}{s \bullet m \bullet K}$, the unit for specific heat capacity is $\frac{J}{kg \bullet K}$, and the time has unit of second. Consequently, the dimensional analysis for the Eq. 7.2d is

$$\begin{aligned} \text{Right side: } & \rho c_T \frac{\partial T}{\partial t} = \frac{kg}{m^3} \frac{J}{kg \bullet K} \frac{K}{s} = \frac{J}{m^3 s} \\ \text{Left side: } & k \frac{\partial^2 T}{\partial y^2} = \frac{J}{s \bullet m \bullet K} \bullet \frac{K}{m^2} = \frac{J}{m^3 s} \end{aligned} \quad (6.96)$$

Comparing Eq. 6.96 with Eq. 6.95, it is found that the mass of water (Unit: kg) in the coupled hydro-mechanical (consolidation) problem is corresponding to heat energy (unit: J) in the coupled thermal stress problem.

Other relationships can also be determined. If we define $K_w = \frac{k}{g}$, the K_w has a unit of

$$K_w = \frac{k}{g} = \frac{m}{s} \frac{1}{(10m/s^2)} = \frac{m}{s} \frac{1}{(10m/s^2)} \times \frac{kg/m^2}{kg/m^2} = \frac{kg}{s \bullet m \bullet kPa} \quad (6.97)$$

Comparing K_w with heat conductivity (unit: $\frac{J}{s \cdot m \cdot K}$), it is found that the unit of the mass of water kg is corresponding to heat energy unit J and the matric suction unit kPa is corresponding to the temperature unit K . Comparing K_w with heat conductivity, specific water capacity and specific heat capacity, and the coefficient of expansion due to pore water pressure (matric suction) and the coefficient of expansion due to temperature, we can find the most fundamental parallel between the coupled thermal stress problem and the coupled consolidation problem is that:

(1). State variable: mass of water (kg) in the coupled consolidation problem corresponds to energy (J) in the coupled thermal stress problem

(2). Stress state variable: pore water pressure ($u_a - u_w$) or u_w (or matric suction, kPa) in the coupled consolidation problem corresponds to temperature T or $(-T)$ (K) in the coupled thermal stress problem.

These conclusions are consistent with the discussions in the previous sections. All the material properties parameters can be transferred between the coupled thermal stress problem and the coupled consolidation problem by substituting the state variable and the stress state variable from one problem into the other. The following equations show their relationship, where \leftrightarrow stands for the transformation.

(1). Water conductivity versus heat conductivity:

$$\begin{aligned} \frac{K_w}{g} &= \frac{m}{s} \frac{1}{(10m/s^2)} = \frac{m}{s} \frac{kg/m^2}{kg(10m/s^2)/m^2} = \frac{kg}{s \cdot m \cdot kPa} \\ &= \frac{kg \leftrightarrow J}{s \cdot m \cdot kPa \leftrightarrow K} = \frac{J}{s \cdot m \cdot K} = K_T \end{aligned}$$

or

$$K_T g = \frac{J}{s \cdot m \cdot K} \frac{m}{s^2} = \frac{J}{K s^3} = \frac{kg}{kPa s^3} = \frac{kg m^2}{kN s^3} = \frac{m}{s} = K_w$$

(2). Water specific capacity versus heat specific capacity:

$$C_w = \frac{1}{kPa} = \frac{kg}{kg \cdot kPa} = \frac{kg \leftrightarrow J}{kg \cdot kPa \leftrightarrow K} = \frac{J}{kg \cdot K} = C_T$$

(3). Coefficient of expansion due to matric suction variation versus coefficient of expansion due to temperature variation:

$$\alpha_w = \frac{1}{kPa} = \frac{1}{kPa \leftrightarrow K} = \frac{1}{K} = \alpha_T$$

(4). Water content versus energy in unit mass.

$$w = \frac{m_w}{m_s} = \frac{\rho_w V_w}{\rho_d V} = \frac{\rho_w}{\rho_d} \theta_w = \frac{kg}{kg} = \frac{kg \leftrightarrow J}{kg} = \frac{J}{kg}$$

More comparisons in symbols and units between the coupled consolidation theory and the coupled thermal stress problem are shown in Tables 6.2 and 6.3, respectively.

Table 6.2. The Comparisons in Symbols between the Coupled Consolidation Theory and the Coupled Thermal Stress Problem

	Coupled Consolidation Theory		Coupled Thermal Stress Problem	
	Physical Meaning	Symbol	Physical Meaning	Symbol
Mechanical	Stress	$\bar{\sigma} - u_a$	Stress	σ
	Strain	ε	Strain	ε
	Displacement	u, v, w	Displacement	u, v, w
	Young's Modulus	E	Young's Modulus	E
	Poisson's Ratio	μ	Poisson's Ratio	μ
	Coefficient of Expansion due to Water Pressure Variation	α	Coefficient of Expansion due to Temperature Variation	α
Thermo-dynamic (Water Phase Continuity)	Coefficient of permeability	k	Coefficient of conductivity	k
	Specific Water Capacity	C_w	Specific Heat Capacity	C_T
	Dry Unit Density	ρ_d	Density	ρ
	Volumetric Water Content Variation	$-m_1^w \frac{\partial(\sigma_m - u_a)}{\partial t}$	Heat Generation	S
	Time	t	Time	t

Table 6.3. The Comparisons in Units between the Coupled Consolidation Theory and the Coupled Thermal Stress Problem

	Coupled Consolidation Theory		Coupled Thermal Stress Problem	
State variable	Mass of water	kg	J	Energy
Stress state variable	Pore water pressure	kPa	K	Temperature
Common	coordinate($x, y, \text{ and } z$)	m	m	coordinate($x, y, \text{ and } z$)
	Mass density	10^3 kg/m^3	10^3 kg/m^3	Mass density
	Acceleration of gravity	m/s^2	m/s^2	Acceleration of gravity
Equilibrium	Young's Modulus	kPa	kPa	Young's Modulus
	Coefficient of Expansion	kPa^{-1}	K^{-1}	Coefficient of Expansion
Equation	Pore water pressure	kPa	K	Pore water pressure
Continuity	Permeability k_w	m/s	$\text{JK}^{-1} \text{s}^{-3}$	Conductivity $K_T g$
	$K_w = k_w / g$	$\text{kg}(\text{kPa})^{-1} \text{m}^{-1} \text{s}^{-1}$	$\text{JK}^{-1} \text{m}^{-1} \text{s}^{-1}$	Heat conductivity
	Specific water capacity	$(\text{kPa})^{-1}$	$\text{J}(\text{kg})^{-1} \text{K}^{-1}$	Specific heat capacity
Equation	Source term S	s^{-1}	s^{-1}	r/ρ
	water generation S'	$(\text{kg})\text{m}^{-3} \text{s}^{-1}$	$\text{Jm}^{-3} \text{s}^{-1}$	r

6.5 Uncoupled Consolidation Theory for Saturated-Unsaturated Soils

The coupled hydro-mechanical stress problem handles the behavior of a soil under any condition. In practice, the behavior of a soil after a load application is of special interest. The environment is assumed unchanged and the soil is allowed to drain. Usually the pore pressure in the soil increases at the instant of load application. As time goes, the excess pore water pressure will dissipate and the soil volume will decrease. It is a time-dependent process. This phenomenon is called consolidation. In other words, consolidation is a special case of the coupled hydro-mechanical stress problem in which the soil behavior will change by following a special stress path.

This chapter attempts to investigate the consolidation theory of saturated-unsaturated soil. Before the discussion of the coupled consolidation theory for saturated-unsaturated soils, first of all let us discuss the uncoupled consolidation theory for unsaturated soils.

For saturated soils, a true three dimensional consolidation theory of consolidation couples the equilibrium of total stresses and the continuity of the soil water mass. A pseudo three-dimensional theory uncouples these two phenomena, under the assumption that the total stresses are constant. This condition is only strictly true in two special cases, one dimensional condition is one such case and Poisson's ratio is equal to 0.5 is the other. For uncoupled two- or three- dimensional consolidation theory, the assumption that the total mechanical stress remains constant is not true. However, the assumption will greatly simplify the problem and give out helpful information for the practice. For the uncoupled consolidation theory for unsaturated soils, we can also make the same assumption. Firstly the one dimensional consolidation theory for unsaturated soils is discussed.

6.5.1 Literature Review

The development of consolidation theory for saturated-unsaturated soils is summarized as follows.

Terzaghi (1923) used the effective stress as the stress state variable to describe the behaviors of a saturated soil, which can be stated as follows:

- (1). Changes in volume and shearing strength of a soil are due to extensively to change in effective stress;
- (2). The effective stress σ' is defined as the excess of the total applied stress σ over the pore water pressure u_w , that is,

$$\sigma' = \sigma - u_w \quad (6.98)$$

Terzaghi derived the one-dimensional consolidation theory for saturated soils. The assumptions used are:

- (1). The soils is homogeneous and saturated;
- (2). The soil particles and the water is incompressible;
- (3). The water flow is vertical only;

(4). The Darcy's law is valid and the coefficient of volume change and permeability remain constant during consolidation; and

(5). The strains are small.

By combining the stress strain relationship with the continuity equation, Terzaghi proposed the following differential equation for the consolidation of a saturated soil.

$$C_v \frac{\partial^2 u_w}{\partial y^2} = \frac{\partial u_w}{\partial t}$$

or

$$k \frac{\partial^2 u_w}{\partial y^2} = \frac{\gamma_w}{1 + e_0} \frac{\partial e}{\partial \sigma'} \frac{\partial u_w}{\partial t} \quad (6.99)$$

where C_v = coefficient of consolidation; k = coefficient of permeability at saturation; γ_w = water density; $\frac{\partial e}{\partial \sigma'}$ is the slope of void ratio versus effective stress curve.

Terzaghi described the process of consolidation as following steps:

(1). At the instant of load application, there is no void ratio change, that is, undrained loading. The total normal pressure has increased by the applied load, but the effective stress remains unchanged. Therefore, the excess pore water pressure at $t=0$ is equal to the applied load.

(2). At any time t , such that $0 < t < \infty$, the excess pore water pressure will dissipate under constant total stress at any horizon. Eq. 6.99 describes the pore water pressure changes with respect to depth and time during the consolidation process. The changes in pore water pressure result in changes in effective stress. The effective stress changes can be substituted into the constitutive equation in order to compute the volume change, which is equal to the volume of water flowing out of the saturated soils. Consequently, the void ratio, water content, and density throughout the consolidation process can be computed.

(3). At $t = \infty$, all the excess pore pressure will dissipate.

For an unsaturated soil, the problem is much more complicated. Because of the existence of the air phase, there is an immediate volume change at the instant of load application. The volume change will lead to increase in pore water pressure (i.e., decrease in matric suction) and change in soil structure. On the one hand, soil volume will decrease due to the compression caused by the applied load and, on the other hand, soil volume tends to increase due the increase in pore water pressure. This is true except for collapsible soils. The final immediate volume change will depend on the combination of the two effects. Furthermore, unlike saturated soils, the increase in pore water pressure for unsaturated soils is not necessarily equal to the applied load any more. As time goes on, the increase in pore water pressure will also dissipate gradually. Two more questions are raised in solving the problem of consolidation of unsaturated soils:

(1). How much is the settlement at different time?

(2). What is the increase in pore water pressure, or, what is the matric suction at different time?

For unsaturated soils, the soil properties are very sensitive to the soil structure change and vary greatly. As a result, a third question also appears: what's the mechanical stress's influence on the soil properties?

Biot (1941) proposed a general theory of consolidation for a saturated soil or an unsaturated soil with occluded air bubbles by using two constitutive equations, one relating total stress σ and strain, and the other for the pore water pressure u_w . The difference between the Biot's consolidation theory and the Terzaghi's theory lies in that the Biot's consolidation theory considered the total stress is not constant during the consolidation process due to the non-uniformity of the excess pore water pressure dissipation and the resulting total stress variations. The total stress variations during the consolidation process will result in Mandel-Cryer effect for saturated soils. In his paper, Biot explained the physical meanings of m_2^s and m_2^w in a way similar to the previous discussion. However, he proved that $m_2^s = m_1^w$ (that is, $3\alpha = m_1^w$) by assuming the existence of a potential energy of the soil. Consequently there are only four material parameters, i.e. E, μ, α , and $\rho_d C_w$ instead of five parameters, i.e. $E, \mu, \alpha, \rho_d C_w$, and

m_1^w in Fredlund's constitutive laws. For saturated soils, the conclusion is right because $m_1^s = m_2^s = m_1^w = m_2^w$ due to the effective stress principle. While for unsaturated soils, these two parameters represent different physical meanings and should be independent to each other. For example, for collapsible soils m_2^s and m_1^w have different sign. More discussions about these arguments will be discussed later.

Fredlund and Hansan (1979) presented two partial differential equations which could be solved for the pore air pressure and the pore water pressure during the consolidation of an unsaturated soil. The air phase is assumed to be continuous. Darcy's law and Fick's laws were applied to the flow of the water and the air phases, respectively. The excess pore water pressure and pair pressure due to the load application were derived by using the compressibility of air-water mixture. Both equations were solved simultaneously by the finite difference method to calculate the time rate of the pore air pressure and water pressure dissipation. The material parameters are assumed to be constants.

Fredlund and Rahardjo (1986) used the two partial differential equations to simulate the total and water volume change behaviors of compacted Kaoline specimens during the total stress and matric suction changes. However, pore water pressure changes in the specimens were not measured during the tests.

Similar consolidation equations have also been proposed by Lloret and Alonso (1980). Air phase was considered as continuous. Eulerian descriptions were used to derive the differential equations for the air phase and water phase. The excess pore water pressure and pair pressure due to the load application were derived by using the compressibility of air-water mixture. The material parameters were taken from the constitutive surfaces measured by Matyas and Radhakrishna (1968). The determinations of the material parameters for the differential equation for the air phase were unknown.

In 1984, Dakshanamurthy et al. extended the consolidation theory for unsaturated soils proposed by Fredlund and Hansan (1979) to the three dimensional case. The continuity equations were coupled with the equilibrium equations in deriving the three dimensional formulation.

Rahardjo (1990) conducted one-dimensional consolidation test on an unsaturated silty sand in a specially designed K_0 cylinder. The pore air and water pressure were measured simultaneously. The total and water volume change were measured independently. The results indicated an essentially instantaneous dissipation of the excess pore-air pressure for the particular soil. On the other hand, the excess pore water pressure was found to be a time-dependent process which could be closely simulated by using the water flow partial differential equation.

All the current methods count on numerical methods to solve the differential equations for the air phase and water phase due to the nonlinear properties of unsaturated soils. To obtain the parameters in the constitutive laws, nearly all the researchers use the constitutive surfaces, which are expressed as a function of $\sigma - u_a$ and $u_a - u_w$.

The possible problems associated with their works are:

(1). The water is tactically considered to be incompressible because the continuity equation is used to derive the differential equation for the water phase. However, the water is considered compressible when the excess pore water pressure and air pressure are calculated. The inconsistency in the compressibility of water cause the expressions of the excess pore water pressure and air pressure are overly complicated.

(2). The material parameters are assumed to be constants, which oversimplified the problem. For unsaturated soils, available data revealed that the material properties are highly nonlinear.

(3). Some researchers use the Skempton's equation to verify their results for the excess pore water pressure parameters. However, the Skempton's equation is proved incorrect in this dissertation.

(4). Most researchers assume the air coefficients of permeability to perform the numerical simulation. Research indicates that the air coefficients of permeability are much bigger than those of water. If the air phase is continuous, the excess pore water pressure should dissipate much faster than the excess pore water pressure.

(5). Henry's law is used to include the air dissolution to water when calculating the excess pore water pressure and air pressure. However, as discussed above, if the air

phase is continuous, the excess pore air pressure will dissipate instantly and the pore air pressure will not change much. The volume of air dissolved in the soil water should not change very much and Henry's law should not be considered. If the air is occluded in the soil, the differential equation for the air phase can not be derived because the assumption that the air phase is continuous is not satisfied. As a consequence, under both conditions, there are some problems involved in the past research.

6.5.2 Assumptions Made for the Uncoupled Consolidation Problem

The purpose of this section is to develop a simple calculation method for the uncoupled consolidation theory for unsaturated soils. The method is developed by using the conventional assumption for the consolidation theory by Terzaghi (1936) with the following additions:

- (1). The air phase is continuous and the excess pore water pressure is dissipated instantly;
- (2). The total mechanical stress remains constant during the consolidation process;
- (3). All the other material parameters are functions of both mechanical stress and matric suction.

Condition (1) is considered to be reasonable because the air coefficients of permeability are much greater than the water coefficients of permeability, a detailed discussion will be presented at the end of this Chapter.

Condition (2) is right for one dimensional case, but not true for two or three dimensional case. However, the assumption will greatly simplify the problem and provide useful information in practice. A detailed discussion for the coupled consolidation theory for unsaturated soils will be discussed in the next section

Firstly the consolidation theory by Terzaghi (1936) is reviewed by considering saturated soils as a special case of unsaturated soils, and then the method is extended to unsaturated soils. A new method is proposed to calculate the settlements for unsaturated throughout the consolidation process. An example is used to demonstrate the method. Finally some discussions are presented

6.5.3 Using Constitutive Surface to Explain the Consolidation Theory for Saturated Soils

The constitutive surfaces of saturated-unsaturated soils have been discussed in Chapter V. In this section, the consolidation theory for saturated soils is explained by the constitutive surfaces.

6.5.3.1 Stress Paths for the Consolidation of Saturated Soils

Fig. 6.10 and 6.11 show the schematic plots of the void ratio and water content constitutive surfaces of a saturated soil, respectively. The degree of saturation surface is not plotted here and it is equal to 1. Terzaghi's consolidation theory is reviewed by using these two constitutive surfaces and considering a saturated soil as a special case of an unsaturated soil. The stress paths of consolidation for a saturated soil can be illustrated by curve ABC in Fig. 6.10 and 6.11. Curve ABC in Fig. 6.10 and 6.11 show the void ratio and water content variations during the consolidation process of the soil, respectively.

The initial conditions of the soils are shown as Point A in the Fig. 10 and 11, i.e. $u_w = (u_w)_A$ and $\sigma = \sigma_A$. The corresponding void ratio and water content are also shown in these two surfaces respectively.

An external load $\Delta\sigma = \sigma_C - \sigma_A$ is applied to the soil. According to the Terzaghi's consolidation theory, at the instant of load application, i.e. $t=0$, all the load is taken by the pore water. The increase in total normal stress and pore water pressure at any point in the soils are equal to the applied load $\Delta\sigma$ everywhere. There is no volume change and no water drainage at this stage. The void ratio and the water content variations in this process are illustrated by the line from point A to point B in Fig. 6.10 and 6.11, respectively.

Recall the void ratio constitutive surface for a saturated soil (Fig. 6.10) is,

$$e = f(\sigma') = f(\sigma - u_w) = f((\sigma - u_a) + (u_a - u_w)) \quad (5.3)$$

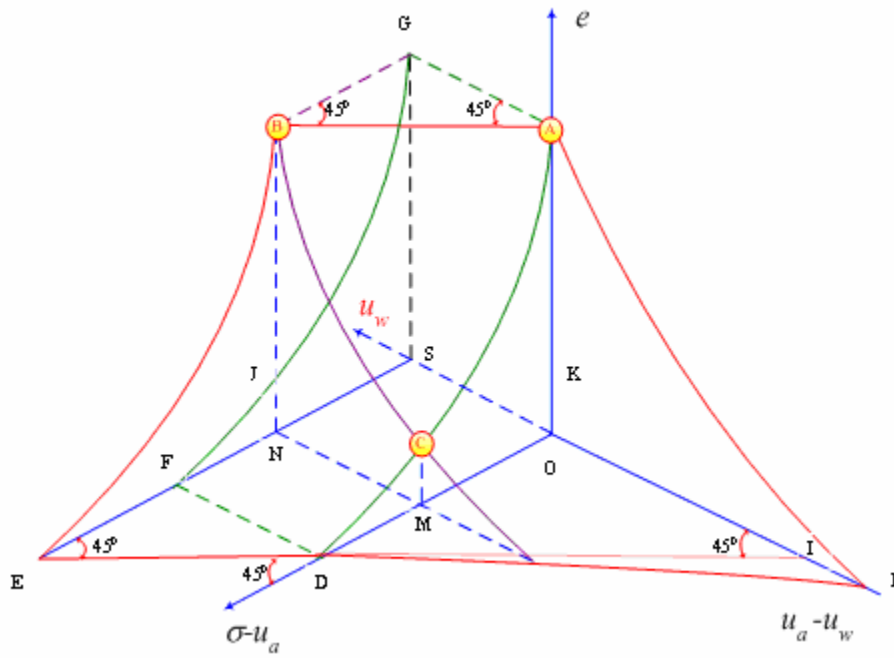


Fig. 6.10. Void ratio constitutive surface for a saturated soil

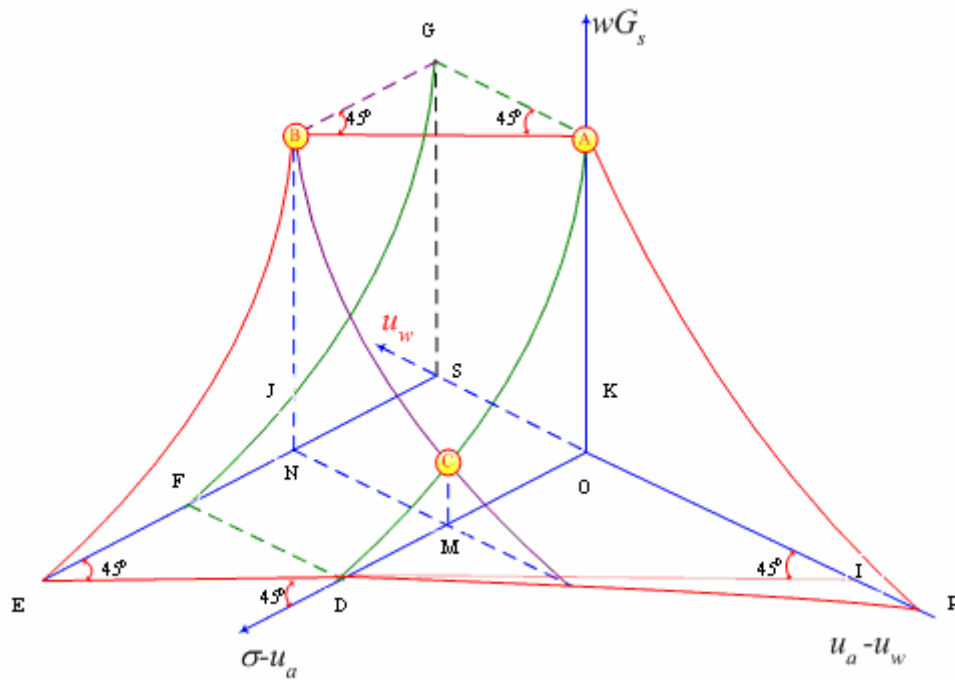


Fig. 6.11. Water content constitutive surface for a saturated soil

and the water content constitutive surface for a saturated soil (Fig. 6.11) is,

$$wG_s = Se = e = f(\sigma') = f(\sigma - u_w) = f((\sigma - u_a) + (u_a - u_w))$$

The angle $\angle BAG$ in both Fig. 6.10 and Fig. 6.11 are equal to 45° because the line AB in the two Figures stands for the constant void ratio and water content for the saturated soil due to the undrained loading. The total normal stress and pore water pressure increase $\Delta\sigma$ simultaneously.

At any time t , such that $0 < t < \infty$, water is drained and the excess pore water pressure will dissipate with time. The volume of the soil will decrease and the volume change is equal to the net water flow out. For one dimensional consolidation, the total mechanical stress keeps constant during the consolidation process. This stage can be explained by curve BC in Fig. 6.10. Curve BC shows the void ratio decreases at a constant total stress level. The pore water pressure decreases, and at the same time the effective stress increases while their sum, the mechanical stress, keeps constant.

Correspondingly, curve BC in Fig. 6.11 shows the same change in the mechanical stress and the pore water pressure, and the water content decreases. The water content on the curve BC in Fig. 6.11 decreases in the exactly same way as void ratio curve BC in Fig. 6.10 because for saturated soils $wG_s = e$. The stress path of curve BC in Fig. 6.10 is the same as that of curve BC in Fig. 6.11.

Curve AC in Fig. 6.10 stands for the void ratio versus total (or effective) stress curve while curve BC in Fig. 6.10 stands for the void ratio versus pore water pressure curve during the consolidation process. These two curves decrease in the same way because the total stress is constant during the one dimensional consolidation for the saturated soil. The pore water pressure variation is the same as that in effective stress. Hence, in Fig. 6.10 the curve BC has the exactly same shape as the curve AC.

Similarly, Curve AC in Fig. 6.11 stands for the water content versus total (or effective) stress curve while curve BC in Fig. 6.11 stands for the water content versus pore water pressure curve during the consolidation process. These two curves decrease

in the same way as Curve AC and BC in Fig. 6.10 because the volume change of the saturated soil is equal to the volume of water flow out of the soil.

At time $t=\infty$, all the excess pore water pressure is dissipated completely, which is point C in Fig. 6.10 and 6.11

In short, Fig. 6.10 and 6.11 have the same shape but have different meanings, Fig. 6.10 indicates the relationship between void ratio and the mechanical stress and the pore water pressure (matric suction), while Fig. 6.11 illustrates the relationship between water content and the mechanical stress and the matric suction. Curve ABC in Fig. 6.10 represents the void ratio variations during the consolidation process, while Curve ABC in Fig. 6.11 stands for the water content wGs variations along the same stress path.

6.5.3.2 Derivation of Differential Equation for the Consolidation of Saturated Soils

The derivation of the Terzaghi's consolidation theory can be reviewed simply as follows. The continuity equation of water flow through a soil element is,

$$\text{Net water flow in} = \text{rate of change of stored water}$$

which gives

$$\frac{\partial}{\partial z} \left(k_z \frac{\partial h}{\partial z} \right) = \frac{\partial \theta}{\partial t} = \frac{G_s}{1+e_0} \frac{\partial w}{\partial t} = \frac{G_s}{1+e_0} \left(\frac{\partial w}{\partial u_w} \right)_{BC} \frac{\partial u_w}{\partial t} \quad (6.100a)$$

where z = coordinate in vertical direction; k_z = permeability coefficient; h = total hydraulic head; G_s = soil specific gravity; θ = volumetric water content; e_0 = initial void ratio; t = time; and $\left(\frac{\partial w}{\partial u_w} \right)_{BC}$ = slope of the curve BC in Fig. 6.11.

The left side of the Eq. 6.100a represents the net water flow in or out of a soil element, the $\frac{\partial \theta}{\partial t}$ at the right side stands for the volumetric water content variation of the soil element. It should be calculated by the soil water characteristic curve of the soil. As shown in Fig. 6.11, the drainage process is represented by the curve BC. Curve BC is in

fact the soil water characteristic curve for the saturated soil at the constant mechanical stress level $\sigma = \sigma_B$.

Combining Bernoulli's Eq. 6.68 with 6.100a and neglecting the influence of elevation head gives,

$$\frac{\partial}{\partial z} \left(k_z \frac{\partial u_w}{\partial z} \right) = \frac{\partial \theta}{\partial t} = \frac{G_s}{1+e_0} \frac{\partial w}{\partial t} = \frac{G_s}{1+e_0} \left(\frac{\partial w}{\partial u_w} \right)_{BC} \frac{\partial u_w}{\partial t} \quad (6.100b)$$

For a saturated soil, the volume change in a unit time is equal to the net water flow into the soil, hence,

$$\frac{\partial \theta}{\partial t} = - \frac{1}{1+e_0} \frac{\partial e}{\partial t} \quad (6.101)$$

At the same time, the volume change in a unit time is obtained by the void ratio versus the effective stress relationship from the consolidation test, which is the curve AC in Fig. 6.10, hence,

$$\frac{1}{1+e_0} \frac{\partial e}{\partial t} = \frac{1}{1+e_0} \left(\frac{\partial e}{\partial \sigma'} \right)_{AC} \frac{\partial \sigma'}{\partial t} \quad (6.102)$$

Combining Eq. 6.101 with Eq. 6.102 gives,

$$\frac{1}{1+e_0} \left(\frac{\partial e}{\partial \sigma'} \right)_{AC} \frac{\partial \sigma'}{\partial t} = \frac{1}{1+e_0} \left(\frac{\partial e}{\partial \sigma'} \right)_{AC} \frac{\partial (\sigma - u_w)}{\partial t} = \frac{1}{1+e_0} \left(\frac{\partial e}{\partial \sigma'} \right)_{AC} \left(\frac{\partial \sigma}{\partial t} - \frac{\partial u_w}{\partial t} \right) \quad (6.103)$$

Considering that for one dimensional consolidation, the total mechanical stress is constant during the consolidation process. Therefore, $\frac{\partial \sigma}{\partial t} = 0$. Combining Eq. 6.100 and 6.103 and neglecting the influence of elevation head gives,

$$\frac{\partial}{\partial z} \left(k_z \frac{\partial u_w}{\partial z} \right) = \frac{1}{1 + e_0} \left(\frac{\partial e}{\partial \sigma'} \right)_{AC} \frac{\partial u_w}{\partial t} = \frac{\alpha_v}{1 + e_0} \frac{\partial u_w}{\partial t} \quad (6.104)$$

Eq. 6.104 is the differential equation of the Terzaghi's consolidation theory, where $\alpha_v = \left(\frac{\partial e}{\partial \sigma'} \right)_{AC}$ is coefficient of compressibility of the soil. Comparing Eq. 6.100 and 6.104 gives

$$G_s \left(\frac{\partial w}{\partial u_w} \right)_{BC} = - \left(\frac{\partial e}{\partial \sigma'} \right)_{AC} \quad (6.105)$$

It indicates that the Terzaghi's consolidation equation replaces the soil-water characteristic curve BC in Fig. 6.11 with the consolidation curve AC in Fig. 6.10 to calculate the soil volumetric water content variation during the consolidation process. Eq. 6.105 is satisfied for saturated soils only because of the effective stress principle and the 100% of degree of saturation for saturated soils in the process of consolidation. Eq. 6.105 can also be derived from the effective stress principle (Eq. 4.3 and 4.4), too.

6.5.4 One Dimensional Consolidation Theory for Unsaturated Soils

6.5.4.1 Stress Paths for the Consolidation of an Unsaturated Soil

The constitutive surfaces of an unsaturated soil provide the constitutive relationship between the void ratio, water content and degree of saturation and the two stress state variables, i.e. the net normal mechanical stress $\sigma - u_a$ and the matric suction $u_a - u_w$. The method for constructing the constitutive surfaces for unsaturated soils has been

discussed in Chapter V. The previous section illustrated the consolidation process for a saturated soil by using the void ratio and water content constitutive surfaces. The consolidation for an unsaturated soil can be investigated in the same way.

Considering an unsaturated soil with an initial condition,

$$\sigma - u_a = (\sigma - u_a)_A, \quad u_a - u_w = (u_a - u_w)_A \quad (6.106)$$

The environmental suction is $(u_a - u_w)_A$. An external load $P = (\sigma - u_a)_B - (\sigma - u_a)_A$ is applied on the soil. The soil is allowed to drain and both the externally applied load and the surrounding suction keep unchanged until infinite time period $t = \infty$.

Fig. 6.12 and 6.13 show the schematic plots of the water content and void ratio constitutive surface for an unsaturated soil. The consolidation process for this soil is also illustrated by curve ABC in both Figures. Point A in the Fig. 6.12 and 6.13 represent the initial water content and void ratio under the initial conditions defined by Eq. 6.106, respectively. If expressed mathematically, it means that both the void ratio and the water content are functions of two stress state variables, the mechanical stress and the matric suction. If these two variables are known, the corresponding void ratio and water content can be determined by the corresponding constitutive surface. The consolidation process can be described as follows:

(1). At the instant of load application, $t = 0$, there is no water drainage, namely, soil is compressed under undrained loading condition. Curve AB in Fig. 6.12 shows the undrained loading process. The water content of the soil keeps constant on curve AB in Fig. 6.12. Due to the load application, the mechanical stress $(\sigma - u_a)$ will increase. The increase in mechanical stress will cause the soil pore size to decrease. Correspondingly, the matric suction $(u_a - u_w)$ will decrease (pore water pressure will increase from a more negative value to a less negative value). Point B is the final status for this process. From Point A to Point B along Curve GAB, there is no water content variation, i.e. $w_A = w_B$.

RN is curve AB's projection on the total normal stress and the matric suction plane, illustrating the stress path during this process.

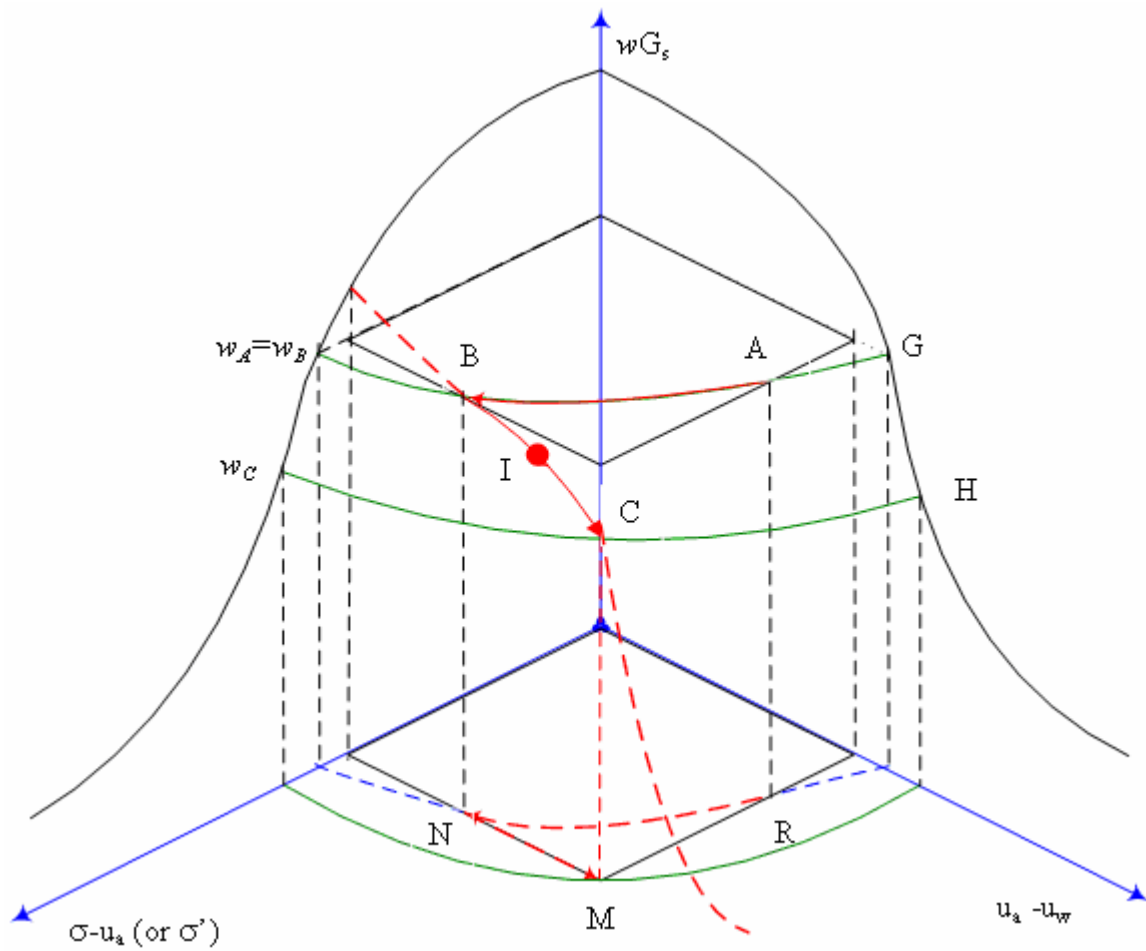


Fig. 6.12. Consolidation stress path on the water content constitutive surface for unsaturated soils

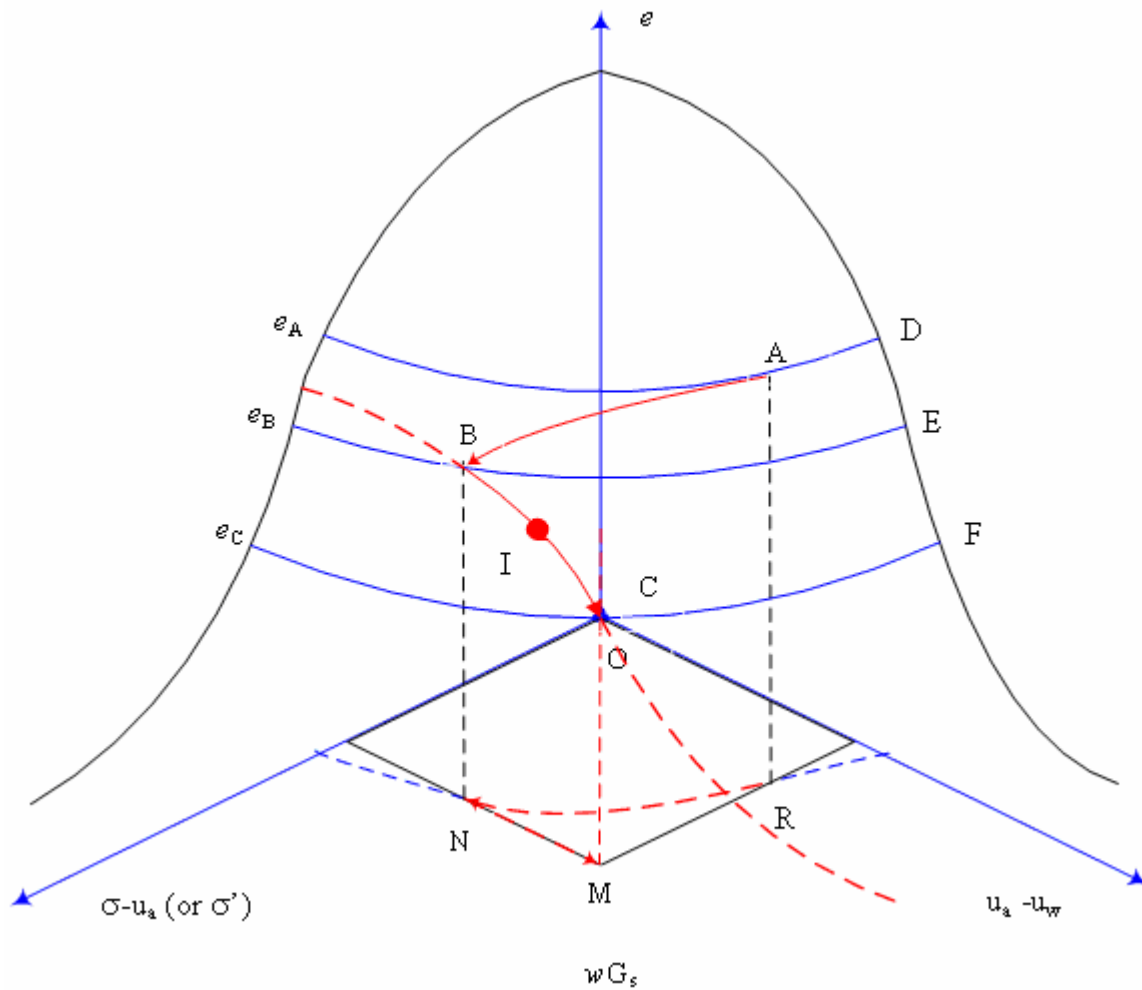


Fig. 6.13. Consolidation stress path on the void ratio constitutive surface for unsaturated soils

Unlike a saturated soil, the unsaturated soil is compressed at the instant of load application due to the existence of air phase. The void ratio variations during the process can be explained by void ratio constitutive surface in Fig. 6.13. Along the same stress path RN as that in Fig. 6.12, the void ratio of the soil will vary from Point A to Point B along curve AB in Fig. 6.13. Curve AD, BE and CF correspond to constant void ratio curves at different void ratio level e_A, e_B, e_C , and $e_A > e_B > e_C$. Curve AB in the Fig. 6.13

indicates that the void ratio of the soil decreases from e_A to e_B under undrained loading condition at the instant of load application $t=0$.

(2). At any time t , such that $0 < t < \infty$, the excess pore water pressure will dissipate, i.e. the matric suction in the soil ($u_a - u_w$) will increase due to the suction differences between the soil and the environment suctions. When the excess pore water pressure dissipates (soil suction increases), the water in the soil is drained out and the soil volume decreases. This process is a time-dependent process.

For one dimensional consolidation, the total normal stress doesn't change during the process, that is, $\sigma - u_a = (\sigma - u_a)_B$. Therefore, the water is drained along a constant mechanical stress curve BC as shown in Fig. 6.12 and 6.13. Fig. 6.12 shows that the water content decreases from Point B to Point C with dissipation of the excess matric suction. Fig. 6.13 shows that the void ratio of the soils decreases with dissipation of the excess pore water pressure (matric suction) along the same stress path.

(3). At time $t=\infty$, all the excess pore water pressure is dissipated completely. Hence, $u_a - u_w = (u_a - u_w)_A$.

6.5.4.2 Settlement Calculations for the Unsaturated Soil during the Consolidation Process

The consolidation settlement of the unsaturated soil can be calculated by making use of the constructed constitutive surfaces. As we know, for a saturated soil, the immediate settlement at the instant of load application is zero. As a consequence, the total settlement is equal to the consolidation settlement. The consolidation settlement calculation for an unsaturated soil is different from that for a saturated soil. It includes two components: one is the immediate settlement of the soil at the instant of load application and the other is the consolidation settlement of the soil due to the excess pore water pressure dissipation. To calculate the immediate settlement, the void ratio at the point A and the point B are needed and the void ratio at the point B and the point C are needed for the consolidation settlement calculation in Fig. 6.13.

To calculate the settlement of the soil, first of all the material parameters m_1^s and m_2^s for any point on the curve AB and BC must be calculated by taking the derivative of the void ratio constitutive surface with the mechanical stress and matric suction, respectively. Secondly, for the immediate settlement calculation, integration of the void ratio along the constant water content stress path RN in Fig. 6.13 is needed. While for the consolidation settlement, integration of the void ratio along the constant mechanical stress NM in Fig. 6.13 is needed. The unsaturated soil properties are usually highly nonlinear and AB and BC are usually curves in Fig. 6.13. As a consequence, the calculation is very difficult to perform and usually numerical method is needed.

A simpler method is to use the constitutive surfaces to calculate these settlements directly. The procedures of the calculation are described as follows:

(1). Calculate the initial water content and void ratio of the soil under the known initial conditions (Eq. 6.106). The mathematical expression of the void ratio and water content constitutive surfaces can be obtained by the method proposed in Chapter IV and Chapter V. With the known initial conditions (Eq. 6.106), the void ratio, water content and degree of saturation constitutive surface can be used to get the initial void ratio, water content and degree of saturation, respectively.

Actually, with any combination of two known variables in the five variables, i.e. mechanical stress, matric suction, void ratio, degree of saturation and water content, all the other three soils status variables can be calculated by the known constitutive surfaces of the soil.

(2). Determine the soil status at the instant of load application Point B in Fig. 6.12 and 6.13. For point B, there are two known variables. One is the total mechanical stress, which is equal to the initial mechanical stress plus the applied external load, i.e. $(\sigma_m - u_a)_B = (\sigma_m - u_a)_A + P$. The other one is the water content at Point B. Because it is an undrained loading, there is no water content variation from point A to point B in Fig. 6.12 and $w_B = w_A$ while the initial water content w_A known. The conditions can be expressed as

$$(\sigma_m - u_a)_B = (\sigma_m - u_a)_A + P, w_B = w_A \quad (6.107)$$

where P = the applied load.

All the other soil status variables can be gained by combining the Eq. 6.107 and the known constitutive surfaces. The procedures are described as follows. First of all, use the water content constitutive surface to calculate the matric suction under the condition of Eq. 6.107. Secondly, determine the void ratio and degree of saturation from the void ratio and the degree of saturation constitutive surfaces, respectively.

(3). Determine the soil status at $t=\infty$ for point C in the Fig. 6.12 and 6.13. For point C, two conditions are known. One is the matric suction at point C, which is equal to the surrounding suction because all the excess matric suction is dissipated at time $t=\infty$. Hence, $(u_a - u_w)_C = (u_a - u_w)_A$. The other is the applied load, which doesn't change during the consolidation process. Hence, $\sigma - u_a = (\sigma - u_a)_B$. All the other parameters such as e_C , S_c , and w_C can be determined by the corresponding constitutive surfaces.

Once all the state variables at the different stages (or Point A, B, and C) are determined, the corresponding settlements can be calculated as what we have done for saturated soils. The immediate compression at the instant of load application (stage 1) is

$$\Delta H_1 = \frac{\Delta e_1}{1 + e_0} H = \frac{e_B - e_A}{1 + e_0} H \quad (6.108)$$

the consolidation settlement (stage 2) is

$$\Delta H_2 = \frac{\Delta e_2}{1 + e_0} H = \frac{e_C - e_B}{1 + e_0} H \quad (6.109)$$

and the total settlement is equal to the sum of the immediate settlement and the consolidation settlement, which is

$$\Delta H = \Delta H_1 + \Delta H_2 = \frac{e_c - e_A}{1 + e_0} H \quad (6.110)$$

where ΔH_1 , ΔH_2 , ΔH = immediate compression, consolidation settlement and total settlement, respectively; e_A, e_B, e_C = void ratio at point A, B and C, respectively; H = thickness of soil layer; e_0 = initial void ratio; Δe_1 = void ratio variation at the instant of the load application; and Δe_2 = void ratio variation during the consolidation process.

For any arbitrary point I on the curve BC, the corresponding consolidation settlement is

$$\Delta H_i = \frac{e_i - e_B}{1 + e_0} H \quad (6.111)$$

and the total settlement is

$$\Delta H = \Delta H_1 + \Delta H_i = \frac{e_B - e_A}{1 + e_0} H + \frac{e_i - e_B}{1 + e_0} H = \frac{e_i - e_A}{1 + e_0} H \quad (6.112)$$

where ΔH_i = consolidation settlement at any time $t=t_i$; and e_i = void ratio at any time $t=t_i$.

6.5.4.3 Time Rate of Consolidation for Unsaturated Soils

A complete consolidation theory for an unsaturated soil must include two parts: 1. the total settlement calculation of the soil, which is accomplished as the previous section, 2. the time rate of the consolidation. The consolidation for an unsaturated soil is also a time dependent process.

As we discussed previously, the net normal mechanical stress during the consolidation is a constant, i.e. $\sigma - u_a = (\sigma - u_a)_B$. Therefore the only unknown stress state variable during the consolidation is the matric suction. Once the matric suction at

different time is known, all the state variables for the soil are known. Consequently the corresponding consolidation and total settlements can be calculated by Eq. 6.111 and 6.112, respectively. The matric suction dissipations are illustrated by curve BC as shown in Fig. 6.12, and the corresponding void ratio variation is shown as Curve BC in Fig. 6.13. Consequently, the procedures to solve the time rate of the consolidation problem are:

- (1). Find the matric suction $(u_a - u_w)_i$ at any time $t = t_i$;
- (2). Calculate the void ratio e_i at that time $t = t_i$ with the two known variables, i.e. $(\sigma - u_a)_i = (\sigma - u_a)_B$ and $(u_a - u_w)_i$;
- (3). Calculate the corresponding consolidation settlement and total settlement by Eq. 6.111 and 6.112.

To find the matric suction $(u_a - u_w)_i$ at any time $t = t_i$, it is required to solve the differential equation for water continuity under the condition that mechanical stress $\sigma - u_a = (\sigma - u_a)_B$. The continuity equation can be derived in the same way as the Eq. (6.100) that has been done previously. The following Eq. can be gotten:

$$\frac{\partial}{\partial z} \left(k_z \frac{\partial h}{\partial z} \right) = \frac{\partial \theta}{\partial t} = \frac{G_s}{1+e} \frac{\partial w}{\partial t} = \frac{G_s}{1+e} \left(\frac{\partial w}{\partial u_w} \right)_{BC} \frac{\partial u_w}{\partial t} \quad (6.113)$$

where $\left(\frac{\partial w}{\partial u_w} \right)_{BC}$ = the slope of the Curve BC in Fig. 6.12.

Eq. 6.113 is the continuity equation for water phase of the soil at the net normal mechanical stress $\sigma - u_a = (\sigma - u_a)_B$ level. Curve BC in Fig. 6.12 is actually the soil water characteristic curve of the soil at the net normal mechanical stress $\sigma - u_a = (\sigma - u_a)_B$ level.

Unlike that of a saturated soil, the volume change of an unsaturated soil is not equal to the volume change of the water phase any more. Therefore, there is no simple relationship between Curve BC in Fig. 6.12 and Curve AC in Fig. 6.13 any more. Eq.

6.113 can be solved by combining the boundary conditions for any specific problem and the relationship between matric suction variations and needed times can be obtained. The corresponding settlement can be obtained too. For unsaturated soils, both the permeability k and the slope of soil water characteristic curve $\left(\frac{\partial w}{\partial u_w}\right)_{BC}$ are functions of matric suction and vary in a large range. It makes the differential equation highly nonlinear so that usually numerical methods are usually used to solve the Eq. 6.113.

6.5.4.4 Mitchell's Derivation

Mitchell (1980) transformed the nonlinear differential equation for the water phase (Eq. 6.113) into a linear differential equation by using the following assumptions:

- (1). The permeability function is

$$k = \frac{k_0 (u_a - u_w)_0}{(u_a - u_w)} \quad (6.114)$$

where $(u_a - u_w)_0$ = matric suction at the field capacity, usually equal to 10kPa; and k_0 = permeability at total suction is equal to 10kPa.

Directly measuring the water permeability of an unsaturated soil is extremely difficult. Available data reveal that the water permeability will decrease rapidly with increase in matric suction. Eq. 6.114 reasonably reflects this tendency.

- (2). The soil-water characteristic curve is expressed as,

$$w = C_w \log_{10} (u_a - u_w) + D \quad (6.115)$$

where C_w = slope of the soil water characteristic curve when it is plotted in a semi-log scale.

Usually the soil water characteristic curve is also highly nonlinear and varies in a large range. Generally the log linear assumption for the soil-water characteristic curve is considered as good enough for practical purpose.

Denoting that $U = \log_{10}(u_a - u_w)$, then Eq. 6.113 can be transformed into

$$\alpha \frac{\partial^2 U}{\partial z^2} = \frac{dU}{dt} \quad (6.116)$$

where $\alpha = \frac{k_0 u_0}{0.4343 \frac{G_s}{1+e} C_w}$, which is called diffusion coefficient and it is a constant.

Eq. 6.116 is has the same style as the Terzaghi's consolidation theory. It is linear and has close-form solution for some special boundary conditions.

For a soil with initial matric suction state $U = U_0$ and boundary conditions $\frac{\partial U}{\partial z} = 0$ at $z=0$, $U = U_H$ at $z=H$ for any time $0 < t < \infty$, the solution of Eq. 6.116 (Mitchell 1980) is,

$$U = U_H + \frac{4(U_H - U_0)}{\pi} \sum_{n=1}^{\infty} \frac{(-1)^n}{2n-1} e^{-\frac{(2n-1)^2 \pi^2 \alpha t}{4H^2}} \cos \frac{(2n-1)\pi z}{2H} \quad (6.117)$$

where $T_v = \frac{\alpha t}{H^2}$; $U_0 = \log_{10}(u_a - u_w)_B$; and $U_H = \log_{10}(u_a - u_w)_A$.

Eq. 6.117 can be used to get the relationship between matric suction variation and time. Finally, the consolidation for the unsaturated soils can be solved. Actually, all the approaches which have been developed for the consolidation calculation for saturated soils can be used for unsaturated soils in a similar way. The differences between the Terzaghi's consolidation theory and the method proposed above lies in: first of all, the diffusion coefficient for the Terzaghi's consolidation theory is different from that in Eq. 6.116. Second, the solution for the pore water pressure variation with time for the Terzaghi's consolidation theory is given in terms of a Cartesian scale while the solution

of the pore water pressure variation given by Eq. 6.116 is in terms of the matric suction in log scale. Thirdly, the boundary conditions in the Terzaghi's consolidation theory are always zero while the boundary conditions for Eq. 6.116 are arbitrary for unsaturated soils.

For a soil surface is subjected to suction $U(0,t) = U_e + U_0 \cos(2\pi nt)$, Mitchell (1980) gives out the solution for Eq. 6.116,

$$U(z,t) = U_e + U_0 e^{-\sqrt{\frac{n\pi}{\alpha}}z} \cos\left(2\pi nt - \sqrt{\frac{n\pi}{\alpha}}z\right) \quad (6.118)$$

Due to Eq. 6.116 is linear, the principle of superposition can be applied. For the situation when a soil surface is subjected to arbitrary suction, series can be used to handle more complex boundary conditions at the soils surface by using Eq. 6.116 with different combinations of U_e , U_0 and n .

It is also noted that if only the permeability function has the style of $k = \frac{K_0}{u_a - u_w}$, the differential equation can be transformed into linear differential equation, where K_0 is a best-fitted parameter.

6.5.4.5 An Example for an Expansive Soil

6.5.4.5.1 Basic Descriptions of the Problem

An example is given to show the method proposed above. Fig. 6.14 shows the model for the example. Assuming a 3m thick soil layer with an initial condition

$$\begin{aligned} (\sigma - u_a)_A &= 10 \text{ kPa}, & \text{or } \log_{10}(\sigma - u_a)_A &= 1, \\ (u_a - u_w)_A &= 3981 \text{ kPa} & \log_{10}(u_a - u_w)_A &= 3.6 \end{aligned}$$

A surcharge of $P = (\sigma - u_a)_B - (\sigma - u_a)_A = 398.10 - 10 = 388.10 \text{ kPa}$ is applied to the ground surface and the surrounding environment has a constant suction of 3981 kPa all the time. The soil is impermeable at the bottom of the layer. The void ratio, water content and degree of saturation constitutive surfaces of the soil are defined by Eq. 5. 17, 5.20 and 4.11 and the corresponding surfaces are plotted as shown in Fig. 5. 12, 5.13, and 5.14, respectively.

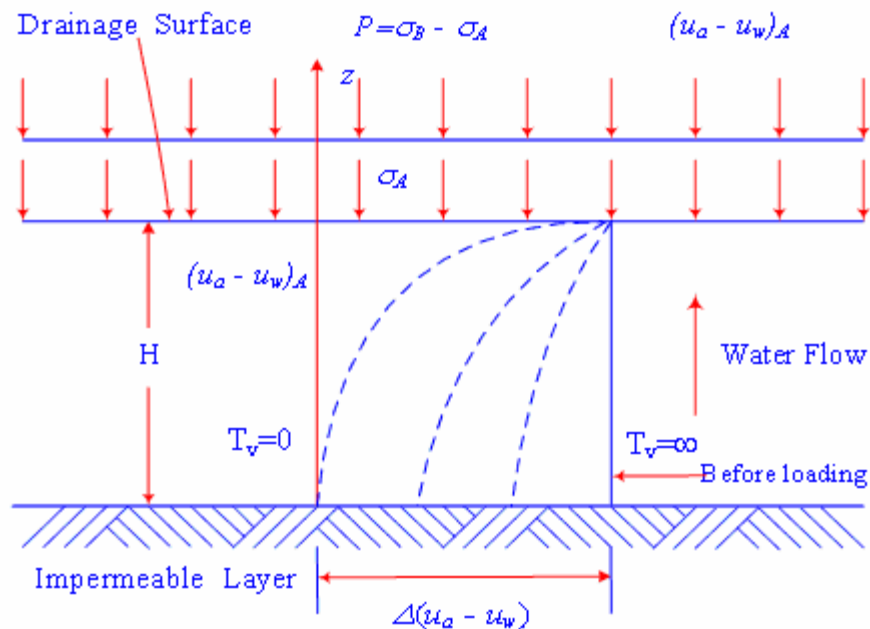


Fig. 6.14. Model for an expansive soil example

The soil state variables at different stages can be obtained. As have described before, with any combination of two known variables in the five variables, i.e., net normal mechanical stress, matric suction, void ratio, degree of saturation and water content, all the other three state variables can be calculated by the constitutive surfaces of the soil. The known variables at different stages are:

- (1). Initial condition: the matric suction and the net normal mechanical stress,
- (2). At the instant of load application: the water content and the mechanical stress,

(3). At time $t=\infty$: the matric suction and the mechanical stress.

Table 6.4. Summary of the Results for the Consolidation of an Unsaturated Soil

State variables \ Stage	Initial condition	after loading	Final Condition
	Point A	Point B	Point C
$\sigma-u_a$ (kPa)	10	398.1	398.1
u_a-u_w (kPa)	3981.1	488.7	3981.1
e	0.476	0.470	0.411
$W(\%)$	17.74	17.74	15.3
$S(\%)$	98.7	99.9	98.7

The corresponding results are listed in Table 6.4. As can be seen, at the instant of load application the mechanical stress changes from 10 kPa to 398.1kPa and the matric suction decreases from 3981.1kPa to 488.7kPa. The void ratio decreases from 0.476 to 0.470 and degree of saturation increases from 98.7% to 99.9%. During the process, the water content keeps unchanged, which is 17.74%.

From $t=0$ to time $t=\infty$, the void ratio decreases from 0.470 to 0.411, the degree of saturation decreases from 99.9% to 98.7%, and water content decreases from 17.74% to 15.3%, indicating there is some water drainage. During the process, the mechanical stress does not change. Finally the soil matric suction will reach equilibrium with the surrounding environment, which is 3981.1kPa.

6.5.4.5.2 Settlement Calculation

The immediate settlement at the instant of load application can be calculated by Eq. 6.108:

$$\Delta H_1 = \frac{\Delta e_1}{1+e_0} H = \frac{e_B - e_A}{1+e_0} H = \frac{0.470 - 0.476}{1+0.476} \times 3 = -0.0122 \text{ (m)}$$

The consolidation settlement can be calculated by Eq. 6.109:

$$\Delta H_2 = \frac{\Delta e_2}{1+e_0} H = \frac{e_C - e_B}{1+e_0} H = \frac{0.411 - 0.470}{1+0.476} \times 3 = -0.120 \text{ (m)}$$

The total settlement can be calculated by Eq. 6.110:

$$\Delta H = \Delta H_1 + \Delta H_2 = \frac{e_C - e_A}{1+e_0} H = -0.0122 - 0.120 = -0.132 \text{ (m)}$$

6.5.4.5.3 Time Rate of the Consolidation Settlement

The consolidation occurs at the net normal mechanical stress level $(\sigma - u_a) = 398.10 \text{ kPa}$, the corresponding soil-water characteristic curve Fig. 6.15 and void ratio versus matric suction curve Fig. 6.16 can be obtained from the void ratio and water content constitutive surfaces by taking $(\sigma - u_a) = 398.10 \text{ kPa}$ into Eq. 5.17, 5.20 and 5.21, or and the corresponding surfaces as shown in Fig. 5.12, 5.13 and 5.14, respectively. As we discussed previously, most current researchers investigate the consolidation of unsaturated soils by assuming a constant material parameters and usually these material parameters are obtained from the boundary curves as shown in Fig. 5.6. Fig. 6.15 and Fig. 6.16 also show the soil-water characteristic curve and void ratio versus matric suction curve when the mechanical stress is equal to 1Kpa, i.e. $(\sigma - u_a) = 1\text{kPa}$. It can be seen that the soil-water characteristic curve and void ratio versus matric suction curve when the mechanical stress is equal to 398.1kPa are greatly different from those when the mechanical stress is equal to 1 kPa. As a consequence, the calculation by assuming the material parameters are constant will result in great errors.

The regression of the soil water characteristic curve at the range from 488.7kPa (Point B as shown in Fig. 6.12) to 3981.1kPa (Point C in Fig. 6.12) is:

$$w = -0.0267 \times \log_{10}(u_a - u_w) + 0.2516 \quad (6.119)$$

where C_w in Eq. 6.115 is equal to 0.0267.

The permeability function of the soil is assumed to be defined by Gardner's Equation (Gardner 1958) as follows:

$$K = \frac{1.0 \times 10^{-8}}{1 + 0.1 \times \left(\frac{u_a - u_w}{1 \times 9.8} \right)^2}$$

The best-fitted permeability function curve with Eq. 6.114 (Fig. 6.17) is

$$K = \frac{7.0 \times 10^{-9}}{(u_a - u_w)}$$

That is, $k_0 u_0 = 7.0 \times 10^{-8}$ m/s. The corresponding diffusion coefficient of the soils is:

$$\alpha = \frac{k_0 u_0}{0.4343 \rho_d C} = 3.36 \times 10^{-7}$$

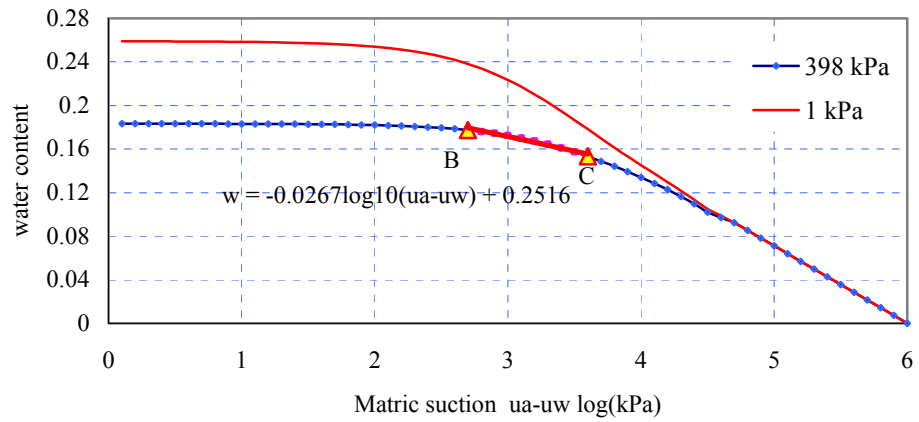


Fig. 6.15. Soil water characteristic curves at different mechanical stress levels

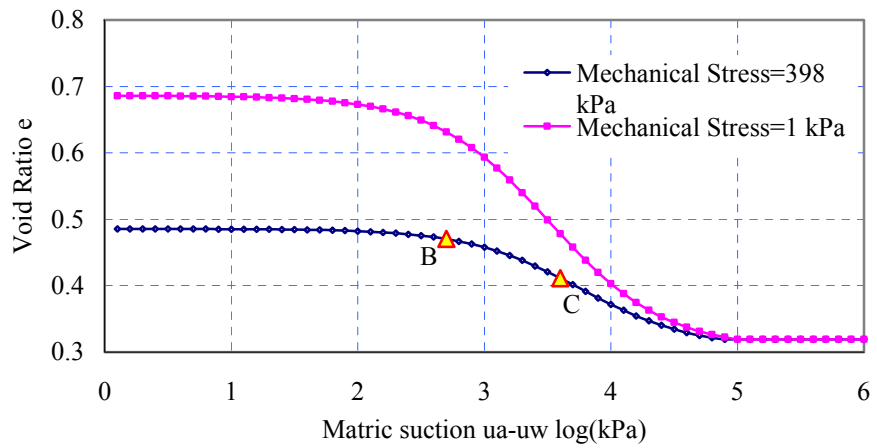


Fig. 6.16. Void ratio versus matric suction at different mechanical stress levels

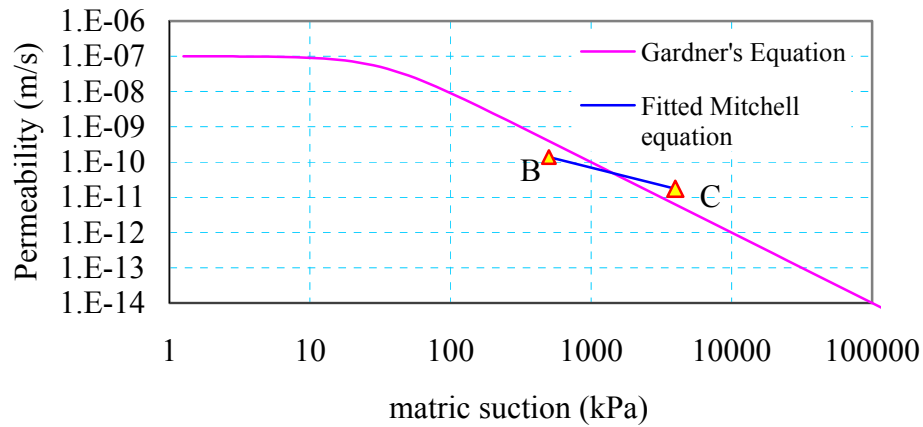


Fig. 6.17. Permeability function for the soil

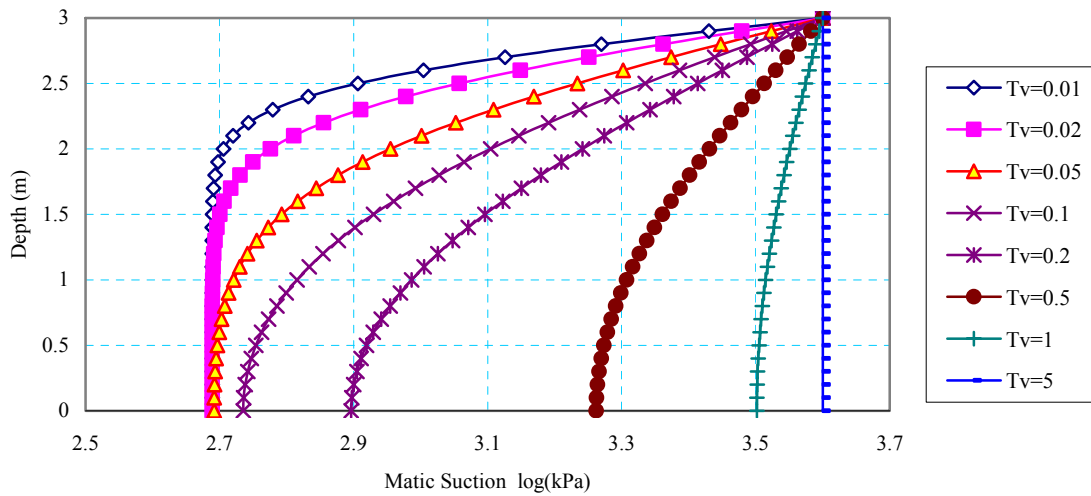


Fig. 6.18. Suction distribution profiles at different times

Combining $U_0 = \log_{10}(u_a - u_w)_B = 2.69$ and $U_H = \log_{10}(u_a - u_w)_A = 3.6$ with Eq. 6.117, the suction distribution profiles at different time can be obtained. The results are shown in Fig. 6.18. After the suction distribution profile at different time is calculated, the corresponding void ratio profile can be obtained by using the void ratio versus

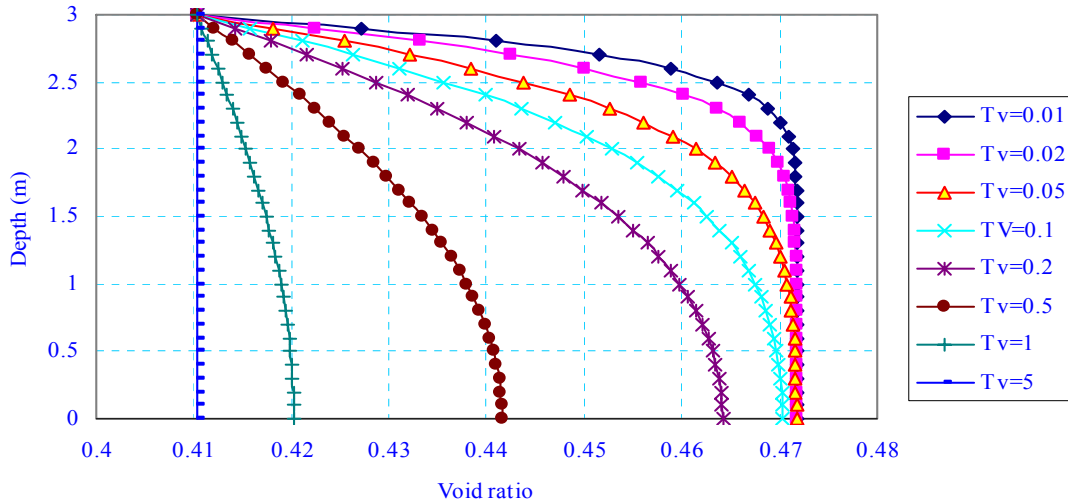


Fig. 6.19. Void ratio distribution profiles at different times

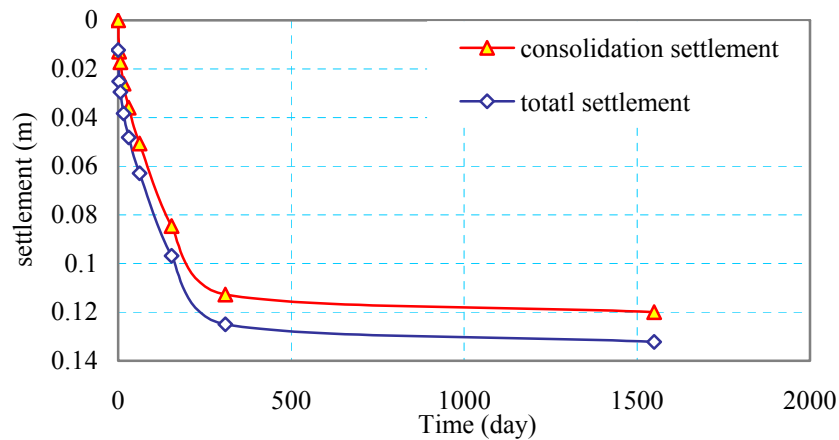


Fig. 6.20. The consolidation settlements and total settlements at different times

matric suction curve at $(\sigma - u_a) = 398.1 \text{ kPa}$ as shown in Fig. 6.16 and the results are shown in Fig. 6.19. The corresponding total settlements and consolidation settlements at different time can be calculated by using Fig. 6.19 and Eq. 6.111 and 6.112, and the results are shown in Fig. 6.20. Fig. 6.20 shows the consolidation settlement and the total settlement of the soil. The difference between them is the immediate settlement.

6.5.4.6 Discussion

6.5.4.6.1 Excess Pore Water Pressure Parameter

In this section, all the problems involved in the consolidation of the unsaturated soils are solved. At the instant of load application, the degree of saturation increases a little bit (from 98.7% to 99.9%). The immediate settlement is only 10% of the total settlement, and the reason for this is the initial degree of saturation for the soil is high. The matric suction changes dramatically and the pore water pressure parameter, i.e. the ratio between the variation in matric suction and the applied load, is

$$\frac{\Delta(u_a - u_w)}{\Delta\sigma} = \left| \frac{(3981.1 - 488.7)}{(398.1 - 10)} \right| = 9.0$$

which is totally different from the excess pore water pressure parameters for saturated soils obtained by a lot previous researchers. Skempton (1954) and Bishop (1954) derived the following equation for the excess pore pressure parameter:

$$\frac{\Delta u_w}{\Delta \sigma_3} = B = \frac{1}{1 + \frac{n C_v}{C_c}} \quad (6.120)$$

where Δu_w = change in pore water pressure; $\Delta \sigma_3$ = isotropic change in total stress; n = porosity; C_v = compressibility of water; and C_c = compressibility of the soil skeleton.

From Eq. 6.120, Skempton and Bishop concluded that the pore water pressure parameter for unsaturated soils is $0 < B < 1$. The conclusion is supported by some observations (Skempton 1954; Bishop 1954) and is extensively accepted in the past.

The calculated excess pore water pressure parameter from the above example is conflicted with the Skempton's equation. A scrutiny finds that there is mistake in the derivation of the Skempton's equation. The Skempton's equation was originally derived for the calculation of the excess pore water pressure parameters for unsaturated soils

while the effective stress principle ($\Delta\sigma' = \Delta\sigma_3 - \Delta u_w$) for saturated soils was used in the derivation. It is incorrect because the effective stress principle does not hold for unsaturated soils any more. Instead, for unsaturated soils, Bishop's equation should be used to calculate the equivalent effective stress, i.e. $\Delta\sigma' = \Delta\sigma_3 - \chi\Delta u_w$. Finally the new excess pore water pressure parameter should be

$$\frac{\Delta u_w}{\Delta\sigma_3} = B = \frac{1}{\chi + \frac{nC_v}{C_c}} \quad (6.121)$$

where χ = parameter in Bishop's equation.

Because χ can be less than 1, it is possible to have a B greater than 1. Skempton's calculations for the pore water pressure parameters are also questionable because the initial pore water pressure was tacitly considered as zero.

Fig. 6.21 and 6.22 show the schematic plots for the reasoning. The soils tested by Skempton were initially unsaturated and the initial conditions of the soil are point 1 in both Figures. The soil is then compressed into a saturated soil by an externally applied load. It can be seen that the water content keeps constant at the instant of load application (from point 1 to point 2 in Fig. 6.21). At the same time the void ratio decreases when the soil is unsaturated (from Point 1 to Point 0 in Fig. 6.22) until the soil reaches saturation. Once the soil is saturated, an increase in the mechanical stress will not cause any void ratio variations any more (from Point 0 to Point 2 in Fig. 6.22) and the variations in total stress will cause the same magnitude of the pore water pressure variations, i.e. B=1. It can be seen from these two Figures that a load applied to an unsaturated soil will never cause a positive pore water pressure greater than itself, since

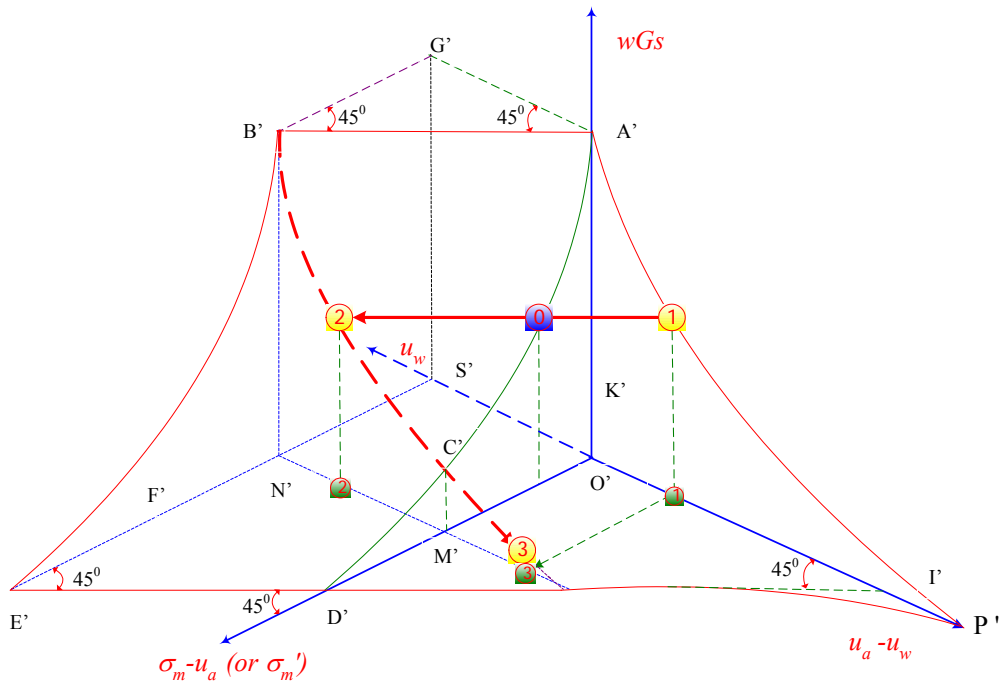


Fig. 6.21. Water content variations during the consolidation process of a soil

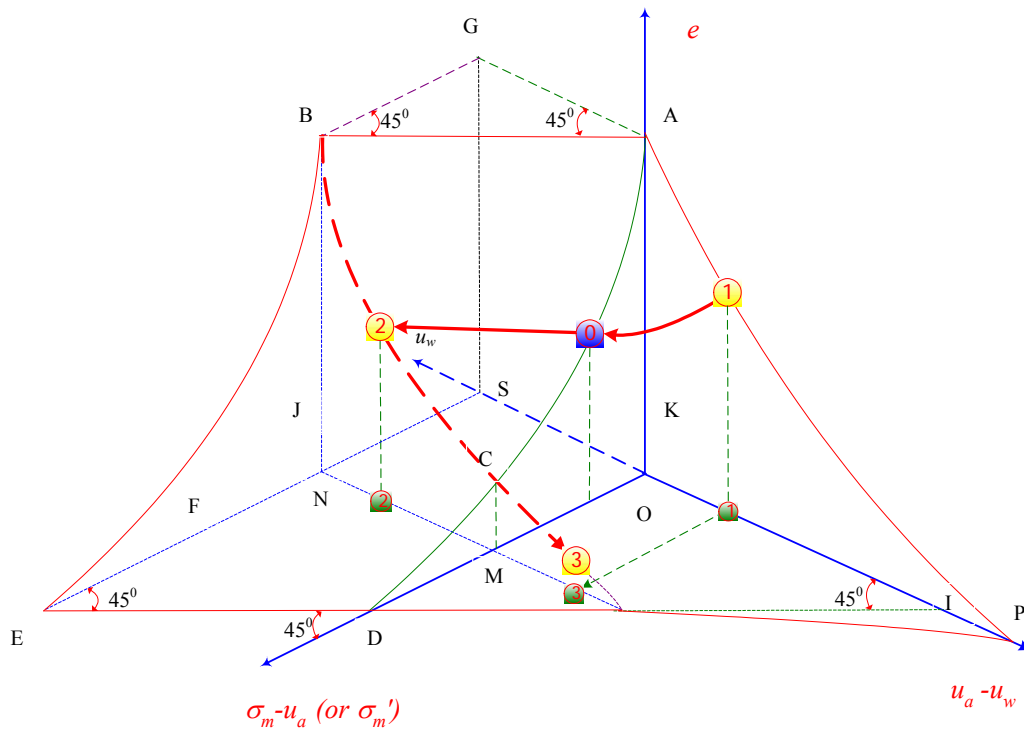


Fig. 6.22. Void ratio variations during the consolidation process of a soil

portion of the applied load is used to make the soil to be saturated, i.e. to make the soil suction decrease to zero, and the left is used to increase the pore water pressure for zero to a positive value. By assuming tacitly that the initial pore water pressure was zero (point 0), Skempton got an excess pore water pressure parameter B which is always between 0 and 1. In other words, when calculating the applied load, Skempton considered that the soil status was changed from point 1 to point 2 in Fig. 6.21 and 6.22. However, when calculating the pore water pressure variation, he considered the soil status was changed from point 0 to point 2. The pore water pressure variations in the unsaturated portion (From Point 1 to Point 0) were not considered.

The bimodal structure of the soil can also be used to explain the calculation results in the example. A single clay particle is surrounded by absorbed water and forms a double diffusion layer. Individual clay particles are always aggregated or flocculated together. The clay aggregates are then grouped together to form granular-like structure. The pores formed by the clay aggregates, which are called macropores, are much bigger than the internal pores, which are called micropores, in the aggregates. Micropores have much higher air entry values than macropores. When soil is drying, air will first enter into the macropores while the micropores are still saturated. If a load is applied to the unsaturated soil, the interparticle stress between aggregates will be much higher than the applied total stress thanks to the actual cross section is smaller than the total section area. Therefore, the intergranular stresses between the clay aggregates are higher than the applied total stress. Recall that the aggregates are actually saturated internally, the excess pore water pressure due to the load application will equal to the interparticle stress according to the effective stress principle. Consequently, the excess pore water pressure is expected to be greater than the applied load, which corresponds to $B > 1$. Fig.6.23 shows the explanation of the excess pore water pressure by using the bimodal structure of soils.

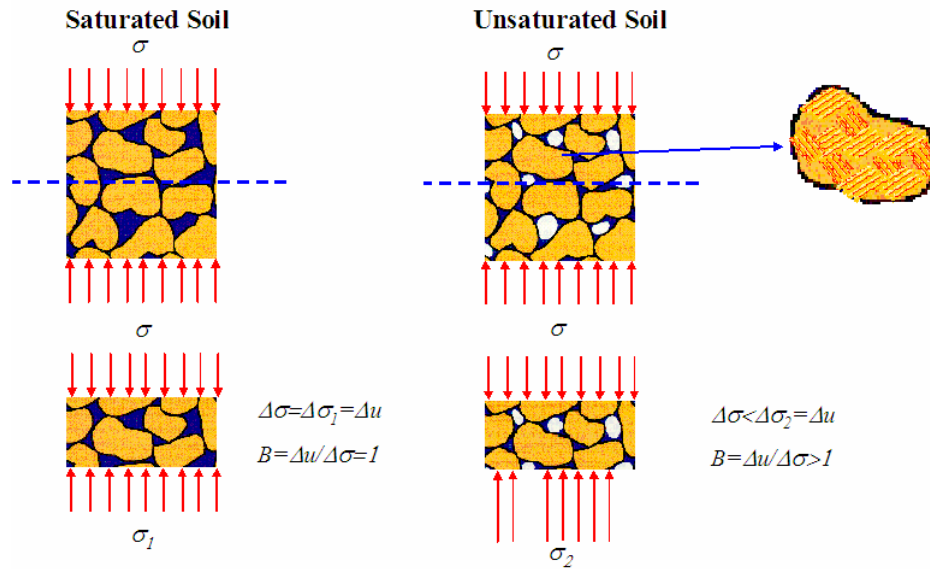


Fig. 6.23. Explanation of the excess pore water pressure by the bimodal structure of soils

Fredlund and Hasan (1980) also derived the pore pressure parameters for unsaturated soils under undrained loading based on the compressibility of air-water mixture. The pore air and water pressure parameter were all between 0 and 1, indicating there is some problem in the simulation.

In the “experimental verification of the theory of consolidation for unsaturated soils”, Rahardjo and Fredlund (1995) conducted one-dimensional consolidation test on an unsaturated silty sand in a specially designed K_0 cylinder. The pore air and water pressure were measured simultaneously. Observations indicated that a 1.0 kPa variation in the mechanical stress $\sigma - u_a$ caused 24.5 kPa variation in the matric suction $u_a - u_w$ for one unsaturated silt ($B=24.5$) and a 1.2 kPa variation in the mechanical stress $\sigma - u_a$ caused 20.4 kPa variation in the matric suction $u_a - u_w$ for another unsaturated silt ($B=17$). Observations also found that pore-air pressure dissipation occurred essentially instantaneously. Both tests indicated that $B > 1$. Unfortunately, no attention was paid to the phenomenon.

6.5.4.6.2 Influence of the Mechanical Stress on Soil Behaviors

Fig. 6.15 and 6.16 indicates that soil properties are influenced by the mechanical stress dramatically. In Fig. 6.15 and 6.16, the void ratio versus matric suction curve and soil water characteristic curve at the mechanical stress $(\sigma - u_a) = 1 \text{ kPa}$ and $(\sigma - u_a) = 398.10 \text{ kPa}$ are shown. It is shown that there is great influence of the mechanical stress on the soil-water characteristic curve at the low suction range but little or no influence at the high suction level. The air entry value seems to be higher at high mechanical stress level than at lower mechanical stress level. It is reasonable because when the soil is compressed, the soil pore size will decrease so that a higher matric suction value is needed for the air to enter the soil pores. For the void ratio versus matric suction curves (Fig. 6.9), the maximum void ratio (the swell limit) is approximately 0.68 for $(\sigma - u_a) = 1 \text{ kPa}$ and 0.48 for $(\sigma - u_a) = 398.10 \text{ kPa}$, respectively. The minimum void ratio values (the shrinkage limit) are basically the same ($e=0.31$) for both curves, indicating the volume change of the soil is influenced greatly by mechanical stress. In fact, the void ratio constitutive surface can be considered as a collection of shrink test curves at different stress levels which swell limits decrease with the increase in mechanical stress level. It can also be visualized as a collection of “consolidation curves” at different matric suction levels. In the same way, the water content constitutive surface can be considered as a collection of soil-water characteristic curve at different mechanical stress level while the air entry values increase with the increase in mechanical stress level. All these results indicate that the method proposed in Chapter V for constructing the constitutive surfaces for unsaturated soils works very well and are consistent with most of the current observations presented in Chapter II.

The influence of the mechanical stress is included in the method proposed for the calculation of the consolidation of unsaturated soils because the soil water characteristic curve and the void ratio versus matric suction curve used in the calculation are at $(\sigma - u_a) = 398.10 \text{ kPa}$. Therefore this method will have a higher accuracy than previous uncoupled analysis in which the soil water characteristic curve and the void

ratio versus matric suction curve used are at $(\sigma - u_a) = 0$ kPa (or constant material parameters). Another advantage for the proposed method is that the obtained constitutive surfaces can be obtained at very high suction level, for example, shows a surface with whole possible suction range (from 0 to 1,000,000kPa), which is very desirable when the high-quality data in this range are not easy to obtain.

6.5.4.6.3 Essentiality of the Proposed Method

Due to the highly nonlinear properties for unsaturated soils, to date most researchers used numerical methods to solve the consolidation or volume change problem for unsaturated soils (Fredlund and Hansan 1980; Lloret and Alonso 1980), which is not desirable for practical purpose. In this chapter, a simple method is proposed to calculate the excess pore water pressure, immediate, consolidation and total settlement for the one dimensional consolidation for unsaturated soils. Just by “reading” the soil state variables from the constitutive surfaces, the proposed method greatly simplifies the calculation and avoids any complicated numerical iteration caused by the nonlinearity. Reasonable results are obtained. In the following discussion, the theoretic basis for the proposed method is further explained.

If the pore air pressure is constant, the constitutive laws for the volume change of unsaturated soils are as follows:

$$d\varepsilon_v = \frac{dV_v}{V_0} = m_1^s d(\sigma) + m_2^s d(-u_w) \quad (6.122)$$

$$d\theta = \frac{dV_w}{V_0} = m_1^w d(\sigma) + m_2^w d(-u_w) \quad (6.123)$$

At the instant of load application, the stress path for the undrained loading is AB for the void ratio variations and the water content variations as shown in Fig. 6.12 and 6.13, respectively.

To obtain the immediate compression due to the undrained loading, numerical integrations for Eq. 6.122 is needed along the corresponding stress path AB in Fig. 13:

$$\begin{aligned}
 \Delta \varepsilon_v &= \int_A^B d\varepsilon_v = \int_A^B m_1^s d(\sigma) + \int_A^B m_2^s d(-u_w) \\
 &= \int_A^B \frac{1}{1+e_0} \left(\frac{\partial e}{\partial \sigma} d\sigma + \frac{\partial e}{\partial (-u_w)} d(-u_w) \right) \\
 &= \int_A^B \frac{de}{1+e_0} = \frac{e_B - e_A}{1+e_0} = \frac{\Delta e}{1+e_0}
 \end{aligned} \tag{6.124}$$

From Eq. 6.124, it can be seen that the immediate compression calculation involving two processes: (1). taking the derivatives of the void ratio constitutive surface to get the material parameters m_1^s and m_2^s , and then calculate the volumetric strain due to small stress increments, (2). integrating the small volumetric strains into the volumetric strain. These two processes are reverse to each other. By “taking the readings” for the initial and final void ratio, the same calculation result can be obtained without involving any nonlinear deriving and integrating process. The calculation is expected to have a higher accuracy than the results obtained from the numerical methods because there will be some calculation errors during the integration and the derivation processes for a nonlinear problem

The calculation for the excess pore water pressure can be performed in the similar way. Excess pore water pressure calculation due to an undrained loading (From point A to point B in Fig. 6.12) can be calculated numerically in the following way:

For undrained loading:

$$\Delta \theta_w = \int_A^B d\theta_w = \int_A^B m_1^w d(\sigma) + \int_A^B m_2^w d(-u_w) = 0 \tag{6.125}$$

Therefore,

$$\int_A^B \frac{G_s}{1+e_0} \left(\frac{\partial w}{\partial \sigma} d\sigma + \frac{\partial w}{\partial(-u_w)} d(-u_w) \right) = 0 \quad (6.126)$$

That is,

$$\int_{\sigma_A}^{\sigma_B} \frac{G_s}{1+e_0} \left(\frac{\partial w}{\partial \sigma} d\sigma \right) + \int_{u_A}^{u_B} \frac{G_s}{1+e_0} \left(\frac{\partial w}{\partial(-u_w)} d(-u_w) \right) = 0 \quad (6.127)$$

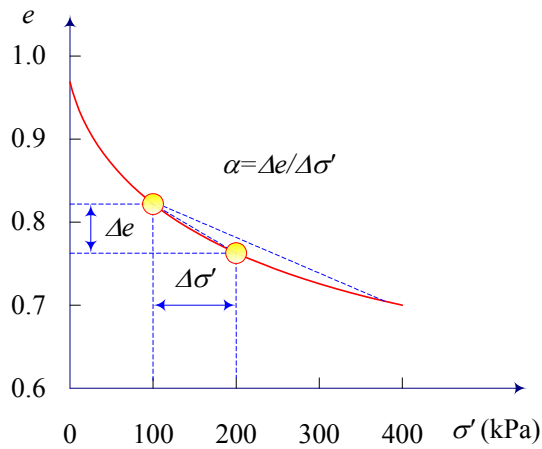
For Eq. 6.127, the initial mechanical stress and matric suction are known and the final mechanical stress is known. Hence, to solve Equation is to find pore pressure u_B from the constant water content path AB as shown in Fig. 12. To accomplish this, derivation of the water content constitutive surface is need to get the material parameters m_1^w and m_2^w and integration of the same surface is needed to get the water content variations. These two processes are reverse to each other. An alternative is to “read” the water content from the constitutive surface directly. The resulting result is expected to have a higher accuracy than that obtained from the numerical method.

In conclusion, the proposed method avoided the need of deriving and integrating for the constitutive surfaces. It is expected that the obtained results will be more accurate than numerical method if the problem is a nonlinear problem.

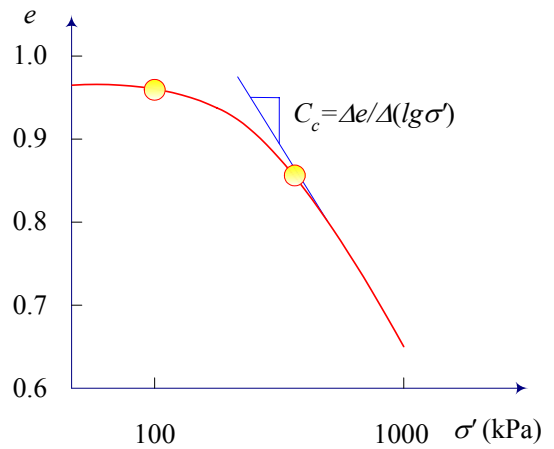
The same method can be applied to the settlement calculation for a saturated soil as shown in Fig. 6.24. Namely, there is no need to calculate the compressibility of the soil (α_v or C_c) for the settlement calculation purpose only. What we need do is to get the effective stress of the soil, find the corresponding void ratio from the void ratio versus effective stress curve (which can be obtained from the one dimensional test), and then use Eq. 6.110 and 6.112 to get the corresponding total settlement and consolidation settlement. The only difference is that for a saturated soil, ΔH_1 in Eq. 6.112 is zero because there is no initial compression for the saturated soil. By doing this, a more accurate result can be obtained.

$$S = \frac{e_1 - e_0}{1 + e_0} H = \frac{\Delta e}{1 + e_0} H = \frac{\alpha \Delta \sigma'}{1 + e_0} H$$

$$S = \frac{e_1 - e_0}{1 + e_0} H = \frac{\Delta e}{1 + e_0} H = \frac{C_c \Delta (\lg \sigma')}{1 + e_0} H$$



(a)



(b)

Fig. 6.24. Compression curves of a saturated soil and settlement calculations

6.5.4.6 An Example for a Collapsible Soil

6.5.4.6.1 Problem Statement

The proposed method can also be used for the calculation of the consolidation for collapsible soils. Two constitutive surfaces, void ratio and degree of saturation surfaces, are taken from the experimental work of Pereira and Fredlund (1997). The mathematical expressions of the void ratio constitutive surfaces are:

$$e = e_u + \frac{e_s - e_u}{\left[1 + \left(\frac{u_a - u_w}{c} \right)^b \right]} \tag{6.128}$$

Where

$$e_u = 0.67 - 0.0073 \ln(\sigma^*)$$

$$e_s = 1.226(\sigma^*)^{-0.1359}$$

$$c = c_1(\sigma^*)^2 + c_2(\sigma^*) + c_3$$

$$b = b_1(\sigma^*)^{b_2}$$

$$c_1 = 9.4 \times 10^{-4}$$

$$c_2 = 7.46 \times 10^{-2}$$

$$c_3 = -4.07$$

$$b_1 = 49.01$$

$$b_2 = -6.1 \times 10^{-1}, \text{ and}$$

$$\sigma^* = \text{net confining stress}$$

The mathematical expressions of the degree of saturation constitutive surfaces are as following:

$$S = S_0 + \frac{1 - S_0}{\left[1 + \left(\frac{u_a - u_w}{c} \right)^d \right]} \quad (6.129)$$

where

$$S_0 = a + b \ln(\sigma^*)$$

$$a = 0.354$$

$$b = 3.65 \times 10^{-3}$$

$$c = 7.91, \text{ and}$$

$$d = 0.977$$

The corresponding water content surface can be calculated as:

$$wG_s = Se = \left[S_0 + \frac{1 - S_0}{\left[1 + \left(\frac{u_a - u_w}{c} \right)^d \right]} \right] \left[e_u + \frac{e_s - e_u}{\left[1 + \left(\frac{u_a - u_w}{c} \right)^b \right]} \right] \quad (6.130)$$

Fig. 6.25 and Fig. 6.26 show the water content, void ratio, and degree of saturation constitutive surfaces for the collapsible soil.

Assuming a 3m thick soil layer with initial conditions that

$$\begin{aligned}(\sigma - u_a)_A &= 150 \text{ kPa}, \\(u_a - u_w)_A &= 350 \text{ kPa}\end{aligned}$$

A surcharge of $P = (\sigma - u_a)_B - (\sigma - u_a)_A = 300 - 150 = 150 \text{ kPa}$ is applied to the ground surface. Assume the ground surface has a constant suction of 350 kPa all the time. The soil is impermeable at the bottom of the layer (Fig. 6.27).

6.5.4.6.2 Determinations of Soil State Variables at Different Stages of the Consolidation Process

From the initial conditions, the void ratio, the degree of saturation can be calculated from Eq. 6.128 and 6.129. The corresponding water content can be calculated from Eq. 6.128 or the relationship $w = Se/G_s$, where $G_s = 2.64$. The calculation results are summarized in Table 6.5 (column 3).

Table 6.5. Calculation Results for the Consolidation of a Collapsible Soil

	Unit	Point A	Point B	Point C
Mechanical stress	(kPa)	150	300	300
Matric Suction	(kPa)	350	48.95	350
Void ratio e		0.723	0.602	0.697
water content w	(%)	10.6	10.6	10.3
Degree of Saturation S	(%)	38.7	46.5	39.0

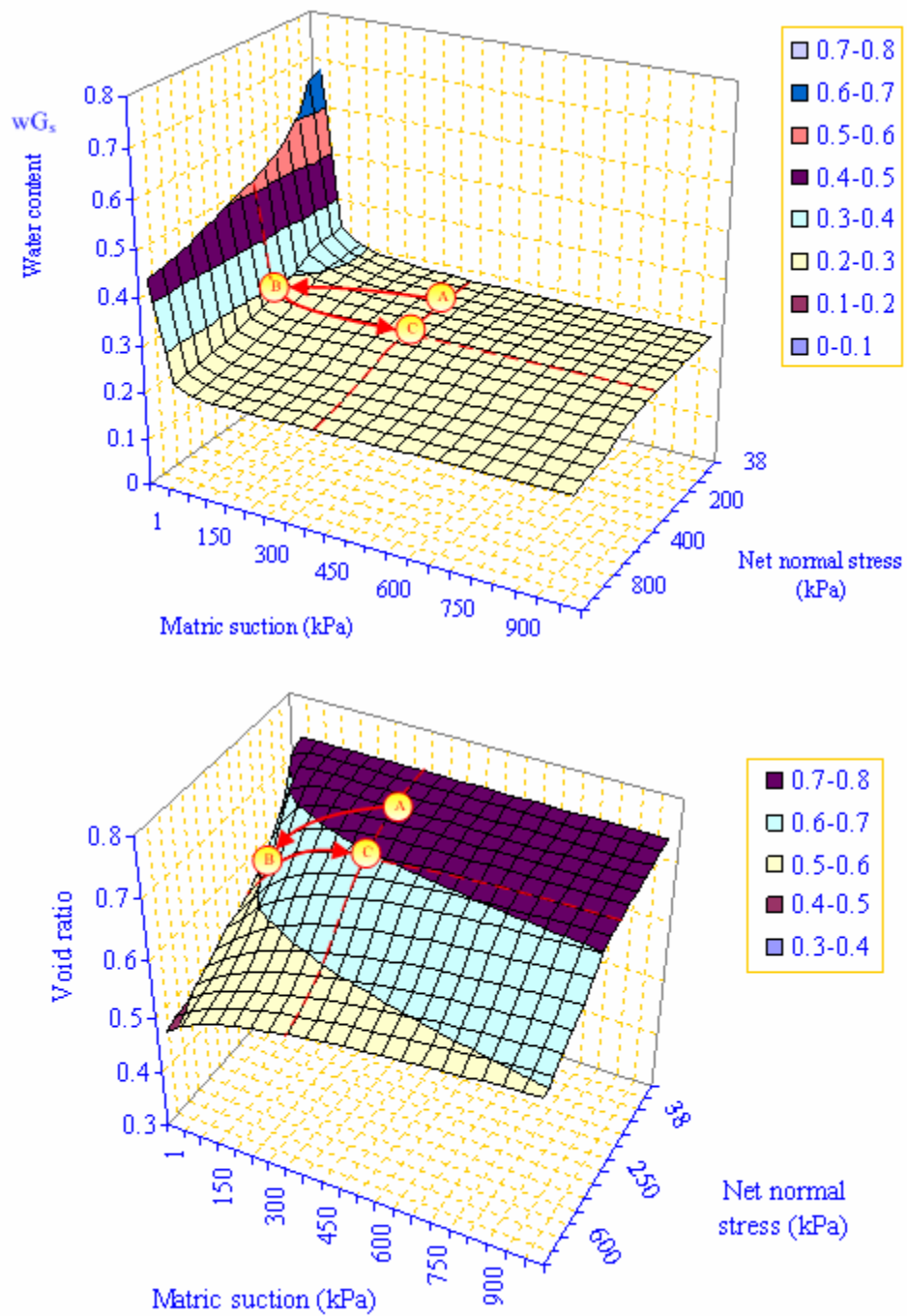


Fig. 6.25. Water content and void ratio constitutive surfaces for a collapsible unsaturated soil

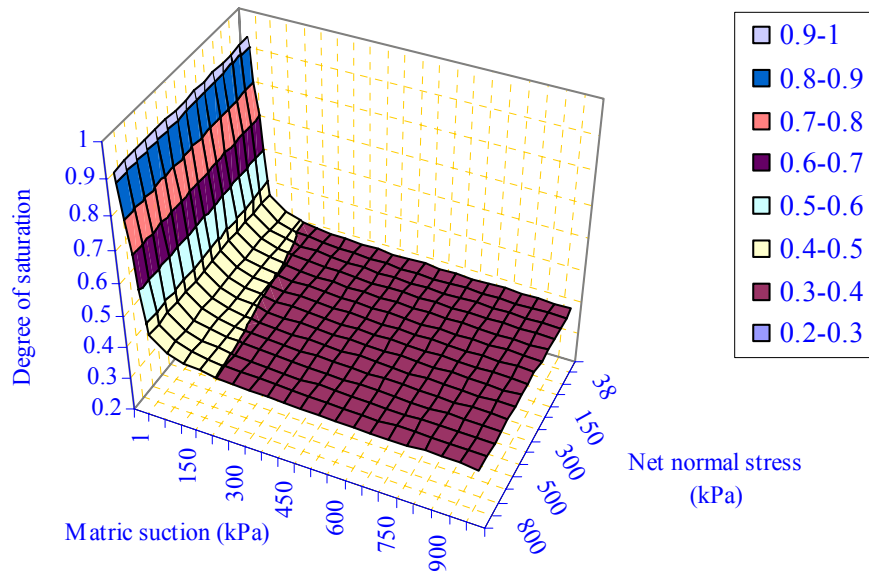


Fig. 6.26. Degree of saturation constitutive surface for a collapsible unsaturated soil

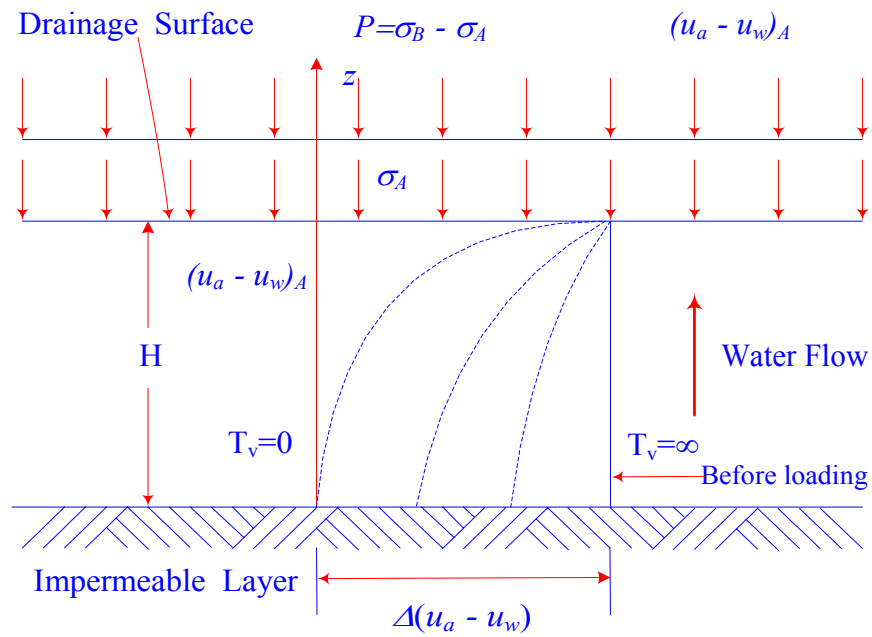


Fig. 6.27. Consolidation for a collapsible soil

At the instant of load application, the mechanical stress will increase from 150kPa to 300kPa, while the water content remains unchanged (10.6%). From these two

conditions, the matric suction can be solved, which is 48.95kPa. The corresponding void ratio and degree of saturation can be computed by inputting the matric suction and the mechanical stress in to Eq. 6.128, 6.129 and 6.130, respectively. The results are shown in the Table 6.5 (column 4).

If the load keeps the same (300kPa) all the time and the excess pore water pressure is allowed to dissipate under the constant surrounding matric suction (350kPa), finally the excess pore water pressure will dissipate completely at $t = \infty$ and the suction at any point of the soil layer will be 350kPa. From these two conditions, the void ratio, degree of saturation and water content of soil can be computed from Eq. 6.128, 6.129 and 6.130. The results are shown in the Table 6.5 (column 5).

The initial condition is taken as point A, the stage at the end of load application is taken as point B and the final stage at $t = \infty$ is taken as point C. These three points are also plotted on the void ratio and water content constitutive surfaces in Fig. 6.25. The stress paths of the consolidation process are also shown on the two constitutive surfaces.

Fig. 6.28 is the schematic plot of the void ratio and water content constitutive surfaces in the Fig. 6.25. From Fig. 6.28, at the instant of load application (from point A to point B), the water content is the same while the void ratio decreases (and degree of saturation increases). The matric suction decreases due to the load application. From point B to point C, the excess pore water pressure (excess matric suction) decreases along the constant mechanical stress curve (as shown in Fig. 6.28) while the void ratio increases along the constant mechanical stress curve. The increase in void ratio means the soil is swelling. The results are reasonable because the characteristic of a collapsible soil is when adding water to the collapsible soil, it will collapse (decrease in volume). Adding water to soil will cause soil matric suction to decrease. Therefore, the characteristic of a collapsible soil is that when matric suction decreases, the soil volume will decrease. From point B to point C, the matric suction of the soil increases. Therefore, the volume for the collapsible soil should also increase. It is also noted that all these calculations are performed under the assumption that the soil is elastic. Under most conditions, a collapsible soil is changed into a stable structure soil (expansive soil)

after the collapse is accomplished. Under this condition, the plasticity of the soil must be considered, which is out of the range of this research. If the collapse is not accomplished, the swelling may also be possible. Further research is needed in this direction. The investigation of the behavior of a collapsible soil under the elastic assumption is useful and a basis for the research of plastic behaviors.

6.5.4.6.3 Settlement Calculation

The immediate settlement at different stages can be calculated by Eq. 6.108:

$$\Delta H_1 = \frac{\Delta e_1}{1+e_0} H = \frac{e_B - e_A}{1+e_0} H = \frac{0.6025 - 0.7231}{1+0.7231} \times 3 = -0.210067 \text{ (m)}$$

The consolidation settlement can be computed by Eq. 6.109:

$$\Delta H_2 = \frac{\Delta e_2}{1+e_0} H = \frac{e_C - e_B}{1+e_0} H = \frac{0.6975 - 0.6025}{1+0.7231} \times 3 = 0.1654 \text{ (m)}$$

Therefore, total settlement can be obtained from Eq. 6.110:

$$\Delta H = \Delta H_1 + \Delta H_2 = \frac{e_C - e_A}{1+e_0} H = -0.2101 + 0.1654 = -0.0447 \text{ (m)}$$

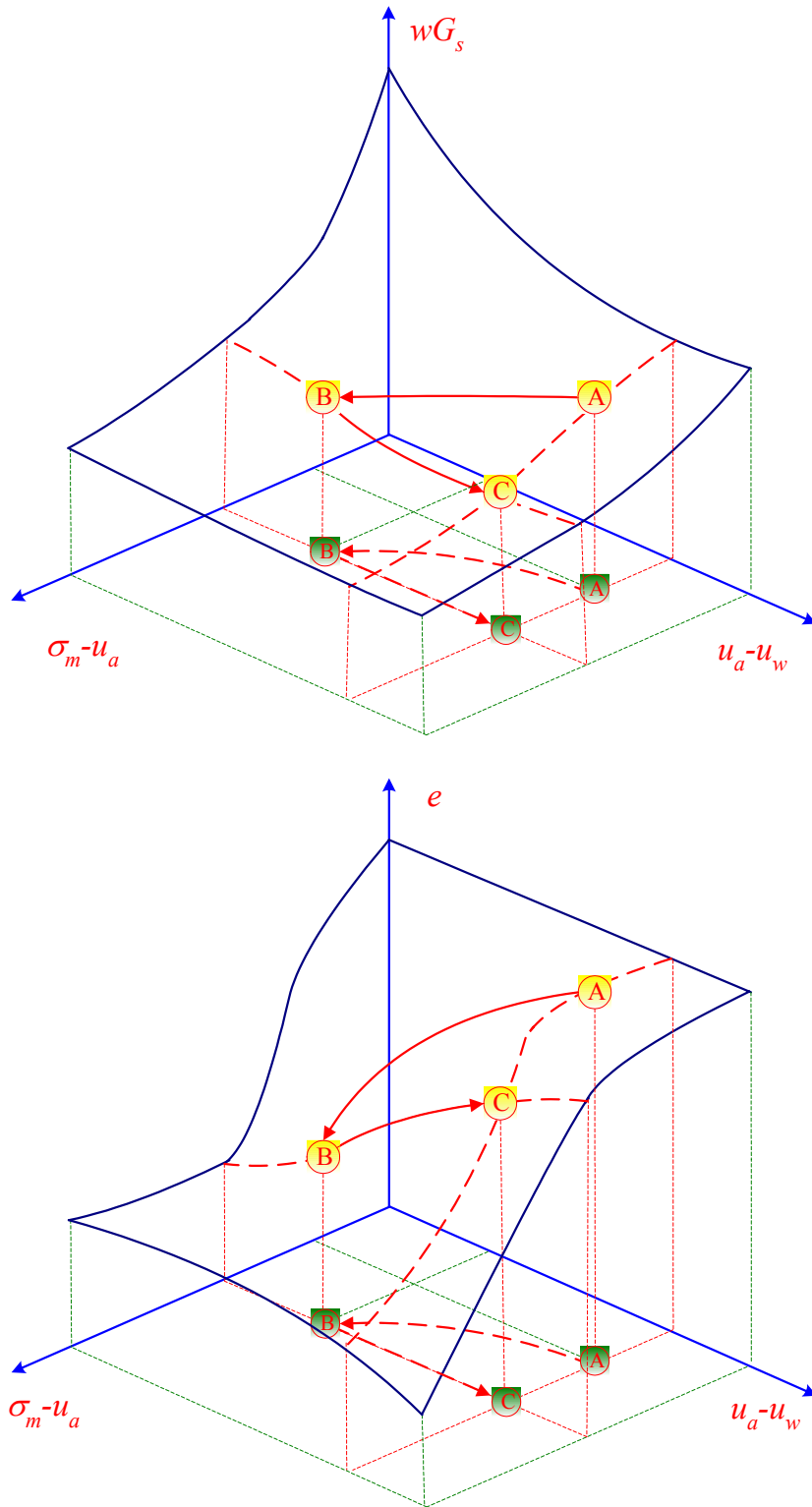


Fig. 6.28. Schematic plot of the consolidation process for the collapsible soil

The time rate of the consolidation settlement can also be solved in the same way as that proposed in the previous section. When calculating the time rate of the consolidation settlement, we need solve the differential equation for the water flow under the condition that mechanical stress is equal to 300 kPa. The permeability function of the soil is taken as that proposed by Pereira and D.G. Fredlund (1997),

$$k_w = k_p \left(\frac{\psi_{cr}}{(u_a - u_w)} \right)^\lambda \quad (6.131)$$

where $k_w \leq k_s$, $k_p = -1.39 \times 10^{-7} + 6.259 \times 10^{-8} \ln(\sigma^*)$, $k_s = 1.17 \times 10^{-6} - 1.8 \times 10^{-7} \ln(\sigma^*)$, is the coefficient of permeability fro the soil at saturation condition; $\psi_{cr} = 3.0$; and $\lambda = 2.90$.

When the mechanical stress is 300kPa, the permeability function of the soil is as shown in Fig. 6.29. The regression function for the soil permeability in the suction range between 48.95 kPa and 350 kPa is

$$k = \frac{k_0 (u_a - u_w)_0}{(u_a - u_w)} = \frac{4 \times 10^{-10}}{(u_a - u_w)} \quad (6.132)$$

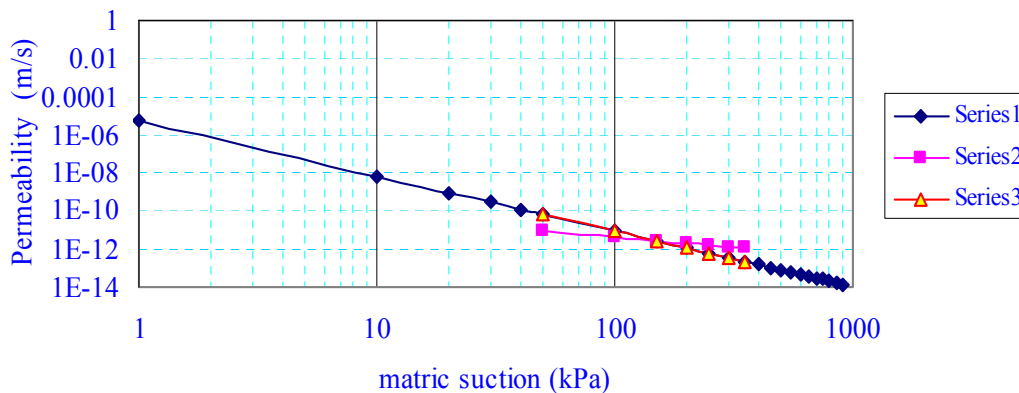


Fig. 6.29. Permeability function of the collapsible soil when the mechanical stress is equal to 300kPa

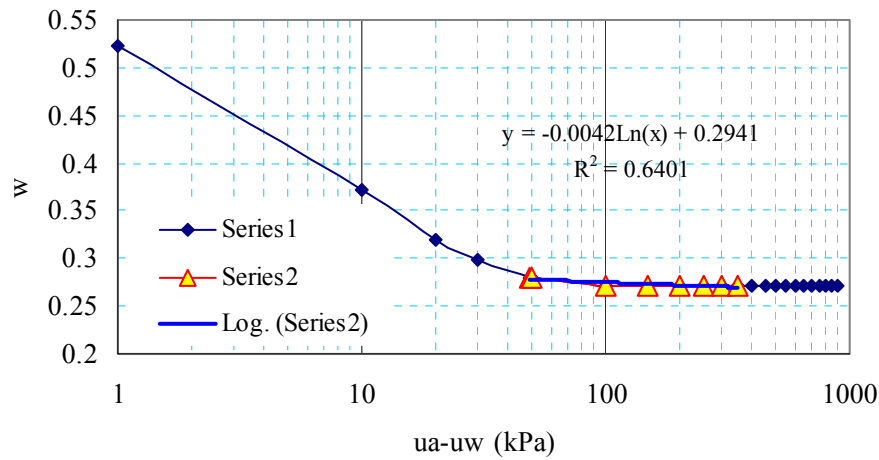


Fig. 6.30. Soil water characteristic curve of the collapsible soil when the mechanical stress is equal to 300kPa

The regression curve for the soil-water characteristic curve when the mechanical stress is 300kPa can be calculated from Eq. 6. 130 (or Fig. 6.26). The regression curve for the suction ranging from 48.95kPa to 350 kPa can be expressed as,

$$w = C_w \log_{10}(u_a - u_w) + D = -0.0036 \log_{10}(u_a - u_w) + 0.1114 \quad (6.133)$$

where C_w =slope of the soil water characteristic curve when it is plotted in a semi-log scale. Correspondingly,

$$\alpha = \frac{k_0 u_0}{0.4343 \frac{G_s}{1+e} C_w} = \frac{4 \times 10^{-10}}{0.4343 \frac{2.64}{1+0.6626} 0.0036} = 1.6112 \times 10^{-7}$$

Eq. 6.117 is then used to calculate the matric suction profiles at different time, and the results are shown in Fig. 6.30. The relationship between the void ratio and matric suction when the mechanical stress is equal to 300kPa i.e. $\sigma - u_a = 300kPa$, is

determined by Eq. 6.128, and the results are shown in Fig. 6.30. The void ratio profiles for the soil at different time can be calculated by combining the results from Fig. 6.31 and 6.32, which are plotted in Fig. 6.33. The consolidation settlement and the total settlement can be calculated by Eq. 6.111 and 6.112, and the results are plotted in Fig. 6.34. Fig. 6.34 indicates that under elastic assumption, the collapsible soil will rebound when the excess matric suction dissipates.

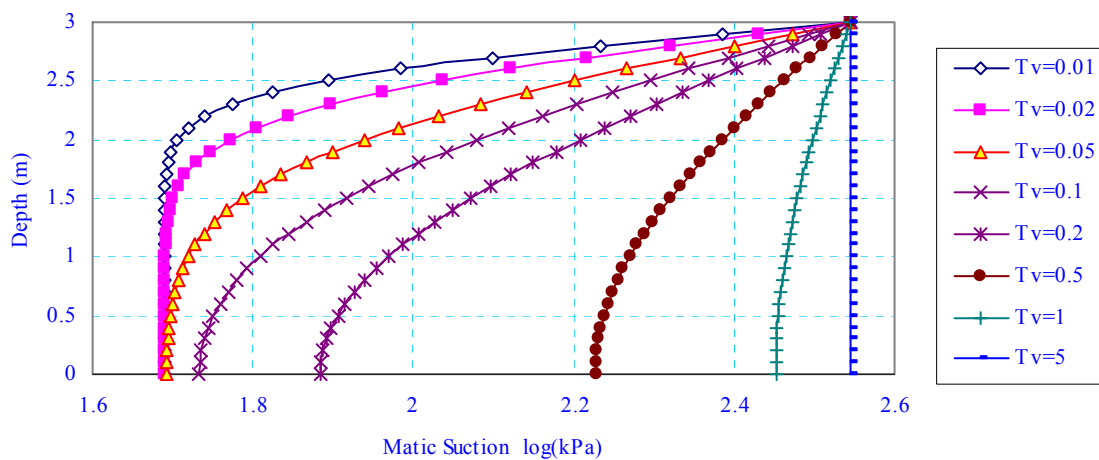


Fig. 6.31. Matric suction profiles for the collapsible soil at different times

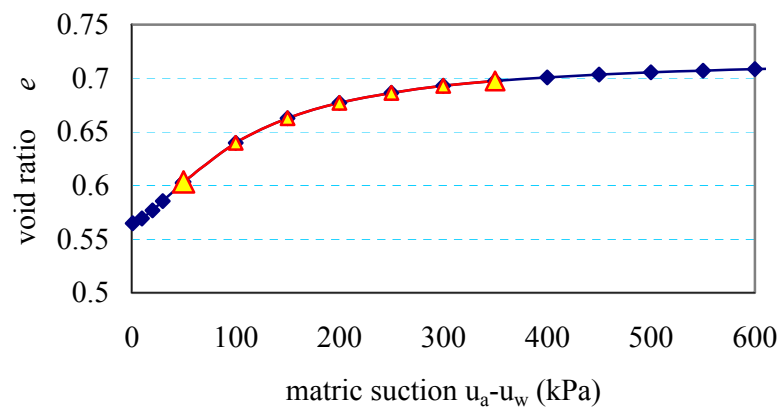


Fig. 6.32. The void ratio versus matric suction curve for the collapsible soil at $\sigma - u_a = 300 \text{ kPa}$

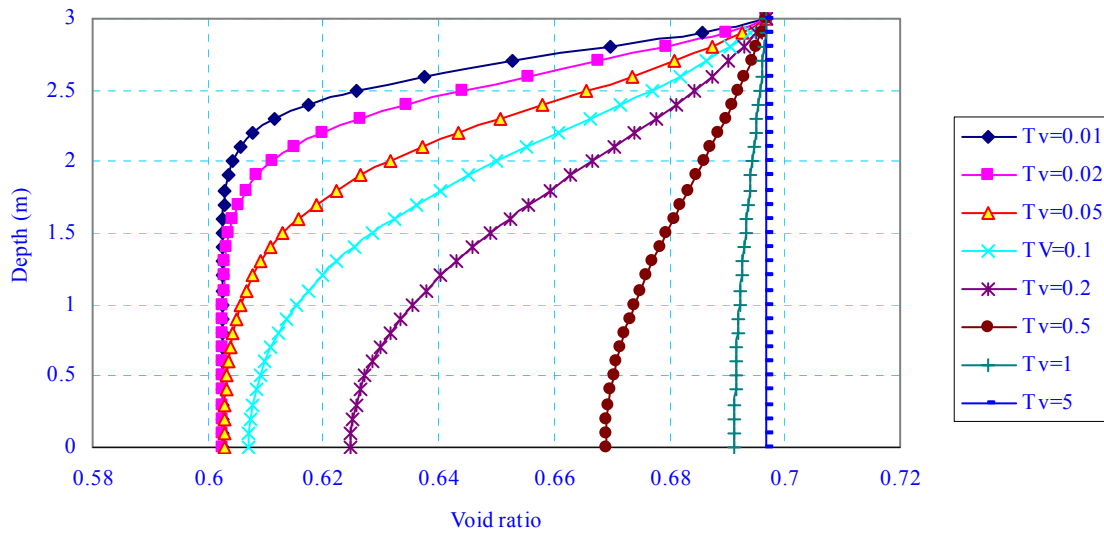


Fig. 6.33. Void ratio profiles for the collapsible soil at different times

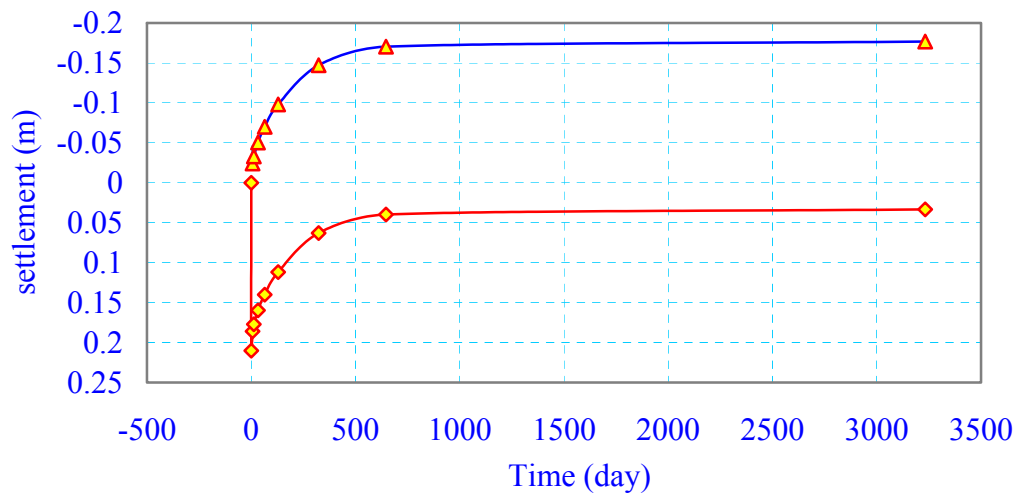


Fig. 6.34. Settlements of a collapsible soil at different times

6.5.5 Signs for the Parameters in the Constitutive Laws

Two typical unsaturated soils, an expansive soil and a collapsible soil, are used in the previous sections to illustrate the proposed method for the uncoupled consolidation

theory for unsaturated soils. From these two soils, signs of the parameters in the constitutive laws, m_1^s, m_2^s, m_1^w , and m_2^w in Eq. 6.76 and 6.77 or a_t, a_m, b_t , and b_m in Eq. 6.79, 6.80, 6.81 and 6.82, are investigated.

Recall that a_t is the slope of void ratio versus mechanical stress curve under constant matric suction condition. Curve AC in Fig. 6.13 shows the void ratio versus mechanical stress curve under constant matric suction for an unsaturated expansive soil. It indicates that when the compressive mechanical stress increases, the void ratio decreases. In other words, when a load is applied to an unsaturated expansive soil, the soil volume will decrease. Therefore, a_t or m_1^s has a negative sign.

Curve AC in Fig. 6.28 shows the void ratio versus mechanical stress curve under constant matric suction for an unsaturated collapsible soil. It indicates that when the compressive mechanical stress increases, the void ratio decreases. In other words, when a load is applied to an unsaturated collapsible soil, the soil volume will decrease. Therefore, a_t or m_1^s has a negative sign. In a summary, a_t or m_1^s has a negative sign for both expansive and collapsible soils.

a_m is the slope of void ratio versus matric suction curve under constant mechanical stress condition. Curve BC in Fig. 6.13 shows the void ratio versus the matric suction curve under the constant mechanical stress condition for an unsaturated expansive soil. It indicates that when the matric suction increases, the void ratio decreases. Correspondingly, a_m or m_2^s has a negative sign.

Curve BC in Fig. 6.28 shows the void ratio versus the matric suction curve under the constant mechanical stress condition for an unsaturated collapsible soil. It indicates that when the matric suction decreases, the void ratio decreases, which is a typical characteristic of collapsible soil. Therefore, a_m or m_2^s has a positive sign.

Similarly, we can find the signs for b_t (m_1^w) and b_m (m_2^w) from Fig. 12 for expansive soils and Fig. 6.28 for collapsible soils. It is found that both b_t (m_1^w) and a_m or m_2^s are negative for both expansive soils and collapsible soils. Recall that b_t is the slope of

water content versus mechanical stress under constant matric suction condition. A negative b_t (m_1^w) means when a load is applied to an unsaturated soil, the load tends to squeeze water out of the soil.

Also, because b_t is the slope of soil water characteristic curve (water content versus matric suction under constant mechanical stress condition), that b_m (m_2^w) is negative for both expansive soils and collapsible soils means when water is added to an unsaturated soil, it will always cause matric suction to decrease.

Fredlund and Rahardjo (1993) stated that b_m (or m_2^w) is positive for collapsible (metastable-structured) soils. Pereira and Fredlund (1997) also made the same statement. However, the soil water characteristic curves calculated from the void ratio and degree of saturation constitutive surface, that is, Eq. 6.128 and 6.129 or Fig. 6.25 and 6.26 respectively, indicate that b_m (or m_2^w) is negative. In another literature by Pereira (1996), calculations of m_2^w for the same soil show that m_2^w is negative. However, the author made a conclusion that m_2^w is positive, conflicting with his own calculations. A positive b_m (or m_2^w) value means that when adding water to a soil, the matric suction of the soil will increase. It is impossible and not reasonable.

The signs for all the parameters for different soils are summarized in Table 6.6. The calculation results of material parameters m_1^s , m_2^s , m_1^w , and m_2^w for the collapsible soil can also be found in the literature (Pereira 1996). It indicates for the collapsible soil, only m_2^s is positive.

Table 6.6. Summary of the Signs of Parameters in the Constitutive Laws

Soil \ Sign	a_t (or m_1^s)	a_m (or m_2^s)	b_t (or m_1^w)	b_m (or m_2^w)
Expansive Soils	-	-	-	-
Collapsible Soils	-	+	-	-

The signs for all the parameters for different soils can be explained by the bimodal model introduced in the Chapter II completely. Here no more discussion is made. It is noted that the shear dilation has not been considered. If there is shear dilation, the sign of the above material parameters can also be changed. a_t (m_1^s) and b_t (m_1^w) could be positive. More research is needed on this topic.

6.5.6 Validity of the Effective Stress Principle

During the past decades considerable work has been done to explain or predict the volume change behavior in terms of effective stresses. Bishop (1959) extended Terzaghi's classical expression of the effective stress principle for saturated soils to Bishop's equation for unsaturated soils. Aitchison (1961) and Jennings (1961) also proposed the similar equations. However, it was shown that there was no simple general χ value for most unsaturated soils and that χ is a variable related to total stress, pore water pressure, stress path and soil types.

Jennings and Burland (1962) concluded that the effective stress principle was not valid for collapsible soils because "With reference to Bishop's equation, a process of soaking the soil will bring about a reduction of the matric suction, which representing a decrease in effective stress. On the basis of the effective stress principle this decrease in effective stress should be accompanied by an increase in the volume of the soil. Consequently, in every case when the partially saturated soil was soaked under constant applied load, it undergoes additional settlement or "collapsed". This occurred even when soaking took place at small values of applied load. Clearly, the collapse is the reverse of the behavior predicted on the basis of the effective stress principle".

Matyas and Radhakrishna (1968) used the two stress state variables $\sigma - u_a$ and $u_a - u_w$ to describe the volume change behavior of unsaturated soils. They found that the volume of unsaturated soils can be uniquely expressed as a function of the two stress state variables $\sigma - u_a$ and $u_a - u_w$. They also used their test result to calculate the χ value

for a collapsible soil and found that a negative χ value for the soil. As a consequence they concluded that the effective stress principle is not valid.

These conclusions and the following null tests by Fredlund and Morgenstern (1977) lead to an extensive acceptance of the two stress state variable concept.

However, the above reasoning is questionable. Most Authors have tacitly assumed that χ “should be positive and less than unity” (Matyas and Radhakrishna 1968). The tacit assumption leads to an increase in matric suction will always cause increase in effective stress and decrease in volume, which is the contrary to the collapsible soil behaviors. However, the assumption is questionable. Combine Eq. 6.44, 6.66, 6.79 and 6.80, gives,

$$\chi = 3\alpha B = \frac{m_2^s}{m_1^s} = \frac{a_m}{a_t} \quad (6.134)$$

Table 6.6 shows that a_t or m_1^s is negative for both expansive soils and collapsible soils while a_m or m_2^s is negative for expansive soils but positive for collapsible soil. As a consequence, χ is positive for expansive soils and negative for collapsible soils.

If χ is negative, the collapsible soil behaviors can be explained by the effective stress principle too. When a collapsible soil is soaked, the matric suction of the soil will decrease. The decrease in matric suction will cause an increase in effective stress according to Bishop’s Equation because χ is negative. The soil volume therefore will decrease. Actually, as far as the equivalent effective stress itself is concerned, the corresponding effective stress can always be found for any combination of total mechanical stress and matric suction for any volume change (swell or collapse).

Most researchers assumed that χ should be positive and less than unity because they considered the effective stress defined by Bishop’s Equation is a microscopic intergranular effective stress while it is actually a macroscopic equivalent effective stress, which will be explained in the following section.

6.5.7 Bimodal Explanation of Soil Behaviors: Expansive or Collapsible

The soil behavior can be explained by the bimodal pore distribution discussed in the Chapter II. Single clay particles are surrounded by water and form a double diffusion layer. They grouped together to form aggregates. Under most cases, the aggregates are saturated internally due to the micropores formed by the single clay particles are so small and the corresponding air entry values are so high. Terzaghi's effective stress principle therefore holds internally in the aggregates. The soil is then composed of a lot of "granular" aggregates. Between aggregates there are a lot of macropores. The single soil particles and water are incompressible while as a consequence of grouping of aggregates, the soil structure is compressible, especially when there is air in the macropores.

When an externally loaded unsaturated soil is soaked in the water, soil will absorb water and the matric suction will decrease. The intergranular effective stress internally in the aggregates therefore will decrease. The double diffusion layers for the single clay particles will become thick and the soil aggregates will swell. The decrease in matric suction will also cause the soil structure become more compressible due to the more deformable aggregates. Under the same load, the soil volume will decrease.

A reduction in matric suction therefore has a two-fold effect on soil structure, namely a reduction in intergranular stress and a reduction in the rigidity of the soils structure. The former will cause soil aggregates to expand and then the soil to swell while the latter will cause soil structure easy to compress. The macroscopic volume change of the soil will depend on the combination of these two effects. If the soil volume increases, the soil is an expansive soil (χ is positive). Otherwise, the soil will be a collapsible soil (χ is negative). The effective stress defined by Bishop's equation therefore should be a macroscopic concept instead of the intergranular stress.

It is possible that some expansive soils can also exhibit some degree of collapse behavior (Jennings and Burland 1962), depending on the applied external stresses. If the external applied stress is small, when soaking an expansive soil in water, it is possible that the increase in the soil volume caused by the decrease in intergranular stress will be

greater than the decrease in the soil volume caused by the decrease in the rigidity of the soil structure. The soil therefore exhibits as an expansive soil.

On the contrary, if the applied external stress is high, at some point, it is possible that, when the same soil is soaked in water, the increase in the soil volume caused by the intergranular stress decrease will be less than the decrease in the soil volume caused by the decrease in the rigidity of the soil structure. The soil therefore exhibits as a collapsible soil. After the collapse, the soil structure will be more stable. It is possible that a further increase in the applied external load will make the soil an expansive soil again.

6.5.8 Two- or Three Dimensional Uncoupled Consolidation Theory for Unsaturated Soils

The above discussion is for one dimensional coupled and uncoupled case. For two – or three dimensional uncoupled consolidation, there is no close-form solution for the differential equation for the water phase. Numerical method must be used instead. Firstly the excess pore water pressure can be determined in the same way as the above discussion. The calculation results are then used as the initial conditions for the numerical simulation.

The uncoupled two- and three- consolidation theory for saturated-unsaturated soils are discussed under the assumption that the total stresses remain constant during the process of consolidation. The assumption is not true. However, the assumption greatly simplifies the problem and the results obtained under this assumption can provide helpful information for the consolidation behavior of the unsaturated soil.

To discuss the uncoupled two and three-dimensional consolidation theory, firstly the constitutive surfaces for the soils must be known. The similar method as we proposed in the previous section can be used. The only difference is that the constitutive surface for the three dimensional consolidation will use the average total mechanical stress and matric suction as the mechanical stress axis and matric suction axis respectively while the one dimensional consolidation theory uses the vertical mechanical stress σ_v and

matrix suction. The reason for this is the volumetric strain for three-dimensional consolidation occurs in three directions while it occurs in only vertical direction for one-dimensional consolidation.

6.6 The Coupled Consolidation Theory for Saturated-Unsaturated Soils

In the uncoupled consolidation theory for saturated-unsaturated soils, it is assumed that the total stress remain constant during the process of consolidation, which is not strictly true for two- or three- dimensional conditions. A thermodynamic analogue can be used to illustrate the problem more clearly.

A solid steel cylinder with a diameter of R is inserted into a steel ring with the exact same inner diameter as shown in Fig. 6. 35. The cylinder and the ring are in good contact but there is no stress between them. Both of them have an initial temperature of 20°C . The ring is then allowed to cool down to 10°C while the cylinder keeps its initial temperature, 20°C . Stress will be generated between the ring and the cylinder due to the non-uniform temperature distribution and the resulting differential deformation, namely, the ring tends to shrink and reduce its inner diameter to a value less than R while the cylinder is tending to keep the same diameter R . In this case, we can see the differential deformations can generate stresses in the material.

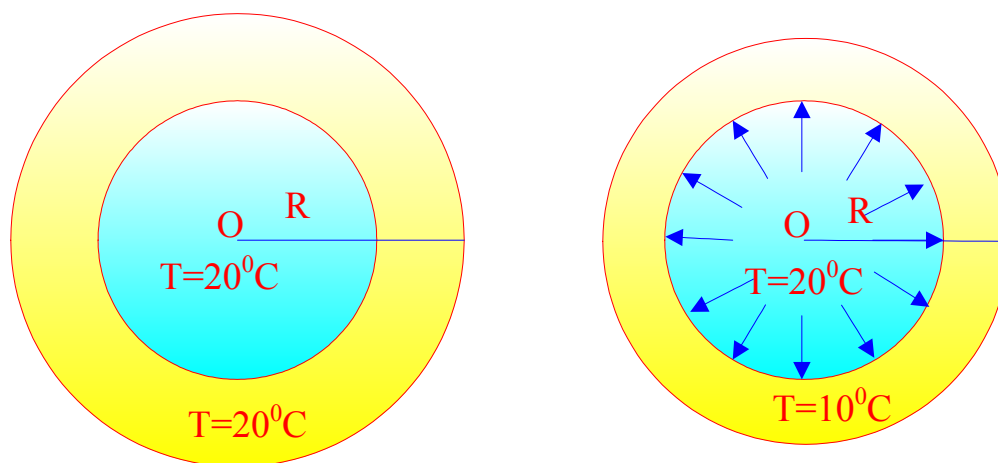


Fig. 6.35. Cooling down of a ring attached on a solid cylinder

A similar phenomenon can occur during the consolidation of a soil. In this section, the coupled consolidation theory for saturated-unsaturated soils is discussed.

6.6.1 The Coupled Consolidation Theory for Saturated Soils

6.6.1.1 The Biot's Consolidation Theory for Saturated Soils

Biot (1941) proposed a two- or three- dimensional consolidation theory for saturated soils. It is also called true two- or three- dimensional consolidation theory because it considered that the total stress is varying during the consolidation process. The differential equations for Biot's three dimensional consolidation theory are:

$$\begin{aligned} G\nabla^2 u + \frac{G}{1-2\mu} \frac{\partial \varepsilon_v}{\partial x} - \frac{\partial u_w}{\partial x} + X &= 0 \\ G\nabla^2 v + \frac{G}{1-2\mu} \frac{\partial \varepsilon_v}{\partial y} - \frac{\partial u_w}{\partial y} + Y &= 0 \\ G\nabla^2 w + \frac{G}{1-2\mu} \frac{\partial \varepsilon_v}{\partial z} - \frac{\partial u_w}{\partial z} + Z &= 0 \end{aligned} \quad (6.135)$$

$$\frac{k}{\rho_w g} \left[\left(\frac{\partial^2 u_w}{\partial x^2} \right) + \left(\frac{\partial^2 u_w}{\partial y^2} \right) + \left(\frac{\partial^2 u_w}{\partial z^2} \right) \right] = - \frac{\partial \varepsilon_v}{\partial t} \quad (6.136)$$

Eq. 6.135 and 6.136 can also be derived by considering the saturated soils as a special case of unsaturated soils. Recall the void ratio constitutive surface for a saturated soil is,

$$e = f(\sigma') = f(\sigma - u_w) = f((\sigma - u_a) + (u_a - u_w)) \quad (5.3)$$

and the water content constitutive surface for a saturated soil is,

$$wG_s = Se = e = f(\sigma') = f(\sigma - u_w) = f((\sigma - u_a) + (u_a - u_w))$$

There is no air in the saturated soil, namely $u_a = 0$. Therefore we have,

$$\begin{aligned} m_1^s &= \frac{1}{1+e_0} \frac{\partial e}{\partial(\sigma-u_a)} = \frac{1}{1+e_0} \frac{\partial f(\sigma-u_w)}{\partial \sigma} \\ m_2^s &= \frac{1}{1+e_0} \frac{\partial e}{\partial(u_a-u_w)} = \frac{1}{1+e_0} \frac{\partial f(\sigma-u_w)}{\partial(-u_w)} \\ m_1^w &= \frac{G_s}{1+e_0} \frac{\partial w}{\partial(\sigma-u_a)} = \frac{G_s}{1+e_0} \frac{\partial f(\sigma-u_w)}{\partial \sigma} \\ m_2^w &= \frac{G_s}{1+e_0} \frac{\partial w}{\partial(u_a-u_w)} = \frac{G_s}{1+e_0} \frac{\partial f(\sigma-u_w)}{\partial(-u_w)} \end{aligned}$$

that is,

$$m_1^s = m_2^s = m_1^w = m_2^w = \frac{1}{1+e_0} \frac{\partial f}{\partial \sigma'} \quad (6.137)$$

Recall the relationship,

$$\lambda = \frac{E\mu}{(1+\mu)(1-2\mu)}, G = \frac{E}{2(1+\mu)}$$

$$m_1^s = \frac{1}{B} = \frac{3(1-2\mu)}{E}$$

$$m_2^s = 3\alpha$$

$$m_2^w = \frac{G_s}{1+e_0} \frac{dw}{d(u_a-u_w)} = \rho_d C_w$$

and the definition of the two parameters β_{w1} and β_{w2} in Eq. 6.90, we have,

$$\beta_{w1} = \frac{m_1^w}{m_1^s} = 1$$

$$\beta_{w2} = (m_2^w - m_1^w \frac{m_2^s}{m_1^s}) = 0$$

Substituting into Eq. 6.65 and 6.90, we can get the exactly same equation as Eq. 6.135 and 6.136.

It will be much clear if we further derive the Eq. 6.136 in the Following way. Considering for saturated soils,

$$d\varepsilon_v = \frac{1}{1+e_0} \frac{\partial e}{\partial \sigma'} d\sigma' = \frac{\alpha_v}{1+e_0} d(\sigma_m - u_w) \quad (6.138)$$

Eq. 6.136 can be also written as,

$$C_{v3} \left[\left(\frac{\partial^2 u_w}{\partial x^2} \right) + \left(\frac{\partial^2 u_w}{\partial x^2} \right) + \left(\frac{\partial^2 u_w}{\partial x^2} \right) \right] = \frac{\partial u_w}{\partial t} - \frac{\partial \sigma_m}{\partial t} \quad (6.139a)$$

where $C_{v3} = \frac{k(1+e_0)}{\alpha_v \gamma_w}$

Eq. 6.139a can also be obtained by substituting Eq. 6.137 and 6.138 into Eq. 6.65 and 6.73. Therefore, Eq. 6.65 and 6.73 are the differential equations for both saturated and unsaturated soils. The only difference between a saturated soil and an unsaturated soil is that for a saturated soil Eq. 6.137 must be satisfied while for an unsaturated soil there is no such relationship existing among these material parameters. Eq. 6.65 and 6.73 must be solved simultaneously. The externally applied load will be used as boundary conditions to calculate the excess pore water pressure.

In Terzaghi's consolidation theory, the total stress is considered to be constant during the consolidation process. Hence, $\frac{\partial \sigma_m}{\partial t} = 0$. Eq. 6.139a therefore is changed into,

$$C_{v3} \left[\left(\frac{\partial^2 u_w}{\partial x^2} \right) + \left(\frac{\partial^2 u_w}{\partial x^2} \right) + \left(\frac{\partial^2 u_w}{\partial x^2} \right) \right] = \frac{\partial u_w}{\partial t} \quad (6.139b)$$

Eq. 6.135 and Eq. 6.139b are the differential equations for the three dimensional uncoupled consolidation theory for saturated soils (Terzaghi 1943). These two equations are uncoupled because Eq. 6.139b includes only one unknown: pore water pressure. Usually Eq. 6.139b is solved firstly and then the results are put into Eq. 6.135 to solve the total and effective stresses. The initial condition for 6.139b is excess pore water pressure. Therefore, the excess pore water pressure must be calculated before solving Eq. 6.139b, which is equal to the applied load according to Terzaghi's consolidation theory.

6.6.1.2 Mandel-Cryer Effect

When Biot's consolidation theory is used to analyze the consolidation process of a saturated soil, unlike that in Terzaghi's consolidation theory, the excess pore water pressure will increase at the initial stage sometimes, gradually reach the peak, and then dissipate gradually. The maximum excess pore water pressure during the consolidation is greater than the applied load, which is different from what assumed by Terzaghi's consolidation theory.

This phenomenon was firstly studied by Mandel (1953) when he analyzed the consolidation of a saturated soil cylinder under an axis-symmetric external load. Cryer (1963) also found the similar phenomenon in the consolidation of a soil ball with a uniform radial external load. This phenomenon is then called Mandel-Cryer effect. Gibson et al. (Gibson et al. 1963) verified the effect by performing the consolidation test for a soil ball. Fig. 6.36 shows the schematic comparison between Terzaghi's and Biot's consolidation theory.

Mandel-Cryer effect can be explained by Fig. 6.37 and 6.38(Qian and Ying 1993). Fig. 6.37 is a soil cylinder with uniform compression load P. Fig. 6.38 is the pore water

pressure distribution along with the radius. At $t=0$, $u_0=P$ is shown as line ML in Fig. 6.38. At $t=t_1$, there is drainage at the boundary and the pore water pressure at point A decreases. For a saturated clay soil, because the permeability of the soil is usually is very low, the initial dissipation of the excess pore water pressure will be limited in a certain range, say, between r_A and r_B . There is no drainage in the range between the center point O and r_B . The excess pore water pressure distribution should have been as Curve MNA. However, the water drainage will cause the effective stress to increase in the outer shell and the outer shell tends to shrink inwards. At the same time, the range between the center point and r_B has no drainage and no volume change. Therefore, the outer shell will apply some compressive force on the inner sphere besides the applied load P just like what has been discussed in Fig. 6.35. Consequently the total mechanical stress at the inner part will be higher than the applied load, which is sustained by the pore water and cause a pore water pressure higher than the applied load. The actual pore water pressure distribution will be Curve M'N'A instead of MNA. With the consolidation proceeding, the pore pressure will increase till it reaches a peak. After the pore water pressure reaches the peak, the decrease caused by the dissipation of pore water pressure is greater than the increase in the pore water pressure caused by the mechanical stress variation. The pore water pressure in the soil will decrease gradually and finally be in equilibrium with the environment. Past research indicates that the Mandel-Cryer effect depends on soil permeability and Poisson's Ratio. When Poisson's Ratio equal to 0.5 there is no such effect. The smaller the Poisson's ratio, the more serious the Mandel-Cryer effect is.

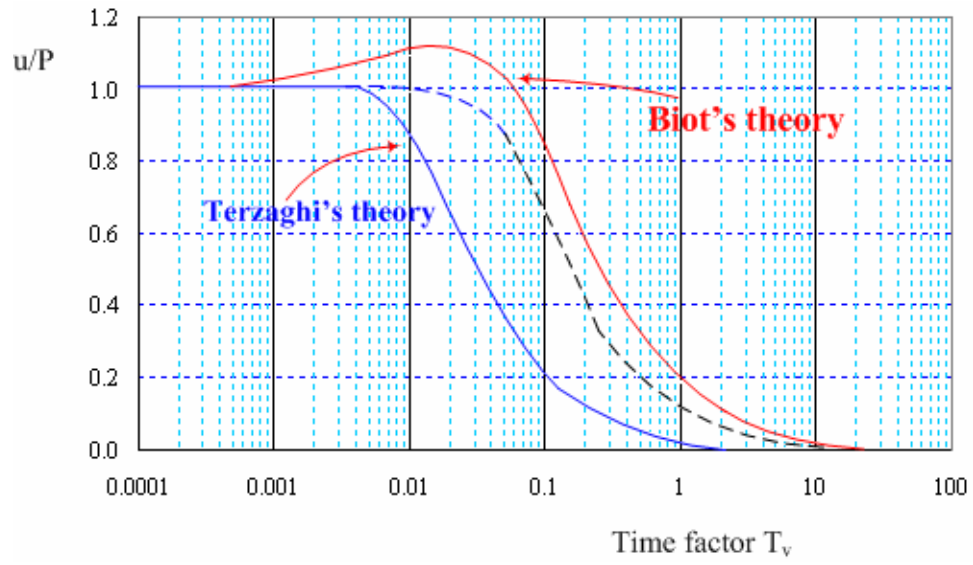


Fig. 6.36. Mandel-Cryer effect (Qian and Ying 1993)

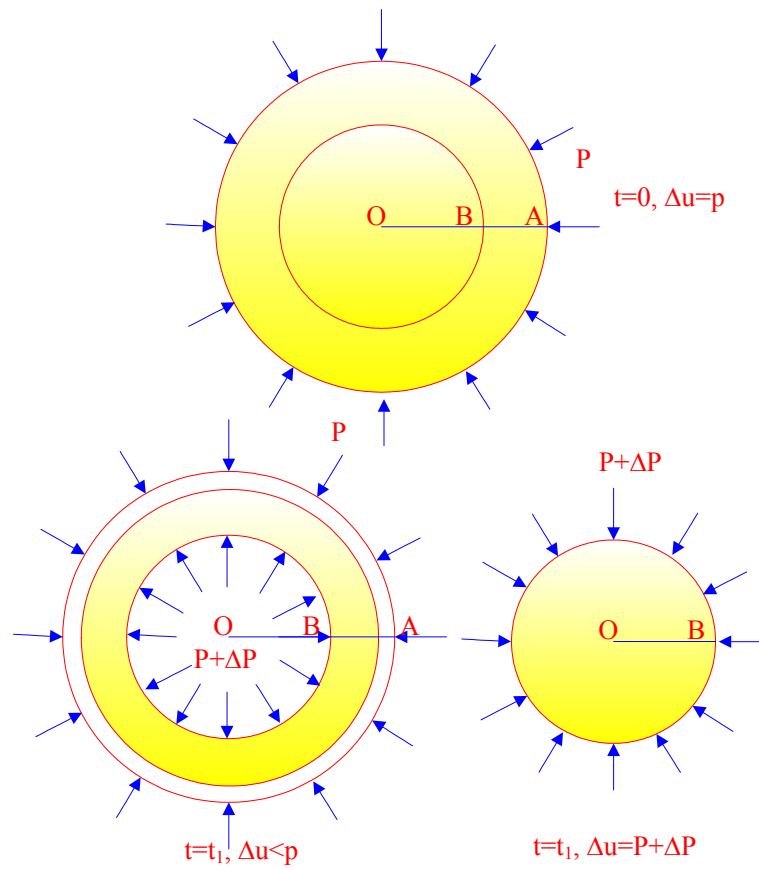


Fig. 6.37. Total stress variations during the consolidation process of a soil cylinder

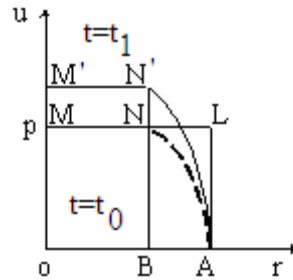


Fig. 6.38. Explanation of the Mandel-Cryer effect (Qian and Ying 1993)

In conclusion, there is some difference in the solutions between the coupled and uncoupled consolidation theory for saturated soils. For unsaturated soils, no research has been done in this direction so far according to my knowledge. Such research requires the utilization of numerical methods. Therefore, before the further discussion in solving the differential equations for the coupled consolidation theory for unsaturated soils, a method is proposed to solve the coupled consolidation theory for saturated-unsaturated soils by modifying the existing program for the analysis of the coupled thermal stress.

6.6.2 Using the Coupled Thermal Stress Analysis Program to Solve the Differential Equations for the Coupled Consolidation Theory for Saturated-Unsaturated Soils

6.6.2.1 Modification of the Coupled Thermal Stress Analysis Program in ABAQUS

Numerical method is needed when solving the coupled consolidation theory for saturated-unsaturated soils. At present available commercial programs for solving the coupled differential equations for the consolidation of unsaturated soils are still scarce. Pereira (1996) developed a computer program called COUPSO based on the Eq. 6.65 and 6.90. Olivella et al. (1996) developed a computer program called CODE_BRIGTH to couple the deformation, transport of brine, gas and heat transport problem. It is more complicated and should be able to solve the coupled consolidation problem for unsaturated soils. In this section, how to modify the current available coupled thermal stress program to solve the coupled consolidation problem for saturated-unsaturated soils

is discussed. It is meaningful. First of all available computer programs for this problem are still scarce and programming a new code is time-consuming and very expensive. By modifying the available commercial code for the coupled thermal stress problem, we can fully utilize available resources to perform complicated research for saturated-unsaturated soils. It is very cost-saving and can be extensively used. Second, it is advantageous for the next step research. The objective of the dissertation is to investigate the behaviors of foundations and structures on expansive soils. The simulation involves the volume change of expansive soil, namely the coupled consolidation problem for saturated-unsaturated soils, the soil structure interaction by contact (jointed) elements, and the simulation of the walls by general shell elements. So far to my knowledge, no available program can perform such a complicated simulation in the geotechnical engineering, especially for unsaturated soils. On the contrary, there are a lot of well-established commercial programs in mechanical engineering, which can handle the coupled thermal stress analysis, contact simulation and shell behavior analysis at the same time. By modifying the available thermal stress problem to solve the coupled consolidation problem for saturated-unsaturated soils, the complicated problem can be solved at the lowest price.

In the previous section, it is found that there are close similarities between the coupled thermal stress problem and the coupled consolidation theory for unsaturated soils. These similarities provide the opportunity to use the coupled thermal stress analysis to solve the coupled consolidation problem for unsaturated soils. From the previous discussion (Eq. 6.91 and 6.92), it can be seen that the only difference between them is that the coupled thermal stress problem does not consider the heat generation due to the mechanical stress variation, that is m_1^w is always zero. In other words, the only difference is that in Eq. 6.92d, it lacks a $m_1^w \frac{\partial \sigma_m}{\partial t}$ term. This means when we use the coupled thermal stress analysis to solve the consolidation of soils, there is no excess pore water pressure when there is load application because $d(u_a - u_w)$

$= -\frac{m_1^w}{m_2^w} d(\sigma_m - u_a) = 0$. To solve this problem, it is proposed to consider the $m_1^w \frac{\partial \sigma_m}{\partial t}$ as a “heat generation” or “source” term because $m_1^w d\sigma_m$ is the heat generation due to mechanical stress variation for the coupled thermal stress problem. $m_1^w \frac{\partial \sigma_m}{\partial t}$ therefore is the heat generation due to mechanical stress variation in a unit time.

ABAQUS is used in this dissertation to perform the whole simulation for the coupled consolidation of saturated-unsaturated soils. In ABAQUS, the “coupled thermal stress analysis” option is provided. The Eulerian description of Eq. 6.92d is used, which is as following,

$$\int_V \rho \dot{U} dV = \int_S q dS + \int_V r dV$$

or,

$$\int_V \rho \left(\dot{U} - \frac{r}{\rho} \right) dV = \int_S q dS \quad (6.140)$$

where V = volume of solid material; S = surface area; ρ = material density; \dot{U} = the material time rate of the internal energy; q = heat flux per unit area of the body; flowing into the body, and r = heat supplied externally into the body per unit volume.

Comparing Eq. 6.91d, 6.92d, and 6.142, we have,

$$S = S(\sigma_m) = r = m_1^w \frac{\partial \sigma_m}{\partial t} \quad (6.141)$$

ABAQUS does provide an option called “heat generation” for the coupled thermal stress analysis. The heat generation term in Eq. 6.141 however is a function of

mechanical stress variations. The mechanical stress variations are unknown during the consolidation process and need be calculated by solving the differential equations. This kind of situation can not be handled by the heat generation directly. Subroutines are therefore needed to calculate the mechanical stress variation and the corresponding source term. Two user subroutines, UMATHT and USDFLD, are used to accomplish this objective (Appendix C.1.2). A utility subroutine GETVRM is used to access the mechanical stresses at every material point in the calculation domain and a user subroutine called USDFLD is used to calculate the mean mechanical stress and the mean mechanical stress variation between the current step and the previous step, and then the mechanical stress variation is transferred into the subroutine UMATHT.

The subroutine UMATHT can be used to define the thermal constitutive behavior of the material as well as the internal heat generation during the heat transfer process. It is therefore used to define the constitutive law for the water phase for the consolidation problem for saturated-unsaturated soils. In ABAQUS, the original constitutive law for the heat transfer for the coupled thermal stress problem is Eq. 6.16a ($dE_T = \rho C_T dT$), which is written as,

$$DU = DUDT * DTEMP \quad (6.142)$$

where DU=thermal energy variation; DUDT =the specific heat capacity; and DTEMP = temperature variation.

The mass density is input in the main program. Recall that the commensurate constitutive law for the coupled consolidation theory for soils is Eq. 6.18($dE = m_1^w d\sigma + \rho C_T dT$), Eq. 6.142 is therefore modified as,

$$DU = DUDT * DTEMP + E1W * DSIGMAM \quad (6.143)$$

where $E1W$ = heat generation parameter m_1^w ; and $DSIGMAM$ = the mechanical stress variation between the previous and current calculation step $d\sigma_m$, which is obtained from the user subroutine USDFLD(Appendix C.1.2.1.).

6.6.2.2 Verification: Solving the Biot's Consolidation Theory by Using the Modified Coupled Thermal Stress Program

As discussed previously, Eq. 6.65 and 6.73 are differential equations for the consolidation for both saturated and unsaturated soils. Saturated soils are a special case of unsaturated soils with the relationship $m_1^s = m_2^s = m_1^w = m_2^w$. As a consequence, the proposed modification for the simulation of the consolidation for unsaturated soils should also be able to solve the coupled consolidation problem for saturated soils.

An example is used to verify the proposed modification. Qian and Ying (1993) analyzed the consolidation of a soil cylinder by using the Biot's consolidation theory. Assume that there is a clay column with a radius $R=15m$ (Fig. 6.39). The soil properties are listed as follows:

Young's Modulus	$E=10,000kPa$
Poisson's Ratio	$\mu=0.3$
Coefficient of permeability of	$k=1.16 \times 10^{-6}cm/s$

A load $P=1,000kPa$ is applied uniformly in the radial direction, and the soil water is drained in the radial direction freely.

To perform a coupled consolidation analysis by using the modified coupled thermal stress problem, the following material parameters are needed: coefficient of expansion α , heat generation parameter m_1^w and specific heat capacity. The soil density is assumed to be 1 in order that m_2^w can be used as specific heat capacity directly in the program. From Eq. 6.83, 6.84 and 6.85, we have,

$$m_1^s = \frac{1}{B} = \frac{3(1-2\mu)}{E} = \frac{3 \times (1-2 \times 0.3)}{1 \times 10^4} = 1.2 \times 10^{-4}$$

For saturated soils, $m_1^s = m_2^s = m_1^w = m_2^w$. Correspondingly

$$\alpha = \frac{m_2^s}{3} = 4 \times 10^{-5}$$

$$m_2^w = \rho C_T = m_1^w = 1.2 \times 10^{-4}$$

The mesh generation is shown in Fig. 6.39 and the input files for this problem are attached in Appendix C.1. The calculation results are shown in Fig. 6.40, which the same as that was obtained by Qian and Ying (1993).

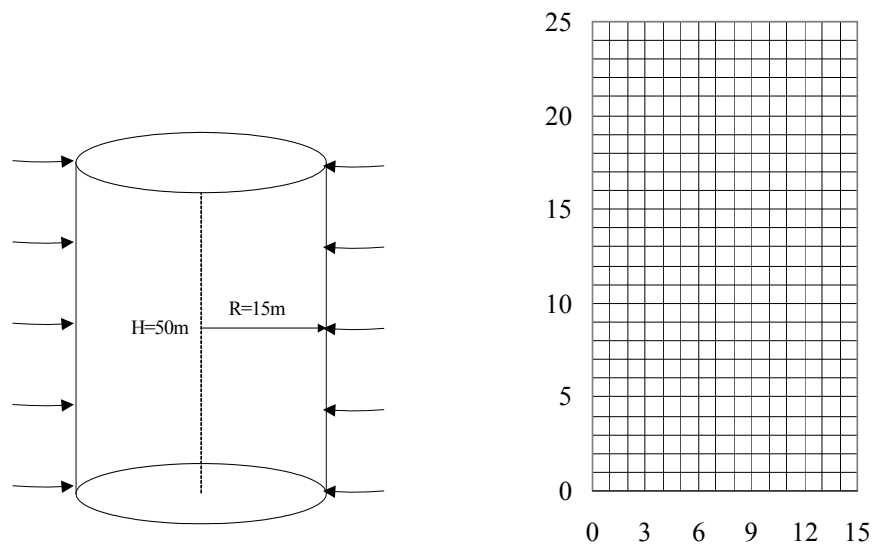


Fig. 6.39. Consolidation of a soil cylinder

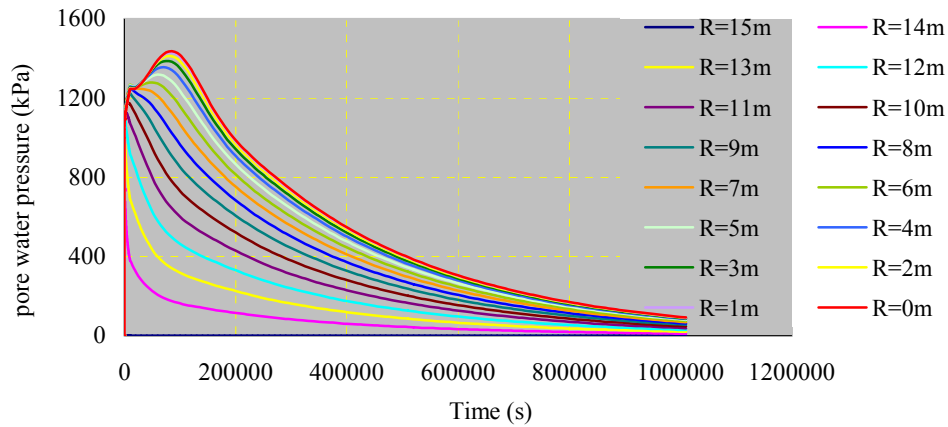


Fig. 6.40. Pore water pressure variation at different times for a cylinder during the consolidation process

In a summary, the proposed method can be used to simulate the coupled consolidation theory for saturated-unsaturated soils. It can also be seen that there is a relationship between the parameters of saturated soils. As a consequence of the effective stress principle and 100% degree of saturation, a saturated soil basically is such a special material as that 1 kPa externally load will cause the soil pore water pressure to increase 1kPa, while 1kPa increase in the pore water pressure will cause an increase in the soil volume which has the same quantity as the decrease caused by a 1kPa external all around load.

6.6.3 The Coupled Consolidation Theory for Unsaturated Soils

For unsaturated soils, the relationships between m_1^s , m_2^s , m_1^w , and m_2^w are arbitrary because the effective stress principle is not satisfied and the degree of saturation is not 100% any more. A simple discussion can prove this comment. For an unsaturated soil, if Bishop's equation is used, the void ratio can be expressed as,

$$e = f(\sigma') = f((\sigma - u_a) + \chi(u_a - u_w))$$

Hence,

$$m_2^s = \frac{1}{1+e_0} \frac{\partial e}{\partial(u_a - u_w)} = \frac{\chi}{1+e_0} \frac{\partial f}{\partial(\sigma')} = \chi m_1^s \quad (6.144)$$

For unsaturated expansive soils, $0 < \chi < 1$. For unsaturated collapsible soils, $\chi < 0$. Simultaneously, because $Se = wG_s$, we have,

$$\begin{aligned} m_1^w &= \frac{S}{1+e_0} \frac{\partial e}{\partial(\sigma - u_a)} + \frac{e}{1+e_0} \frac{\partial S}{\partial(\sigma - u_a)} = Sm_1^s + \frac{e}{1+e_0} \frac{\partial S}{\partial(\sigma - u_a)} \\ m_2^w &= \frac{S}{1+e_0} \frac{\partial e}{\partial(u_a - u_w)} + \frac{e}{1+e_0} \frac{\partial S}{\partial(u_a - u_w)} = Sm_2^s + \frac{e}{1+e_0} \frac{\partial S}{\partial(u_a - u_w)} \end{aligned} \quad (6.145)$$

From Eq. 6.144 and 6.145, we can see the relationships between m_1^s , m_2^s , m_1^w , and m_2^w are arbitrary for unsaturated soils.

Biot (1941) proposed a general consolidation theory for a saturated soil and the soil with occluded air bubbles, which is similar to Eq. 6.65 and 6.73. By assuming there is a potential energy of the soil, Biot proved that $m_2^s = m_1^w$. However, it is questionable because these two parameters have completely different physical meanings. Eq. 6.144 and 6.145 also show that there is no clear relationship between m_2^s and m_1^w for unsaturated soils. The relationship $m_2^s = m_1^w$ only holds for saturated soils.

From Table 6.6, it can be seen that the signs of the parameters in the constitutive laws for expansive soils is different from that for collapsible soils. As a consequence, we need consider them separately. The coupled consolidation for unsaturated soils is a very complicated problem. In this section, parameter studies are used to investigate the consolidation for unsaturated soils.

6.6.3.1 The Coupled Consolidation for Unsaturated Expansive Soils

From Table 6.6, it can be seen that all the parameters in the constitutive laws for expansive soils have a negative sign.

An unsaturated expansive soil cylinder is used to perform the simulation for the coupled consolidation. It is assumed that the soil cylinder has the same dimension as shown in Fig. 6.39 and the mesh generation is also the same to make the analysis comparable. The soil properties are as follows:

Poisson's Ratio	$\mu=0.3$
Coefficient of permeability	$k=1.16 \times 10^{-6} \text{ cm/s}$

The initial conditions of the soil cylinder are that the matric suction is -3,000kPa and the mechanical stress is 0 kPa for the whole calculation domain. A load $P=1,000\text{kPa}$ is applied uniformly in the radial direction, and the soil water is drained in the radial direction freely.

Eight combinations as shown in Table 6.7 are used to perform the parameter studies to investigate the influences of parameters variations on the generation and dissipation of the excess pore water pressure. It is noted that the following combinations may not represent real soils. The results are only used to represent the possible tendency for the generation and dissipation of the excess pore water pressure in the numerical analysis. The results are shown in Fig. 6.41a-i.

The simulation results are shown as Fig. 6.41 a-i. A summary for the soil at the center of the cylinder are plotted in Fig. 6.42. From these Figures, the following observations can be made:

Comparing Fig. 6.41a and b, it is found that an increase in the Young's Modulus of the soil will cause the Mandel-Cryer effect severe. The corresponding Young's Modulus for Fig. 6.41a and b are 20,000kPa and 5,000kPa, respectively. Fig. 6.41a and b have the same initial excess pore water pressure, but in Fig. 6.41a the Mandel-Cryer effect is

more severe. The explanation for this is that the same thermal strain can cause a higher increase in mechanical stress when the soil is more rigid.

Table 6.7. Parameters Studies for an Expansive Soil

	m_1^s $\times 10^{-4}$ (kPa ⁻¹)	m_2^s $\times 10^{-4}$ (kPa ⁻¹)	m_1^w $\times 10^4$ (kPa ⁻¹)	m_2^w $\times 10^{-4}$ (kPa ⁻¹)	χ	B_w	$\Delta(u_a - u_w)$ (kPa)	$\frac{k_w}{m_2^w}$ $\times 10^{-5}$	M-C effect
(1)	-0.6	-1.2	-1.2	-1.2	2	1	1000	9.7	yes
(2)	-2.4	-1.2	-1.2	-1.2	0.5	1	1000	9.7	yes
(3)	-1.2	-0.6	-1.2	-1.2	0.5	1	1000	9.7	yes
(4)	-1.2	-2.4	-1.2	-1.2	2	1	1000	9.7	yes
(5)	-1.2	-1.2	-0.6	-1.2	1	0.5	500	9.7	yes
(6)	-1.2	-1.2	-2.4	-1.2	1	2	2000	9.7	yes
(7)	-1.2	-1.2	-1.2	-0.6	1	2	2000	19.4	yes
(8)	-1.2	-1.2	-1.2	-2.4	1	0.5	500	4.8	yes

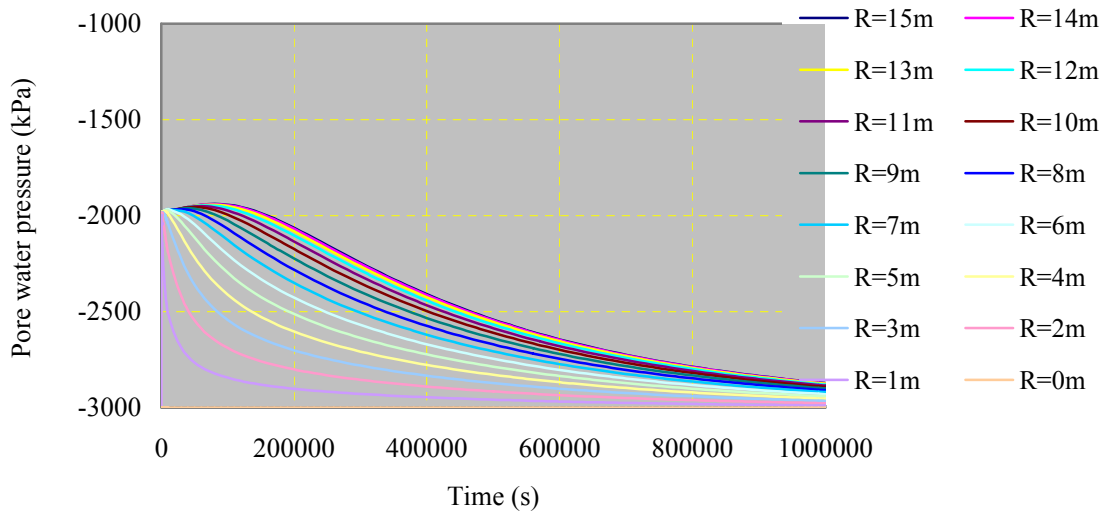


Fig. 6.41a. Simulation of $2m_1^s = m_2^s = m_1^w = m_2^w = -1.2 \times 10^{-4}$

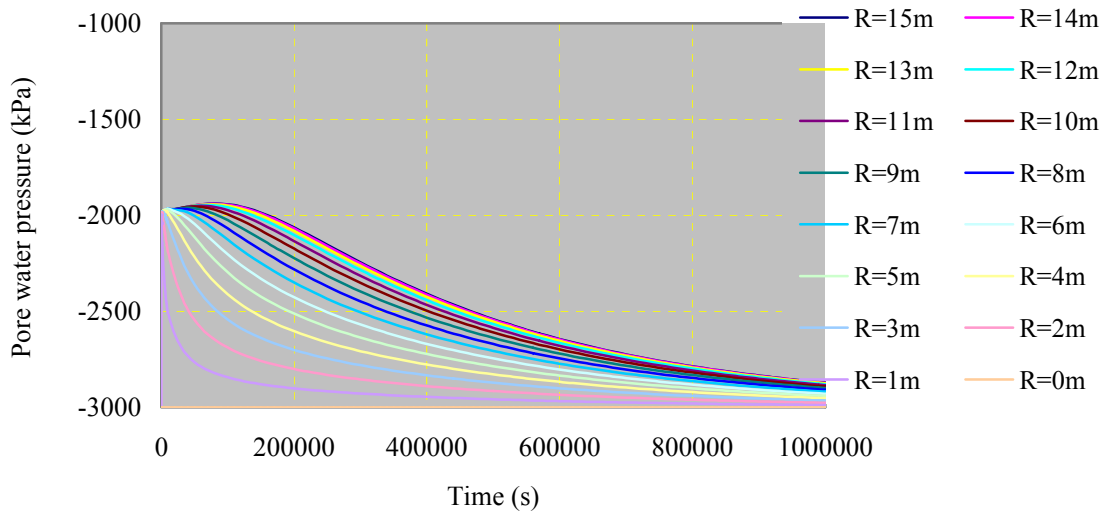


Fig. 6.41b. Simulation of $\frac{1}{2}m_1^s = m_2^s = m_1^w = m_2^w = -1.2 \times 10^{-4}$

Comparing Fig. 6.41c and d, it is found that an increase in the coefficient of expansion of soil will cause the Mandel-Cryer effect severe. The corresponding coefficient of expansion for Fig. 6.41c and d are $-6 \times 10^{-5} \text{ kPa}^{-1}$ and $-2.4 \times 10^{-4} \text{ kPa}^{-1}$, respectively. Fig. 6.41c and d have the same initial excess pore water pressure, but in Fig. 6.39d the Mandel-Cryer effect is more severe. The explanation for this is that when the coefficient of expansion of a soil is bigger, the resulting thermal strain will be bigger, which in turn results in a higher increase in the mechanical stress and the excess pore water pressure.

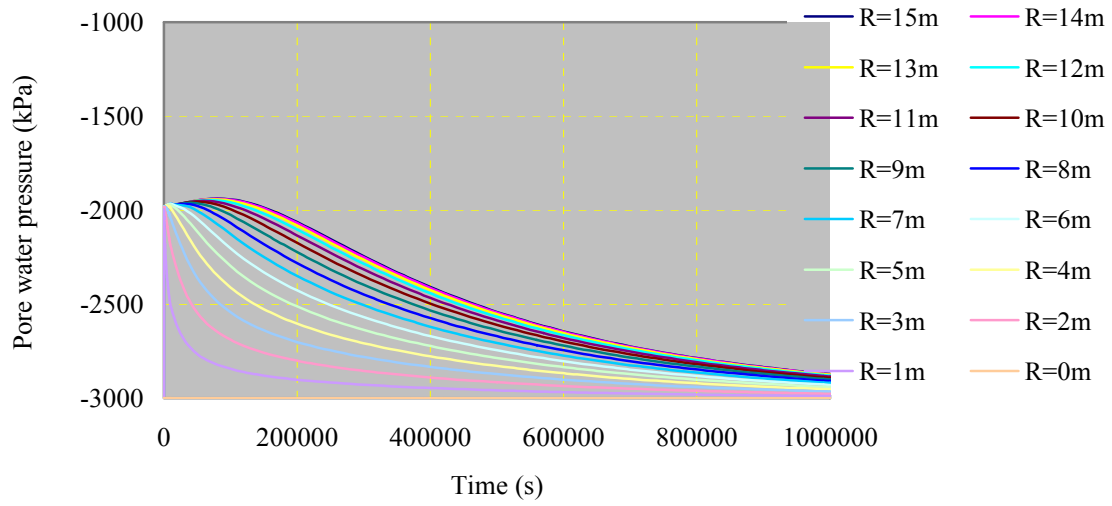


Fig. 6.41c. Simulation of $m_1^s = 2m_2^s = m_1^w = m_2^w = -1.2 \times 10^{-4}$

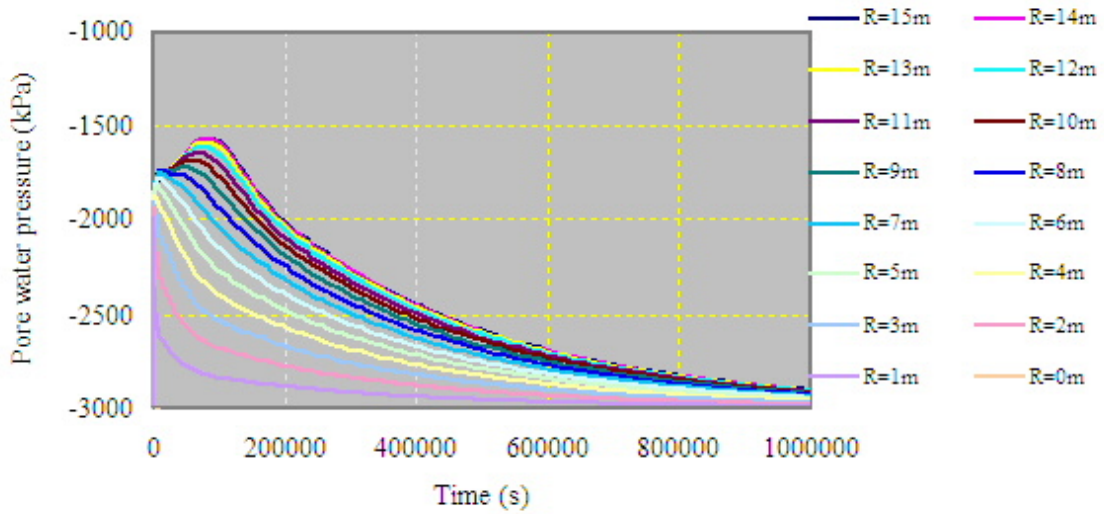


Fig. 6.41d. Simulation of $m_1^s = \frac{1}{2}m_2^s = m_1^w = m_2^w = -1.2 \times 10^{-4}$

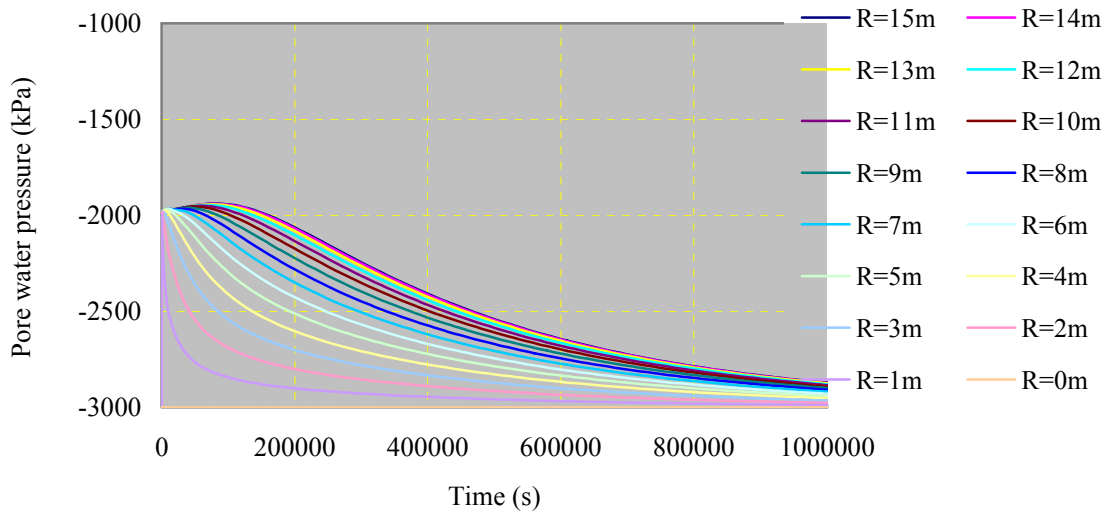


Fig. 6.41e. Simulation of $m_1^s = m_2^s = 2m_1^w = m_2^w = -1.2 \times 10^{-4}$

It is also found that Fig. 6.41a and 6.41d are exactly the same, and so are Fig. 6.41b and c. The conclusion is that an increase in the Young's Modulus has the same effect on the decrease in the coefficient of coefficient of expansion, namely, if the χ is the same for the soils, the Mandel-Cryer effect will be the same. The dissipation process is also the same because the permeability coefficients and specific water capacities of the soil is the same.

Comparing Fig. 6.41e and 6.41f, it is found that an increase in m_1^w will result in a higher excess pore water pressure. The reason for this is because m_1^w is related to the ability of “water generation” due to the mechanical stress. The bigger the m_1^w , the more water can be squeezed out, and the higher the excess pore water pressure under the undrained loading.

Comparing Fig. 6.41g and 6.41h, it is found that an increase in m_2^w will result in a lower excess pore water pressure. The reason for this is because m_2^w is related to the specific water capacity, and a bigger the m_2^w will result in a less excess pore water pressure if the water content variation is the same.

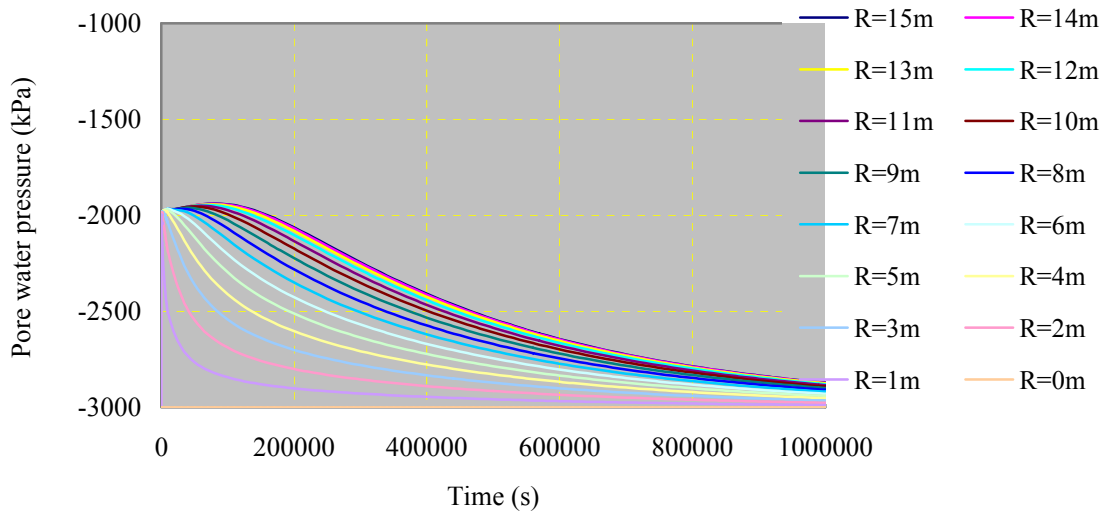


Fig. 6.41f. Simulation of $m_1^s = m_2^s = \frac{1}{2} m_1^w = m_2^w = -1.2 \times 10^{-4}$

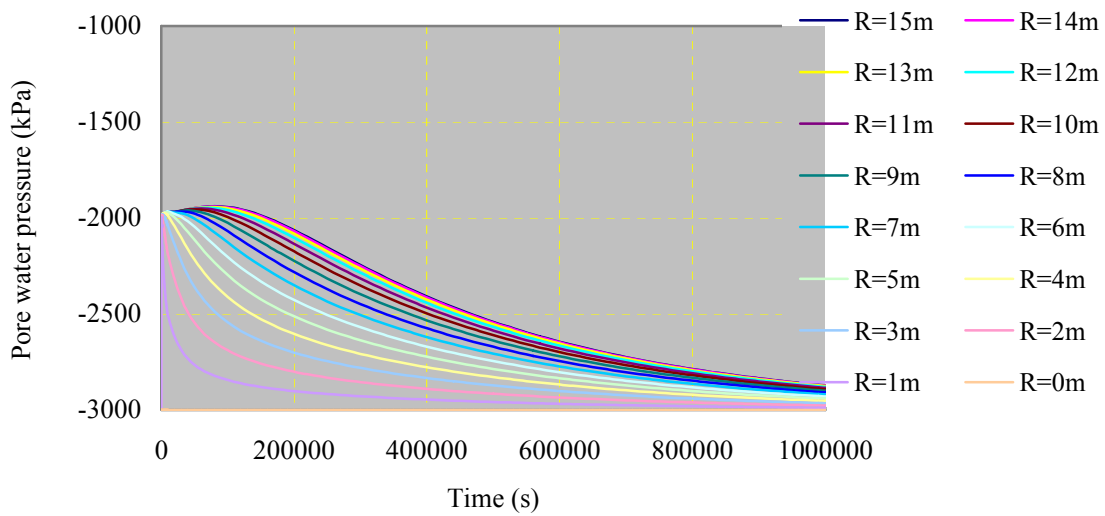


Fig. 6.41g. Simulation of $m_1^s = m_2^s = m_1^w = 2m_2^w = -1.2 \times 10^{-4}$

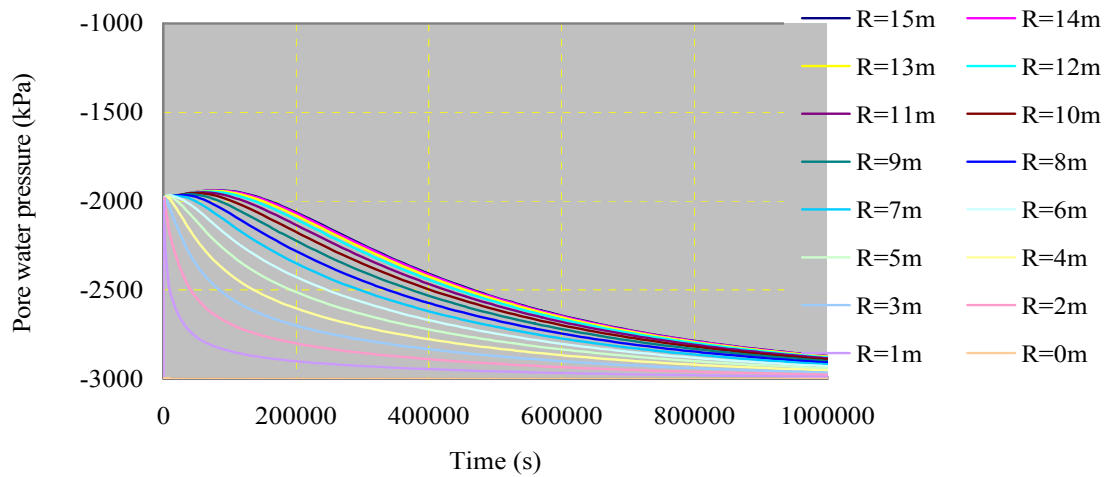


Fig. 6.41h. Simulation of $m_1^s = m_2^s = m_1^w = \frac{1}{2} m_2^w = -1.2 \times 10^{-4}$

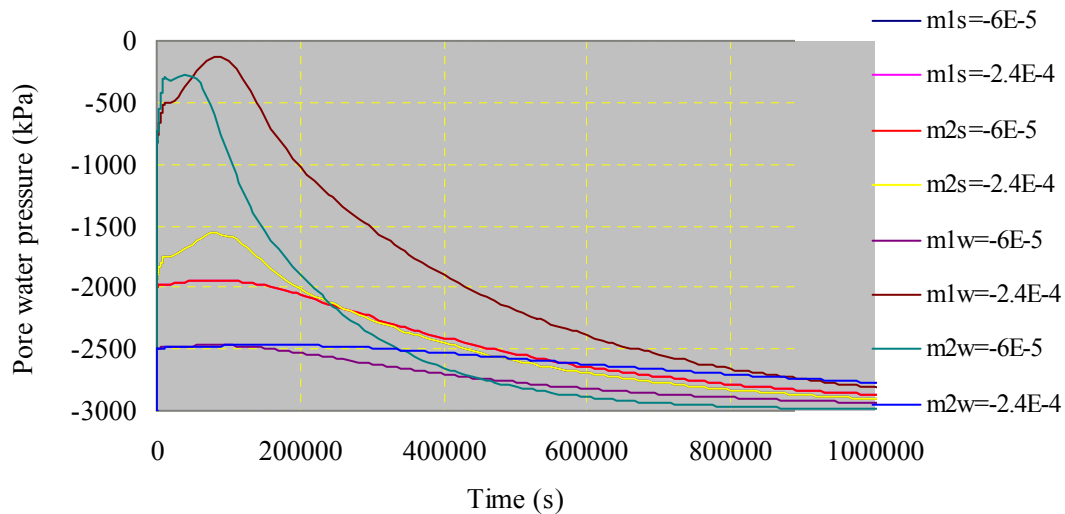


Fig. 6.42. Summary of the simulation for expansive soils

Comparing Fig. 6.41 e and 6.41h and Fig. 6.41 f and g respectively, it is found that the highest excess pore water pressure is not the same and the dissipation rate is not the same. The reason for this is because combination (7) and (8) have different diffusion coefficients ($\alpha = k_w / m_2^w$) although their permeability coefficients are the same. It is the

diffusion coefficient ($\alpha = k_w/m_2^w$) instead of permeability coefficient k_w only that dominates the Mandel-Cryer effect. For a soil with a lower diffusion coefficient, the Mandel-Cryer effect will be more severe, namely the peak excess pore water pressure will be higher and the dissipation process is slower.

In conclusion, for saturated soils, the Mandel-Cryer effect exists under any condition. The initial excess pore water pressure depends on the ratio between m_1^w and m_2^w , i.e., Eq. 6.60 $d(u_a - u_w) = -\frac{m_1^w}{m_2^w} d(\sigma_m - u_a)$. All the parameters m_1^s , m_2^s , m_1^w , m_2^w , μ and k_w will influence the Mandel-Cryer effect. The dissipation process is mainly determined by the diffusion coefficient $\alpha = k_w/m_2^w$.

6.6.3.2 The Thermodynamic Analogue to the Consolidation Theory for Saturated-Unsaturated Expansive Soils

The explanation for the Mandel-Cryer effect in the saturated-unsaturated expansive soils is as follows. Under the above initial conditions, when the external load ΔP is applied to the soil, the mechanical stress in the cylinder will increase ΔP everywhere due to the symmetry in the shape of the cylinder and the applied load. At the instant of load application, the pore water pressure of the soil will increase Δu (matric suction will decrease) at any point of the cylinder due to the load application. The relationship between the ΔP and Δu is defined by Eq. 6.60a. The load application tends to compress the soil cylinder while the increase in the pore water pressure tends to make the soil swell in that the increase in the pore water pressure results in a decrease in the effective stress for expansive soils. The final result will depend on the combination of these two effects. As time goes, the excess pore water pressure is dissipated by losing water from the exposed surface. The excess pore water pressure at the surface of the cylinder will dissipate faster than that at the inner shells and the excess pore water pressure at the inner shell therefore will be higher than that at the outer shell. The decrease in the excess pore water pressure will cause soil to shrink in that the equivalent effective stress is

increased. Obviously the outer shell of the soil will shrink more than the soil at the inner shells if there is no prevention from the inner shell. However, the assumption is not satisfied and the prevention from the inner shell will cause mechanical forces between soil shells. The resulting mechanical forces will result in an increase in mechanical stresses in the inner shells, which in turn cause the excess pore water pressure in the inner shell to increase. The soil shells have to reach equilibrium by adjusting the mechanical stress and the excess pore water pressure. As a consequence, during the consolidation process there are two tendencies in the excess pore water pressure variations for the soil at the inner shells of the cylinder: a decrease in the pore water pressure due to the dissipation of the excess pore water pressure and an increase in the pore water pressure due to the increase in the mechanical stress. The actual pore water pressure will depend on the combination of these two effects. At the early stage of the consolidation process, the second effect is dominant. At a later stage of the consolidation process, the first effect will be dominant. As a consequence, the pore water pressure at the inner shells of the soil cylinder will increase firstly, gradually reach a peak and then decrease gradually. This is a typical phenomenon of the Mandel-Cryer effect.

The thermodynamic analogue to process of consolidation was first proposed by K. Terzaghi to facilitate the visualization of the mechanics of consolidation and swelling. As we have discussed previously, there is also a similarity between the coupled thermal stress problem and the coupled consolidation theory for saturated-unsaturated soils. The thermodynamic analogue to the consolidation of the simulated cylinder can be described as follows. A cylinder with infinite length has an initial temperature of u_0 and mechanical stress of 0 kPa at every point of the cylinder. The cylinder is placed in an environment with a constant temperature u_0 . An externally radial load ΔP is applied to the cylinder instantaneously. At the instant of load application, the cylinder is compressed radically and every point of the cylinder has a mechanical stress of ΔP . Simultaneously, part of the work done by the externally applied load is converted into heat energy. Considering that at the instant of load application the time is so short that there is no heat exchange between the cylinder and the surrounding environment. All the

resulting heat generation is therefore used to increase the temperature of the cylinder from u_0 to $u_0 + \Delta u$ everywhere. As a consequence the cylinder has two instant tendencies in volume change: compression due to the applied load and expansion due to the temperature increase. The final volume of the cylinder depends on the combination effect of these two effects. The cylinder is then cooling down from the exposed surface toward the center of the cylinder. The surface of the cylinder will cool down at a faster rate than the inner shell, which results that temperature at the surface is lower than that at the inner shell. The decrease in temperature will cause the cylinder to shrink. Therefore the outer shell of the cylinder will shrink more than the inner shell if there is no prevention from the inner shell. Obviously this assumption is not satisfied and the inner shell will prevent the outer shell from shrinking more than the inner shell itself can. This prevention will result in force and the inner shell of the cylinder will have a mechanical stress higher than ΔP , that is, the mechanical stress in the cylinder will not equal to the applied load any more (or, during the consolidation, the total stress does not keep constant). Similarly, the increase in mechanical stress in the inner shell will cause an increase in temperature in the inner shell. The cylinder has to reach equilibrium by adjusting the temperature and deformation. The temperature at the inner part of the cylinder will keep increasing until reaching a peak when the temperature increase resulted by the mechanical stress increase is equal to the temperature decrease caused by the cooling process. Thereafter the temperature will decrease gradually in that the cooling process is dominant. Consequently, during the cooling process, the temperature in the inner part of the cylinder will increase firstly, gradually reach a peak, and then decrease gradually. This is a typical Mandel-Cryer effect. For an expansive soil, if we change the temperature in the above description into the pore water pressure and the heat energy into mass of water, we can get the same conclusion.

The thermodynamic analogue for the coupled consolidation for a saturated soil can also be explained in a similar way. The corresponding cylinder will have following characteristics: when an external load ΔP is applied to the cylinder, at the instant of the load application it will cause the temperature in the cylinder to increase a magnitude of

ΔP . The load application will compress the cylinder while the temperature increase will make the cylinder to expand. The compression caused by an external load ΔP is equal to the expansion resulted by the temperature increase. As a consequence, both the total stress and temperature increase ΔP and there is no volume change at the instant of load application. Under these conditions, the requirement $m_1^s = m_2^s = m_1^w = m_2^w$ is satisfied. During the heat dissipation process, this relationship is always satisfied and the Mandel-Cryer effect exists.

6.6.3.3 The Coupled Consolidation for Unsaturated Collapsible Soils

A collapsible soil is different from an expansive soil in that the collapsible soil will experience a decrease in volume when the matric suction decreases (or pore water pressure increases). The difference, when expressed in the material parameters, can be seen from Table 6.6. For collapsible soils, m_1^s , m_1^w , and m_2^w are negative and m_2^s is positive while all these parameters are negative for expansive soils.

Table 6.8 Parameters Studies for a Collapsible Soil

	m_1^s $\times 10^{-4}$ (kPa ⁻¹)	m_2^s $\times 10^{-4}$ (kPa ⁻¹)	m_1^w $\times 10^4$ (kPa ⁻¹)	m_2^w $\times 10^{-4}$ (kPa ⁻¹)	χ	B_w	$\Delta(u_a - u_w)$ (kPa)	$\frac{k_w}{m_2^w}$ $\times 10^{-5}$	M-C effect
(1)	-0.6	1.2	-1.2	-1.2	2	1	1000	9.7	yes
(2)	-2.4	1.2	-1.2	-1.2	0.5	1	1000	9.7	yes
(3)	-1.2	0.6	-1.2	-1.2	0.5	1	1000	9.7	yes
(4)	-1.2	2.4	-1.2	-1.2	2	1	1000	9.7	yes
(5)	-1.2	1.2	-0.6	-1.2	1	0.5	500	9.7	yes
(6)	-1.2	1.2	-2.4	-1.2	1	2	2000	9.7	yes
(7)	-1.2	1.2	-1.2	-0.6	1	2	2000	19.4	yes
(8)	-1.2	1.2	-1.2	-2.4	1	0.5	500	4.8	yes

Eight combinations as shown in Table 6.8 are used to perform the parameter studies to investigate the influences of parameters variations on the dissipation of excess pore water pressure for collapsible soils. The results are shown in Fig. 6.43a-h and the summary for the pore water pressure dissipation of a point at the center of the cylinder is shown in Fig. 6.44.

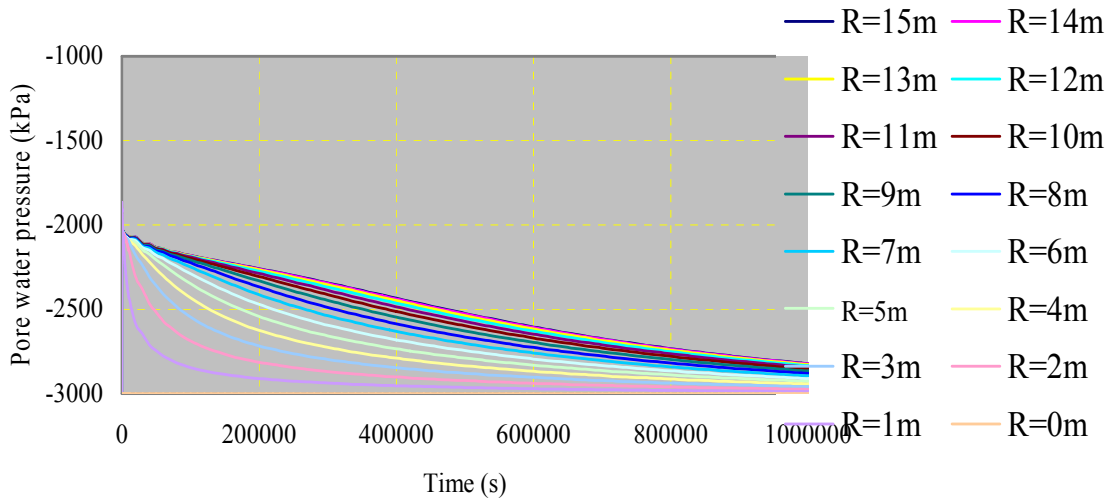


Fig. 6.43a. Simulation of $2m_1^s = -m_2^s = m_1^w = m_2^w = -1.2 \times 10^{-4}$

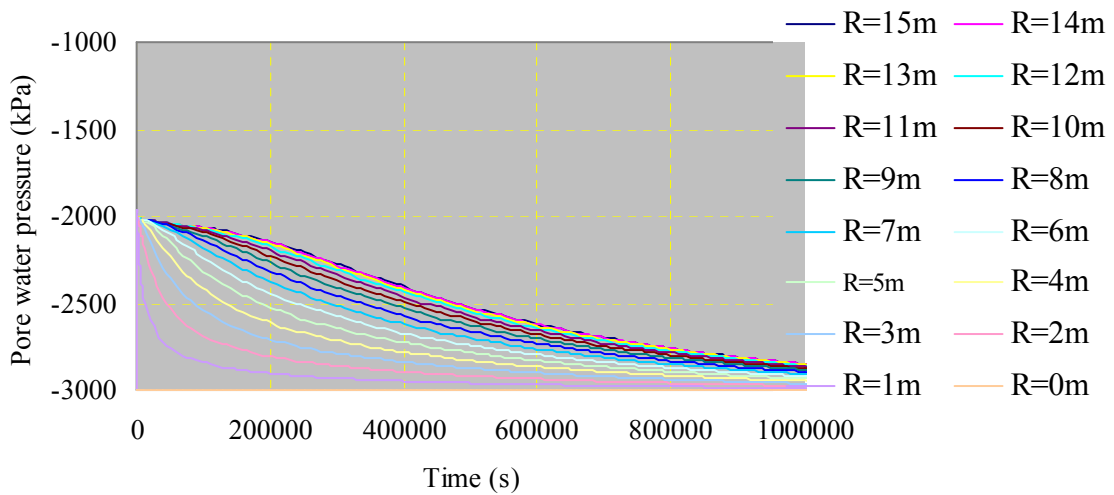


Fig. 6.43b. Simulation of $\frac{1}{2}m_1^s = -m_2^s = m_1^w = m_2^w = -1.2 \times 10^{-4}$

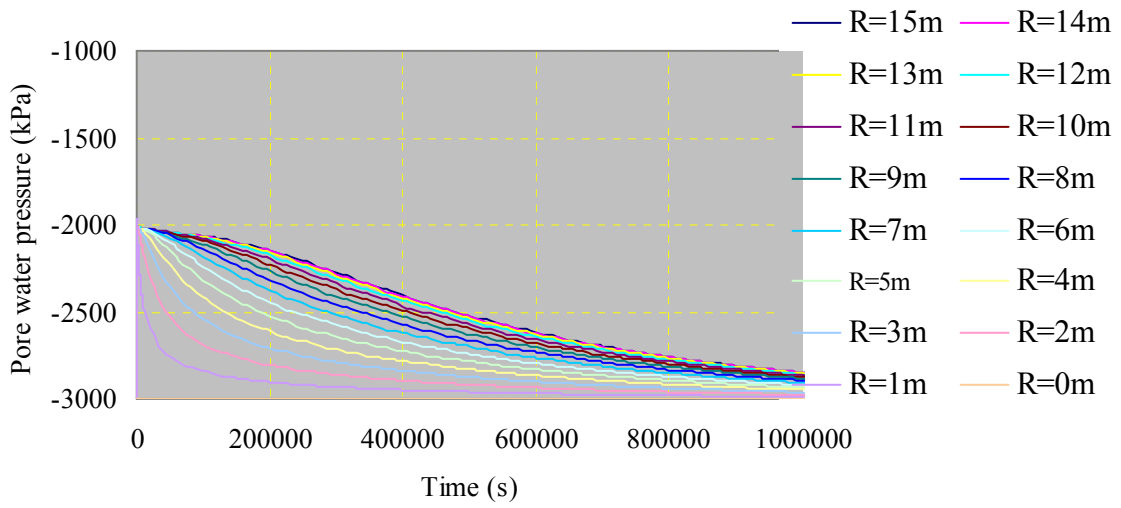


Fig. 6.43c. Simulation of $m_1^s = -2m_2^s = m_1^w = m_2^w = -1.2 \times 10^{-4}$

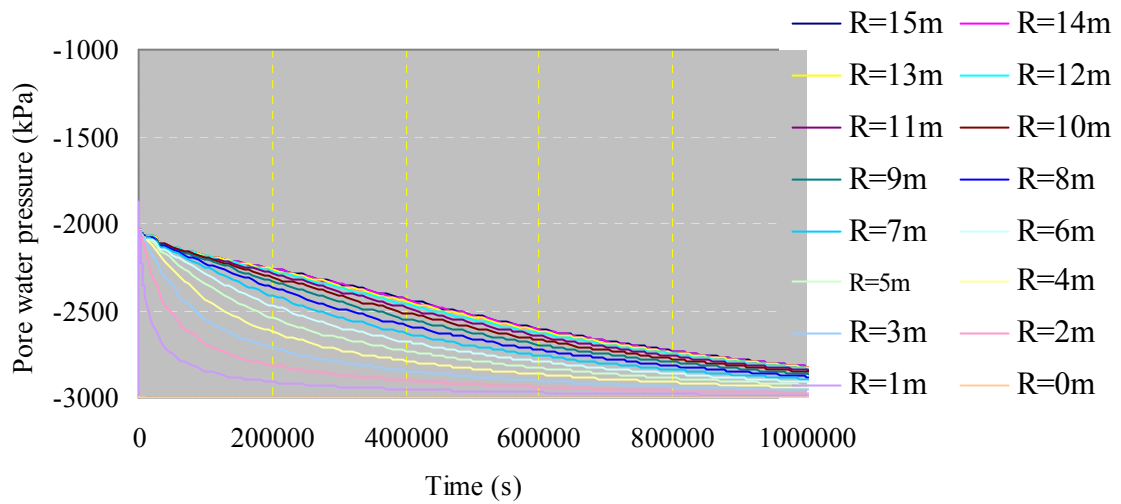


Fig. 6.43d. Simulation of $m_1^s = -\frac{1}{2}m_2^s = m_1^w = m_2^w = -1.2 \times 10^{-4}$

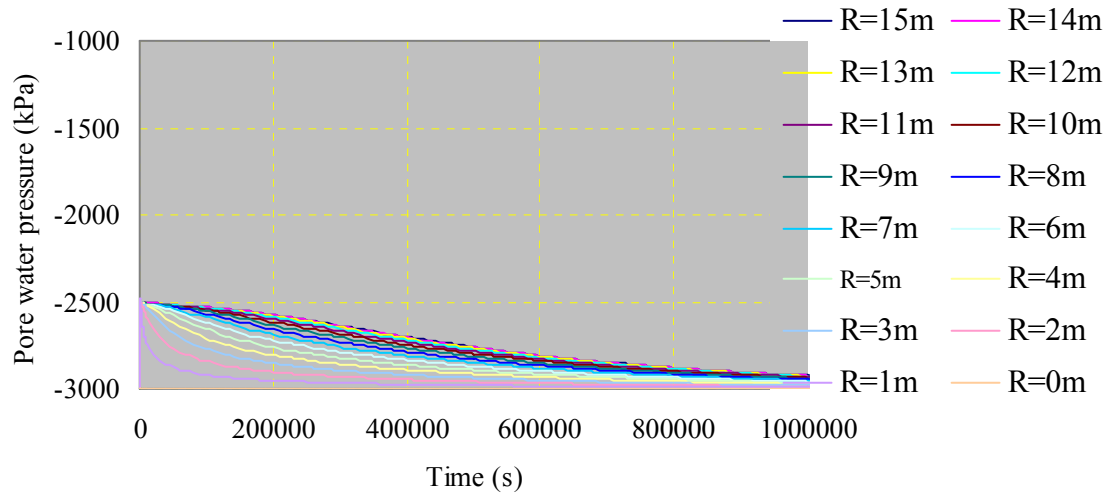


Fig. 6.43e. Simulation of $m_1^s = -m_2^s = 2m_1^w = m_2^w = -1.2 \times 10^{-4}$

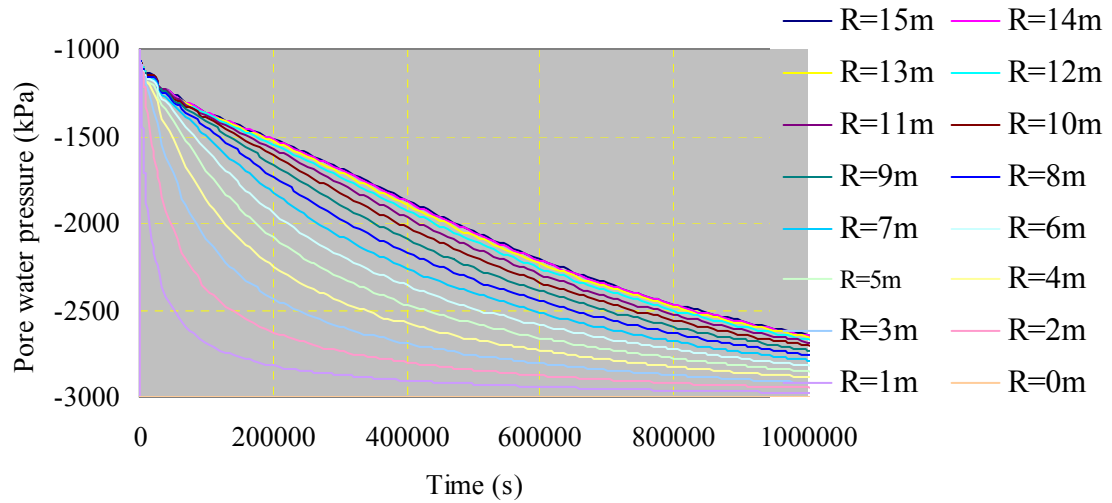


Fig. 6.43f. Simulation of $m_1^s = -m_2^s = \frac{1}{2}m_1^w = m_2^w = -1.2 \times 10^{-4}$

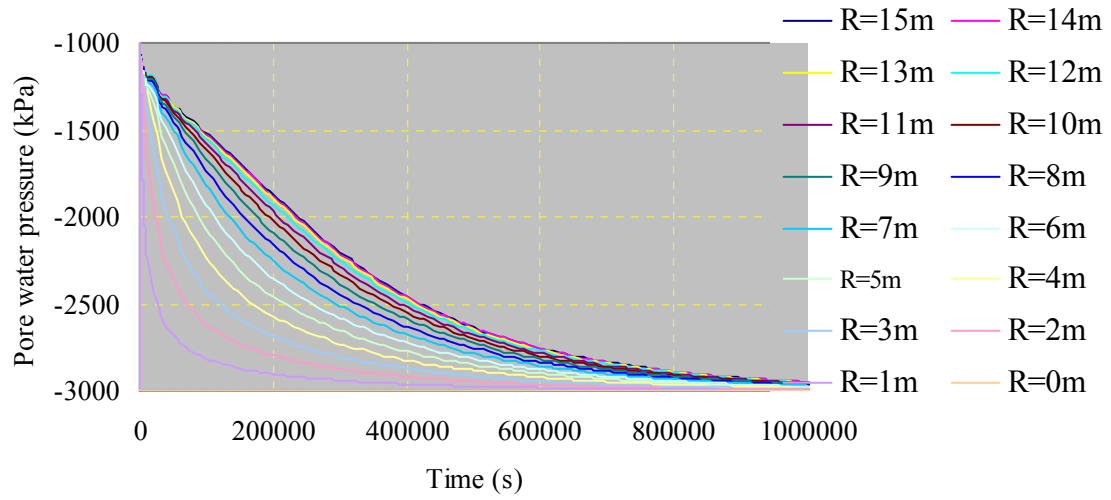


Fig. 6.43g. Simulation of $m_1^s = -m_2^s = m_1^w = 2m_2^w = -1.2 \times 10^{-4}$

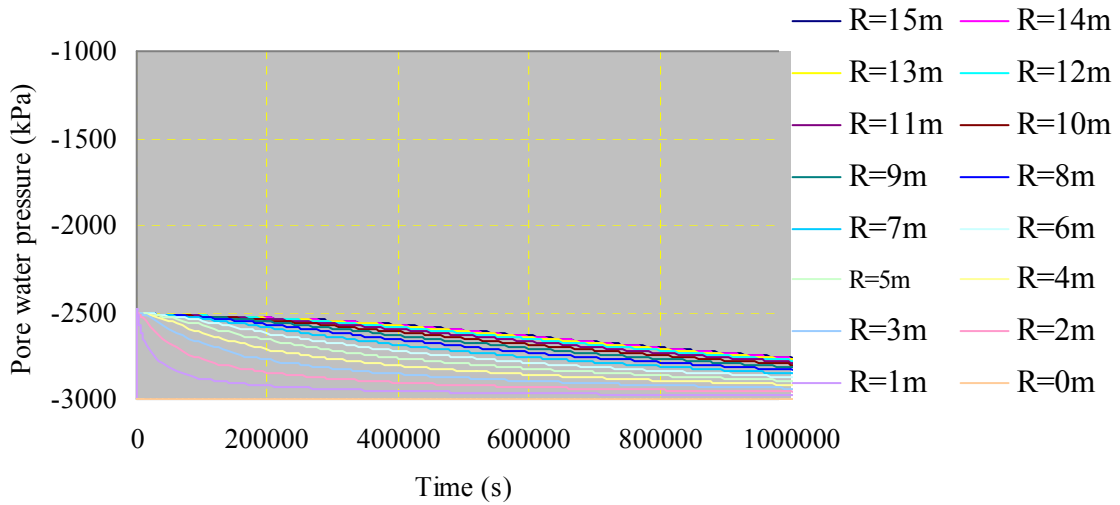


Fig. 6.43h. Simulation of $m_1^s = -m_2^s = m_1^w = \frac{1}{2}m_2^w = -1.2 \times 10^{-4}$

The corresponding Young's Modulus for Fig. 6.43a and b are 20,000kPa and 5,000kPa, respectively. Comparing Fig. 6.43a and b, it is found that an increase the Young's Modulus of the soil will cause the pore water pressure dissipate faster.

The corresponding coefficient of expansion for Fig. 6.43c and d are $-6 \times 10^{-5} \text{ kPa}^{-1}$ and $-2.4 \times 10^{-4} \text{ kPa}^{-1}$, respectively. Comparing Fig. 6.43c and d, it is found that an increase in the coefficient of expansion of soil will cause excess pore water pressure to dissipate faster.

It is also found that Fig. 6.43a and d are exactly the same, and so are Fig. 6.43b and c. The conclusion is that an increase in Young's Modulus has the same effect on the decrease in the coefficient of expansion. Namely when χ is the same for the soils, the dissipation process is also the same because the permeability coefficients and specific water capacities of the soil is the same.

Comparing Fig. 6.43e and f, it is found that an increase in m_1^w will result in a higher excess pore water pressure.

Comparing Fig. 6.43g and h, it is found that an increase in m_2^w will result in a lower excess pore water pressure.

Comparing Fig. 6.43 e and h and Fig. 6.43 f and g respectively, it is found that the dissipation rate is not the same. The reason for this is because combination (7) and (8) have different diffusion coefficients ($\alpha = k_w / m_2^w$) although their permeability coefficients are the same.

A summary for the soil at the center of the cylinder are plotted in Fig. 6.44. None of these Figures indicates the existence of the Mandel-Cryer effect is observed. To make the investigation more clear, the following parameters studies have been performed to study the difference in excess pore water pressure dissipation between coupled and uncoupled analysis and the consolidation process for expansive and collapsible soils.

1. $m_1^s = m_2^s = m_1^w = m_2^w = -1.2 \times 10^{-4}$, coupled consolidation analysis;
2. $m_1^s = -m_2^s = m_1^w = m_2^w = -1.2 \times 10^{-4}$, coupled consolidation analysis;
3. The same conditions as that in 1 and 2, uncoupled consolidation analysis.

The initial conditions of the soil cylinder is that the matric suction is -1,000kPa and the mechanical stress is 0 kPa for the whole calculation domain. The surrounding matric suction is -1,000kPa and remains unchanged until the completion of the consolidation

process. All the other conditions are the same as that used in the parameters studies for unsaturated expansive soils.

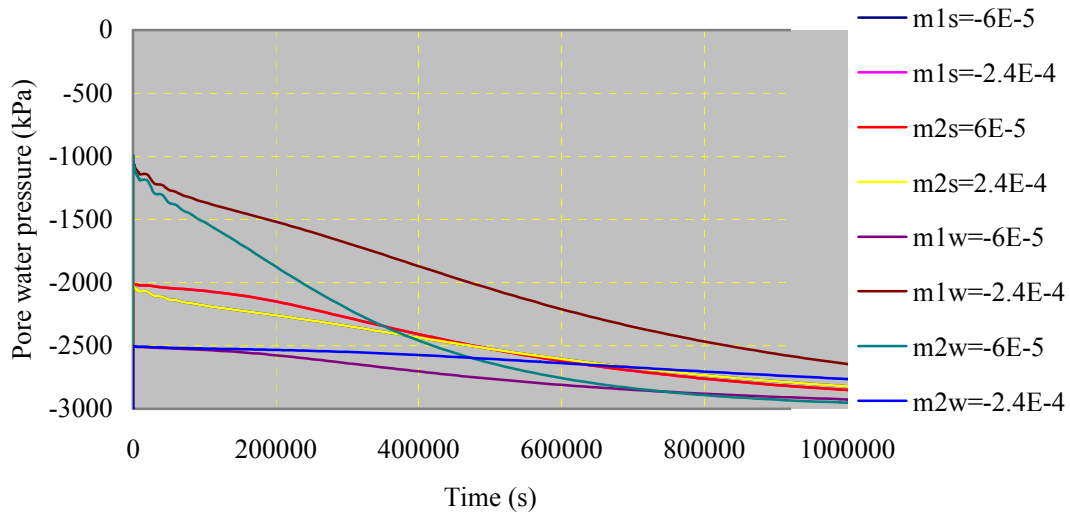


Fig. 6.44. Summary of simulation for collapsible soils

In this parameters study, case 1 stands for an expansive soil (all the parameters are negative), case 2 stands for a collapsible soil because m_2^s is positive.

The pore water pressures at the cent of the cylinder for these analyses are shown as in Fig. 6.45.

Because the applied loads are the same and $m_1^w = m_2^w$ the excess pore water pressure at the instant of load application is 1,000 kPa for these two soils. The excess pore water pressure at the instant of load application is 1000kPa. The initial matric suction is -1,000kPa, therefore, the pore water pressure at the instant of load application is 0 kPa for both soils.

In the uncoupled analysis, the mechanical stresses are assumed to be constant during the uncoupled analysis. The initial conditions are that the pore water pressures are 0 kPa for both soils. Because the coefficients of permeability k_w and m_2^w are the same for these

two soils, the excess pore water pressure will dissipate along the same line as shown in Fig. 6.45.

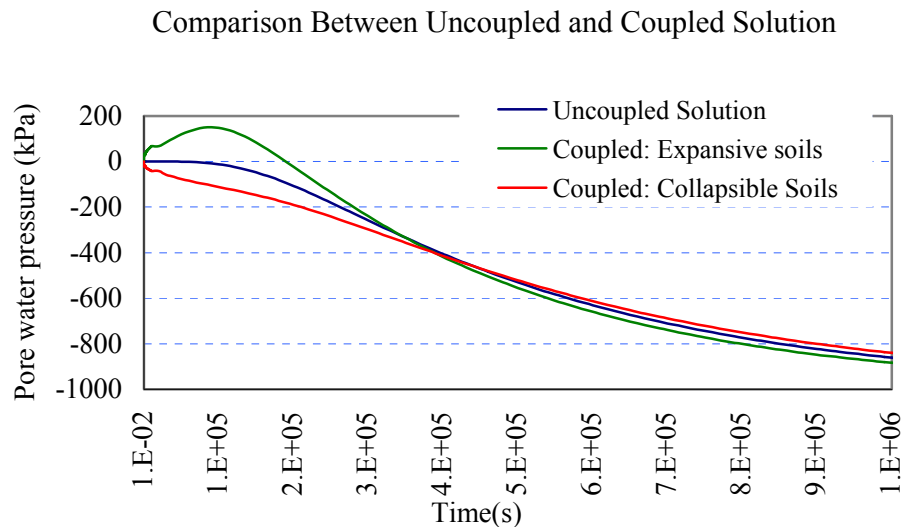


Fig. 6.45. Comparison between the coupled and uncoupled solutions for expansive soils and collapsible soils

In the coupled analysis, the initial conditions for these two soils are that the applied loads are both equal to 1,000kPa. The program will automatically calculate the excess pore water pressure at the instant of load application.

For the expansive soil ($m_2^s = -1.2 \times 10^{-4}$), during the coupled consolidation analysis, Mandel-Cryer effect exists. The pore water pressure will increase firstly, gradually reach a peak and then decrease gradually until all the excess pore water pressure is dissipated completely. The reason for this is the same as that for a saturated soil. With a negative m_2^s value, the soil will shrink when the excess pore water pressure dissipates. The outer shell of the soil cylinder will shrink faster than the inner shell (Fig. 6.37). The differential deformation will cause compressive stresses to the inner shell. As a consequence, the pore water pressure in the inner shell will increase at the early stage of the consolidation.

For the collapsible soil ($m_2^s = 1.2 \times 10^{-4}$), it is found that the excess pore water pressure dissipates in a faster way than that in the uncoupled consolidation analysis. The explanations for this phenomenon are listed as follows:

When the external load ΔP is applied to the soil, at the instant of load application, the mechanical stress in the cylinder will increase ΔP everywhere due to the symmetry in the shape of the cylinder and the applied load (Fig. 6.37). The pore water pressure of the soil will increase Δu (matric suction will decrease) at any point of the cylinder due to the load application. The load application tends to compress the soil cylinder. Unlike an expansive soil, the increase in pore water pressure will cause the collapsible soil to collapse (reduction in the soil volume). Consequently, at the instant of load application, the volume of the collapsible soil will decrease and the pore water pressure will increase.

As time goes, the excess pore water pressure is then dissipated by losing water from the exposed surface. The excess pore water pressure at the surface of the cylinder will dissipate faster than that at the inner shell and the excess pore water pressure at the inner shell therefore will be higher than that at the outer shell. The decrease in the excess pore water pressure will cause the collapsible soil to swell, which is the reverse of the collapsible behavior. Obviously the outer shell of the soil will swell more than the soil at the inner shell if there is no traction from the inner shell. However, the assumption is not satisfied and the traction from the inner shell will cause tensile forces between soil shells. The resulting tensile forces will result in a decrease in mechanical stresses in the inner shell (unloading), which in turn cause the excess pore water pressure in the inner shell to decrease. The soil shells have to reach equilibrium by adjusting the mechanical stress and excess pore water pressure. Therefore, during the consolidation process the excess pore water pressure at the inner shell of the collapsible soil cylinder will decrease due to two reasons: the dissipation of excess pore water pressure and the decrease in pore water pressure due to the tensile stress (unloading) between the soil shells. As a consequence, the pore water pressure will dissipate rapidly at the early stage of the consolidation of the collapsible soil. At the late stage of the consolidation of the collapsible soil, when there is excess pore water pressure dissipation at the outer shell,

the excess pore water pressure at the inner shell will decrease due to the tensile stress between shells. The hydraulic gradient is then reduced by the tensile stress instead of dissipation. The dissipation rate of the excess pore water pressure is the reduced. At the late stage of the consolidation of the collapsible soil has a dissipation rate less than the uncoupled analysis (Fig. 6. 45).

The rapid dissipation of the pore water pressure will be dramatic at the early stage of the consolidation and the excess pore water pressure will be dissipated at a slower rate than the uncoupled analysis at the late stage of consolidation. In a word, it seems that there is a “reverse” Mandel-Cryer effect in the consolidation for collapsible soils. All the behaviors exhibited in the Fig. 43.a-h can be explained the reverse Mandel-Cryer effect in the same way as that for an unsaturated expansive soil (Fig. 6.41 a-h). All the parameters m_1^s , m_2^s , m_1^w , m_2^w , μ and k_w will influence the “reverse” Mandel-Cryer effect.

It should also be kept in mind that the above discussion is based on the elastic assumption. It is possible that a collapsible soil (metastable-structured soil) will become as expansive soil (stable-structured soil) after collapse. A further investigation on the possibility of the above reverse Mandel-Cryer effect is highly desirable in the future research.

6.6.3.4 Thermodynamic Analogue to the Consolidation Process of a Collapsible Soil

The thermodynamic analogue to the consolidation of the collapsible soil cylinder can be described as follows. A cylinder with infinite length has an initial temperature of u_0 and mechanical stress of 0 kPa at every point of the cylinder. The cylinder is placed in a environment with a constant temperature u_0 . The characteristics of the cylinder material are that when the temperature of the material increase, the material will shrink. An externally radial load ΔP is applied to the cylinder instantaneously. At the instant of load application, the cylinder is compressed radically and every point of the cylinder has a mechanical stress of ΔP . Simultaneously, part of the work done by the externally applied load is converted into heat energy. Considering that at the instant of load application the

time is so short that there is no heat exchange between the cylinder and the surrounding environment. All the resulting heat generation is therefore used to increase the temperature of the cylinder from u_0 to $u_0 + \Delta u$ everywhere. As a consequence the cylinder volume will decrease due to two reasons: compression caused by the applied load and shrinkage due to the temperature increase. The cylinder is then cooling down from the exposed surface toward the center of the cylinder. The surface of the cylinder will cool down at a faster rate than the inner shell, which results that temperature at the surface is lower than that at the inner shell. The decrease in temperature will cause the cylinder to expand. Therefore the outer shell of the cylinder will expand more than the inner shell if there is no traction from the inner shell. Obviously this assumption is not satisfied and there is a tensile force to prevent the outer shell from swelling more than the inner shell itself can. The tensile force will result in that the inner shell of the cylinder will have a mechanical stress lower than ΔP (unloading).

Similarly, the decrease in mechanical stress in the inner shell will cause a decrease in temperature in the inner shell. The cylinder has to reach equilibrium by adjusting the temperature and deformation. At the early stage of the consolidation of the collapsible soil, the excess temperature at the inner shell will decrease due to two reasons: the dissipation of heat energy and the decrease in temperature due to unloading. These two reasons cause the temperature at the inner shell to decrease dramatically at the early stage of the consolidation process. The decrease in temperature due to the tensile stress on the other hand will reduce the temperature gradient between the soil shells. This effect will tend to slow down the dissipation of the excess temperature. At the late stage of the consolidation, it will cause a slower dissipation rate than the uncoupled analysis. As a consequence, for the collapsible soil, the excess pore water pressure has a higher dissipation rate at the early stage and a lower dissipation rate at the late stage of the consolidation than that in the uncoupled analysis due to the mechanical stress variation. There is a reverse "Mandel-Cryer effect during the consolidation process of the collapsible soil.

6.7 Some Discussions on the Consolidation Theory for Unsaturated Soils

6.7.1 Stress State Variables and Constitutive Laws

Three main reasons led to the extensive acceptance of the two stress state variables concept: (1). the effective stress principle failed to explain the collapsible soil behavior (Jennings and Burland 1962; Matyas and Radhakrishna 1968); (2). the χ value was very hard to obtain; (3). the oedometer and triaxial null tests performed by Fredlund and Morgenstern (1977) indicated that the volume change of unsaturated soils can be described by $(\sigma - u_a)$ and $(u_a - u_w)$ or their combinations. The discussions presented in this chapter reveal that the collapsible soil behaviors actually can be explained by the effective stress principle and the effective stress principle therefore is valid for all the soils. The χ value is very hard to obtain because $\chi = 3\alpha B$, while α and B are functions of both mechanical stress and matric suction. The reason why there is need for two stress state variables should be that the effective stress alone is not sufficient to explain and predict the soil volume change behaviors. The changes in the soil volume due to mechanical stress variation and that due to matric suction variation are two complete different physical phenomena and have totally different constitutive laws. The matric suction (or pore water pressure) alone can not be used to describe the volume change due to mechanical stress variation while the mechanical stress (or effective stress) alone can not be used to describe the water flow. Even for saturated soils, two stress state variables, σ and u_w , instead of the effective stress only, are needed for the description of the soil behaviors. For saturated soils, the effective stress can be used to determine the volume change and shear strength. However, the variations of effective stress are related to the total stress and pore water pressure. The diffusion equation 6.99 in Terzaghi's consolidation theory is actually the differential equation for water phase. To predict the behaviors of saturated soils, pore water pressure is still needed.

Actually, how many stress state variables should be used to describe the soil behaviors depends on how many physical phenomena are of interest. For example, currently the mechanical stress and matric suction are extensively used stress state variables to investigate the volume change behavior of unsaturated soils. If the salt

concentration in an unsaturated soil varies greatly and influences the soil behaviors greatly, a fourth stress state variable, i.e. osmotic suction should be included. In the same way, if the temperature in the soil varies greatly and influences the soil behavior greatly, a fifth stress state variable, i.e. temperature should be included. When a stress state variable is not of interest, it is considered as always constant. For example, if only two stress state variables, σ and u_w , are used to investigate behaviors of a soil, then the assumption is that the soil is under isothermal conditions, the pore air pressure is constant, and the salt concentration is constant. The temperature, pore air pressure, and osmotic suction therefore are not of interest and are not used as stress state variables.

To understand the behavior of unsaturated soils, all these stress state variables such as mechanical stress, pore water pressure, and pore air pressure must be known. Any complete set of stress state variables proposed for the volume change behavior should be able to express the entire three stress state variables after linear combinations. Fredlund (1973) proposed the use of two stress state variables, i.e. $(\sigma - u_a)$ and $(u_a - u_w)$ (Eq. 6.74) for unsaturated soils. However, combinations in Eq. 6.74 apparently fail to achieve this requirement. For example, for a complete dry soil with rigid soil structure, the pore air pressure alone is of interest. However, from the combinations proposed above the pore air pressure can not be calculated. In other words, for the combination (1), actually even if the $(\sigma - u_a)$ and $(u_a - u_w)$ are all known, we still can not calculate the pore air pressure from these two stress state variables. No matter how we combine these two stress state variables, the mechanical stress σ , pore water pressure u_w , and air pressure u_a can not be calculated. As a consequence, Eq. 6.74 is actually not a complete set of stress state variables, i.e. $(\sigma - u_a)$ and $(u_a - u_w)$ are necessary but not sufficient to determine the unsaturated soils behaviors.

Therefore, the proposed sets of stress state variables in Eq. 6.74 bear some hidden assumptions. For the above combinations proposed by Fredlund (1973), the hidden assumptions are that only the mechanical stress and the matric suction are of interest and

the air pressure is constant (atmospheric pressure) and will not influence the soil behaviors.

If the pore air pressure is of interest, a third stress state variable (for example, the pore air pressure) should be used as the third stress state variable. Otherwise, the combinations proposed will be unable to provide the information about the air pressure. The following combinations can be used:

- 1). σ , $-u_w$ and u_a , or $(\sigma - u_{a0})$, $(u_{a0} - u_w)$ and $(u_a - u_{a0})$,
 - 2). $(\sigma - u_a)$, $(u_a - u_w)$ and u_a ;
 - 3). $(\sigma - u_a)$, $(u_a - u_w)$ and σ ;
 - 4). $(\sigma - u_a)$, $(u_a - u_w)$ and $-u_w$; etc
- (6.146)

where σ is total mechanical stress; u_w is pore water pressure; u_{a0} is atmospheric pressure, and u_a is pore air pressure. u_{a0} is the atmospheric pressure, which can be taken as a constant.

Eq. 6.146 can also be converted into other styles by using linear combinations. It is proposed to use (1) in Eq. 6.146 as a complete set of stress state variables to investigate the volume change behavior of the unsaturated soils. The reasons are listed as follows:

1. It is convenient to use $(\sigma - u_a)$ and $(u_a - u_w)$ as stress state variables to obtain the constitutive surfaces and the corresponding material parameters for unsaturated soils. However, it is not convenient to investigate the soil behavior by using $(\sigma - u_a)$ and $(u_a - u_w)$ as stress state variables because when it is not easy to separate the influence of the mechanical stress, pore water pressure and air pressure. Fredlund and Rahardjo (1993) derived the differential equations for the consolidation for unsaturated soils by using $(\sigma - u_a)$ and $(u_a - u_w)$ as stress state variables. However, all the stress state variables are separated finally in terms of σ , $-u_w$ and u_a . The $(\sigma - u_a)$ and $(u_a - u_w)$ actually were not used as whole to be stress state variables.

2. For the water phase, the driving force for the water flow is the hydraulic head instead of matric suction. The hydraulic head is related directly to pore water pressure by the energy equation. It is more convenient to use pore water pressure as stress state variable to construct the constitutive law, and to derive the differential equation for the water phase. For the similar reason, the air pressure should be used to construct the constitutive law, and to derive the differential equation for the air phase.

Other supporting evidences include that most current researchers use three stress state variables, i.e. σ , $-u_w$ and u_a , instead of two stress state variables, to study the consolidation of unsaturated soils although it was asserted that two stress state variables were used (Fredlund and Hansan 1980, Lloret et al. 1980, and Fredlund and Rahradjo,1993). $(\sigma - u_a)$ and $(u_a - u_w)$ were only used to construct the constitutive surfaces while σ , $-u_w$ and u_a were used for the differential equations.

6.7.2 Discussions Associated with the Constitutive Relations

Fredlund and Morgenstern (1977) performed null tests in which the individual components of the stress state variables i.e. σ , $-u_w$ and u_a , were varied while the stress state variables, i.e. $(\sigma - u_a)$ and $(u_a - u_w)$ were maintained constant. Experimental data indicated that essentially no overall volume change or water content change during the null tests. Based on the test results together with other evidences, mainly Bishop's derivation for the effective stress principle and some experimental data, they concluded that the $(\sigma - u_a)$ and $(u_a - u_w)$ or their combinations can be used to describe the soil volume change (or shear strength) behavior. Furthermore, Fredlund and Morgenstern (1976) proposed that only two constitutive relationships, i.e. one for soil structure (Eq. 6.65) and the other for water phase (Eq. 6.66) are needed for the soil volume change. The air phase constitutive relation can be expressed as the difference between the soil structure volume change and the change in the volume of water present in the element (Eq. 6.67).

The reasoning and the proposed constitutive laws, however, are questionable. One reason has been discussed in the previous section that the proposed combination of stress state variable is not a complete set of stress state variables. A further discussion on the proposed constitutive laws reveals that the proposed constitutive laws also contain some tacit assumptions.

In most cases, the mechanical stress, pore water pressure and air pressure are of interest for an unsaturated soil. Correspondingly three constitutive relations are needed. One for soil structure, one for water phase and the third one is for the air phase. A general constitutive law for unsaturated soils can be written as follows,

$$\begin{aligned}
 \text{Soil structure: } \frac{dV_v}{V_0} &= k_1^s d\sigma_m + k_2^s du_w + k_3^s du_a \\
 \text{Water phase: } \frac{dV_w}{V_0} &= k_1^w d\sigma_m + k_2^w du_w + k_3^w du_a \\
 \text{Air phase: } \frac{dV_a}{V_0} &= k_1^a d\sigma_m + k_2^a du_w + k_3^a du_a
 \end{aligned} \tag{6.147}$$

Where, k_1^s , k_2^s , k_3^s , k_1^w , k_2^w , k_3^w , k_1^a , k_2^a , and k_3^a are material parameters.

That is, the soil structure change is caused by three components, one component is due to the normal mechanical stress variation, one is due to the matric suction variation, and the air pressure variation will also influence the volume change of the soil structure. For the water phase and the air phase, it is the same. A similar form was proposed by Bishop in the derivation of Bishop's equation, that is,

$$\sigma' = \sigma - k_1 u_w - k_2 u_a \tag{6.148}$$

where σ' =effective stress, and k_1 and k_2 = material parameters.

Eq. 6.148 states that the soil volume change is determined by the mechanical stress, pore water pressure and air pressure, which presents the same information as that in Eq. 6.147.

Under this condition, all the void ratio, water content and air volume of the soil should be functions of the mechanical stress, pore water pressure and air pressure, i.e.,

$$e = f(\sigma, u_w, u_a), \quad wG_s = g(\sigma, u_w, u_a), \quad v_a = h(\sigma, u_w, u_a) \quad (6.149)$$

Correspondingly, the definition of the parameters in the Eq. 6.147 should be a function of the three stress state variables:

$$\begin{aligned} k_1^s &= \frac{1}{1+e_0} \frac{de}{d\sigma} & k_2^s &= \frac{1}{1+e_0} \frac{de}{du_w} & k_3^s &= \frac{1}{1+e_0} \frac{de}{du_a} \\ k_1^w &= \frac{1}{1+e_0} \frac{dwG_s}{d\sigma} & k_2^w &= \frac{1}{1+e_0} \frac{dwG_s}{du_w} & k_3^w &= \frac{1}{1+e_0} \frac{dwG_s}{du_a} \\ k_1^a &= \frac{1}{1+e_0} \frac{dv_a}{d\sigma} & k_2^a &= \frac{1}{1+e_0} \frac{dv_a}{du_w} & k_3^a &= \frac{1}{1+e_0} \frac{dv_a}{du_a} \end{aligned} \quad (6.150)$$

The physical meanings of the material parameters in Eq. 6.150 can also be explained in a way similar to that for the consolidation theory and all these parameters should be functions of the mechanical stress, pore water pressure and air pressure.

Null test only proved the soil volume and water volume can be expressed as Eq. 6.76 and 6.77, that is,

$$\frac{dV_v}{V_0} = m_1^s d(\sigma_m - u_a) + m_2^s d(u_a - u_w) \quad (6.76)$$

$$\frac{dV_w}{V_0} = m_1^w d(\sigma_m - u_a) + m_2^w d(u_a - u_w) \quad (6.77)$$

Compare Eq. 6.76 and 6.77 with the first two equations in Eq. 6.147, we can found the relationship between the parameters:

$$\begin{aligned} k_1^s &= m_1^s, & k_2^s &= -m_2^s, & k_3^s &= -(k_1^s + k_2^s) \\ k_1^w &= m_1^w, & k_2^w &= -m_2^w, & k_3^w &= -(k_1^w + k_2^w) \end{aligned} \quad (6.151)$$

That is, the null tests only prove that there are some relationships between the material parameters in the constitutive laws for the soil structure and water phase.

In the null tests, the soil volume and water volume maintained constant, the air volume therefore must be constant, too. It means that the air phase volume is a function of $(\sigma - u_a)$ and $(u_a - u_w)$, which is expressed in Eq. 6.78. However, it does not mean that $(\sigma - u_a)$ and $(u_a - u_w)$ can be used as a complete set of stress state variables to describe the volume change behavior of the soils. It is well known that air phase has high compressibility and the fundamental law for the air phase is the mass conversation instead of continuity equation. In the differential equation for the air phase, the air density or the air pressure is used as a third stress state variable. In other words, in the null tests, the air concentration in the soil was actually varying because the air pressures were varying. The air phase constitutive equation therefore should include a term in a relation to the pore air pressure variation instead of Eq. 6.78. Fredlund and Rahardjo (1993) derived the differential equation for the air phase in the following way. The net mass rate of air flow across the element is equal to the difference between the mass rates of the air entering and leaving the element within a period of time:

$$\frac{\partial(M_a/V_0)}{\partial t} = \frac{\partial\left(D_a^* \frac{\partial J_a}{\partial y}\right)}{\partial y} \quad (6.152)$$

where M_a is the air mass in the soil element; V_0 is the initial total volume; D_a^* is the coefficient of transmission for the air phase and J_a is the mass rate of air flowing across a unit area of the soil. Eq. 6.152 is finally converted into the following style:

$$\left(\frac{w_a}{RT}\right)u_a \frac{\partial(V_a/V_0)}{\partial t} + (1-S)n \left(\frac{w_a}{RT}\right) \frac{\partial u_a}{\partial t} = D_a^* \frac{\partial^2 u_a}{\partial y^2} - \frac{\partial D_a^*}{\partial y} \frac{\partial u_a}{\partial y} \quad (6.153)$$

where, V_a/V_0 is determined by Eq. 6.78. It is obvious that the pore air pressure is used as stress state variable in the differential equation 6.153.

Actually the mass conservation is also the fundamental law for deriving the differential equation for water phase (Lloret and Alonso 1980). The only difference is that water can be considered as incompressible. The mass conservation for the water phase is therefore can be represented by the continuity equation.

In conclusion, to investigate and predict the behaviors of unsaturated soils, Three stress state variables, i.e. σ , $-u_w$ and u_a , are needed.

It is admitted that it is more convenient to use $(\sigma - u_a)$ and $(u_a - u_w)$ as stress state variables to obtain the constitutive surfaces and the corresponding material parameters for the constitutive laws as shown in 6.151. Void ratio, water content and unit air volume in a soil are functions of three stress state variables, i.e. σ , $-u_w$ and u_a as shown in Eq. 6.149, which is four- dimensional and very difficult to obtain. When $(\sigma - u_a)$ and $(u_a - u_w)$ are used as stress state variables, the void ratio, water content and unit air volume can be expressed as a function of $(\sigma - u_a)$ and $(u_a - u_w)$ only with the conclusion obtained from the null tests. The void ratio, water content and unit air volume are then surfaces in the $(\sigma - u_a)$ and $(u_a - u_w)$ space, which provides a useful and invaluable tool for unsaturated soil mechanics. More null tests are highly desirable to further verify the conclusion that the volume of the soil structure and water phase are functions of the $(\sigma - u_a)$ and $(u_a - u_w)$ only for all the unsaturated soils. Otherwise, Eq.

6.147 instead of Eq. 6.76, 6.77 and 6.78 should be used. However, to obtain mathematical expression of the void ratio, void ratio, water content and unit air volume under the σ , $-u_w$ and u_a space is very time consuming and costive. It is also noted that the null tests only prove that the volume of soil structure and water phase are functions of the $(\sigma - u_a)$ and $(u_a - u_w)$ only. Whether this conclusion can be extended to the shear strength for unsaturated soils or not is highly questionable. A null test for the shear strength for unsaturated soils is therefore highly desirable.

The previous discussion of coupled thermal stress problem also provides an example for the constitutive relations for two stress state variables, i.e. mechanical stress and temperature.

For soils with more stress state variables are of interest, more constitutive relations are needed. For example, for a soil with mechanical stress, matric suction, air pressure and temperature are of interest, a fourth constitutive relation is needed for the energy variation. It is a coupled thermo-hydro-air pressure-mechanical (THM) problem and the fundamental laws for the problems are the conservations of momentum, mass and energy. More discussions about the THM problems can be seen in Gens et al. (1997)

6.7.3 Air in Soil

Air phase in the soil has two possibilities of existence. One possibility is that the air phase is continuous and connected to the atmosphere. The other possibility is that the air is occluded by the soil skeleton and has no connection with atmosphere. The ratio between the two possibilities depends on the degree of saturation of the soil. Fredlund and Rahardjo (1993) proposed that “an unsaturated soil can be further subdivided, depending upon whether the air phase is continuous or occluded. The subdivision is primarily a function of the degree of saturation. An unsaturated soil with continuous air phase generally has a degree of saturation less than approximately 80%. Occluded air bubbles commonly occur in unsaturated soils having a degree of saturation greater than approximately 90%. The transition zone between continuous air phase and the occluded

air bubbles occurs when the degree of saturation is between approximately 80-90%”. However, it is possible that there are occluded air bubbles even in dry soils.

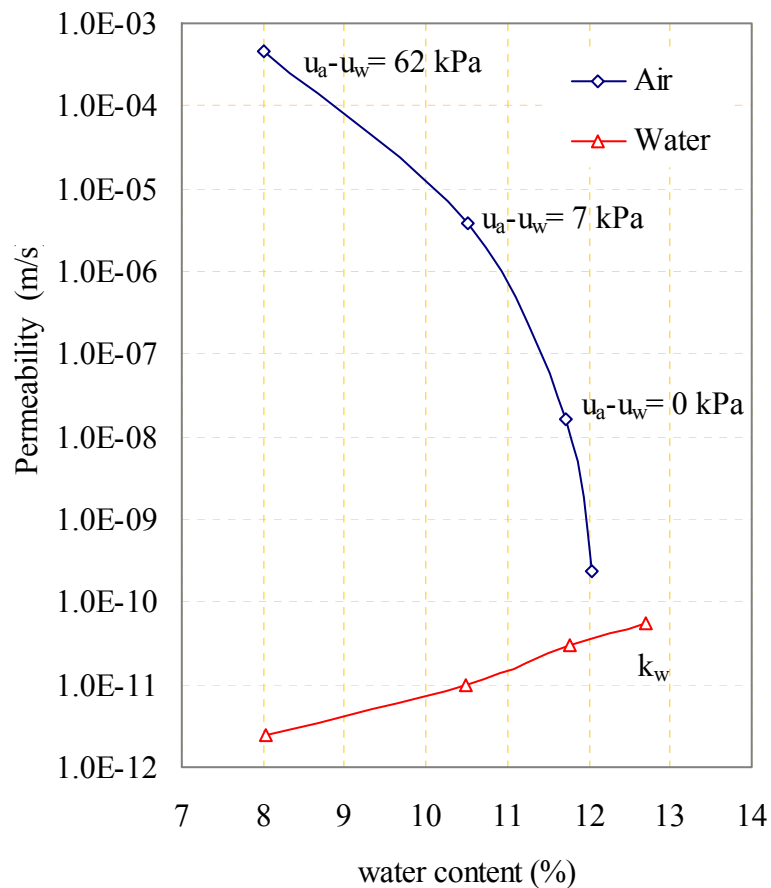


Fig. 6.46. The air and water coefficients of permeability for a Westwater soil (Barden and Pavlakis 1971)

When there is load application on the soil, the air under these two conditions behaves differently. If the air in the soil is continuous, both the air pressure and water pressure will increase at the instant of load application. The excess air pressure will dissipate much faster than excess pore water pressure because the viscosity of air is much smaller than that of water. The difference causes that the air coefficients of permeability are much bigger than water coefficients of permeability (Fredlund and Rahardjo 1993). For

example, for a Westwater soil, the ratio between air coefficients of permeability and water coefficients of permeability is from 10^3 to 10^9 as shown in Fig. 6.46 (Barden and Pavlakis 1971). Consequently the excess pore air pressure can be considered to dissipate instantaneously. Rahardjo (1990) conducted one-dimensional consolidation test on an unsaturated silty sand in a specially designed K_0 cylinder. The pore air and water pressure were measured simultaneously. The results indicated an essentially instantaneous dissipation of the excess pore-air pressure for the particular soil. On the other hand, the excess pore water pressure was found to be a time-dependent process which could be closely simulated by using the water flow partial differential equation. Under this condition, the pore air pressure can be assumed constant throughout the consolidation process.

Another reason for assuming a constant pore air pressure during the consolidation process is because the pore air pressure may not vary much when there is load application. When the soil is completely saturated, the water compressibility (approximately $4 \times 10^{-7} \text{ kPa}^{-1}$, Dorsey 1940) is far less than the compressibility of soil structure. An externally applied stress is nearly entirely transferred to the water phase. The effective stress for the saturated soil remains unchanged and there is no volume change. If the soil is unsaturated, the compressibility of the air (when u_a is 202.6 kPa, the isothermal compressibility of the air is $4.94 \times 10^{-3} \text{ kPa}^{-1}$) is bigger than the compressibility of the soil structure (usually between $5 \times 10^{-4} \text{ kPa}^{-1}$ and 10^{-5} kPa^{-1}) as shown in Fig. 6.47. Therefore, most of the applied load is transferred to the soil structure. The pore air pressure variation is not significant.

Consequently, when the air phase in the soil is continuous it is reasonable to assume the pore air pressure will dissipate instantly, or the air pressure is constant and equal to the atmospheric pressure throughout the process. Under this assumption, there are only two stress state variables, i.e. σ and $-u_w$. The constitutive laws for unsaturated soils are expressed as Eq. 6.122. and 6.123. The constitutive surface can be used to get the material parameters needed for the constitutive laws. The excess pore water pressure can be obtained by Eq. 6.63.

When the air phase is not continuous, the air phase can be considered as part of the soil structure. Under this condition, the differential equation of the air phase can not be derived.

In a summary, when the air phase is continuous, it is reasonable to assume that the excess pore water pressure is dissipated instantaneously. When the air phase is not continuous, the differential equation for the air phase can not be derived. When the soil is saturated, there is no need for the consideration of the air pressure. Under all the conditions, it seems the differential equation for the air phase is not needed. When the soil is saturated, Biot's consolidation theory can be used, which has the same constitutive law as that in Eq. 6.122 and 6.123.

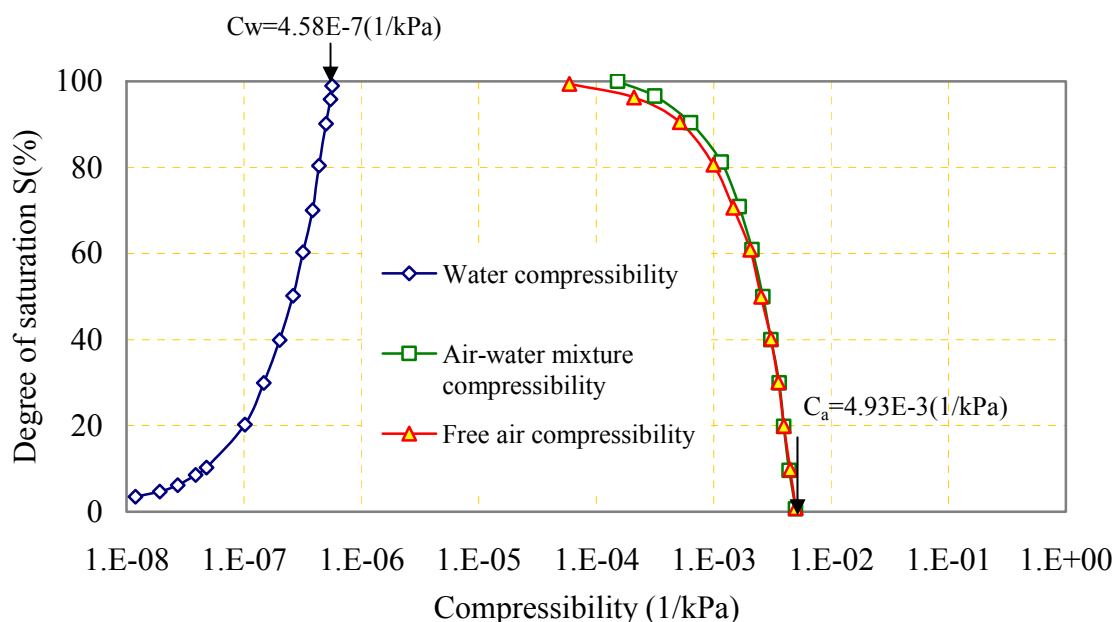


Fig. 6.47. Compressibility of water, free air and air-water mixture (Modified from Fredlund and Rahardjo 1993)

Fredlund and Rahardjo (1993) stated that for the soil with occluded air bubbles, excess pore water pressure and pore air pressure are basically equal. The phenomenon may be accounted for the low matric suction and high degree of saturation. Under these

condition, Fredlund and Rahardjo proposed that the air bubbles are considered to have no contact with soil skeleton, that is, the contractile skin does not exist and the air bubbles are surrounded by pore water completely just like air bubbles in the water of a lake. Biot (1941) derived a general consolidation theory for saturated soils or unsaturated soils with occluded air bubbles. The theory is basically the same as the theory proposed in the previous section with the constant pore air pressure assumption (Eq. 6.122 and 6.123) except that Biot proved that $m_2^s = m_1^w$, which may be a mistake. The material parameters will change due to the existence of the occluded air phase, which is reflected by the constitutive surface. Therefore, the proposed theory is applicable for the case when there are occluded air bubbles. In conclusion, for either continuous air phase occluded air phase or saturated soils, the same constitutive laws (Eq. 6.122 and 6.123) can be applied. In other words, the consolidation theory discussed in this chapter is applicable for soils under any condition.

6.7.4 Excess Pore Water Pressure Parameter and Pore Air Pressure Parameter

When the assumption that the pore air pressure is constant throughout the consolidation process is made, the excess pore air pressure parameter is zero. The air phase will not be considered and the corresponding method to calculate the excess pore water pressure has been discussed in the previous sections.

When the air phase is continuous and the pore air pressure is of interest, to perform an uncoupled analysis for an unsaturated soil, it is required to estimate the excess pore water and air pressure. Fredlund and Rahardjo (1993) derived the excess pore air and water pressure by using the air water mixture compressibility. The derivation actually can be simplified by the following two conditions:

- (1). The water phase is incompressible;
- (2). The soil volume change is equal to the air phase volume change.

There are two unknowns, namely the excess pore water and air pressure. By using the above two conditions, two equations can be obtained. The excess pore water and air pressure therefore can be solved. These two conditions can be expressed as follows:

$$\begin{aligned}\frac{dV_w}{V_0} &= m_1^w d(\sigma_m - u_a) + m_2^w d(u_a - u_w) = 0 \\ \frac{dV_v}{V_0} &= m_1^s d(\sigma_m - u_a) + m_2^s d(u_a - u_w) = \frac{(1-S+hS)n}{\bar{u}_a} du_a\end{aligned}\tag{6.154}$$

From Eq. 6.154, the excess pore water and air pressure du_w and du_a can be solved in terms of the applied load $d\sigma_m$. Fredlund and Rahardjo (1993) derived equations for the excess pore water and air pressure for unsaturated soils under undrained loading. The compressibility of the air-water mixture is used, namely, the water is considered to be compressible. However, the water was considered to be incompressible when deriving the differential equation for the water phase because the continuity equation was used. As discussed previously, the compressibility of water is much lower than that of air and soil structure. Therefore, it is reasonable to consider the water to be incompressible without causing significant errors. If the condition that the water is incompressible is put in to Fredlund and Rahardjo's derivation for the excess pore water and air pressure, Eq. 6.154 can be obtained. Eq. 6.154 is therefore a simplified version of the Fredlund and Rahardjo's derivation.

CHAPTER VII

EVAPOTRANSPIRATION, INFILTRATION AND BOUNDARY CONDITIONS

7.1 Introduction

In the previous chapter, when we discuss the volume change of soils, only two stress state variables, i.e. total stress and matric suction, are used. Other factors such as temperature, air pressure and salt concentration will also influence the volume change behaviors of the soil. They are not considered under most conditions because of two reasons. (1). The stress state variables representing these factors do not change very much. For example, the temperature in a deep soil layers can be considered as constant. (2). Their influences are small enough to be neglected. For example, the pore air pressure variations have much less influence on soil volume than the mechanical stress and matric suction variations. In other words, the coupled consolidation simulation for the volume change of a soil is a simplified condition for the real problem.

To investigate the behaviors of residential buildings on expansive soils, the evaporation process at the soil-atmosphere must be considered. Let us discuss how many stress state variables need be used to model the evaporation process at the soil-atmosphere interface if direct numerical simulation of the evaporation process is performed. Atmosphere is a mixture of different kinds of gases and water vapor. Soil at the ground surface usually are unsaturated and have three phases as shown in Fig. 7.1: solid, liquid (water+ air dissolved), and air (mixture of dry air and water vapor) phase. Water can be either liquid or evaporated in the gas phase. Air can be either gas or dissolved in the water.

Chapter III discussed the factors influencing the evapotranspiration. Two processes are involved in the evaporation or transpiration. The first is on an energy basis in which energy is needed to change the state of the molecules of water from liquid to vapor. The second one is on an aerodynamic basis in which the saturated water vapor is removed by a process of eddy diffusion. When all the physical phenomena involved in the

evaporation process are expressed as numerical models, the stress state variables and the corresponding constitutive laws needed for the simulation of the ground soil are listed in Table 7.1 and 7.2.

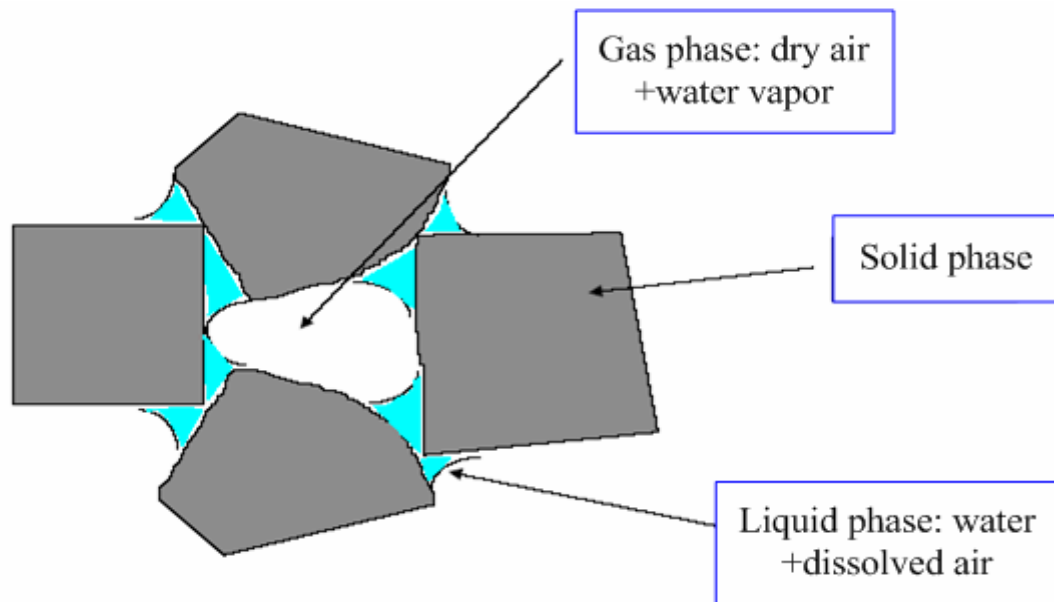


Fig. 7.1. Schematic representation of an unsaturated porous material (Olivella et al. 1996)

Table 7.1. Equations and Variables Summary (Olivella et al. 1996)

Fundamental laws	Stress state variables	Symbol
Equilibrium of stresses	displacements	u, v, w
Balance of water mass	Pore water pressure	u_w
Balance of air mass	Pore air pressure	u_a
Balance of internal energy	Temperature	T

The fundamental laws needed for the derivations of differential equations are: mass balance of solid, mass balance of water, mass balance of air, momentum balance for the medium, and internal energy balance for the medium.

For the air, all the stress state variables and the corresponding constitutive laws and fundamental laws are needed except that used for the liquid phase. Unlike the volume change, all these factors influence the evaporation process greatly and are not negligible. Three primary reasons make it nearly impossible for the numerical simulation of the evaporation at the soil-atmosphere surface: (1). the boundary conditions for the atmosphere are very difficult to determine; (2). the boundary conditions such as temperature and matric suction at the soil-atmosphere are extremely difficult to determine; (3). the material parameters needed for the constitutive laws are a function of all the stress state variables listed in the Table 7.2 and are extremely difficult to obtain. To date the numerical simulations for the evaporation processes are highly restricted in theoretic investigations rather than practical applications. Wilson (1990) derived differential equations for the coupled water and heat flow at the soil-atmosphere interface. Only conductions of the air, water and heat are considered. Much more complicated physical processes such convection, radiation, eddy diffusion, and the latent heat associated with water phase changes, which are also extremely important for the evaporation process, are not considered. Very few progresses in the numerical simulation of the evaporation process at the soil-atmosphere surface are achieved. When there is vegetation, the problem is much more complicated.

Table 7.2. Constitutive Equations and Equilibrium Restrictions (Olivella et al. 1996)

Constitutive equations	Darcy's law	liquid and gas advective flux
	Fick's law	vapor and air nonadvective fluxes
	Fourier's law	conductive heat flux
	Retention curve	Liquid phase degree of saturation
	Mechanical constitutive model	Stress tensor
	Phase density	liquid density
	Gases law	gas density
Equilibrium restrictions	Henry's law	Air dissolved mass fraction
	Psychrometric law	Vapor mass fraction

7.2 Boundary Conditions and Evapotranspiration

To compute the volume change of saturated and unsaturated soils, the boundary conditions at the ground surface must be known. There are three types of flux boundary conditions, namely, the prescribed pore water pressure (matric suction), prescribed water flux and forced convection boundary condition.

Proscribed pore water pressure boundary condition is also called the first kind of boundary condition. It specifies the either the hydraulic head or pore water pressure (matric suction) at the ground surface. Direct determination of the matric suction at the soil surface is extremely difficult because the existence of soil cracks and vegetations at the ground surface. Forced convection boundary condition (B.C. Third Kind) is similar to what Dalton's Equation which will be discussed later. It requires the knowledge about the wind speed and the matric suction at the ground surface and in the air. It is very hard to get, either.

The prescribed water flux boundary condition specifies the rate of water loss or gain at the soil surface. Although there is no theoretic method to evaluate the evaporation accurately, empirical methods for estimating the evaporation have been well established in the agriculture engineering field. "In May 1990, FAO organized a consultation of experts and researchers in collaboration with the International Commission for Irrigation and Drainage and with the World Meteorological Organization, to review the FAO methodologies on crop water requirements and to advise on the revision and update of procedures. The panel of experts recommended the adoption of the Penman-Monteith combination method as a new standard for reference evapotranspiration and advised on procedures for calculating the various parameters. The FAO 56 Penman-Monteith method was developed by defining the reference crop as a hypothetical crop with an assumed height of 0.12 m, with a surface resistance of 70 s m^{-1} and an albedo of 0.23, closely resembling the evaporation from an extensive surface of green grass of uniform height, actively growing and adequately watered. The method overcomes the shortcomings of the previous FAO Penman method and provides values that are more consistent with actual crop water use data worldwide. Furthermore, recommendations

have been developed using the FAO 56 Penman-Monteith method with limited climatic data, thereby largely eliminating the need for any other reference evapotranspiration methods and creating a consistent and transparent basis for a globally valid standard for crop water requirement calculations (Allen et al. 1998)”.

In this chapter, attempts are made to transplant the FAO 56 Penman-Monteith method from the agricultural engineering to the geotechnical engineering field. It appears to be logical to estimate the evaporation at the ground surface by the FAO 56 Penman-Monteith method, and then use it as a controlling condition to simulate the volume change of the soil. Before the actual application is described an introduction of the FAO 56 Penman-Monteith method is given.

7.3 Potential Evapotranspiration

7.3.1 Introduction

The FAO 56 Penman-Monteith method uses standard climatic data that can be easily measured or derived from commonly measured data. All calculation procedures have been standardized according to the available weather data and the time scale of computation. The calculation methods, as well as the procedures for estimating missing climatic data, are presented in the publication “ Crop evapotranspiration - Guidelines for computing crop water requirements - FAO Irrigation and drainage paper 56.”(Allen et al. 1998)

Two processes are involved in the evaporation or transpiration of the water. The first is on an energy basis in which energy is needed to change the state of the molecules of water from liquid to vapor. The second one is on an aerodynamic basis in which the saturated water vapor is removed by a process of eddy diffusion (Fig. 7.2).

7.3.2 Energy Basis

At the soil-atmosphere interface, there is a continuous of flow of water molecules from the water surface to the air and a return to the liquid surface. When a condition of the equilibrium with pure water exists, the two flows are equal and the air is saturated with

water vapor. The partial pressure exerted by the vapor at this time is called saturated vapor pressure. Under most conditions, the air is not saturated. Fig. 7.3 shows the hourly relative humidity and the corresponding suction in the air in an arbitrary day at a site at Arlington, Texas. For the capillary water in the soil where the air-water surface is curved in a concave shape, the saturation vapor pressure is reduced. It is not uncommon the air has a relative humidity of less than 100%. A 90% relative humidity corresponds to suction as high as 10^5 kPa. As a consequence there is always some vapor pressure deficiency and the soil water always tends to be vaporized at the soil-air interface.

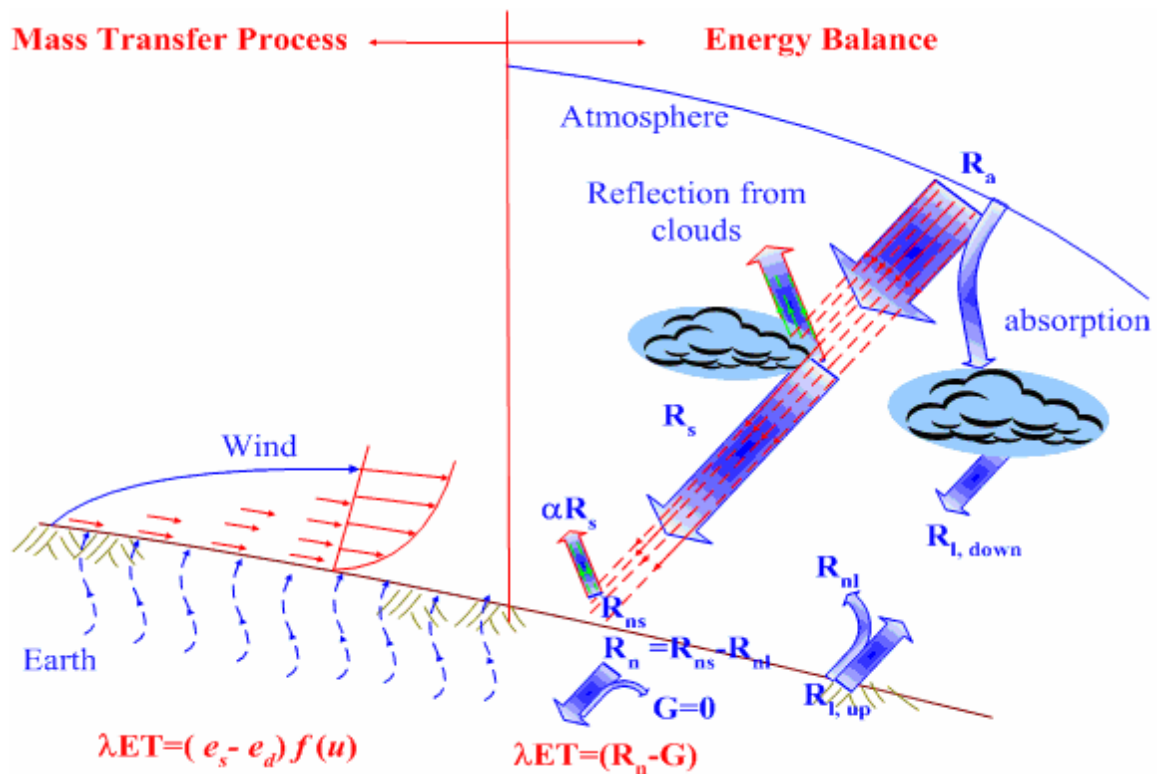


Fig. 7.2. Two bases for the FAO 56 Penman-Monteith method (After Allen et al. 1998)

Energy is needed for the evaporation. This energy is known as the latent heat of vaporization λ , which is a function of temperature. For example, at 20°C , λ is equal to 2.45 MJ/kg approximately. In other words, 2.45 MJ are needed to vaporize 1 kg or

0.001m³ water. Therefore, an energy input of 2.45MJ/m² from the sun is able to vaporize 0.001m or 1mm of water. Then the latent evaporation energy of 1 mm water is equivalent to 2.45MJ/m².

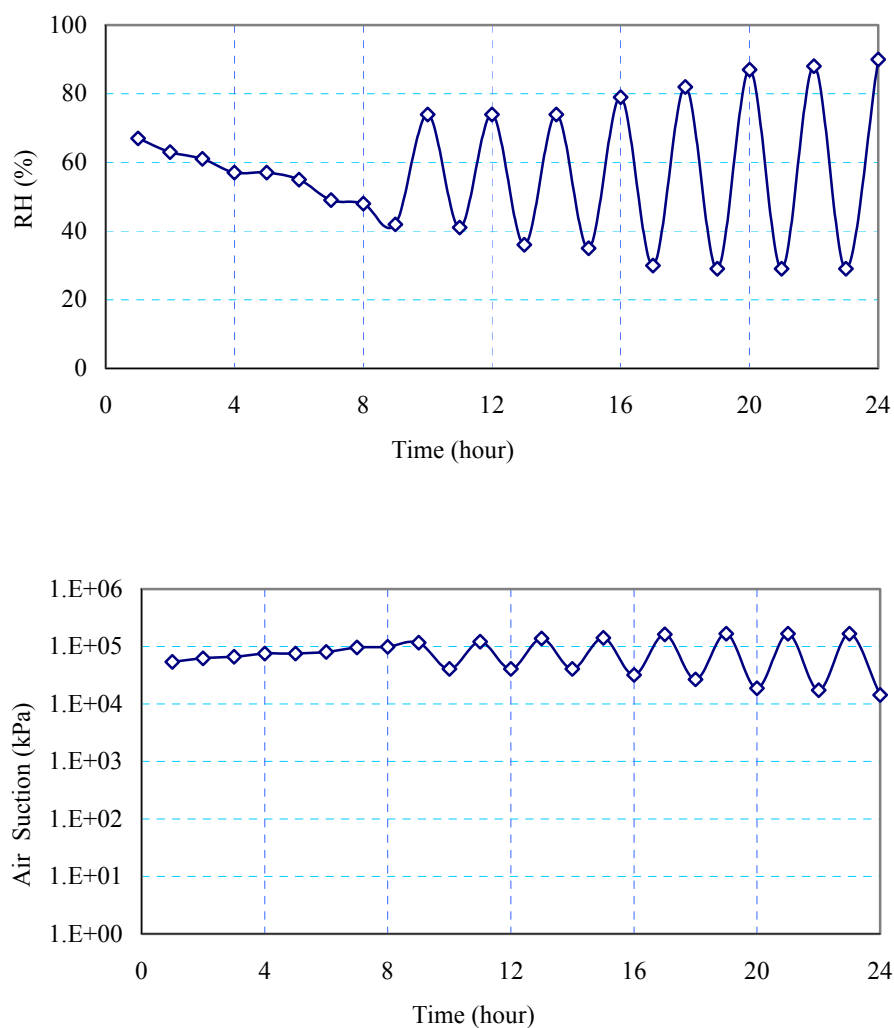


Fig.7.3. The air relative humidity (RH) and total suction at different times in a day (08/01/99, Arlington, TX)

The principle source of heat energy for evaporation is solar radiation for the sun. As shown in Fig. 7.2, for the same location on the earth at the same day in the year, the solar

radiation received at the top of the earth's atmosphere on a horizontal surface is the same every year, which is called the extraterrestrial (solar) radiation, R_a . When there are clouds, some of the radiation is scattered, reflected or absorbed by the atmospheric gases, clouds and dust. The amount of radiation reaching a horizontal plane is known as the solar radiation, R_s , which is also referred to as shortwave radiation because the sun emits energy by means of electromagnetic waves characterized by short wavelengths. A considerable amount of solar radiation reaching the earth's surface is reflected. The fraction of the solar radiation R_s that is not reflected from the surface is called the net solar radiation, R_{ns} . The solar radiation absorbed by the earth is converted to heat energy. The earth also loses this energy by several processes, including emission of radiation. The radiative energy emitted by the earth has wavelengths longer than those from the sun because the earth is at a much lower temperature than the sun. Therefore, the terrestrial radiation is referred to as longwave radiation. The earth's surface both emits (R_l , up) and receives longwave radiation from the atmosphere (R_l , down). The difference between outgoing and incoming longwave radiation is called the net longwave radiation, R_{nl} . As the outgoing longwave radiation is almost always greater than the incoming longwave radiation, R_{nl} represents an energy loss. Consequently, the energy available to heat the soil and the soil water is the difference between the net solar radiation, R_{ns} and the net outgoing longwave radiation R_{nl} , which is called the net radiation, R_n . Part of the energy is used to heat the soil, which is called soil heat flux (G), and the rest is used for vaporizing the soils water as shown in Fig. 7.2. This is the theoretic basis for the radiation method. The soil temperature at the ground surface is needed to estimate the energy for evapotranspiration, which is usually very difficult to measure.

7.3.3 Aerodynamic Basis

The transfer of water vapor from the ground surface to the atmosphere may be described by Dalton's Equation,

$$E = (e_s - e_a) f(u) \quad (7.1a)$$

where E is the evaporation in unit time, e_s is the vapor pressure at the evaporation surface, e_a is the vapor pressure in the atmosphere above, and $f(u)$ is a function of the horizontal wind velocity. For water, e_s is known if the surface temperature is known.

The total suction of a soil can be calculated by the Kelvin's Equation as followings:

$$\psi = -\frac{RT}{v_{w0}w_v} \ln\left(\frac{P}{P_0}\right) \quad (2.1)$$

where ψ =total suction (kPa); R =universal gas constant, equal to 8.31432 J/(mol•K); T =absolute temperature, (k); v_{w0} = specific volume of water(m³/kg); w_v =molecular mass of water vapor (kg/kmol); P = partial pressure of pore-water vapor (kPa); and P_0 = saturation pore water pressure at the same temperature; $RH = \frac{P}{P_0}$ is also called relative humidity.

As can be seen from the definition of the total suction (Eq. 2.1), the e_s and e_a actually reflects the total suction difference between the air and the evaporation surface. That is, the evaporation from the soil surface depends on the suction in both the air and the soil, and the wind speed. To use Eq. 7.1a to calculate the evaporation from the soil surface, the surface temperature (or the total suction at the evaporation surface) must be known for the evaporation surface, which, as we discussed before, is very difficult to obtain. Wilson (1990) used the Dalton's Equation to simulate the evaporation of a sand column.

7.3.4 Penman's Derivation

Both the aerodynamic basis and the energy basis involve knowing the surface temperature, which is extremely difficult to obtain. A method was suggested by Penman (1948) to eliminate the parameters measured with most difficulty-surface temperature. It provided an opportunity to make theoretical estimates of evaporation rates from standard meteorological data. Penman's derivation is as follows:

The heat budget H is used in evaporation, E , heating of the air, K , and heating of the soil, S .

$$H = E + K + S \quad (7.2)$$

Over a single day, the change in the stored heat, S , is negligible compared with other changes. Thus, Eq. 7.2 can be safely reduced to

$$H = E + K \quad (7.3)$$

The transport of vapor and the transport of heat by eddy diffusion are, in essentials, controlled by the same mechanism, and apart from the differences in the molecular constants, the one is expected to be governed by $(e_s - e_d)$ where the other is governed by $(T_s - T_a)$. To a very good approximation, therefore, it is possible to write down the ratio of K/E in the form,

$$K / E = \beta = \gamma(T_s - T_a) / (e_s - e_d) \quad (7.4)$$

where, T_s , T_a , and T_d are temperatures of surface, air and dewpoint. Thus,

$$H = E(1 + \beta), \quad E = H / (1 + \beta) \quad (7.5)$$

Let E_a be the value of E obtained by putting e_a instead of e_s . Then,

$$E_a = (e_a - e_d) f(u) \quad (7.1b)$$

where e_s , e_a and e_d are the saturation vapor pressure at the temperature of T_s , T_a , and T_d , respectively, i.e.

$$\frac{E_a}{E} = 1 - \frac{(e_s - e_a)}{(e_s - e_d)} = 1 - \phi \quad (7.6)$$

From Eq. 7.4 and 7.5,

$$E = H / (1 + \beta) = \frac{H}{\left[1 + \gamma \frac{T_s - T_a}{e_s - e_d} \right]} \quad (7.7)$$

If we set

$$\Delta = \frac{e_s - e_d}{T_s - T_a} \quad (7.8)$$

where Δ is the slope of the e vs. T curve at $T=T_a$, then

$$\frac{H}{E} = (1 + \beta) = 1 + \gamma \frac{T_s - T_a}{e_s - e_d} = 1 + \gamma \frac{e_s - e_d}{\Delta(e_s - e_d)} = 1 + \frac{\gamma}{\Delta} \quad (7.9)$$

From Eq. 7.7 and 7.9,

$$E = \frac{H + \frac{\gamma}{\Delta} E_a}{\left(1 + \frac{\gamma}{\Delta} \right)} = \frac{\Delta H + \gamma E_a}{(\Delta + \gamma)} = \frac{\Delta H + \gamma(e_a - e_d) f(u)}{(\Delta + \gamma)} \quad (7.10)$$

Eq. 7.10 is the Penman (1948)'s Equation. This equation can be used for the potential evaporation estimate for the bare soil, vegetation and water surface. All the

factors influencing evaporation or transpiration including net radiation, air temperature, wind speed and relative humidity are considered.

7.3.5 The FAO 56 PM Method

There are about seven versions of combination methods: 1948 original Penman method (Penman 1948), 1963 Penman method (Penman 1963), FAO 24 modified Penman method (Doorenbos and Pruitt 1977), IFAS Florida Modified Penman method (Jones et al. 1984), ASCE Penman Monteith method (Jensen et al.1990), ASCE Penman-Monteith method (Allen et al.1998), ASCE 2000 Penman-Monteith method (Walter et al.2000), and the FAO 56 Penman-Monteith method (Allen et al. 1998). The FAO 56 Penman – Monteith method is well established as the most accurate and robust methods to estimate reference ET, and the past decade of research has solidified its status as the international standard.

The FAO 56 Penman-Monteith method was developed by defining the reference crop as a hypothetical crop with an assumed height of 0.12 m, with a surface resistance of 70 s m⁻¹ and an albedo of 0.23, closely resembling the evaporation from an extensive surface of green grass of uniform height, actively growing and adequately watered. From the original Penman-Monteith equation and the equations of the aerodynamic and canopy resistance, the FAO Penman-Monteith equation has been derived in Chapter II:

$$ET_0 = \frac{0.408\Delta(R_n - G) + \gamma \frac{900}{T + 273} u_2 (e_s - e_a)}{\Delta + \gamma(1 + 0.34u_2)} \quad (3.5)$$

where ET_0 =reference evapotranspiration (mm day⁻¹); R_n =net radiation at the crop surface (MJ m⁻² day⁻¹); G =soil heat flux density (MJ m⁻² day⁻¹); T = air temperature at 2 m height (°C); u_2 =wind speed at 2 m height (m s⁻¹); e_s =saturation vapor pressure (kPa); e_a =actual vapor pressure (kPa); $e_s - e_a$ =saturation vapor pressure deficit (kPa); Δ =slope vapor pressure curve (kPa °C⁻¹); and γ =psychrometric constant (kPa °C⁻¹).

The method overcomes the shortcomings of the previous FAO Penman method and provides values that are more consistent with actual crop water use data worldwide. Furthermore, recommendations have been developed using the FAO Penman-Monteith method with limited climatic data, thereby largely eliminating the need for any other reference evapotranspiration methods and creating a consistent and transparent basis for a globally valid standard for crop water requirement calculations. Fig. 7.4 shows the calculation procedure of the FAO 56 Penman Monteith Method.

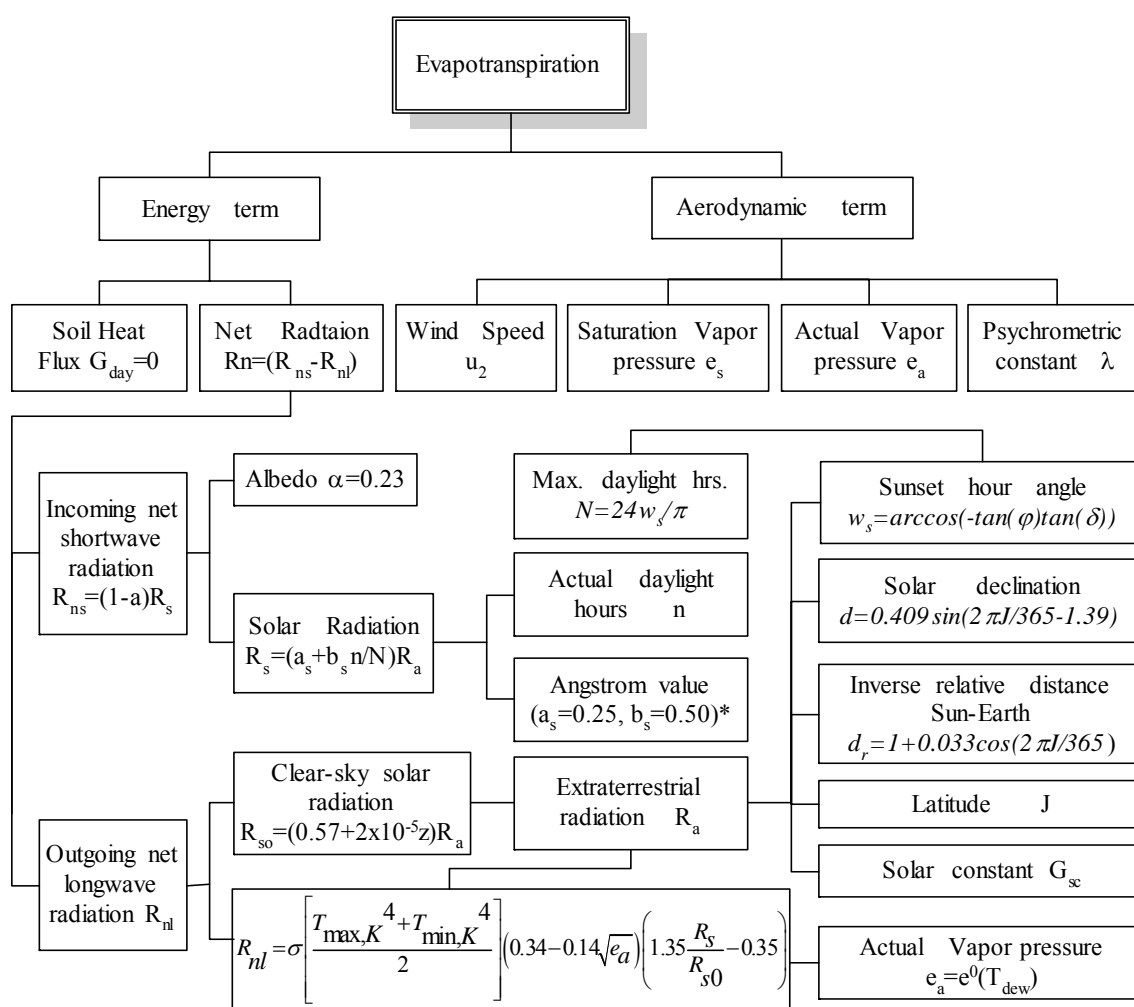


Fig.7.4. Calculation procedures of the FAO 56 Penman-Monteith method

7.3.6 An Example: Reference ET for the Site at Arlington, Texas

The site described in Chapter IV is used as an example to calculate the reference ET. The calculation will be used in the future numerical simulation in Chapter VIII.

7.3.6.1 Extraterrestrial Radiation (R_a)

The principle source of heat energy for ET is solar radiation for the sun. As shown in Fig. 7.2, the solar radiation received at the top of the earth's atmosphere on a horizontal surface is called the extraterrestrial (solar) radiation, R_a . If the sun is directly overhead, the surface is perpendicular to the sun's rays at the top of the earth's atmosphere and the radiation is constant (about 0.082 MJ m⁻² min⁻¹). It is also called the solar constant. The actual intensity of radiation is determined by the angle between the direction of the sun's rays and the normal to the surface of the atmosphere. This angle will change during the day and will be different at different latitudes and in different seasons. However, for the same place and the same day in the year, it is the same. The extraterrestrial radiation, R_a , for each day of the year and for different latitudes can be estimated from the solar constant, the solar declination and the time of the year by:

$$R_a = \frac{24(60)}{\pi} G_{sc} d_r [\omega_s \sin \varphi \sin \delta + \cos \varphi \cos \delta \sin \omega_s] \quad (7.11)$$

where R_a =extraterrestrial radiation (MJ m⁻² day⁻¹); G_{sc} =solar constant, 0.0820 MJ m⁻² min⁻¹; d_r =inverse relative distance Earth-Sun; $d_r = 1 + 0.0033 \cos(2\pi J / 365)$; ω_s =sunset hour angle (rad); $\omega_s = \arccos(-\tan(\varphi) \tan(\delta))$; φ =latitude (rad); δ =solar declination, $\delta = 0.409 \sin(2\pi J / 365 - 1.39)$ (rad); J = the number of the day in the year.

All the data needed for Eq. 7.11 are the latitude of the site and the day number for each day. The site has latitude of 32.7330 N, and a elevation of 198.12m (650ft).

R_a is expressed in the above equation in MJ m⁻² day⁻¹. The corresponding equivalent evaporation in mm/day is obtained by multiplying R_a by 0.408. Daily values

of R_a between 08/01/1999 and 05/30/2003 for the site at Arlington, Texas are plotted in Fig. 7.5.

7.3.6.2 Solar or Shortwave Radiation (R_s)

When there are clouds, some of the radiation is scattered, reflected or absorbed by the atmospheric gases, clouds and dust (Fig. 7.2). The amount of radiation reaching a horizontal plane is known as the solar radiation, R_s . For a cloudless day, R_s is roughly 75% of extraterrestrial radiation. On a cloudy day, the radiation is scattered in the atmosphere, but even with extremely dense cloud cover, about 25% of the extraterrestrial radiation may still reach the earth's surface mainly as diffuse sky radiation. Solar radiation is also known as global radiation, meaning that it is the sum of direct shortwave radiation from the sun and diffuse sky radiation from all upward angles.

R_s can be calculated with the Angstrom formula which relates solar radiation to extraterrestrial radiation and relative sunshine duration:

$$R_s = \left(a_s + b_s \frac{n}{N} \right) R_a \quad (7.12)$$

where R_s = solar or shortwave radiation ($\text{MJ m}^{-2} \text{ day}^{-1}$); n = actual duration of sunshine (hour); N = maximum possible duration of sunshine or daylight hours (hour); n/N = relative sunshine duration (-); R_a = extraterrestrial radiation ($\text{MJ m}^{-2} \text{ day}^{-1}$); a_s = regression constant, expressing the fraction of extraterrestrial radiation reaching the earth on overcast days ($n = 0$); $a_s + b_s$ fraction of extraterrestrial radiation reaching the earth on clear days ($n = N$).

Because the actual duration of sunshine n is not available for the site, the Hargreaves' radiation formula was used to calculate the R_s ,

$$R_s = k_{R_s} \sqrt{(T_{\max} - T_{\min})} R_a \quad (7.13)$$

where R_a =extraterrestrial radiation ($\text{MJ m}^{-2} \text{d}^{-1}$); T_{\max} =maximum air temperature ($^{\circ}\text{C}$); T_{\min} =minimum air temperature ($^{\circ}\text{C}$); k_{R_s} =adjustment coefficient (0.16.. 0.19); k_{R_s} is taken as $0.18 (^{\circ}\text{C}^{-0.5})$.

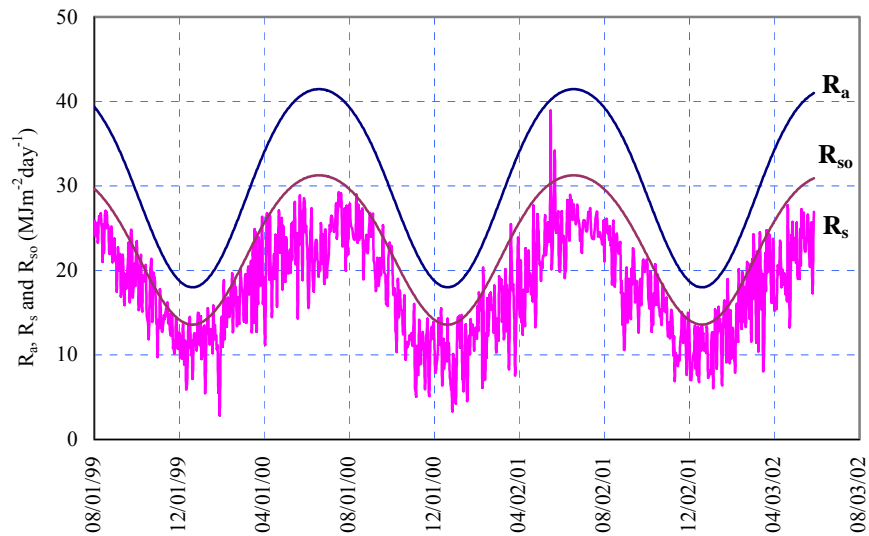


Fig. 7.5. Daily values of R_a , R_{s0} and R_s between 08/01/1999 and 05/30/2003 for the site at Arlington, Texas

7.3.6.3 Clear-Sky Solar Radiation (R_{s0})

The clear-sky radiation, R_{s0} , when $n = N$ for R_s , is calculated by the following equation:

$$R_{s0} = (0.75 + 2 \times 10^{-5}z)R_a \quad (7.14)$$

where z = station elevation above sea leveling meter, which is 198.12m (650ft) for the site.

Daily values of R_s and R_{s0} between 08/01/1999 and 05/30/2003 for the site at Arlington, Texas are shown in Fig. 7.5.

7.3.6.4 Net Solar Radiation (R_{ns})

A considerable amount of solar radiation reaching the earth's surface is reflected. The fraction of the solar radiation R_s that is not reflected from the surface is called the net solar radiation, R_{ns} . The net solar radiation, R_{ns} , is the fraction of the solar radiation R_s that is not reflected from the surface. It is calculated by the following equation,

$$R_{ns}=(1-\alpha)R_s \quad (7.15)$$

For the green grass reference crop, α is assumed to have a value of 0.23.

7.3.6.5 Net Longwave Radiation (R_{nl})

The rate of longwave energy emission is proportional to the absolute temperature of the surface raised to the fourth power. This relation is expressed quantitatively by the Stefan-Boltzmann law. The net energy flux leaving the earth's surface is, however, less than that emitted and given by the Stefan-Boltzmann law due to the absorption and downward radiation from the sky. Water vapor, clouds, carbon dioxide and dust are absorbers and emitters of longwave radiation. Their concentrations should be known when assessing the net outgoing flux. As humidity and cloudiness play an important role, the Stefan-Boltzmann law is corrected by these two factors when estimating - the net outgoing flux of longwave radiation. It is thereby assumed that the concentrations of the other absorbers are constant:

$$R_{nl} = \sigma \left[\frac{T_{\max,K}^4 + T_{\min,K}^4}{2} \right] (0.34 - 0.14\sqrt{e_a}) \left(1.35 \frac{R_s}{R_{s0}} - 0.35 \right) \quad (7.16)$$

where R_n =net outgoing longwave radiation ($\text{MJ m}^{-2} \text{ day}^{-1}$); σ =Stefan-Boltzmann constant ($4.903 \cdot 10^{-9} \text{ MJ K}^{-4} \text{ m}^{-2} \text{ day}^{-1}$); $T_{\max, K}$ =maximum absolute temperature during the 24-hour period ($K = ^\circ\text{C} + 273.16$); $T_{\min, K}$ =minimum absolute temperature during the 24-hour period ($K = ^\circ\text{C} + 273.16$); e_a =actual vapor pressure (kPa); R_s/R_{s0} =relative

shortwave radiation (limited to £ 1.0); R_s =measured or calculated (Eq. 7.13) solar radiation ($\text{MJ m}^{-2} \text{ day}^{-1}$); R_{s0} =calculated (Eq. 7.14) clear-sky radiation ($\text{MJ m}^{-2} \text{ day}^{-1}$).

An average of the maximum air temperature to the fourth power and the minimum air temperature to the fourth power is commonly used in the Stefan-Boltzmann equation for 24-hour time steps. The term $(0.34 - 0.14\sqrt{e_a})$ expresses the correction for air humidity, and will be smaller if the humidity increases. The effect of cloudiness is expressed by $\left(1.35 \frac{R_s}{R_{s0}} - 0.35\right)$. The term becomes smaller if the cloudiness increases and hence R_s decreases. The smaller the correction terms, the smaller the net outgoing flux of longwave radiation. Note that the R_s/R_{s0} term in Eq. 7.14 must be limited so that $R_s/R_{s0} \leq 1.0$.

7.3.6.6 Net Radiation (R_n)

The net radiation (R_n) is the difference between the incoming net shortwave radiation (R_{ns}) and the outgoing net longwave radiation (R_{nl}):

$$R_n = R_{ns} - R_{nl} \quad (7.17)$$

Fig. 7.6 shows the daily values of R_{ns} , R_{nl} and R_n between 08/01/1999 and 05/30/2003 for the site at Arlington, Texas.

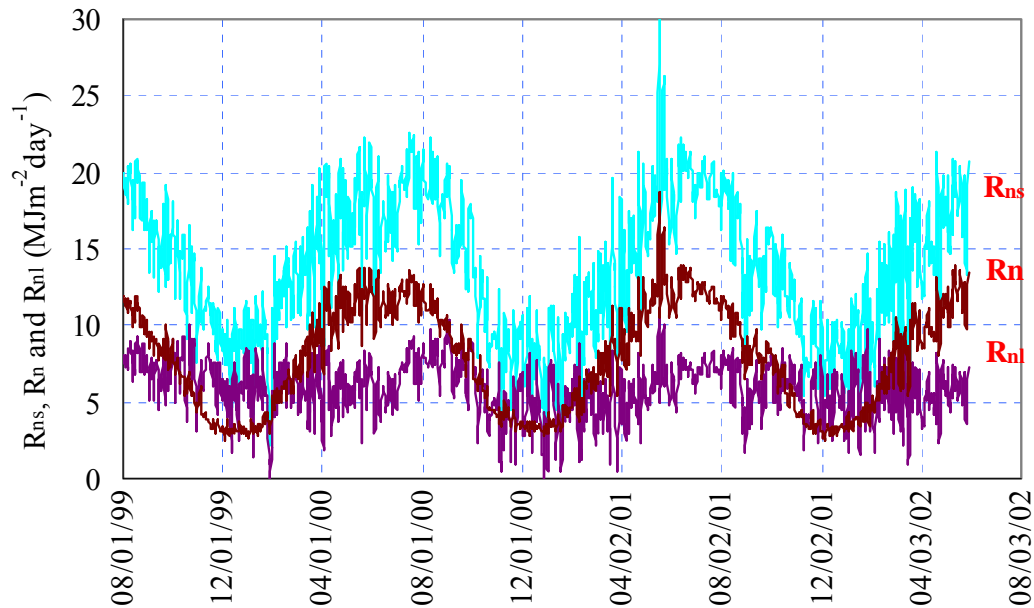


Fig. 7.6. Daily values of R_{ns} between 08/01/1999 and 05/30/2003 for the site at Arlington, Texas

7.3.6.7 Soil Heat Flux (G)

Complex models are available to describe soil heat flux. Because soil heat flux is small compared to R_n , particularly when the surface is covered by vegetation and calculation time steps are 24 hours or longer, a simple calculation procedure is presented here for long time steps, based on the idea that the soil temperature follows air temperature:

$$G = C_s \frac{T_i - T_{i-1}}{\Delta t} \Delta z \quad (7.18)$$

where G soil heat flux ($\text{MJ m}^{-2} \text{ day}^{-1}$); C_s soil heat capacity ($\text{MJ m}^{-3} \text{ }^\circ\text{C}^{-1}$); T_i air temperature at time i ($^\circ\text{C}$); T_{i-1} air temperature at time $i-1$ ($^\circ\text{C}$); Δt length of time interval (day); Δz effective soil depth (m).

As the soil temperature lags air temperature, the average temperature for a period should be considered when assessing the daily soil heat flux, i.e., Δt should exceed one day. The depth of penetration of the temperature wave is determined by the length of the time interval. The effective soil depth, Δz , is only 0.10-0.20 m for a time interval of one or a few days but might be 2 m or more for monthly periods. The soil heat capacity is related to its mineral composition and water content.

As the magnitude of the day, soil heat flux beneath the grass reference surface is relatively small, it may be ignored and thus:

$$G_{\text{day}} \cong 0 \quad (7.19)$$

7.3.6.8 Saturation Vapor Pressure

Saturation vapor pressure is related to air temperature. It can be calculated from the air temperature by:

$$e^{\circ}(T) = 0.6108 \exp \left[\frac{17.27T}{T + 237.4} \right] \quad (7.20a)$$

where $e^{\circ}(T)$ saturation vapor pressure at the air temperature T (kPa); T air temperature ($^{\circ}\text{C}$)

7.3.6.9 Actual Vapor Pressure (e_a)

Actual vapor pressure (e_a) can be derived from dewpoint temperature,

$$e_a = e^{\circ}(T_{\text{dew}}) = 0.6108 \exp \left[\frac{17.27T_{\text{dew}}}{T_{\text{dew}} + 237.4} \right] \quad (7.20b)$$

7.3.6.10 Slope of Saturation Vapor Pressure Curve (Δ)

$$\Delta = \frac{4098 \left[0.6108 \exp \left(\frac{17.27T}{T + 237.4} \right) \right]}{(T + 237.4)^2} \quad (7.21)$$

7.3.6.11 Atmospheric Pressure (P)

$$P = 101.3 \left(\frac{293 - 0.0065z}{293} \right)^{5.26} \quad (7.22)$$

where P atmospheric pressure (kPa); z elevation above sea level (m).

7.3.6.12 Latent Heat of Vaporization (λ)

$\lambda = 2.45 \text{ MJ kg}^{-1}$ is taken in the simplification of the FAO 45 Penman-Monteith equation. This is the latent heat for an air temperature of about 20°C.

7.3.6.13 Psychrometric Constant (γ)

The psychrometric constant, γ , is given by:

$$\gamma = \frac{C_p P}{\varepsilon \lambda} = 0.665 \times 10^{-3} P \quad (7.23)$$

where γ = psychrometric constant (kPa °C⁻¹); P = atmospheric pressure (kPa); λ = latent heat of vaporization, 2.45 (MJ kg⁻¹); C_p = specific heat at constant pressure, 1.013 10⁻³ (MJ kg⁻¹ °C⁻¹); ε = ratio molecular weight of water vapor/dry air = 0.622.

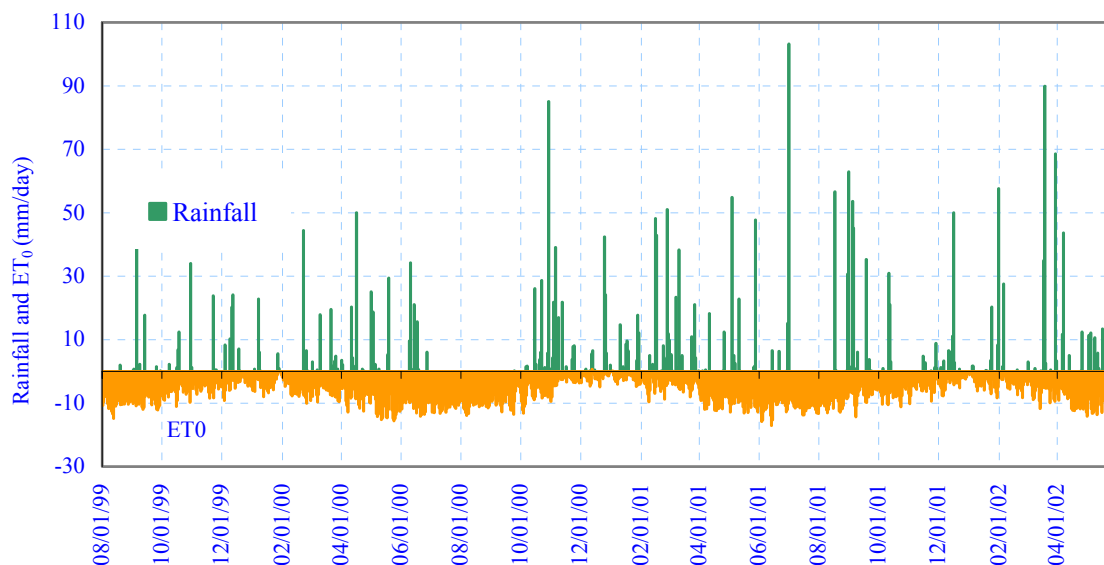


Fig. 7.7. Daily evapotranspiration and rainfall of the site between 08/01/1999 and 05/30/2003

By following the procedures in Fig. 7.4, the potential evaporation between 08/01/1999 and 05/30/2003 can be calculated and the result is shown in Fig. 7.7. Fig. 7.7 also shows the daily rainfall data for this period. It can be seen that at the first year the rainfall and the evaporation is basically evenly distributed, and then there was a dry season from July to October, 2000. The dry season was followed by a wet season from October 2000 to March 2001, and then the rainfall and the evapotranspiration was evenly distributed again.

7.4 Crop Evapotranspiration under Standard Conditions

The above calculation is the reference crop evapotranspiration by assuming that the reference crop has an assumed height of 0.12 m, with a surface resistance of 70 s/m and an albedo of 0.23, which closely resembles the evaporation from an extensive surface of green grass of uniform height, actively growing and adequately watered. The calculation

expresses the evaporating ability of the atmosphere at a specific location and time of the year and does not consider the crop characteristics and soil factors.

The crop evapotranspiration differs distinctly from the reference grass evapotranspiration (ET_o) as the ground cover, canopy properties and aerodynamic resistance of the crop are different from grass. For example, the site at Arlington, Texas was covered by the Johnson grass, which is a warm season, perennial grass. The maximum grass height is as high as 1.0m. In the FAO 56 PM Method, the effects of characteristics that distinguish the cropped surface from the reference surface are integrated into the crop coefficient. Two calculation approaches are used to change the reference grass evapotranspiration in to cropped evapotranspiration (the potential evapotranspiration for actual crop (vegetation)): the single and the dual crop coefficient approach. The single crop coefficient approach was used in this dissertation to show the procedure of the simulation. By multiplying ET_o by the crop coefficient, ET_c , which is called crop evapotranspiration under standard conditions, is determined.

$$ET_c = K_c ET_o \quad (7.24)$$

where ET_c =crop evapotranspiration (mm/day); K_c =crop coefficient (dimensionless); ET_o =reference crop evapotranspiration (mm/day).

ET_c represents the evapotranspiration from disease-free, well-fertilized crops, grown in large fields, under optimum soil water conditions and achieving full production under the given climatic conditions. Factors influencing the crop coefficient include the crop type, climate, soil evaporation and crop growth stages. For our research, the Arlington site was covered by the Johnson grass, which is a warm season, perennial grass. The maximum grass height is as high as 1.0m. Texas ET Network (<http://texaset.tamu.edu/>) recommends that the crop coefficient for this kind of grass is 0.6 through much of the year. For the dual crop coefficient approach, the principle is similar.

7.5 Crop Evapotranspiration under Non-Standard Conditions

7.5.1 Introduction

The actual evapotranspiration or infiltration also depends on the soil status. When the soil is wet, the water is relatively free to move and easily taken up by the plant roots. (The potential evaporation from the surface of lake and the wet soil are basically the same because the soil particles are surrounded by water and can move from one particle to the other relatively easily). However, the potential for the soil to absorb water is low. Conversely, in dry soils, water is strongly bounded by absorptive force to the soil matrix, and is less easily to lose by evaporation or extracted by the vegetation. If a dry soil and a wet soil are submerged into water, the dry soil will absorb more water if all the other conditions are the same.

The evapotranspiration under non-standard conditions ($ET_c \text{ adj}$) is the evapotranspiration from crops or vegetations grown under management and environmental conditions that differ from the standard conditions. The actual evapotranspiration in the field may deviate from ET_c due to non-optimal conditions such as the presence of pests and diseases, soil salinity, low soil fertility, water shortage or waterlogging. This may result in scanty plant growth, low plant density and may reduce the evapotranspiration rate below ET_c . The effects of soil water stress are described by multiplying the basal crop coefficient by the water stress coefficient, K_s

$$ET_c \text{ adjusted} = K_s \times K_c \times ET_0 \quad (7.25)$$

7.5.2 Determination of the Water Stress Coefficient

Soil water availability refers to the capacity of a soil to retain water available to vegetations. It is considered that after a heavy rain, water in the macropores of the saturated soil will drain until field capacity is reached. Usually, the matric suction at the field capacity is considered as 10 kPa ($pF=2$). In absence of water supply, the water content in the root zone decreases as a result of water uptake by the vegetation or tree. As water uptake progresses, the remaining water is held to the soil particles with greater

force because the double diffusion layer becomes thin and the electromagnetic force increases, which makes it more difficult for the vegetation or tree to extract it. Eventually, the wilt point for vegetation or tree is reached and the water uptake is zero. Usually, the suction at the permanent wilt point is at 32,000 kPa (pF=5.5). The suction value at a bare soil surface may be higher than 32,000 kPa (pF=5.5). However, the range in which the suction values are higher than 32,000 kPa usually is limited in a small depth and of little significance. The total available water in the root zone is defined as the difference between the water content at field capacity and wilting point:

$$TAW = 1000(\theta_{FC} - \theta_{WP}) H \quad (7.26)$$

where TAW=the total available soil water in the root zone (mm); θ_{FC} =the water content at field capacity (m^3/m^3); θ_{WP} =the water content at permanent wilting point (m^3/m^3); H= the rooting depth (m).

TAW is the amount of water that vegetation can extract from its root zone, and its magnitude depends on the type of soil and the rooting depth. As can be seen for the water content constitutive surface, TAW is also a function of the mechanical stress. A higher mechanical stress corresponds to smaller macropores in the soil. The bigger the mechanical stress, the smaller the TAW is.

Although water is theoretically available until wilting point, vegetation water uptake is reduced well before wilting point is reached. Where the soil is sufficiently wet, the soil supplies water fast enough to meet the atmospheric demand of the vegetation, and water uptake equals E_{Tc}. As the soil water content decreases, water becomes more strongly bound to the soil matrix and is more difficult to extract. When the soil water content drops below a threshold value, soil water can no longer be transported quickly enough towards the roots to respond to the transpiration demand and the vegetation begins to experience stress. The fraction of TAW that vegetation can extract from the root zone without suffering water stress is the readily available soil water:

$$RAW = p TAW = p 1000(\theta_{FC} - \theta_{WP}) H \quad (7.27)$$

where RAW= the readily available soil water in the root zone (mm); p= average fraction of Total Available Soil Water (TAW) that can be depleted from the root zone before moisture stress (reduction in ET) occurs (0-1).

TAW can be calculated from the water content constitutive surface. If the burying depth of the soil is known, the corresponding mechanical stress can be obtained from the total unit weight of the soil and Poisson's ratio. The corresponding matric suctions for the field capacity and the permanent wilt point are 10 kPa and 32,000 kPa, respectively. As a consequence, the corresponding θ_{FC} and θ_{WP} can be calculated from the water content constitutive surface.

Water content in the root zone can also be expressed by root zone depletion, D_r , i.e., water shortage relative to field capacity.

$$D_r = 1000(\theta_{FC} - \theta) H \quad (7.28)$$

where θ is the current volumetric water content.

At field capacity, the root zone depletion is zero ($D_r = 0$). When soil water is extracted by evapotranspiration, the depletion increases and stress will be induced when D_r becomes equal to RAW. After the root zone depletion exceeds RAW (the water content drops below the threshold θ_i), the root zone depletion is high enough to limit evapotranspiration to less than potential values and the actual evapotranspiration begins to decrease in proportion to the amount of water remaining in the root zone.

For $D_r > RAW$, K_s is given by:

$$K_s = \frac{TAW - D_r}{TAW - RAW} = \frac{TAW - D_r}{(1-p)TAW} = \frac{\theta - \theta_{WP}}{(1-p)(\theta_{FC} - \theta_{WP})} \quad (7.29)$$

where K_s = a dimensionless transpiration reduction factor dependent on available soil water (0 - 1); D_r =root zone depletion (mm); TAW=total available soil water in the root zone (mm); p =fraction of TAW that a crop can extract from the root zone without suffering water stress .

When the root zone depletion is smaller than RAW, $K_s = 1$.

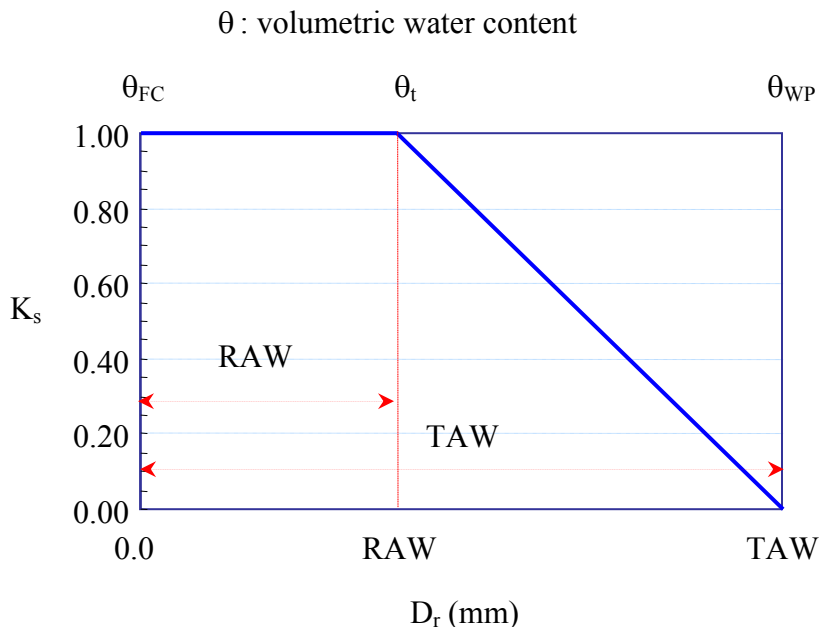


Fig. 7.8. Water stress coefficient, K_s (After Allen et al. 1998)

Fig. 7.8 actually reflects that the actual evapotranspiration is dependent on matric suction and decreases with an increase in suction because the matric suction is related to the water content through the soil-water characteristic curve. Fig. 7.9 shows the relationship between the water stress coefficient K_s and the matric suction for soil SW145 at the ground surface (mechanical stress is 1kPa) and the $p=0.5$. The matric suction for the field capacity is 10kPa and for the permanent wilt point it is 31622kPa (5.5pF).

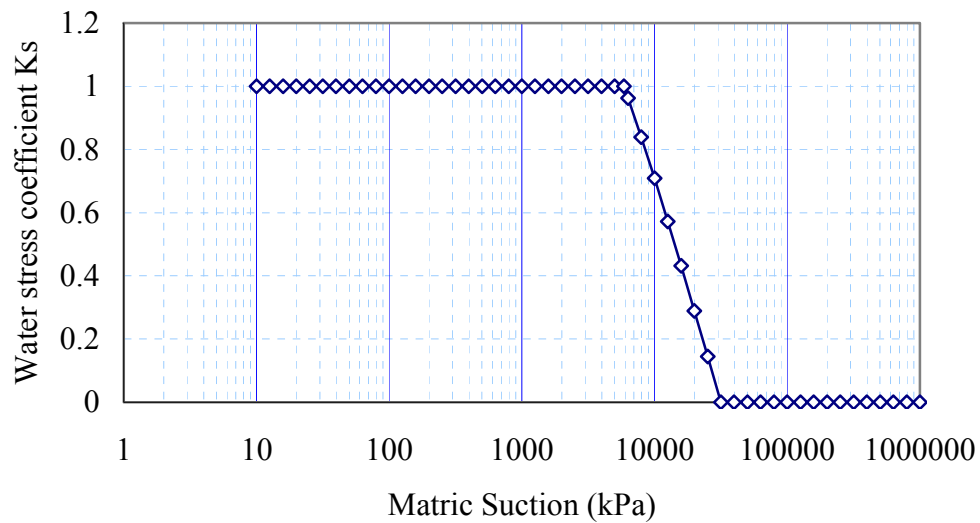


Fig. 7.9. Water stress coefficient, K_s for the site at Arlington, Texas.

Texas ET Network (<http://texaset.tamu.edu/>) recommends that the average water stress coefficient for low stress is 0.8 through much of the year, which corresponds to a $p=0.6$ approximately. The low water stress condition was chosen because more restrictions were applied for the actual evapotranspiration. Fig. 7.10 shows the cumulative rainfall, cumulative actual evapotranspiration and their difference for the Arlington site when $K_s=0.8$ and the $K_c=0.6$. The difference approximately represents the net water input to the soil.

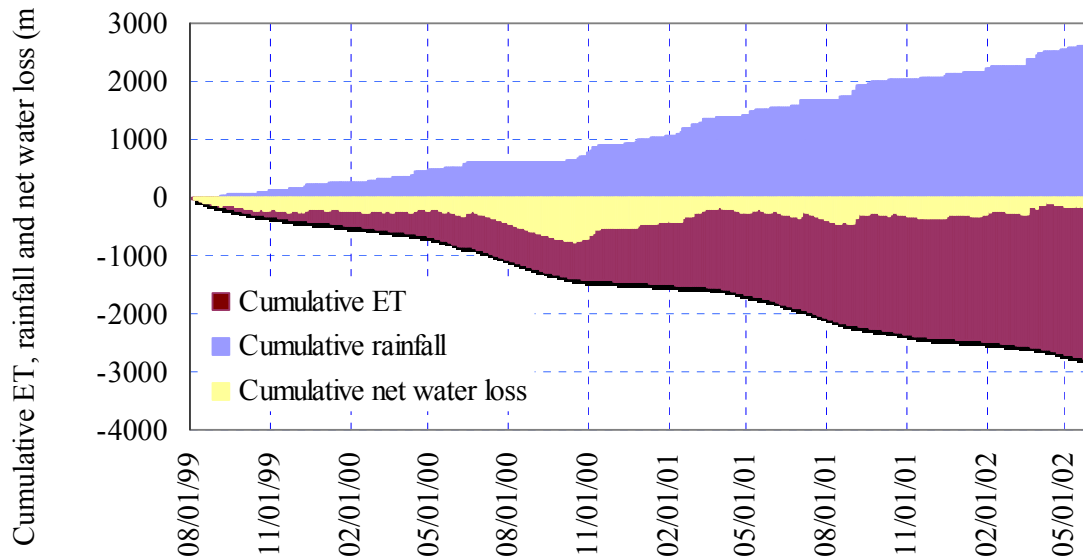


Fig. 7.10. Cumulative evapotranspiration, rainfall and net water loss over a period of two years for a site at Arlington, Texas

7.6 Water Balance and Net Water Loss

Before the further discussion of the application of the actual evapotranspiration to the boundary conditions, the water balance at the root zone is discussed. To determine the actual evapotranspiration at the grass root zone, a daily water balance computation for the grass root zone is required. The grass root zone can be presented by means of a container with a soil solid base (Fig. 7.11). The water content in the container may fluctuate. If the mean mechanical stress is constant (the container will be squeezed by the mechanical stress), the container will have a fixed ability to hold water, which is between the saturation (swell limit, matric suction equal to zero) and zero. The daily water content can be expressed in terms of depletion at the end of the day as followings:

$$D_{r,i} = D_{r,i-1} - (P - RO)_i - I_i - CR_i + ET_{c,i} + DP_i \quad (7.30)$$

where $D_{r,i}$ =root zone depletion at the end of day i (mm); $D_{r,i-1}$ =water content in the root zone at the end of the previous day, $i-1$ (mm); P_i =precipitation on day i (mm); RO_i =runoff from the soil surface on day i (mm); I_i =net irrigation depth on day i that infiltrates the soil (mm); CR_i =capillary rise from the groundwater table on day i (mm); $ET_{c,i}$ =actual evapotranspiration on day i (mm); DP_i =water loss out of the root zone by deep percolation on day i (mm).

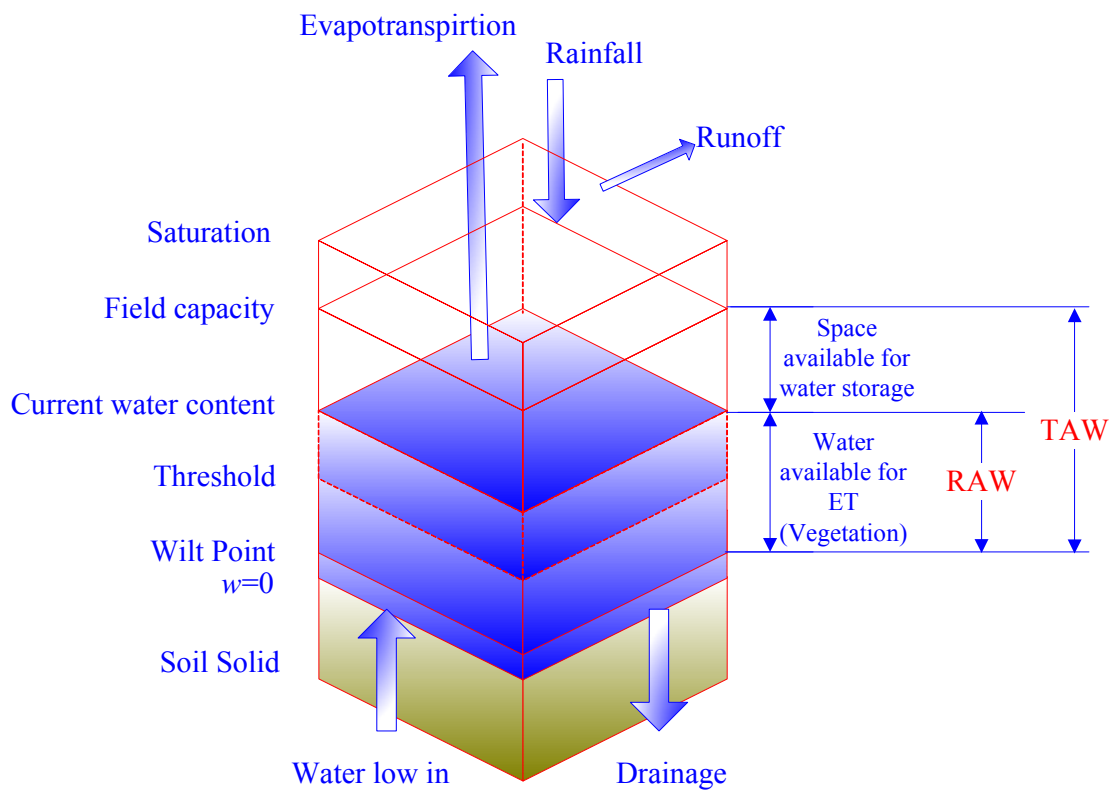


Fig. 7.11. Water balance of the grass root zone(After Allen et al. 1998)

Eq. 7.30 represents that rainfall, irrigation and capillary rise of groundwater towards the root zone add water to the root zone and decrease the root zone depletion. Soil evaporation, crop transpiration and percolation losses remove water from the root zone and increase the depletion.

The initial depletion of the root zone can be calculated from the constitutive surfaces. The initial depletion is defined as:

$$D_{r, i-1} = 1000(\theta_{FC} - \theta_{i-1}) H \quad (7.31)$$

where θ_{i-1} is the soil volumetric water content for the effective root zone at the end of day i . Similar to the calculation of TAW, if the current soil status(mechanical stress and the matric suction) is known, the θ_{i-1} can be determined from the constitutive surfaces of the soil. Note that the θ_{FC} is at the same mechanical stress level but have a matric suction of 10 kPa.

For the Arlington site, there is no irrigation included, that is, $I_i=0$. The amount of water transported upwards by capillary rise from the water table to the root zone depends on the soil type, the depth of the water table and the wetness of the root zone. The FAO 56 PM method considers that CR can normally be assumed to be zero when the water table is more than about 1 m below the bottom of the root zone. The ground water table is at 4.2m below the ground surface. Therefore, it can be safely assumed that the $CR=0$ for our simulation. More information on CR is presented in FAO Irrigation and Drainage Paper No. 24. Consequently, Eq. 7.30 is converted into,

$$D_{r, i} = D_{r, i-1} - (P - RO - DP)_i + ET_{c, i} \quad (7.32)$$

Eq. 7.32 means the variation in depletion depends on the difference between the net infiltration $(P - RO - DP)_i$ and the actual evapotranspiration $ET_{c, i}$. If the net infiltration $(P - RO - DP)_i$ is known, the final depletion of the soil can be known because the $ET_{c, i}$ can be calculated by the FAO 56 PM method. Actually, if the initial conditions of the soil is known and the net infiltration and actual evapotranspiration are known, the average depletion can be calculated by using the finite element method. Note that the water balance we discussed is for the root zone, it could be used as a controlling condition to calculate the influence of the weather on the soil, which, in turn, can be used

to calculate the influence of weather on the structure. In the root zone, the water loss or water gain is an average estimate. However, it can provide us relatively accurate information about the whole calculated domain.

In Fig. 7.11 it is assumed that water can be stored in the root zone until field capacity is reached. The FAO 56 PM Method proposes that, although following heavy rain or irrigation the water content might temporally exceed field capacity, the total amount of water above field capacity is assumed to be lost the same day by deep percolation, following any evapotranspiration for that day. By assuming that the root zone is at field capacity following heavy rain or irrigation, the minimum value for the depletion $D_{r,i}$ is zero. As a result of percolation and evapotranspiration, the water content in the root zone will gradually decrease and the root zone depletion will increase. In the absence of any wetting event, the water content will steadily reach its minimum value θ_{WP} . At that moment no water is left for evapotranspiration in the root zone, K_s becomes zero, and the root zone depletion has reached its maximum value TAW. The limits imposed on $D_{r,i-1}$ and $D_{r,i}$ are consequently:

$$0 < D_{r,i} < TAW \quad (7.33)$$

If there is no rain during the day, that is, $P=0$, there will not be runoff, $RO=0$. The FAO 56 PM method consider that as long as the soil water content in the grass root zone is below field capacity (i.e., $D_{r,i} > 0$), the soil will not drain and $DP_i = 0$. Consequently, $(P - (RO + DP))_i = 0$. The net water loss therefore is,

$$D_{r,i} = D_{r,i-1} + ET_{c,i} \quad (7.34)$$

Eq. 7.33 must be satisfied, hence,

$$0 < D_{r,i} = D_{r,i-1} + ET_{c,i} < TAW \quad (7.35)$$

Substituting Eq. 7.31 into 7.35 gives,

$$ET_{c,i} < 1000 \left((\theta_{FC} - \theta_{wp}) - (\theta_{FC} - \theta_{i-1}) \right) H \quad (7.36)$$

that is

$$ET_{c,i} < 1000 \left((\theta_{i-1} - \theta_{wp}) \right) H \quad (7.37)$$

$1000 \left((\theta_{i-1} - \theta_{wp}) \right) H$ is the water available for evapotranspiration. If the calculated $ET_{c,i}$ is greater than $1000 \left((\theta_{i-1} - \theta_{wp}) \right) H$, $ET_{c,i} = 1000 \left((\theta_{i-1} - \theta_{wp}) \right) H$. In summary, for a day with no rainfall, we have

$$\begin{aligned} NWL &= ET_{c,i}, \quad \text{if } ET_{c,i} < 1000 \left((\theta_{i-1} - \theta_{wp}) \right) H \\ NWL &= 1000 \left((\theta_{i-1} - \theta_{wp}) \right) H, \quad \text{if } ET_{c,i} \geq 1000 \left((\theta_{i-1} - \theta_{wp}) \right) H \end{aligned} \quad (7.38)$$

where NWL is the final net water loss or gain.

If there is rainfall during the i th day, the precipitation is equivalent to daily rainfall. It is noted that in only very rare cases, it will rain 24 hours incessantly. Therefore, there is evapotranspiration even during a raining day and the evapotranspiration is expected to be significant because the water is freely available. The FAO56 PM Method proposes that daily precipitation in amounts less than about $0.2 ET_0$ is normally entirely evaporated and can usually be ignored in the water balance calculation, especially when the single crop coefficient approach is being used. Consequently, the effective precipitation is the difference between the daily precipitation and the actual evapotranspiration. It is the actual amount of water available to the soil. The FAO 56 PM method consider that as long as the soil water content in the grass root zone is below field capacity (i.e., $D_{r, i} > 0$), the soil will not drain and $DP_i = 0$. Similarly, it is

reasonable to assume that if the soil water content in the grass root zone is below field capacity (i.e., $D_{r,i} > 0$), there is no runoff.

Therefore, when there is rainfall during a day, two categories of condition needed to be considered. One is when the rainfall is less than the evapotranspiration during the day. The other is when the rainfall is greater than the evapotranspiration during the day.

For the first condition, the daily total evapotranspiration is greater than the rainfall $ET_{c,i} - P_i > 0$, there is net evapotranspiration and no runoff or deep percolation.. The net evapotranspiration will cause the soil to lose water until the soil reaches wilt point. The water needed to make the soil reach the wilt point depends on the current water content, the wilt point water content and the depth of the root zone, which is $1000(\theta_{i-1} - \theta_{wp})H$. $1000(\theta_{i-1} - \theta_{wp})H$ is the maximum water the soil can lose. Eq. 7.32 is then written as,

$$D_{r,i} = D_{r,i-1} + (ET_{c,i} - P_i) \quad (7.39)$$

Eq. 7.33 must be satisfied, hence, we have,

$$NWL = ET_{c,i} - P_i, \text{ if } 0 < ET_{c,i} - P_i < 1000((\theta_{i-1} - \theta_{wp}))H \quad (7.40)$$

$$NWL = 1000((\theta_{i-1} - \theta_{wp}))H, \text{ if } ET_{c,i} - P_i > 1000((\theta_{i-1} - \theta_{wp}))H \quad (7.41)$$

Eq. 7.40 represents that if there is evapotranspiration $ET_{c,i} - P_i > 0$, and the net evapotranspiration ($ET_{c,i} - P_i$) is less than the water available in the soil to lose $1000(\theta_{i-1} - \theta_{wp})H$, then the net water loss (NWL) equals to the net evapotranspiration $ET_{c,i} - P_i$. Eq. 7.41 represents that if there is evapotranspiration $ET_{c,i} - P_i > 0$, and the net evapotranspiration ($ET_{c,i} - P_i$) is larger than the water available in the soil, then the actual water loss will be the water available to lose, i.e. $1000(\theta_{i-1} - \theta_{wp})H$ in the soil.

For the second case, if the rainfall is greater than the evapotranspiration $P_i - ET_{c,i} > 0$, there is net infiltration. The infiltration will increase the water content in the soil until the soil arrives at the field capacity. The water needed to make the soil reach the field capacity depends on the current water content, the field capacity and the depth of the root zone, which is $1000(\theta_{FC} - \theta_{i-1})H$. $1000(\theta_{FC} - \theta_{i-1})H$ is the maximum water the soil can absorb. In other words, if it is a really heavy rain, after subtracting the actual evapotranspiration and the amount of water needed for the root zone to reach field capacity, there is still some surplus, then the surplus will be either runoff or deep percolation. Considering Eq. 7.32 and 7.33, gives,

$$NWL = ET_{c,i} - P, \text{ if } 0 < P_i - ET_{c,i} < 1000((\theta_{CF} - \theta_{i-1}))H \quad (7.42)$$

$$NWL = 1000((\theta_{CF} - \theta_{i-1})), \text{ if } P_i - ET_{c,i} > 1000((\theta_{CF} - \theta_{i-1}))H \quad (7.43)$$

Eq. 7.42 represents that if there is net infiltration $P_i - ET_{c,i} > 0$, and the net infiltration ($P_i - ET_{c,i}$) is less than the space available in the soil to store water until it reach the field capacity, $1000(\theta_{FC} - \theta_{i-1})H$, then the net water gain equals to the net infiltration ($P_i - ET_{c,i}$). Eq. 7.43 represents that if the net infiltration ($P_i - ET_{c,i}$) is more than the maximum amount of water the soil can absorb, i.e. $1000(\theta_{FC} - \theta_{i-1})H$, the surplus will be runoff.

7.7 Boundary Conditions for Different Surface Conditions

For the coupled mechanical stress and matric suction analysis, two kinds of boundary conditions are needed, one is mechanical boundary condition and the other is the flux boundary condition. If the boundary conditions are known, finite element method or finite difference method can be used to solve the differential equations and the soils status in the whole calculation domain can be computed. The corresponding deformation of the soil can also be calculated. The estimate of net water loss by using the daily weather data as discussed above can be potentially used for the determination of the upper boundary conditions for the coupled mechanical stress and matric suction analysis. Generally, there could be either bare soil or turf grass or trees around a house. For

different kinds of ground surfaces, the methods for the boundary conditions should also be different.

7.7.1 Bare Soils

If the ground surface is bare soils, the water is removed directly from the soil surface by evaporation. If the soil surface is intact without any cracks, it is reasonable to use the secondary boundary conditions, that is, the rate of water flow leaving the soil surface is known,

$$k \frac{\partial h}{\partial z} \Big|_{bare\ soil\ surface} = \frac{10^{-3} ET_{c,i}}{86400} (m/s) \quad (7.44)$$

if it is written in terms of pore water pressure (matric suction) and the elevation head is neglected,

$$\frac{k}{\rho_w g} \frac{\partial u_w}{\partial z} \Big|_{bare\ soil\ surface} = \frac{ET_{c,i}}{8.64 \times 10^7} (m/s) \quad (7.45)$$

where k = the permeability coefficient of the bare soil, m/s; h = hydraulic head, m; z = the coordinate in the vertical direction, m; ρ_w = the mass density of water, 10^3 kg/m^3 ; u_w = pore water pressure, kPa; g = the acceleration of gravity, g/m^2 ; and $ET_{c,i}$ is the actual evapotranspiration and equal to $K_s K_c ET_0$, mm/day.

If there is rainfall and there is net water gain, the boundary condition is

$$\frac{k}{\rho_w g} \frac{\partial u_w}{\partial z} \Big|_{bare\ soil\ surface} = \frac{ET_{c,i} - P_i}{8.64 \times 10^7} (m/s) \quad (7.46)$$

Note that the similar discussion is needed as what we have had for the net water loss. Actually, it is much better to use,

$$\frac{k}{\rho_w g} \frac{\partial u_w}{\partial z} \Big|_{bare\ soil\ surface} = \frac{NWL}{8.64 \times 10^7} (m/s) \quad (7.47)$$

where NWL is net water loss as discussed previously.

In the absence of any supply of water to the soil surface, or if the soil underneath is unable to supply water fast enough to satisfy the evaporation demand, evaporation will decrease rapidly and may cease within a few days, that is, K_s will drop to zero depending on the soil suction (water content). K_s can be estimated by the method proposed by the FAO 56 PM method as discussed above.

7.7.2 Grass Root Zone

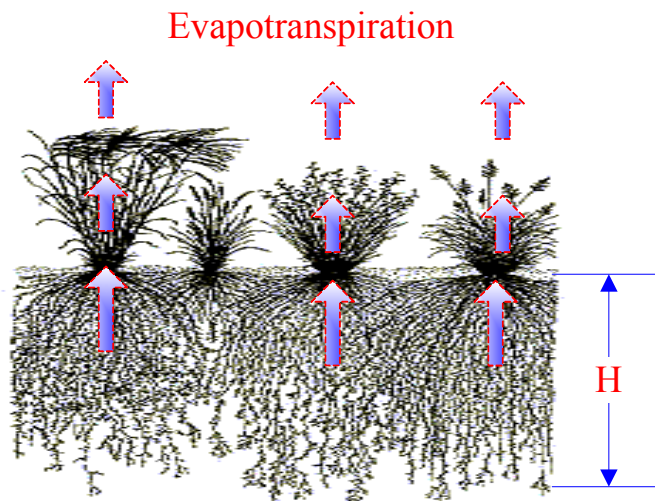


Fig. 7.12. Water loss in the grass root zone (adapted from prairie grass root system, available at <http://www.cod.edu/Visitors/prairie/heritage.htm>)

If the ground surface is covered by grass, water is lost mainly by transpiration from the grass (Fig. 7.12). The water, together with some nutrients, is taken up by the grass roots locally at the grass root zone and transported through the grass. The vaporization occurs at the grass leaf surface. Research indicates that nearly all water taken up is lost by transpiration and only a tiny fraction is used within the grass. Consequently, it appears to be logical to use the water source term to represent the local water loss in the grass root zone. The water source term is defined as the rate of water loss or gain in volume per unit soil volume. For the grass root zone, the water source term can be calculated by

$$S = \frac{\dot{V}_{NWL}}{V_s} = \frac{10^{-3} NWL \times A}{86400H \times A} = \frac{NWL}{H} (s^{-1}) \quad (7.48)$$

where S is the water source term, (s^{-1}); NWL is the net water loss per day (from unit evaporation surface), (mm/day); H is the depth of the grass root zone, (m); and A is the area of the evaporation surface.

By using the water source term to simulate the local water loss for the grass root zone, the average water loss in the grass root zone can be simulated. An assumption hiding behind this is that the rainfall can infiltrate freely into the grass root zone because the precipitation is added directly to the water balance of grass root zone. Note that there are always a lot of cracks at the ground surface, this assumption is considered to be reasonable.

If there are cracks at the bare soil surface, the rainfall can infiltrate into the soil more easily along the cracks. Similarly, the evaporation will occur at the crack in a much easier way. It is very difficult to estimate the influence of the crack. It is recommended to use the same treatment for the grass root zone, to treat the bare soil with cracks. In other words, evaporation is assumed to occur internally in the soil and the precipitation can infiltrate freely and uniformly into the cracked zone. More research in this direction is needed.

7.7.3 Tree Root Zone

Tree root zone (or some deep grass root zone) is usually deeper than grass root zone. It is considered that usually the precipitation can not infiltrate directly in the deep tree root zone. In this case, it is proposed that the tree root zone can be considered as the condition when the precipitation is always zero. Like grass root zone, water together with some nutrients is taken up by the tree roots locally at the tree root zone and transported through the grass. The vaporization occurs at the tree leaf surface as shown in Fig. 7.13.

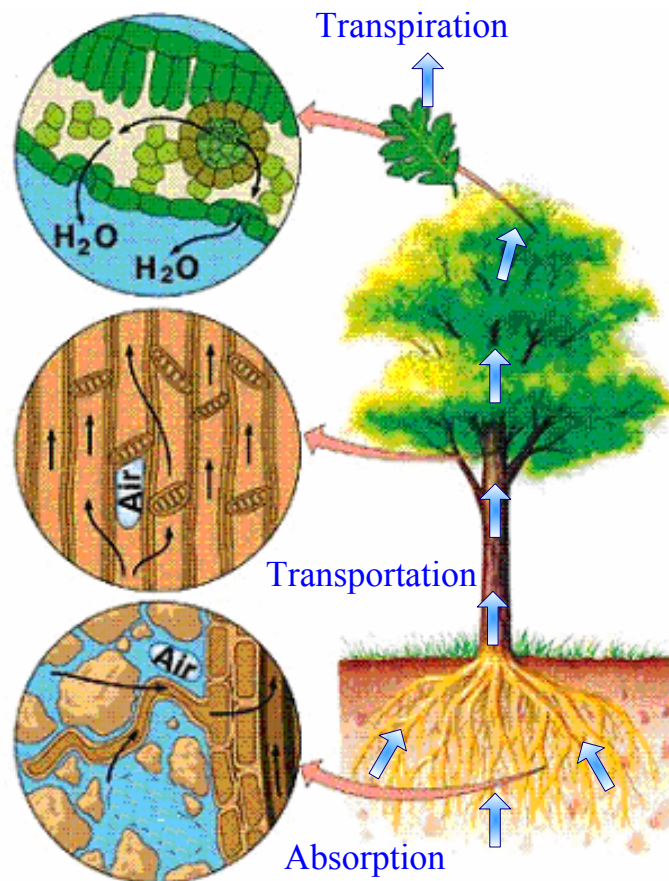


Fig. 7.13. Water losses in the tree root zone (adapted from tree picture, Botany Visual Resources Library by Randy Moore, Dennis Clark and Darrell Vodopich, 1998. available at <http://www.science.siu.edu/plant-biology/PLB117/JPEGs%20CD/0693.JPG>)

A water source term can be used to simulate the water loss due to tree.

$$S = \frac{V_{NWL}^{\bullet}}{V_s} = \frac{10^{-3} NWL \times A}{86400 H \times A} = \frac{NWL}{H} (s^{-1}) \quad (7.49)$$

where NWL is calculated by Eq. 7.40 and 7.41.

7.8 Discussion

The boundary matric suction when there are grasses at the ground surface are actually not specified. The boundary conditions are controlled by the water source term and calculated by the computer program itself. When we calculate the water source term, the average loss of the water is used by dividing the net water loss by depth. It is not strictly true. However, it gives a relatively accurate water loss under the averaged senses. As a consequence, the proposed method may not give an accurate calculation result of the water content for every single point in the grass root zone or tree root zone. However, it is considered to be logical that the proposed method can produce an accurate “averaged” effect of water loss for the grass root zone or the tree root zone and a more accurate simulation result for the surrounding soils.

As discussed previously, when the water balance in the grass root zone is calculated, the CR_i (capillary rise from the groundwater table on day i) and the DP_i (loss out of the root zone by deep percolation on day i (mm)) are both taken as zero. It is not exactly right. Actually these two parts can be visualized as the water flow in and out of the grass root zone even when there is no rain. Usually it is considered their quantities are so small that they are negligible comparing with the evapotranspiration. Moreover, when performing the simulation, there will be some water flowing into the grass root zone or out of the grass root zone, depending on the soil conditions and their environment. Further research is needed in this direction.

CHAPTER VIII

VERIFICATION OF THE PROPOSED METHOD

8.1 Introduction

A site at Arlington, Texas is chosen to implement the proposed methods for the construction of constitutive surfaces, the coupled consolidation theory for saturated and unsaturated soils and determination of the boundary conditions by using the FAO 56 PM method. The site is introduced in Chapter IV. The soil stratigraphy, weather condition, field observations and laboratory tests results are presented in Chapter IV too. Chapter V proposes a method to construct the constitutive surfaces for saturated and unsaturated soils by using the results obtained from Chapter IV. The consolidation theory for saturated and unsaturated soils has been discussed in the Chapter VI. The theory is applicable for both expansive and collapsible soils. Both coupled and uncoupled cases have been discussed. Chapter VII introduces a method to estimate the potential and actual evapotranspiration by using the FAO-56 PM method for different ground surfaces. It actually provides a method to determine the boundary conditions for the coupled consolidation analysis. In this chapter, all the discussions are used in one program to simulate the footings' movements at a site at Arlington, Texas. The simulation result is compared with the field observation.

8.2 Model Used in the Simulation

A site at Arlington, Texas is used to implement the theories proposed in the previous chapters. The stratigraphy of the site has been introduced in Chapter IV. Fig. 8.1 shows the dimension and the stratigraphy used for the simulation. As shown in Fig. 8.1, 0-1.8m is the Dark Gray silty clay, while the soil surface is covered by the Johnsongrass, which is warm season, perennial grass. The grass root zone is assumed to be 0.47m. 1.8-4.0m is the Brown silty clay. The ground water level is at a depth of 4.2m. The matric suction at the 4.0m deep is assumed to be 10kPa, which is corresponding to the field

capacity for most soils. The footing is made of concrete, having a dimension of $2\text{m} \times 2\text{m} \times 0.6\text{m}$ (Length \times width \times height). The concrete mass density is assumed to be 2400kg/m^3 , the acceleration of gravity is 10m/s^2 . The soil domain used for the simulation is $10\text{m} \times 10\text{m} \times 4\text{m}$ (Length \times width \times height). 10m is considered to be a length far away so that there is no influence of the footing.

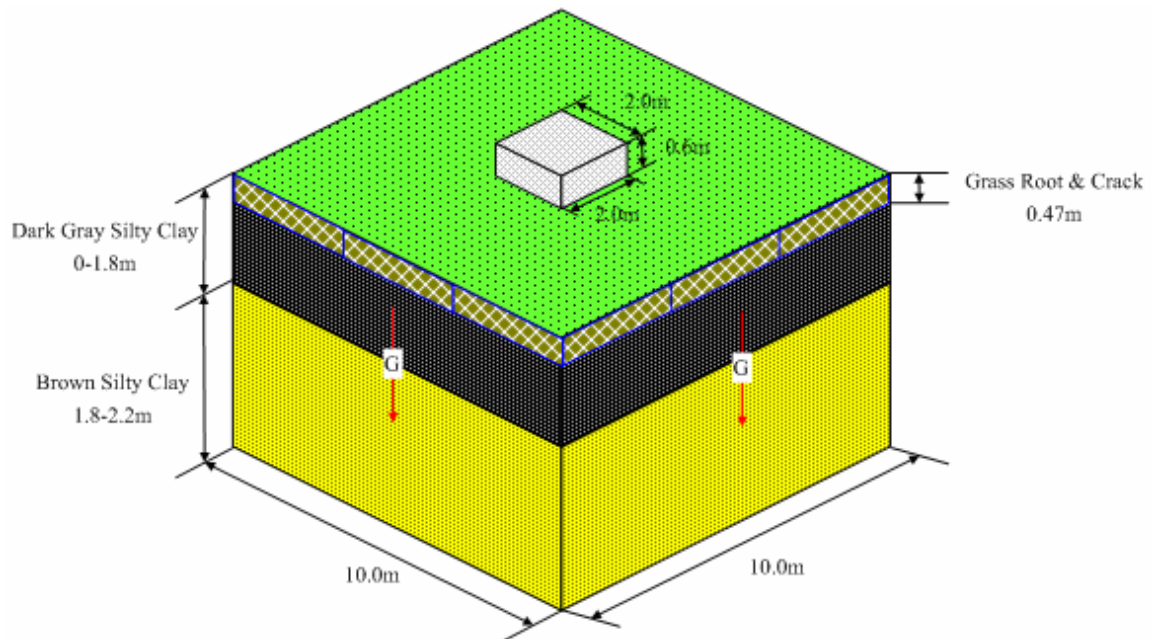


Fig. 8.1. Model used for the simulation

In Chapter VI, it is proved that ABAQUS/STANDARD can be used for the couple consolidation simulation for saturated and unsaturated soils. In this Chapter, ABAQUS/STANDARD will be used for the simulation of the movements for the site at Arlington, Texas. Fig. 8.2 shows the mesh used for the simulation. In the horizontal (x and y) direction, the mesh is uniform, and both length and width have a dimension of 1m . In the vertical direction, the mesh size decreases with depth. The reason for this is that the surface is the place where matric suctions and stresses vary most frequently. The mesh is generated by the ABAQUS/CAE with a bias of 1.1 in the vertical direction,

which means that the height of the mesh is 1.1 times of the height of the mesh on top of it. Compared with the soil block, the concrete footing is actually a rigid body. The mesh generation for the concrete footing is $1\text{m}\times 1\text{m}\times 0.3\text{m}$. The mesh generation is attached in the Appendix D.1.

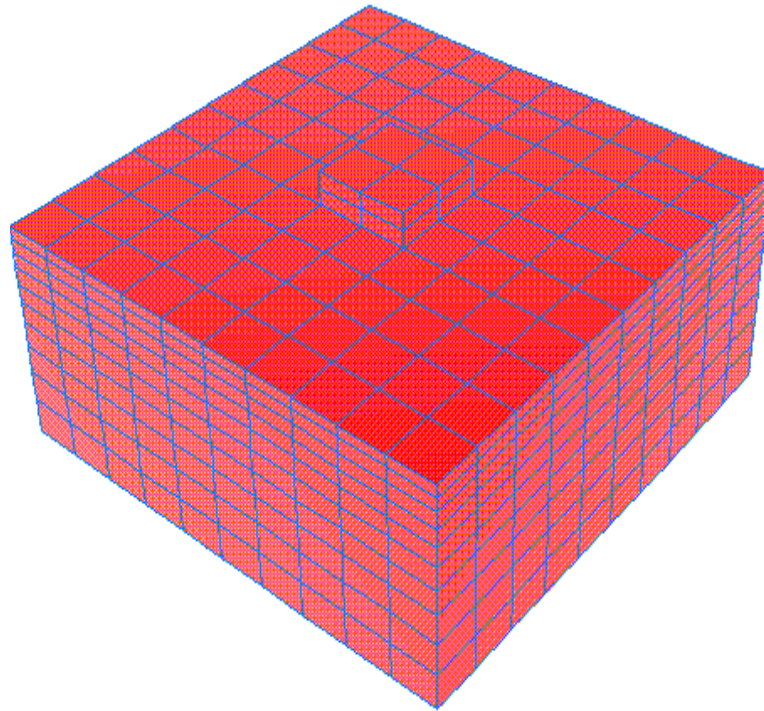


Fig. 8.2. Mesh generation of the model

The soils are assumed to have an initial geostatic status in mechanical stress with a K_0 value equal to 0.67. This corresponds to a Poisson's ratio equal to 0.4. It is assumed that the Poisson's ratio is a constant for the two soils. The initial matric suction is determined by the boring log, which will be discussed later.

8.3 Material Properties Used in the Analysis

Three kinds of material properties are involved in the simulation, that is, the concrete (footing), Dark Gray silty clay (with a depth of 0.0-1.8m), and 1 the Brown silty clay

(with a depth of 1.8-4.0m). In addition, the material properties for the contact (jointed) elements at the soil-concrete footing interface are also needed.

For the simulation of the volume change of the soils, a coupled hydro-mechanical stress analysis is needed and the thermodynamic part corresponds to the water phase continuity of the soil. For the simulation of the concrete footing, only the mechanical stress analysis is of interest. For the simulation of the soil-concrete footing interface, contact (jointed) elements are needed. The contact elements are used to calculate the force transferring from the concrete footing to the soil underneath. The lower side of the contact elements is soil surface, while the upper side is the bottom of the concrete footing. As a consequence, the simulation for the lower side of the contact elements is the coupled hydro-mechanical stress analysis (or the coupled thermal stress analysis) and at the upper side only the mechanical stress analysis is of interest. A special technique, which is called “pseudo matric suction (thermal) analysis” here, is proposed for the contact elements and the concrete footing to solve the dilemma. The basic concept for the “pseudo matric suction (thermal) analysis” is to perform the coupled hydro-mechanical stress analysis (or the coupled thermal stress analysis) for the whole system even there is no water (or heat) flow in the concrete footing and the contact elements. Mathematically, no water (heat) flow is equivalent to that the water flow equals to zero. If only the assumed water flow does not cause any stresses in the footing, it will solve the conflict and bring convenience for the simulation. The final simulation result will be the same as that in the real conditions. The effect is achieved by specially specifying the material properties of the concrete footing and contact elements, which will be discussed later.

The differential equation used for the coupled mechanical stress and matric suction analysis is

$$\begin{aligned}
 (\lambda + G) \frac{\partial \varepsilon_v}{\partial x} + G \nabla^2 u - (3\lambda + 2G) \alpha \frac{\partial (u_a - u_w)}{\partial x} + X &= 0 \\
 (\lambda + G) \frac{\partial \varepsilon_v}{\partial y} + G \nabla^2 v - (3\lambda + 2G) \alpha \frac{\partial (u_a - u_w)}{\partial y} + Y &= 0
 \end{aligned} \tag{3.22}$$

$$\begin{aligned}
& (\lambda + G) \frac{\partial \varepsilon_v}{\partial z} + G \nabla^2 w - (3\lambda + 2G) \alpha \frac{\partial (u_a - u_w)}{\partial z} + Z = 0 \\
& \frac{\partial}{\partial x} \left(k \frac{\partial u_w}{\partial x} \right) + \frac{\partial}{\partial y} \left(k \frac{\partial u_w}{\partial y} \right) + \frac{\partial}{\partial x} \left(k \left(\frac{\partial u_w}{\partial z} + 1 \right) \right) \\
& = m_1^w \frac{\partial (\sigma_m - u_a)}{\partial t} + m_2^w \frac{\partial (u_a - u_w)}{\partial t} + S'
\end{aligned} \tag{3.23}$$

8.3.1 Material Properties for the Concrete Footing

The mass density for ordinary concrete is $2.4 \times 10^3 \text{ kg/m}^3$ (the input is 2.4 to be consistent with other units, which is discussed in Chapter VI). The Young's Modulus of the concrete footing is assumed as $E=4 \times 10^6 \text{ kPa}$ and Poisson's Ratio is assumed as $\mu=0.15$.

The coupled thermal stress analysis is performed for the whole model. For the concrete, the thermodynamic part corresponds to the water phase continuity of the soil.

To make sure the thermodynamic analysis will not influence the mechanical analysis of the concrete footing, the following material properties are assigned to the concrete:

(1). The coefficient of expansion due to pore water pressure (temperature) variations of the concrete footing is zero, i.e. $\alpha = 0$ in Equation 3.22. There is no (thermal) strain in the concrete footing even when there is pore water pressure (temperature) variation. As a consequence, there is no mechanical stress variation due to the pore water pressure (temperature) variation and the coupled thermal stress analysis has been uncoupled. To avoid possible singularity in the analysis, the concrete is assumed to have a coefficient of expansion of $10^{-30} \text{ kPa}^{-1}$ instead of (the corresponding value in the coupled thermal stress analysis is 10^{-30} K^{-1}). Compared with the expansion coefficient of the soil (which is usually between 10^{-4} kPa^{-1} and 10^{-8} kPa^{-1}), the expansion coefficient of the concrete footing is considered to be so small that there is no significant deformation occurrence due to the matric suction (temperature) variation.

(2). There is no water (heat) generation due to the mechanical stress variation and no water (or sink) source, i.e. $m_1^w = 0$ and $S=0$ in Equation 3.23.

(3). There is no water flow out of the boundary of the concrete footing. Namely, there is zero water flux at the concrete footing surface. At the bottom of the concrete footing, the zero water flux is realized by assigning a zero gap conductance for the contact elements, which will be discussed later.

(4). The specific water capacity of the concrete is assigned to be 10^{-6}kPa^{-1} . The coefficient permeability of the concrete is assigned to be 10^{-2}m/s , which corresponds to a heat conductivity of $10^{-3} \text{ J}/(\text{s} \cdot \text{m} \cdot \text{K})$ (or $\text{kg}/\text{s} \cdot \text{m} \cdot \text{kPa}$) in the coupled thermal stress problem.

Condition (2) and (3) make sure that there is no water content (heat) variation in the concrete footing. A high coefficient of permeability of the concrete in condition (4) is to make sure that the pore water pressure in the concrete footing is uniformly distributed and will not cause any differential pore water pressure. Condition (1) is to make sure even there are pore water pressure variations there is no strain (and stress) generation. Actually condition (1) only is enough to make sure the stresses and strains in the concrete are not affected by the imposed water flow analysis. In this way, a coupled thermal stress problem analysis is performed while the result is the same as that obtained from a single mechanical stress analysis.

The material properties are defined in the ABAQUS/STANDARD by using the following commands:

```
*Material, name=Material-block
*Conductivity
1e-3.,
*Density
2.4,
*Elastic
4e+06, 0.15
*Expansion
1e-30,
*Specific Heat
```

1e-6.,

The material properties for the concrete footing are defined in the main program in the Appendix D.1.1. because all the material parameters are constants and there is no water (heat) generation.

8.3.2 Material Properties for the Contact Element

The soil-concrete footing interaction is simulated by contact elements. The theory for contact elements will be presented in Chapter IX. The contact elements are elements with zero thickness. The upper side of the contact element is the bottom surface of the concrete footing and the lower side is the ground surface where the concrete footing is based on. ABAQUS defines contact between two bodies in terms of two surfaces that may interact; these surfaces are called a “contact pair.” ABAQUS defines the contact conditions between two bodies using a strict “master-slave” algorithm. Each potential contact condition is defined in terms of a “slave” node and a “master” surface. The slave nodes are constrained not to penetrate into the master surface; however, the nodes of the master surface can, in principle, penetrate into the slave surface. In this simulation, the bottom face of the concrete footing is assigned to be the master surface and the ground surface is assigned to be the slave surface. Namely, the concrete can penetrate into the soil while the soil can not penetrate into the concrete.

The default “hard” contact relationship, which allows no penetration of the slave nodes into the master surface and no transfer of tensile stress across the interface, is used for the normal mechanical interaction at the soil-concrete interface. The hard contact relationship allows the compressive load to be transferred to the soil while the tensile stress is not allowed to transfer. Instead, there is separation between the footing and the soil.

The possible friction between the concrete footing and the ground soil is simulated by the Coulomb friction model as described in the next chapter. Because the footing is symmetric and small compared with the simulated domain, the frictional stress and tangential movements between the soil and the footing is expected to be small in this

simulation. To prevent any possible sliding, the friction coefficient is assigned to be 0.3. The commands for the mechanical behavior of the contact elements are:

```
*Surface Interaction, name=IntProp-1
*Surface Behavior, pressure-overclosure=HARD
*Friction
0.3
```

No water flow exists between the footing and the ground soil. This condition is simulated by the “thermal interaction” option in ABAQUS. Zero water flow between the footing and the ground soil is realized by assigning a very small gap conductance, namely, the contact element itself is impermeable. The command is written as followings:

```
*Gap Conductance
1e-30,0.
0.,0.5
```

The first number in the above command represents the gap conductance, and the second number represents the gap between the footing and the soil. The gap conductance is a function of the height of the gap. When the footing and the soil is in contact with each other, the gap conductance equals to $10^{-30} \text{ J}/(\text{m}^2 \text{ s } ^\circ\text{C})$. When there is a gap with a height of 0.5m, the gap conductance equals to zero. When the gap height is between 0 and 0.5m, the gap conductance will be linearly interpolated. No water (heat) generation due to the friction is allowed in the contact elements.

8.3.3 Material Parameters for Saturated and Unsaturated Soils

Six material property parameters, i.e. Young’s Modulus E , Poisson’s ratio μ , coefficient of expansion α , specific water capacity C_w (or m_2^w), and the water generation parameter m_1^w are needed for the coupled mechanical stress and matric suction analysis. Poisson’s ratio usually does not change very much for soils and is taken as 0.4 in this simulation. All the other material properties of the soil are not constants but functions of both mechanical stress and matric suction. A new method has been proposed in the Chapter

V to construct the constitutive surfaces for unsaturated soils. The constructed constitutive surfaces are continuous and the first derivatives are also continuous too. From the constructed surfaces, all the parameters can be determined. The computations for the material parameters are as followings.

When the soil is saturated, the material parameters can be calculated as followings:

$$m_1^s = m_2^s = m_1^w = m_2^w = \frac{1}{1+e_0} \frac{de}{d\sigma'} \quad (6.137)$$

In this dissertation, the void ratio versus effective stress curve when the pore water pressure is zero is regressed by Sigmaplot and the corresponding mathematical expression is:

$$e = y_1 + \frac{a_1}{1 + \exp\left(-\frac{\log_{10}(\sigma') - x_1}{b_1}\right)} = y_1 + \frac{a_1}{1 + \exp\left(-\frac{\log_{10}(\sigma_m - u_w) - x_1}{b_1}\right)} \quad (8.1)$$

Where, a_1 , b_1 , x_1 , and y_1 are regression constants.

$$\frac{de}{d(\sigma')} = -\frac{a_1 \left[1 + \exp\left(-\frac{\log_{10}(\sigma') - x_1}{b_1}\right)\right]^{-2} \exp\left(-\frac{\log_{10}(\sigma') - x_1}{b_1}\right)}{(\sigma') b_1 \ln 10} \quad (8.2)$$

As a consequence, Young's Modulus E , coefficient of expansion α , specific water capacity C_w (or m_2^w) for the saturated soil can be obtained by combining Equation 6.42a, 6.59, 6.137 and 8.2.

In this dissertation, the void ratio versus matric suction curve when the mechanical stress is zero is regressed by Sigmaplot and the corresponding mathematical expression is:

$$e = y_2 + \frac{a_2}{1 + \exp\left(-\frac{\log_{10}(u_a - u_w) - x_2}{b_2}\right)} \quad (8.3)$$

where, a_2 , b_2 , x_2 , and y_2 are regression constants.

Correspondingly, the constructed void ratio constitutive surface has the following style,

$$(\sigma_m - u_a)10^{\left[y_1 - b_1 \ln\left(\frac{a_1}{e - x_1} - 1\right)\right]} + (u_a - u_w)10^{\left[y_2 - b_2 \ln\left(\frac{a_2}{e - x_2} - 1\right)\right]} = 1 \quad (8.4)$$

Equation 8.4 is the mathematical expression of the void ratio constitutive surface. From which the Young's Modulus and coefficient of expansion of the soil can be obtained. Equation 8.4 can be rewritten as,

$$\begin{aligned} & F(e, (\sigma_m - u_a), (u_a - u_w)) \\ & = (\sigma_m - u_a)10^{\left[y_1 - b_1 \ln\left(\frac{a_1}{e - x_1} - 1\right)\right]} + (u_a - u_w)10^{\left[y_2 - b_2 \ln\left(\frac{a_2}{e - x_2} - 1\right)\right]} - 1 = 0 \end{aligned} \quad (8.5)$$

The void ration e in Equation 8.5 is a function of both mechanical stress and matric suction, i.e.

$$e = f((\sigma_m - u_a), (u_a - u_w)) \quad (8.6)$$

Taking the derivative of the Equation 8.6 with respect to $\sigma - u_a$, we have,

$$\frac{d}{d(\sigma_m - u_a)} F(e, (\sigma_m - u_a), (u_a - u_w)) = \frac{\partial F}{\partial e} \frac{\partial e}{\partial (\sigma_m - u_a)} + \frac{\partial F}{\partial (\sigma_m - u_a)} = 0 \quad (8.7)$$

Therefore, we have,

$$\frac{\partial e}{\partial(\sigma_m - u_a)} = - \frac{\frac{\partial F}{\partial(\sigma_m - u_a)}}{\left[(1+e_0) \frac{\partial F}{\partial e} \right]} \quad (8.8)$$

where,

$$\frac{\partial F}{\partial(u_a - u_w)} = 10^{\left[y_2 - b_2 \ln \left(\frac{a_2}{e - x_2} - 1 \right) \right]} \quad (8.9)$$

$$\frac{\partial F}{\partial(\sigma_m - u_a)} = 10^{\left[y_1 - b_1 \ln \left(\frac{a_1}{e - x_1} - 1 \right) \right]} \quad (8.10)$$

$$\frac{\partial F}{\partial e} = - \frac{\frac{\partial F}{\partial(\sigma_m - u_a)} \frac{a_1 b_1 \ln 10}{(e - x_1)(a_1 - e + x_1)}}{\frac{\partial F}{\partial(u_a - u_w)} \frac{a_2 b_2 \ln 10}{(e - x_2)(a_2 - e + x_2)}} \quad (8.11)$$

Consequently, we have,

$$E = \frac{3(1-2\mu)}{m_1^s} = -3(1-2\mu) \left[(1+e_0) \frac{\partial F}{\partial e} \right] / \frac{\partial F}{\partial(\sigma_m - u_a)} \quad (8.12)$$

In a similar way we can have,

$$\alpha = \frac{m_2^s}{3} = \frac{1}{3(1+e_0)} \frac{\partial e}{\partial(u_a - u_w)} = - \frac{\frac{\partial F}{\partial(u_a - u_w)}}{\left[3(1+e_0) \frac{\partial F}{\partial e} \right]} \quad (8.13)$$

From Equation 8.1, the mathematical expression of the water content versus effective stress curve when the pore water pressure is zero can be obtained,

$$w = \frac{e}{G_s} = \frac{y_1}{G_s} + \frac{\frac{a_1}{G_s}}{1 + \exp\left(-\frac{\log_{10}(\sigma') - x_1}{b_1}\right)} = y_{11} + \frac{a_{11}}{1 + \exp\left(-\frac{\log_{10}(\sigma_m - u_w) - x_1}{b_1}\right)} \quad (8.14)$$

where $y_{11}=y_1/G_s$; and $a_{11}=a_1/G_s$

In this dissertation, the water content versus matric suction curve when the mechanical stress is zero is regressed by Sigmaplot with the same style as shown in Equation 8.1. Correspondingly, the water content constitutive surface has the following style,

$$(\sigma_m - u_a)10^{\left[y_{11} - b_1 \ln\left(\frac{a_{11}}{w - x_1} - 1\right) \right]} + (u_a - u_w)10^{\left[y_3 - b_3 \ln\left(\frac{a_3}{w - x_3} - 1\right) \right]} = 1 \quad (8.15)$$

where a_3 , b_3 , x_3 , and y_3 are regression constants for the water content versus matric suction curve when the mechanical stress is zero.

Equation 8.15 can be rewritten as,

$$\begin{aligned} & H(e, (\sigma_m - u_a), (u_a - u_w)) \\ & = (\sigma_m - u_a)10^{\left[y_{11} - b_1 \ln\left(\frac{a_{11}}{wG_s - x_1} - 1\right) \right]} + (u_a - u_w)10^{\left[y_2 - b_2 \ln\left(\frac{a_2}{wG_s - x_2} - 1\right) \right]} - 1 = 0 \end{aligned} \quad (8.16)$$

The void ratio e in Equation 8.16 is a function of both mechanical stress and matric suction, i.e.

$$wG_s = h((\sigma_m - u_a), (u_a - u_w)) \quad (8.17)$$

Taking the derivative of the Equation 8.17 with respect to $\sigma - u_a$, we have,

$$\frac{d}{d(\sigma_m - u_a)} H(e, (\sigma_m - u_a), (u_a - u_w)) = \frac{\partial H}{\partial(wG_s)} \frac{\partial(wG_s)}{\partial(\sigma_m - u_a)} + \frac{\partial H}{\partial(\sigma_m - u_a)} = 0 \quad (8.18)$$

$$\text{where } \frac{\partial H}{\partial(u_a - u_w)} = 10^{\left[y_3 - b_3 \ln\left(\frac{a_1}{e - x_1} - 1\right) \right]}; \quad \frac{\partial H}{\partial(\sigma_m - u_a)} = 10^{\left[y_1 - b_1 \ln\left(\frac{a_1}{e - x_1} - 1\right) \right]};$$

$$\frac{\partial H}{\partial(wG_s)} = - \frac{\partial H}{\partial(\sigma_m - u_a)} \frac{a_1 b_1 \ln 10}{(e - x_1)(a_1 - e + x_1)} - \frac{\partial H}{\partial(u_a - u_w)} \frac{a_3 b_3 \ln 10}{(e - x_3)(a_3 - e + x_3)}$$

Therefore, we have,

$$\frac{\partial(wG_s)}{\partial(\sigma_m - u_a)} = - \frac{\frac{\partial H}{\partial(\sigma_m - u_a)}}{\left[(1 + e_0) \frac{\partial H}{\partial(wG_s)} \right]} \quad (8.19)$$

and

$$m_1^w = \frac{1}{1 + e_0} \frac{\partial(wG_s)}{\partial(\sigma_m - u_a)} = - \frac{\frac{\partial H}{\partial(\sigma_m - u_a)}}{\left[(1 + e_0) \frac{\partial H}{\partial(wG_s)} \right]} \quad (8.20)$$

In a similar way we can have,

$$m_2^w = \frac{1}{1 + e_0} \frac{\partial(wG_s)}{\partial(u_a - u_w)} = - \frac{\frac{\partial H}{\partial(u_a - u_w)}}{\left[(1 + e_0) \frac{\partial H}{\partial(wG_s)} \right]} \quad (8.21)$$

At the high suction range, the degree of saturation surface is obtained firstly by assuming that degree of saturation is a function of matric suction only. The obtained degree of saturation surface has the following style,

$$S = y_4 + \frac{a_4}{1 + \exp\left(-\frac{\log_{10}(u_a - u_w) - x_4}{b_4}\right)} \quad (8.22)$$

Under this condition, the material parameters m_1^w and m_2^w can be calculated as following way.

$$m_1^w = \frac{e}{1 + e_0} \frac{\partial S}{\partial(\sigma_m - u_a)} + \frac{S}{1 + e_0} \frac{\partial e}{\partial(\sigma_m - u_a)} = \frac{S}{1 + e_0} m_1^s \quad (8.23)$$

$$m_2^w = \frac{e}{1 + e_0} \frac{\partial S}{\partial(u_a - u_w)} + \frac{S}{1 + e_0} \frac{\partial e}{\partial(u_a - u_w)} = \frac{e}{1 + e_0} \frac{\partial S}{\partial(u_a - u_w)} + \frac{S}{1 + e_0} m_2^w$$

where

$$\frac{dS}{d(u_a - u_w)} = -\frac{a_4 \left[1 + \exp\left(-\frac{\log_{10}(u_a - u_w) - x_4}{b_4}\right) \right]^{-2} \exp\left(-\frac{\log_{10}(u_a - u_w) - x_4}{b_4}\right)}{(u_a - u_w) b_4 \ln 10}$$

The excess pore water pressure parameters and the χ is Bishop's equation can also be obtained by equation 6.61 and Equation 6.134. Above calculations need some iteration for computing the void ratio and water content as discussed in Chapter V. A computer program called SurfaceCalculation (Appendix B.2) is used to perform the iteration. The calculation results for the soil SW145, SW189 and Sporc are presented in the Appendix B.1.1, B.1.2, and B.1.3., respectively.

The relationships between the state variables and the stress state variables needed for constructing the constitutive surfaces of the soils for the soil at a depth between 0

and 1.8m SW145 and the soil at a depth between 1.8 and 4.0m SW189 are summarized in Table 8.1 and Table 8.2, respectively. The c values in the two tables are the suction values at the shrinkage limits and these values will be used for the constant volume assumption for the higher suction range.

Table 8.1 Regression Parameters for Boundary Curves for Soil Sample SW145

	Regression Parameters for Boundary Curves			
	e vs. $(\sigma-u_a)$	e vs. (u_a-u_w)	w vs. (u_a-u_w)	S vs. (u_a-u_w)
a	0.49127602	0.387060	0.285551272	1.02479000
b	-0.42147606	-0.456384	-0.671559558	-0.32401330
x	2.75275012	3.624239	4.386436815	4.97954342
y	0.19544900	0.299088	-0.026264216	-0.02478979
c				32637

Table 8.2 Regression Parameters for Boundary Curves for Soil Sample SW189

	Regression Parameters for Boundary Curves			
	e vs. $(\sigma-u_a)$	e vs. (u_a-u_w)	w vs. (u_a-u_w)	S vs. (u_a-u_w)
a	0.6641108	0.3604135	0.4379930	1.0654200
b	-0.6811336	-0.5072783	-1.3789691	-0.5193185
x	3.3957253	2.7015441	4.5734664	4.8246437
y	0.1730660	0.4739990	-0.1242133	-0.0968234
c				20000

8.3.4 Permeability Functions of the Soils

Permeability coefficients are also needed for the analysis. Permeability coefficients of saturated soils are a function of void ratio only. The permeability for saturated soils can be measured by both laboratory tests and field tests. In his dissertation, the saturated permeability coefficients are obtained from the one dimensional consolidation tests by calculating the C_v . For unsaturated soils, the coefficient of permeability is a function of both mechanical stress and matric suction. Since mechanical stress, matric suction, void ratio, degree of saturation and water content are interrelated by the constitutive surfaces,

the permeability of unsaturated soils can be expressed as a function of any two of the five state variables. The reason for this is that the soil status can be determined by any two of the five state variables if the three constitutive surfaces for the void ratio, degree of saturation and water content are known.

$$k_w = f(\sigma - u_a, u_a - u_w); \quad k_w = f(S, e); \quad k_w = f(S, w); \quad k_w = f(e, w) \quad (8.24)$$

Basically, they are the same because

$$e = f(\sigma - u_a, u_a - u_w); \quad S = f(\sigma - u_a, u_a - u_w); \quad w = f(\sigma - u_a, u_a - u_w) \quad (8.25)$$

If the soil structure is incompressible, then the void ratio is constant and it is possible to decouple the two parameters into two parts (1) the saturated permeability which reflects the influence of the constant void ratio (and mechanical stress), and (2) another function which account for the influence of matric suction (or water content or degree of saturation). Under this condition, only one parameter in the three parameters, i.e., matric suction, degree of saturation and water content is needed to determine the unsaturated permeability. Currently, most permeability functions for unsaturated soils are based on this tacit assumption. For our investigation, the soils are deformable unsaturated soils. Consequently, two state variables are needed for the permeability function. This is the reason in this dissertation, the permeability function based on one parameter isn't chosen.

Even for incompressible unsaturated soils, it is very difficult to measure the permeability, still not to say for deformable unsaturated soils. It is a very time-consuming process to measure the permeability for unsaturated soils. The duration of the test increases as the water content in the soils decreases. The permeability values can differ by several orders in magnitude, causing direct measurement to be very difficult as there is no apparatus that can measure such a wide range of permeability efficiently. There are also some methods for the field measurements. However, the

results are usually more variable, due partly to the difficulty in determine the boundary conditions and the heterogeneity in the soil such as cracks.

The coefficient of permeability for a deformable unsaturated soils have been investigated experimentally and theoretically (Staple and Lehande 1954; Mitchell et al. 1965; Barden and Pavlakis 1971; Reicosky et al. 1981; Nimmo and Akstin 1988; Fleureau and Taibi 1994; Huang et al 1997).

Taylor (1948) derived an equation for the coefficient of permeability of saturated soils as follows,

$$k = C_1 \frac{\rho_w g}{\mu} \frac{e^3}{1+e} \quad (8.26)$$

Where k =permeability; C_1 =is a constant related to the soil water system; ρ_w =mass density of water; g =acceleration of gravity; μ =viscosity of water; e =void ratio

Mitchell et al (1965) obtained the permeability function for a deformable unsaturated soil based on Taylor's (1948) derivation of the permeability function for a saturated soils as followings,

$$k = C_2 \frac{\rho_w g}{\mu} \frac{e^3}{1+e} S^3 \quad (8.27)$$

where C_2 =is a constant related to the soil water system; S = degree of saturation

Huang et al (1997) proposed a permeability function for deformable unsaturated porous soil. The proposed function takes into account the influence of both the degree of saturation and the void ratio as followings,

$$k = k_{e0} 10^{b(e-e_0)} \frac{\int_0^{S_e} \frac{n(S_e - \sum_e)}{\psi^2} d\sum_e}{\int_0^1 \frac{n(S_e - \sum_e)}{\psi^2} d\sum_e} \quad (8.28)$$

where \sum_e is the dummy variable of integration representing effective degree of saturation; S_e is effective degree of saturation; n is porosity; ψ is matric suction; e_0 is the void ratio at saturation; and k_{e0} is the saturated permeability.

Equation 8.28 is also simplified by assuming that the volume change during the desaturation range is negligible.

$$k = k_{e0} 10^{b(e-e_0)} \frac{\int_0^{S_e} \frac{(S_e - \sum_e)}{\psi^2} d\sum_e}{\int_0^1 \frac{n(S_e - \sum_e)}{\psi^2} d\sum_e} \quad (8.29)$$

In this dissertation, the Mitchell's equation is used to calculate the permeability surface for saturated- unsaturated soils. The reasons for the choice are as followings:

1. It is a theoretical equation taking into account the influence of both degree of saturation and void ratio, that is, two state variables are involved.

2. The Taylor's equation, which is a special case of the Mitchell's equation when the soil is saturated, has been verified in some degree. Lambe and Whitman (1969) concluded that the $\log k_s$ versus e relationship is approximately a straight line for most soils.

3. It is observed that the most of the volume change occurs when the degree of saturation is still high. Mitchell's experimental data suggested that the k versus S^3 relationship is approximately linear for degree of saturation between 80% and 100%. For the degree of saturation lower than 80% , the matric suction is really high and the water flow is small. In our program, the maximum matric suction will be at the soil

surface and the water flow is actually controlled by the evapotranspiration. The permanent wilt point is used as another controlling factor for the water flow. Therefore, it is considered that the Mitchell's equation is a good choice for our simulation.

The Mitchell's equation can be written alternatively as,

$$k = f(e)S^3 \quad (8.30)$$

where $f(e)$ is the permeability function when the soil is saturated, which can be obtained from the one dimensional consolidation curve.

Once the $f(e)$ is obtained, the permeability surface for the soils can be obtained from the known constitutive surfaces $e = f(\sigma - u_a, u_a - u_w)$ and $S = f(\sigma - u_a, u_a - u_w)$. The permeability obtained is a function of both mechanical stress and matric suction. It is a surface in the permeability-mechanical stress-matric suction coordinate system. The assumptions of this method are (1), when the soil is saturated, the one dimensional consolidation test is a good enough method to obtain the saturated permeability function, and (2) when the soil is unsaturated, the permeability will linearly proportional to the S^3 term. The first assumption is considered to be reasonable and the second assumption subjects to argument. Further investigation is desirable in this direction. The obtained permeability function for the soil SW145 is,

$$k = 10^{(8.8874e-15.2329)} S^3 \quad (8.31)$$

The obtained permeability function for the soil SW189 is,

$$k = 10^{(9.5134e-17.5882)} S^3 \quad (8.32)$$

The permeability coefficient surfaces for the soil SW145 and SW189 are shown as in Fig. 8.3 and Fig. 8.4, respectively.

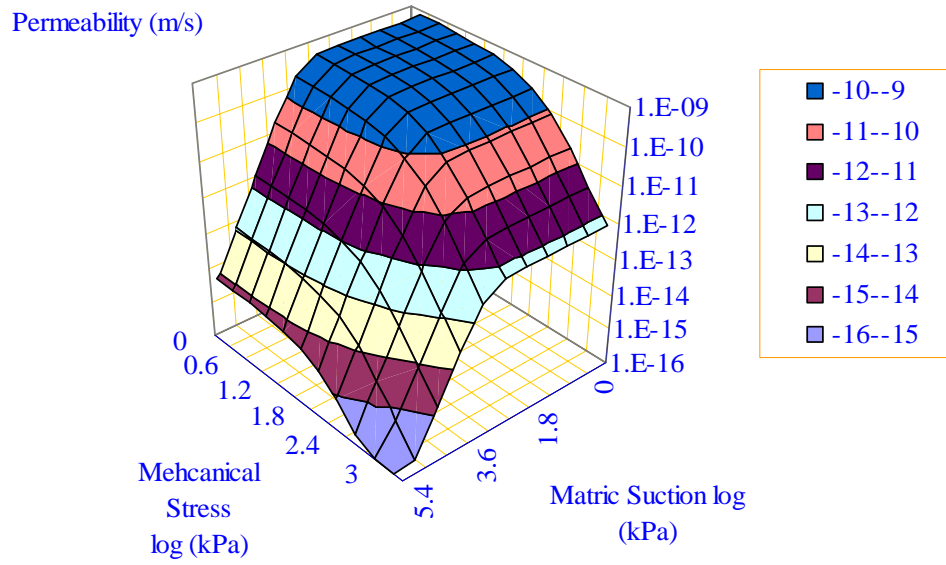


Fig. 8.3. The permeability coefficient surface for the soil SW145

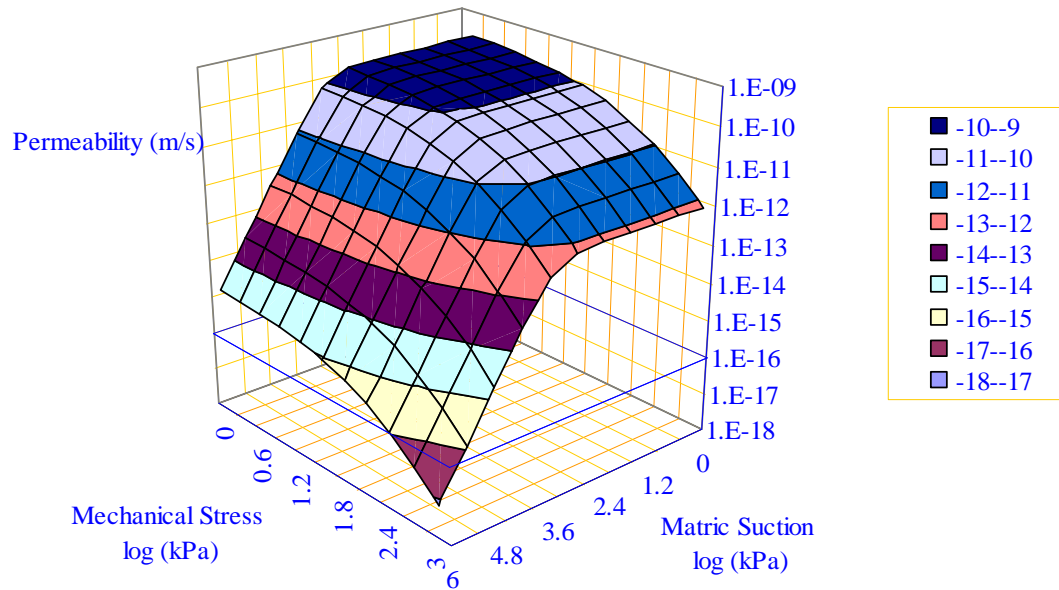


Fig. 8.4. The permeability coefficient surface for the soil SW189

8.4 Modifying the Coupled Thermal Stress Problem to Include the Influence of Gravity

The similarities between the coupled thermal stress and couple consolidation analysis have been discussed in Chapter VI. The difference between the coupled thermal stress problem and the coupled consolidation analysis for saturated-unsaturated soils lies in that the gravity does not influence the temperature distribution for heat transfer, but it does influence the pore water pressure distribution for the consolidation analysis. Namely, water will flow under the influence of gravity from a higher elevation to a lower elevation while the temperature distribution or heat flow has nothing to do with the elevation of the material. As a consequence the differential equation for the water phase continuity equation is different from that for the heat flow. The differential equation for a heat transfer problem is,

$$\left[\frac{\partial}{\partial x} \left(k \frac{\partial T}{\partial x} \right) + \frac{\partial}{\partial y} \left(k \frac{\partial T}{\partial y} \right) + \frac{\partial}{\partial z} \left(k \frac{\partial T}{\partial z} \right) \right] = \rho_d C_T \frac{\partial T}{\partial t} + S \quad (8.33)$$

The differential equation for a water flow problem is,

$$\left[\frac{\partial}{\partial x} \left(\frac{k}{g} \frac{\partial u_w}{\partial x} \right) + \frac{\partial}{\partial y} \left(\frac{k}{g} \frac{\partial u_w}{\partial y} \right) + \frac{\partial}{\partial z} \left(\frac{k}{g} \left(\frac{\partial u_w}{\partial z} + \rho_w g \right) \right) \right] = \rho_d C_w \frac{\partial u_w}{\partial t} + S \quad (8.34)$$

Comparing Equation 8.33 and 8.34, it is found that the difference exists in the z direction because the gravity exists in z direction only. A discussion for a one dimensional steady state vertical flow will make the difference more clearly.

The differential equation for the one dimensional steady state vertical heat flow is,

$$\frac{\partial}{\partial z} \left(k \frac{\partial T}{\partial z} \right) = 0 \quad (8.35)$$

The solution for Equation 8.35 is,

$$k \frac{\partial T}{\partial z} = C \quad (8.36)$$

where C is constant.

If the boundary condition is that there is no vertical flow at the upper and the low boundaries, i.e. $k \frac{\partial T}{\partial z} = 0$, then the solution for Equation 8.36 is,

$$T = C_1 \quad (8.37)$$

where C_1 is constant.

Equation 8.37 means that the material finally will have the same temperature everywhere if there is no heat exchange with the environmental.

Let us consider a one dimensional steady state vertical water flow now. The corresponding differential equation for the one dimensional steady state vertical water flow can be obtained from Equation 8.34, which is,

$$\frac{\partial}{\partial z} \left(k \frac{\partial h}{\partial z} \right) = 0 \quad (8.38)$$

The solution for Equation 8.38 is,

$$k \frac{\partial h}{\partial z} = C_2 \quad (8.39)$$

where C_2 is constant.

If there is no vertical flow at the upper and lower boundaries, i.e. $\frac{\partial h}{\partial z} = 0$, then the solution for Equation 8.39 is,

$$h = C_3 \quad (8.40)$$

where C_3 is constant.

If the ground water level is taken as reference elevation, then $C_3=0$.

Bernoulli's equation states that the total head of water equals to the sum of the elevation head, pressure head and the velocity head, i.e.,

$$h = z + \frac{u_w}{\rho_w g} + \frac{v^2}{2g} \quad (6.67)$$

where h is the total hydraulic head; z is the elevation head; u_w is the pore water pressure; ρ_w is the density of water; g is the gravity acceleration; and v is the velocity of the water flow.

Usually the velocity head in a soil is much too small to be of any consequence and thus can be neglected. Equation 6.67 is converted to:

$$h \approx z + \frac{u_w}{\rho_w g} \quad (6.68a)$$

As a consequence, the pore water pressure distribution is,

$$u_w = -\rho_w g z = -10z \quad (8.41)$$

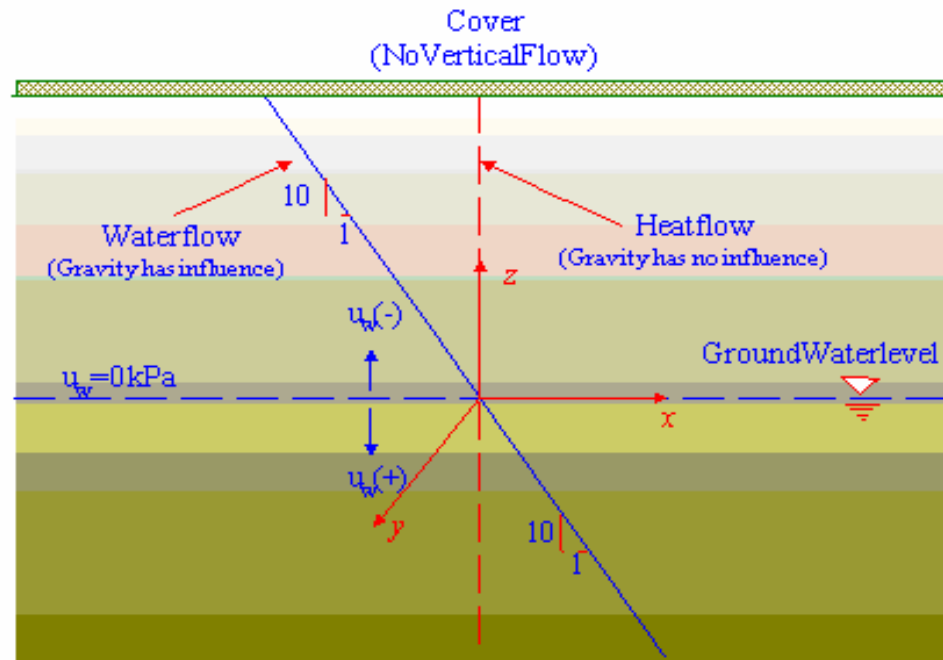


Fig. 8.5. Comparisons between the heat flow and the water flow under equilibrium

A real problem can show the difference in solution between Equation 8.33 and 8.34. For example, if the soil is covered by a larger enough cover for a very long time and there is no vertical flow under the cover (Fig. 8.5). If the heat transfer equation 8.35 is used to solve the water flow problem by using the thermodynamic analogue, the solution will be the vertical line in the Fig. 8.5, which means the pore water pressure is the same along the whole soil profile. If the Equation 8.34 or 8.38 is used to solve the same problem, the solution will be the inclined line with a slope of 1:10 as shown in Fig. 8.5.

In classical soil mechanics for saturated soils, the influence of the elevation head is neglected because all the parameters for a saturated soil are considered as constants. The simplification will cause little error. Fredlund and Rahardjo (1993) proposed that the influence of the gravity could also be neglected under some conditions for unsaturated soils. However, it is not true because all the material parameters for an unsaturated soil are highly nonlinear and are functions of mechanical stress and matric suction. Neglecting the influence of gravity will cause errors in matric suction

calculations, which in turn will cause the errors in calculating the material properties. Finally it will lead to mistakes for the whole simulation. Consequently, when we use the thermodynamic analogue to consolidation process to compute the volume change of an unsaturated soil, the program should be modified to accommodate the influence of gravity. In ABAQUS/Standard, the modification is made as followings by using the user subroutine UMATHT. The heat flux vectors for the equation 8.33 are

```
do i=1, ntgrd
    flux(i) = -cond*dtemdx(i)
end do
```

where ntgrd stands for number of spatial gradients of temperature, for three dimensional case, ntgrd=3; flux(i) is the heat flux vector in the ith direction; cond is the heat conductivity; and dtemdx(i) is the current values of spatial gradients of temperature in the ith direction.

As discussed above, the gravity only influences the water flow in the z direction. Hence, the modification is made as followings

```
do i=1, ntgrd-1
    flux(i) = -cond*dtemdx(i)
end do
flux(ntgrd)=-cond*(dtemdx(ntgrd)+10)
```

The verification program for the modification is attached in the Appendix D.2.

8.5 Initial Conditions, Boundary Conditions and Loadings

8.5.1 Initial Conditions

The soils are assumed to have an initial geostatic status for mechanical stress. Because the starting point for the simulation is assumed to be 08/01/1999, which is between the

second boring (07/13/1999) and the third borings (10/25/1999), the initial matric suctions are obtained as followings:

(1). Average the water content profile for the four footings (RF1, RF2, W1, and W2) on 07/13/1999 and the water content profile for the two footings (W1 and W2, RF1 and RF2 have no data) on 10/25/1999 (Fig. 8.6).

(2). Interpolate the water content for 08/01/1999, and find the corresponding water content at the nodes with different depth (Fig. 8.6).

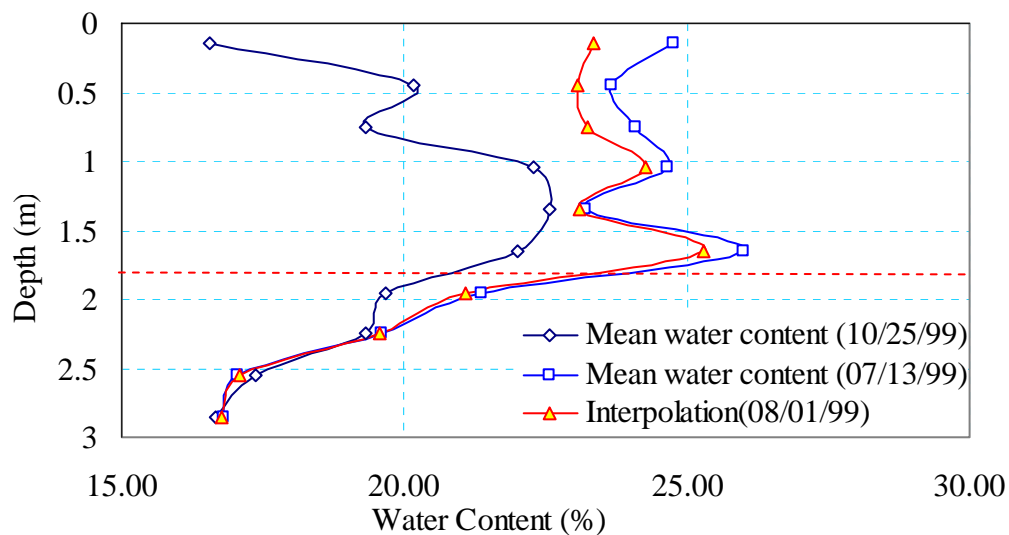


Fig. 8.6. Interpolation of the water content profile for 08/01/1999

(3). Find the corresponding mean mechanical stress from the depth. The density of the soil is 20kN/m^3 , and the Poisson's ratio is 0.4, then $K_0=0.67$. Consequently, $\sigma_m = 0.778\sigma_v$. The mean mechanical stress versus water content profile is shown as in Fig. 8.7. As shown in Fig. 8.2, the domain is divided 10 layers, for each layer (layer 1-layer 8), the water content is interpolated by using the result from Fig. 8.7.

(4). Make use of the water content constitutive surface to obtain the corresponding matric suction profile as shown in Fig. 8.8. Because the water content constitutive surfaces are known for the two soil layers and both the water content and mechanical stress at the soil profile are obtained from step 3, the matric suction along the depth can

be obtained by iteration. The Solver in Microsoft Excel is used to perform the iteration. The matric suctions at the surface nodes are assumed to be 1000kPa. The matric suctions below 3.0m are obtained by assuming the matric suction at the depth of 4.0m is 10 kPa, and then interpolated with the matric suctions at layer 8. The result is plotted in Fig. 8.8.

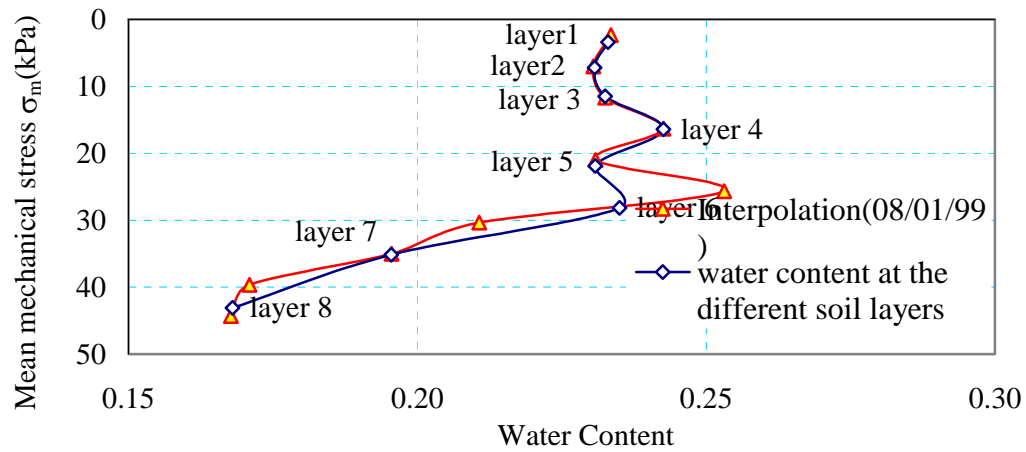


Fig. 8.7. Mechanical stresses versus water content at different soil layers

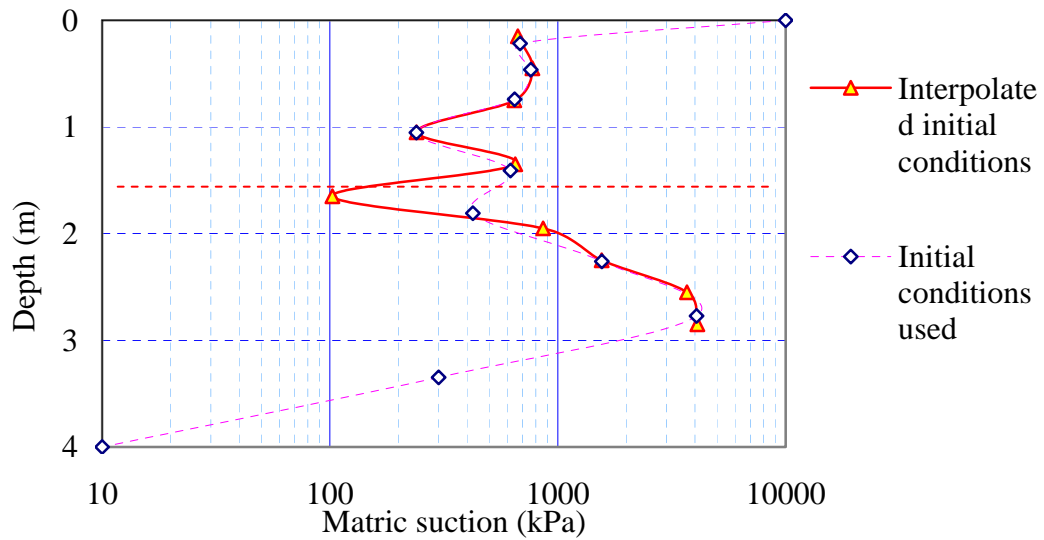


Fig. 8.8. Calculated matric suction profiles for 08/01/1999

8.5.2 Boundary Conditions

8.5.2.1. Mechanical Boundary Conditions

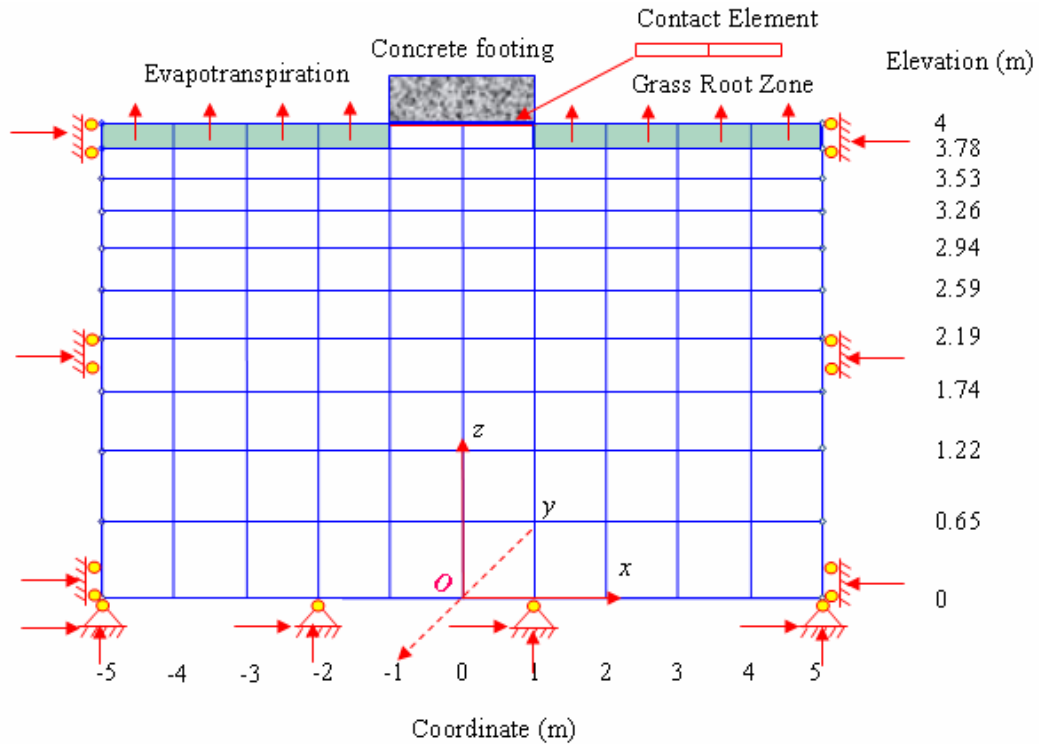


Fig. 8.9. Boundary conditions for the simulation domain (sideview)

Fig. 8.9 shows the boundary conditions for the model in Fig. 8.2. Point O is the origin of the coordinate system, and only the xOz plane is shown. The horizontal displacement at (in x direction) is restrained, that is, no horizontal displacement at both the left and right side.

$$x = -5\text{m or } x = 5\text{m}, u_x = 0$$

For the yOz plane, similarly,

$$y = -5\text{m or } y = 5\text{m}, u_y = 0$$

which is not shown in the Fig. 8.9. The restraints are applied by using the XSYMM (Symmetry about a plane $x = -5\text{m or } x = 5\text{m}$, degrees of freedom 1,5,6=0) and YSYMM (Symmetry about a plane $y = -5\text{m or } y = 5\text{m}$, degrees of freedom 2,5,6=0) option in the

ABAQUS/Standard. For the nodes at the bottom of the domain, the displacements in both x, y, and z direction are restrained,

$$z=0 \text{ m, } u_x= u_y= u_z=0$$

The restraints are applied by using the PINNED (degrees of freedom 1,2,3=0) option in the ABAQUS/Standard.

At the soil surface outside from the concrete footing, there is no mechanical load. The load the concrete footing applied to the soil is its gravity. The soil-structure interaction is simulated by using contact element. The load transfer depended on whether the bottom of the concrete footing is in contact with the soil surface or not. When surfaces are in contact, any contact pressure can be transmitted between them. The surfaces separate if the contact pressure reduces to zero. Separated surfaces come into contact when the clearance between them reduces to zero, i.e.

$$P=0 \text{ for } h<0 \text{ (open), and}$$

$$h=0 \text{ for } P>0 \text{ (closed).}$$

“Hard contact” option in ABAQUS/Standard is used to define the contact pressure-overclosure relationship. Shear force at the interface between the concrete footing and the ground soil surface will depends on the computation result. Because the footing is symmetric and the boundary conditions for it in all the directions are the same, the horizontal displacement between the soil surface and the concrete surface is expected to be small. The definition of the material properties for the contact element has been discussed previously.

8.5.2.2. Water Flow (Heat Transfer) Boundary Conditions

As has been discussed before, heat transfer boundary conditions represent the water flux boundary conditions. At the place far away from the footing, it is assumed there is only vertical flow, that is, the horizontal flow on both the left q_x and right sides q_y are zero, which are as followings,

$$x= -5\text{m or } x=5\text{m, } q_x=0$$

for the yOz plane, similarly,

$$y = -5\text{m or } y = 5\text{m, } q_y = 0$$

These conditions are not shown in the Fig. 8.9. The restraints are applied automatically by ABAQUS/Standard without specially specifying. For the nodes at the bottom of the domain, it is assumed the soil matric suction is constant and equaled to -10 kPa through the simulation due to the ground water level is at 4.0m depth,

$$z = 0 \text{ m, } u_w = -10\text{kPa}$$

For the soil underneath the concrete footing, there is no vertical flow. Because the coupled consolidation of the soils are simulated by the coupled thermal stress problem, the vertical zero water flux for the soil underneath the concrete footing is simulated by defining the material properties of the contact element between the soil surface and the bottom surface of the concrete footing. The definition of the material properties for the contact element has been discussed previously.



Fig. 8.10. Grass at the site at Arlington, Texas

At the soil surface outside from the concrete footing, the soil is covered by Johnsongrass (*Sorghum halepense*) as shown in Fig. 8.10, which is the most widely distributed naturalized warm-season, perennial grass in North America. Therefore, the boundary conditions are controlled by the vegetation evapotranspiration. The method for estimating the evapotranspiration for the vegetation has been discussed in the Chapter VII. Depending on the daily weather data, the evapotranspiration for the grass is different. The single crop coefficient for the Johnsongrass is assumed as $K_c = 0.6$. Texas ET Network (<http://texaset.tamu.edu/>) recommends that the average water stress coefficient for low stress is 0.8 through much of the year, which corresponds to a $p = 0.6$ approximately. The adjusted coefficient for the water and environmental stress depends on the matric suction in the grass root zone (Fig. 7.9). For the grass root zone, the water source term can be calculated by Equation 7.48 and the net water loss for the grass root zone is calculated by Equation 7.42 and 7.43.

8.5.3 Loadings

During the simulation, body forces caused by the gravity are applied to both the concrete footing and soil block. The acceleration of gravity is taken as 10m/s^2 . The weight of the footing is transferred to the soil surface by contact element. There is no thermal load applied during the simulation. The weather's influence is simulated as the source term and is discussed in the boundary conditions section.

8.6 Programming

8.6.1 Introduction

ABAQUS/Standard is used to perform the simulation and the coupled temperature-displacement option is used. One input file for the main program and four user subroutines are used to perform the simulation. The main program defines mesh, material properties for concrete and contact elements, soil structure interaction, initial conditions, boundary conditions and analysis steps for the simulation. The soil properties are calculated and transferred into main program by user subroutines. User

subroutine USDFLD firstly obtain the temperature (matric suction) and mechanical stress of the previous step for each element from the main program, and then the soil state variables (void ratio, degree of saturation and water content) are calculated from the constitutive surfaces. The needed soil parameters such as Young's modulus E , coefficients of expansion α , specific water capacity C_w or m_2^w , water generation parameters m_1^w , coefficient of permeability, and the mean mechanical stress variations are also calculated. If the element is at the grass root zone, the matric suction is used to calculate the current water content, water stress coefficient K_s . The actual evapotranspiration can be calculated by analyzing the soil water balance.

The Young's Modulus is transferred to the user subroutine UMAT to calculate the stiffness matrix for the equilibrium equation. The coefficient of expansion is transferred to the user subroutine UEXPAN. The specific water capacity, water generation parameter, coefficient of permeability and water source term are transferred to the user subroutine UMTHT to calculate the water continuity.

The mechanical stress and the matric suction can be calculated by using finite element method to solve the coupled consolidation theory differential equations if the initial conditions and the boundary conditions are known. The calculated mechanical stress and the matric suction are used as the initial condition for the next step. In this way, the simulation can be performed.

8.6.2 Main Program

8.6.2.1 Introduction

The fully coupled thermal-stress analysis in ABAQUS is used to simulate the coupled consolidation theory for saturated-unsaturated soils to obtain the thermal and mechanical solutions simultaneously. The coupled temperature-displacement elements are used for this purpose.

The temperatures (pore water pressure or matric suction) are integrated using a backward-difference scheme, and the nonlinear coupled system is solved using Newton's method. The flow chart of the main program is shown in Fig. 8.11.

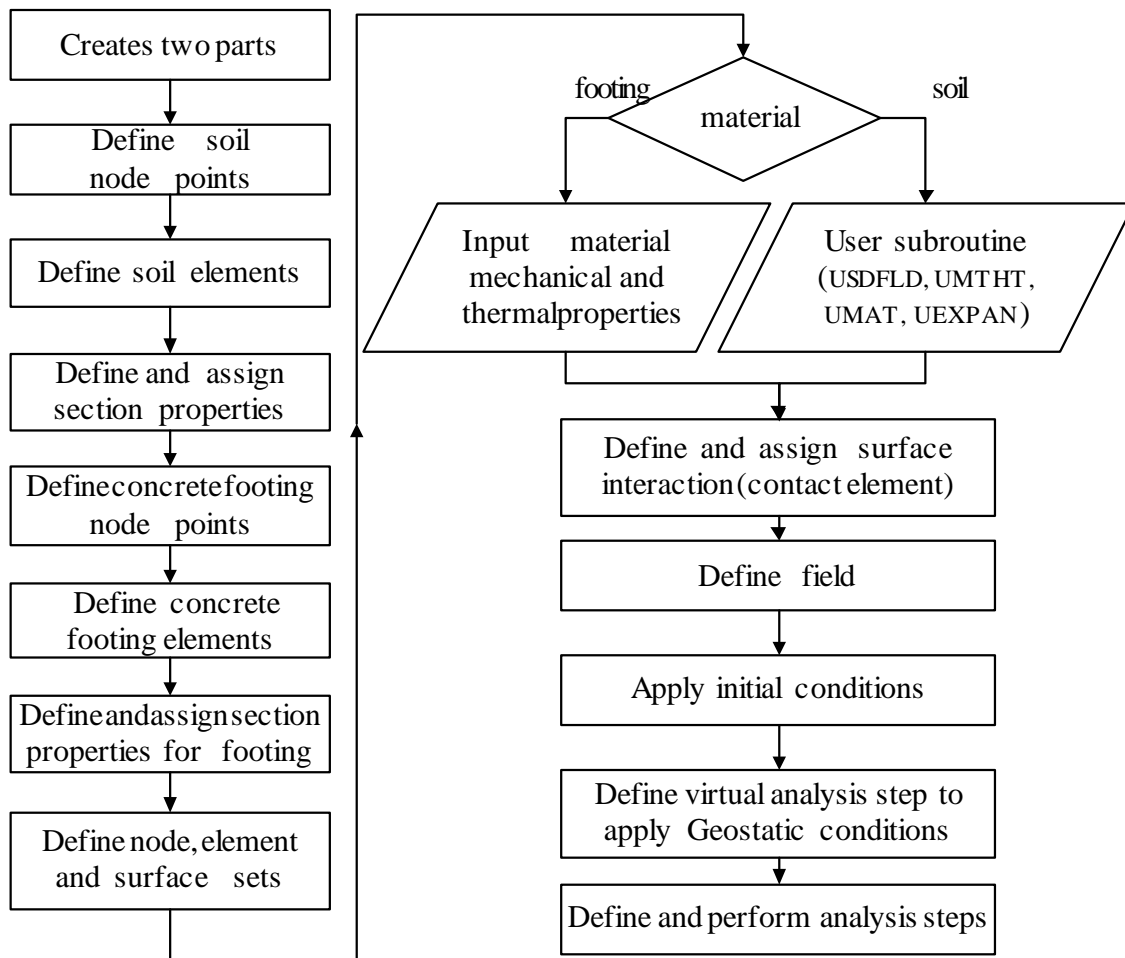


Fig. 8.11. Flowchart of the main program

The program is attached in the appendix D.1. Because the soil properties are functions of both mechanical stress and matric suction, a special user subroutine USDFLD in ABAQUS/Standard written by Fortran is used to obtain the reference evapotranspiration and rainfall data from external file, and to obtain the mechanical stress and matric suction from the previous calculation step. Then the mechanical stress and the matric suction are used to calculate the soil state variables such as void ratio, water content and degree of saturation. The calculation results, combined with the two stress state variables, are used to calculate the soil parameters for the constitutive relationships such as the Young's Modulus, coefficient of expansion, specific water

capacity and water generation parameters. Some other parameters such as permeability coefficient, mean mechanical stress variation and the water source term due to the weather are also calculated in the user subroutine USDFLD. The soil parameters for the constitutive relationships are then transferred to the user subroutines UMTHT, UMAT, and UEXPAN to calculate the parameters for the calculations.

8.6.2.2 User Subroutine USDFLD

The user subroutine USDFLD is used to calculate parameters for the simulation. The flowchart of the user subroutine USDFLD is shown in Fig. 8.12. Firstly, the utility routine GETVRM is called to get the temperature (matric suction) and the mechanical stress from the main program respectively. The mean mechanical stress is calculated and compared with the mean mechanical stress at the previous step to get the mean mechanical stress variations. The two stress state variables are used to calculate the state variables of the soil, i.e., void ratio, water content and degree of saturation, from the constitutive surfaces constructed in Chapter V. The void ratio and the degree of saturation are used to determine the permeability coefficient of the soil at current status. The derivatives of the constitutive surfaces are also calculated to get the m_1^s , m_2^s , m_1^w , and m_2^w . These parameters are used to calculate the Young's Modulus, coefficient of expansion, water generation due to mechanical stress and the water specific capacity. The Young's Modulus is transferred into the user subroutine UMAT to calculate the material Jacobian matrix, $\partial\Delta\sigma/\partial\Delta\varepsilon$. The coefficient of expansion is transferred into the user subroutine UEXPAN. The mean mechanical stress variation, water specific capacity m_2^w , water generation parameter m_1^w , and permeability coefficient are transferred into the user subroutine UMTHT to calculate parameters for the thermal constitutive relations, that is, the continuity of the water phase.

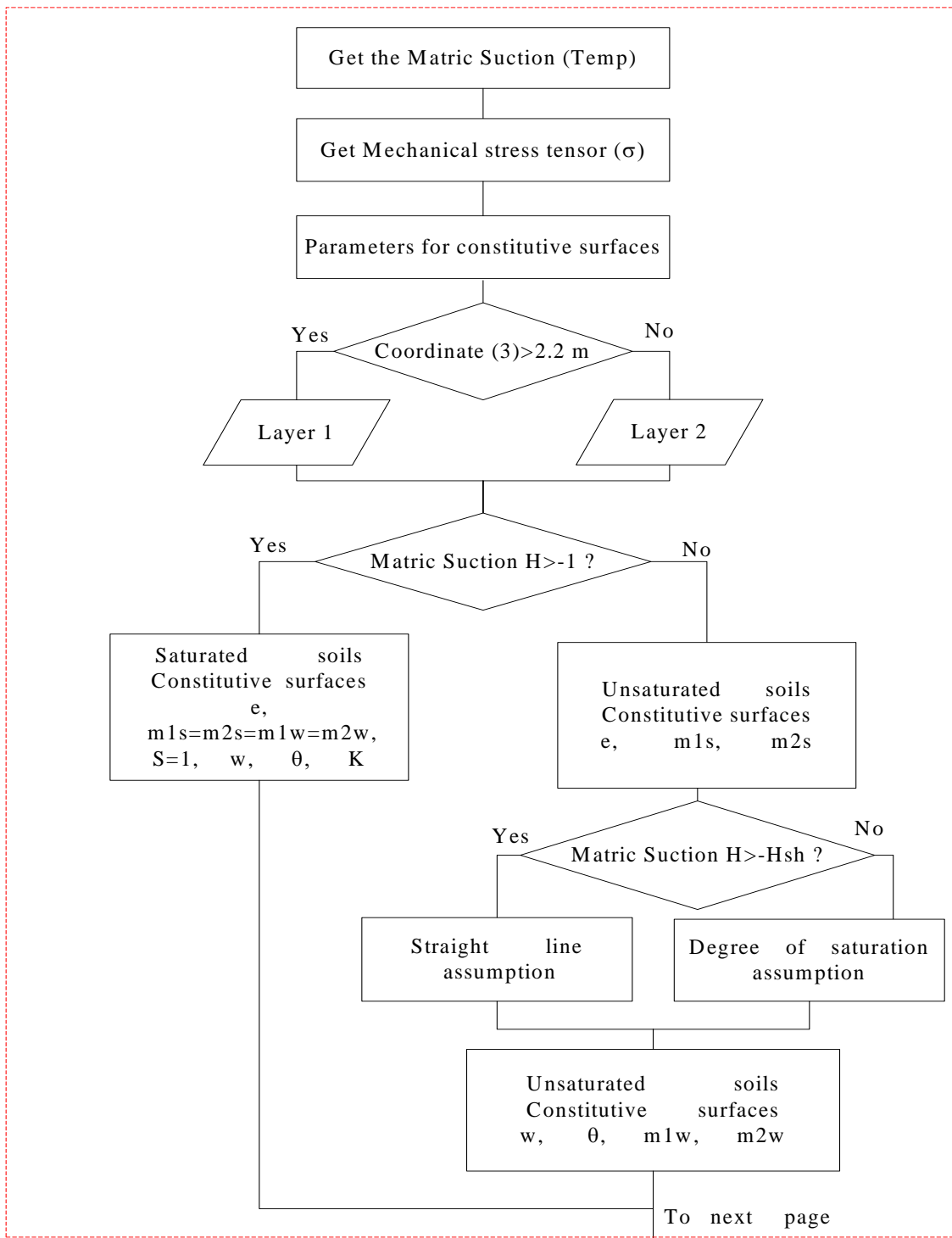


Fig. 8.12. Flow chart for the user subroutine USDFLD. (a) constitutive surfaces and their derivatives

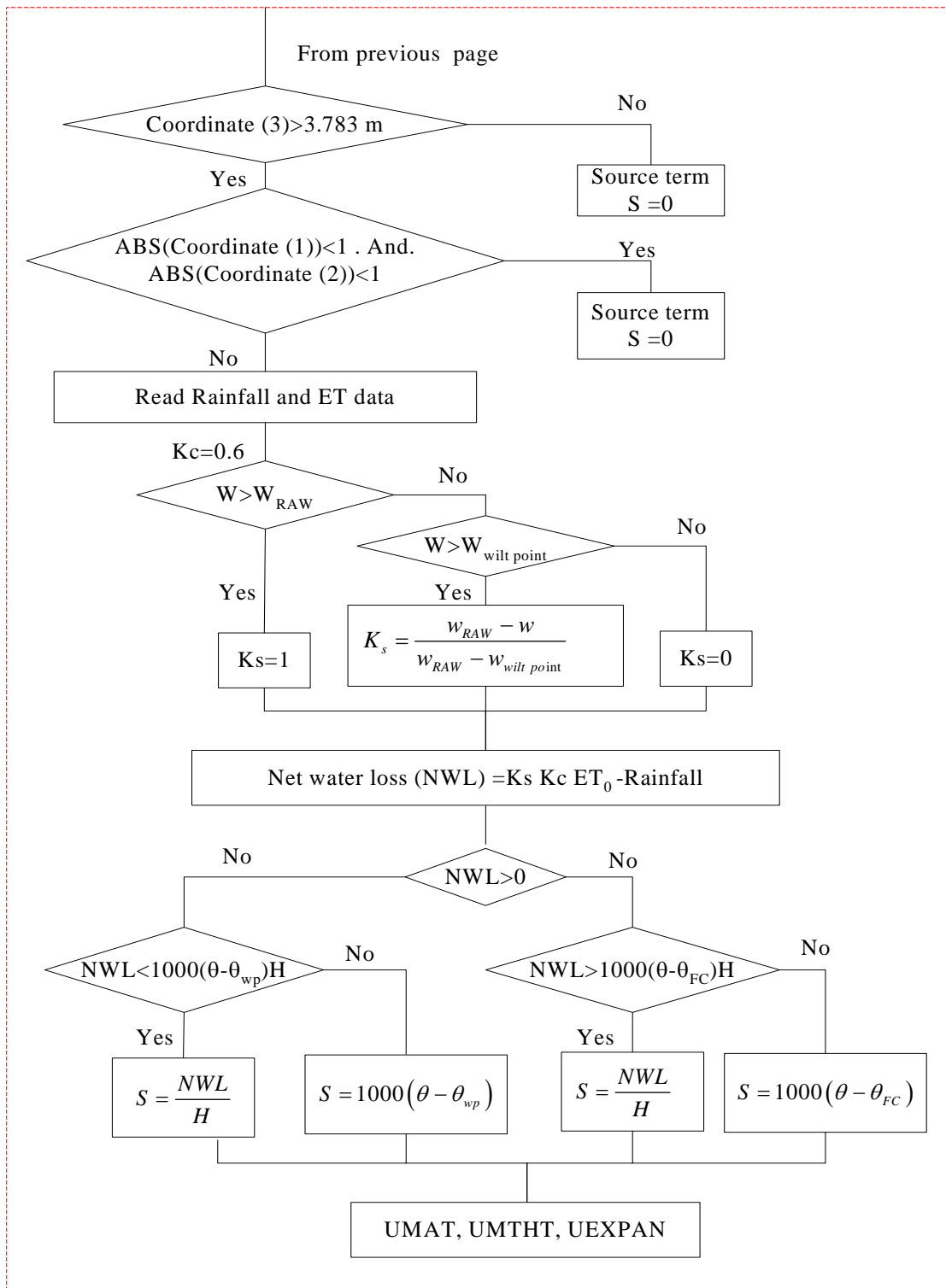


Fig. 8.12. (Continued) (b) Flow chart for the source term calculation

The sink term at the grass root zone caused by the evapotranspiration and the rainfall infiltration are also calculated. The vegetation at the site is Johnson grass, K_c is taken as 0.6. Depending on the water content (i.e., matric suction) in the soil, the water stress factor K_s is calculated according to the discussion in the chapter 7. The sink term is also transferred into the user subroutine to calculate the continuity for the water phase. The user subroutine USDFLD is attached in Appendix D.1.2.1.

8.6.2.3 User Subroutine UMTHT

The difference between the consolidation for saturated-unsaturated soils and the coupled thermal stress problem due to heat conduction is that during the consolidation of the saturated-unsaturated soil, the pore water pressure (temperature) will change. The pore water pressure variation corresponds to variation in the mass of water per unit mass of soil. The corresponding part in the heat transfer is the internal heat generation. The thermodynamic explanation of the consolidation is when the load is applied to the material, and the volume of the material will change. In this process, work is done to the material due to the load application. The work is changed into heat energy due to internal friction. The heat generation due to friction can be treated in the same as what we used to treat the internal heat generation.

The user subroutine UMTHT in conjunction with the user subroutine USDFLD is used to define the thermal constitutive behavior of the material as well as internal heat generation during heat transfer processes.

The permeability coefficient, specific water (heat) capacity, variation in mean mechanical stress and the water source term (internal heat generation) are calculated firstly in the user subroutine USDFLD from the soil constitutive surfaces and weather condition, depending on the matric suction and mechanical stress from the previous step, and then are transferred into the user subroutine UMTHT.

The heat generation due to the mean mechanical stress variation and the heat generation due the grass root zone absorption are put together as a source term. If the

soil is not in the grass root zone, only the heat generation due to mechanical stress variation is calculated because $S=0$.

The user subroutine UMTHT is attached in Appendix D.1.2.2.. The flow chart for the user subroutine UMTHT is,

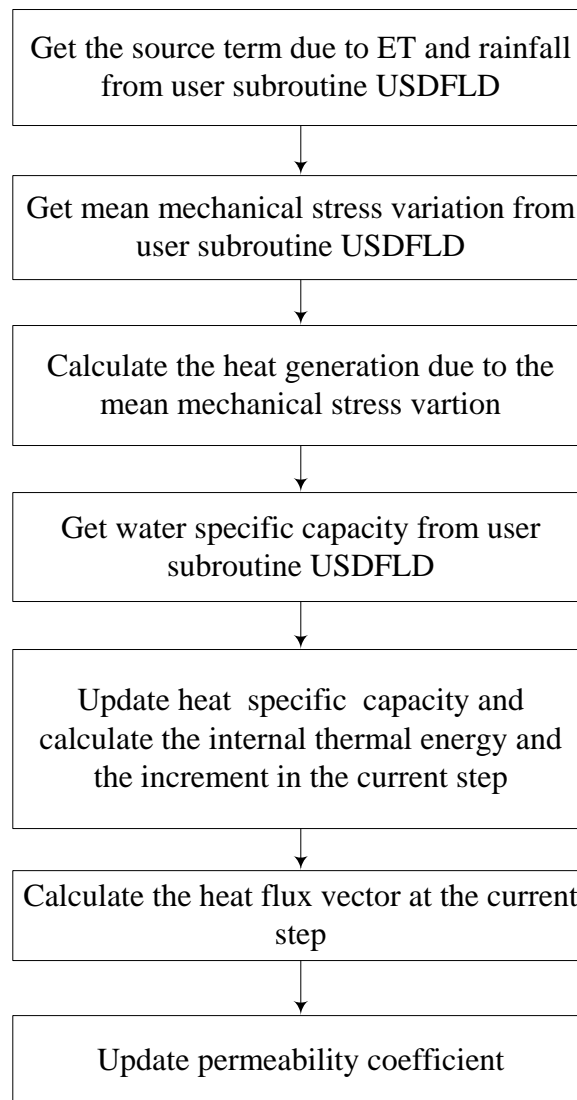


Fig. 8.13. Flow chart for the user subroutine UMTHT

8.6.2.4 User Subroutine UMAT

The user subroutine USDFLD is used to calculate the Young's Modulus from the soil constitutive surfaces because the Young's Modulus is a function of both mechanical stress and matric suction. The Young's Modulus is then transferred into the user subroutine UMAT to calculate the material Jacobian matrix, $\partial\Delta\sigma/\partial\Delta\varepsilon$ for the mechanical constitutive model.

$$[D] = \frac{E(1-\mu)}{(1+\mu)(1-2\mu)} \begin{vmatrix} 1 & \frac{\mu}{1-\mu} & \frac{\mu}{1-\mu} & 0 & 0 & 0 \\ & 1 & \frac{\mu}{1-\mu} & 0 & 0 & 0 \\ & & 1 & 0 & 0 & 0 \\ & & & \frac{(1-2\mu)}{2(1-\mu)} & 0 & 0 \\ & & & & \frac{(1-2\mu)}{2(1-\mu)} & 0 \\ & & & & & \frac{(1-2\mu)}{2(1-\mu)} \end{vmatrix}$$

(8.42)

Only the symmetric part of the matrix is calculated by taking one half the sums of the matrix and its transpose because the soils are considered as homogenous and isotropic.

The elastic matrix is used in conjunction with the array of strain increments to calculate the new mechanical stress. The strain increments are the mechanical strain increments (the total strain increments minus the thermal strain increments) because the *EXPANSION, USER option is used in the same material definition.

The user subroutine UMAT is attached in Appendix D.1.2.3..

8.6.2.5 User Subroutine UEXPAN

The user subroutine UEXPAN is used to calculate the thermal strain due to temperature variation. Firstly, the coefficient of expansion calculated from the user subroutine USDFLD is transferred into the user subroutine UEXPAN and then the thermal strain is calculate by multiplying the coefficient of expansion and the temperature variation.

The user subroutine UEXPAN is attached in Appendix D.1.2.4..

8.7 Results and Discussion

Fig. 8.13 shows the calculation results for the simulation. The displacements at the four corners of the concrete footing were taken out and compared with the observation. The observation for the four footings is shown in the Fig. 8.14. The cumulative curve for the Rainfall minus evapotranspiration under water stress condition is also shown in the Fig.. The $K_c=0.6$ and $K_s =0.8$, which are recommended by the Texas ET network. In the simulation the K_s is dependent on the actual soil status. The cumulative difference between the rainfall and the evapotranspiration under water stress conditions are plotted because it approximately reflected the net water loss over the two year's period, and it is the net water loss that influence the soil conditions. The simulation results for the footing movements over the two year's period are also shown in Fig. 8.13. Compared with the observations for the four footings, the simulation results matched the observations reasonably well in both tendency and the magnitude, reflecting that the proposed method for the modeling of grass root zone and for the construction of the constitutive surfaces are good enough for practical applications.

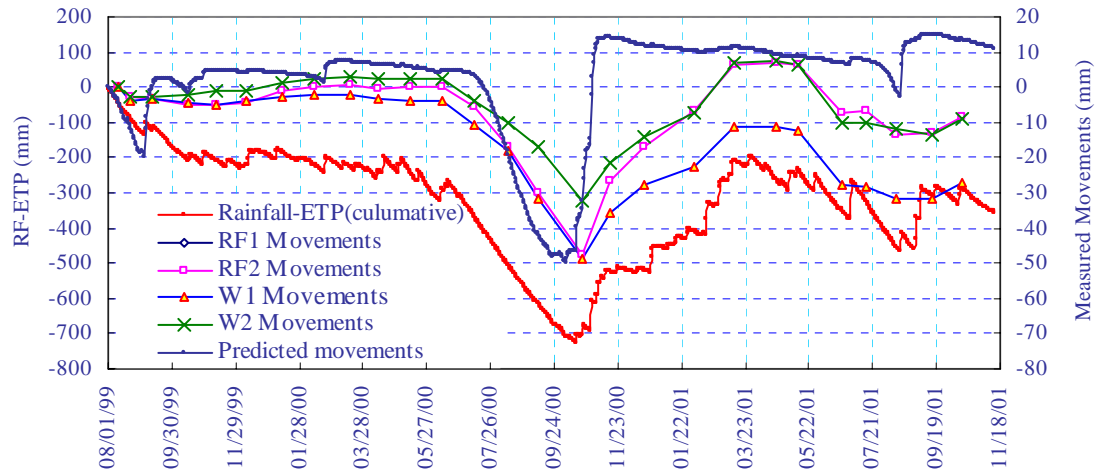


Fig. 8.14. Comparisons between the observation and simulation results

However, the footing moved upward faster than the observation. The reason for this may be that the daily net water loss is calculated in the simulation. However, generally speaking, a rainfall event only lasts a few hours during the day. It is very rare to rain 24 hours continuously. If the rainfall density is greater than the ability of soil to absorb water, usually there is some kind of runoff. However, when a daily rainfall is compared with the evapotranspiration and the actual soil status, the rainfall is averaged during the whole day and the rainfall density is actually underestimated. With a lower rainfall density and a longer time, the soil has opportunities to absorb more water than it actually should do at the very beginning. If there is a long rainfall period, the soil surface will tend to be saturated and has less ability to absorb more water. Consequently, the footing will move upward faster than the actual observation when there is rainfall.

CHAPTER IX

CURRENT DESIGN METHODS AND NUMERICAL SIMULATIONS OF RESIDENTIAL BUILDINGS ON EXPANSIVE SOILS

9.1 Introduction

The consolidation theory in Chapter VI explains the volume change behaviors for saturated-unsaturated soils when there are both load applications and water content variations. The laboratory tests and the corresponding method to construct the constitutive surfaces for saturated-unsaturated soils are discussed in Chapter IV and Chapter V. The method to obtain the material parameters needed for the consolidation theory is discussed in Chapter VIII. Chapter VII discusses the method to determine the boundary conditions by using daily weather data. Chapter VIII discusses the numerical methods to solve the differential equations for the consolidation of saturated-unsaturated soils and the method proposed in Chapter VII is used to verify the actual observations at a site at Arlington, Texas. As a consequence, all the problems associated with the soil behaviors have been discussed.

However, the final objective for the whole research still has not been reached. The question is: how should we design foundations on expansive soils? In this chapter, current design methods for foundations on expansive soils are reviewed. Based on the discussions in the previous chapters, a complete system for the simulations of residential buildings on expansive soils is proposed. The coupled consolidation theory is used to simulate the volume change behavior for saturated-unsaturated soils. Contact (jointed) elements are used to simulate the slab-soil interaction at the interface while general purpose shell elements are used to simulate the behavior of slabs and walls. Pseudo moisture variation simulation is proposed to solve the problem during the conversion from the coupled hydro-mechanical stress analysis and the mechanical stress analysis. Some tentative results as well as recommendations for future research are presented. The smeared crack model is proposed to simulate cracking in the residential buildings.

9.2 Review of Current Design Methods for Foundations on Expansive Soils

Current available design methods for foundations on expansive soils include: the Building Research Advisory Board (BRAB) method (1968), the Wire Reinforcement Institute (WRI) Method (1996), the Post-Tensioning Institute (PTI) Method (1996), the Portland Cement Association (PCA) Method (Spears and Panarese, 1990) and the Corps of Engineers (COE) method (1987).

9.2.1. The BRAB Method (1968)

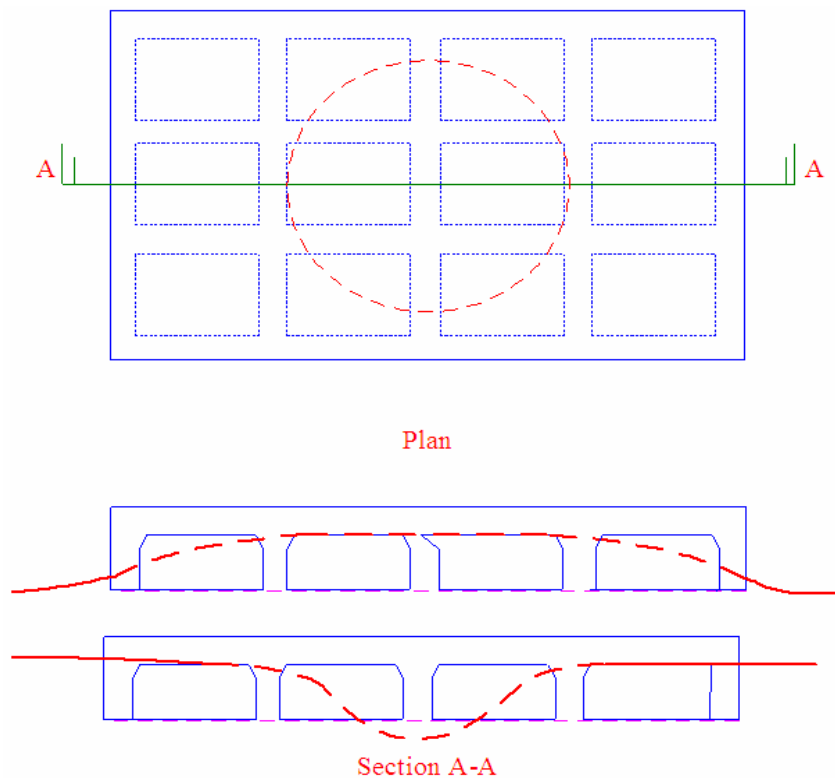


Fig. 9.1. Assumption of the BRAB method (BRAB 1968)

The BRAB method assumes that there is an area of loss of support as shown in Fig. 9.1, the diameter of which is a function of the soil (P.I., degree of compaction, etc.) and which is allowed to move to any position under the building. This procedure designed

only one or two beams at a time. The BRAB report showed support conditions which allowed all beams in a given direction to be considered at one time. The moment equations developed by BRAB give a maximum moment, both positive and negative at midspan (Fig. 9.2). The most critical locations are assumed to be under load bearing walls and columns. This procedure is developed entirely from looking at slabs that seem to work and those which do not, and writing an equation which would produce sections equal to those which had been performing satisfactorily. Formulas are developed which take into account loss in the center as shown above, loss at edges and corners as well as provisions for inclusion of concentrated loads.

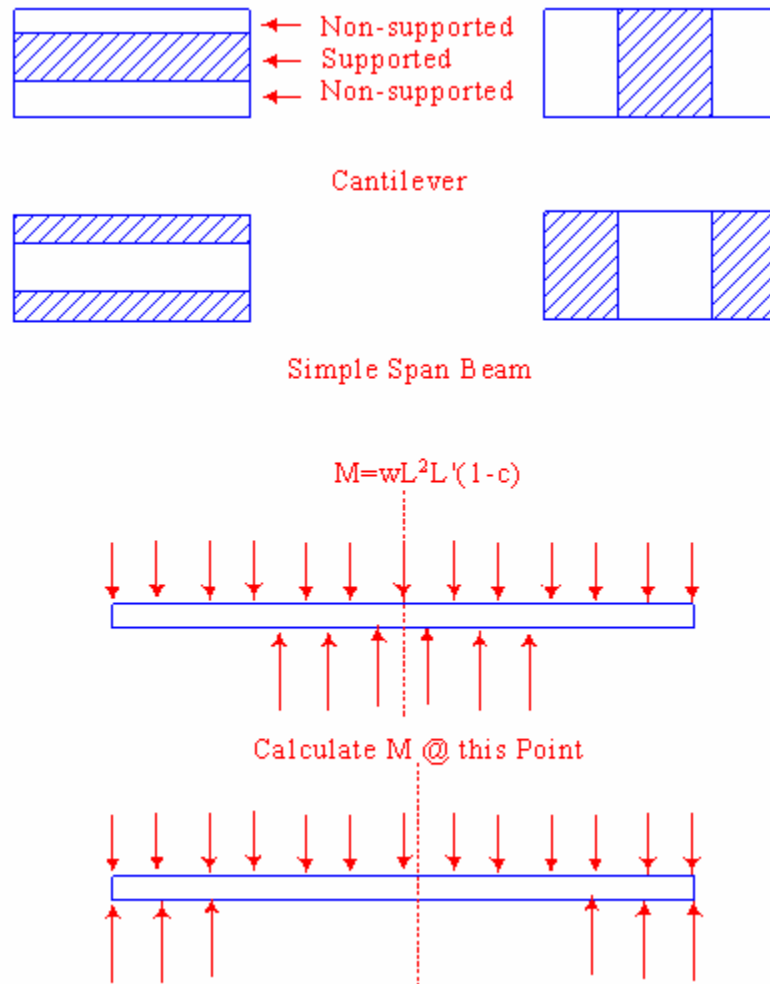


Fig. 9.2. Assumed support conditions and locations of maximum moment (BRAB 1968)

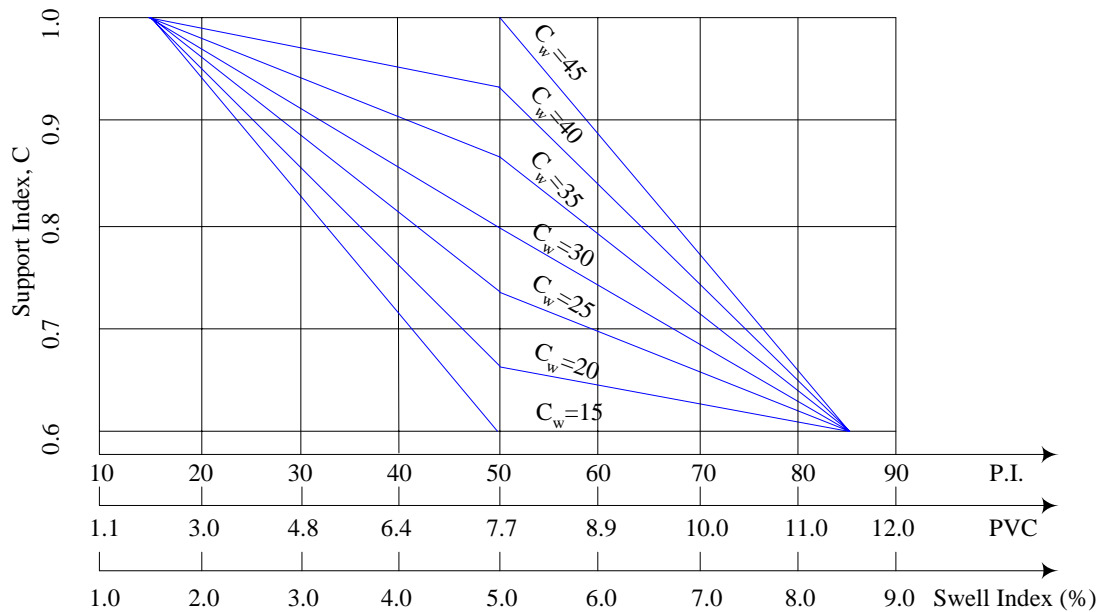


Fig. 9.3. Supporting index, C, based on criterion for soils sensitivity and climatic rating (BRAB 1968)

The BRAB method first chooses the climatic rating index (C_w) for the continental United States, and then uses the climatic rating index (C_w) and the plasticity index or the PVC or the swell index to determine the supporting index (C) as shown in Fig. 9.3. The support index can be increased to a modified support index (C_m) or decreased to a reduced support index (C_r) according to the site soil condition and type. Slabs of irregular shape are then divided into overlapping rectangles of length (L) and width (L'). The load is considered to be a uniformly distributed superstructure. The effective load for each rectangular dimension is determined according to its aspect ratio. The maximum bending moment, shearing force and differential deflection can be calculated from the following equations, respectively:

$$M_{\max} = \frac{wL^2L'(1-C)}{8}, \quad V_{\max} = \frac{wLL'(1-C)}{2}, \quad \text{and} \quad \Delta_{\max} = \frac{wL^4L'(1-C)}{48EI} \quad (9.1)$$

where w = the deflection of the slab.

The BRAB method takes into account the influence of the climate and the soil properties based on empirical data. The problem associated with the BRAB method is that for slabs with different dimensions at the same site, the designs by this method are the same, a result that is not reasonable. Research indicates that designs based on the BRAB method are usually over conservative.

9.2.2 The WRI Method

The Wire Reinforcement Institute (WRI) design procedure was developed by Walter (1996). It is a modified version of the BRAB method. The WRI design procedures can be summarized as follows:

Firstly the effective plasticity index of the underlying 15 feet by using weighting factors 3, 2, and 1 for the first, second, and third 5-feet-layer respectively, and the effective plasticity index can be modified for natural ground slope and overconsolidation by using the correction coefficients.

Secondly, slabs of irregular shape are divided into overlapping rectangles of length (L) and width (L') and the climatic rating index (C_w) is chosen in the same way as that in BRAB method.

Thirdly, the soil-climate support index was chosen from Fig. 9.4, and the beam spacing is chosen according to Fig. 9.5

The cantilever length is determined as a function of soil (I_c), and the length modification factors for long and short directions, k_l and k_s , respectively, are determined From Fig. 9.6. The modified cantilever lengths (L_c) in both directions are multiplied by I_c and the number of beams in both direction are calculated:

$$N_l = \frac{L'}{S} + 1 \quad N_s = \frac{L}{S} + 1 \quad (9.2)$$

The maximum bending moment, shearing force and differential deflection are calculated for each direction from:

$$M = \frac{wL'(L_c)^2}{2}, \quad V = wL'(L_c), \quad \Delta = \frac{w(L_c)^4 L'}{4E_c I} \quad (9.3)$$

where M = Moment, positive or negative; Δ = Deflection in inches; E_c = Creep modulus of elasticity of concrete; I = Moment of inertia of section.

The beam depth for reinforced steel and prestressed steel can also be calculated by using the following equations:

$$\begin{aligned} \text{Reinforced Steel} \quad d &= \sqrt[3]{\frac{664ML_c}{B}} \\ \text{Prestressed Steel} \quad d &= \sqrt[3]{\frac{553ML_c}{B}} \end{aligned} \quad (9.4)$$

where M = Moment in KF; L_c = Cantilever length (k Ic).

The WRI method is based on the same assumptions as those in the BRAB method.

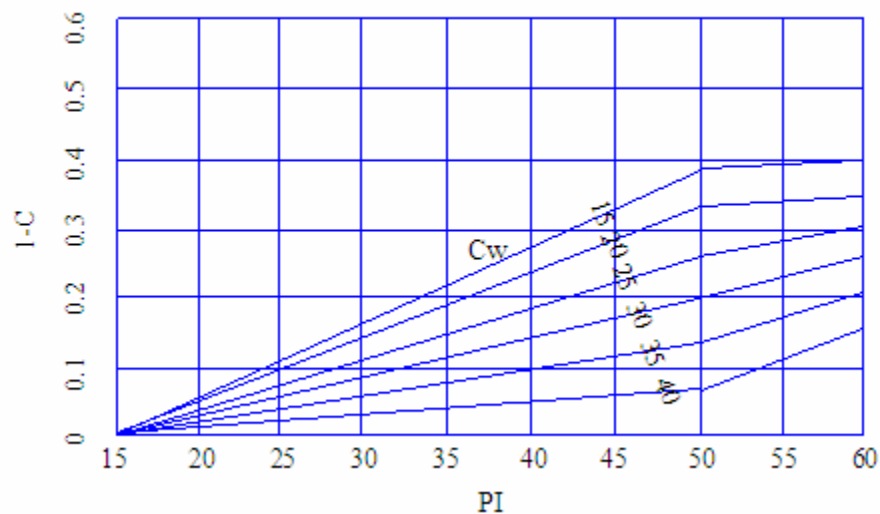


Fig. 9.4. The soil-climate support index (WRI 1996)

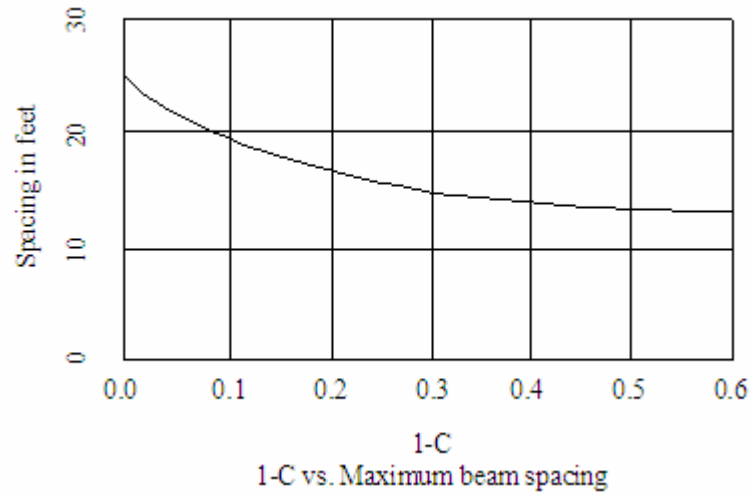


Fig. 9.5. Beam spacing determination (after WRI 1996)

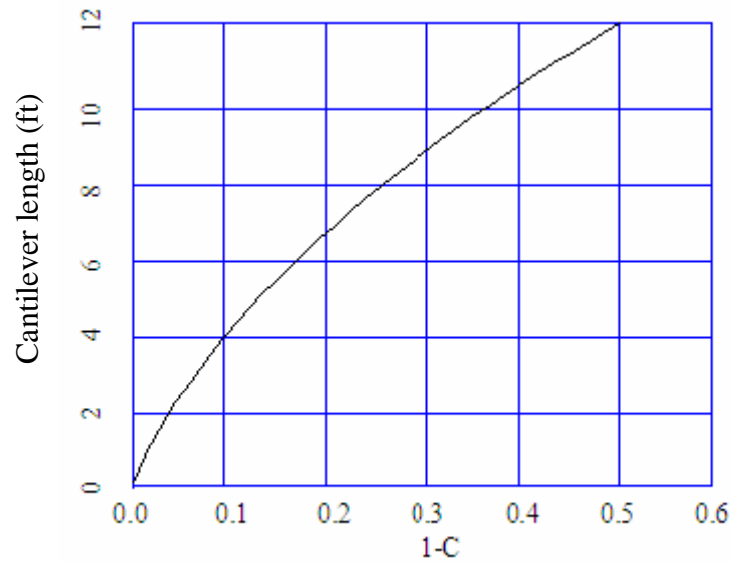


Fig. 9.6. Length modification factors for long and short directions (after WRI 1996)

9.2.3 Post-Tensioning Institute (PTI) Method

The Post-Tensioning Institute design method is the most systematic and well theoretic-based method so far for the design of slab on expansive soils. The movement prediction

is based on the suction method (Lytton 1977; Mckeen 1980). The soil-structure interaction is based on Wray's (1978) analysis of a plate resting on a semi-infinite elastic continuum. The main procedures are listed as followings,

The Atterberg limits, the percent passing #200 sieve, and percent passing 2 micron sieve are used to estimate the soil properties such as suction compression index, slope of soil water characteristic curve, and Mitchell's diffusion coefficient. The Thornthwaite Moisture Index (TMI) in combination with the Atterberg limits is used to determine the depth of active moisture zone, constant suction at the depth of active moisture zone, and the edge moisture distance. A program called VOLFLO is used to calculate the differential movements for the edge lift case or center lift case, depending on different boundary conditions. The center of the slab is assumed to be at the equilibrium profile. The finite difference method is used to perform a two dimensional steady state suction distribution analysis under the assumption that there is no vertical flow. The calculated differential movement is input into a program called PTISLAB to calculate the maximum moment, shear force and deflection and so forth. PTISLAB uses some regression equations, which are obtained from Wray's finite element analysis of a plate resting on a semi-infinite elastic continuum, to calculate the maximum moment, shear force and so on.

Bulut (2001) performed a three dimensional finite element analysis to simulate slabs with irregular shapes to improve the design of PTI method. The Mindlin plate theory was used and the soil-structure interaction was performed by iteration to calculate the actual supporting area. The movement prediction was from the VOLFLO program. It was also proposed that Gay's program (1994) can be used to calculate the differential movements. Gay's program is a two dimensional transient coupled thermal stress program.

The PTI method actually includes all the factors influence the behavior of slab on expansive soils, weather, soil properties, slab behaviors, and soil-structure interaction. It is the most complete method so far. It is founded on Dr. Lytton's theory for the volume

change of unsaturated soils. It is the best method available. It is also verified by a lot of practical applications and is one of the most extensively used methods.

9.2.4 The PCA Method

The PCA method is based on the computerized solution by Packard and uses influence chart by Pickett and Ray with the concept of equivalent single wheel loading centrally located at the interior of the slab. The slab analyzed has a radius of three times the radius of relative stiffness. The effect of slab discontinuity beyond this limit is not included in the charts. The PCA method is a thickness selection process and it suggests that the slab be strengthened at the joints to account for lack of continuity, which is commonly done by thickening at edges or by use of smooth dowels or tie bars.

9.2.5 The COE Method

The COE method is based on Westergaard's formulae for edge stresses in the concrete slab. This approach calculates the ability to support the load using both the unloaded slab and the loaded slab at the edge or joint in question. The joint transfer coefficient is needed and is assumed to be 0.75, which means the load support is reduced by 25 percent at the joint. The modulus of elasticity of the concrete is taken as 4000ksi, and the Poisson's ratio is assumed to be 0.20. The impact factor is taken as 25 percent and the safety factor is approximately 2. Nomographs are provided and the required variables are modulus of rupture, subgrade modulus, and the load. Loading is handled by placing loads in categories and by using a design index category. The index basically fixes the wheel area, wheel spacing, axle loading and other constants such as the safety factor.

9.2.6 The ACI Method

The ACI method does not deal directly with the slab thickness required for the applied load on the surface of the slab. Rather it deals with concrete mix expansion and shrinkage. ACI 223 specifies the proper amount of reinforcement, in the form of

reinforcing steel, and its location within the depth of the slab for specific values of anticipated expansion and shrinkage.

9.2.7 Discussion

From the review of current design methods, the research needed for foundations on expansive soils can be summarized as following,

- (1). The influence of weather should be included;
- (2). The behaviors of the soils must be included and the research is in the range of unsaturated soils. Two stress state variables must be used, that is, the mechanical stress and matric suction. The volume change of expansive soils is dominated by the matric suction variations or water content variations.
- (3). Soil structure interaction should be considered. The separation between the slab and the ground surface should be considered. If the structure or the load is not symmetric, the friction between the slab and the ground surface should be considered.
- (4). The maximum moment, the maximum shear force and the deflection are needed to design the slab on expansive soils.

Although all these information have been included more or less, there are a lot of drawbacks for current methods as followings:

- (1). Except the PTI method, all the other methods are based on empirical relations and are oversimplified.
- (2). The coupled influence of soil structure interaction has not been considered. For example, most of these methods calculate the soil deformation due to moisture variation, and then a load is applied on the curved soil surface. The consolidation of the soil under the mechanical load has not been considered.
- (3). The soil structure interaction can not represent the actual conditions. All methods use the Winkler's foundation model to simulate the soil structure interaction and the results are not realistic as we discussed previously. The best model has been used is the Bussineq's solution (Bulut, 2001). However, the friction between the slab and soil can not be simulated.

In conclusion, theories for every portion of the problem have been well developed while a complete system for the problem is still not available. In this chapter, a complete system is proposed to solve the problem in one program. Readily available daily weather data such as solar radiation, temperature, relative humidity, wind speed and rainfall will be used as input to estimate the soil-atmosphere boundary conditions. Coupled consolidation theory for saturated-unsaturated soils will be used to simulate the soil deformation and all the material parameters are functions of both mechanical stress and matric suction. Contact elements will be used to simulate the soil-slab interaction and general shell elements will be used to simulate the behavior of the slab and the wall.

It is assumed that the weather conditions and patterns are repeatable and will not change very much in the future and therefore the historic weather data is a reasonably good representative of the weather pattern in the future. It is considered that the current condition is the same as that at the same day in 5 or 10 years ago and can be used initial conditions for the simulation, depending on the requirement on the reliability for the design. If there is requirement for higher safety concerns, a longer period should be adopted. The historic weather data for 5 years or ten years ago will be used as the daily weather data in the future 5 or 10 years respectively. As we discussed before, the house will damage only under extreme severe conditions. As a consequence, a transient simulation for the structure behaviors should be performed and the most dangerous conditions in the simulation period should be found and used for the design purpose. In this way, the problem caused by expansive soils can be solved in a unified system with reasonable consideration. Before discussing the proposed system, we will review some basic theory for needed models firstly.

9.3 Theory of Contact Elements

9.3.1 Basic Theory of Contact (Jointed) Elements

Goodman (1968) proposed a two dimensional 4-node jointed element with zero thickness to simulate the interaction between jointed rocks. Since then, jointed elements have been extensively used in the rock mechanics, but few examples have been seen in

soil structure interaction. The contact elements used in the actual simulation of foundation on expansive soils are much more complicated and are built-in options in the ABAQUS/Standard. Some details will be introduced in the further discussion. This section introduces the basic theory of contact element only (Zhu, 1998).

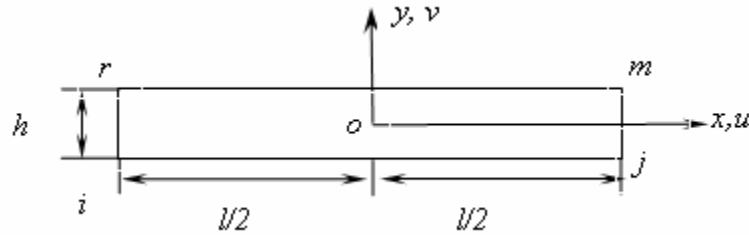


Fig. 9.7. A contact element

A contact element is an element with zero thickness. Fig. 9.7 shows a contact element with a width of h , length of l and thickness of t . There are four nodes in the elements and the origin is at the center of the element. The node forces of the element are:

$$\{F\}^e = [U_i \ V_i \ U_j \ V_j \ U_m \ V_m \ U_r \ V_r]^T \quad (9.5)$$

Nodal displacements are:

$$\{\delta\}^e = [u_i \ v_i \ u_j \ v_j \ u_m \ v_m \ u_r \ v_r]^T \quad (9.6)$$

Assume that the displacements are linearly distributed between the upper and lower sides. So we have,

$$\begin{aligned} u_{upper} &= \frac{1}{2}\left(1 - \frac{2x}{l}\right)u_r + \frac{1}{2}\left(1 + \frac{2x}{l}\right)u_m \\ u_{lower} &= \frac{1}{2}\left(1 - \frac{2x}{l}\right)u_i + \frac{1}{2}\left(1 + \frac{2x}{l}\right)u_j \end{aligned} \quad (9.7)$$

The horizontal differential displacement is,

$$\Delta u = u_{upper} - u_{lower} = \frac{1}{2} \left[(u_r - u_i)\left(1 - \frac{2x}{l}\right) + (u_m - u_j)\left(1 + \frac{2x}{l}\right) \right] \quad (9.8)$$

The vertical differential displacement is,

$$\Delta v = v_{upper} - v_{lower} = \frac{1}{2} \left[(v_r - v_i)\left(1 - \frac{2x}{l}\right) + (v_m - v_j)\left(1 + \frac{2x}{l}\right) \right] \quad (9.9)$$

Assume that the shear stress in the element is proportional to the horizontal displacement, that is,

$$\tau_s = \lambda_s \Delta u + \tau_{s0} \quad (9.10)$$

and the normal stress in the element is proportional to the vertical displacement, that is,

$$\sigma_n = \lambda_n \Delta v + \sigma_{n0} \quad (9.11)$$

where λ_n , λ_s = the normal and tangential stiffness factors, respectively, and τ_{s0} , σ_{n0} = initial shear stress and normal stress respectively.

Assume,

$$\{\Delta \delta\} = \begin{Bmatrix} \Delta u \\ \Delta v \end{Bmatrix}, \quad [\lambda] = \begin{bmatrix} \lambda_s & 0 \\ 0 & \lambda_n \end{bmatrix}, \quad \{\sigma_0\} = \begin{Bmatrix} \tau_{s0} \\ \sigma_{n0} \end{Bmatrix} \quad (9.12)$$

From Eq. 9.10 and 9.11, we have,

$$\{\sigma\} = \begin{Bmatrix} \tau_s \\ \sigma_n \end{Bmatrix} = [\lambda]\{\Delta\delta\} + \{\sigma_0\} \quad (9.13)$$

From Eq. 9.8 and 9.9, we have,

$$\{\Delta\delta\} = \begin{Bmatrix} \Delta u \\ \Delta v \end{Bmatrix} = [M]\{\delta\}^e \quad (9.14)$$

Where

$$[M] = \frac{1}{2} \begin{bmatrix} -z_1 & 0 & -z_2 & 0 & z_2 & 0 & z_1 & 0 \\ 0 & -z_1 & 0 & -z_2 & 0 & z_2 & 0 & z_1 \end{bmatrix} \quad (9.15)$$

$$z_1 = 1 - \frac{2x}{l}, z_2 = 1 + \frac{2x}{l} \quad (9.16)$$

Assume the nodal virtual displacement is $\{\delta^*\}^e$. The virtual differential displacement in the element is,

$$\{\Delta\delta^*\} = [M]\{\delta^*\}^e \quad (9.17)$$

The virtual work done by the unit force at unit length is,

$$t\{\Delta\delta^*\}^T \{\sigma\} = \{\delta^{*e}\}^T t[M]^T ([\lambda]\{\Delta\delta\} + \{\sigma_0\}) \quad (9.18)$$

Integrating along with the unit length, the virtual work done by unit force can be obtained, which should equal to the virtual work done by the unit nodal forces. So we have,

$$\{F\}^e = \left(t \int_{-l/2}^{l/2} [M]^T [\lambda][M] dx \right) \{\Delta\delta\}^e + \int_{-l/2}^{l/2} [M]^T [\sigma_0] dx \quad (9.19)$$

The second term at the right side of Eq. 9.19 is the nodal force derived from initial stress. The nodal load caused by the initial stress can be gotten by changing the sign of the second term. The first term at the right side of Eq. 9.19 is the nodal forces caused by the nodal displacement. From Eq. 9.19 the nodal force of the element is obtained

$$\{F\}^e = [k]^e \{\Delta\delta\}^e \quad (9.20)$$

Where

$$[k]^e = t \int_{-l/2}^{l/2} [M]^T [\lambda][M] dx \quad (9.21)$$

The nodal force caused by initial force is,

$$\{P\}_{\sigma_0}^e = -t \int_{-l/2}^{l/2} [M]^T [\sigma_0] dx \quad (9.22)$$

Substitute Eq. 9.15 into Eq. 9.21, and note that,

$$\int_{-l/2}^{l/2} z_1^2 dx = \frac{4l}{3}, \quad \int_{-l/2}^{l/2} z_1 z_2 dx = \frac{2l}{3}, \quad \int_{-l/2}^{l/2} z_2^2 dx = \frac{4l}{3} \quad (9.23)$$

The element stiffness matrix can be obtained as followings,

$$[k]^e = \frac{lt}{6} \begin{bmatrix} 2\lambda_s & 0 & \lambda_s & 0 & -\lambda_s & 0 & -2\lambda_s & 0 \\ 0 & 2\lambda_n & 0 & \lambda_n & 0 & -\lambda_n & 0 & -2\lambda_n \\ \lambda_s & 0 & 2\lambda_s & 0 & -2\lambda_s & 0 & -\lambda_s & 0 \\ 0 & \lambda_n & 0 & 2\lambda_n & 0 & -2\lambda_n & 0 & -\lambda_n \\ -\lambda_s & 0 & -2\lambda_s & 0 & 2\lambda_s & 0 & \lambda_s & 0 \\ 0 & -\lambda_n & 0 & -2\lambda_n & 0 & 2\lambda_n & 0 & \lambda_n \\ -2\lambda_s & 0 & -\lambda_s & 0 & \lambda_s & 0 & 2\lambda_s & 0 \\ 0 & -2\lambda_n & 0 & -\lambda_n & 0 & \lambda_n & 0 & 2\lambda_n \end{bmatrix} \quad (9.24)$$

According to Eq. 9.13, the stress in the element is uniform along the y direction, while linearly distributed along x direction. Hence, it is reasonable to assume that the initial stress is linearly distributed along the x direction, that is,

$$\begin{aligned} \tau_{s0} &= \frac{1}{2} \left[\left(1 - \frac{2x}{l}\right) \tau_{si0} + \left(1 + \frac{2x}{l}\right) \tau_{sj0} \right] \\ \tau_{n0} &= \frac{1}{2} \left[\left(1 - \frac{2x}{l}\right) \tau_{ni0} + \left(1 + \frac{2x}{l}\right) \tau_{nj0} \right] \end{aligned} \quad (9.25)$$

where τ_{si0} , τ_{ni0} , τ_{sj0} and τ_{nj0} = the initial stress at node i and j .

The nodal load caused by the initial stress is

$$\{P\}_{\sigma_0}^e = -t \int_{-l/2}^{l/2} [M]^T [\sigma_0] dx = -\frac{tl}{6} \begin{bmatrix} -2 & 0 & -1 & 0 \\ 0 & -2 & 0 & -1 \\ -1 & 0 & -2 & -1 \\ 0 & -1 & 0 & -2 \\ 1 & 0 & 2 & 0 \\ 0 & 1 & 0 & 2 \\ 2 & 0 & 1 & 0 \\ 0 & 2 & 0 & 1 \end{bmatrix} \quad (9.26)$$

If the initial stress in the element is uniform, that is, the nodal loads caused by the initial stress is

$$\{P\}_{\sigma_0}^e = \frac{tl}{2} [\tau_{s0} \quad \sigma_{n0} \quad \tau_{s0} \quad \sigma_{n0} \quad -\tau_{s0} \quad -\sigma_{n0} \quad -\tau_{s0} \quad -\sigma_{n0}]^T \quad (9.27)$$

The element stiffness matrix can also be derived in the following way. As shown in Fig. 9.7, the stresses in the element are,

$$\{\varepsilon\} = \begin{Bmatrix} \gamma_s \\ \varepsilon_n \end{Bmatrix} = \begin{Bmatrix} \Delta u/h \\ \Delta v/h \end{Bmatrix} = \{w\}/h \quad (9.28)$$

Substituting Eq. (9.14) into Eq. 9.28, we have,

$$\{\varepsilon\} = [B]\{\delta\}^e \quad (9.29)$$

where

$$[B] = \frac{1}{h}[M] \quad (9.30)$$

The strains in the element are

$$\{\sigma\} = \begin{Bmatrix} \tau_s \\ \sigma_n \end{Bmatrix} = \begin{bmatrix} G & 0 \\ 0 & E \end{bmatrix} \begin{Bmatrix} \gamma_s \\ \varepsilon_n \end{Bmatrix} = [D]\{\varepsilon\} \quad (9.31)$$

Where

$$[D] = \begin{bmatrix} G & 0 \\ 0 & E \end{bmatrix} \quad (9.32)$$

The element stiffness matrix can be calculated as

$$[k]^e = \int [B]^T [D][B] dV \quad (9.33)$$

where $dV = t dx$ $[B] = \frac{1}{h}[M]$.

Hence,

$$[k]^e = t \int_{-1/2}^{1/2} [M]^T [\lambda][M] dx \quad (9.34)$$

Denote that

$$\lambda_n = \frac{E}{h}, \quad \lambda_s = \frac{G}{h} \quad (9.35)$$

Therefore,

$$[D] = e[\lambda] \quad (9.36)$$

Substituting Eq. 9.36 into Eq. 9.33, Eq. 9.21 can be obtained.

9.3.2 Determination of Stiffness Factors

Stiffness factors λ_n and λ_s are needed when using the contact elements to simulate the soil-structure interaction. Obviously these factors should be measured through experiments. In this section, some problems related to the determination of the stiffness factors λ_n and λ_s are discussed.

9.3.2 .1 The Normal Stiffness Factor λ_n

Usually contact element can not sustain normal tensile stress. When the two sides of the contact element are separated, i.e., $h > 0$, the shear stress is also zero. As a consequence, we have $\lambda_n = \lambda_s = 0$ for $h > 0$ or $P = 0$, where P is the contact pressure.

Usually λ_n and λ_s used in actual computation are numbers close to zero to avoid “overflow” when the soil and foundation are separated.

When the normal stresses are compressive stresses, the normal stiffness factor λ_n should be taken as a very large value. From Eq. 9.40, when $h \rightarrow 0$, $\lambda_n \rightarrow \infty$. Usually λ_n is taken as a very large number, for example, 10^9kPa/m^3 .

ABAQUS use the “hard contact” relationship to represent the contact pressure-overclosure relationship described as above, which is also shown in Fig. 9.8. When surfaces are in contact, any contact pressure can be transmitted between them. The surfaces separate if the contact pressure reduces to zero. Separated surfaces come into contact when the clearance between them reduces to zero, that is,

$$\begin{aligned} P &= 0, \text{ for } h < 0 \text{ (open), and} \\ h &= 0, \text{ for } P > 0 \text{ (closed)} \end{aligned} \quad (9.37)$$

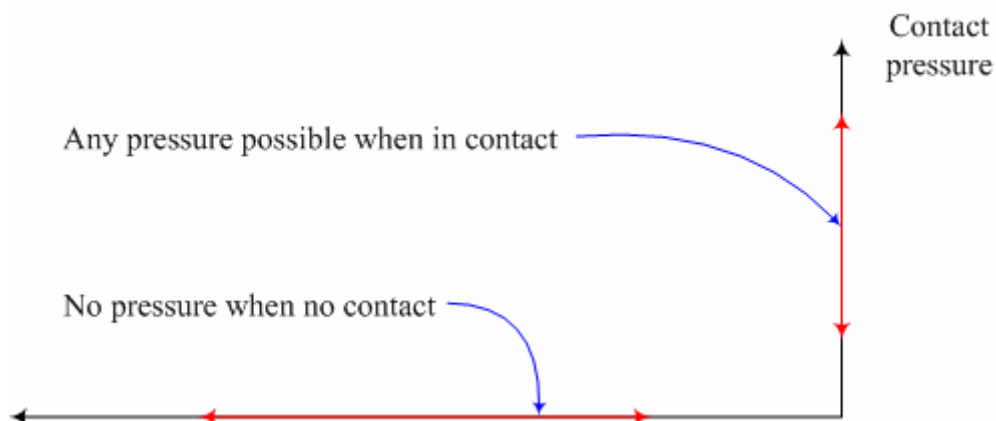


Fig. 9.8. Hard contact (ABAQUS/Standard 2002)

9.3.2.2 The Tangential Stiffness Factor λ_s

The tangential stiffness factor λ_s in Eq. 9.15 should also be measured from laboratory or field experiments. The calculation of actual shear stress between the slab and the soil underneath is a very complicated problem. The shear stress will be dependent on the material properties at the interface. The material for foundation is usually concrete, and the main influence factor is its roughness. The soils underneath can vary a lot and the properties are mainly determined by its current status, for example, mechanical stress and matric suction (or water content). As a consequence, the shear stress can be expressed as following style:

$$\tau_s = f(\sigma - u_a, u_a - u_w, u_a) \quad (9.38)$$

Fredlund and Rahardjo (1993) proposed the shear strength equation for unsaturated soils by using the two stress state variables concept:

$$\tau_{ff} = (\sigma_f - u_a)_f \operatorname{tg} \phi' + (u_a - u_w)_f \operatorname{tg} \phi^b + c' \quad (9.39)$$

where τ_{ff} = shear strength of an unsaturated soil; $(\sigma_f - u_a)_f$ = the normal mechanical stress at failure at the failure plane; $(u_a - u_w)_f$ = the matric suction at failure at the failure plane; ϕ' = internal friction angle associated with the normal mechanical stress $(\sigma_f - u_a)_f$; ϕ^b = rate of increase in shear strength with the matric suction $(u_a - u_w)_f$; c' = effective cohesion coefficient.

Eq. 9.39 is questionable because the two stress state variables concept is based on the results of the null tests (Fredlund 1973). However, the null tests only proved that the volume changes of the soil structure and water volume are functions of $\sigma - u_a$ and

$u_a - u_w$ only. The conclusion that the shear strength of unsaturated soils can be expressed as Eq. 9.39 can not be made.

When the influence of pore air pressure for the shear strength is negligible and the variations in $\sigma - u_a$ and $u_a - u_w$ are small, Eq. 9.38 can be expressed as

$$\tau_s = f(\sigma, -u_w) \quad (9.40)$$

The empirical method can be used to Eq. 9.40, which gives,

$$\tau_s = A\sigma + Bu_w + C \quad (9.41)$$

where A, B and C =material parameters for small variations in σ and $-u_w$.

Eq. 9.41 can be considered as a special case of Eq. 9.39 when the pore air pressure is zero or constant. However, it should be kept in mind that their theoretic backgrounds are different. For large variations in $\sigma - u_a$ and $u_a - u_w$, ϕ' , ϕ^b and c' in Eq. 9.39 are expected to be function of $\sigma - u_a$ and $u_a - u_w$, too.

Another issue should be kept in mind is that the shear strength of unsaturated soils are not necessarily the shear strength at the soil-slab interface. Specific experiments different from the measuring of the shear strength of unsaturated soils are needed to investigated the shear strength at the soil-slab interface. A possible method is to use direct shear apparatus to measure it. The upper side is the concrete material used in real conditions and the lower side is the real soils for specific project. The concrete should be in good contact with the soil. A procedure similar to the direct shear test can be performed to measure the relationship between the horizontal movements, shear strength and applied normal load.

Eq. 9.40 indicates that λ_s is a function of mechanical stress and matric suction. As a consequence, both mechanical stress and matric suction should be controlled in the test. However, it will be very difficult to control the matric suction in the direct shear test

because it is varying with the applied load. As we discussed in Chapter VI, there is matric suction variation at the instant of load application. A better way to perform the test seems to control the water content of the soil in different tests. Under elastic assumption, if the applied mechanical stress and water content are known, the corresponding matric suction can be obtained from the water content surface of the soil by using the assumption that the water content is constant during the direct shear test. In this way, Eq. 9.40 and λ_s in Eq. 9.10 can be obtained. The obtained tangential stiffness factor λ_s can be handled by the user subroutine UFRIC in ABAQUS. In this dissertation, no such test data are available and a default Coulomb friction model is used.

In the basic form of the Coulomb friction model, two contacting surfaces can carry shear stresses up to a certain magnitude across their interface before they start sliding relative to one another; this state is known as sticking. The Coulomb friction model defines this critical shear stress, τ_{critic} , at which sliding of the surfaces starts as a fraction of the contact pressure, P , between the surfaces ($\tau_{critic} = \mu P$). The stick/slip calculations determine when a point transitions from sticking to slipping or from slipping to sticking. The fraction, μ , is known as the coefficient of friction.

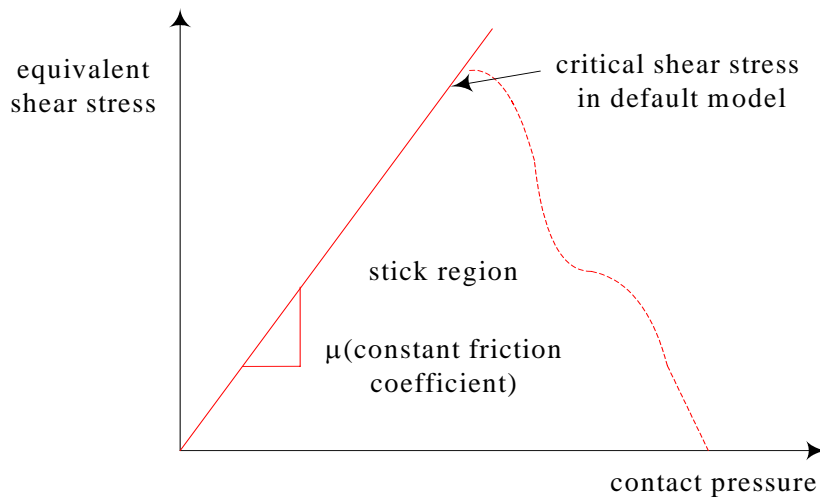


Fig. 9.9. Slip regions for the basic Coulomb friction model (ABAQUS/Standard 2002)

The basic friction model assumes that μ is the same in all directions (isotropic friction). For a three-dimensional simulation there are two orthogonal components of shear stress, τ_1 and τ_2 , along the interface between the two bodies. These components act in the slip directions for the contact surfaces or contact elements.

ABAQUS combines the two shear stress components into an “equivalent shear stress,” $\bar{\tau}$, for the stick/slip calculations, where $\bar{\tau} = \sqrt{\tau_1^2 + \tau_2^2}$. In addition, ABAQUS combines the two slip velocity components into an equivalent slip rate,

$$\dot{\gamma}_{eq} = \sqrt{\left(\dot{\gamma}_1\right)^2 + \left(\dot{\gamma}_2\right)^2}.$$

The stick/slip calculations define a surface (see Fig. 9.9 for a two-dimensional representation) in the contact pressure–shear stress space along which a point transitions from sticking to slipping. In the following examples, the default model is used, in which the friction coefficient is defined as a function of the equivalent slip rate and contact pressure. The static and kinetic friction coefficients are specified directly in the main program. ABAQUS can handle more complicated tangential behaviors at the soil-structure interface as discussed above. More details can be found in the ABAQUS Analysis User's Manual.

9.4 Theory of General Shell Elements

The thicknesses of slabs and walls of a residential building are significantly smaller than the other dimensions. When three dimensional continuum elements are used, the stiffness matrix of the slab and walls are too stiff to obtain accurate simulation results and singularity may arise. As a consequence, the slabs and walls are generally considered as plates or shells and the plate or shell theory can be used for the simulation of slab and wall behaviors. The general shell elements are proposed to simulate the behaviors of slabs and walls. They provide robust and accurate solutions to both thick and thin plate and shell. The general shell elements have five degrees of freedom and can be used to simulate plate bending with shear deformation and plate stretching. When the principle of virtual work is applied, only the strain energy caused by σ_z is neglected.

Therefore it is expected to be more accurate. The Mid-surface of the shell can be arbitrary. Due to their various advantages, it is recommended to use the shell element to simulate the behavior of the slab and walls of the residential building. The basic theory for the general shell elements are introduced simply as followings (Wang and Shao, 1999).

9.4.1 Determination of the Element Shape

Fig. 9.10 shows a typical thick shell element. If the general coordinates of every pair of nodes i_{top} and i_{bottom} are given, the algebraic shape of the element can be determined approximately. Denote that ξ and η are the curved coordinates at the center surface of the shell, ζ is the coordinate in the thickness direction, and $-1 \leq \xi, \eta, \zeta \leq 1$. The generic coordinates of an arbitrary point in the shell element can therefore be expressed as,

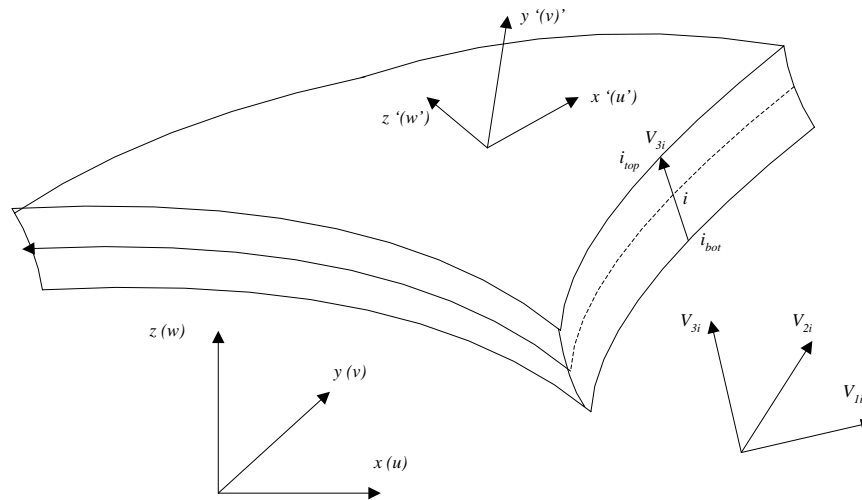


Fig. 9.10. A general shell element

$$\begin{Bmatrix} x \\ y \\ z \end{Bmatrix} = \sum_{i=1}^n N_i(\xi, \eta) \begin{Bmatrix} x_i \\ y_i \\ z_i \end{Bmatrix}_{center} + \sum_{i=1}^n N_i(\xi, \eta) \frac{\zeta}{2} \begin{Bmatrix} \Delta x_i \\ \Delta y_i \\ \Delta z_i \end{Bmatrix} \quad (9.42)$$

where

$$\begin{Bmatrix} x_i \\ y_i \\ z_i \end{Bmatrix}_{center} = \frac{1}{2} \left(\begin{Bmatrix} x_i \\ y_i \\ z_i \end{Bmatrix}_{lower} + \begin{Bmatrix} x_i \\ y_i \\ z_i \end{Bmatrix}_{upper} \right) \quad (9.43)$$

is the generic Cartesian coordinates of the nodes at the center surface.

$$v_{3i} = \begin{Bmatrix} v_{3ix} \\ v_{3iy} \\ v_{3iz} \end{Bmatrix} = \begin{Bmatrix} x_i \\ y_i \\ z_i \end{Bmatrix}_{top} - \begin{Bmatrix} x_i \\ y_i \\ z_i \end{Bmatrix}_{bottom} = \begin{Bmatrix} \Delta x_i \\ \Delta y_i \\ \Delta z_i \end{Bmatrix} \quad (9.44)$$

is the vector from node i_{top} to node i_{bottom} . v_{3i} is taken as the normal direction at the center surface, and $|V_{3i}|$ is therefore the thickness at the point i , i.e.

$$t_i = |V_{3i}| = \sqrt{\Delta x_i^2 + \Delta y_i^2 + \Delta z_i^2} \quad (9.45)$$

The direction cosines l_{3i} , m_{3i} and n_{3i} of the unit vector v_{3i} for the vector V_{3i} are as followings:

$$v_{3i} = \begin{Bmatrix} l_{3i} \\ m_{3i} \\ n_{3i} \end{Bmatrix} = \frac{1}{t_i} \begin{Bmatrix} \Delta x_i \\ \Delta y_i \\ \Delta z_i \end{Bmatrix} \quad (9.46)$$

9.4.2 Displacement Functions

According to the basic assumption of the general shell, i.e. the mid surface normals remain straight line after deformation, the displacement u , v , and w of an arbitrary point in the shell element can be determined by three translations u_i , v_i , and w_i along x , y and z

direction as well as two small rotations α_i and β_i about the vector V_{3i} . Generic displacements in terms of nodal displacements are:

$$\begin{Bmatrix} u \\ v \\ w \end{Bmatrix} = \sum_{i=1}^n N_i(\xi, \eta) \begin{Bmatrix} u_i \\ v_i \\ w_i \end{Bmatrix}_{center} + \sum_{i=1}^n N_i(\xi, \eta) \zeta \frac{t_i}{2} \begin{bmatrix} l_{1i} & -l_{2i} \\ m_{1i} & -m_{2i} \\ n_{1i} & -n_{2i} \end{bmatrix} \begin{Bmatrix} \alpha_i \\ \beta_i \end{Bmatrix} \quad (9.47)$$

where l_{1i}, m_{1i}, n_{1i} and l_{2i}, m_{2i}, n_{2i} are the direction cosines of V_{1i} and V_{2i} , respectively.

$$V_{1i} = \begin{Bmatrix} l_{1i} \\ m_{1i} \\ n_{1i} \end{Bmatrix}, \quad V_{2i} = \begin{Bmatrix} l_{2i} \\ m_{2i} \\ n_{2i} \end{Bmatrix} \quad (9.48)$$

to make the discussion simpler, the subscription ‘‘center’’ is omitted and Eq. (9.47) can be rewritten as:

$$\begin{Bmatrix} u \\ v \\ w \end{Bmatrix} = [N_1 N_2 \dots N_n] \begin{Bmatrix} a_1 \\ a_2 \\ \vdots \\ a_n \end{Bmatrix} \quad (9.49)$$

where $a_i = [u_i \ v_i \ w_i \ \alpha_i \ \beta_i]^T$ ($i=1, 2, \dots, n$)

$$N_i = \begin{bmatrix} N_i & 0 & 0 & N_i \zeta \frac{t_i}{2} l_{1i} & -N_i \zeta \frac{t_i}{2} l_{2i} \\ 0 & N_i & 0 & N_i \zeta \frac{t_i}{2} m_{1i} & -N_i \zeta \frac{t_i}{2} m_{2i} \\ 0 & 0 & N_i & N_i \zeta \frac{t_i}{2} n_{1i} & -N_i \zeta \frac{t_i}{2} n_{2i} \end{bmatrix} \quad (9.50)$$

Unit vectors can be defined as followings:

$$v_{1i} = \frac{i \times V_{3i}}{|i \times V_{3i}|}, \quad v_{2i} = \frac{V_{3i} \times v_{1i}}{|V_{3i} \times v_{1i}|} \quad (9.51)$$

where i is a unit vector along x direction.

If V_{3i} is parallel to i , i in above equation should substituted by the unit vector j along y direction.

9.4.3 Determinations of Stress and Strain

To take use of the assumption that the mid surface normals remain straight line after deformation, the stress should be computed in a local coordinate in which the axis z' is the normal direction. Firstly two tangential vectors can be obtained from the surface on which $\xi = \text{constant}$ such as:

$$\begin{aligned} \frac{\partial r}{\partial \xi} &= \frac{\partial x}{\partial \xi} i + \frac{\partial y}{\partial \xi} j + \frac{\partial z}{\partial \xi} k \\ \frac{\partial r}{\partial \eta} &= \frac{\partial x}{\partial \eta} i + \frac{\partial y}{\partial \eta} j + \frac{\partial z}{\partial \eta} k \end{aligned} \quad (9.52)$$

where i, j, k = the unit vectors in x, y , and z direction, respectively.

The vector in the normal direction can be obtained from the above two vectors,

$$V_3 = \frac{\partial r}{\partial \xi} \times \frac{\partial r}{\partial \eta} = \begin{vmatrix} i & j & k \\ \frac{\partial x}{\partial \xi} & \frac{\partial y}{\partial \xi} & \frac{\partial z}{\partial \xi} \\ \frac{\partial x}{\partial \eta} & \frac{\partial y}{\partial \eta} & \frac{\partial z}{\partial \eta} \end{vmatrix} \quad (9.53)$$

or,

$$V_3 = \begin{vmatrix} \frac{\partial x}{\partial \xi} \\ \frac{\partial y}{\partial \xi} \\ \frac{\partial z}{\partial \xi} \end{vmatrix} \times \begin{vmatrix} \frac{\partial x}{\partial \eta} \\ \frac{\partial y}{\partial \eta} \\ \frac{\partial z}{\partial \eta} \end{vmatrix} = \begin{vmatrix} \frac{\partial y}{\partial \xi} \frac{\partial z}{\partial \eta} - \frac{\partial y}{\partial \eta} \frac{\partial z}{\partial \xi} \\ \frac{\partial x}{\partial \eta} \frac{\partial z}{\partial \xi} - \frac{\partial x}{\partial \xi} \frac{\partial z}{\partial \eta} \\ \frac{\partial x}{\partial \xi} \frac{\partial y}{\partial \eta} - \frac{\partial x}{\partial \eta} \frac{\partial y}{\partial \xi} \end{vmatrix} \quad (9.54)$$

After V_3 is determined, the unit vectors in x' and y' directions can be determined in the similar way,

$$v_1 = \frac{i \times V_3}{|i \times V_3|}, \quad v_2 = \frac{V_3 \times v_1}{|V_3 \times v_1|} \quad (9.55)$$

and

$$v_3 = \frac{V_3}{|V_3|} \quad (9.56)$$

Therefore, the transformation between the global and local coordinate can be obtained,

$$X = \theta X' \quad X' = \theta^T X \quad (9.57)$$

in which,

$$X = [x \ y \ z]^T, \quad X' = [x' \ y' \ z']^T$$

$$\theta = [v_1 \ v_2 \ v_3] = \begin{bmatrix} l_1 & l_2 & l_3 \\ m_1 & m_2 & m_3 \\ n_1 & n_2 & n_3 \end{bmatrix} \quad (9.58)$$

Denote that u' , v' , w' are the displacements in the x' , y' and z' directions, respectively. According to the shell theory, $\sigma_z = 0$. As a consequence, the strains related to the computation of energy due to computation are:

$$\varepsilon' = \begin{Bmatrix} \varepsilon_{x'} \\ \varepsilon_{y'} \\ \gamma_{x'y'} \\ \gamma_{y'z'} \\ \gamma_{z'x'} \end{Bmatrix} = \begin{Bmatrix} \frac{\partial u'}{\partial x'} \\ \frac{\partial v'}{\partial y} \\ \frac{\partial u'}{\partial y'} + \frac{\partial v'}{\partial x'} \\ \frac{\partial v'}{\partial z'} + \frac{\partial w'}{\partial y'} \\ \frac{\partial u'}{\partial z'} + \frac{\partial w'}{\partial x'} \end{Bmatrix} \quad (9.59)$$

Two coordinate transformations are needed to express ε' in terms of nodal parameters a_i . Firstly, the derivatives of the displacements in the global coordinate are transformed into those in the local coordinate, and their relationships are:

$$\begin{bmatrix} \frac{\partial u'}{\partial x'} & \frac{\partial v'}{\partial x'} & \frac{\partial w'}{\partial x'} \\ \frac{\partial u'}{\partial y'} & \frac{\partial v'}{\partial y} & \frac{\partial w'}{\partial y'} \\ \frac{\partial u'}{\partial z'} & \frac{\partial v'}{\partial z'} & \frac{\partial w'}{\partial z'} \end{bmatrix} = \theta^T \begin{bmatrix} \frac{\partial u}{\partial x} & \frac{\partial v}{\partial x} & \frac{\partial w}{\partial x} \\ \frac{\partial u}{\partial y} & \frac{\partial v}{\partial y} & \frac{\partial w}{\partial y} \\ \frac{\partial u}{\partial z} & \frac{\partial v}{\partial z} & \frac{\partial w}{\partial z} \end{bmatrix} \theta \quad (9.60)$$

Secondly, the derivatives of u , v , and w with respect to x , y , and z are transformed into those with respect to the natural coordinates ξ, η, ζ , and their relationships are:

$$\begin{bmatrix} \frac{\partial u}{\partial x} & \frac{\partial v}{\partial x} & \frac{\partial w}{\partial x} \\ \frac{\partial u}{\partial y} & \frac{\partial v}{\partial y} & \frac{\partial w}{\partial y} \\ \frac{\partial u}{\partial z} & \frac{\partial v}{\partial z} & \frac{\partial w}{\partial z} \end{bmatrix} = J^{-1} \begin{bmatrix} \frac{\partial u}{\partial \xi} & \frac{\partial v}{\partial \xi} & \frac{\partial w}{\partial \xi} \\ \frac{\partial u}{\partial \eta} & \frac{\partial v}{\partial \eta} & \frac{\partial w}{\partial \eta} \\ \frac{\partial u}{\partial \zeta} & \frac{\partial v}{\partial \zeta} & \frac{\partial w}{\partial \zeta} \end{bmatrix} \quad (9.61)$$

in which,

$$J = \begin{bmatrix} \frac{\partial x}{\partial \xi} & \frac{\partial y}{\partial \xi} & \frac{\partial z}{\partial \xi} \\ \frac{\partial x}{\partial \eta} & \frac{\partial y}{\partial \eta} & \frac{\partial z}{\partial \eta} \\ \frac{\partial x}{\partial \zeta} & \frac{\partial y}{\partial \zeta} & \frac{\partial z}{\partial \zeta} \end{bmatrix} \quad (9.62)$$

Substituting Eq. (9.42) into (9.62), and taking use of Eq. (9.49), (9.50), (9.60) , (9.61) , etc, ε' can be expressed as,

$$\varepsilon' = [B'_1 B'_2 \dots B'_n] \begin{Bmatrix} a_1 \\ a_1 \\ \vdots \\ a_n \end{Bmatrix} \quad (9.63)$$

The stresses in the local coordinate can be expressed as:

$$\sigma' = [\sigma_{x'} \ \sigma_{y'} \ \tau_{x'y'} \ \tau_{y'z'} \ \tau_{z'x'}]^T = D\varepsilon' \quad (9.64)$$

in which,

$$D = \frac{E}{1-\eta^2} \begin{bmatrix} 1 & \eta & 0 & 0 & 0 \\ & 1 & 0 & 0 & 0 \\ & & \frac{1-\eta}{2} & 0 & 0 \\ & & & \frac{1-\eta}{2k} & 0 \\ & & & & \frac{1-\eta}{2k} \end{bmatrix} \quad (9.65)$$

where E , η are the Young's modulus and Poisson's ratio, respectively; $k=1.2$, which is a modification factor by considering that the shear stresses distribute non-uniformly along the thickness direction.

The stiffness matrix can be calculated by replacing the $B^T DB$ in the global coordinate with the $B^T DB$ in the local coordinate.

$$K' = \int_{-1}^1 \int_{-1}^1 \int_{-1}^1 B'^T DB' |J| d\xi d\eta d\zeta \quad (9.66)$$

where B' and D are the strain and elastic matrix in the local coordinate, respectively.

After the displacements are obtained, Eq. (9.63) and (9.64) can be used to calculate ε' and σ' . The stresses in the global coordinate can be calculated as:

$$\begin{bmatrix} \sigma_x & \tau_{xy} & \tau_{xz} \\ \tau_{xy} & \sigma_y & \tau_{yz} \\ \tau_{xz} & \tau_{yz} & \sigma_z \end{bmatrix} = \theta \begin{bmatrix} \sigma_{x'} & \tau_{x'y'} & \tau_{x'z'} \\ \tau_{x'y'} & \sigma_{y'} & \tau_{y'z'} \\ \tau_{x'z'} & \tau_{y'z'} & \sigma_{z'} \end{bmatrix} \theta^T \quad (9.67)$$

9.5 Pseudo Moisture Variation Simulations

Numerical simulations of the behaviors of residential buildings on expansive soils have been investigated in the past by a lot of researchers. The main drawback of the past

investigations lies in that nearly all the investigations such as the volume change of expansive soils, simulation of soil-structure interaction and the behaviors of structures were performed separately. However, in reality the building, foundation and ground soils are working in a unified system. Foundations are the supporting link between the building and the ground. They transmit the loads from the walls, floors and roof into the ground. At the same time they transfer any ground movement back to the structure, possibly causing distortions and damages. On the one hand, any variations in the building loads will cause the stress variations at the soil-structure interface, which in turn, will cause the mechanical stress and matric suction variations in the soil, and finally influence the evapotranspiration process. On the other hand, any variations in the evapotranspiration process will finally lead to the stress redistributions in the building. Under these conditions, any attempt to investigate the behaviors of residential building on expansive soils by studying the influencing factors separately, which is meaningful and brings huge simplifications to research, will distort the reality in some degree and lead to misleading results. The best way therefore is to investigate the problem in a unified system as it is. In this dissertation, it is proposed that all the numerical simulations should be accomplished in one whole program, i.e. the simulation of the evapotranspiration, volume change of the soil, soil-structure interaction and behaviors of the building should be performed in one whole program and their interactions should be considered at the same time. In this way, the results obtained are the most closest to real situations and useful for guiding actual foundation designs.

For the simulation of the volume changes of expansive soils, the coupled hydro-mechanical stress analysis is used. The coupled thermal stress analysis can be used for the analysis due to their similarities. The FAO 56 Penman-Montieth method can be used to estimate the water loss at the soil-atmosphere interface. For the simulation of the foundations and the walls, the shell elements are proposed due their thicknesses are much smaller than the other two dimensions. Only the mechanical stress distributions and variations in the shell are of interest. The contact elements are used to simulate the load transfer from the foundation to the soils underneath. No water is allowed to flow

through the contact elements to the concrete foundations. The upper side of the contact element is the bottom surface of the foundation and its lower side is the ground soil. Correspondingly, a new problem emerges when applying the proposed unified system for the simulations of residential buildings on expansive soils. There is an inconsistency between the simulation of the soils and that of the foundations and walls: for the soil the coupled hydro-mechanical analysis is required while a single mechanical stress analysis is required for the foundations and walls. This inconsistency will cause difficulties in programming at the soil-structure interface. Fig. 9.11 shows the possible problem.

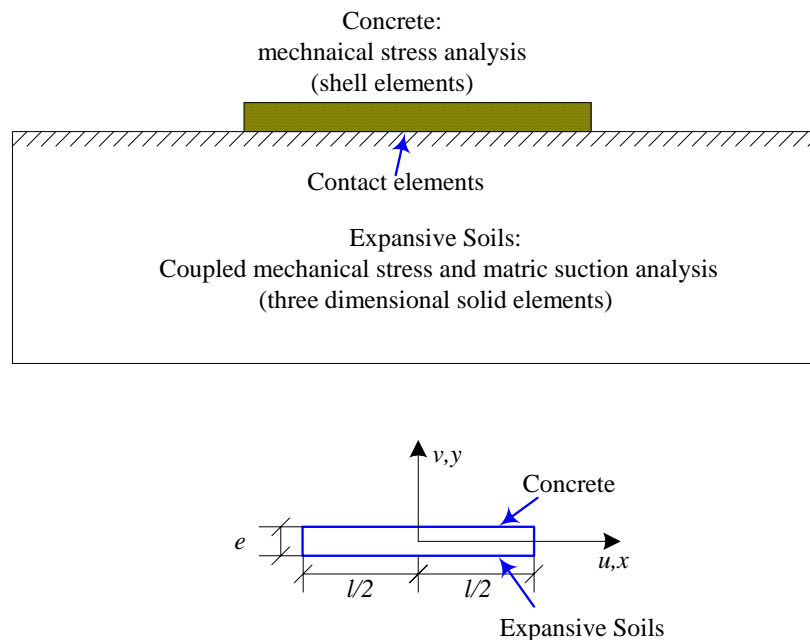


Fig. 9.11. Soil-structure interactions and contact elements

A technique called pseudo moisture variation simulation is proposed to solve this dilemma. The idea is to perform a coupled hydro-mechanical stress analysis for the soil-structure interaction, foundations and walls even though there is no water flow. In this way, the simulation for residential buildings on expansive soils can be integrated into a single coupled hydro-mechanical stress problem. A coupled thermal stress analysis can be performed for the whole system by applying the thermodynamic analogue to the

consolidation process. It is applicable because mathematically no water flow is equivalent of zero water flow. In this section, ABAQUS will be used to show the application of the proposed pseudo moisture variation simulation.

9.5.1 Simulation of the Volume Change of the Ground Soils

For the simulation of the volume change of the ground soil, the coupled hydro-mechanical stress analysis will be performed as it is in the real condition. In ABAQUS, the coupled thermal stress analysis can be used to perform the coupled hydro-mechanical stress analysis by following the proposed modifications in Chapter VI and VIII.

9.5.2 Simulation of the Soil-Structure Interaction

The coupled hydro-mechanical stress contact elements are used for the simulation of the soil structure interaction. The mechanical stress analysis part will be the same as that in the real conditions. For the water flow part, the condition that there is no water flow can be realized by assigning proper conduction properties for the contact elements. Water flow is represented by heat flow and pore water pressure (matric suction) is represented by temperature in ABAQUS. In ABAQUS, Heat conduction across the interface is assumed to be defined by

$$q = k(T_A - T_B) \quad (9.68)$$

where q = the heat flux per unit area crossing the interface from point A on one surface to point B on the other; T_A and T_B =the temperatures of the points on the surfaces; and k = the gap conductance.

In reality, there is no (or very small) water flow from the soil to the concrete foundation. As a consequence, the zero water flow condition can be realized easily by assigning a zero gap conductance to the contact elements. A very small number close to zero is used instead in actual simulations in order to avoid any possible overflow problem.

9.5.3 Simulation of the Foundations and Walls

The coupled hydro-mechanical stress shell elements are used for the simulation of the foundations and walls of residential buildings. The mechanical stress analysis part will be the same as that in the real conditions. For the water flow part, some conditions must be satisfied to assure that the simulation results can reflect the real mechanical behaviors of the foundations and walls of residential buildings. In other words, the pseudo moisture variation simulation should not influence the actual mechanical behavior of the foundation and walls. The moisture variation is represented by thermal energy variation in ABAQUS, it is therefore required that there are no thermal stress generation in the corresponding coupled thermal stress analysis for the foundations and walls. Thermal stresses are usually resulted from the restriction of thermal strains. Therefore, two methods can be used to avoid the thermal stress generation: one is to make sure that there is no thermal strain and the other is to make sure that there is no restriction for the thermal strains. Obviously the second method is not easy to be satisfied because any change in the mechanical restrictions will also results in changes in mechanical stress analysis. Therefore, the first method is proposed. From Chapter VI, thermal strain is calculated as,

$$\begin{aligned} (d\varepsilon_x)_T &= (d\varepsilon_y)_T = (d\varepsilon_z)_T = \alpha d(-T_x) \\ &= \alpha d(-T_y) = \alpha d(-T_z) = \alpha d(-T) \end{aligned} \quad (6.3)$$

To have a zero thermal strain, the easiest way is to assign a zero coefficient of expansion α , i.e. $\alpha = 0$. Usually a very small number close to zero is used instead in actual simulation to avoid any possible overflow problem.

Another way to achieve zero thermal strain is to make the temperature variation $d(-T)$ is equal to zero. It can be realized by assign a zero heat supply or generation to the material and a uniform distributed initial thermal conditions.

9.6 Two Examples

Two examples are used to illustrate the proposed system. One is to illustrate the edge lift case, and the other is used to illustrate the center lift case.

9.6.1 Description of the Problem

Fig. 9.12a shows the slab used for the simulation, which consists of three $8\text{ m} \times 8\text{ m} \times 0.4\text{ m}$ slabs and numbered as I, II and III, respectively. Fig. 9.12b shows the walls used in the simulation, which have thicknesses and height of 0.1 m and 2 m , respectively. To make the further explanation a little easier, the walls are numbered from 1 to 10. Fig. 9.12c shows a structure formed by the slabs and walls as shown in Fig. 9.12a and 9.12b, which representing a residential building used for the examples. More complicated structure can be used such as a building with roof, doors and windows. However, the structure as shown in Fig. 9.12c is used to make it easier to present the simulation results. Fig. 9.12e shows the soil domain used for the simulation. The $48\text{ m} \times 48\text{ m} \times 6\text{ m}$ of ground soil includes the same two soil layers as those at the site at Arlington, Texas: 1st layer is the dark gray silty clay with a thickness of 1.8 m within which there is a grass root zone with a thickness of 0.47 m at the ground surface, and 2nd layer is the brown silty clay with a thickness of 4.2 m . A right-handed, rectangular Cartesian system is used in the simulations. The origin O of the coordinate is taken at the bottom center of the ground soil and the building is built on the center of the ground soil. A tree with a $6\text{ m} \times 6\text{ m} \times 1.5\text{ m}$ tree root zone as shown in Fig. 9.12d is planted close to the building. The locations of the tree are different. In one case, the tree is planted at the corner formed by the wall 6 and wall 8, which is used to illustrate the edge lift condition. In another case, the tree is planted at the corner formed by the wall 3 and wall 6, which is used to illustrate the center lift condition.

9.6.2 Material Properties

9.6.2.1 Soil Properties

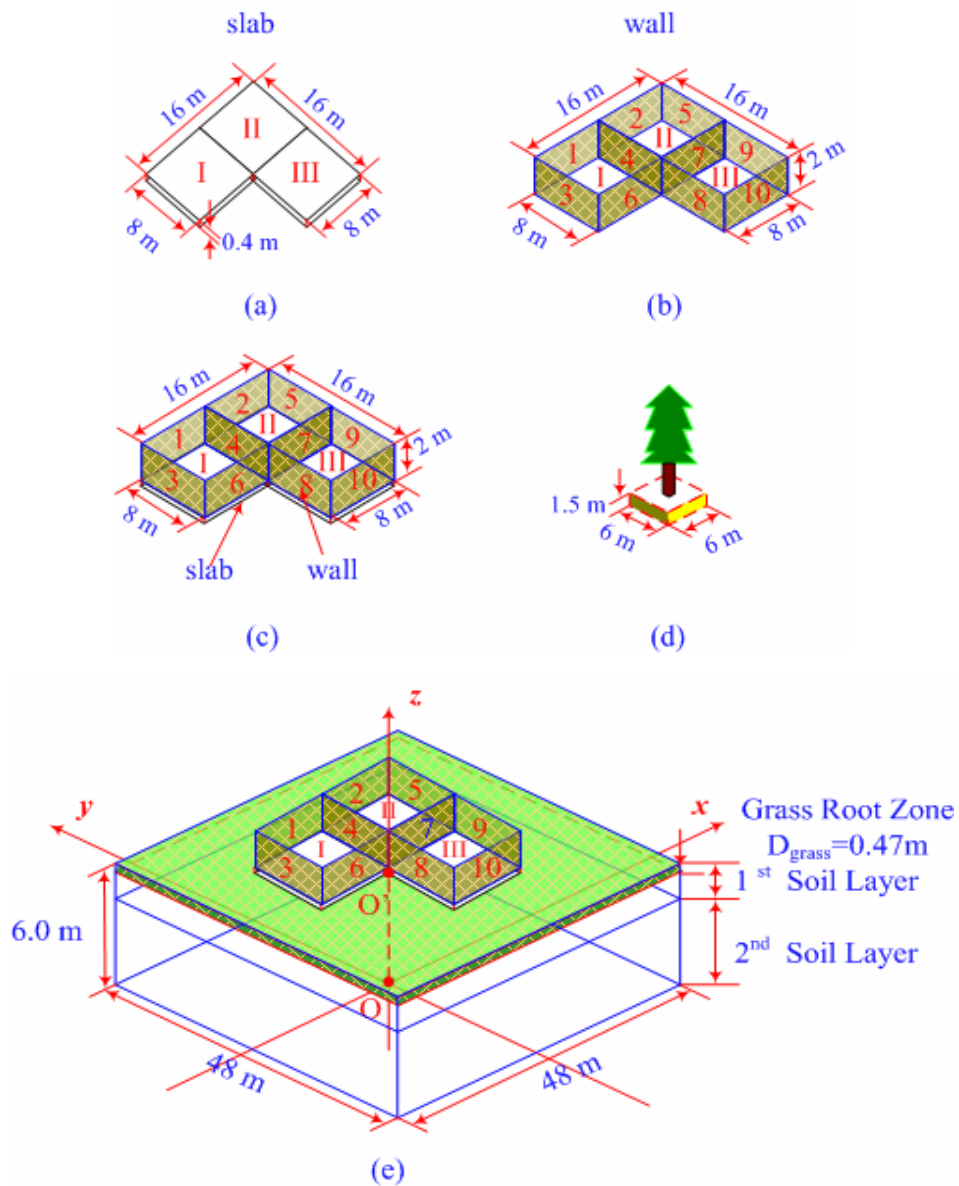


Fig. 9.12. Simulation domain. (a) slab; (b) walls; (c) house formed by the slabs and walls; (d) tree root zone; (e) soil domain and the building

The soils in the examples are assumed to have the same properties as those at the site at Arlington, Texas. The first soil layer is the dark gray silty clay with a thickness of 1.8 m within which there is a grass root zone with a thickness of 0.47 m. The soil properties are

represented by the soil SW145 in the Appendix B.1.1. The second soil layer is the brown silty clay with a thickness of 4.2m. The soil properties are represented by the soil SW189 in the Appendix B.1.2.

9.6.2.2 Material Properties for Slabs and Walls

Both the slabs and walls are assumed to be made of concrete. The mass density for ordinary concrete is $2.4 \times 10^3 \text{ kg/m}^3$ (the input is 2.4 to be consistent with other units, which is discussed in Chapter VI). The Young's Modulus of the concrete footing is assumed as $E=4 \times 10^6 \text{ kPa}$. Considering that the strain in the slabs and the walls are small while the rotation is large, the section Poisson's ratio is defined as zero $\mu=0.0$. The shell thickness remains constant and the shell elements are suited for small-strain, large-rotation analysis.

The material thermal properties are also needed for the pseudo moisture variation simulation. As we discussed previously, the pseudo moisture simulation must not cause any stress or moment variation in the slabs and the walls. To realize this, the coefficients of expansion of the slabs and walls are close to zero. In the program, they are assumed to be $1 \times 10^{-30} \text{ kPa}^{-1}$ (which is corresponding to a thermal coefficient of expansion 10^{-30} K^{-1}). The specific water capacity of the concrete is assigned to be 10^{-5} kPa^{-1} (which corresponding to a specific heat capacity of $10^{-5} \text{ J/kg} \cdot \text{K}$), which means any water content change will cause very small pore water pressure variation. The coefficient permeability of the concrete is assigned to be 10^{-8} m/s , which corresponds to a heat conductivity of $10^{-9} \text{ J/(s} \cdot \text{m} \cdot \text{K)}$ (or $\text{kg/s} \cdot \text{m} \cdot \text{kPa}$) in the coupled thermal stress problem.

9.6.3 Material Properties at the Soil-Slab Interface

9.6.3.1 Soil-Structure Interaction Simulation in ABAQUS/Standard

There are built-in options in ABAQUS/Standard for the contact elements. Two methods are used for modeling contact interactions: using surfaces or using contact elements and the former one is used in this dissertation. Both of them are based on the contact element

theory described above. The small-sliding contact in ABAQUS/Standard is used to simulate the soil-structure interaction between the soil and the slab. With this formulation the contacting surfaces can undergo only relatively small sliding relative to each other, but arbitrary rotation of the bodies is permitted.

ABAQUS/Standard defines the contact conditions between two bodies using a strict “master-slave” algorithm. The slave nodes are constrained not to penetrate into the master surface. However, the nodes of the master surface can, in principle, penetrate into the slave surface and the contact direction is always normal to the master surface. Generally, the master surface should be chosen as the surface of the stiffer body. As a result, the bottom surfaces of the concrete slabs are chosen as the master surface and the ground soil surface is chosen as slave surface because the slabs are stiffer than the soil.

If during iteration a slave node is found to have penetrated the master surface by more than a specific distance, ABAQUS/Standard abandons the increment and tries again with a smaller increment size. This distance is known as H_{crit} . In this simulation, the deflection of the slab may be significant. As a result, a bigger H_{crit} is used to avoid the possible difficulties in the simulation of the slab-soil interaction. In both simulations, H_{crit} is taken as 1.1.

To make the simulation of the soil-slab interaction more accurate, the two surfaces at the soil-slab interface that form a contact pair can be adjusted in ABAQUS/Standard so that they are precisely in contact at the start of the simulation. ABAQUS/Standard moves any slave nodes penetrating the master surface in the initial configuration so that they just contact the master surface by using the ADJUST parameter. The condition that ADJUST=0.0 is used, which causes ABAQUS/Standard to adjust only those slave nodes that are penetrating the master surface.

9.6.3.2 Normal and Tangential Behaviors at the Soil-Slab Interface

The material properties at the slab-soil interface are needed for the simulation. The “hard” contact relationship is used to simulate the normal behavior at the soil-slab interface.

For the tangential behaviors, both conditions when the soil and the slab either slip relatively or stick together should be considered. The friction coefficient when there is no relative slip is different from that when there is relative slip. The former is typically referred to as the “static” friction coefficient, and the latter is referred to as the “kinetic” friction coefficient. Typically, the static friction coefficient is higher than the kinetic friction coefficient. In the default model in ABAQUS, the static friction coefficient corresponds to the value given at zero slip rate, and the kinetic friction coefficient corresponds to the value given at the highest slip rate. The transition between static and kinetic friction is defined by the values given at intermediate slip rates. In this model it is assumed that the friction coefficient decays exponentially from the static value to the kinetic value according to the formula:

$$\mu = \mu_k - (\mu_s - \mu_k) e^{-d_c \dot{\gamma}_{eq}} = 0.1 + 0.4 e^{-4 \dot{\gamma}_{eq}} \quad (9.69)$$

where μ_k = the kinetic friction coefficient, is taken as 0.1 in the following examples; μ_s = the static friction coefficient, is taken as 0.5 in the following examples; d_c = a user-defined decay coefficient, is taken as 4 in the following examples; and $\dot{\gamma}_{eq}$ = the slip rate (Oden and Martins 1985).

In the following simulations, the static friction coefficient, the kinetic friction coefficient and the decay coefficient are assumed to be 0.5, 0.1, and 4, respectively. The corresponding exponential decay friction model is shown in Fig. 9.13.

9.6.3.3 Hydraulic (Thermal) Properties at the Soil-Slab Interface

It is assumed that in the following simulations, there is no water flow through the soil-slab interface. This condition is realized by defining a very low “gap conductance” to the contact elements. The hydraulic conductance of the contact elements is assumed to be 10^{-30} s^{-1} when the contact element’s thickness is zero (i.e. the slab and the soil are in contact with each other), which corresponds to a gap conductance of $10^{-30} \text{ J}/(\text{m}^2 \text{ s } ^\circ\text{C})$.

The hydraulic conductance of the contact elements is assumed to be 0 when the contact element's thickness is equal to or greater than 0.2m (i.e. the slab and the soil are separate and have a clearance of 0.2 m). ABAQUS/Standard will interpolate the hydraulic conductance of the contact element linearly with the gap clearance.

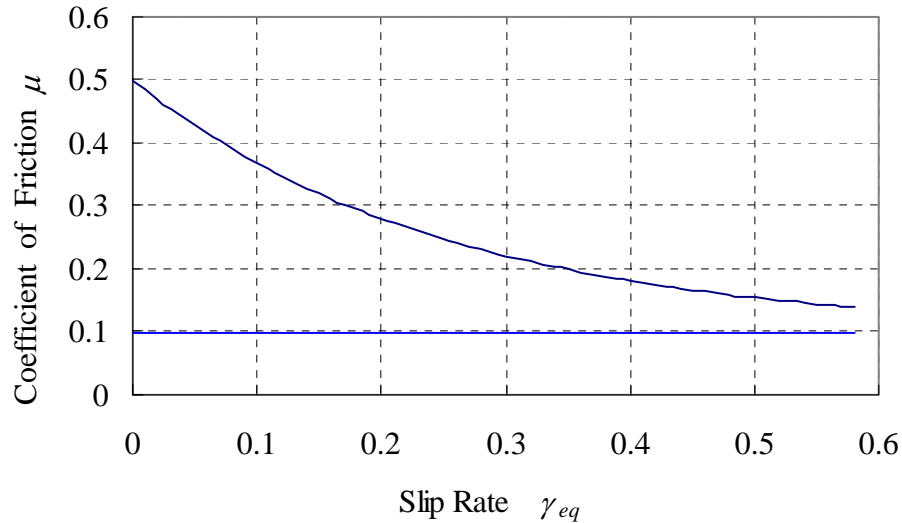


Fig. 9.13. Exponential decay friction model

9.6.4 Boundary Conditions and Loadings

9.6.4.1 Mechanical Boundary Conditions

Fig. 9.14 shows the mechanical boundary conditions used for the simulations. The mechanical boundary conditions for the simulated domain are as followings. In the x direction, at the far sides of the simulated domain, the displacement in x direction and the rotation along y and z axis are restricted, that is,

$$x = -24\text{m or } x = 24\text{m}, \quad u_x = \varphi_{xy} = \varphi_{zx} = 0$$

Similarly, in the y direction, at the far sides of the simulated domain, the displacement in y direction and the rotation along x and z axis are restricted, that is,

$$y = -24\text{m or } y = 24\text{m}, \quad u_y = \varphi_{xy} = \varphi_{zy} = 0$$

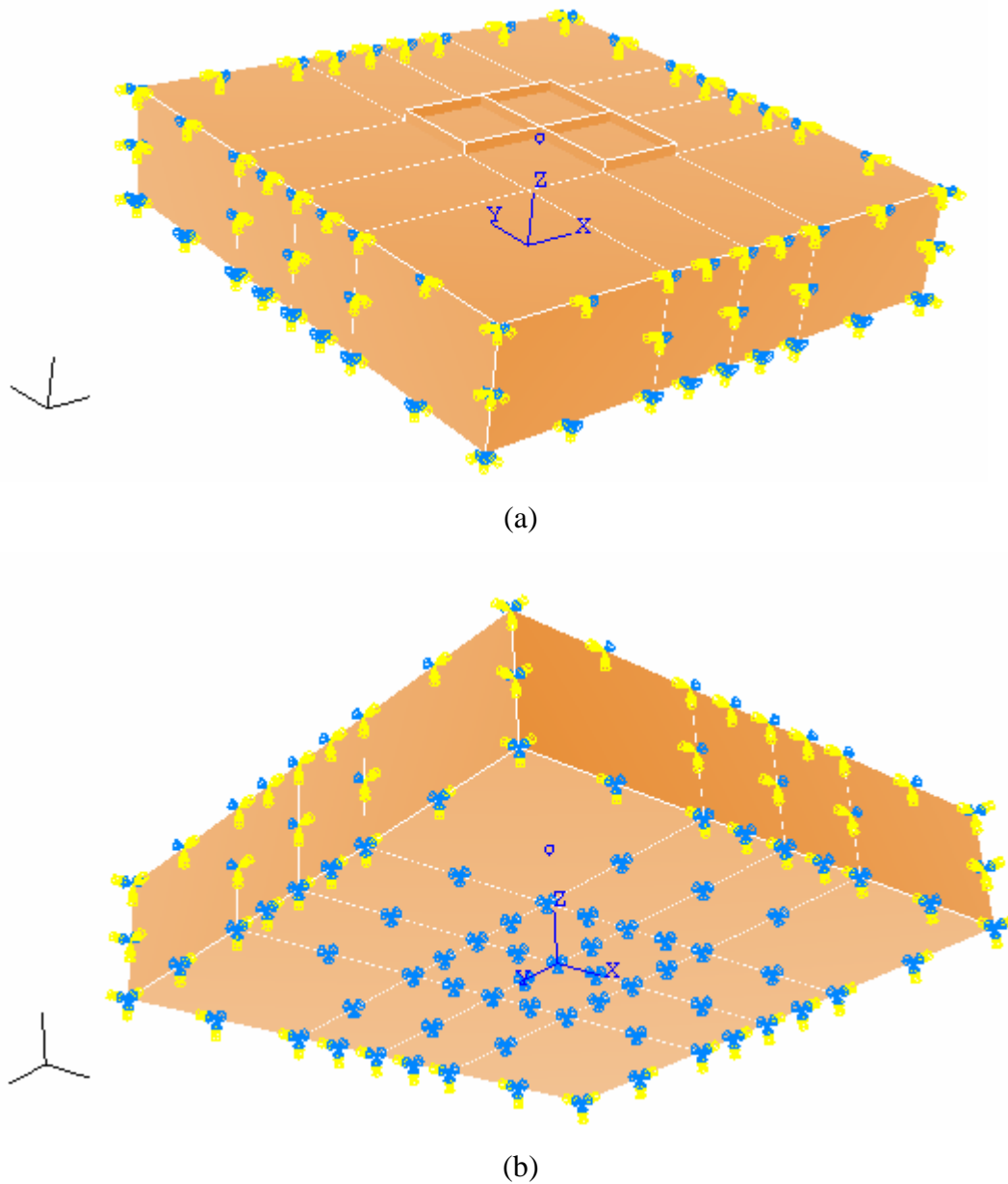


Fig. 9.14. Mechanical boundary conditions for the simulations.(a) view from the top(b) view from the bottom

For the nodes at the bottom of the soil domain, the displacements in both x , y , and z direction were restrained,

$$z=0 \text{ m, } u_x= u_y= u_z=0$$

At the soil surface outside from the concrete footing, there was no mechanical load. The house is built on the ground soil surface and there is no mechanical restriction for the building..

9.6.4.2 Hydraulic (Heat Transfer) Boundary Conditions

In the following simulations, the hydraulic boundary conditions are implemented by the heat transfer boundary conditions. At the place far away from the footing, it is assumed that there is no horizontal flow because the boundary is considered to be infinite and symmetric, that is,

$$x= -24\text{m or } x=24\text{m, } q_x= q_y=0$$

$$y= -24\text{m or } y=24\text{m, } q_x= q_y=0$$

The restraints are applied automatically by ABAQUS without specially specifying. For the nodes at the bottom of the domain i.e. $z=0$, it was assumed the soil matric suction is constant and equaled to -10 kPa through the simulation, which is considered as ground water level and corresponding to the matric suction at the field capacity.

For the soil underneath the concrete slabs, there is no vertical flow. This condition is realized by assigning a very small gap conductance to the contact elements at the soil-slab interface.

9.6.4.3 Weather Conditions, Grass and Tree Root Zone

The site where the house is built is assumed to be at Arlington, Texas. The weather conditions are the same as those shown in Fig. 4.6. At the soil surface outside from the concrete slab, the soil is assumed to be covered by Johnsongrass (*Sorghum halepense*) and the weather conditions are the same as that at the site at Arlington, Texas. The method for estimating the evapotranspiration for the vegetation has been discussed in the Chapter VII. Depending on the daily weather data, the evapotranspiration for the grass was different. The single crop coefficient for the Johnsongrass is assumed as $K_c= 0.6$. The adjusted coefficient for the water and environmental stress depends on the matric

suction or water content in the grass root zone (Fig. 7.9). Please see detailed explanations in Chapter VII and VIII.

For the grass root zone, the water source term can be calculated by Eq. 7.48 and the net water loss for the grass root zone is calculated by Eq. 7.42 and 7.43.

In these two examples, a tree is planted near the house to show the influence of the tree root zone. Tree root zone is deeper than grass root zone. It is considered that the precipitation can not infiltrate directly in the deep tree root zone. In this case, it is proposed that the tree root zone can be considered as the condition when the precipitation is always zero. Like grass root zone, water together with some nutrients is taken up by the tree roots locally at the tree root zone and transported through the tree. The single crop coefficient for the tree is assumed as $K_c = 0.3$. The adjusted coefficient for the water and environmental stress depends on the matric suction in the tree root zone is assumed to be the same as that in Fig. 7.9. The vaporization occurs at the tree leaf surface as shown in Fig. 7.13. For the tree root zone, the water source term can be calculated by Eq. 7.49 and the net water loss for the grass root zone is calculated by Eq. 7.40 and 7.41.

The soil properties and the actual evapotranspiration due to the grass root zone and the tree root zone are calculated by the user subroutines USDFLD similar to what we described in Chapter VIII. The corresponding flowchart is shown in Fig. 9.15. The detailed program is attached in the Appendix E.

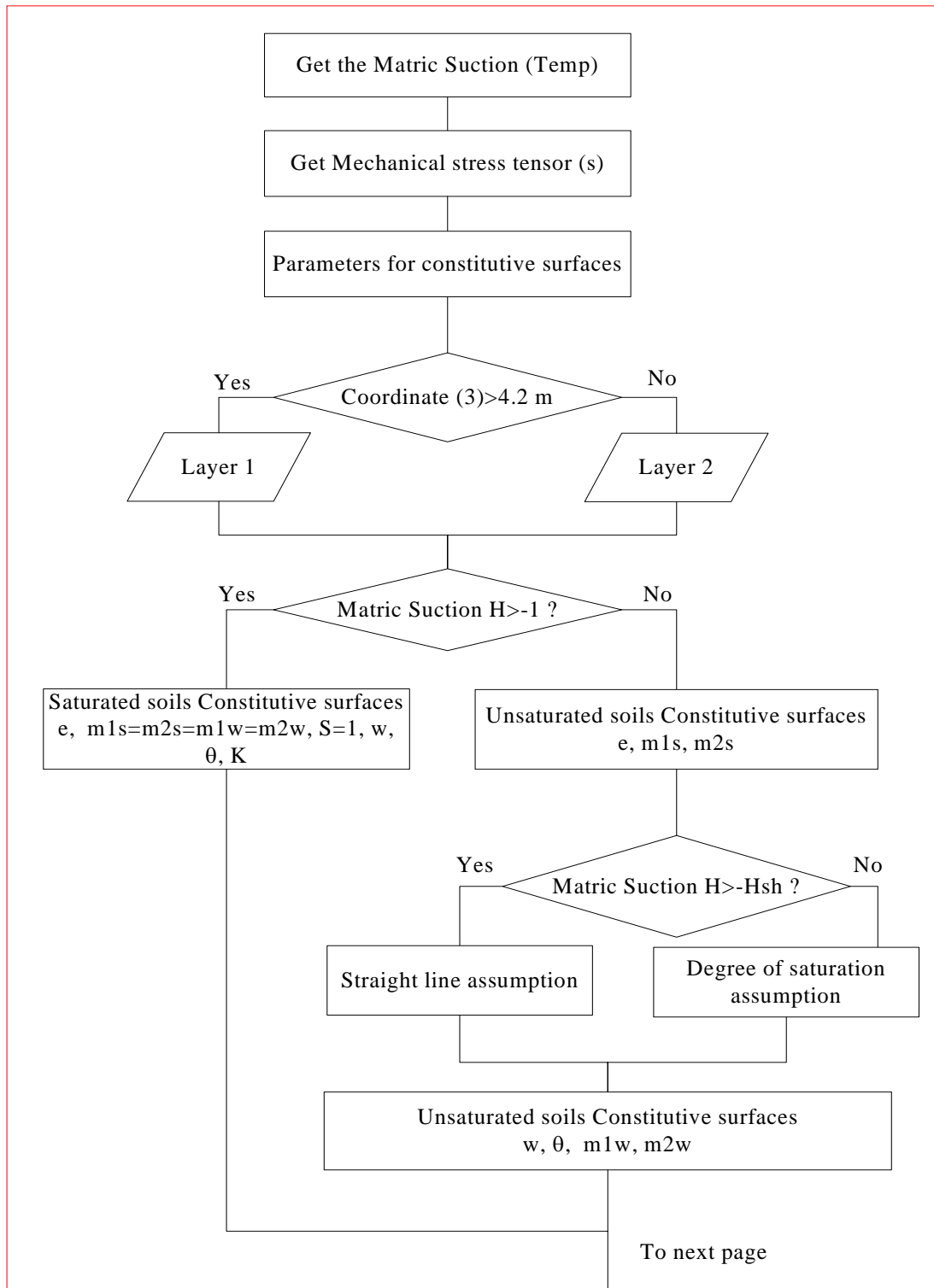


Fig. 9.15. Flow chart for the user subroutine USDFLD. (a) flow chart for the constitutive surfaces and the derivatives

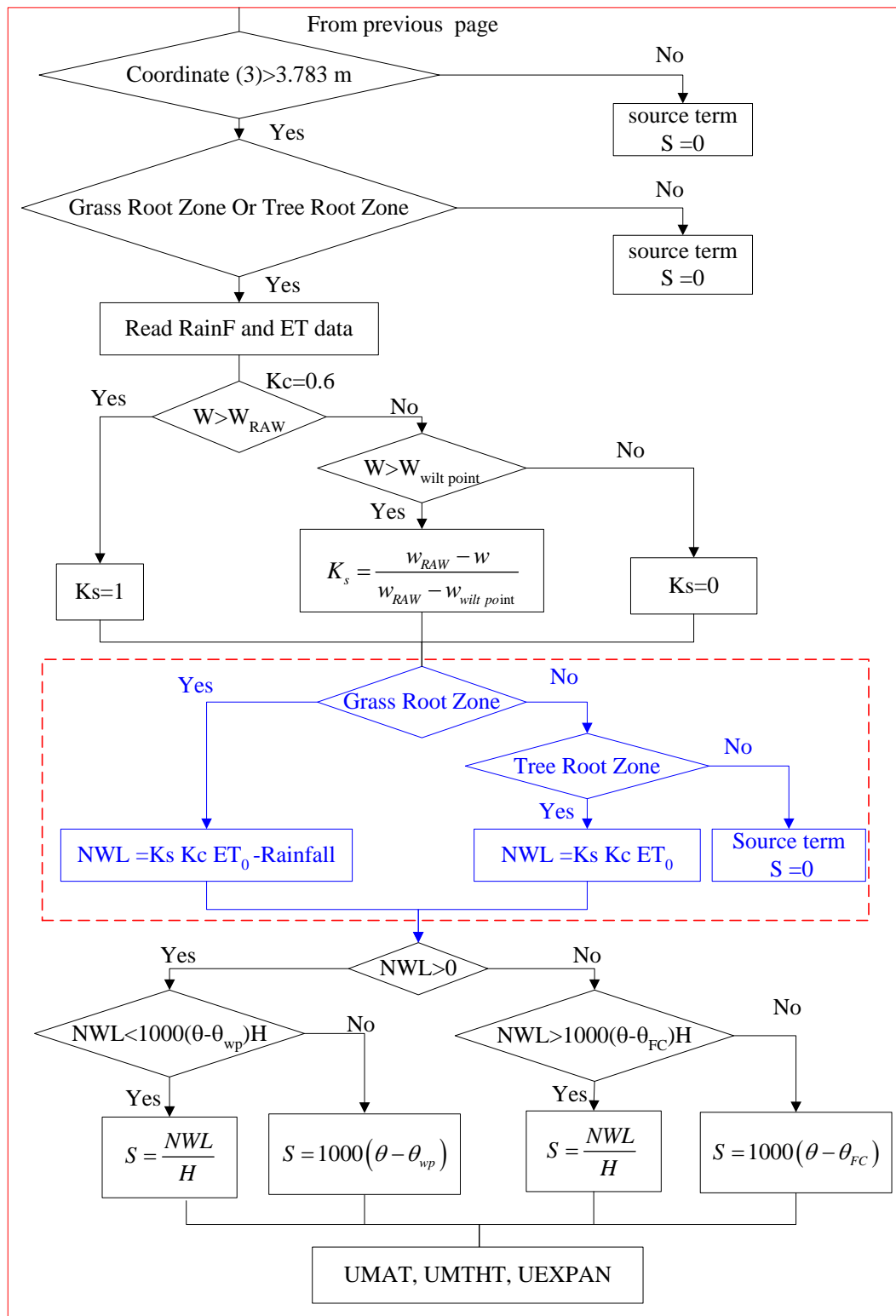


Fig. 9.15. (Continued)(b) flow chart for the source term calculation

9.6.4.4 Loadings

During the simulation, body forces caused by the gravity are applied to both the building and soil block. For the soil domain, the soil density is taken as 1000kg/m^3 while the acceleration of gravity is taken as 20m/s^2 . In this way, an equivalent soil density of 2000kg/m^3 is obtained. The reason for using 1000kg/m^3 instead of 2000kg/m^3 directly is because in the coupled thermal stress problem, the mass density is the same for both mechanical stress and heat transfer simulation. For the coupled consolidation theory, the mass density in the differential equation for the water flow is the dry unit density while the mass density should be the total unit density when calculating the body force for the mechanical stress equilibrium.

The load the building applied to the soil is its gravity. The soil-structure interaction is simulated by contact elements. The load transfer depends on whether the bottom of the concrete footing is in contact with the soil surface or not. When surfaces are in contact, any contact pressure can be transmitted between them. The surfaces separate if the contact pressure reduces to zero. Separated surfaces come into contact when the clearance between them reduces to zero. Fig. 9.16 shows the loading conditions in the following simulations.

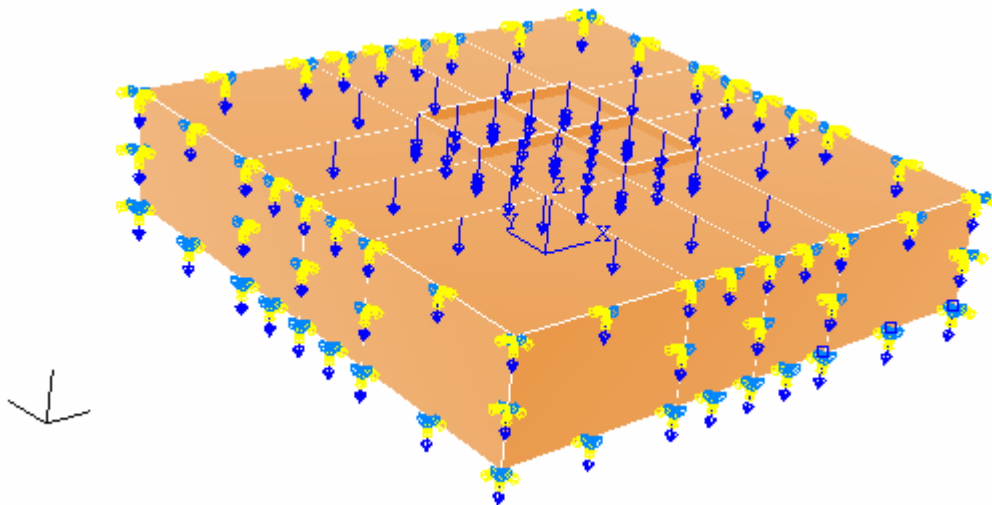


Fig. 9.16. Loads applied in the simulations

There is no thermal load applied during the simulation. The weather's influence is simulated by the source term and is discussed in the boundary conditions section.

9.6.5 Mesh Generation and Shear Locking

9.6.5.1 Mesh Generation for Soil Domain

The three dimensional coupled temperature-displacement element C3D8T is used for the simulation of the volume change of the soil. It is a 8-node thermally coupled brick element, which uses trilinear interpolation for the geometry and displacements. The temperature (pore water pressure) is interpolated linearly.

Fig. 9.17 shows the mesh generation of the example problems. Non-uniform mesh is used to make the simulation more efficiently. In the horizontal plane (xoy plane), at the center of the simulated domain where the building is built a finer mesh is used with uniform intervals. As shown in Fig. 9.17a, along x direction, in the range of $-8m < x < 8m$, a uniform interval of 0.5m are used. In the range of $-24m < x < -8m$ and $8m < x < 24m$, 8 intervals are seeded and the intervals are denser towards the center of the simulated domain with a bias of 2.0. In the y direction, the same procedure is applied. In the z direction, 8 intervals are seeded and intervals are denser towards the ground soil surface with a bias of 2.0 because the soil volume and water content usually vary significantly. The mesh generation for the soil domain is shown in Fig. 9.17b.

9.6.5.2 Mesh Generation, Shear Locking and Reduced Integration for the Slabs and Walls

The slabs and the walls are meshed with a uniform element size of 0.5m. The mesh for the whole simulated domain is shown in Fig. 9.17b.

The S8RT general shell element is used for the simulation of the slabs and walls. It is a 8-node thermally coupled quadrilateral general thick shell element, which use quadratic interpolation for the geometry and displacements. The temperature is interpolated linearly in the shell surface. It has six nominal active degrees of freedom ($u_x, u_y, u_z, \phi_x, \phi_y, \phi_z$) at all eight nodes and three temperatures 11, 12, 13 through the

thickness at the corner nodes only. Although three rotation components are used, but only two are actively associated with stiffness in ABAQUS/Standard. For plate or shell, the thickness in one dimension is very small compared with the other two dimensions, there is a singularity because of artificial energy when three dimensional continuum elements are used for the simulation. A small stiffness is associated with the rotation about the normal to avoid this difficulty, i.e. only five degrees of freedom ($u_x, u_y, u_z, \phi_x, \phi_y$) are actually used. The default stiffness values used are sufficiently small such that the artificial energy content is negligible.

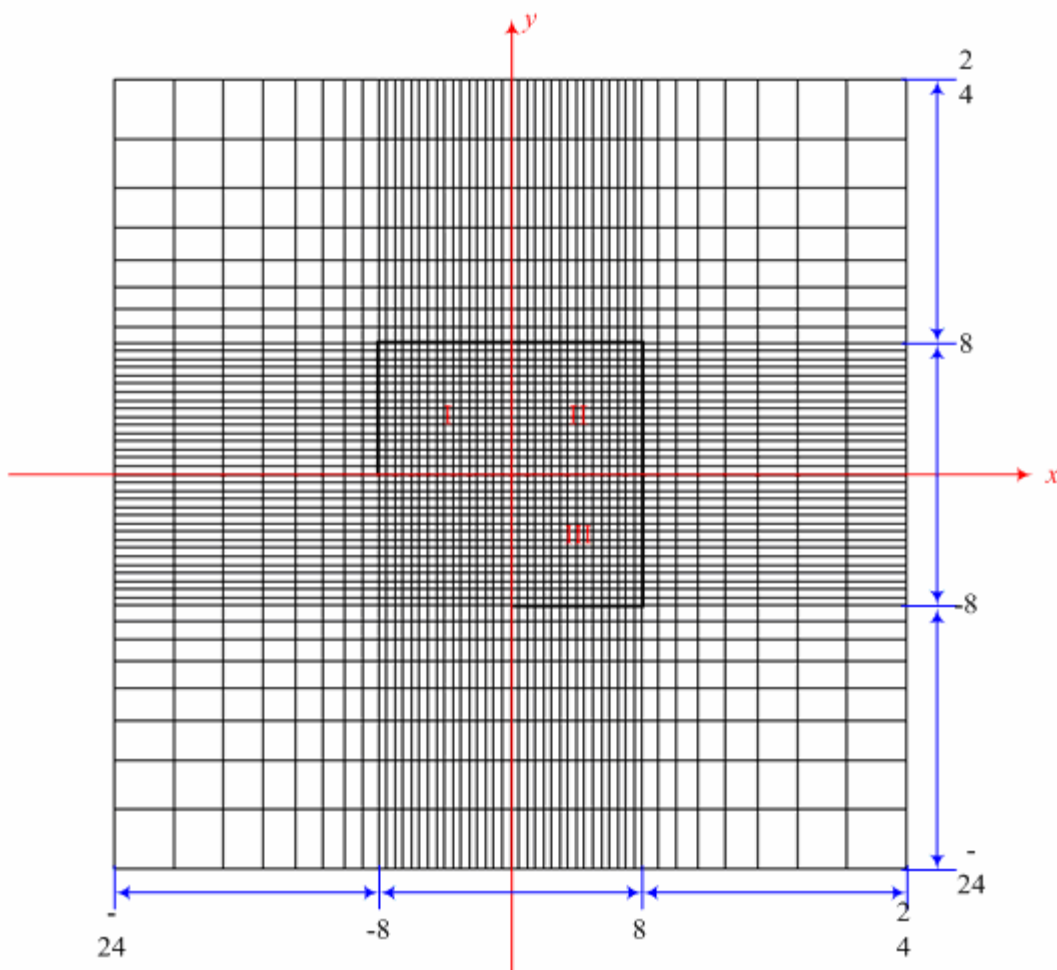


Fig. 9.17. Mesh generation of the example problems. (a) top view

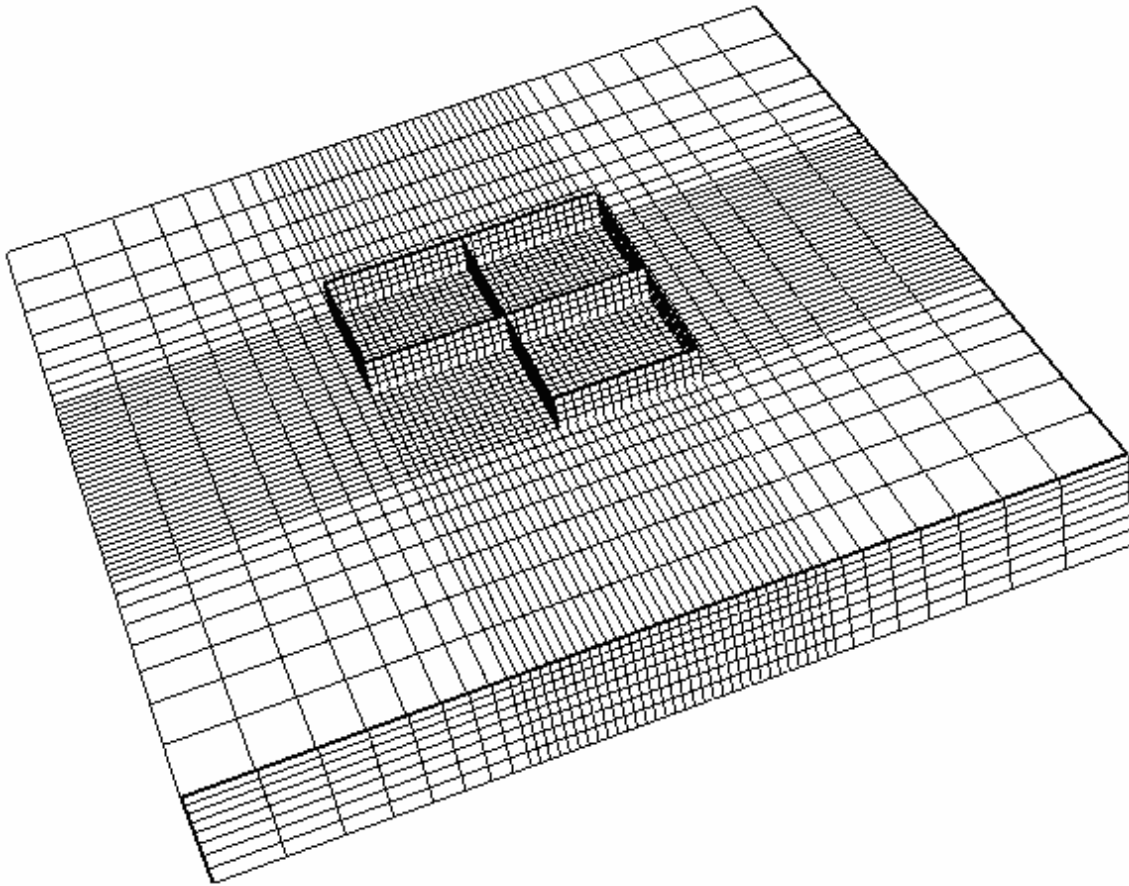


Fig. 9.17. (Continued) (b) Three dimensional view

ABAQUS/Standard provides element type S8RT for use in thick shell problems. However, the slabs and walls in the residential buildings have thicknesses less than about $1/15$ of a characteristic length on the surface of the shell, which should be considered as a thick shell according the ABAQUS/Standard. As a consequence, when using the S8RT element to simulate the behavior of the slabs and walls, the artificial energy content in the simulation is too high, i.e. the stiffness matrix of the element is increased improperly. Under this condition, shear locking occurs. Pawsey and Clough (1971) and Zienkiewicz et al. (1971) found that by using reduced integration, the drawback can be overcome and the general shell elements can not only used for thick plate or shell, but also for thin plate or shell. In this dissertation, reduced integrations are

used to the general shell elements to simulate the behaviors of the slabs and walls in the residential building, which are usually considered as thin plate or shell.

ABAQUS/Standard does provide reduced integration for stiffness matrix of the S8RT element while the mass matrix and distributed loadings are still integrated exactly. For slabs, the thickness is 0.4 m and the 5×5 Gaussian integration points are replaced by the 3×3 Gaussian integration points. The reduced integrations are implemented by the following commands:

```
*Shell Section, elset=_G21, material=Material-1
0.4, 3
```

where _G21= the element set for the slabs.

For walls, the thickness is 0.1m and the 3×3 Gaussian integration points are used. The reduced integrations are implemented by the following commands:

```
*Shell Section, elset=_G22, material=Material-1
0.1, 3
```

where _G22= the element set for the walls.

The definitions for the shell section for slabs and walls can be found in the main program Appendix E.

9.6.6 Initial Conditions and Simulation Procedure

The initial matric suction in the soil is assumed to be -500kPa throughout the whole soil domain. At the first step a steady state analysis is performed to make the soil suction to reach equilibrium with a matric suction of -10 kPa at the ground water level. The weather conditions as shown in the Fig. 4.6 are then applied to the grass and the tree and the simulation last one year. The following examples show the partial simulation results

for different conditions. All the simulation results are movies changing daily with time or weather conditions.

9.6.7 An Example for Center Lift Case

9.6.7.1 Introduction

The tree is planted at the corner formed by the wall 3 and the wall 6 of the building as shown in Fig. 9.18. The tree root zone is below the grass root zone. The coordinate of the tree root zone is: from -13 m to -7m in x axis, from 3 m to -3m y axis and from 4.23m to 5.53m in z axis. The plane view of the simulation domain is shown in Fig. 9.19a and the profiles at different locations A-A', B-B', and C-C' in Fig. 9.19a are shown in Fig. 9.19b, c and d, respectively.

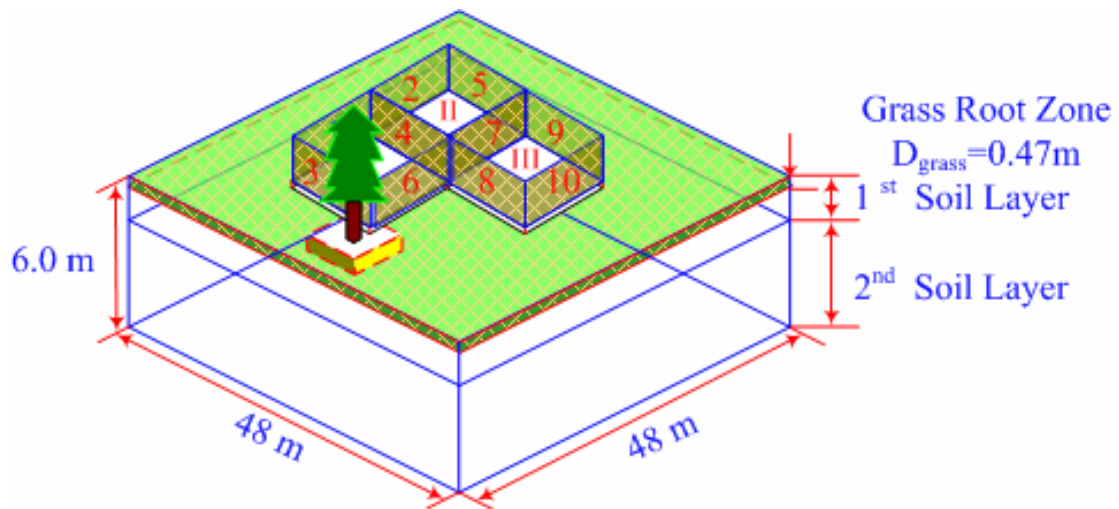


Fig. 9.18. An example when there is a tree at the corner of wall 3 and wall 6

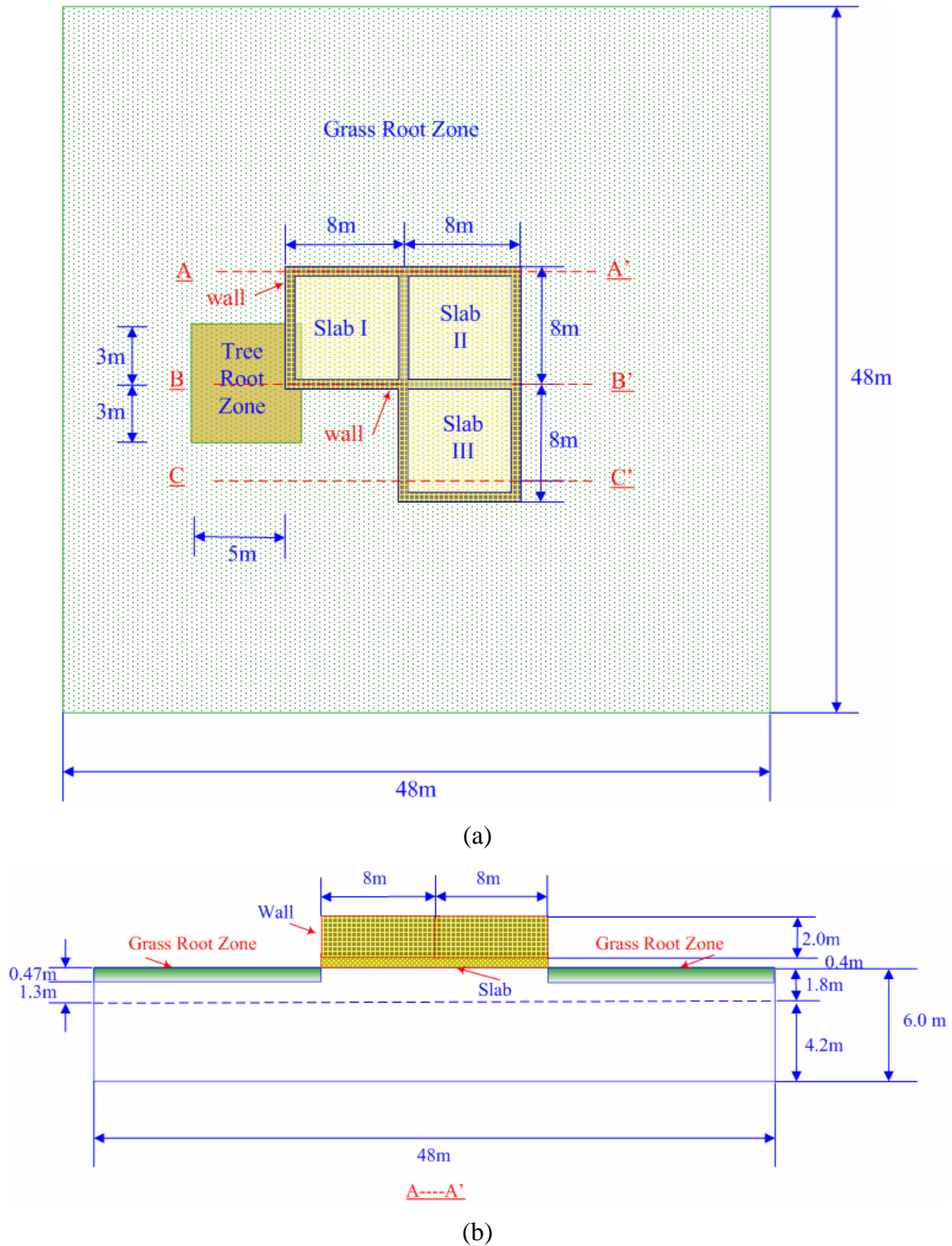


Fig. 9.19. Top view and profiles of the simulation domain for a center lift case. (a) view from the top (b) A-A' profile

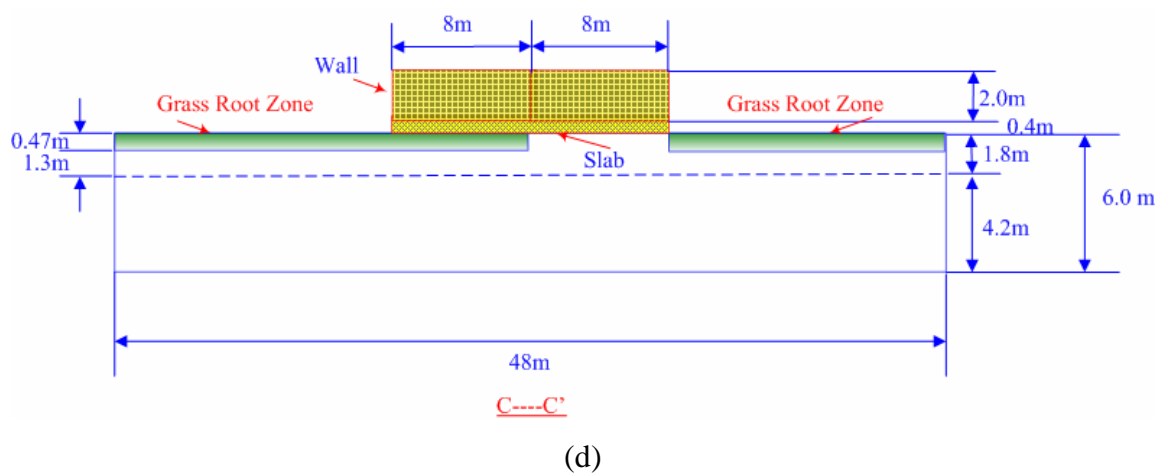
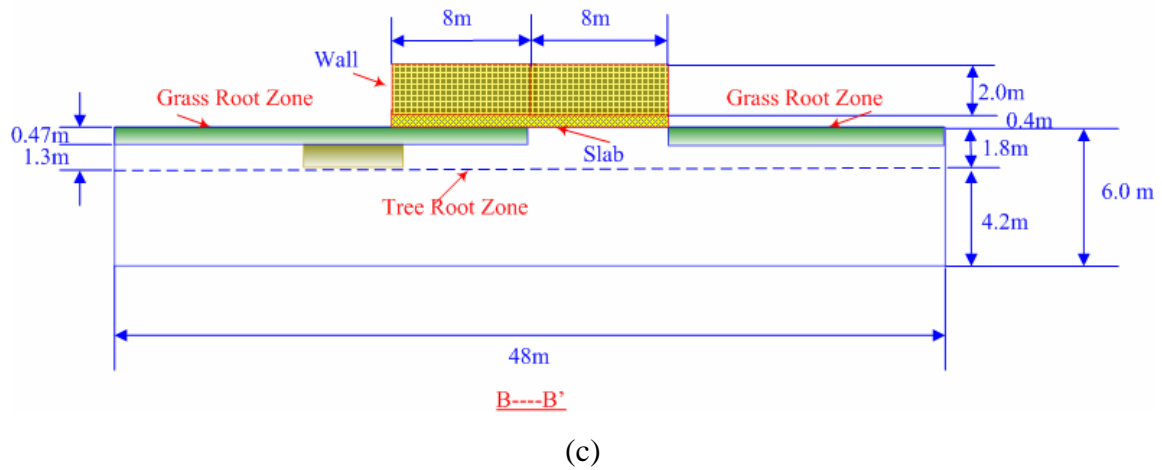


Fig. 9.19. (Continued) (c) B-B' profile (d) C-C' profile

9.6.7.2 Suction Distributions

Fig. 9.20 shows the matric suction distributions for the simulated domain at the 301st days. It can be seen that the matric suctions at the ground soil surface are higher than those below the surface and the matric suction underneath the slab is lower than that outside of the slab because the slabs prevent the soils underneath from losing water. The suction value in the tree root zone is much higher than the other places because the tree root can absorb water from the soil more easily.

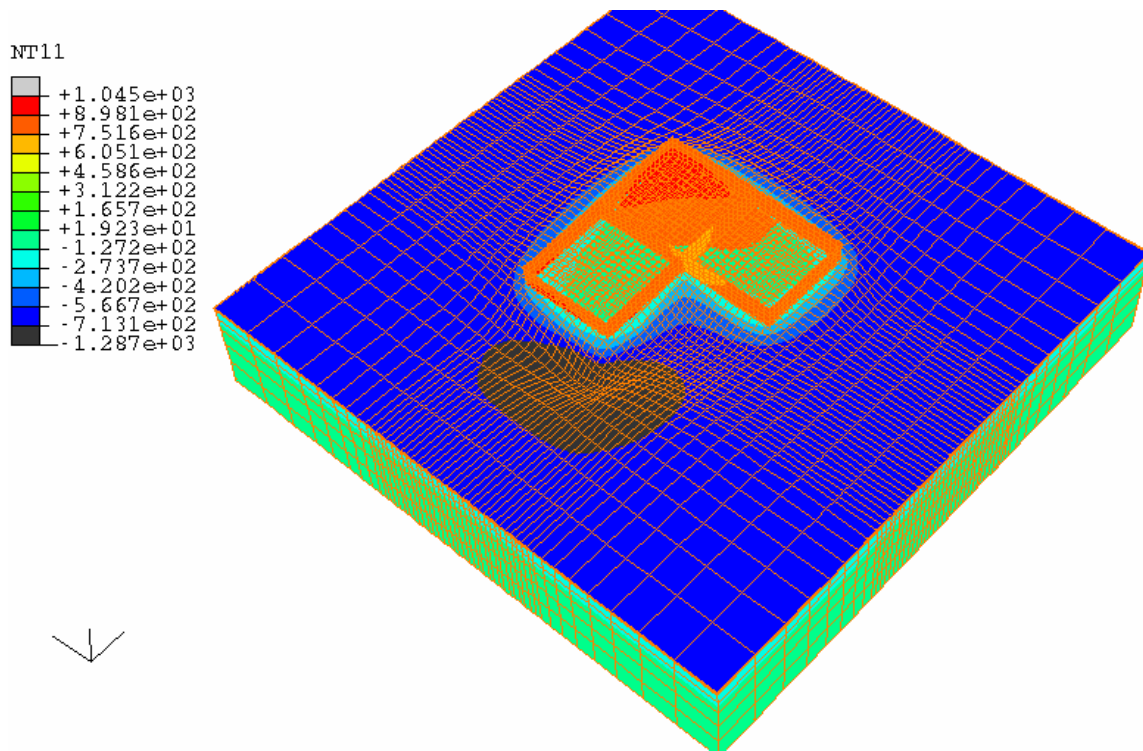


Fig. 9.20. Suction distributions at the 301st day for a center lift case

9.6.7.3 Deformations

Fig. 9.21 shows the deformations of the whole simulated domain at the 301st day. As can be seen, the soil underneath the slab has a higher elevation than the soils outside of the slab due to the lower suction values underneath the slab. The settlement at the center of the tree root zone is bigger than any other place due to the higher suction values caused by the tree root. A sink pit is formed close to the corner formed by the wall 3 and wall 6. At the place far from the building, at the soil deformation is the same, indicating the influence of the tree and the slabs are limited in certain range.

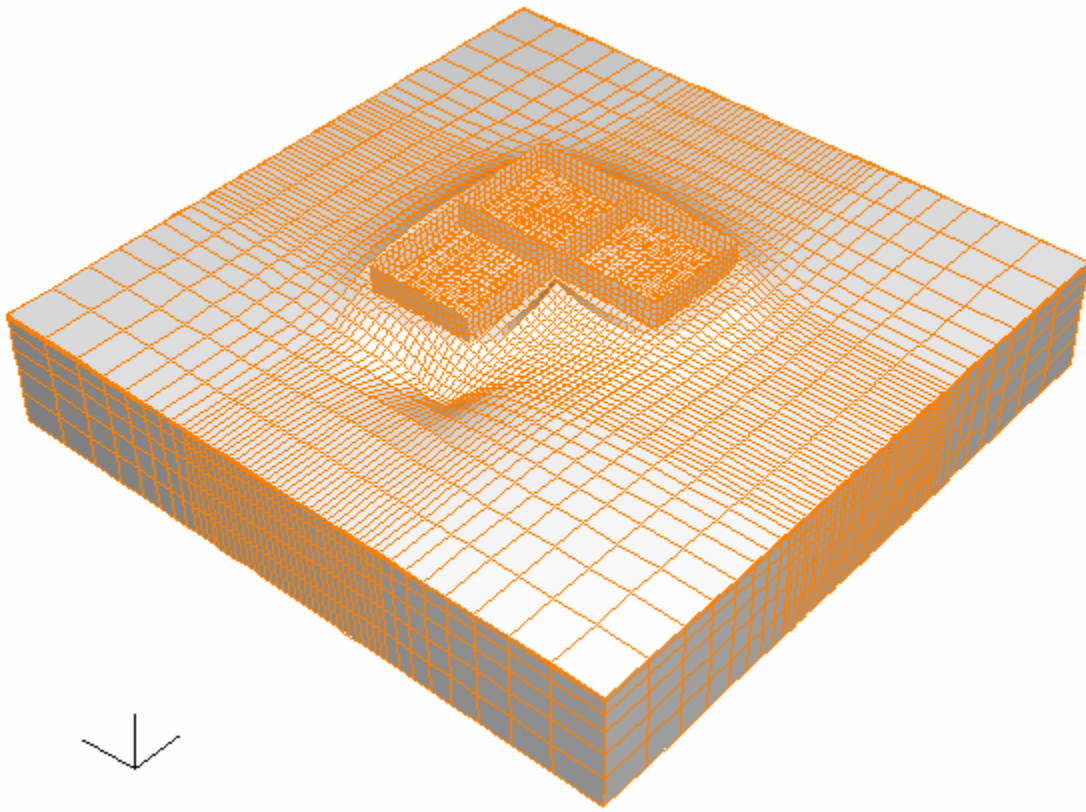


Fig. 9.21. Deformations at the 301st day for a center lift case

9.6.7.4 Openings between the Soils and the Slabs

The shrinkage caused by the tree root zone can be large enough to cause gaps between the slabs and the ground soils. Fig. 9.22 show there is a gap between the soil and the slab at the corner close to the tree at the 301st day while other places the soils and the slabs are in contact with each other.

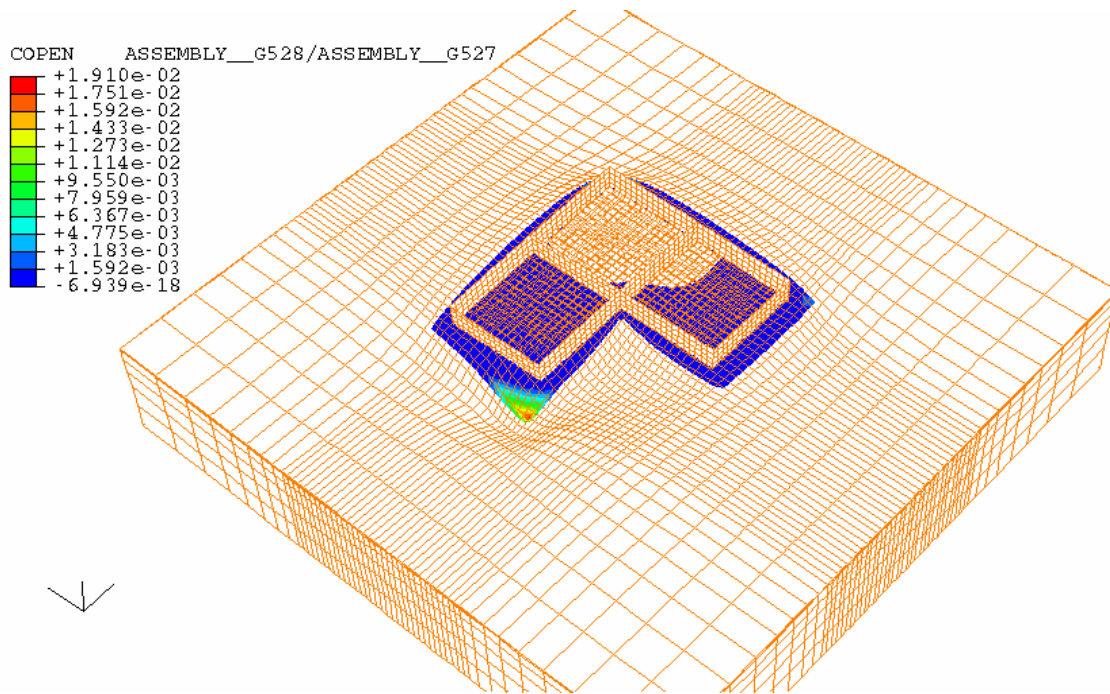


Fig. 9.22. Openings between the soils and the slab at the 301st day for a center lift case

9.6.7.5 Contact Pressures

Fig. 9.23 indicates that at the 301st day, when the weather is dry, the contact pressures at the edge of the slabs are smaller than those in the center of the slabs. This situation is caused by soil shrinkage at the edge of the house. When there is shrinkage at the edge of the house, the soils at the edge have less support to the slab. As a consequence, the load from the superstructure is transferred to the soils underneath the center of the slab. The soils underneath the center of the slab have to give more support to the slabs and the reaction forces from the soils are higher. It can also be found that the reaction force of the soils is zero at the corner where the tree is planted. Compare Fig. 9.22 and 9.23, it can be found at the corner where the slab loses support, the reaction forces are zero. The soils and the slabs are in contact with each other except the corner near the tree root zone.

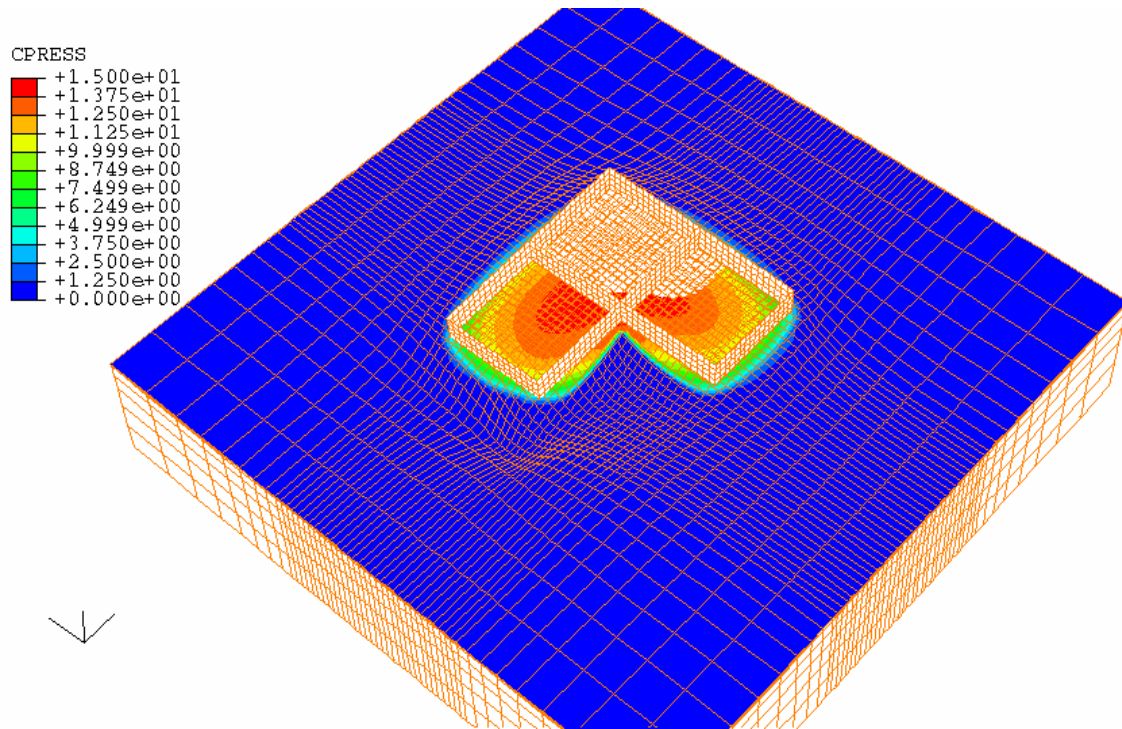


Fig. 9.23. Contact pressure between the soils and the slab at the 301st day for a center lift case

The reaction forces are different at different locations. The differential reaction forces are corresponding to differential deflections in the slab. Consequently, there are bending moments even when the slabs and the soils are in contact with each other. As we discussed previously, the BRAB method and the WRI method calculate the bending moment under the assumptions that there are some areas where the slab and the soil are not in contact. The supporting index and the dead weight of the structure are used to calculate the maximum bending moment of the slab. From this analysis, it can be found that, even when the soil and the slab are in contact, there are bending moments in the slab. Furthermore, not all loads from the superstructure can generate bending moments in the slab because part of the loads is contracted by the reaction forces from the soils. As a consequence, the loads and the distances which actually cause bending moments

are not equal to the dead weight of the structure and the lengths of losing support. This problem will be further discussed later.

9.6.7.6 Slips and the Shear Forces between the Soil and the Slabs

The structure is not symmetric, which causes the building tends to slip. Fig. 9.24 shows the accumulated slips of the soil surface along x direction (CSLIP1) between the slab and the soil at the soil-slab interface at the 301st day. The accumulated slips underneath wall 3 and wall 8 are negative while the accumulated slips underneath the wall 5 and wall 9 are positive, indicating the soil is moving outwards from the center of the slab due to the soil shrinkage. It can also be seen that the slips of the soils underneath the wall 3 is much bigger than any other places because the tree root zone causes more shrinkage of the soils. The center of the slab is sticking with the soils and the relative slips are very small (light green stands for zero slip).

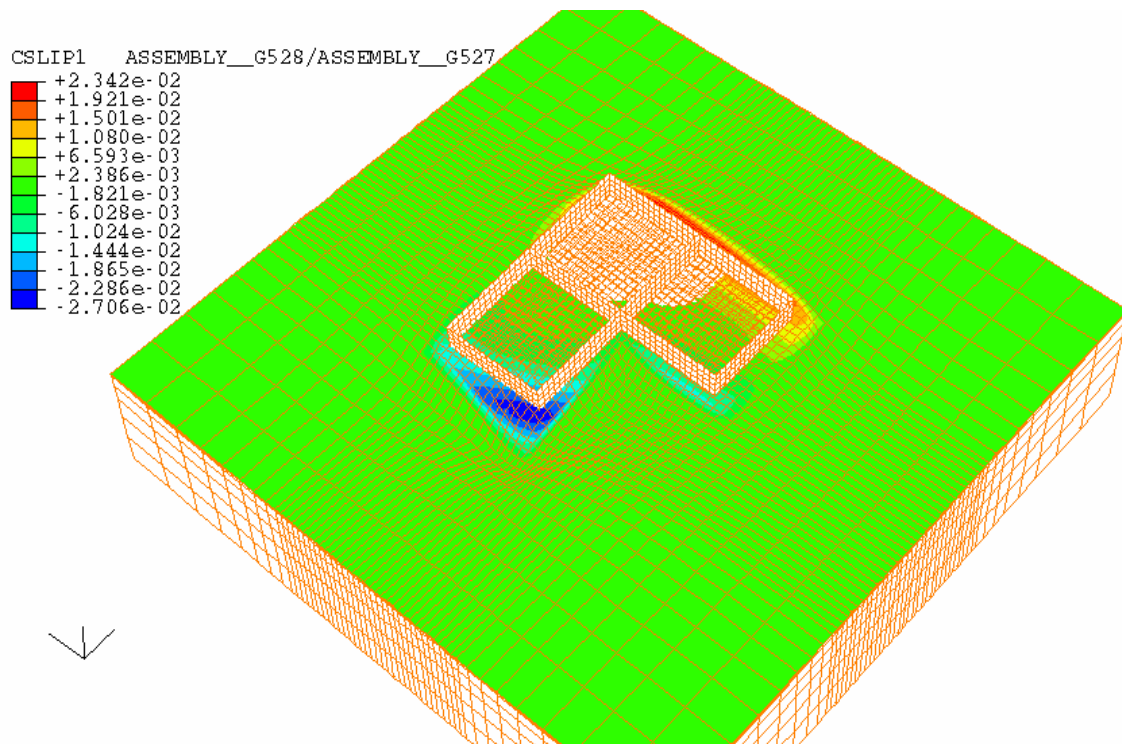


Fig. 9.24. Slips between the soils and the slab at the 301st day for a center lift case

The shear stresses between the slab and the soil at the soil-slab interface along the x direction are shown in Fig. 9.25. The maximum shear stresses along x direction are found near the corner where the tree is planted. At the corner where there is gap, the shear stresses are zero. The shear stresses underneath the edge of the slab are higher than those at the center of the slab. The shear stresses at the center of the slab are close to zero because the relative slips are close to zero. The results for relative slips and shear stresses are consistent with each other.

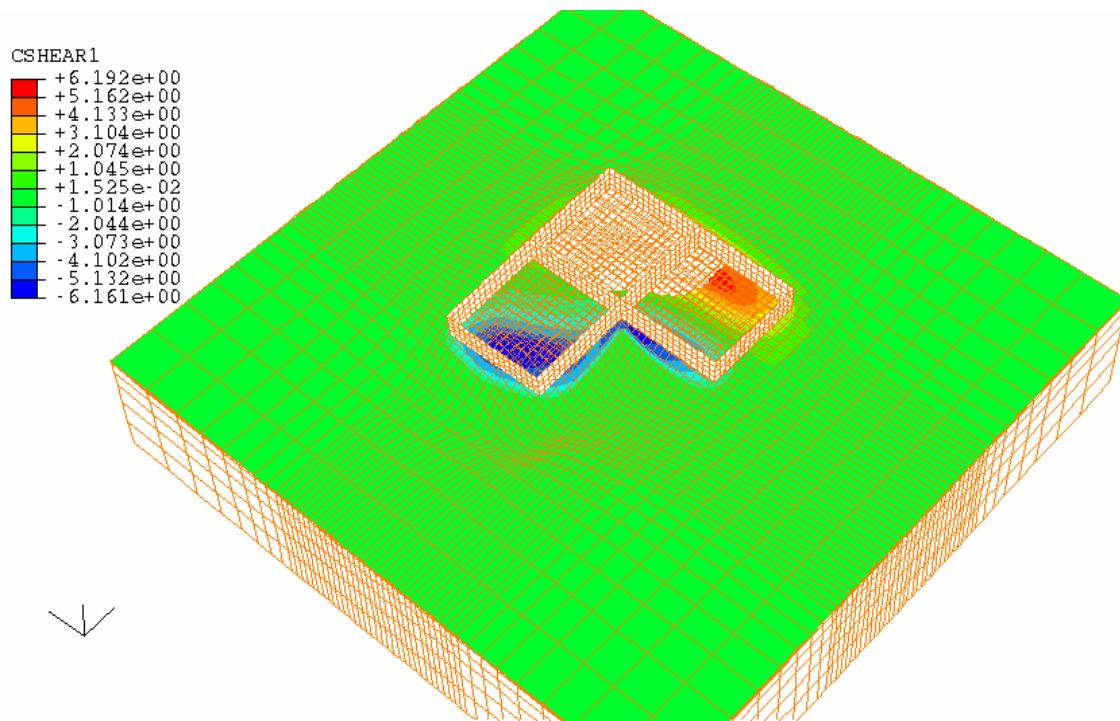


Fig. 9.25. Shear stresses between the soils and the slab at the 301st day for a center lift case

9.6.7.7 Deflections of the Slab and the Gaps between the Soil and the Slab

The shapes of the ground soil surface and the slab along the B-B' profile at the 1st day (08/01/1999), the 101st day (11/09/1999), the 201st day (2/17/2000), and the 301st day (5/27/2000) are shown in Fig. 9.26. At the start of the simulation (08/01/1999), the soil surface is flat. Due to the weight of the structure, there are settlements and the slab are not flat but the deflections are so small that it looks like flat in the Fig. 9.26. From 08/01/1999 to 11/09/1999, even the rainfall and evapotranspiration is basically evenly distributed, there is some evaporations due to the soils in the simulation are very wet at the start of the simulation. As a consequence, the soils and the slabs goes down and there is a gap between the soils and the slab at the left side near the tree root zone. At the right side, the soil and the slab are still in contact, but the deflection of the slab becomes bigger.

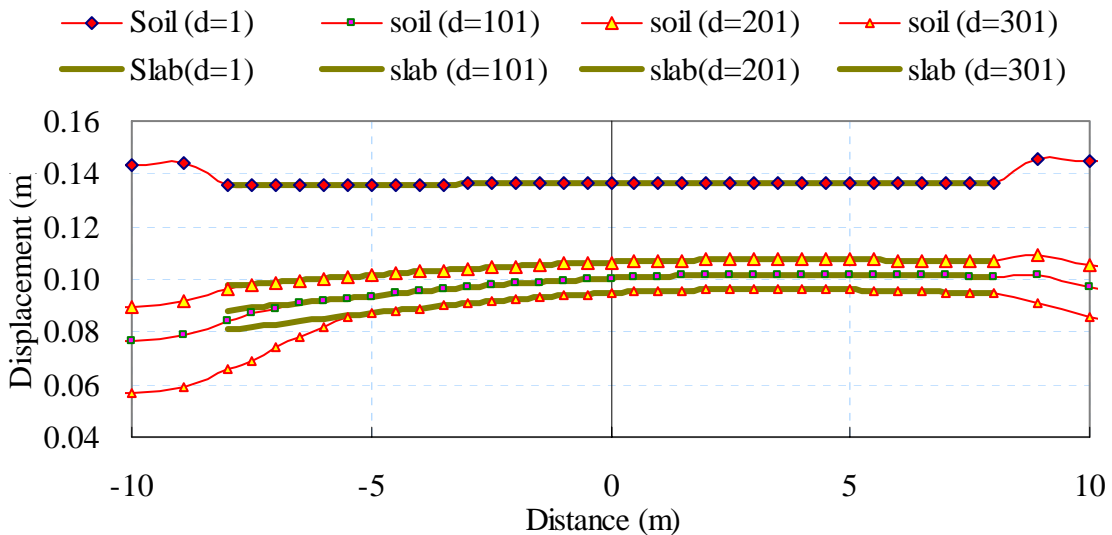


Fig. 9.26. Shapes of the ground soil surface and the slab at different times

From 11/09/1999 to 02/17/2000, it is a relatively wet season, and the soil starts to swell, the elevation of the slab and the soils go upward. The gap between the soils and the slab at the left side disappears due to the swell of the soil but the soil elevation is still lower than that of the slab. At the right side, the soil elevation is higher than the slab. Under this condition, an edge lift case occurs. However, due to the weight of the walls at

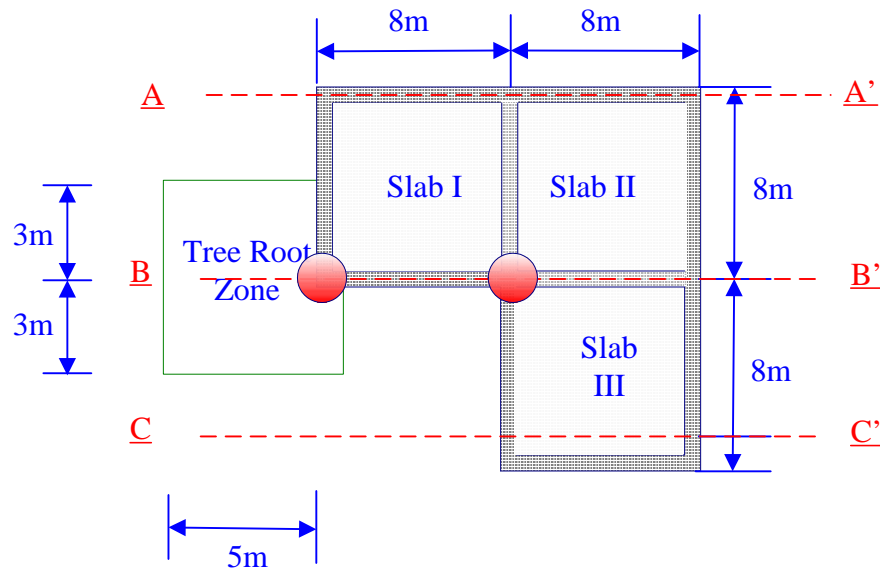
the edge of the slab, the deflection of the slab is still downward and the edge lift condition is not obvious. From 02/17/2000 to 05/27/2000, there is evaporation again, the soils shrink and the elevation of the building decreases. The gap between the soils and the slab near the tree root zone reappears at the 301st day.

This procedure can be clearer if we look at the displacement of the slab and the soil at two different locations at the same time. Two observation points are used to illustrate the variations in deflection of the slab and the gap between the slab and the soil. Fig. 9.27a shows the locations of the two observation points, one is at the center of the B-B' line ($x=0.0\text{m}$) and the other is at the left end of the center line where the tree is planted ($x=-8.0$). Fig. 9.27b shows the vertical displacements of the soils and the slab at these two points. The displacement differences in the slab at these two different actually reflect the deflection of the slab while the displacement differences at the same location between the soil and the slab reflect their contact conditions.

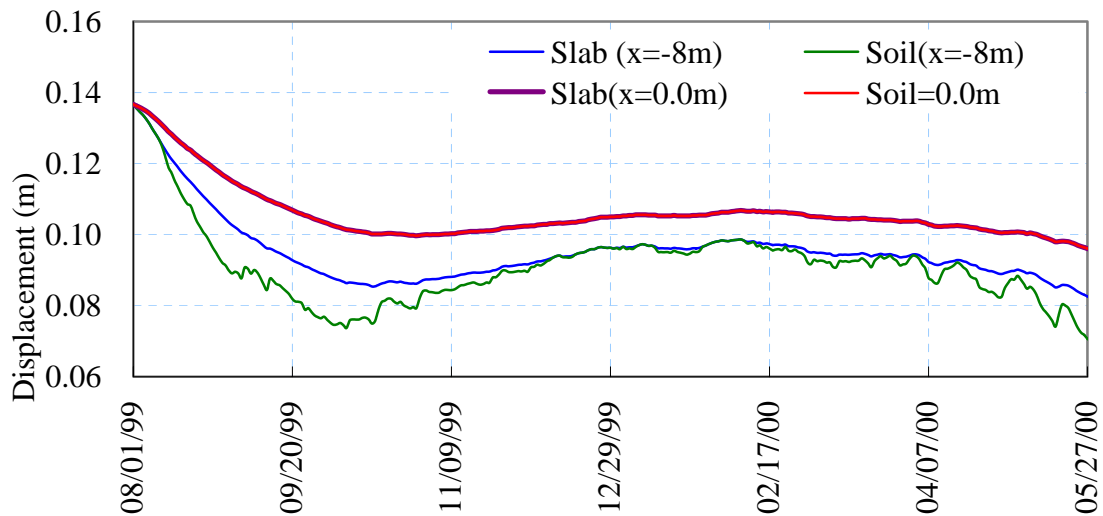
For the point at the center of the line B-B', it can be seen that the slab and the soil have the same displacements throughout the simulation period, indicating the slab and the soil are always in contact with each other. The starting point of the displacements is 0.14m, indicating there is a swell after the first step of steady state analysis.

For the point at the left side, at the beginning from 08/01/1999 to 08/01/1999 the soil and the slab have the same displacement at the edge of the slab and are in contact. Then there are differences in displacements between the slab and the soil from 08/11/1999 to 12/10/1999, the differences vary with time (weather conditions) and are equal to the height of the gaps at that point between the soil and the slab. From 12/11/1999 to 02/08/2000, the displacement of the soil and the slab are basically the same, indicating the gap recovers due to the wet winter season. There is a short period during this season where there are small gaps between the soil and the slab, which is caused by a short period dry weather and the corresponding soil shrinkage as shown in the Figure. From 02/08/2000 to 05/27/2000, the gap between the soil and the slab reappears and becomes bigger because the weather becomes hotter and hotter.

It can also be seen from Fig. 9.27b that before a gap appears the soils shrink first and the elevation goes down while when the gap recovers the soils always swell upwards first. The simulation results are consistent with the actual conditions in the field very well.



(a)



(b)

Fig. 9.27. Displacements of the ground soils and the slab at two locations for a center lift case. (a) locations of the observation points; (b) displacements at different points

9.6.7.8 Moment Distributions along X Direction in the Slab

From the simulation, the moments in the slab at any time can be also obtained. Of course, they vary with the weather conditions and time. Actually with the simulation performed, movie can be used to show the moments variations along with daily weather conditions.

To make the results presentation easier, the centers of all three slabs are chosen to show the moments variations with time. Fig. 9.28a shows the locations of the three points. Fig. 9.28b shows the moments variations in the x directions for the three points through the simulation. Fig. 9.28b can be more easily explained in combination with Fig. 9.26 and Fig. 9.27b. As can be seen in Fig. 9.26, at the start of the simulation, the slabs are placed on the ground soils. Because the soil surface is originally flat, the deflection of the slab are very small (Fig. 9.26) and there is no gap between the soil and the slab. As a consequence, the moments in the slabs are small and basically the same (Fig. 9.28b). As time goes on, the soils at the edge and the tree root zone lose water due to evapotranspiration. The water loss is different at different locations. The water loss at the edge of the building is greater than that in the center while the water loss at the tree root zone is greater than that at the other places. The differences in water loss cause differential movements of the soil underneath the building, which cause the moments increase in the slabs. The moments in the slabs depend on weather conditions, the severer the weather conditions, the greater the differential movements, the greater the deflections in the slabs and the greater the moments in the slabs. The maximum moments are seen on 10/08/1999 when there is the biggest gap between the soil and the slab. Compare Fig. 9.28b and 9.27b, we can see they match very well.

It can be seen that the maximum moments occur in slab II because slab I and slab II also contributes moments to it. The second largest moment is in slab II instead of in slab I. This conclusion, at the first glance, conflicts with all the currently available design methods. Fig. 9.29 shows the explanation of the above calculation results. Fig. 9.29 shows a slab with two concentrated loads applied on both ends. The left side of the slab loses support from soil and the soil is replaced by the reaction forces at the bottom of the slab. If the two concentrated loads are the same, the maximum moment in the slab will

not be at the center but some place in the right half of the slab. For slab I in the simulation, the corner close to the tree root zone has less support from the soils underneath. As a result, the moments in the slab are smaller than any other slabs.

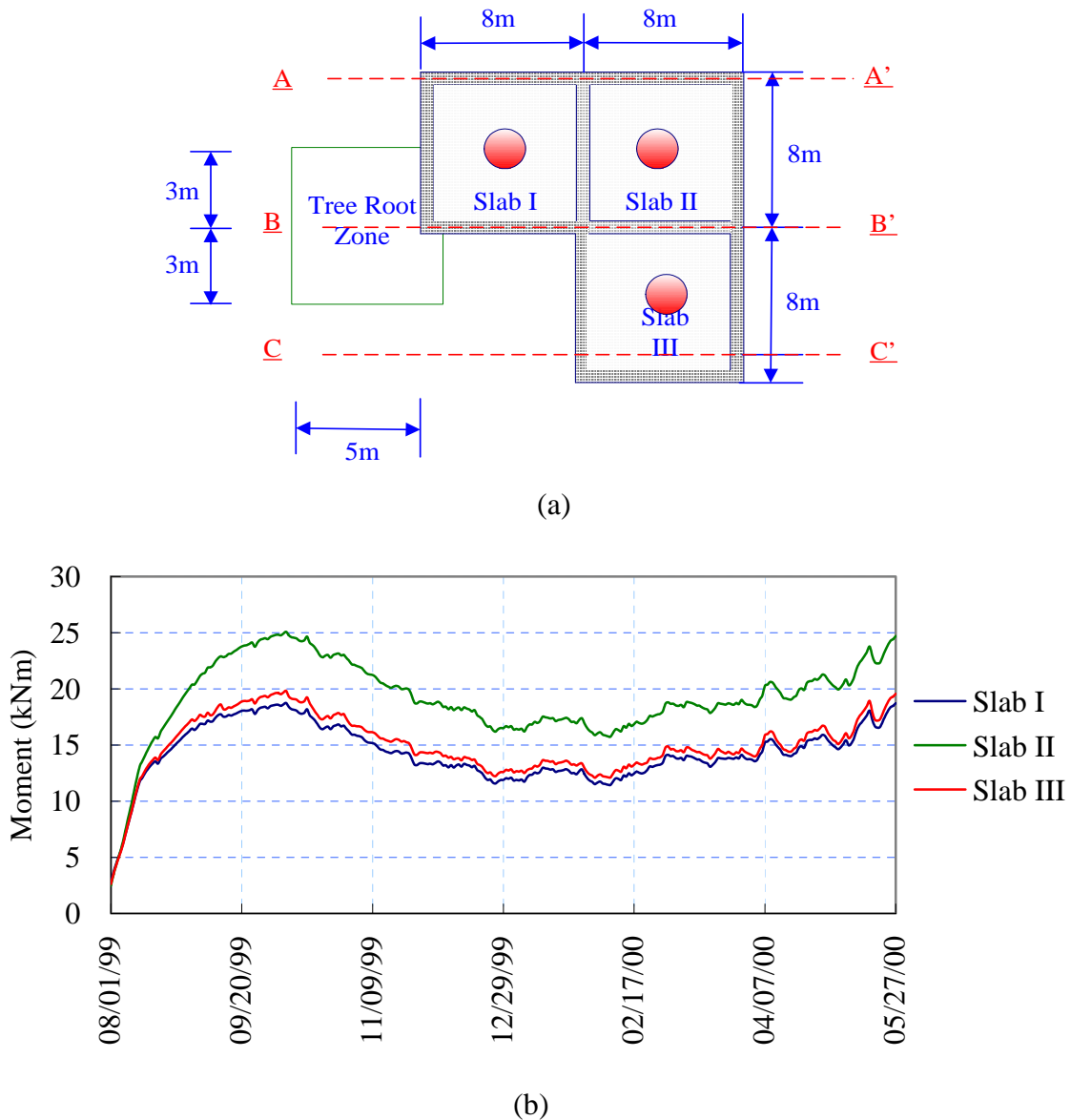


Fig. 9.28. Moments at three different locations at different times. (a) locations of the observation points; (b) moments at different locations

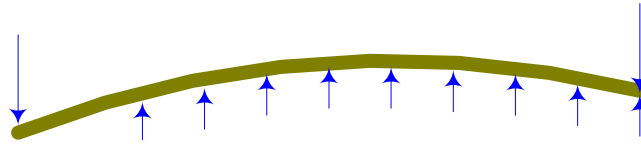


Fig. 9.29. A slab on the ground losing support from soils at the left side

All the currently available methods tacitly consider the most dangerous place is at the place where the slab loses support and the moment there is used as the maximum moment for design. The first half of the above assumption is right. However, the second half is incorrect. Before further discussion for this, more results about the moment distributions in the slabs are presented and discussed. The moment distributions in the slabs can be plotted as three dimensional surfaces. However, it is much easier to explain the results by using two dimensional plots. In the following discussions, both three dimensional moment surfaces and two dimensional moment curves are presented. Fig. 9.30 shows the locations where the moments are taken out and plotted as two dimensional curves. The B-B' profile have a coordinate of $y=0.0\text{m}$. The moments in slab I and slab II at different locations, $y=0.25\text{m}$, $y=2.25\text{m}$, $y=4.25\text{m}$, $y=6.25\text{m}$, and $y=7.25\text{m}$, are taken out for the following discussions.

Fig. 9.31a shows the moment distributions along x direction of slab I, slab II, and slab III at the start of simulation (08/01/1999). Fig. 9.31b shows the moment distributions along x direction in slab I and slab II at different profiles at the same time. It can be seen the maximum moments are in the center of the slab and the minimum moments are at the edge of the slab. The moment distribution are basically symmetric to the $x=0$ axis, indicating that slab III has little influence on the moment distributions along x direction of slab I and slab II. At the border of slab I and slab II, the moments are negative because of the weight of wall 4. The moments in all three slabs are small (less than 4 kN.m) because the slabs and the soils are in good contact and the differential movements are small at that time.

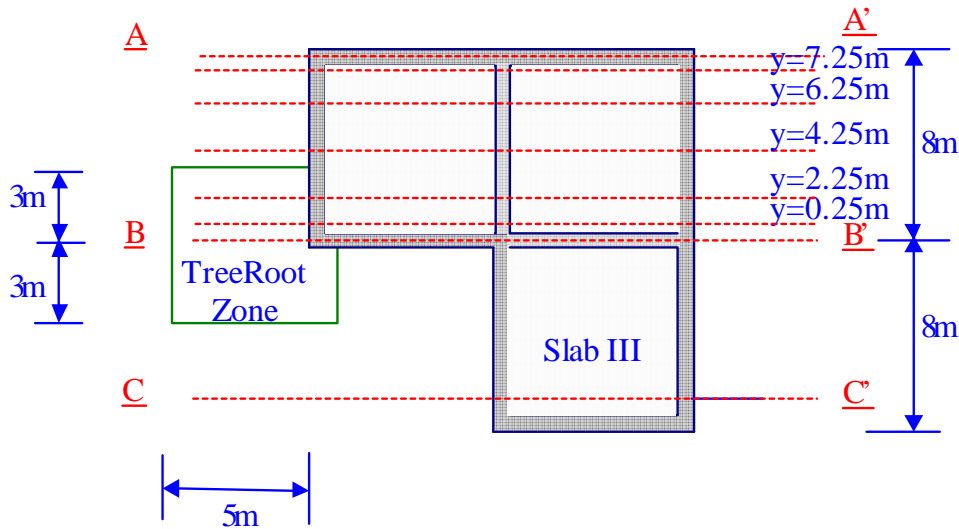


Fig. 9.30. Locations where the moments are presented

Fig. 9.32a shows the moment distributions along x direction of slab I, slab II, and slab III at the start of simulation (11/09/1999). Fig. 9.32b shows the moment distributions along x direction in slab I and slab II at different profiles at the same time. It can be seen that at $y=7.75\text{m}$ and $y=6.25$ where it is far way from the tree root zone and slab III, the moment distributions are approximately symmetric to the $x=0$ axis, indicating both the tree root zone and slab III have no influence in the moment distributions. At $y=0.25\text{m}$ and $y=2.25$ where it is close the tree root zone, the moments in slab I are smaller than their counterpart in slab II because the soils at the corner of the tree root zone provide less support to the slab. The condition is similar to what has been shown in the Fig. 9.29. The maximum moment in slab I moves to the point $(x=-1.75, y=-4.25)$, a position far away from the tree root zone diagonally from the center of the slab. The reason for this is because of the less support provided by the soil in the corner of the tree root zone. The maximum moment in slab II moves to the point $(x=2.25, y=2.25)$ because slab II is influenced by slab I, slab III and the tree root zone.

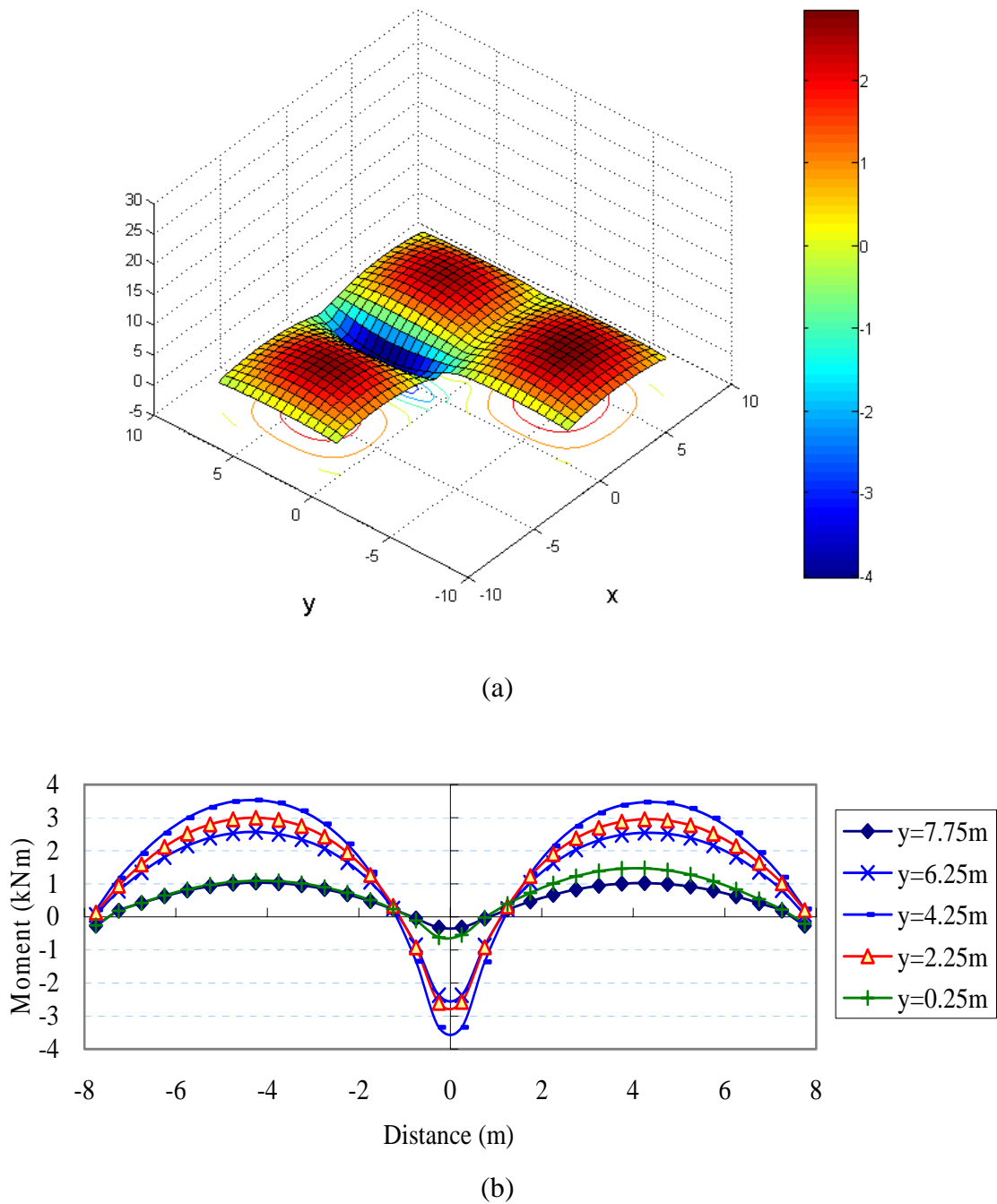
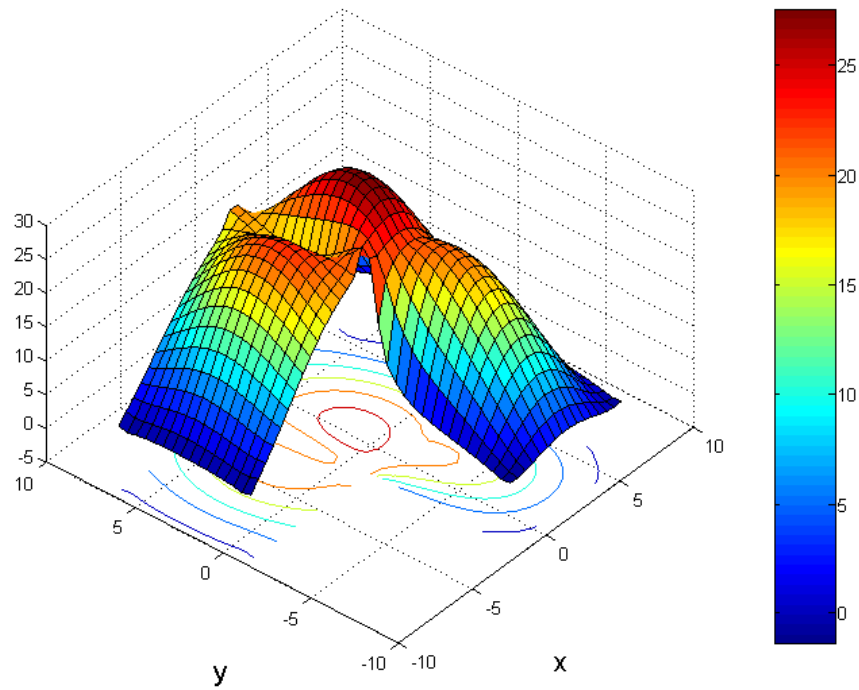
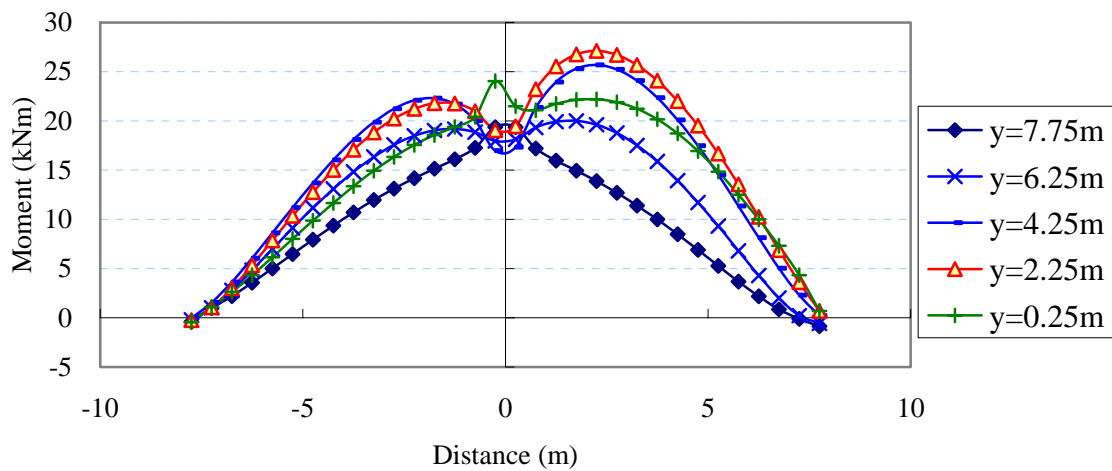


Fig. 9.31. Slab moments along the x direction at the 1st day (08/01/1999) for a center lift case. (a) three dimensional moment distributions; (b) two dimensional moment distributions



(a)



(b)

Fig. 9.32. Slab moments along the x direction at the 101st day (11/09/1999) for a center lift case. (a) three dimensional moment distributions; (b) two dimensional moment distributions

Because of the weight of wall 4, the moment at the border of slab I and slab II drops. The maximum drop is seen approximately at the center of the wall 4 ($x=0$, $y=4.25$) as shown in Fig. 9.32b. Fig. 9.33 and Fig. 9.34 show the moment distributions in the slabs at the 201st and 301st day, respectively. Similar conclusions can be reached. Fig. 9.35 shows the moment distributions at different times at the locations of $x=0.25\text{m}$, $x=4.25\text{ m}$, and $x=7.25\text{m}$, respectively. Fig. 9.36 shows the maximum and the minimum moment in the slabs during the period from 08/01/1999 to 05/27/2000.

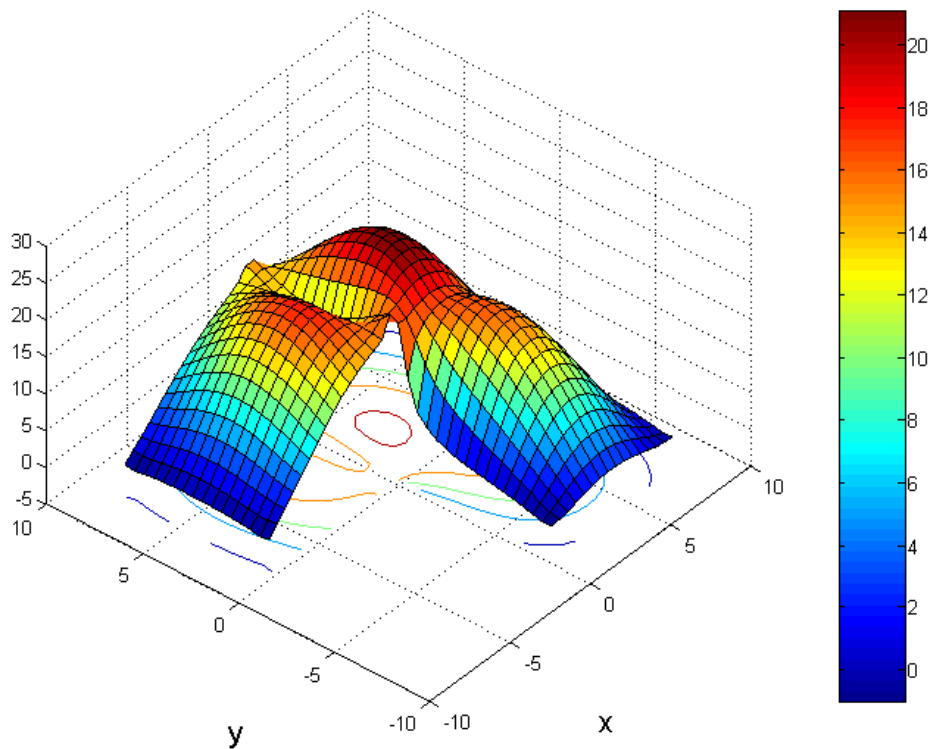


Fig. 9.33. Slab moments along the x direction at the 201st day (02/17/2000) for a center lift case. (a) three dimensional moment distributions

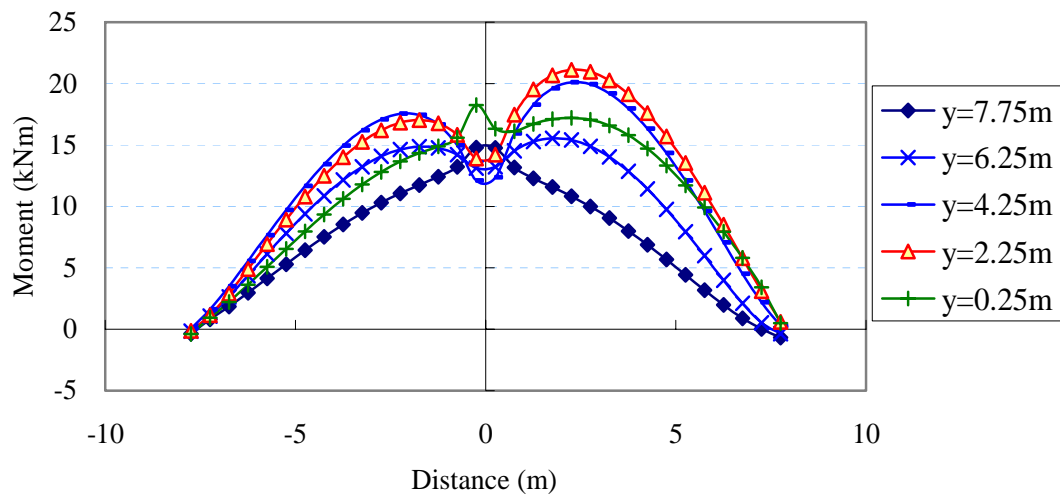


Fig. 9.33. (Continued) (b) two dimensional moment distributions

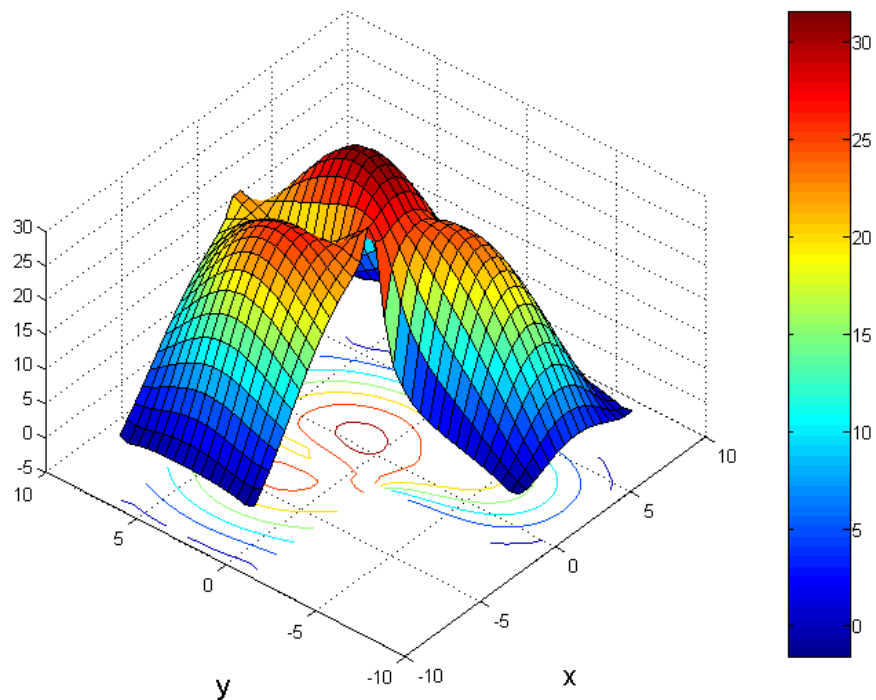


Fig. 9.34. Slab moments along the x direction at the 301st day (05/27/2000) for a center lift case. (a) three dimensional moment distributions

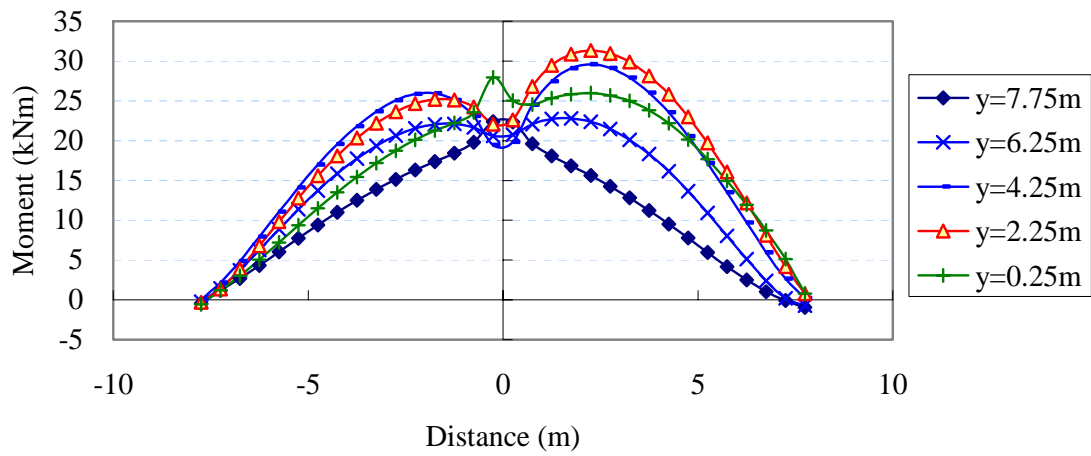
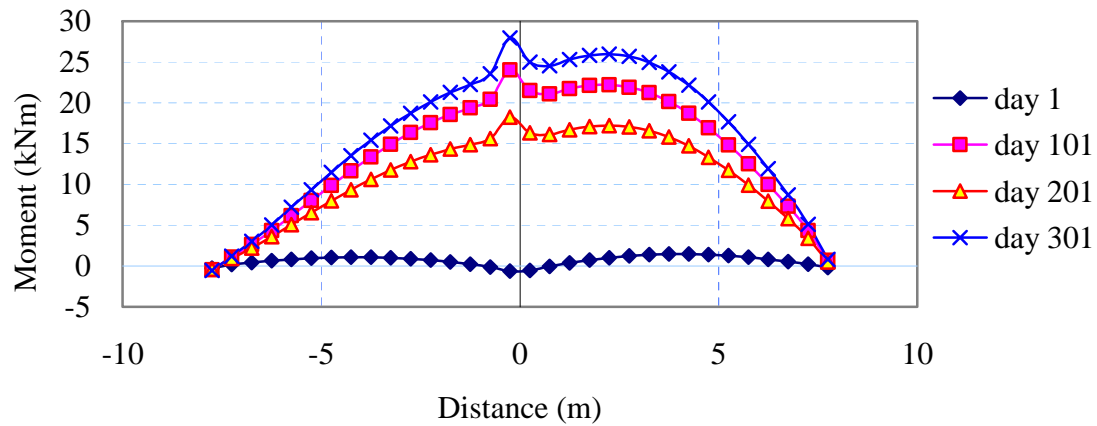
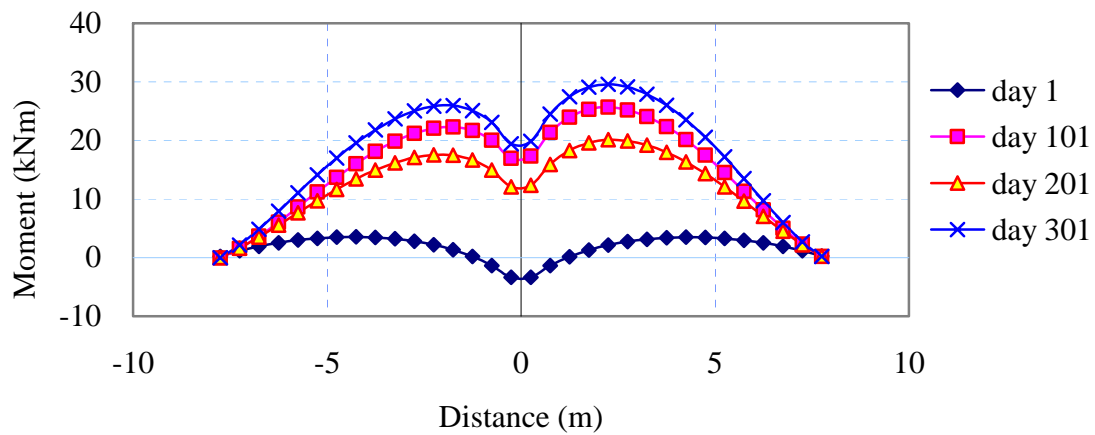


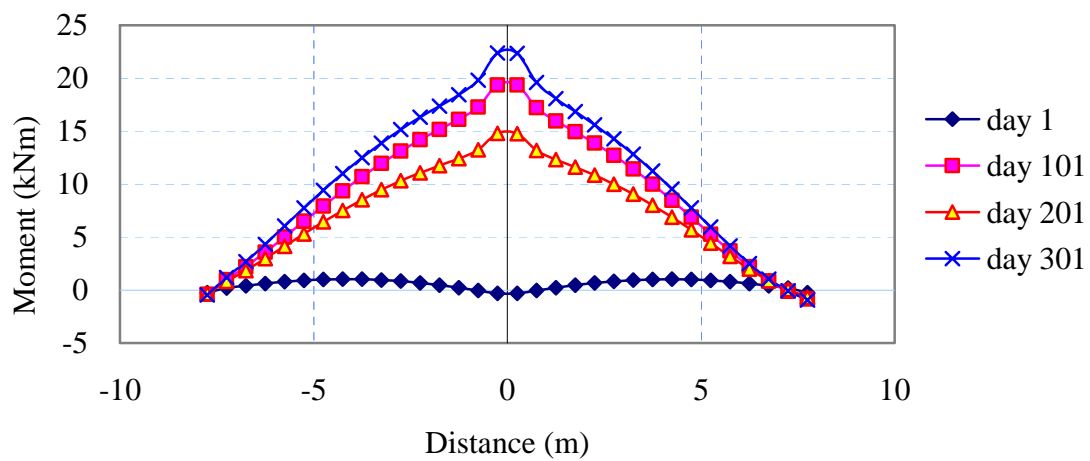
Fig. 9.34. (Continued) (b) two dimensional moment distributions



9.35. Slab moments along the x direction at the different locations and times for a center lift case. (a) moments at $x=0.25\text{m}$



(b)



(c)

Fig. 9.35. (Continued) (b) moments at $x=4.25\text{m}$; (c) moments at $x=7.25\text{m}$

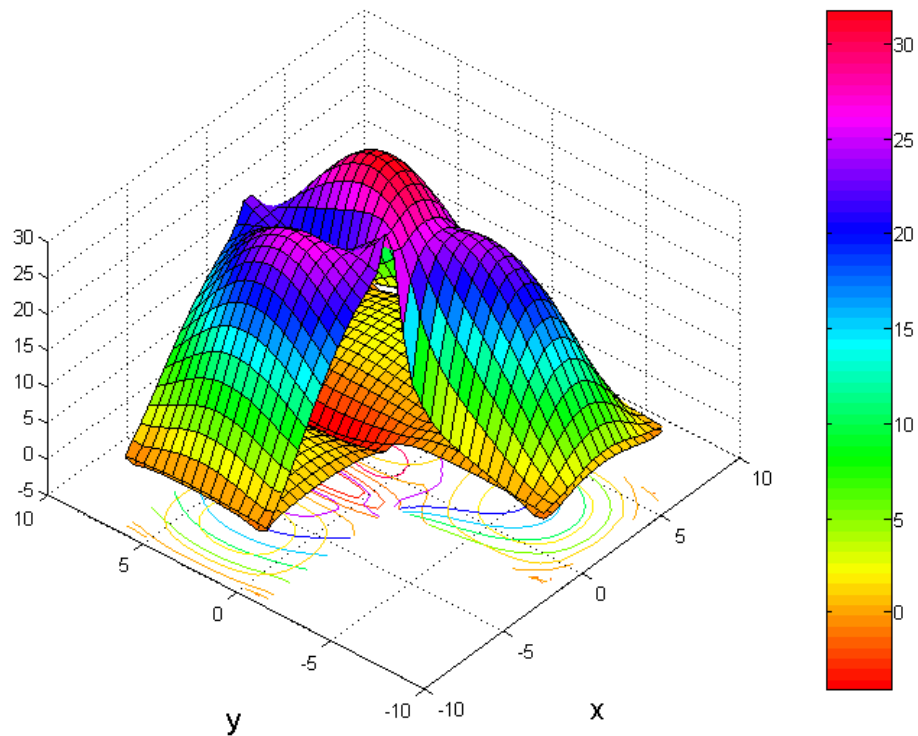


Fig. 9.36. Maximum and minimum slab moments along the x direction in 300 days for a center lift case

9.6.7.9 Moment Distributions along y Direction in the Slab

The moment distributions along y direction at the 1st day, the 101st day, the 201st day and the 301st day are shown in the Fig.s from 9.37 to 9.40. The maximum and minimum moments during this period is shown in Fig. 9.41.

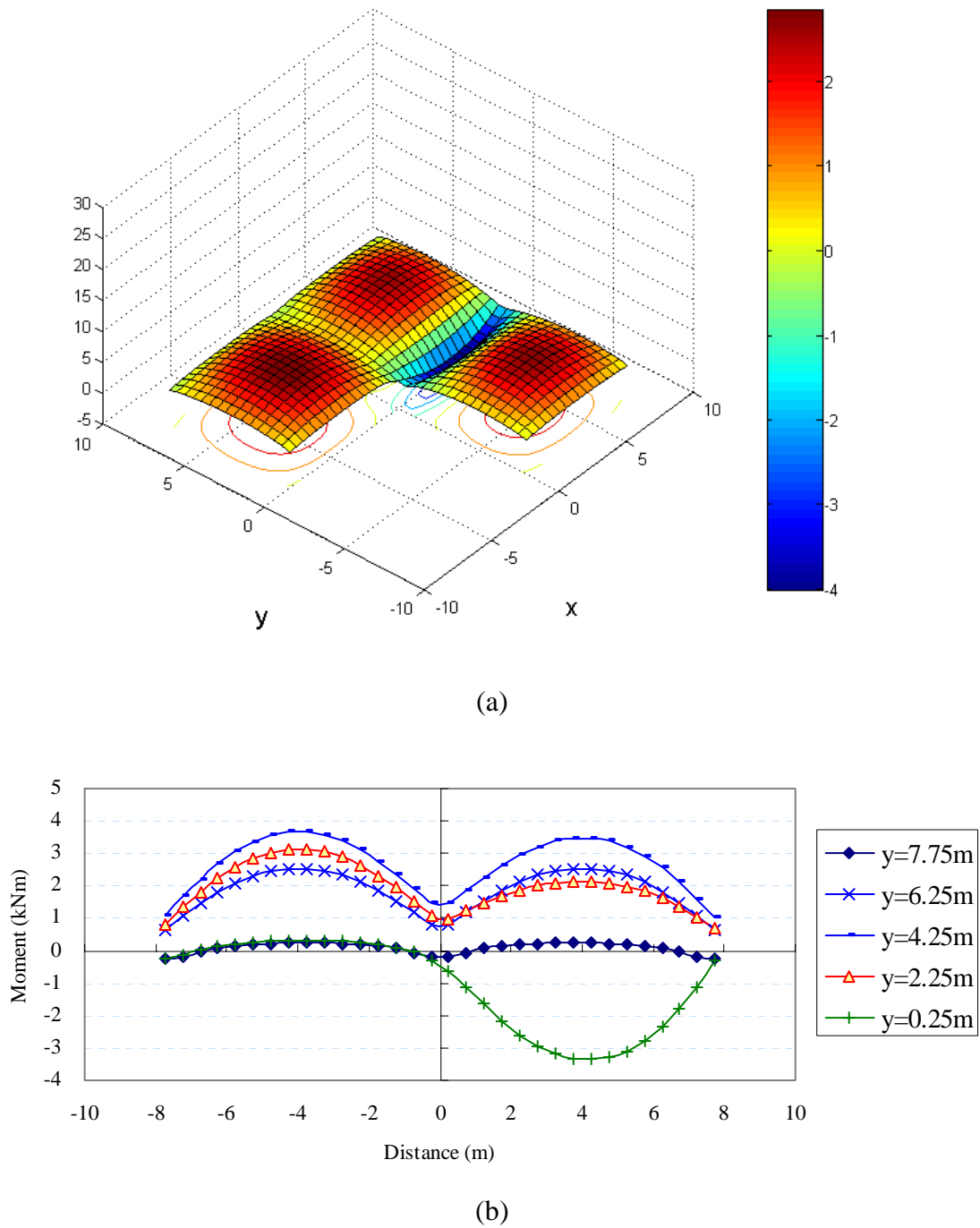


Fig. 9.37. Slab moments along the y direction at the 1st day for a center lift case. (a) three dimensional moment distributions; (b) two dimensional moment distributions

Fig. 9.37a shows the moment distributions along y direction of slab I, slab II, and slab III at the start of simulation (11/09/1999). Fig. 9.37b shows the moment distributions along x direction in slab I and slab II at different profiles at the same time. The moments in all three slabs are small because the soil conditions are the same at all places, the slabs and soils are in good contact, and the deflections in the slabs are small. It can be seen that the moment distributions are approximately symmetric to the $x=0$ axis at all locations except that at $y=0.25\text{m}$, indicating that slab III has no influence in the moment distributions along y direction at the locations far away from the slab III. The moments at $y=0.25\text{m}$ and close to the border of slab II and slab III changes dramatically to negative, mainly because of the weight of wall 7. However, the influence of the wall 7 is limited in a small range.

From Fig. 9.37 to 9.40, it can be seen that as time goes on, the soils at the edge of the slabs lose water due to evaporation and shrinks, which provide less or no support to the slabs at the same locations, depending whether there is a tree or not or whether the weather is severe enough. As a result, the moments in the center of the slabs increase. The soils in the tree root zone can provide less support to the slab, which cause the moments along y direction in slab I is smaller than those in slab II. From Fig. 9.38b, it can be seen that at locations far away from the tree root zone and slab III such as the profiles of $y=6.25\text{m}$ and $y=7.75\text{m}$, the moment distributions in slab I and slab II are symmetric. For the profiles $y=2.25\text{m}$ and $y=4.25\text{m}$ where the moment distributions are not influenced by slab III as shown in Fig. 9.37b, the moment distributions are not symmetric any more. The moments in slab I are smaller than those in slab II. A reasonable explanation for this is that due to the existence of the tree, the soils at that zone can provide less or no support to the slab. As a result, the moments near the tree root zone are smaller than any other places. The moment distribution at the profile $y=0.25\text{m}$ is greatly different from that in Fig. 9.37b. It can be seen from Fig. 9.38b that the moment of slab II at the profile $y=0.25\text{m}$ is much bigger than its counterpart in slab I. the only explanation fro this is that the bigger moment in slab II at that profile is caused

by slab III. Due to the weight of wall 7, the moment of slab II at the profile $y=0.25\text{m}$ drops a little bit. The same phenomena can be seen from Fig. 9.39 and 9.40.

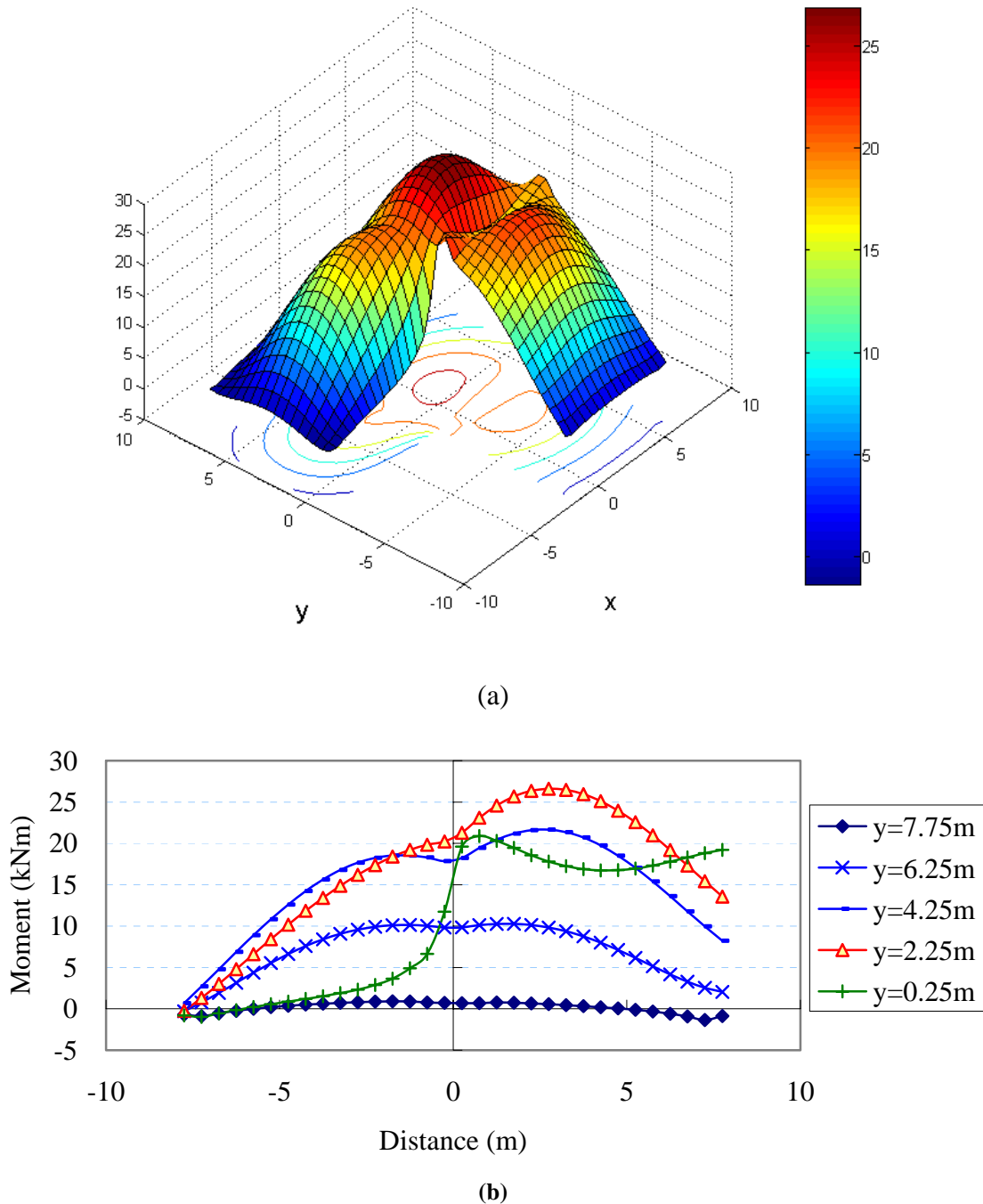


Fig. 9.38. Slab moments along the y direction at the 101st day for a center lift case. (a) three dimensional moment distributions; (b) two dimensional moment distributions

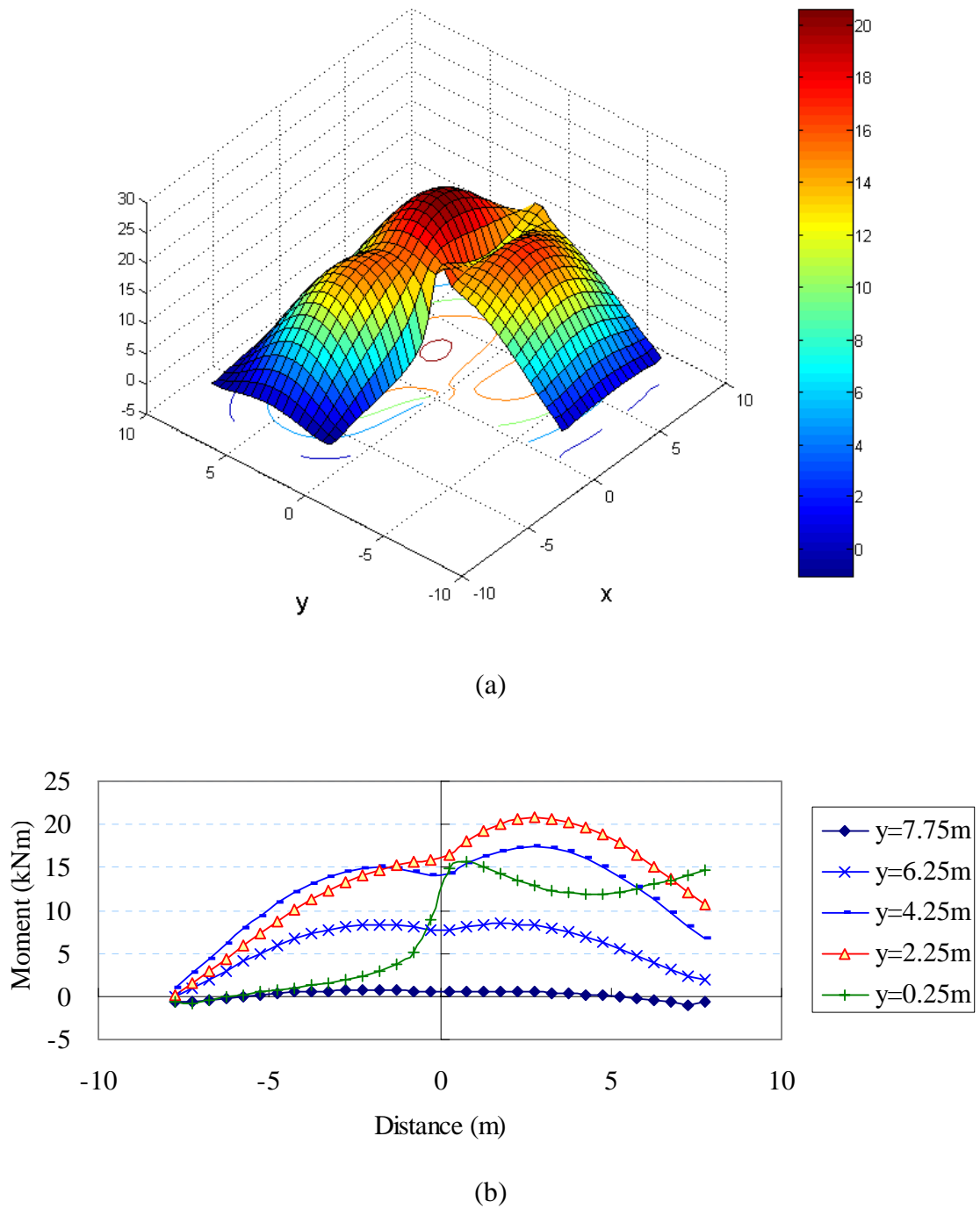


Fig. 9.39. Slab moments along the y direction at the 201st day for a center lift case. (a) three dimensional moment distributions; (b) two dimensional moment distributions

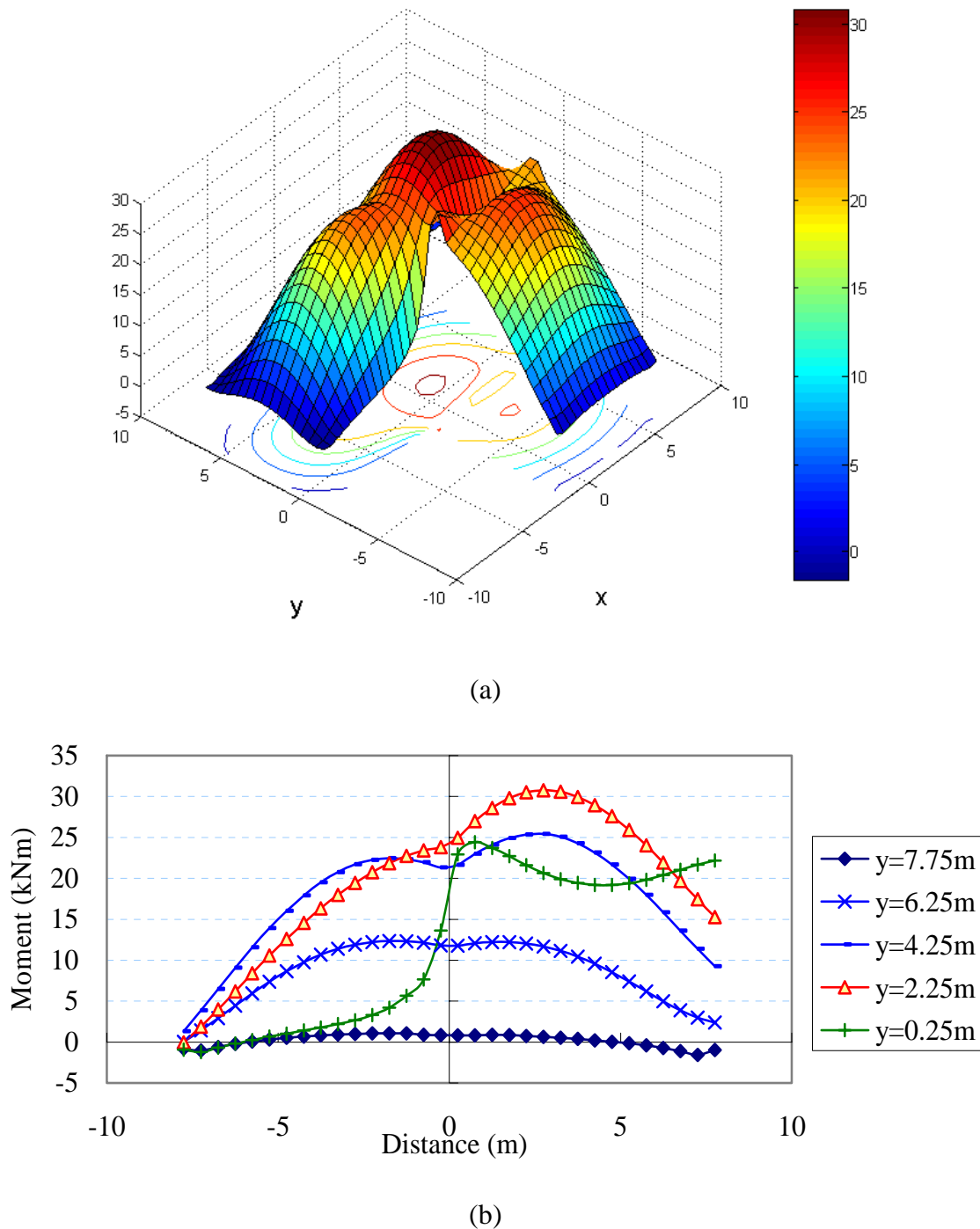


Fig. 9.40. Slab moments along the y direction at the 301st day for a center lift case. (a) three dimensional moment distributions; (b) two dimensional moment distributions

The maximum and the minimum moments in the slabs during the period can also be obtained by comparing the moment distributions for each day, which is shown in Fig. 9.41. Fig. 9.41 is actually the upper and lower envelopes of the moment in the slabs in 300 days.

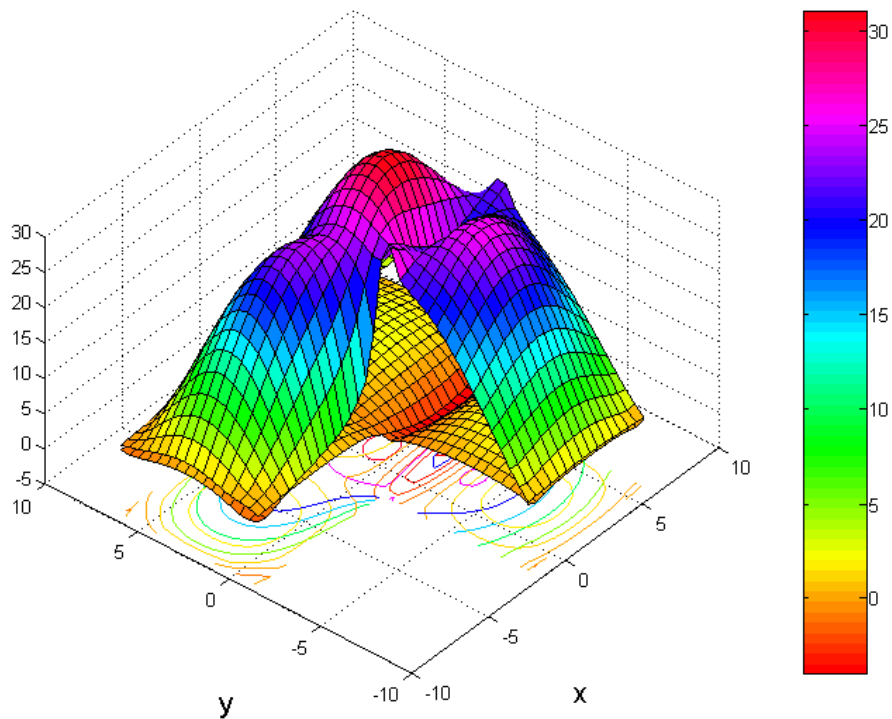


Fig. 9.41. Maximum and minimum slab moments along the y direction in 300 days for a center lift case

9.6.7.10 Stresses in the Structure

Fig. 9.42 shows the Von Mises stresses in the whole simulated domain. The definition of the Von Mises stress is,

$$\begin{aligned}
 q &= \sqrt{\frac{3}{2} S : S} \\
 &= \frac{1}{\sqrt{2}} \sqrt{(\sigma_1 - \sigma_2)^2 + (\sigma_1 - \sigma_3)^2 + (\sigma_2 - \sigma_3)^2}
 \end{aligned}
 \tag{9.70}$$

where q = the Mises equivalent stress; S = the deviatoric stress, defined as $S = \sigma + pI$; and $\sigma_1, \sigma_2, \sigma_3$ = the major, medium and minor principal stresses, respectively.

As we can see from the Fig. 9.42, the maximum von Mises stresses occur in wall 6 and wall 7, close to the top joint formed wall 4, wall 6, wall 7 and wall 8. Some other places such as the joints formed by the wall 1 and wall 2, wall 5 and wall 9, and wall 4 and wall 8 also have higher von Mises stresses. The higher von Mises stresses are always at the top of the walls. The von Mises stresses in the slabs are not as severe as those in the walls.

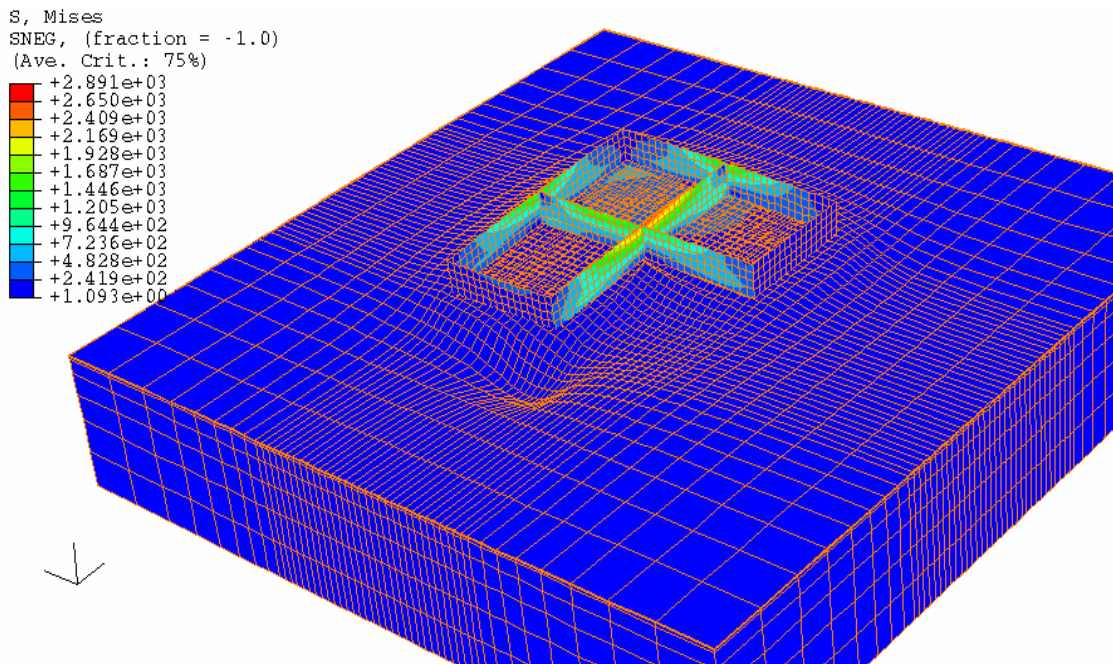


Fig. 9.42. Shear stresses between the soils and the slab at the 301st day for an edge lift case.

Von Mises stress is a stress-invariant used in yield criteria. It is calculated independent of the coordinate reference frame and it does not carry directional stress information, such as normal and shear stresses, but carries enough to identify hot-spots where failure might occur. The von Mises conditions are used to define some failure

criterion. If the walls and the slabs have the same material properties, the walls which have the higher von Mises stresses may crack firstly before any damage occurs in the slabs where the von Mises stresses are smaller. As a consequence, a question arises: what should be used for criterion of the slab design, the failure of the walls or the failure of the slabs? The answer should be the former because we need design a safe building without cracks in the wall. However, all the current design methods only consider the cracking in the slab without considering the cracking in the walls. It may mistakenly cause unsafe designs.

9.6.8 An Example for Edge Lift Case

9.6.8.1 Introduction

The tree is planted at the corner formed by the wall 6 and wall 8 of the building as shown in Fig. 9.42. The tree root zone is below the grass root zone. The coordinate of the tree root zone is: from 1m to -5m in x and y axis and from 4.23m to 5.53m in z axis. The plane view of the simulation domain is shown in Fig. 9.43a and the profiles at different locations A-A', B-B', and C-C' in Fig. 9.43a are shown in Fig. 9.43b, c and d, respectively.

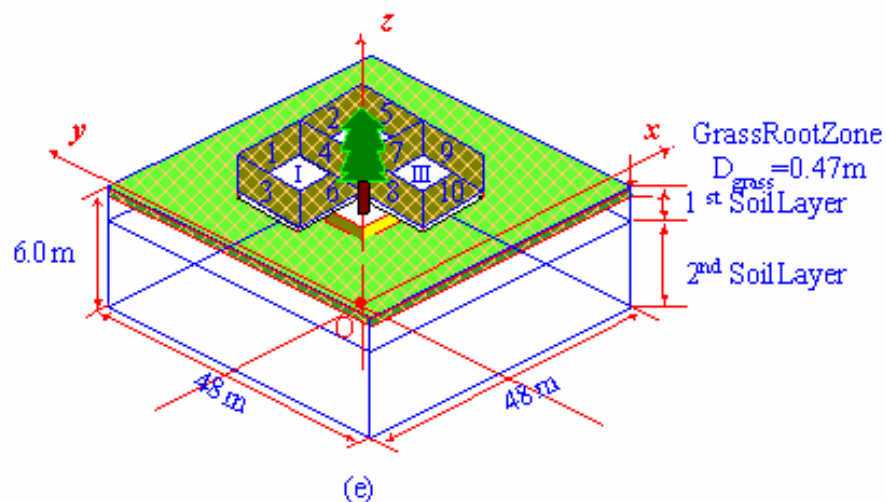


Fig. 9.42. An example when there is a tree at the corner of the house

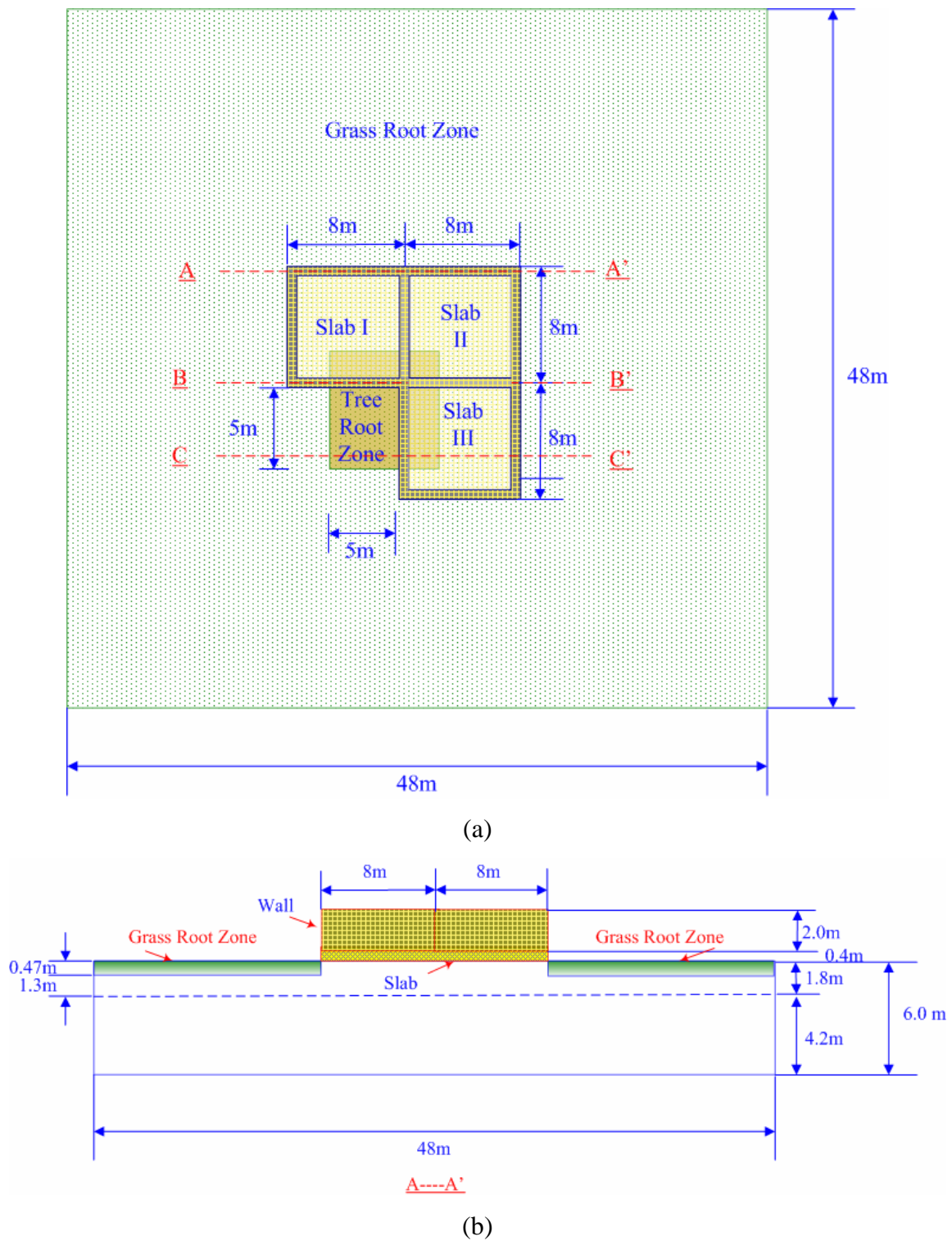


Fig. 9.43. An example when there is a tree at the edge of the house. (a) view from the top; (b) A-A' profile

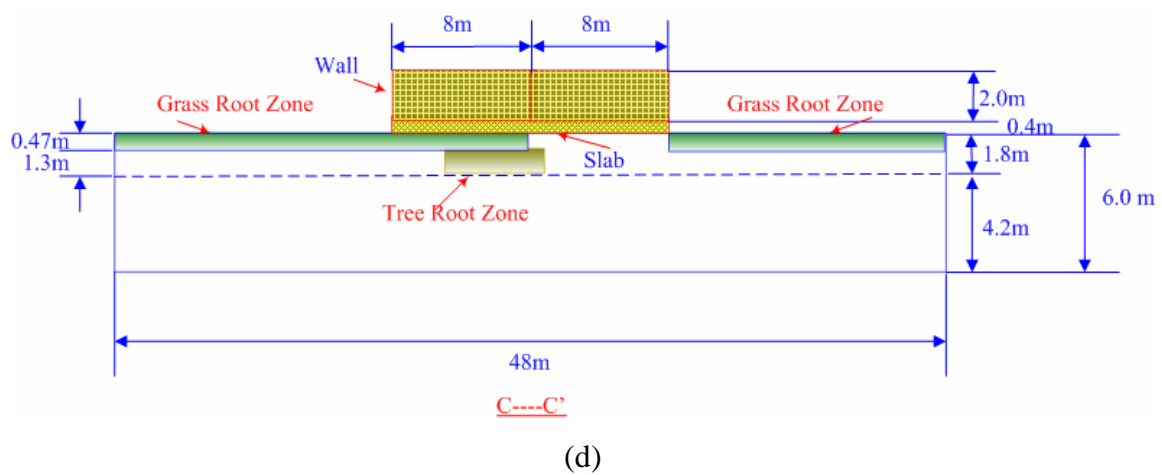
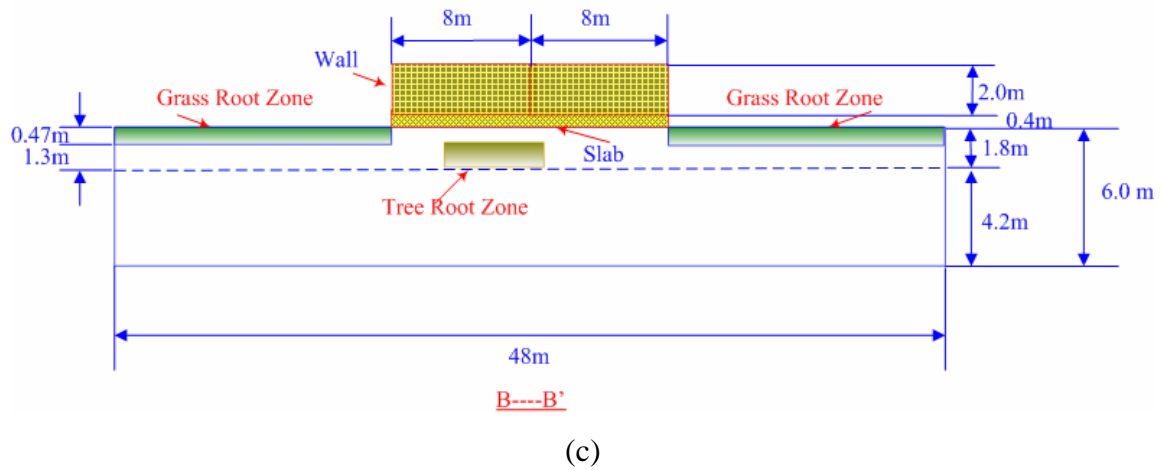


Fig. 9.43. (Continued) (c) B-B' profile; (d) C-C' profile

9.6.8.2 Suction Distributions

Fig. 9.44 shows the matric suction distributions for the simulated domain at the 301st days. It can be seen that the matric suction at the ground soil surface is higher than that at certain depth and the matric suction underneath the slab is lower than that outside of the slab because the slabs prevent the soils underneath from losing water. The suction value in the tree root zone is much higher than the other places because the tree root can absorb water from the soil more easily.

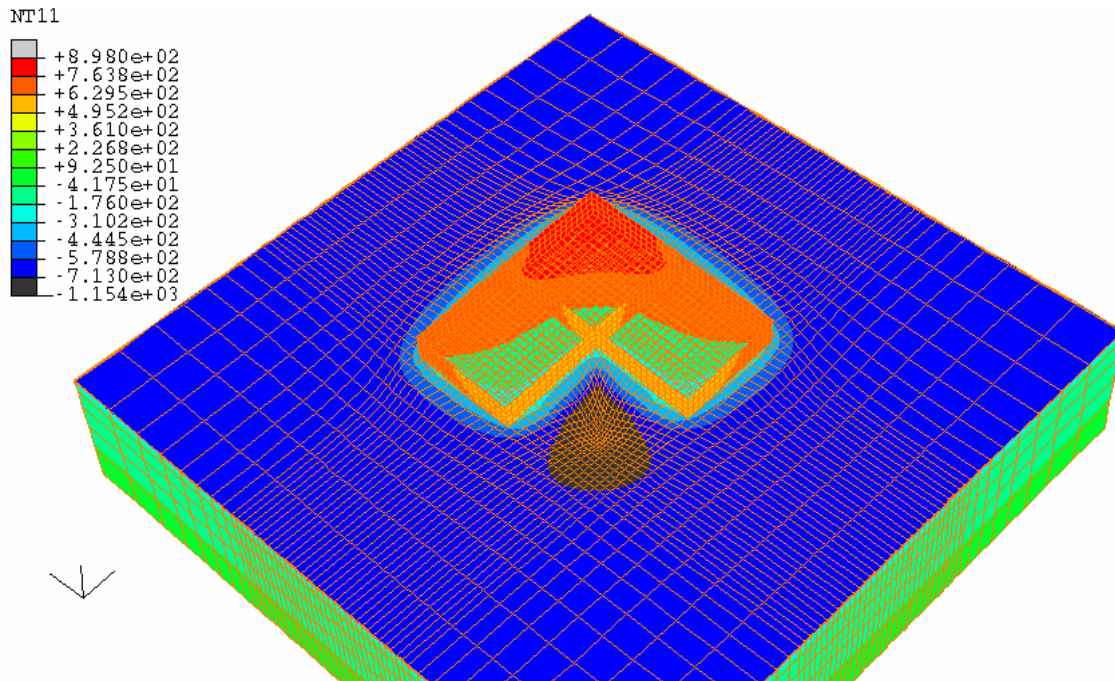


Fig. 9.44. Suction distributions at the 301st day for an edge lift case

9.6.8.3 Deformations

Fig. 9.45 shows the deformations of the whole simulated domain at the 301st day. As can be seen, the soils underneath the slab have a higher elevation than the soils outside of the slab due to the lower suction values underneath the slab. The settlement at the center of the tree root zone is higher than any other place due to the higher suction value caused by the tree root. A sink pit is formed close to the corner formed by the wall 6 and wall 8. At the place far from the building, at the soil deformation is the same, indicating the influence of the tree and the slabs are limited in certain range.

9.6.8.4 Openings between the Soils and the Slabs

The shrinkage caused by the tree root zone can be large enough to cause gaps between the slabs and the ground soils. Fig. 9.46 shows there are two gaps between the soil and the slab at the corner of the slab at the 301st day, one is under the wall 6 and the other is under the wall 8, which are consistent with the position of the tree root zone.

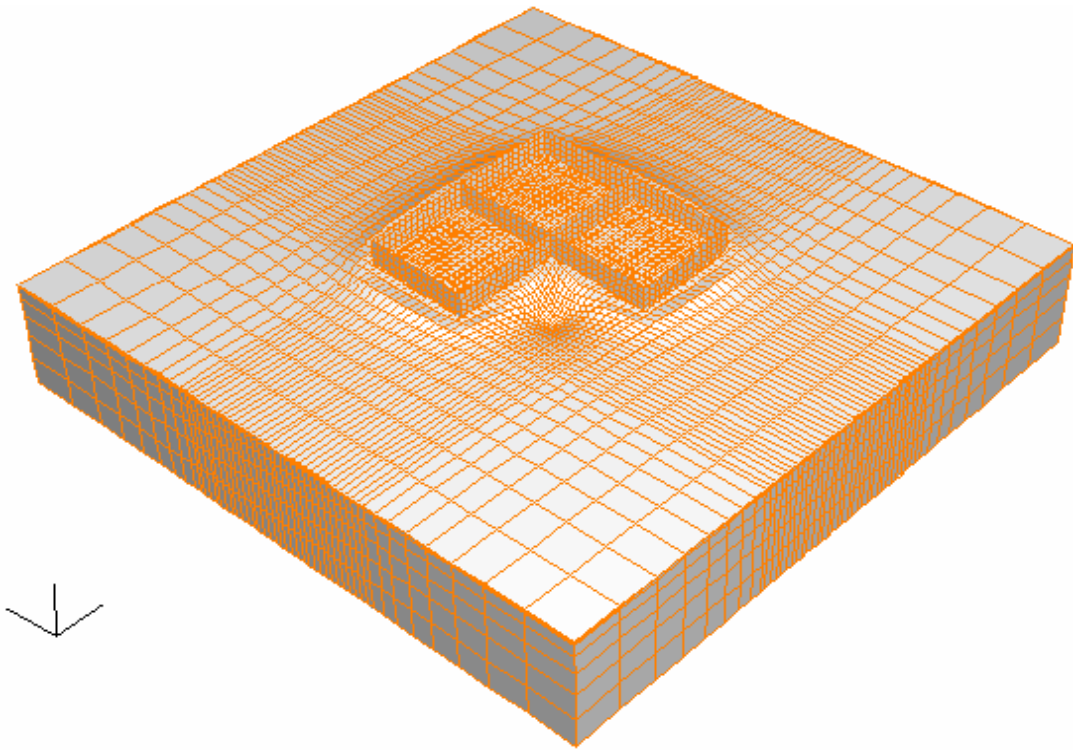


Fig. 9.45. Deformations at the 301st day for an edge lift case

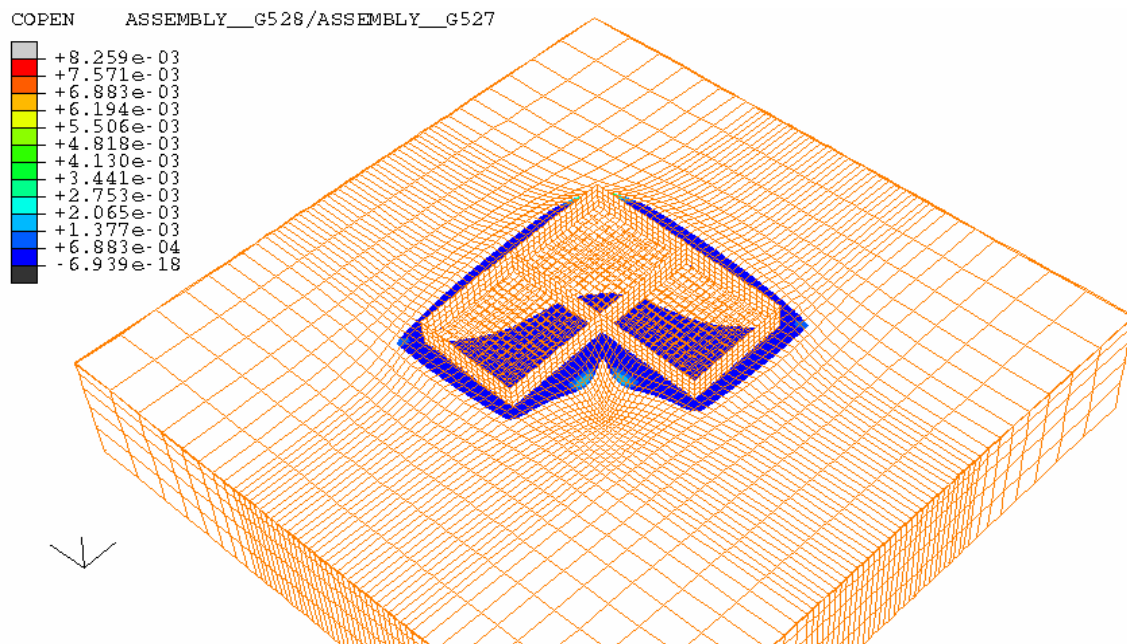


Fig. 9.46. Openings between the soils and the slab at the 301st day for an edge lift case

9.6.8.5 Contact Pressures

Fig. 9.47 indicates that at the 301st day, when the weather is dry, the contact pressures at the edge of the slabs are smaller than those in the center of the slabs. This situation is caused by shrinkage at the edge of the house. When there is shrinkage at the edge of the house, the soils at the edge have less support to the slab. As a consequence, the soils underneath the center of the slab give more support to the slab and the reaction forces from the soils are higher. It can also be found that the reaction force of the soils at the corner where the tree is planted is lower than other places. Compare Fig. 9.46 and 9.47, it can be found at the edge where the slabs lose support, the reaction forces are zero. The soil and the slab are in contact with each other except the edges underneath the tree root zone. However, the reaction forces are different at different locations. At the center of the slab, the reaction forces are higher than those close to the edge.

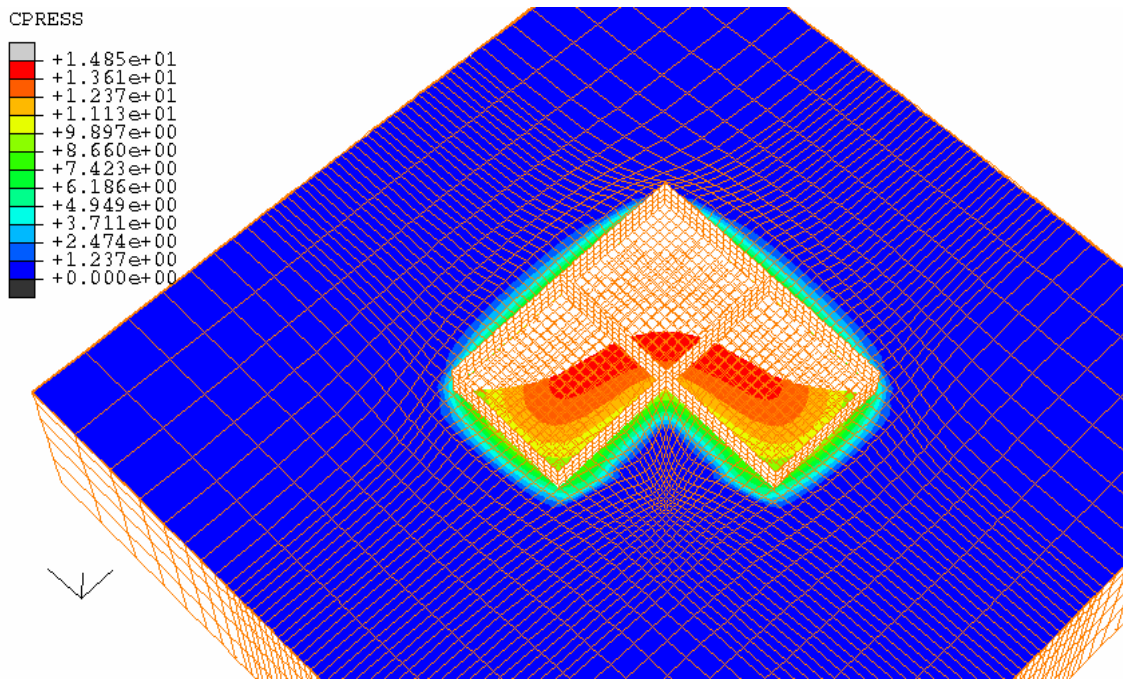


Fig. 9.47. Contact pressure between the soils and the slab at the 301st day for an edge lift case

9.6.8.6 Slips and the Shear Forces between the Soil and the Slabs

The structure is not symmetric, which causes the building tends to slip. Fig. 9.48 shows the accumulated slips of the soil surface (CSLIP) along x direction between the slab and the soil at the soil-slab interface at the 301st day. Underneath the wall 3 and wall 8, the accumulated slips are negative while the underneath the wall 5 and wall 9 the accumulated slips are positive, indicating the soil is moving outwards from the center of the slab due to the soil shrinkage. It can also be seen that the slips of the soils underneath the wall 8 is much bigger than any other place because the tree root zone causes more shrinkage of the soils. The center of the slab is sticking with the soils and the relative slips are very small (light green stands for zero slip).

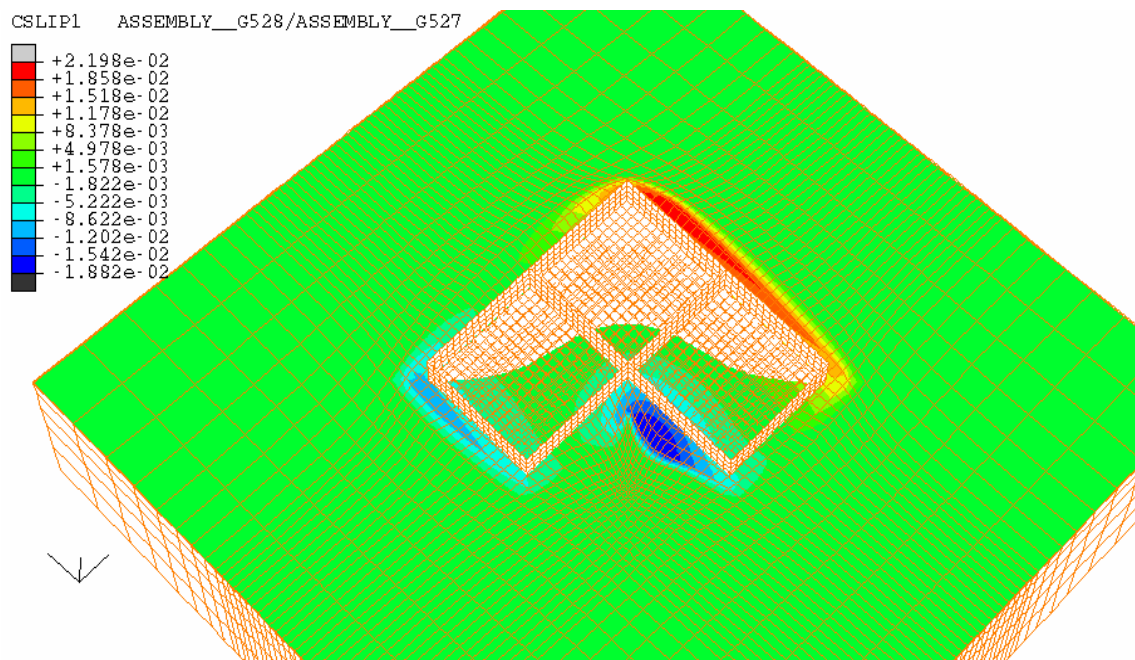


Fig. 9.48. Slips between the soils and the slab at the 301st day for an edge lift case

The shear stresses between the slab and the soil at the soil-slab interface along the x direction are shown in Fig. 9.49. The maximum shear stresses along x direction are found underneath the wall 8 where the maximum relative slips occur. The shear stresses

underneath the edge of the slab, where there are larger slips, are higher than those at the center of the slab. The shear stresses at the center of the slab are close to zero. The results for relative slips and shear stresses are consistent with each other.

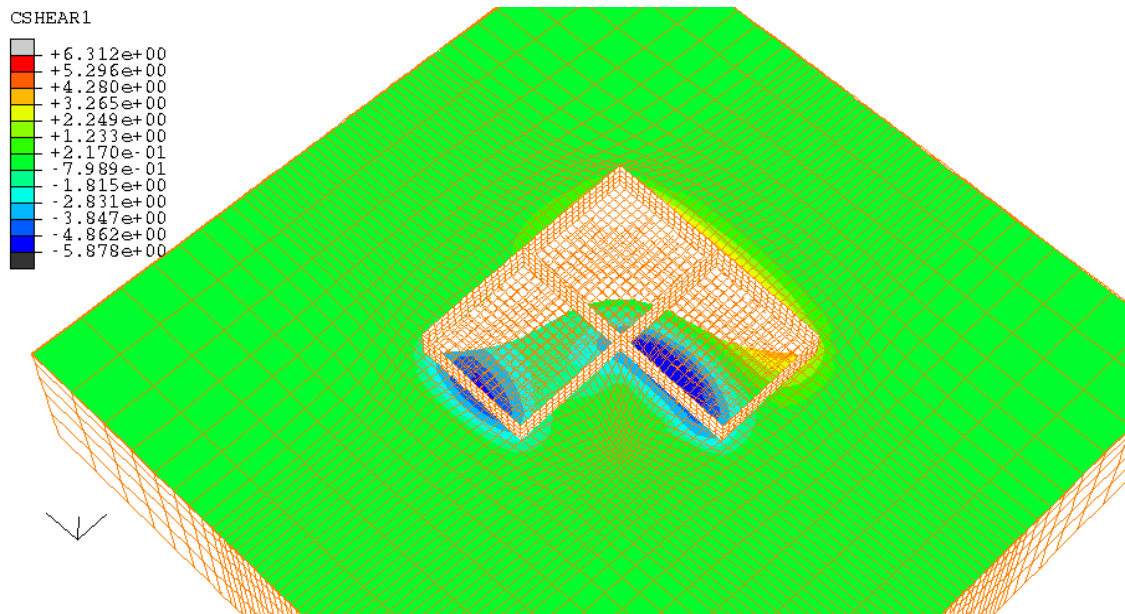


Fig. 9.49. Shear stresses between the soils and the slab at the 301st day for an edge lift case

9.6.8.7 Deflections of the Slab

The shapes of the ground soil surface and the slab along the B-B' profile at 101st day, 201st day and 301st day are shown in Fig. 9.50. Due to the weight of the walls at the edge, the slabs deflect downward at any time even when the soil goes up at the 101st day and 201st day. At the 301st day, the weather is very dry and the soils shrink. Due to the existence of the tree, the soil and the slab separate at the corner. Compare Fig. 9.26 and Fig. 9.50, it can be seen that, when the tree is planted at the corner former by wall 3 and wall 6, the maximum gap between the slab and the ground soil surface is greater than that when the tree is planted at the corner formed by the wall 6 and wall 8. The reasons are two-folds. The first reason is, the former corner is influenced by both the tree root

zone and the grass root zone from three zones while the later corner is influenced by grass root zone from only one zone (all the other three zones are covered by slabs). The second reason is, the loads at these two locations are different. At the later corner, the load is bigger than that at the former one. The load is sustained by the soil nearby, and cause more displacement.

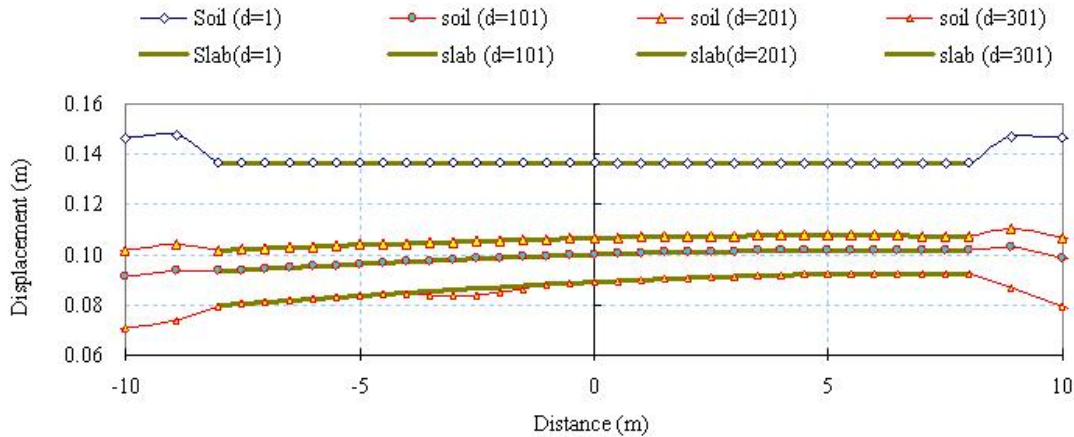


Fig. 9.50. Displacements of the ground soils and the slab along the B-B' at different times for an edge lift case

9.6.8.8 Moment Distributions along x Direction in the Slab

From the simulation, the moments in the slab at any time can be obtained. Of course, they vary with the weather condition and time. Fig. 9.51, 9.52, 9.53 and 9.54 show the moments in the x direction at the 1st day, 101st day, 201st day and 301st day, respectively. The maximum and the minimum moments in the slabs in 350 days are shown in Fig. 9.55. It can be seen that the moments at the center of the slabs are higher than those at the edges. The maximum moment for the three slabs occurs at the center of slab II, which indicating the loads applied on slab I and slab III also have influences on the moment in slab II. The moments at the borders two of the three slabs are smaller than the moments in the center of the slab, indicating that the load distributions influence the moment distributions greatly.

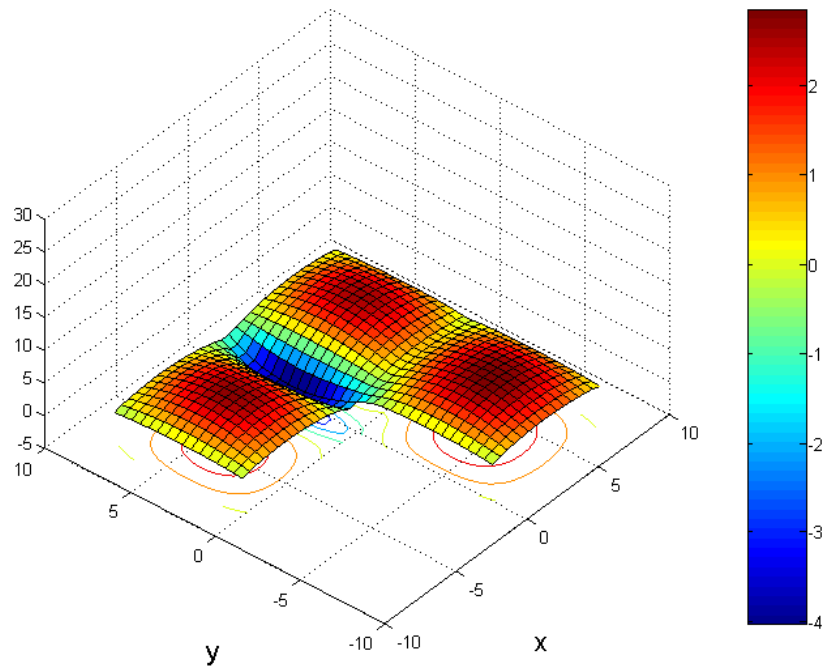


Fig. 9.51. Slab moments along the x direction at the 1st day for an edge lift case

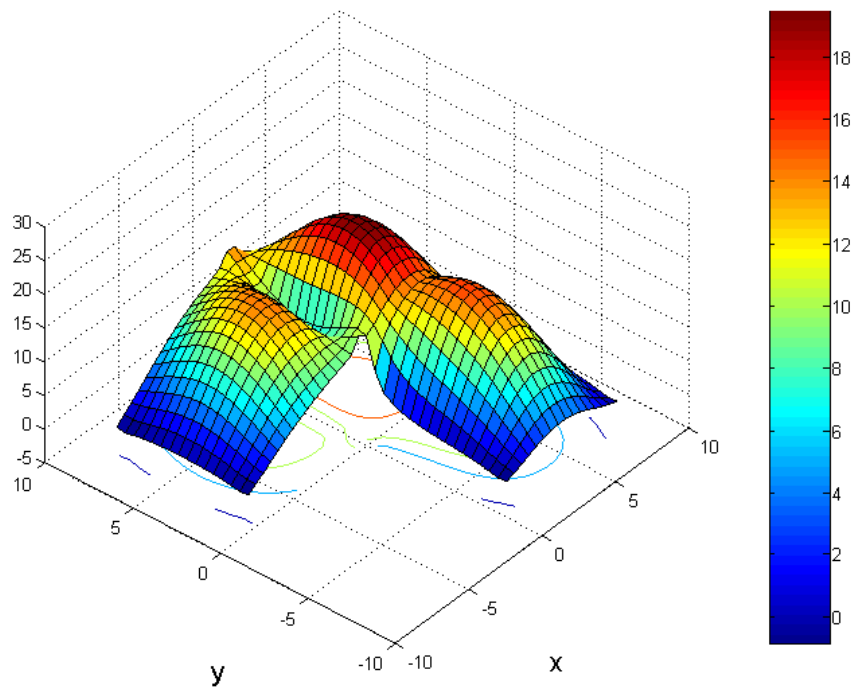


Fig. 9.52. Slab moments along the x direction at the 101st day for an edge lift case

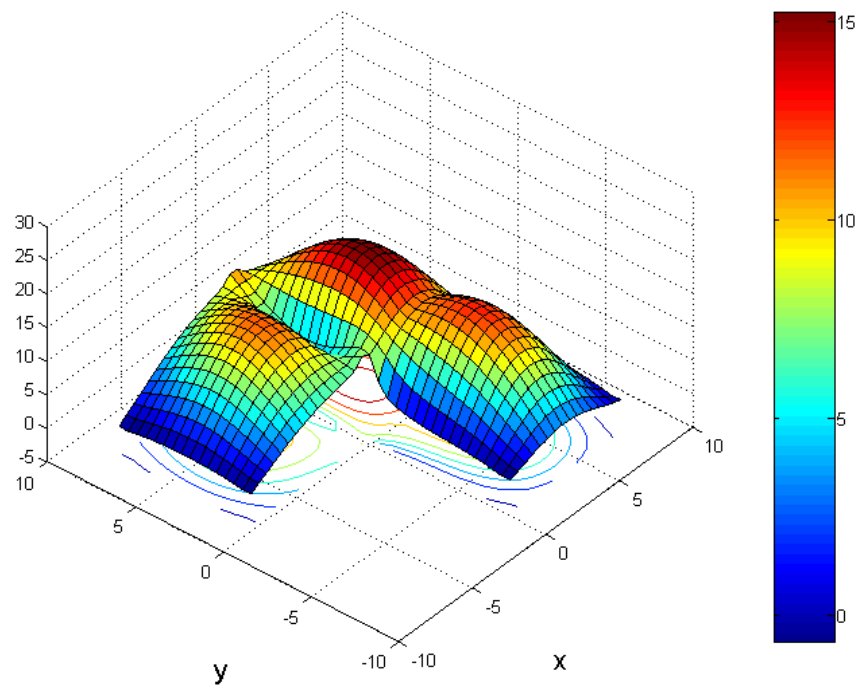


Fig. 9.53. Slab moments along the x direction at the 201st day for an edge lift case

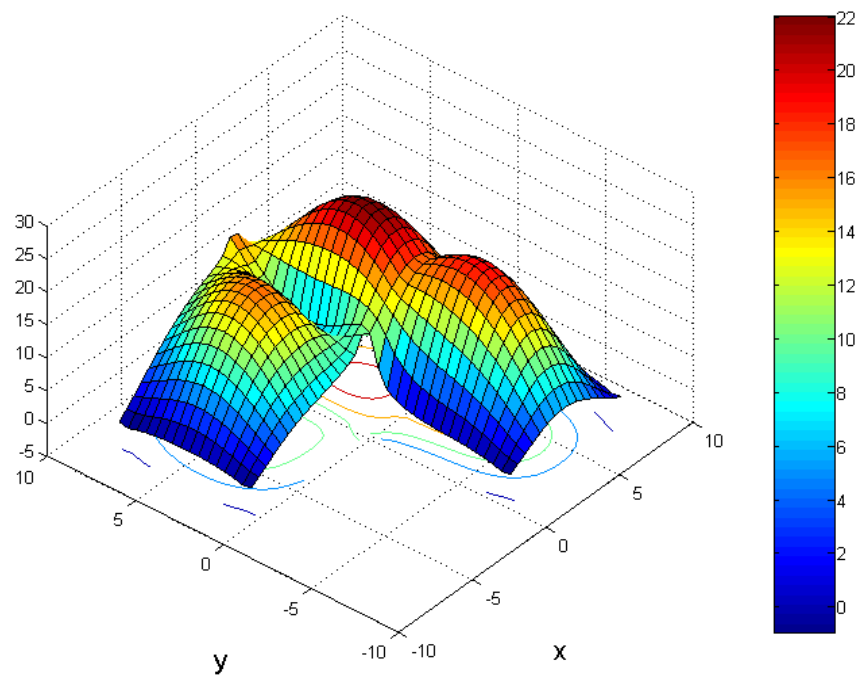


Fig. 9.54. Slab moments along the x direction at the 301st day for an edge lift case

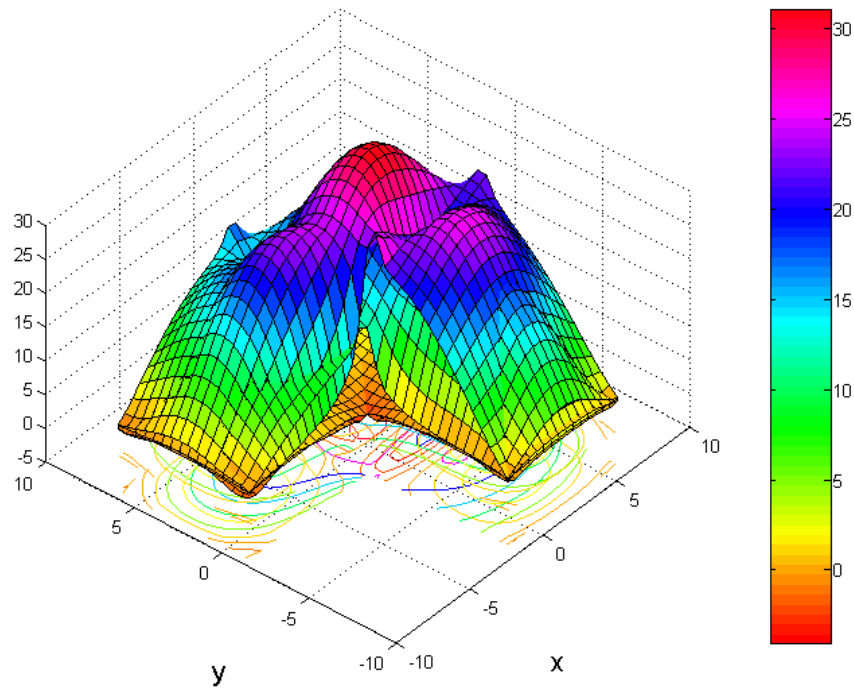


Fig. 9.55. Maximum and minimum slab moments along the x direction in 350 days for an edge lift case

9.6.8.9 Moment Distributions along y Direction in the Slab

Fig. 9.56, 9.57, 9.58, and 9.59 show the moments along the y direction at the 1st day, 101st day, 201st day and 301st day, respectively. The maximum and the minimum moments along the y direction in the slabs are shown in Fig. 9.60. It can be seen that the moments at the center of the slabs are higher than those at the edges. The maximum moment for the three slabs occurs at the center of slab II, which indicating the loads applied on slab I and slab III also have influences on the moment in slab II. The moments at the borders two of the three slabs are smaller than the moments in the center of the slab, indicating that the load distributions influence the moment distributions greatly.

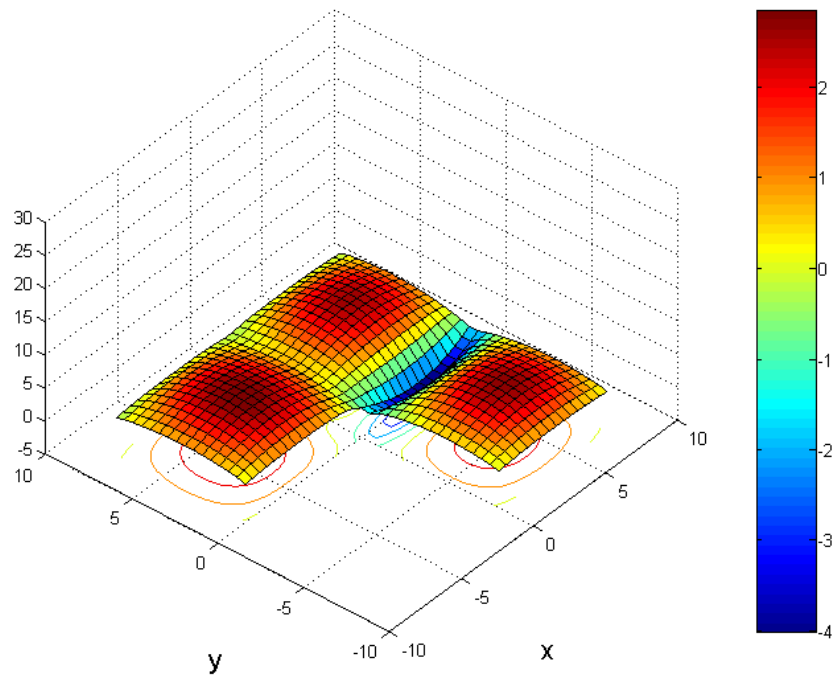


Fig. 9.56. Slab moments along the y direction at the 1st day for an edge lift case

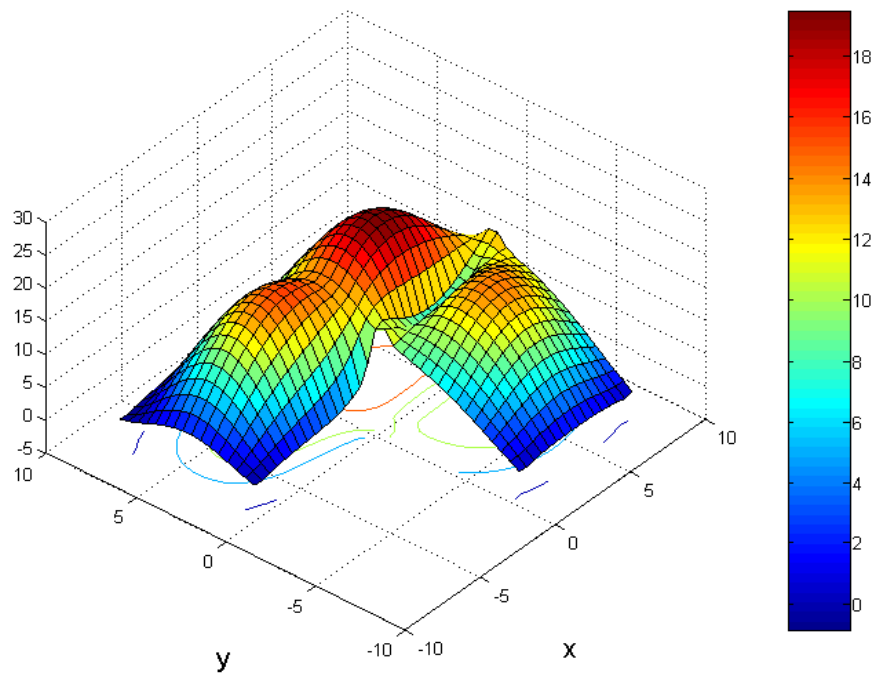


Fig. 9.57. Slab moments along the y direction at the 101st day for an edge lift case

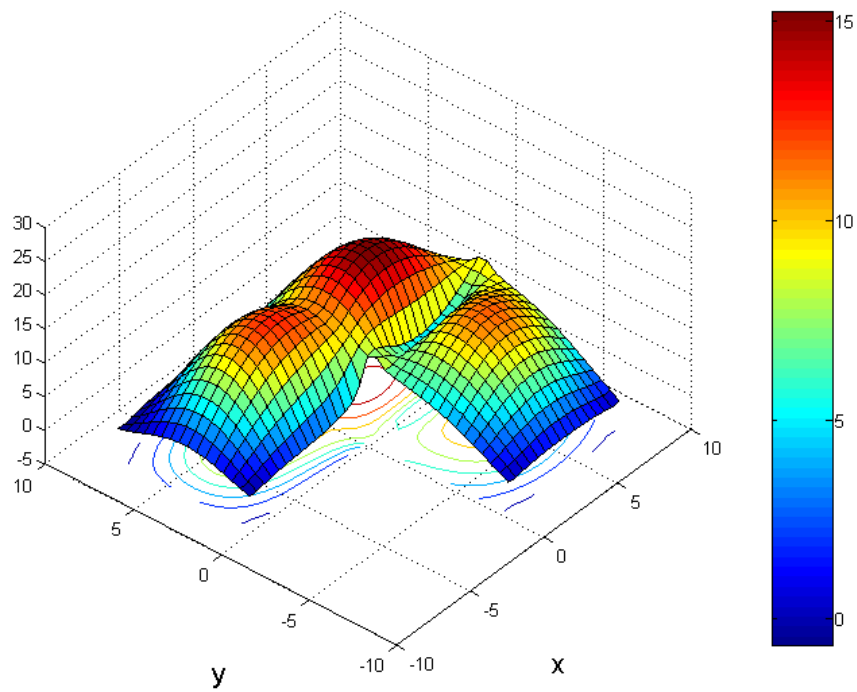


Fig. 9.58. Slab moments along the y direction at the 201st day for an edge lift case

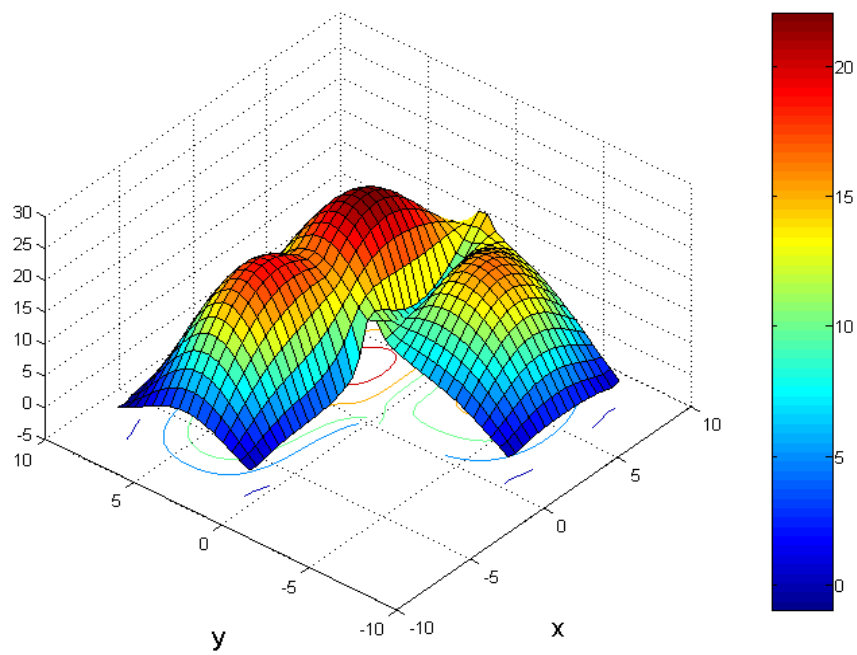


Fig. 9.59. Slab moments along the y direction at the 301st day for an edge lift case

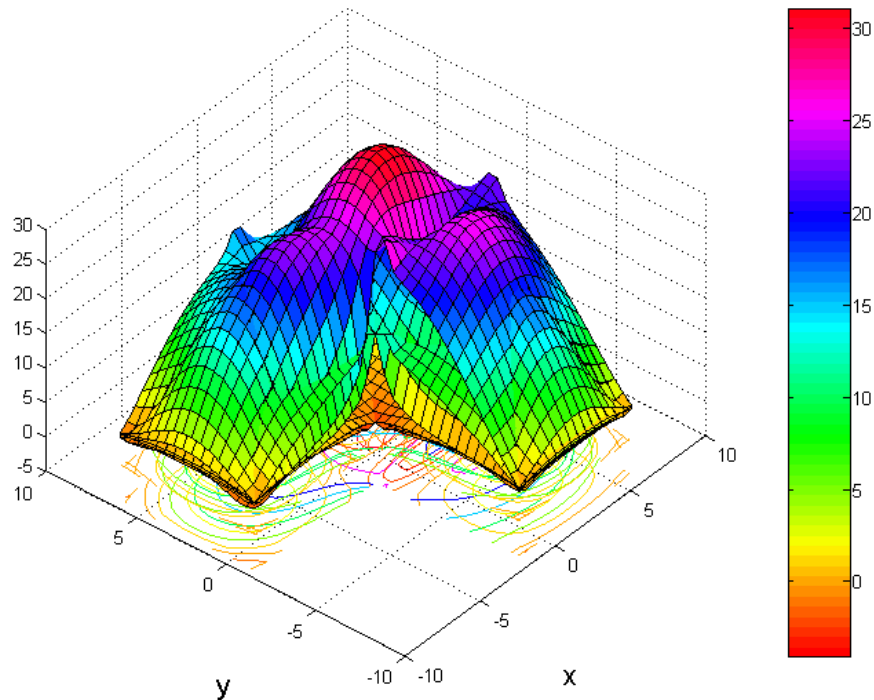


Fig. 9.60. Maximum and minimum slab moments along the y direction in 350 days for an edge lift case

9.6.8.10 Von Mises Stresses in the Structure

Fig. 9.61 shows the von Mises stresses in the whole simulated domain. It can be found that the maximum von Mises stresses occur at the top center of the wall 4 and wall 7, instead of the corner formed by the wall 4, wall 6, wall 7 and wall 8. The reason for this is because the tree at the corner causes the soil to shrink more than any other place. As a result, the soil reaction force at the corner is smaller. The load at the corner is transferred to other places nearby and sustained by the soils underneath. Von Mises stress is a stress-invariant used in yield criteria. Therefore, the most dangerous location in this example is at the top center of the wall 4 and wall 7. If the materials of the slabs and the walls are the same, the top center of the wall 4 and wall 7 will crack firstly.

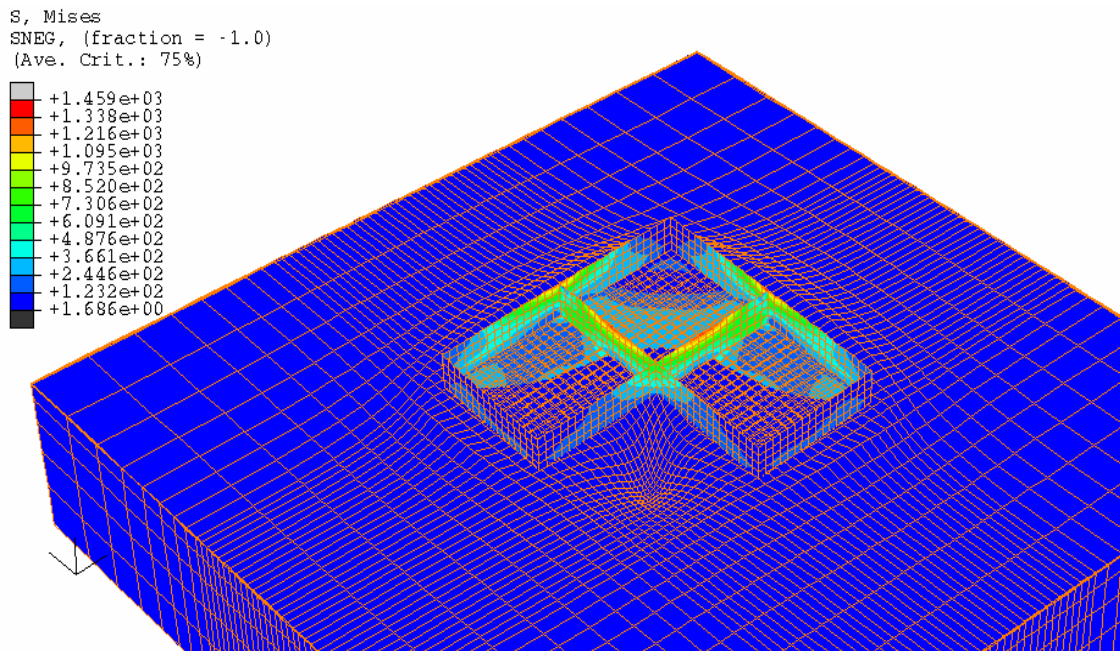


Fig. 9.61. Von Mises stresses in the structure at the 301st day for an edge lift case

9.7 Design Criterion and Cracking Model for Concrete

9.7.1 Design Criterion

As can be seen in the both examples, the maximum von Mises stresses occur in the walls instead of in the slabs. As a consequence, it is possible that under some conditions the slabs work very well while the von Mises stresses in the walls are big enough to cause cracking in the walls. If this condition does exist, a question arises: when we design the slabs on grade, what kind of criterion should be used? Should we just design a safe slab or should we design a slab, whether it cracks or not, to make sure that there is no cracking in both the slab and the wall?

Obviously, it seems we should design a slab to make sure there is no cracking in the walls under any circumstance. To make the design method more reasonable, we need find out whether there is damage to the walls for certain design. However, all the current methods fail to do this. All the current methods concentrate on the moment and

deflection of the slab without considering the cracking in the wall. Therefore, all the current design methods are questionable.

The system proposed above can actually calculate the stresses distributions in the structures. A crack model can be introduced to make the simulation more reasonable and complete.

The smeared cracking model in ABAQUS/Standard, which uses concepts of oriented damaged elasticity (smeared cracking) and isotropic compressive plasticity to represent the inelastic behavior of concrete, is proposed to simulate the cracking in the slabs and walls. The walls can be considered as plain concrete and the slabs can be considered as reinforced concrete. The basic theory of the smeared concrete model is simply introduced as followings.

9.7.2 Smeared Cracking Model for Concrete

9.7.2.1 Smeared Cracking Model for Concrete

Bazant and Cedolin(1979) proposed to determine if the crack propagates by the ratio of ΔU (i.e. the change of the energy of the new cracked unit before and after the propagation) to Δa (i.e. the change of the crack length) instead of the stress intensity factor. The model, which is called the smeared cracking model, does not track individual “macro” crack, rather, the presence of cracks enters into the calculations by the way the cracks affect the stress and material stiffness associated with each material calculation point. Fig. 9.62 shows the smeared crack model for a plane problem. The concrete cracks due to the tension forces in y direction. Before cracking, the concrete is considered as elastic material, the modulus matrix for the material is

$$[D] = \begin{bmatrix} E & 0 & 0 \\ 0 & E & 0 \\ 0 & 0 & G \end{bmatrix}_{\text{intact}} \quad (9.71)$$

where D =stiffness matrix of the material; E = Young's Modulus of the material; and G =shear modulus of the material.

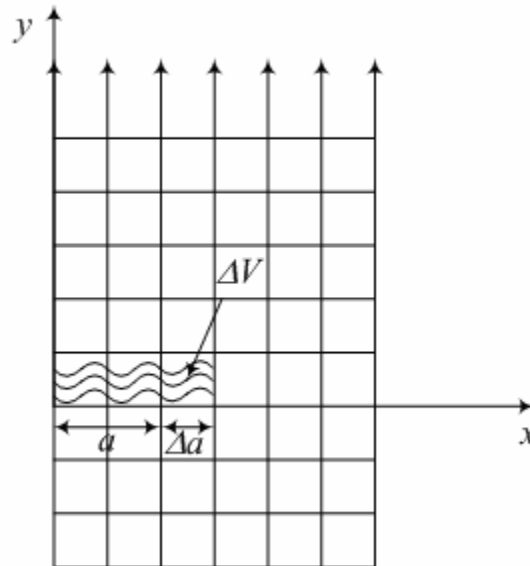


Fig. 9.62. The smeared cracking model

After cracking in y direction, the modulus matrix of the concrete is changed into

$$[D] = \begin{bmatrix} E & 0 & 0 \\ 0 & 0 & 0 \\ 0 & 0 & \beta G \end{bmatrix}_{\text{cracking}} \quad (9.72)$$

The Young's modulus in the direction perpendicular to the crack is zero due to the existence of the cracking while in the direction parallel to the crack, and the Young's Modulus of the material remains unchanged. The shear modulus is also reduced due to the crack.

The smeared cracking model has great advantages over other available cracking models in fracture mechanics because when the crack occurs during the numerical

simulation there is no need to regenerate the mesh. Instead, the mechanical parameters are changed. This treatment brings great convenience in programming.

Some objections have been raised against the smeared cracking model. The major concern is that this approach inherently introduces mesh sensitivity in the solutions, in the sense that the finite element results do not converge into a unique result. A general consensus has been reached that Hilleborg's (1976) approach can be used to deal with this issue for practical purpose with adequate accuracy. The Hilleborg's approach has been used in the smeared cracking model in ABAQUS/Standard.

9.7.2.2 Reinforcement

Usually the slabs are made of reinforcement concrete in which rebars are used to provide tensile strength. One dimensional strain theory elements together with metal plasticity models can be used to describe the behavior of the rebar material. These elements (rods) can be defined singly or embedded in oriented surfaces and are superposed on a mesh of the general purpose shell elements to model the reinforced concrete. The concrete behavior is considered independently of the rebar. Effects associated with the rebar/concrete interface, such as bond slip and dowel action, are modeled approximately by introducing some “tension stiffening” into the concrete modeling to simulate load transfer across cracks through the rebar. More details can be found in the ABAQUS Analysis User's Manual.

9.7.2.3 Crack Detection Surface

Criterion is needed to determine whether there is crack occurrence in the concrete. In the ABAQUS/Standard, if the loading is relatively monotonic and the confining pressures are low, cracking is assumed to occur when the stress reaches a failure surface which is called the “crack detection surface” as shown in Fig. 9.63. When the principal stress components are dominantly compressive, the response of the concrete is modeled by an elastic-plastic theory using a simple form of yield surface which is called “compression surface”. Associated flow and isotropic hardening are used. Both surfaces are linear

relationships between the equivalent pressure stress, p , and the Mises equivalent deviatoric stress, q .

After a crack has been detected, its orientation is stored for subsequent calculations. Cracks are considered to be irrecoverable: they remain for the rest of the calculation (but may open and close). Subsequent cracking at the same point is restricted to being orthogonal to this direction since stress components associated with an open crack are not included in the definition of the failure surface used for detecting the additional cracks. No more than three cracks can occur at any point (two in a plane stress case, one in a uniaxial stress case). Following crack detection, the calculations are affected by the cracks by using a damaged elasticity model as shown in Eq. 9.72.

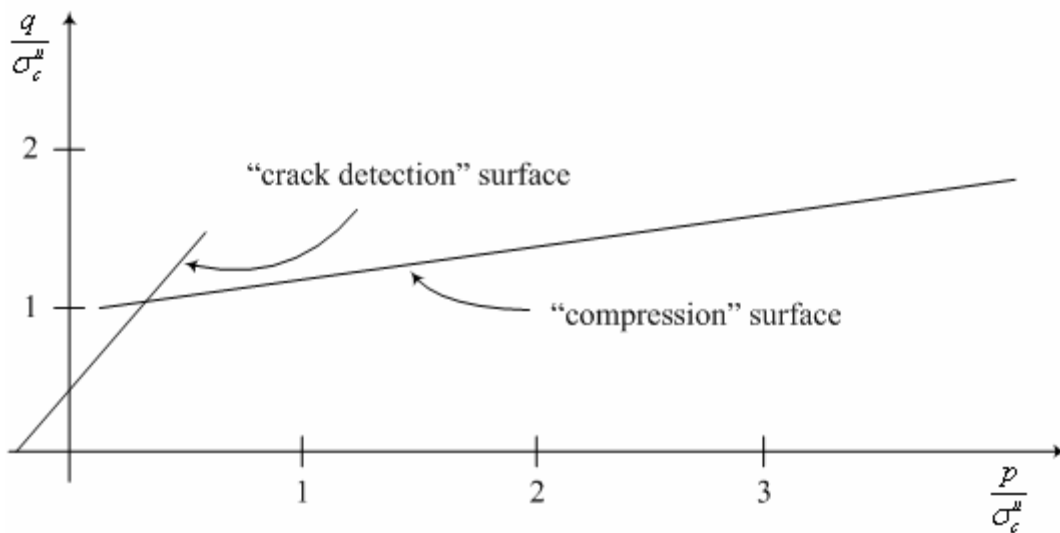


Fig. 9.63. Yield and failure surfaces in the (p - q) plane (ABAQUS/Standard 2002)

9.7.2.4 Postfailure Behavior of the Concrete

To simulate the cracking in the slabs and walls, the postfailure behavior of the concrete must be defined. The slabs are usually made of reinforced concrete. The interaction between the rebars and the concrete tends to reduce the mesh sensitivity because in reinforced concrete, the cracks are relatively evenly distributed. This condition can be

simulated by “Tension stiffening” model in ABAQUS/Standard as shown in Fig. 9.64. It is assumed that the strain softening after failure reduces the stress linearly to zero at a total strain of about 10 times the strain at failure. The strain at failure in standard concretes is typically 10^{-4} , as a result, the tension stiffening reduces the stress to zero at a total strain of about 10^{-3} . This parameter should be calibrated by experiment under some particular case.

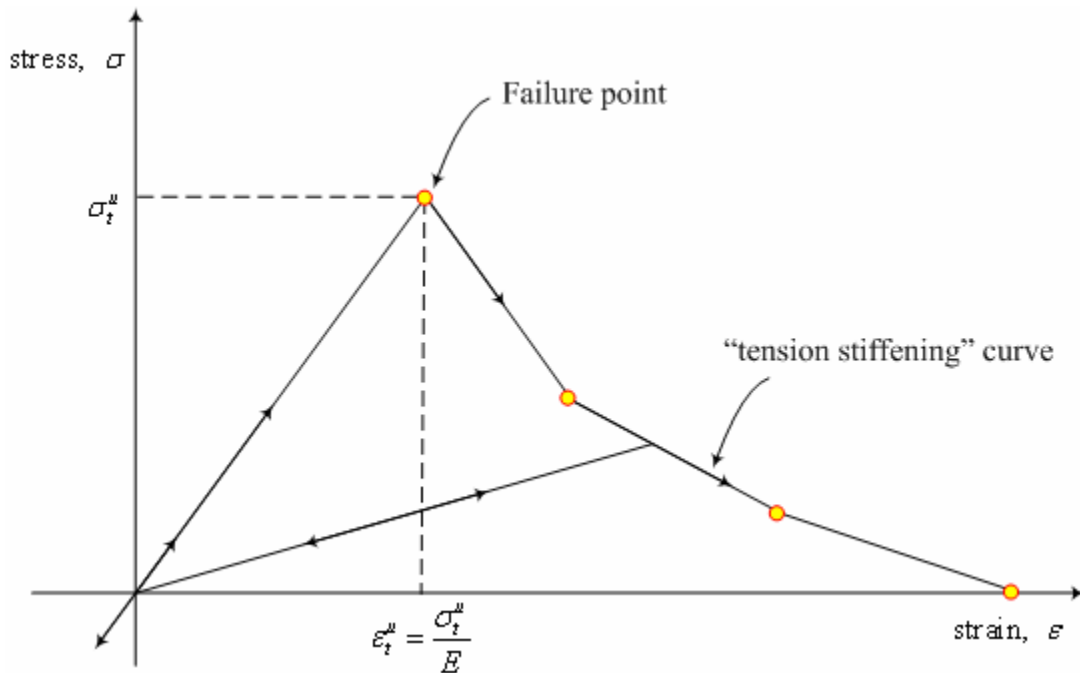


Fig. 9.64. “Tension stiffening” model (ABAQUS/Standard 2002)

The walls can be considered as plain concrete. When there is no reinforcement in the concrete, the strain softening approach for defining tension stiffening may introduce unreasonable mesh sensitivity into the results. Hilleborg et al. (1976) defines the energy required to open a unit area of crack as a material parameter, using brittle fracture concepts. With this approach the concrete's brittle behavior is characterized by a stress-displacement response rather than a stress-strain response. Crisfield (1986) discusses this issue and concludes that Hilleborg's proposal is adequate to allay the concern for many

practical purposes. Under tension a concrete specimen will crack across some section. After it has been pulled apart sufficiently for most of the stress to be removed (so that the elastic strain is small), its length will be determined primarily by the opening at the crack. The opening does not depend on the specimen's length (Fig. 9.65). The ultimate displacement u_0 at which the stress goes to zero, can be estimated from the fracture energy per unit area. More details can be found in the ABAQUS Analysis User's Manual.

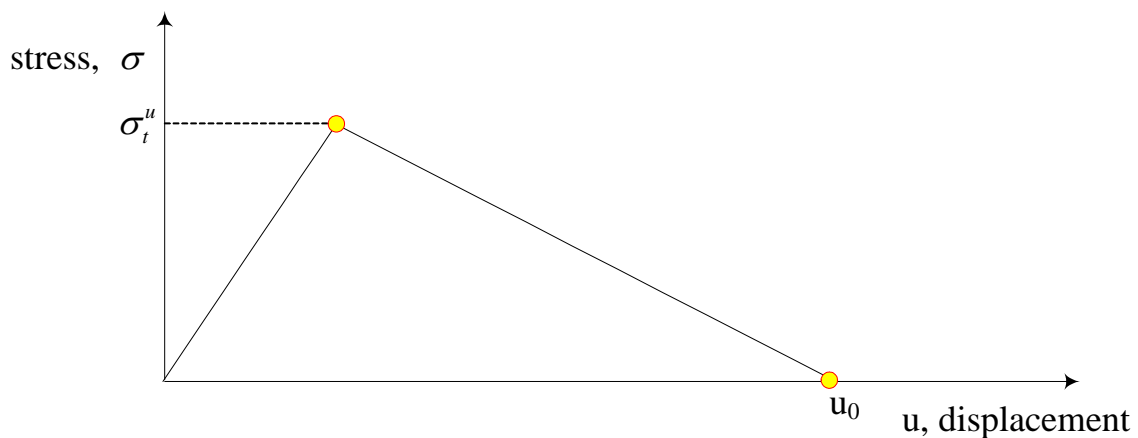


Fig. 9.65. Fracture energy cracking model (ABAQUS/Standard 2002)

9.8 Discussion

Two simple examples have been used to illustrate the simulation of the residential buildings on expansive soils. A lot of parameters such as the dimensions and material properties for the slab and the walls, the normal and tangential behaviors between the soil and the slab and initial soil conditions are assumed due the limited resources and time in this study. More simulations by using real material parameters are needed for the future research and the results should be compared and verified with field observations. Here some discussions about the above simulations can be summarized as followings.

From the simulations, the side lengths of the slabs are 8m, which is reasonably large for a house. The weather can influence the slab from both sides. Therefore, the actual

length which the weather is going to influence is about 4m. From the above simulations, the weather's influence can penetrate through the whole soil underneath the slab. Fig. 9.26 and 9.50 indicate that the slab settle down or go up globally. Under this condition, the edge moisture distance is 4m. In other words, edge moisture distance exists only when the slab is so large that the weather's influence can not penetrate through. For a small slab where the weather's influence can not penetrate through the soil underneath, the edge moisture distance is equal to half of the slab width. Whether the weather's influence can penetrate through the slab or not depends on the width of the slab, the severity of the weather, the soil properties such as permeability coefficient as well as the specific water capacity.

When the weather's influence can penetrate through the soil underneath the slab, the total movements of the slab is different from the differential movements anymore. The total movements such as translation and rotation will not cause stresses or moments in the slab while the differential moments do. As a result, it is very important to distinguish them.

The soil reaction forces underneath the slab are nonuniform. From the above simulations, it can be seen the maximum moments occur at the center of the slabs instead of a certain distance away from the edges as assumed in the BRAB and WRI method. The moment distributions are also influenced by load distribution. The load at the center of the slab can cause negative moments in the slabs.

The criterion of designing a slab on grade is to check whether the slab design is able to ensure that there is no cracking in the superstructure instead of to design a safe slab. The stresses in the walls will be greatly influenced by the deflections in the slab. In this sense, the deflections in the slabs will be a controlling factor in the design of slab on grade.

The proposed model can simulate the behavior of the whole structure. The simulation result can be used to obtain the maximum and the minimum moments and deflections in the structure during certain period, which can also be used to for the design.

Residential building on expansive soils is an integrated system. Any changes in one part will result in the changes in the whole structure. An important characteristic of reinforce concrete is that while the concrete works there is cracking in it. To include a cracking model in the whole system will make the simulation results more realistic and reasonable. In this sense, current research is just a start to a reasonable future design method.

CHAPTER X

PREDICTING THE VOLUME CHANGE OF EXPANSIVE SOILS*

10.1 Introduction

Expansive soils pose great challenges for the design of foundations. One of the most difficult issues for designing foundations on expansive soils is to predict the volume change of the soils. In this chapter, current methods and tests for movement prediction are reviewed and their limitations are discussed. Based on the theory of unsaturated soil mechanics, it is proved that the water content and the mechanical stress can be used to determine the soil status. A simplified method is proposed to construct a void ratio versus mechanical stress and water content surface, which can potentially be used to predict the potential vertical swell and potential vertical shrink of expansive soils at the same time. The new method couples the influence of both mechanical stress and suction and eliminates the limitation of the current methods.

10.2 Current Methods for Predicting the Movements of Expansive Soils

Expansive soil is one of the most widely encountered soils in Texas. The characteristic of expansive soil is that the soil will swell when it absorbs water and shrink when it loses water. The first step for designing foundations on expansive soils is to predict the vertical movements of the ground surface. Every year, the economic loss caused by the damage to houses is considerable, indicating that there is still a great need for evaluating the current methods for predicting the movement of expansive soils.

All the current methods to predict the movements of expansive soils include two components: (1). the continuity equation for the prediction of the moisture variations,

*Reprinted with permission from “Predicting the Volume Change of Shrink-Swell Soils” by Zhang, X. and Briaud, J.-L., 2003. *Proceedings, Texas Section, ASCE Fall Meeting*, Dallas, Texas

and (2). the constitutive law for the prediction of volume change of the soils due to the moisture variation. Currently there are a number of methods for predicting the volume change of expansive soils. According to the state variables used in their constitutive laws, they can be classified into three categories: (1). *Suction based methods* which use the matric suction as a stress state variable, (2). *Water content based methods* which use water content as a state variable, and (3). *Consolidation test based methods* which use the equivalent effective stress as a stress state variables. A brief description of these three methods is given next.

10.2.1 Suction Based Method

Those who contributed most to the suction based method are Lytton (1977), Johnson (1977), Mckeen (1981), and Fargher et al. (1979). The constitutive law of the suction based method is that the volume change of an unsaturated soil due to moisture variations is linearly proportional to the suction variation in log scale, i.e.

$$\gamma_h = \frac{1}{1+e_0} \frac{\Delta e}{\Delta \log(u_a - u_w)} \quad (10.1)$$

where γ_h is the matric suction compression index; equal to the slope of the volumetric strain $\frac{\Delta V}{V}$ (or $\frac{\Delta e}{1+e_0}$) versus the matric suction in log scale $\Delta \log(u_a - u_w)$; e is the void ratio; e_0 is the initial void ratio; and Δ stands for the variation of variables.

The definition of γ_h is very similar to that of the compression index in the saturated soil mechanics except that the stress state variable is suction instead of effective stress. McKeen (1981) proposed that the range over which the matric suction compression index applicable is between 1 and 4.5 in log kPa scale and it has been extensively used in practice.

The continuity equation for the suction based method is Richard' Equation (Hillel 1980):

$$\frac{\partial}{\partial x} \left(k \frac{\partial(u_a - u_w)}{\partial x} \right) + \frac{\partial}{\partial y} \left(k \left(\frac{\partial(u_a - u_w)}{\partial y} + 1 \right) \right) = \rho_d g C_w \frac{\partial(u_a - u_w)}{\partial t} \quad (10.2)$$

where k is the coefficient of hydraulic conductivity for unsaturated soils, which is a function of matric suction, $(u_a - u_w)$ is matric suction, C_w is the specific water capacity of the soil, which is equal to the slope of the soil water characteristic curve $\frac{dw}{d(u_a - u_w)}$, g is the acceleration of gravity, and ρ_d is the dry density of the soil.

The suction based methods form a complete theoretical and practical framework for the volume change problems in unsaturated soils (VOLFLO 1986). The suction based methods are also most frequently used for numerical simulation.

The potential problem associated with the suction based methods in current practice is that relationship between the volumetric strain $\frac{\Delta V}{V}$ and the matric suction in log scale $\Delta \log(u_a - u_w)$ is linear only over a certain suction range and that this range is not known in most cases. A common range (10kPa (2pF) to 31620 kPa (5.5 pF)) is proposed by Mckeen (1992) for all soils and it is considered that all the volume change occurs in this range. In other words, it is considered that for all the soils at the swell limit soil suction is 10kPa (2pF) and at the shrinkage limit soil suction is 31620 kPa (5.5 pF). Using a fixed range to compute the suction compression index γ_h is welcomed by many geotechnical engineers due to the time-consuming process of obtaining the void ratio versus suction curve. However, it is a questionable assumption. Observations indicate that the range of the linear relationship is varying for different soils. Fig. 10.1 is the void ratio versus suction curve of a sample SW145 obtained from a depth of 1.2m to 1.8m at a site in Arlington, Texas. It is very clear that there is a linear relationship between the void ratio and the suction variation in the range from 1000 kPa (4pF) to 20000 kPa

(5.3pF). If the range from 10 kPa (2pF) to 31620 kPa (5.5 pF) is used to determine the matrix suction compression index γ_h , the matrix suction compression index γ_h will be underestimated 50%. Perko et al. (2000) proposed a range from 4.1 pF to 6.25 pF for the linear relationship for a soil. For the movements caused by suction, it is not uncommon to have suction variation from 0 kPa to 100000 kPa, while the log linear relationship is satisfied only over a smaller range. To use the suction method correctly, the range for the linear relationship between the void ratio and the matric suction in log scale should be identified even though more efforts are needed for the laboratory testing. The method proposed in Chapter VI can be used to obtain the void ratio versus matric suction curve.

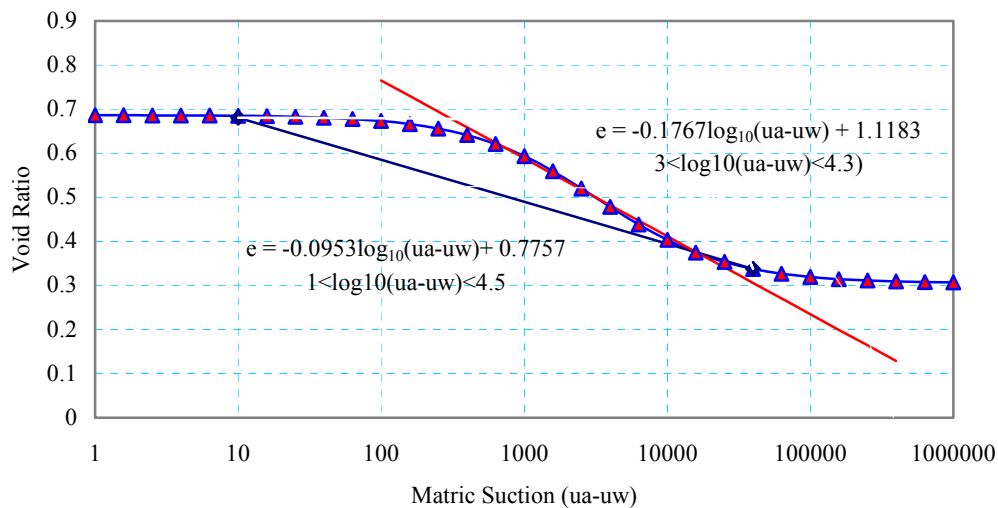


Fig. 10.1. The void ratio versus suction curve for soil sample SW145

10.2.2 Water Content-Based Method

The constitutive law of the water content based methods is proposed by Briaud et al. (2003), indicating that there is a linear relationship between the volume change of unsaturated soil and water content variations:

$$\frac{\Delta V}{V} = \frac{\Delta w}{E_w} \quad (10.3)$$

where E_w is the slope of water content versus volumetric strain curve; V is the volume of the soil; w is the water content; and Δ stands for the variation of variables.

Fig. 10.2 shows the relationship between the water content w and the volumetric strain $\frac{\Delta V}{V}$ curve of a sample SW145 obtained from a depth of 1.2m to 1.8m at a site in Arlington, Texas. Curve 1 shows the free shrink test curve. As we can see, there is an approximate linear relationship over the range between the swell limit and the shrinkage limit. Curve 2 is the void ratio versus water content curve when the degree of saturation curve equals to 100%, curve 3 is the void ratio versus water content curve when the degree of saturation curve equals to 90%. Here we can see the most of the volume change of the soil occurs when the degree of saturation is still high, and that the water content at the shrinkage limit is about 13%.

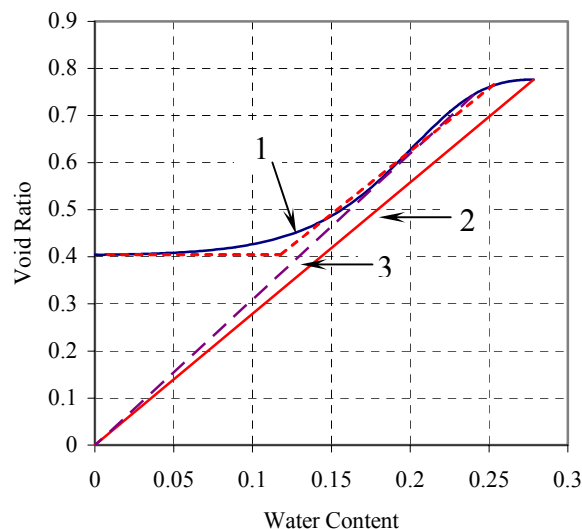


Fig. 10.2. The void ratio versus water content curve for soil sample SW145

The Potential Vertical Rise (PVR) method (McDowell 1956), Vijayvergiya-Ghazzaly method (O'Neill 1980) and shrink test method (Briaud et al. 2003) are typical water content based methods even though their constitutive laws are not expressed

explicitly as Eq. 10.3. The water content methods are considered as empirical methods because none of the current water content methods gives out a continuity equation to predict the water content variation.

For the water content method, there are also limits for the applicable range of the constitutive law. The upper limit is the swell limit and the lower limit is the shrinkage limit. Some water content methods also consider the influence of mechanical stress by adjusting the calculation result with soil dry density. They can be considered as coupled mechanical stress and water content methods. The PVR method gives the upper limit $0.4LL+9$ (swell limit) and the lower limit $0.2LL+7$ (shrinkage limit) and adjusts the potential vertical rise with the soil density and the mechanical stress. However, the PVR method only gives out the potential vertical swell of the soil from the current soil moisture without calculation of the potential vertical shrink, or the potential vertical amplitude of movements, which will be discussed later.

10.2.3 Relationship between the Suction Based Method and the Water Content-Based Method

The suction based methods and the water content methods are not independent. They are related to each other by the soil water characteristic curve. The soil water characteristic curve gives out the relationship between water content and matric suction. It plays a key role in the analysis of unsaturated soils. If we neglect the influence of hysteresis, there is a unique relationship between the water content and the matric suction. To make the discussion a little bit simpler, it is assumed that there is a linear relationship between the water content and the log of the matric suction in the range of interest:

$$(u_a - u_w) = g(w) \quad (10.4a)$$

or

$$w = C_w \log(u_a - u_w) + d \quad (10.4b)$$

where $(u_a - u_w)$ is matric suction; w is water content; C_w is the slope of the soil water characteristic curve; and d is constant.

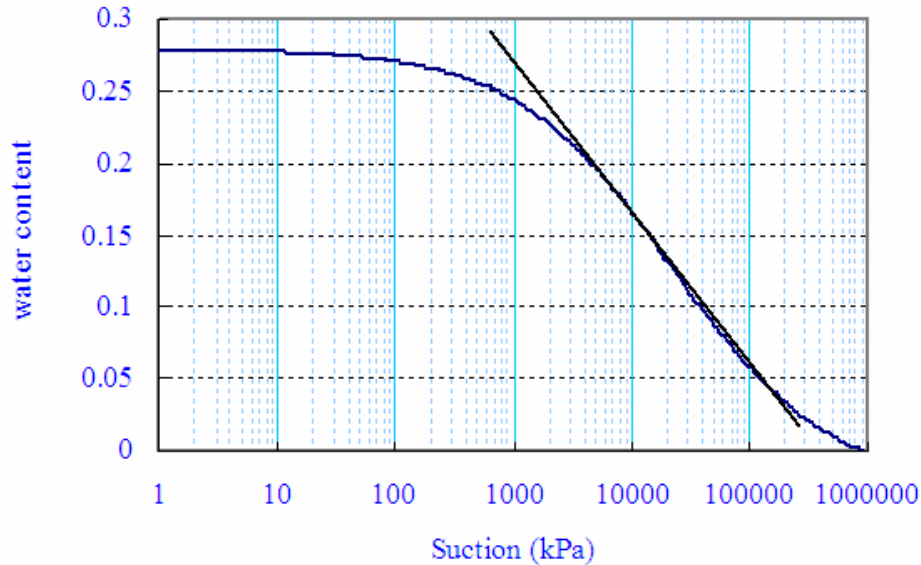


Fig. 10.3. Soil water characteristic curve for soil sample SW145

Fig. 10.3 shows the soil water characteristic curve of a sample SW145 obtained from a depth of 1.2m to 1.8m at a site in Arlington, Texas. By substituting Equation 10.4a into 10.2, we can derive the differential equation of moisture movements in terms of water content,

$$\frac{\partial}{\partial x} (k(w)g'(w) \frac{dw}{dx}) + \frac{\partial}{\partial y} (k(w)(g'(w) \frac{dw}{dy} + 1)) = \rho_d \frac{dw}{dt} \quad (10.5)$$

where $g'(w) = C_w = \frac{du}{dw}$.

Both Eq. 10.2 and 10.5 can be considered as forms of Richard's equation (Swartzendruber 1969). Eq. 10.5 can be used to predict the water content variation by

combining the site-specific boundary conditions. It has been used in soil physics (Philip et al. 1957) but rarely used in geotechnical engineering.

The constitutive law for water content based method can be obtained by substituting Eq. 4b into Eq. 1,

$$\frac{\Delta V}{V} = \frac{\Delta e}{1 + e_0} = \gamma_h \Delta \log(u_a - u_w) = \gamma_h \frac{\Delta w}{C_w} = \frac{\Delta w}{E_w} \quad (10.6a)$$

or ,

$$E_w = \frac{C_w}{\gamma_h} \quad (10.6b)$$

Eq. 10.6b defines the relationship between the suction compression index for suction based method and the swell-shrink modulus for water content method. It indicates that both the water content-based method and the suction based method have the same theoretical basis. They can be interchanged through the soil-water characteristic curve when numerical simulation is performed. But for the water content method, the constitutive law can be obtained from a free shrink test directly. The corresponding advantages of the water content method as an empirical method have been presented by Briaud et al. (2003).

10.2.4 One Dimensional Consolidation Test Based Method

One dimensional consolidation based methods try to use the one dimensional consolidation test to predict the volume change due to suction. The core concept is to find the “equivalent effective stress” variation due to suction variation, and use the one-dimensional consolidation compression index to calculate the volume change due to suction. It is very similar to the Bishop equation, that is,

$$\sigma' = (\sigma - u_a) - \chi(u_a - u_w) \quad (10.7)$$

where χ is a coefficient related to the degree of saturation and is a variable.

The typical consolidation test based methods are Fredlund et al. method (1980), double consolidation method (Jennings et al. 1957), and Salas and Serratosa method (1957). Fredlund's method obtains the equivalent effective stress by projecting the current soil status on the void ratio constitutive surface to the zero suction plane to obtain the equivalent effective stress and use the rebound branch as constitutive law for the volume change calculation as shown in Fig. 10.4. A complicated correction procedure for the swell pressure is needed to get the initial equivalent effective stress, which is shown in Fig. 10.5. No continuity equation is provided for the prediction of the future matric suction variation.

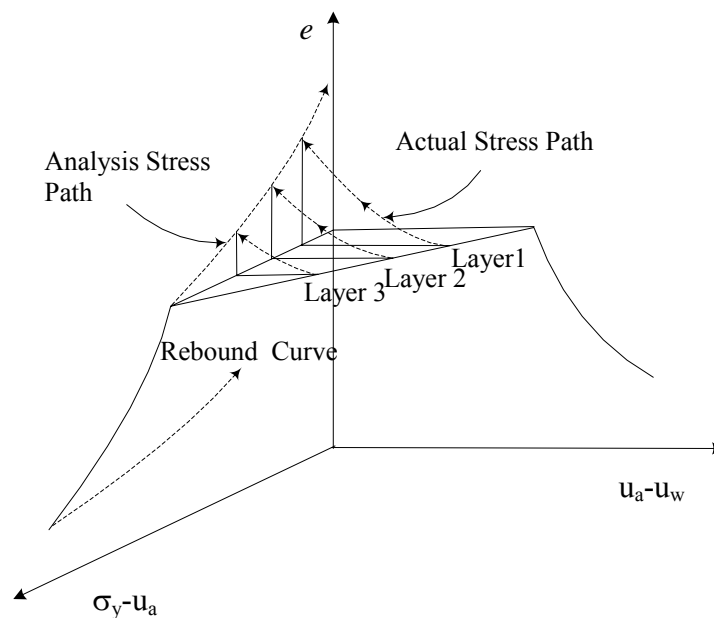


Fig. 10.4. Actual stress path and analysis stress path (after Fredlund et al. 1980)

It is obvious that the volume change of the soil will be influenced by the applied mechanical stress, but it is very difficult to determine the equivalent effective stress accurately, i.e., the χ value in Bishop's equation. Research indicates that χ is a function of both mechanical stress and suction and varies greatly. This difficulty leads to the

emergence of soil mechanics for unsaturated soils, which uses two independent stress state variables as a more convenient way to describe the behavior of unsaturated soils.

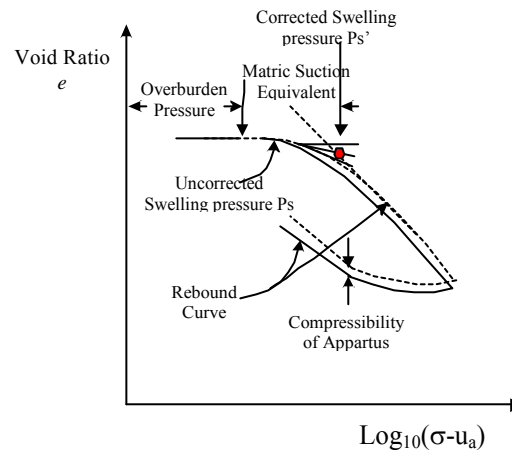


Fig. 10.5. Method for correcting the swell pressure (after Fredlund et al. 1980)

10.3 Variables Needed to Determine the Soil Status

The water content method proposed by Briaud et al. (2003) is actually an uncoupled analysis of the volume change of unsaturated soils where only the influence of moisture variation on the volume change of expansive soils is considered. It is well known that the volume of the expansive soil is also influenced by the mechanical stress. For the coupled analysis of unsaturated soils, Fredlund (1981) proposed that two stress state variables should be used to describe the volume change of soil structure and water phase: net normal mechanical stress and matric suction. The constitutive laws are not curves showed in Fig. 10.1 but surfaces which are called the constitutive surfaces for unsaturated soils. The constitutive surfaces express the soil state variables such as void ratio, water content and degree of saturation of the soils as a function of the two independent stress state variables, that is, the matric suction and the mechanical stress. Theses surfaces are called the void ratio constitutive surfaces, the water content constitutive surface and the degree of saturation constitutive surface, respectively. Fig. 5.12 shows the void ratio constitutive surface for a sample SW145 and its mathematical

expression is Eq. 5.17. The water content constitutive surface for the same soil sample SW145 is shown in Fig. 5.13 and its mathematical expression is Eq. 5.20 and 5.21. The corresponding degree of saturation constitutive surface for the soil sample SW145 is shown in Fig. 5.14.

When the pore air pressure is constant, the two stress state variables are net normal stress and negative pore water pressure, respectively. With these three constitutive surfaces, all the soil state variables, that is, the void ratio, the water content, and the degree of saturation, can be determined if the two stress state variables, matric suction and mechanical stress are known. Actually, any two variables of the five state variables, i.e., void ratio, water content, degree of saturation, net normal stress and matric suction can be used to determine the other three state variables. An interesting combination is when the two known state variables are water content and the mechanical stress. In this case, the water content constitutive surface in Fig. 5.13 can be used to get the corresponding matric suction value of the soil, and then the void ratio constitutive surface and degree of saturation surface (Fig. 5.12 and 5.14, respectively) can be used to get the void ratio and the degree of saturation of the soil. Also, if the future soil status (the water content and the mechanical stress) of the soil is known, the volume change of the soil can be calculated. A routine boring log usually gives out the soil layer distribution with depth and the water content profile. If the soil unit weight is known, the net normal stress can be calculated for soils at different depths. Combining this net normal mechanical stress profile with the water content profile can give the status including the void ratio profile at any depth provided that the three constitutive surfaces have been obtained. If the future soil water content profile and mechanical stress are known, the volume change of the soil can be predicted, which will be discussed later.

The void ratio surface versus the total mechanical stress and the water content is practically useful. The mathematical expression of the void ratio surface versus the net normal stress and the water content can be obtained by combining Eq. 5.17, 5.20 and 5.21 and eliminating the matric suction. The corresponding surface is shown in Fig. 10.6.

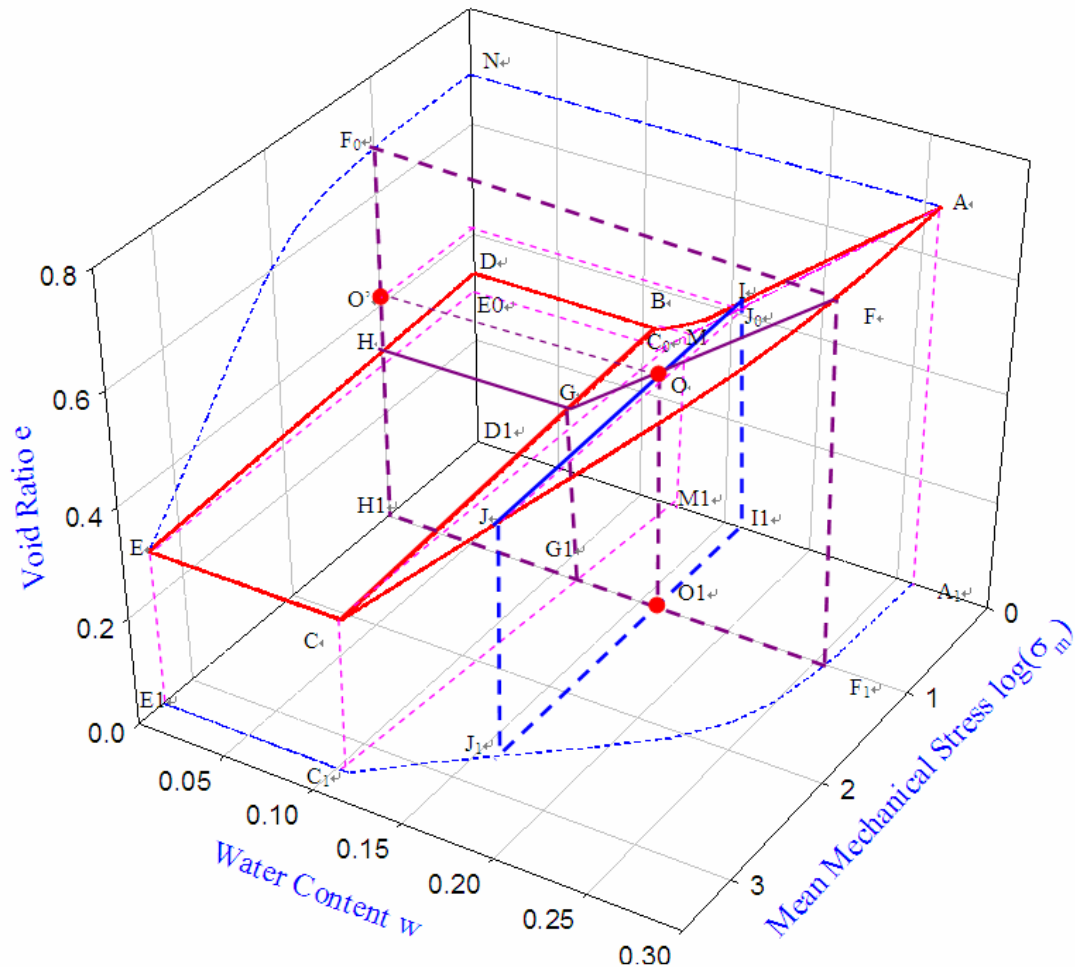


Fig. 10.6. Void ratio versus mechanical stress and water content surface for soil sample SW145

Fig. 10.6 can be thought of as shrink test curves of the soil at different mechanical stress level. Note that the mechanical stress axis is in log scale. To avoid the mathematical problem associated with the origin of log scale for mechanical stress, the mechanical stress for a free shrink test is assumed to be 1 kPa ($\log 1=0$) instead of 0 kPa. Curve ABD is the void ratio versus water content curve for the free shrink test and is the same as what is shown in Fig. 10.2. Segment AB represents the volume change when the soil is drying from the swell limit (which is determined by a free swell test) to the

shrinkage limit. Segment BD represents the constant void ratio after the soil reaches the shrinkage limit. From Point B to D, the soil water content continues to decrease but no volume change occurs.

Curve AFJC is the curve corresponding to void ratios of the one dimensional consolidation test on a fully saturated (swollen) sample in the mechanical stress and water content space. Its corresponding degree of saturation S is 100% and matric suction $u_a - u_w = 0$ kPa. Curve NF₀E represents the void ratio versus mechanical stress in log scale from the one dimensional consolidation test, which is the projection of Curve AFJC on the void ratio versus mechanical stress plane and is the same as Fig. 4.14. For the consolidation test, soil is considered to be completely saturated, that is, $S=100\%$, so the corresponding water contents for different void ratios can be calculated by $W = Se/Gs = e/Gs$. The projection of Curve AFJC on the mechanical stress and water content plane is Curve A₁F₁J₁C₁.

Curve DE represents the zero water content condition at different stress levels. In this case, $S=0$ and $u_a - u_w = 1,000,000$ kPa. Curve BC represents the shrinkage limits for the soil at different mechanical stress levels. The degree of saturation and matric suction corresponding to Curve BC are unknown for different mechanical stress level.

Surface ACBA represents the range where most of the volume change occurs and surface BCEDB represents the range where there is no volume change caused by moisture variation, that is, the zone with water content below the shrinkage limits for different total mechanical stress levels.

Fig. 10.6 indicates that when the total mechanical stress increases the swell limit decreases. Comparatively, the shrinkage limit water content of the soil is not significantly influenced by the mechanical stress, if any. These phenomena can be explained by the bimodal structures of soils in Chapter II. As discussed in Chapter II, the macropores in the soils can be changed while the micropores is unaffected by the applied mechanical stress. When the macropores in the soils are smaller due to applied external mechanical stress, the maximum ability of the soil to hold water is reduced. In other words, a higher mechanical stress level corresponds to a lower swell limit. The soil at

shrinkage limit corresponds to a status at which the soil particle can not be held more closely to each other by suction. The shrinkage limits of the soil at different mechanical stress levels can therefore be considered to be mainly related to the micropores. As discussed in Chapter II, applied external mechanical stresses do not influence the micropores of soils. As a consequence, the shrinkage limit water contents of a soil at different mechanical stress levels can be considered to be constant.

The range of volume change of the soil decreases with an increase in stress level. As shown in Fig. 10.6, Curve FGH represents the shrink test curve when the total mechanical stress is 10 kPa ($\log(\sigma_m - u_a) = 1$). The range for the water content variations when the mean mechanical stress $(\sigma_m - u_a) = 10 \text{ kPa}$ (FG) is smaller than when the mean mechanical stress is zero. So is the void ratio variation range. Fig. 10.6 also shows that the slope of the void ratio versus water content curve, that is, the swell-shrink modulus E_w proposed by Briaud et al. (2003), does not change much. Therefore, the mechanical stress changes mostly the range of water content variation, i.e. the difference between the swell limit and the shrinkage limit (which has been defined as the shrink-swell index by Briaud et al. (2003), and then the range of void ratio variation.

With Fig. 10.6, the void ratio for any soil sample can be determined by its water content and its mechanical stress, which is related to the soil profile and can be determined by its depth and soil density. If the future water content is known, the corresponding volume change of the soil can be calculated.

10.4 A Simplified Method to Obtain the $e-w-\sigma$ Surface

To obtain Fig. 10.6, the three constitutive surfaces of the soil as shown in Figs 5.12, 5.13 and 5.14 are needed. To obtain the constitutive surfaces for unsaturated soils, advanced equipment with both mechanical stress control and matric suction control is needed and the tests are usually very time-consuming. An alternative way is to use the method proposed in Chapter V. Once the constitutive surfaces of the soil are determined, the soil behaviors can be investigated very easily.

Sometimes only the volume change of an unsaturated soil is of interest. Under this condition, a simpler method can be used to construct the void ratio versus mechanical stress and water content surface. As shown in Fig. 10.6, Curve ABD is the void ratio versus water content curve obtained from a free shrink test. Curve AFJC is the curve corresponding to the one dimensional consolidation test in the void ratio, mechanical stress and water content space. If the shrinkage limit water contents of the soil are not influenced by the mechanical stress, the void ratio surface BDEC in Fig. 10.6 can be obtained because there is no more volume change below the shrinkage limits. The void ratio below the shrinkage limits decreases with an increase in mechanical stress but not be influenced by the water content variations. Correspondingly, surface BDEC is parallel to the water content axis.

The shape of surface ABC is still unknown. The consolidation test and free shrink test give the accurate boundary AB and AFC for the surface ABC only. The shape of surface ABC is still unknown.

To complete the surface ABC, it is assumed the void ratio varies linearly with the water content at any constant water content level. For example, Curve IJ, is a straight line on the surface ABC. The physical meaning of the straight line IJ is that, degree of saturation increases linearly with the mechanical stress in log scale until it reaches 100% saturation Point J under undrained compression condition. It is an undrained condition because during the process, the water content keeps constant while the applied mechanical stress increases. The mathematical expression for the whole surface can be obtained in a similar way to what we have used in Chapter V. However, it should be kept in mind that this assumption is not the same as that in Chapter V. Further research is needed in the influence of mechanical stress on the shrinkage limit water content and the degree of saturation. For general engineering use, it is considered that these two assumptions are good enough to evaluate the volume change of expansive soils.

The complete surface obtained can be used to predict the volume change of expansive soils. The application is described as follows:

- (1). Obtain the water content versus depth profile from the boring log plot;

- (2). Calculate the corresponding total mean mechanical stress for each depth;
- (3). Plot the profile on the void ratio versus water content and mechanical stress surface to get the associated distribution.
- (4). Calculate the maximum potential vertical swell and the potential vertical shrink and the sum is the maximum range of the vertical movements.

Fig. 10.6 shows that Point O can be determined once the water content and mechanical stress are known. The potential void ratio increase (potential vertical swell) is Curve OF and the potential void ratio decrease (potential vertical shrink) is Curve OG. The total range of possible void ratio variations is Curve GOF. This method considers the influence of both mechanical stress and matric suction and can be considered as a coupled water content and mechanical stress method.

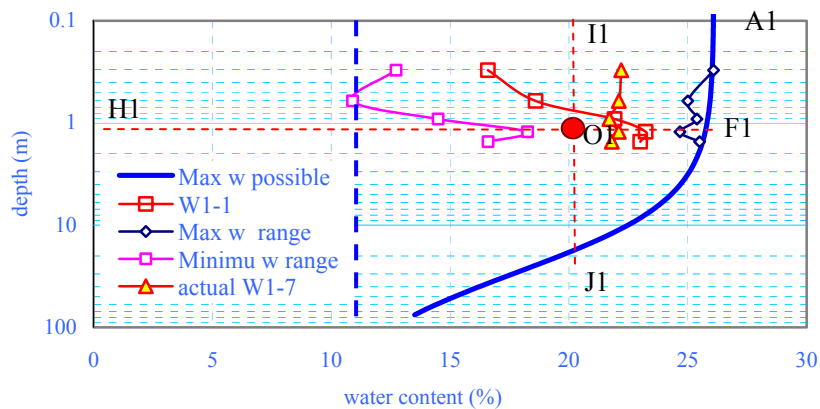
A simplified version of Fig. 10.6 is desirable for practical application. The simplification includes following steps:

Calculate the corresponding total mean mechanical stress for each depth;

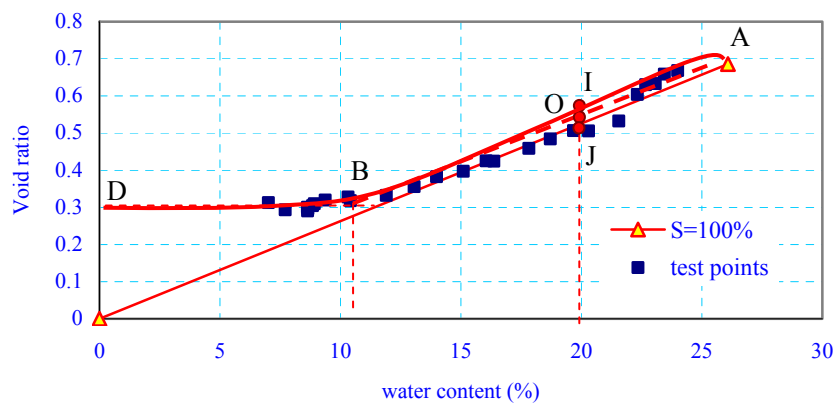
- (1). Plot the relationship between the mechanical stress and the maximum water content $A_1F_1J_1$ in Fig. 10.6 by using the results obtained from one dimensional consolidation test and the shrinkage limit curve BC on a mechanical stress and water content plane, and replace the total mean mechanical stress with the corresponding depth (Fig. 10.7a);
- (2). Plot the relationship between the void ratio and water content ABD and the $S=100\%$ line in Fig. 10.6 on a void ratio and water content plane (Fig. 10.7b);
- (3). Plot the relationship between the mechanical stress and the maximum void ratio NF_0E and the shrinkage limit line BC in Fig. 10.6 on a mechanical stress and void ratio plane, and replace the total mean mechanical stress with the corresponding depth (Fig. 10.7c);
- (4). Plot the water content profile versus depth from the boring log, and plot the results in Fig. 10.7a;

(5). Find the corresponding void ratios for the water content profile and the swell limits and shrinkage limits in Fig. 10.7a by using Fig. 10.7b, and plot the result in Fig. 10.7c.

(6). Calculate the maximum possible volume change, potential vertical swell and potential vertical shrink for the soil profile by comparing the void ratio profile for current condition with the void ratio at the swell limits and shrinkage limits.

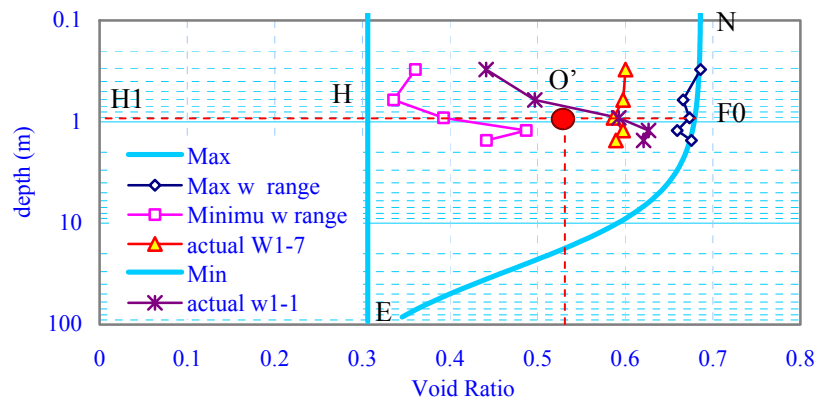


(a)



(b)

Fig. 10.7. Plots for simplified coupled water content method. (a) relationship between the mechanical stress and the maximum water content variation; (b) relationship between the mechanical stress and the maximum void ratio.



(c)

Fig. 10.7. (Continued) (c) relationship between void ratio and water content variation

Noted that in Fig.10.7 the projection of point O on the void ratio –water content plane lies between curve ABD and $S=100\%$, and an interpolation is needed to get a more accurate result.

Fig. 10.7 also shows an example set of calculations for a soil layer from 0 to 1.8m. Four measured water content profiles, w1-1,w1-7, maximum water content range and the minimum water content range, for the same soil layer are shown in Fig. 10.7a, the corresponding void ratios are obtained from Fig. 10.7b and the results are shown in Fig. 10.7c. The calculations are explained in the next section.

10.5 An Example of the Proposed Method

A site in Arlington, Texas is selected to show the application of the proposed method. The predominant soil type at the site is classified as borderline between CL and CH according to the Unified Soil Classification System. The soil stratigraphy, the average soil properties and the parameters for each soil layer are shown in Fig. 4.2. A total of 63 dry borings were performed at the site over a period of two years; 61 borings were done to a depth of 3m and 2 to a depth of 7m. Each boring consisted of pushing Shelby tubes continuously without any drilling and without adding water or drilling

mud. The water level in the 7m deep standpipes varied between 4m and 4.8m below the ground surface over a period of 2 years.

Fig. 10.8 shows all the soil water content profiles obtained over a two year period between June, 1999 and November 2001 for four footings RF1, RF2, W1 and W2. The two thick solid lines are the maximum and the minimum envelopes of the water content variation. Fig. 10.9 shows the corresponding void ratio profile W1-1 and W1-7 of w1 footing at boring 1 (06/24/1999) and boring 7 (11/17/2000) and the maximum water content range for the site as shown in Fig. 10.8. The two solid thick lines in Fig. 10.9 are the swell limits and the shrinkage limits for the soils respectively. The change in the swell limit and the shrinkage limit is due to the change in the soil category.

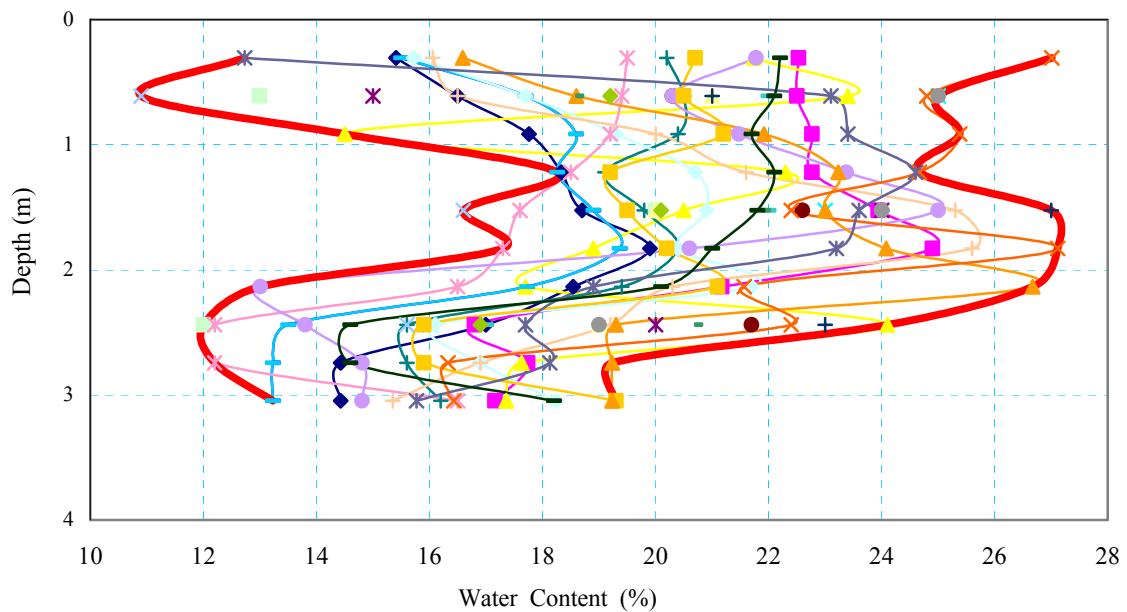


Fig. 10.8. Water content profiles of the site over a period of two years

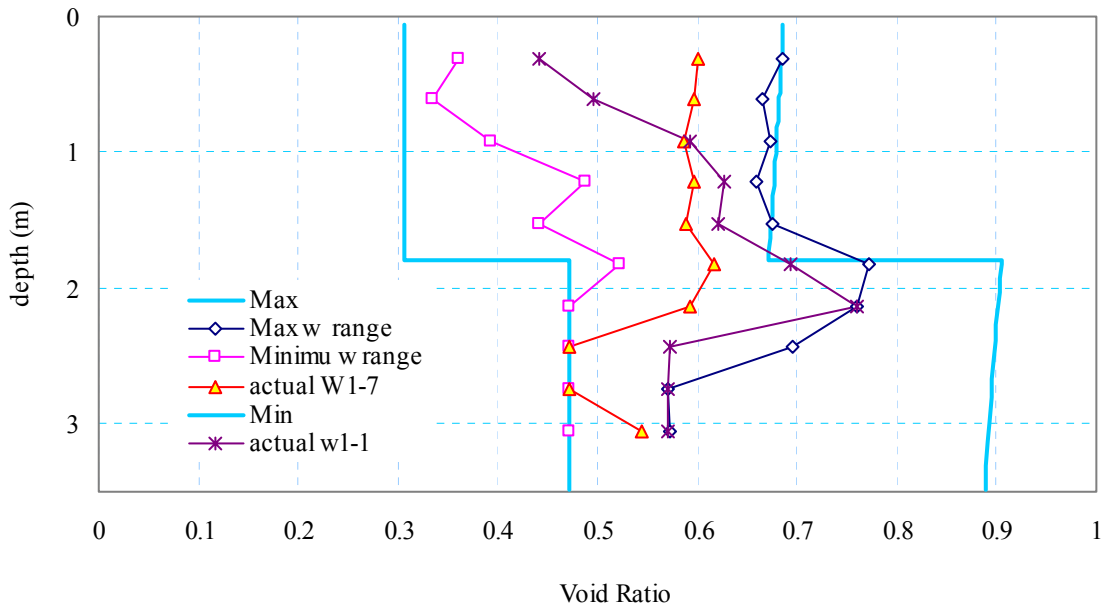


Fig. 10.9. The obtained void ratio profile of the site

The void ratio profile of the 1.8-3.0m soil layer is calculated in the same way as that for the 0-1.8m shown in Fig.7. The result is shown in Fig. 10.9. The vertical volume change can be calculated by the following equation:

$$\Delta H = \sum_{i=1}^n \Delta H_i = \sum_{i=1}^n \frac{\Delta e}{1 + e_0} H_i \quad (10.8)$$

where H_i is the thickness of layer i ; Δe is the range of void ratio variation; and ΔH is the potential vertical movement.

In the example, the maximum possible vertical movement is 0.9623m by comparing the swell limit with the shrinkage limit. The potential vertical shrink for footing W1 is 0.4058m by comparing the W1-1 void ratio profile with the shrinkage limit and the potential vertical swell is 0.5564m. In the same way, the potential vertical shrink and the potential vertical swell for W1-7 can be obtained, which are 0.3512m and 0.6111m

respectively. The total vertical movement for W1-7 is the same as W1-1 for the same boring at different time.

The relative movement for Boring W1 between the W1-1 (06/24/1999) and the W1-7 (11/17/2000) period can be calculated by comparing their void ratio profiles and the movement is -0.0453m (shrink), which is much smaller than the potential vertical movements. The reason will be explained in the next section. Calculations can also be performed between the W1-1 (or W1-7) and the maximum water content and minimum water content ranges due to the climate variation, which will gives the maximum potential vertical movements due to the climate.

10.6 Discussion

10.6.1 Potential Vertical Swell, Potential Vertical Shrink and Total Vertical Movements of Expansive Soils

Slabs built on expansive soils will distort into either a center lift (or edge drop) mode (Fig. 2.13) or an edge lift (center lift) mode (Fig. 2.14) when it experiences a change in its moisture content after construction of the slab (PTI manual 1996). Center lift is considered as a long term condition which occurs when the moisture content of the soil around the perimeter of the slab gradually decreases and the soil shrinks relative to the soil beneath the interior of the slab. Conversely, edge lift is, in general, seasonal or short term condition and occurs when the soil beneath the perimeter becomes wetter than the soil beneath the interior of the slab. The differential movement is needed for design. Fredlund and Rahardjo (1993) suggested that the differential movement of a light structure experiences is very close to the expected total movement. Therefore, the estimate of total movement is useful for the design. To design a structure on expansive soils, both damage modes in Fig. 2.13 and 2.14 should be considered. For the center lift case, the potential shrink of the soil needs to be estimated, and consequently, the potential vertical swell should be considered for the edge lift case.

The PVR method estimates the potential vertical swell only. Fig. 10.10 shows PVR values for the Arlington site during the two years period (06/24/1999-10/13/2001). It can

be seen that the PVR value is a function of time. The reason is that the PVR values are calculated by comparing the current water content with the maximum possible water content of a soil. When the samples for the same soil are obtained at different time of the year, the soil water contents are different, and so are the calculated PVR values. It is obvious that the PVR is not a good value for design purposes or at least misleading. The method proposed by Fredlund has the same problem because it also compares the current status with the future soil, while an effective method of estimating the future status is not given. Usually Fredlund's method assumes that the minimum future suction is equal to zero, which will cause a similar problem to the PVR method. In addition, Fredlund's method has difficulty in predicting the potential vertical shrink because the corresponding matric suction values for the shrinkage limits at different mechanical stress levels can not be predicted.

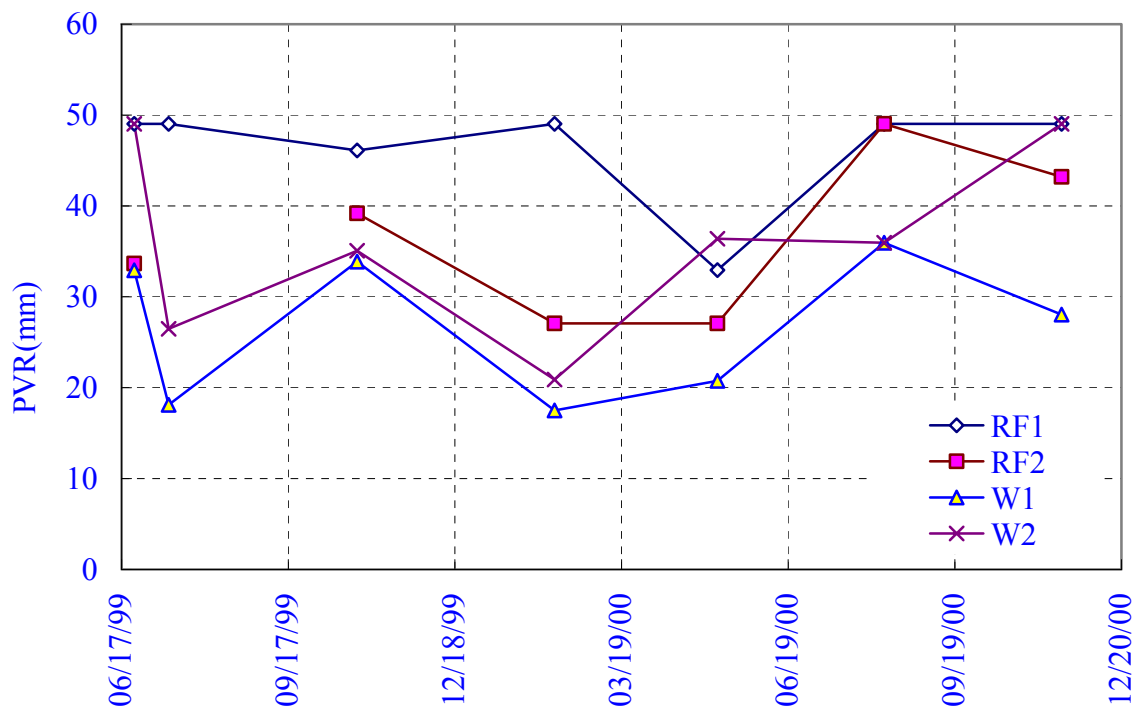


Fig. 10.10. The calculated PVR values for the site over a period of two years

Both the potential swell and the potential shrink at the present time can be obtained from Fig. 10.9 by the proposed method. The potential vertical swell plus potential vertical shrink should be used as a guide for design, which is more reasonable than the PVR value only.

10.6.2 Transient Movements and Maximum Vertical Movements

As we discussed before, the vertical movements for footing W1 between the W1-1 (06/24/1999) and W1-7 (11/17/2000), which is -0.0453m (shrink), is much smaller than the potential total vertical movement of the soil, which is 0.9623m. The reason is that the potential vertical movements correspond to extreme conditions, that is, conditions when the soil is extremely dry (the water content at any position is below the shrinkage limit) or extremely wet (the water content at any position reaches the swell limit) at the whole soil profile.

Under real condition, only the soil at the ground surface is possible to reach these conditions. For the soil at a certain depth, the range of water content variations is much smaller. If the soil is deep enough, the water content will be constant and will not change any more. In addition, the climate varies cyclically each year, which causes the water content in the soil varies cyclically. The cyclic water content variation in the soil profile will cause soils to shrink at some depths while swell at other depths at the same time. By comparing the void ratio profile W1-1 with W1-7, we can find that in the first layer the soil with a depth less than 0.8m swells (void ratio increases) and the soil with a depth greater than 0.8m shrinks. Either the maximum swell or shrink could not be reached. These two different volume changes cause the actual vertical movements far less than the predicted potential vertical movements. Fig. 4.4 shows the observations of the movements for the four footings caused by the climate variation in a period of two years. The actual amplitude of the vertical movements is 0.08m, much less than the maximum potential vertical movements, 0.9623m. In this way, a design for climate-controlled vertical movements and that for extreme conditions are greatly different from each other. Further research is needed in this direction. The numerical simulation will be able to

give a better understanding for the problem. Compared the PVR value range in Fig. 10.10 with the observed vertical movements range in Fig. 4.4, it is found that the PVR method underestimate approximately 2/3 of the range of the vertical movements, which is because the PVR method assumes the volume change of the soil is the same in all directions while the actual vertical movements mainly occurs in the vertical direction due to the lateral restraint.

10.6.3 Methods to Estimate the “Shrink-Swell Potential”

The potential for clay to cause damage by shrinking and swelling is called its shrink-swell potential. For convenience, this parameter is assumed to be proportional to the difference between the liquid limit and the plastic limit, that is, the plastic index. The most recently proposed classifications of shrinkage potential by BRE are shown in Table 1.1. However, this assumption has not been proved.

Briaud et al. (2003) proposed that for natural conditions, the shrinkage limit can be defined as the intersection of the two linear parts of the water content vs. volume change curve and that the range of water content between the shrink limit w_{sh} and the swell limit w_{sw} can be used as a shrink swell index ($I_{ss} = w_{sw} - w_{sh}$). Based on experience on the shrink test and the swell test, the soil shrink-swell potential is classified as Table 1.2. It is more realistic for the estimate of possible damage than the use of the plasticity index. However, the influence of the mechanical stress is not considered. Fig. 10.6 shows the influence of both soil type and mechanical stress.

The reason why we should use the shrink swell index instead of plasticity index to define the shrink-swell potential can also be explained by the bimodal structure of the soil. The soil with the same plasticity index can be considered to have the similar micropores or microstructure. For the soil with the similar microstructure, for example, soils with the same minerals, the macrostructures could be different. The different macrostructures correspond to different engineering properties. The shrink swell index obtained from the undisturbed soil actually reflects the macrostructures of the soils in

some degree. Conversely, the plasticity index is obtained by disturbing the soil completely and it can not reflect the actual macrostructure of the soil.

10.6.4 Influence of Mechanical Stress on Shrink-Swell Modulus

Briaud et al. (2003) proposed a water content method and defined the shrink-swell modulus E_w as the slope of the water content vs. volumetric strain line. Four sets of shrink tests on man-made porcelain clays with overburden pressure were performed to investigate the influence of the mechanical stress on the shrink-swell modulus E_w . The tests tended to indicate that the vertical pressure does not influence E_w . From Fig. 10.6, we can see that the variation range of the shrink-swell modulus E_w is between the free shrink test line AIB and the $S=100\%$ line. In fact, if the soil is saturated, using phase relationships leads to the following equation for E_w (Briaud et al. 2003):

$$E_w = \gamma_w / \gamma_d$$

or

$$E_w = \frac{1 + e_0}{G_s} \quad (10.9)$$

When the degree of saturation for free shrink test is close to 100%, the shrink-swell modulus E_w will not vary very much and be approximately equal to γ_w / γ_d . For a natural soil with a degree of saturation much lower than 100% and with water content above the shrinkage limit, it is expected that the shrink-swell modulus E_w in the free shrink test will vary in a larger range and the influence of the mechanical stress on the shrink-swell modulus E_w will be substantive.

10.7 Conclusion

Current methods for predicting the movement of expansive soils have been reviewed. The difference between them and their relationships are explained. The potential problems associated with their applications in current practice are discussed. The volume change of an unsaturated soil is explained by using constructed constitutive surfaces. The research indicates that the soil status can be determined uniquely by the soil depth, water content and the unit weight of the soils. This conclusion makes a coupled water content and mechanical stress method possible. A simplified version of the coupled water content and mechanical stress method is presented. Three tests, i.e. the free shrink test, the one dimensional consolidation test and the specific gravity test, are needed. An example calculation is performed.

The results indicate that PVR method gives only the potential swell and depends on the timing at which the soil is sampled. As a consequence, the design based on the PVR value is misleading and meaningless. It is the total vertical movement, which is the sum of the potential vertical swell and potential vertical shrink, rather than the PVR that determine the possible damage to a house. Using the plasticity index to determine the shrink-swell potential does not seem to be well founded. A better way is to use the shrink-swell index. However, the influence of the mechanical stress on the shrink-swell index should be investigated. The influence of the mechanical stress on the slope of the shrink test curve is limited when the degree of saturation of the soil (above the shrinkage limit) is high. Future research is needed in this area. Research also indicates that the predicted vertical movements by using extreme conditions as limiting conditions will excessively overestimate the range of climate-controlled movements. For design purposes, it is the differential movement instead of the total movement that creates the damage. More accurate and simpler methods to predict the suction or water content profile are needed to get the differential movements. Numerical methods as what we performed in the previous chapters seem to be a good way to achieve this.

CHAPTER XI

CONCLUSIONS AND FUTURE RESEARCH

In this dissertation, a complete system for the simulation of the behaviors of residential buildings on expansive soils is developed. The strength of this method lies in its use of simple and readily available historic weather data such as daily temperature, solar radiation, relative humidity, wind speed and rainfall as input. Accurate three dimensional predictions are obtained by integrating a number of different analytical and numerical techniques: different simulation methods for different boundary conditions such as tree, grass, and bare soils, coupled mechanical stress and matric suction analysis to describe deformation of saturated-unsaturated soils, jointed elements simulation of soil-structure interaction, analysis of structure stress moment by general shell elements, and assess of structure damage by smeared model. The real-time and dynamic simulation results are consistent with filed measurements very well.

In addition, the consolidation theory for unsaturated soils is investigated. The constitutive surfaces for saturated soils are provided and a new method is proposed to construct the constitutive surfaces for unsaturated soils by using simple laboratory tests. Terzaghi's consolidation theory for saturated soils is explained by using the theory of unsaturated soils mechanics. A new method for the calculation of the one dimensional consolidation for unsaturated soils is proposed. For the first time, the immediate settlement, consolidation settlement, total settlement, time rate of consolidation for unsaturated soils and excessive pore water pressure can be calculated manually in the same way as what we have done for saturated soils with a higher accuracy. It makes the consolidation theory of unsaturated soils as applicable as that of saturated soils. This method can also be used to perform uncoupled two or three dimensional consolidation calculation for both expansive soils and collapsible soils. From the analysis, the equivalent effective stress and excessive pore water pressure can be easily calculated.

At the same time, the physical meanings for the parameters in the constitutive laws

for saturated-unsaturated are illustrated. A new set of the differential equations for the coupled two or three dimensional consolidation of saturated-unsaturated soils are proposed, together with the corresponding method to solve the differential equations. It is also proved numerically and analytically that during the consolidation process the Mandel-Cryer effect exists for unsaturated expansive soils and there is a “reverse” Mandel-Cryer effect for unsaturated collapsible soils. Furthermore, a new method to estimate the volume change of expansive soils is proposed.

The principal conclusions that can be drawn from this study can be outlined in section 11.1. Recommendations for future research are discussed in section 11.2.

11.1 Conclusions

The following conclusions are drawn from the previous chapters:

(1). The bimodal structure model is a good model to explain the soil behaviors. The investigation of soil fabric reveals that there are two distinct structural levels: a micro-structural one and a macro-structural one. Single clay particles are surrounded by water and form a double diffusion layer. They grouped together to form aggregates. Under most cases, the aggregates are saturated internally due to the microspores formed by the single clay particles are so small and the corresponding air entry values are so high. Terzaghi’s effective stress principle therefore holds internally in the aggregates. The soil is then composed of a lot of “granular” aggregates. Between aggregates there are a lot of macropores. The single soil particles and water are incompressible while as a consequence of grouping of aggregates, the soil structure is compressible, especially when there is air in the macropores. Nearly all the soil behaviors can be explained by the bimodal structure of the soils.

(2). Observations indicate that the mechanical stresses mainly influence the macrostructure while the matric suctions influence both the macrostructure and microstructure of soils.

(3). The null tests performed can only prove that there are some relationships between the material parameters in the constitutive laws for the volume change of

unsaturated soils. They can not prove that $(\sigma - u_a)$ and $(u_a - u_w)$ can be used as a complete set of stress state variables to describe the volume change behavior of the soils. Neither did they prove that $(\sigma - u_a)$ and $(u_a - u_w)$ can be used as a complete set of stress state variables to describe the shear strength of the soils.

(4). To understand the behavior of unsaturated soils, three stress state variables such as mechanical stress, pore water pressure, and pore air pressure are needed. $(\sigma - u_a)$ and $(u_a - u_w)$ are actually not a complete set of stress state variables. It is not convenient to investigate the soil behavior by using $(\sigma - u_a)$ and $(u_a - u_w)$ as stress state variables because when it is not easy to separate the influence of the mechanical stress, pore water pressure and air pressure. For the water phase, the driving force for the water flow is the hydraulic head instead of matric suction. The hydraulic head is directly related to pore water pressure by the energy equation. It is more convenient to use pore water pressure as stress state variable to construct the constitutive law, and to derive the differential equation for the water phase. For the similar reason, the air pressure should be used to construct the constitutive law, and to derive the differential equation for the air phase.

(5). The excess air pressure will dissipate much faster than excess pore water pressure because the air coefficients of permeability are much bigger than water coefficients of permeability. When the air phase is not continuous, the air phase can be considered as part of the soil structure. Under both conditions, the differential equation of the air phase is not needed, i.e. only the mechanical stress and pore water pressure are needed as stress state variables.

(6). Two stress state variables (mechanical stress or effective stress and pore water pressure) instead of only one stress state variable (effective stress) are needed to investigate the volume change behaviors of saturated soil. Three stress state variables (mechanical stress or effective stress, pore water pressure and air pressure) instead of two (mechanical stress and matric suction) are needed to investigate the volume change behaviors of saturated soil. The excess pore air pressure can be considered to be

dissipated instantly under some conditions. Under these conditions, two stress state variables are needed to investigate the behaviors of saturated -unsaturated soils.

(7). In the coupled hydro-mechanical stress problem, mechanical stress and matric suction are two independent stress state variables. They have completely different physical meanings. The constitutive relations for these two stress state variables are totally different and the influences on the volume change of the soil are also different. When the matric suction decreases, the soil volume increases in the same magnitude in all three directions. When there is a load application in one direction on the soil, the strains in different directions are different and dependent on Poisson's Ratio. Actually, their relationship is exactly the same as the relationship between the temperature and the mechanical stress in the coupled thermal stress problem. We can not use the mechanical stress to replace matric suction. Neither can we use the matric suction to replace the mechanical stress. They are working independently with different constitutive laws. Therefore, when we describe the volume change behavior of unsaturated soils, both mechanical stress and the matric suction are needed.

(8). The physical meanings of the material parameters in the constitutive laws proposed by Fredlund and Morganstern (1980) are as followings: m_1^s is the inverse of bulk modulus, m_2^s is the triple of coefficient of expansion due to matric suction variation, and m_2^w is the multiply of the dry unit weight of the soil and the specific water capacity. The physical meaning of m_1^w is related to "water generation" or "water source term". Biot (1941) explained the physical meanings of these parameters in the similar way. However, he proved that $m_2^s = m_1^w$ (that is, $3\alpha = m_1^w$) by assuming the existence of a potential energy of the soil, which is questionable because these two parameters have two different physical meanings. Only under the special case when the soil is saturated, it is right.

(9). A saturated soil is a special case of an unsaturated soil. For saturated soil, the material properties satisfy the following relationship: $m_1^s = m_2^s = m_1^w = m_2^w = \frac{1}{1+e_0} \frac{\partial f}{\partial \sigma'}$.

(10). χ in Bishops' Equation is equal to $3\alpha B$. For saturated soils, $3\alpha B$ is equal to unity because of the effective stress principle. For unsaturated soils, the χ is not a constant because of the highly nonlinear properties of unsaturated soils. Both α and B are functions of both mechanical stress and matric suction, depending on material properties. It is not proper to include material properties in the stress state variable. Therefore it is not proper to use effective stress as a stress state variables to investigate the behaviors of unsaturated soil.

(11). The collapsible soil behaviors can be explained by the effective stress principle (Bishop's Equation) too. The only difference is that χ is negative for collapsible soils. The effective stress defined by Bishop's Equation is a microscopic intergranular effective stress while it is actually a macroscopic equivalent effective stress, which will be explained in the following section. The soil behavior can be explained by the bimodal pore distribution.

(12). The excess pore water pressure parameter is $B_w = -\frac{m_1^w}{m_2^w}$.

(13). The statement that m_2^w is positive for collapsible soils is incorrect. A positive m_2^w means that when adding water to a collapsible soil, matric suction of the soil will increase. It conflicts with the physical meaning of m_2^w and experiment data.

(14). The thermodynamic analogue to process of consolidation firstly proposed by Terzaghi can facilitate the visualization of the mechanics of consolidation and swelling. It is found that there are close similarities between the coupled thermal stress problem and the couple consolidation theory for unsaturated soils. Mass of water (kg) in the coupled consolidation problem corresponds to energy (J) in the coupled thermal stress problem and pore water pressure ($u_a - u_w$) or u_w (or matric suction, kPa) in the coupled consolidation problem corresponds to temperature T or $(-T)$ (K) in the coupled thermal stress problem.

(15). The void ratio constitutive surface for a saturated soil is $e = f((\sigma - u_a) + (u_a - u_w))$, and the water content constitutive surface for a saturated soil

is $wG_s = f((\sigma - u_a) + (u_a - u_w))$. They have the exactly same shape but different physical meanings. The water content constitutive surface for a saturated soil is $S=1$.

(16). A new method is proposed to construct the constitutive surfaces for unsaturated soils by using four simple laboratory tests: suction test, one dimensional consolidation test, free shrink test and specific gravity test of a soil.

(17). A new method for the calculation of the one dimensional consolidation for unsaturated soils is proposed. To the author's knowledge, it is for the first time that the immediate settlement, consolidation settlement, total settlement, time rate of consolidation for unsaturated soils and excessive pore water pressure can be calculated manually in the same way as what we have done for saturated soils with a higher accuracy. It makes the consolidation theory of unsaturated soils as applicable as that of saturated soils. This method can also be used to perform uncoupled two or three dimensional consolidation calculation for both expansive soils and collapsible soils. From the analysis, the equivalent effective stress and excessive pore water pressure can be easily calculated.

(18).The uncoupled consolidation process for both saturated and unsaturated soils can be described as followings: At the instant of load application, $t = 0$, there is no water drainage. At any time t , such that $0 < t < \infty$, the excess pore water pressure will dissipate. This process is a time-dependent process. At time $t = \infty$, all the excess pore water pressure will dissipate completely. Unlike a saturated soil, an unsaturated soil will experience a decrease in volume at the instant of load application due to the existence of air phase. The excess pore water pressure parameter is not equal to unity any more.

(19). Skempton's derivation for the excess pore water pressure parameter for unsaturated soils is incorrect. The effective stress principle for saturated soils was used to derive the excess pore water pressure parameter for unsaturated soils. His explanation for the experimental data is also incorrect because the initial pore water pressure is not considered. Computation and analysis indicate that the excess pore water pressure parameter can be greater than unity instead of being always between 0 and 1. To date

most authors use Skempton's equation to verify their consolidation theory for unsaturated soils. As a consequence, their computations are questionable.

(20). The computation of volume change during the consolidation process involves two processes: 1. taking the derivatives of the void ratio constitutive surface to get the material parameters m_1^s and m_2^s , and then calculate the volumetric strain due to small stress increments, 2. integrating the small volumetric strains into volumetric strain. These two processes are reverse to each other. By "taking the readings" for the initial and final void ratio, the same calculation result can be obtained without involving any nonlinear deriving and integrating process. The calculation is expected to have a higher accuracy than the numerical method because there will be some calculation errors during the integration and the derivation process for a nonlinear problem. The proposed method for the consolidation theory for unsaturated soils can also be applied to saturated soils. It is unnecessary to use the compressibility coefficient to calculate the volume change of saturated soils. The void ratio variations can be "read" directly for the void ratio versus mechanical stress curve.

(21). Equation 6.73 and 6.90 are actually the same as the differential equations proposed by Fredlund and Rahardjo (1993) for the coupled consolidation for unsaturated soils, the left sides of both equations represent the net water flow into the unit element and the right sides are the volumetric water content variation. However, Equation 6.73 has some advantages. If Equation 6.73 is used, the water generation can be easily simulated by the heat generation in the coupled thermal stress problem. Consequently, we can modify current programs for the coupled thermal stress problem, which are readily available and well-developed, for the simulation of coupled consolidation problem for saturated-unsaturated soil.

(22). The uncoupled consolidation theory for saturated-unsaturated soils is discussed under the assumption that the total stresses remain constant during the process of consolidation. The assumption is not strictly true. However, the assumption greatly simplifies the problem and the results obtained under this assumption can provide helpful information for the consolidation behavior of the unsaturated soil. Mechanical

stresses are actually varying during the consolidation process. The consolidation theory under the assumption that the mechanical stresses is varying during the process of consolidation is called true two- or three- dimensional consolidation theory or coupled consolidation theory.

(23). Mandel-Cryer effect exists in the coupled consolidation analysis of unsaturated expansive soils.

(24). A collapsible soil is different from an expansive soil in that collapsible soil will experience a decrease in volume when the matric suction decreases (or pore water pressure increases). The difference, when expressed in the material parameters, is that m_1^s , m_1^w , and m_2^w are negative and m_2^s is positive for collapsible soils while all these parameters are negative for expansive soils. A “reverse” Mandel-Cryer effect exists in the coupled consolidation analysis of unsaturated expansive soils.

(25). Six parameters will influence the Mandel-Cryer effect. They are: m_1^s , m_2^s , m_1^w , m_2^w , permeability k and Poisson's ratio μ . An increase in Young's Modulus or decrease in the coefficient of expansion of the soil will cause the Mandel-Cryer effect severe. If the χ is the same, the Mandel-Cryer effect will be the same. An increase in m_1^w or a decrease in m_2^w will result in a higher excess pore water pressure. If the $B_w = -\frac{m_1^w}{m_2^w}$ is the same, the initial excess pore water pressure will be the same. However, the dissipation process depends on the diffusion coefficient ($\alpha = k_w/m_2^w$) instead of permeability coefficient k_w only. For a soil with a lower diffusion coefficient, the Mandel-Cryer effect will be more severe, namely the peak excess pore water pressure will higher and the dissipation process is slower.

(26). Two processes are involved in the evaporation or transpiration. The first is on an energy basis in which energy is needed to change the state of the molecules of water from liquid to vapor. The second one is on an aerodynamic basis in which the saturated water vapor is removed by a process of eddy diffusion. Numerically it is a coupled thermo-hydro-mechanical problem. Due to the difficulties in obtaining the material

properties and determining the boundary conditions, so far it is still unable to simulate the evapotranspiration accurately. An alternative method is to estimate the evapotranspiration empirically. The temperature methods are empirical equations that rely on air temperature as a surrogate for the amount of energy that is available to the reference crop for evapotranspiration. The Radiation methods use a measure of solar radiation coupled with air temperature to predict Evapotranspiration. Both methods have drawbacks. The FAO 56 Penman –Monteith method is well established as the most accurate and robust methods to estimate reference ET, and the past decade of research has solidified its status as the international standard. Different boundary conditions such as tree root zone, grass root zone and bare soils can be handled with different methods. The real-time and dynamic simulation results by using the FAO 56 Penman –Monteith method to estimate the evapotranspiration are consistent with field measurements very well, indicating that the proposed method for the simulation of the influence of weather is reasonable.

(27). Contact elements have better adaptability to simulate the soil-structure interaction for the foundations on expansive soils than Winkler's foundation and Boussinesq's solution. The separation can be handled and the normal and tangential behavior can be modeled in a more flexible way. The results are more close to reality.

(28). General shell elements a useful tool to simulate the behaviors of foundations and walls. Shear locking can be avoided by using reduced integrations. Both thick shell and thin shell can be modeled.

(29). A unified system is proposed for the first time to simulate the behaviors of residential buildings on expansive soils. Tentative simulation results indicate there is need to reexamine the current design methods and criteria.

(30). Current methods for predicting the movements of expansive soils include: suction based methods, water content based methods and consolidation test based methods. Suction based methods use the matric suction as a stress state variable, water content based methods use water content as a state variable while consolidation test based methods use equivalent effective stress as a state variable. Both the water content-

based method and the suction based method have the same theoretical basis. They can be interchanged with each other through the soil-water characteristic curve when numerical simulation is performed. Consolidation test based methods is trying to find the “equivalent effective stress” variation due to suction variation, and use the one-dimensional consolidation compression index to calculate the volume change due to suction. However, it is not easy to find the equivalent effective stress because matric suction and mechanical stress are two independent stress state variables and their constitutive laws for the volume change of expansive soils are totally different and highly nonlinear.

(31). Both the PVR method and the Fredlund’s method predict the potential vertical heave only by comparing the current soil status with the wettest status of a soil. The corresponding results obtained by these two methods therefore depend greatly on the timing of the sampling and are misleading. Soil can not only swell but also shrink. As a consequence, both the potential vertical rise and the potential vertical shrink are critical to the design of the foundation. Under the assumption that the influence of the pore air pressure on the volume change of an expansive soil can be omitted, any two variables of the five state variables, i.e., void ratio, water content, degree of saturation, net normal stress and matric suction can be used to determine the other three state variables. A new coupled water content based method is proposed to estimate the potential vertical rise and the potential vertical shrink at the same time.

(32). Field observations indicate that the actual movements of the soil in the field are much smaller than the potential vertical movements of the soils. The reason for this is that the soils at different depths can not reach the maximum or minimum possible water content at the same time due to the cyclic variation of the weather. It is the differential movements instead of total moments that cause the damage to house.

11.2 Future Research Needed

Recommendations for future research are summarized as follows:

1. A unified system is proposed for the simulation of residential buildings on expansive soils. The system can be more complete by including the cracking models for the slabs and the walls. Smear model can be used to simulate the possible cracking in the slabs and walls. The smeared crack model does not track individual “macro” cracks. Constitutive calculations are performed independently at each integration point of the finite element model. The presence of cracks enters into these calculations by the way in which the cracks affect the stress and material stiffness associated with the integration point.

2. In this dissertation, the slabs used in the simulations have uniform thickness and there is no beam. In practice, there are usually stiffening beams in the slabs. It is better to include the stiffening beams in the system too. The simplest method to include stiffening beams in the slabs is to increase the thickness of the slabs along the corresponding beam locations.

3. A method is proposed to interpolate the constitutive surfaces for unsaturated soils by using four simple laboratory tests. The constitutive surfaces can be measured directly. However, usually this kind of test requires advanced lab equipments and the testing is very time-consuming. So far it is not easy to get high quality data, especially in the high suction range. More research is needed in this direction to find easy and simple way to obtain high quality data for the construction of constitutive surfaces of unsaturated soils.

4. Poisson’s ratio in this dissertation is considered as a constant. However, it should also be a function of both mechanical stress and matric suction. More research is needed in this direction. Triaxial tests with controlling both mechanical stress and matric suction for unsaturated soils are needed to obtain the Poisson’s ratio surface.

5. It is proved numerically and analytically in this dissertation that Mandel-Cryer effect exists for unsaturated expansive soils and reverse Mandel-Cryer effect exists for unsaturated collapsible soils. However, no experiment is performed to verify these

conclusions. Consolidation tests for both unsaturated expansive and collapsible soils are needed to verify the conclusion.

6. The null tests only proved that the volume changes of the soil structure and water volume are functions of $\sigma - u_a$ and $u_a - u_w$ only. The conclusion that the shear strength of unsaturated soils can be expressed as functions of $\sigma - u_a$ and $u_a - u_w$ only can not be made for the null tests. More research is needed to verify the shear strength equation proposed by Fredlund and Rahardjo.

7. Specific experiments different from the measuring of the shear strength of unsaturated soils are needed to investigate the shear strength at the soil-slab interface.

8. In this dissertation, different methods are proposed to simulate the water loss for different vegetations. Only the grass boundary condition is verified by the field observations at a site at Arlington, Texas. More research is needed to verify the conditions when the vegetations are tree or bare soils. For different tree species, the crop coefficients should be different.

9. In this dissertation, the soils are considered as elastic. However, it is well known the soils are elastoplastic materials. Soil will also creep under constant load. More research is needed in this direction to investigate the influence of plasticity and creep.

10. At the ground surface, there are always cracks in the soils. The soil cracks will influence the volume change behavior, permeability and evapotranspiration. More research is needed to determine the cracking mechanism and quantify the influence of cracks on the soils behaviors.

11. As we discussed in Chapter VII, the evapotranspiration problem is actually a coupled thermo-hydro-mechanical problem. All the material parameters in the THM problems are functions of temperature, pore water and air pressure and mechanical stress. The constitutive surfaces for the soils are multidimensional surfaces. How to determine these constitutive surfaces is an extremely difficult problem.

REFERENCES

- ABAQUS/Standard User's Manual* (2002). Vol. I, II, and III, Version 6.3, Hibbit, Karlsson and Sorenson Inc., Pawtucket, RI
- ABAQUS/CAE User's Manual* (2002). Version 6.3, Hibbit, Karlsson and Sorenson Inc., Pawtucket, RI.
- ABAQUS Theory Manual* (2002). Version 6.3, Hibbit, Carlson and Sorenson Inc., Pawtucket, RI
- Ahmad, S., Irons, B.M., and Zienkiewicz, O.C.(1970) "Analysis of Thick and Thin Shell Structures by Curved Elements." *Intl. Journal of Numerical Methods in Engineering*, 2, 419-451.
- Aitchison, G. D. (1961). "Relationship of moisture and effective stress functions in unsaturated soils." *Proceedings, Conference on Pore Pressure and Suction in Soils*. Butterworths, London, pp. 47-52.
- Allen, R.G., Periera, L.S., Raes, D., and Smith, M. (1998). *Crop evapotranspiration: guidelines for computing crop requirements*. Irrigation and Drainage Paper No. 56, FAO, Rome, Italy
- Allen, R.G., Pruitt, W.O. (1991). "FAO 24 reference evapotranspiration factors." *J. Irrig. Drain.* 117(5): 758-774.
- Alonso, E. E., Gens, A., and Josa, A. (1990). "A constitutive model for partially saturated soils." *Geotechnique*, 40(3), 405-430.

- ASTM D2325-68, (1993). "Standard test method for capillary-moisture relationships for coarse and medium textured soils by porous plate apparatus." *1993 Annual Book of ASTM Standards*, Philadelphia, PA.
- ASTM D2435 (1993). "Standard test method for one-dimensional consolidation properties of soils." *1993 Annual Book of ASTM Standards*, Philadelphia, PA.
- ASTM D4546 (1993). "Standard test method for one-dimensional swell or settlement potential of cohesive soils." *1993 Annual Book of ASTM Standards*, Philadelphia, PA.
- ASTM D5298 (1993). "Standard test method for measurement of soil potential suction using filter paper." *1993 Annual Book of ASTM Standards*, Philadelphia, PA.
- Atabek, R. B. , Felix, B., Robinet, J. C. and Lahlou, R. (1991). "Rheological behavior of saturated expansive clay materials." *Workshop on Stress Partitioning in Engineered Clay Barriers*, Duke University, Durham, NC.
- Barden, L., and Pavlakis, G. (1971). "Air and water permeability of compacted unsaturated cohesive soil." *Journal of Soil Science*, 22, 302-317.
- Barry D.A., Parlange, J.Y., Sander, G.C., and Sivaplan, M. (1993). "A class of exact solutions for Richard's equation." *J. Hydro.*, 142(1-4), 29-46.
- Bazant, Z.P., and Cedolin, L. (1979). "Blunt crack band propagation in finite element analysis." *J. Engng. Mech. Div., ASCE* ;105,297–315.
- Biddle, P.G. (1998). *Tree root damage to buildings*. Willowmead Publishing Ltd, Wantage, OX, U.K. (<http://www.willowmead.co.uk/>)

- Biot, M. A. (1941). "General theory of three-dimensional consolidation." *J. Appl. Phys.*, 12(2), 155-164.
- Bishop, A. W. (1954). "The use of pore pressure coefficients in practice." *Geotechnique*, 4(4), 148-152.
- Bishop, A. W., and Blight, G. E. (1963). "Some aspects of effective stress in saturated and unsaturated soils." *Geotechnique*, 13(3), 177-197.
- Blaney, H.F. and Criddle, W.D. (1950). "Determining water requirements in irrigated areas from climatological and irrigation data." *USDA Soil Conservation Service Technical Paper, 96*, 48 pp.
- Building Research Advisory Board (BRAB), (1968), *Criteria for selection and design of residential slabs-on-ground*, National Academy of Sciences, Building Research Advisory Board.
- Briaud, J.L., Zhang, Xiong and Moon, S. (2003). "The shrink test – water content method for shrink and swell predictions." *Journal of Geotechnical and Geoenvironmental Engineering*, ASCE 129(6), 590-600.
- Bulut, R. (2001). "Finite element method analysis of slabs on elastic half space expansive soil foundations." Ph.D. Dissertation, Department of Civil Engineering, Texas A&M University, College Station, TX.
- Buckingham, E. (1907). *Studies of the movement of soil moisture*. U.S.D.A. Bur. of Soils, Bull. 38. U.S. Gov. Print. Office, Washington, DC.

- Chen, Z. S., Zhou, J. X., and Wang, H. J., (1994). *Soil mechanics*. Tsinghua University Press, Beijing, China.
- Childs, E.C. (1969). *An introduction to the physical basis of soil water phenomena*. John Wiley & Sons Ltd., London.
- Childs, E.C., and Collis-George, G.N. (1950). "The permeability of porous materials." *Proceedings, Royal Society of London, Series A*. 201, 392-405.
- Collins, K., and McGown, A. (1974) "The form and function of microfabric features in a variety of natural soils." *Geotechnique*, 24(2), 223-254.
- Crisfield, M. A. (1986). "Snap-through and snap-back response in concrete structures and the dangers of under-integration." *International Journal for Numerical Methods in Engineering*, 22,751–767.
- Cronev, D., and Coleman. J.D. (1961). "Pore pressure and suction in soils." *Proceedings, Conference on Pore Pressure and Suction in Soils*. Butterworths, London, pp. 31-37.
- Cryer, C. W. (1963). "A comparison of three dimensional theories of Biot and Terzaghi." *Quarterly Journal of Mechanics and Applied Mathematics*, 16, 72–81.
- Cui, Y. J., Loiseau, C. and Delage, P. (2002). "Microstructure changes of a confined swelling soil due to suction controlled hydration." *Proc. 3rd Int. Conf. Unsaturated Soils*, Recife, Brazil, 2, 593-598.
- Dakshanamurthy, V., Fredlund, D. G., and Rahardjo, H. (1984). "Coupled three-dimensional consolidation theory of unsaturated porous media." Preprint of Papers:

5th Int. Conf. Expansive Soils, Institute of Engineers, Adelaide, South Australia, May, pp. 99-104.

Departments of the Army and the Air Force (1987) *Concrete floor slabs on grade subjected to heavy loads*, ARMY TM 5-809-12 Air Force AFM 88-3, Chapter 15, August 1987.

Departments of Defense (1977) *Engineering and design: rigid pavements for roads, streets walks and open storage areas*, TM-5-822-6, U.S. Government Printing Office, Washington, DC

Doorenbos, J., and Pruitt, W.O. (1977). *Crop water requirements*. Irrigation and Drainage Paper No. 24, (rev.) FAO, Rome, Italy.

Escario, V. (1969). "Swelling of soils in contact with water at a negative pressure." *Proc. 2nd Int. Conf. Expansive Soils*, Texas A&M Univ., College Station, 1969, pp. 207-217.

Fargher, P. J., Woodburn, J. A. and Selby, J. (1979). "Footings and foundations for small buildings in arid climates." Inst. of Eng. Aust., S. A. Div. and Univ. Adelaide Adult Educ. Dep., Adelaide, Australia.

Fleureau, J.M., and Taibi, S. (1994). "A new apparatus for the measurement of polyphasic permeabilities." *Proceedings, 1st International Conference on Environmental Geotechnics*, Edmonton, Juillet, edited by W.D. Carrier, BiTech Pub., pp. 227-232.

Freeze, R. A., and Cherry, J. A. (1979). *Groundwater*. Prentice-Hall: Englewood Cliffs, NJ

- Fredlund, D. G. (1973). "Volume change behavior of unsaturated soils." Ph.D. dissertation, Univ. of Alberta, Edmonton, Alberta, Canada, 490 pp.
- Fredlund, D. G. and Hasan, J. U. (1979). "One-dimensional consolidation theory: Unsaturated soils." *Canadian Geotechnical Journal*, 16(3), 521-531.
- Fredlund, D. G., Hasan, J. U. and Filson, H. (1980) "The prediction of total heave." *Proc. of the 4th Int. Conf. on Expansive Soils*, Denver, CO, 1, pp. 1-17.
- Fredlund, D. G., and Morgenstern, N. R. (1976). "Constitutive relations for volume change in unsaturated soils." *Canadian Geotechnical Journal*, 13(3), 261-276.
- Fredlund, D. G., and Morgenstern, N. R. (1977). "Stress state variables for unsaturated soils." *ASCE J. Geotech. Eng. Div. GT5*, 103, 447-466.
- Fredlund, D. G. and Rahardjo. H. (1993). *Soil mechanics for unsaturated soils*. John Wiley and Sons, New York.
- Fredlund, D.G., and Xing, A. (1994). "Equations for the soil water characteristic curve." *Canadian Geotechnical Journal*, 31, 533-546.
- Gardner W. R. (1958). "Some steady state solutions of the unsaturated moisture flow equation with application to evaporation from a water table." *Soil Sci.*, 85(4), 228-232.
- Gay, D. A. (1994). "Development of a predictive model for pavement roughness on expansive clay." Ph.D. Dissertation, Department of Civil Engineering, Texas A&M University, College Station, TX.

- Gens, A. and Alonso, E. E. (1992). "A framework for the behavior of unsaturated expansive clays." *Canadian Geotechnical Journal*, 29, 1013-1032.
- Gens, A., Alonso, E.E. and Delage, P. (1997) "Computer modeling and applications to unsaturated soils." *Unsaturated Soil Engineering Practice*, Geotechnical Special Publication No. 68 (ed. Houston, S.L. and Fredlund, D.G.), ASCE, Reston, VA, 299-330.
- Gibson, R.E., Knight, K. and Taylor, P.W. (1963). "A critical experiment to examine theories of three dimensional consolidation." *Proc. European Conf. on SMFR*, Weisbaden, Germany, 1, 69-76.
- Goldberg, R. N. and Nuttall, R. L. (1978). "Evaluated activity and osmotic coefficients for aqueous solutions: The alkaline earth metal halides." *Journal of Physics and Chemistry Reference Data*, 7(1), 263-310.
- Goodman, R.E., Taylor, R.L. and Brekke, T. (1968). "A model for the mechanics of jointed rock." *Proc. ASCE*, 94, SM3, 637-659.
- Green W. H. and Ampt, G.A. (1911). "Studies in soil physics: The flow of air and water through soils." *J. Agri. Sci.*, 4(1),1-24.
- Hargreaves, G.H. and Samani, Z.A. (1982). "Reference crop evapotranspiration from temperature." *Applied Engrg. in Agric.*, 1(2), 96-99.
- Hetenyi, M. (1946). *Beams on elastic foundations*, The University of Michigan Press, Ann Arbor, MI.

- Hilf, J. W. (1956). "An investigation of pore-water pressure in compacted cohesive soils." *Tech. Memo. No. 654*, U.S. Dep. of the Interior Bureau of Reclamation, Design and Construction Div., Denver, CO
- Hilleborg, A., M. Modeer, and Petersson, P. E. (1976). "Analysis of crack formation and crack growth in concrete by means of fracture mechanics and finite elements." *Cement and Concrete Research*, 6, 773–782.
- Hillel, D. (1980). *Fundamentals of soil physics*. Academic Press, New York.
- Hillel, D. (1982). *Introduction to soil physics*. Academic Press, New York
- Ho, D.Y.F., Fredlund, D.G., and Rahardjo, H. (1992). "Volume change indices during loading and unloading of an unsaturated soil." *Canadian Geotechnical Journal*, 29(2), 195-207.
- Holtan, H.N. (1961). "A concept for infiltration estimates in watershed engineering." *USDA-ARS Bulletin 41-51*, Washington, DC. 25 p.
- Holtz R.D. and Kovacs W.D. (1981) *An introduction to geotechnical engineering*, Prentice Hall, Englewood Cliffs, NJ.
- Horton, R.E. (1940). "An approach toward a physical interpretation of infiltration capacity." *Soil Science Soc. Am. Proc.* 4, 399-417.
- Huang, S.Y. (1994). "Evaluation and laboratory measurement of the coefficient of permeability in deformable unsaturated soils." Ph.D. Dissertation, Department of Civil Engineering, University of Saskatchewan, Saskatoon.

- Huang, S.Y., Barbour, S.L. and Fredlund, D.G. (1998), "Development and verification of a coefficient of permeability function for a deformable unsaturated soil." *Canadian Geotechnical Journal*, 35, 411-425.
- Huang, Y. H. (1993). *Pavement analysis and design*, Prentice-Hall, Inc. Englewood Cliffs, NJ].
- Hung, V.Q., Fredlund, D.G., and Pereira, J.H.F. (2002). "Coupled solution of the prediction of volume change in expansive soils." *Proc. 3rd Int. Conf. Unsaturated Soils*, Recife, Brazil, 2, 593-598.
- Hungerford, E. (2001). "Evaluation of EcSS 3000 to mitigate the shrink-swell potential of soils." M.S. Thesis, Department of Civil Engineering, Texas A&M University, College Station, TX.
- Jacobs, J.M. and Satti, S.R. (2001). "Evaluation of reference crop evapotranspiration methodologies and AFSIRS crop water use simulation model." *Res. Rep. No. SJRWMD SJ2001-SP8*. University of Florida, Gainesville, FL. (<http://sjr.state.fl.us/programs/outreach/pubs/techpubs/pdfs/SP/SJ2001-SP8.pdf>)
- Jennings, J. E. (1961). "A revised effective stress law for use in the prediction of the behavior of unsaturated soils." *Proceedings, Conference on Pore Pressure and Suction in Soils*. Butterworths, London, 26-30.
- Jennings, J. E., and Burland, J. B. (1962). "Limitations to the use of effective stresses in partly saturated soils." *Geotechnique*, 12(2), 125-144.

- Jennings, J. E. and Knight, K.(1957). "The prediction of total heave from the double oedometer test." *Proc. Symp. Expansive Clay* , Johannesburg, South Africa, 7(9), 13-19.
- Jensen, M.E., Burman, R.D., and Allen, R.G. (1990). *Evapotranspiration and irrigation water requirements*. ASCE Manuals and Reports on Engineering Practices No. 70, ASCE, New York, NY. (<http://www.fao.org/docrep/X0490E/x0490e00.htm>)
- Johnson, L. D. (1977). "Evaluation of laboratory suction tests for prediction of heave in foundation soils." *Tech. Reports S-77-7*, U.S. Army Engineer Waterways Experiment Station, Vicksburg, MS, 118 pp.
- Jones, D. E. and Holtz, W. G., (1973). "Expansive soils - the hidden disaster." *Journal of Civil Engineering*, ASCE, New York, 43 (8), 49-51.
- Jones, D. E. and Jones, K. A., (1987). "Treating expansive soils." *Civil Engineering*, ASCE, New York, 57(8), 62-65.
- Kostiakov, A.N. (1932). "On the dynamics of the coefficient of water percolation in soils and on the necessity of studying it from a dynamic point of view for purpose of amelioration." *Trans. 6th Com. Int. Soc. Soil Sci.*, Moscow Part A, 17-21.
- Krohn, J. P. and Slosson, J. E. (1980). "Assessment of Expansive Soils in the United States." *Proc. 4th International Conference on Expansive Soils*, Denver, CO, 1, 596-608.
- Lambe, T.W. and Whitman, R.V. (1969). *Soil mechanics*. John Wiley & Sons, New York.

- Lloret, A., and Alonso, E. E. (1980). "Consolidation of unsaturated soils including swelling and collapse behavior." *Geotechnique*, 30(4), 449-477.
- Lloret, A., M.V., Sanchez, M., Gens, A., Pintado, X. and Alonso, E.E. (2003). "Mechanical behavior of heavily compacted bentonite under high suction changes." *Geotechnique*, 53(1), 27-40.
- Lytton, R. L. (1977). "Foundations on expansive soils." *Numerical Methods in Geotechnical Engineering*, Chapter 13, C. S. Desai and J. T. Christian (Eds.), New York: McGraw-Hill, 427-458.
- Lytton, R.L. (1994) "Prediction of movement in expansive clays." *Proceedings of the Settlement '94 Conference* held at Texas A&M University, Geotechnical Special Publication No. 40(2), 1827-1845, ASCE, Reston, VA.
- Mandel, J. (1953). "Consolidation des sols (étude mathématique)." *Géotechnique*, 3, 287-299.
- Matyas, E.L. and Radhakrishna, H. S. (1968). "Volume change characteristics of partially saturated soils." *Geotechnique*, 18(4), 432-448.
- McCloud, D.E. (1955). "Water requirements of field crops in Florida as influenced by climate." *Proc. Soil Sci. Soc. Fla.* 15,165-172.
- McDowell, C. (1956). "Interrelationships of loads, volume change, and layer thickness of soils to the behavior of engineering structures." Highway Research Board, *Proceedings of the Thirty Fifth Annual Meetings*, Publication No. 426, 754-772, Transportation Research Board, Washington, DC.

- McKeen, G.R. (1992). "A model for predicting expansive soil behavior." *Proceedings of the 7th International Conference on Expansive Soils*, 1, 1-6, Texas Tech University, Lubbock, TX.
- McKeen, R. G., (1981). "Suction studies: filter paper method." *Design of Airport Pavements for Expansive Soils: Final Report* , DOT/FAA/RD-81/25, U.S. Dept. of Transportation, Federal Aviation Administration, Systems Research and Development Service, Washington, DC.
- Mein, R. G. and Larson, C. L. (1973). "Modeling infiltration during a steady rain." *Water Resources Research*, 9(2), 384-394.
- Mitchell, J. K. (1976). *Fundamentals of soil behavior*, John Wiley and Sons, New York.
- Mitchell, P. W. (1980). "The structural analysis of footings on expansive soil." Kenneth W. G. Smith & Associates, *Research Report No.1*, Webb & Son, Adelaide, Australia.
- Mitchell, J.K., Hooper, D.R., and Campanella, R.G. (1965). "Permeability of compacted clay." *J. Soil Mech. and Found. Div., ASCE*, SM4, 91, pp. 41–65.
- Nimmo, J.R., and Akstin, K.C. (1988). "Hydraulic conductivity of a sandy soil at low water content after compaction by various methods." *Soil Science Society of America Journal*, 52, 303-310.
- Oden, J. T., and Martins, J. A. C.(1985) "Models and computational methods for dynamic friction phenomena," *Computer Methods in Applied Mechanics and Engineering*, 52, 527–634.

- Olivella, S., Gens, A., Carrera, J., Alonso, E. E. (1996). "Numerical formulation for a simulator (CODE_BRIGHT) for the coupled analysis of saline media." *Engineering Computations*, 13(7), 87-112
- O'Neill, M.W. and Poormoayed, N. (1980). "Methodology for foundations on expansive clays." *ASCE Journal of Geotechnical Engineering Division*, 1345 -1364.
- Parlange, J. Y. (1975). "On solving the flow equation in unsaturated soils by optimization: horizontal infiltration." *Soil Sci.* 122, 236–239.
- Pawsey, S. F., and Clough, R. W. (1971). "Improved numerical integration of thick shell finite elements." *Int. J. Numer. Meth. Engng.*, 3, 575-586.
- Perko, H.A., Thompson, R.W., and Nelson, J.D. (2000). "Suction compression index based on clod test results." *Geotechnical Special Publication No. 99, Advances in Unsaturated Geotechnics*, Proceedings of Sessions of Geo-Denver, Denver, CO.
- Philip J.R. and de Vries D.A. (1957). "Moisture movement in porous materials and temperature gradient." *Transactions of the American Geophysical Union*, 38, 222-232.
- Penman, H.L. (1948). "Natural evaporation from open water, bare soil and grass." *Proceedings of the Royal Society, Series A*, 193,120-145.
- Penman, H.L. (1963). *Vegetation and hydrology*. Tech. Comm. No. 53, Commonwealth Bureau of Soils, Harpenden, England, 125p.

- Pereira, J.H.F. (1996). “*Numerical analysis of the mechanical behavior of collapsing earth dams during first reservoir filling.*” Ph.D dissertation, University of Saskatchewan, Saskatoon, Canada.
- Pereira, J.H.F. and Fredlund, D.G. (1997). “Constitutive Modeling of a Metastable-structured Compacted Soil.” *Proceedings of International Symposium on Recent Developments in Soil and Pavement Mechanics*, Rio de Janeiro, Brazil, pp.317-326.
- Philip, J.R. (1969). “Theory of infiltration.” *Adv. Hydrosci.* 5, 215-290
- Poulos, D. (2000). “Foundation settlement analysis-practice versus research.” Presented at the 8th Spencer J. Buchanan Lecture, Texas A&M University, College Station, TX.
- Post Tensioning Institute (PTI) (1996). *Design and construction of post-tensioned slabs-on-ground*, 2nd Ed., Post Tensioning Institute, Phoenix, AZ.
- Priestley, C.H.B. and Taylor, R.J. (1972). “On the assessment of surface heat flux and evaporation using large-scale parameters.” *Mon. Weather Rev.*, 100, 81-92.
- Pusch, R. (1973). General Report on “Physico-chemical processes which affect soil structure and vice versa.” *Proceedings of the International Symposium on Soil Structure*, Gothenburg, Sweden, Appendix p. 33.
- Pusch, R. (1982). “Mineral-water interactions and their influence on the physical behaviour of highly compacted Na bentonite.” *Canadian Geotechnical Journal*, 19, 381-387

- Pusch, R. and Moreno, L. (2001). "Saturation and permeation of buffer clay." *Proc. 6th Int. Workshop Key Issues in Waste Isolation Research*, Paris, France, 71-81.
- Rahardjo, H. (1990).. "The study of undrained and drained behavior of unsaturated soils." Ph.D. Dissertation, Department of Civil Engineering, University of Saskatchewan, Saskatoon.
- Rahardjo, H. and Fredlund, D.G. (1995). "Experimental verification of the theory of consolidation for unsaturated soils" *Canadian Geotechnical Journal*, 32(5), 749-766.
- Reddy, J. N. (1999). *Theory and analysis of elastic plates*, Taylor & Francis, Philadelphia, PA.
- Reddy, J. N. (1993). *An introduction to the finite element method*, Mc-Graw-Hill Book Company, New York.
- Reicosky, D.C., Yoorchees, W.B., and Radke, J.K. (1981). "Unsaturated water flow through a simulated wheel track." *Soil Science Society of America Journal*, 45, 3-8.
- Richards, L. A. (1931). "Capillary conduction of liquids through porous medium." *J. Physics*, 1, 318-333.
- Romero, E., Gens, A., and Lloret, A. (1999). "Water permeability, water retention and microstructure of unsaturated boom clay." *Engng. Geol.*, 54,117-127.
- Salas, J. A. J., and Serratosa, J. M. (1957). "Foundations on swelling clays." *Proc. 4th Int. Conf. Soil Mech. Found. Eng.*, London, England, 1, 424-428.

Shih, S.F., Allen, L.H., Jr., Hammond, L.C., Jones, J.W., Rogers, J.S., and Smajstrala, A.G. (1981). "Comparison of methods of evapotranspiration estimates." *American Society of Agricultural Engineers Summer Meeting*, Orlando, FL, June 21-24, 81-2015.

Skempton, A.W. (1954). "The pore pressure coefficients, A and B." *Géotechnique*, 4(4), 143-147.

Spears, R.E., and Panarese, W. C. (1990). *Concrete floors on ground*, 2nd Ed, Portland Cement Association, Skokie, IL.

Staple, W.J., and Lehane, J. J. (1954). "Movement of moisture in unsaturated soils." *Canadian Agricultural Science Journal*, 34, 329-342.

Swartzendruber, D. (1969). *The flow of water in unsaturated soils*. Academic Press, New York.

Terzaghi, K. (1936) "The shear resistance of saturated soils." *Proc. 1st Int. Conf. Soil Mech. Found. Eng.*, Cambridge, MA, 1, 54-56.

Terzaghi, K. (1943) *Theoretical soil mechanics*. New York: Wiley.

Thorntwaite, C. W. (1948). "An approach toward a rational classification of climate." *Geographical Review*, 38(1), 55-94.

Timoshenko, S.P. and Goodier, J.N. (1970). *Theory of elasticity*, McGraw-Hill, New York.

- Vlasov, V. Z. and Leont'ev, N. N. (1966). *Beams, plates, and shells on elastic foundation*, Israel Program for Scientific Translations, Jerusalem, Israel.
- VOLFLO (1986). "Volume change and flow calculations in expansive soils." *User's Guide to Program VOLFLO*. Kirby T. Meyers and Associates, Post-Tensioning Institute, Phoenix, AZ.
- VOLFLO Manual (1996). *Volume change and flow calculations in expansive soils*, Program Manual, Geostructural Tool Kit, Inc., Austin, TX.
- Walter, I.A., Allen, R. G., Elliott, R., Mecham, B., Jensen, M. E. et al. (2000). "ASCE standardized reference evapotranspiration equation." *Proc. 4th Decennial Symposium, National Irrigation Symposium. Am. Soc. Agric. Engr.*, St. Joseph, MI, pp. 209-215.
- Wang, M.C. and Shao, M., (1999). "*The finite element method theory and numerical methods*". 2nd Ed., Tsinghua University Press, Beijing, China.
- Wilson, G.W. (1990). "Soil evaporative fluxes for geotechnical engineering problems." Ph.D dissertation, University of Saskatchewan, Saskatoon, Canada.
- Wilson, G.W., Fredlund, D.G. and Barbour, S.L. (1994). "Coupled soil-atmosphere modeling for evaporation." *Canadian Geotechnical Journal*, 31(2),151-161.
- Wire Reinforcement Institute (1996). "*Design of slab-on-ground foundations.*" Technical Report, Wire Reinforcement Institute, Hartford, CT.
- Wray, W.K. (1995). *So your home is built on expansive soils: a discussion of how expansive soils affect buildings*. American Society of Civil Engineers, New York.

- Yong, R.N., and Sheeran, D.E. (1973) "Fabric Unit Interaction and Soil Behavior." *Proceedings of the International Symposium on Soil Structure*, Gothenburg, Sweden, 176-183.
- Yong, R.N., and Warkentin, B.P. (1975). *Soil properties and behaviour*. Elsevier Scientific Publishing Co., Amsterdam, The Netherlands.
- Zhang, X. and Briaud, J.L. (2003). "Predicting the Volume Change of Shrink-Swell Soils." *Proceedings, Texas Section, ASCE Fall Meeting*, Dallas, TX.
- Zhu, B. F. (1998). *The finite element method theory and applications*. 2nd Ed., China WaterPower Press, Beijing, China.
- Zienkiewicz, O. C., Taylor, R. L., and Too, J. M. (1971). "Reduced integration techniques in general analysis of plates and shells." *Int. J. Numer. Methods Eng.*, 3, 275-290.

APPENDIX A
SUMMARY OF THE LABORATORY TESTS

APPENDIX A.1. SUMMARY OF THE FREE SHRINK TESTS

Table A.1.1. Free Shrink Test Data for SW145

Date	Time	level1(mm)		crack(mm)	Average D	Height (mm)				weight	Average H	Volume	γ_d	w	e	S
		diameter 1	diameter 2	diameter3	(mm)	H ₁	H ₂	H ₃	H ₄	(g)	(mm)	(mm ³)	(g/mm ³)			
1st day	12:20	63.32	63.66		63.49	19.10	19.67	20.01	19.54	121.18	19.58	61988.75	1.95	0.240	0.668	0.952
	12:50	63.45	63.35		63.40	19.40	19.89	19.52	19.29	120.64	19.53	61639.50	1.96	0.234	0.659	0.943
	13:20	63.24	63.09		63.17	19.19	19.82	19.31	19.15	120.27	19.37	60689.85	1.98	0.231	0.633	0.965
	13:50	63.65	63.19		63.42	19.16	19.46	19.18	18.90	119.88	19.18	60572.76	1.98	0.227	0.630	0.953
	14:20	63.00	63.02		63.01	19.09	19.42	19.09	18.85	119.54	19.11	59597.22	2.01	0.223	0.604	0.980
	15:21	62.19	62.48		62.34	18.76	18.86	18.53	18.49	118.79	18.66	56946.24	2.09	0.216	0.533	1.073
	17:00	62.13	62.20		62.17	18.54	18.60	18.23	18.37	117.56	18.44	55953.15	2.10	0.203	0.506	1.063
	18:00	62.08	62.00	62.48	62.19	18.45	18.54	18.36	18.37	116.95	18.43	55976.97	2.09	0.197	0.506	1.029
	19:30	61.93	61.79	62.47	62.06	18.16	18.31	18.14	18.31	116.01	18.23	55150.11	2.10	0.187	0.484	1.024
	21:00	61.74	61.59	61.65	61.66	17.95	18.31	18.12	18.23	115.14	18.15	54204.21	2.12	0.178	0.459	1.029
	23:50	61.23	61.14	61.19	61.19	17.98	18.02	17.91	18.08	113.72	18.00	52919.45	2.15	0.164	0.424	1.022
2nd day	9:15	61.10	60.98	61.00	61.03	18.13	18.12	18.09	18.09	113.41	18.11	52964.80	2.14	0.160	0.425	1.000
	10:50	60.68	60.55	60.79	60.67	17.84	18.12	17.90	17.96	112.48	17.96	51912.34	2.17	0.151	0.397	1.008
	13:15	60.49	60.25	60.52	60.42	17.83	18.05	17.97	17.81	111.40	17.92	51365.06	2.17	0.140	0.382	0.970
	15:15	60.18	60.05	60.11	60.11	17.69	17.85	17.72	17.75	110.49	17.75	50383.77	2.19	0.131	0.356	0.972
	18:30	59.72	59.61	59.49	59.61	17.69	17.82	17.72	17.73	109.36	17.74	49503.15	2.21	0.119	0.332	0.950
3rd day	1:40	59.37	59.41	59.27	59.35	17.66	17.78	17.71	17.66	107.91	17.70	48974.00	2.20	0.104	0.318	0.868
	11:00	59.59	59.59	59.52	59.57	17.70	17.78	17.67	17.67	107.81	17.71	49339.19	2.19	0.103	0.328	0.834
	17:00	59.47	59.42	59.27	59.39	17.71	17.78	17.68	17.64	106.88	17.70	49034.53	2.18	0.094	0.320	0.777
	22:00	59.40	59.49	59.11	59.33	17.64	17.69	17.53	17.54	106.44	17.60	48663.09	2.19	0.089	0.310	0.763
4th day	13:50	59.48	59.32	59.00	59.27	17.63	17.65	17.45	17.56	106.37	17.57	48477.93	2.19	0.088	0.305	0.769
	19:51	59.27	59.22	59.04	59.18	17.54	17.64	17.35	17.53	106.18	17.52	48172.66	2.20	0.087	0.296	0.773
	23:00	59.31	59.27	59.16	59.25	17.58	17.43	17.52	17.57	106.16	17.53	48314.27	2.20	0.086	0.300	0.762
5th day	9:30	59.32	59.22	59.03	59.19	17.55	17.41	17.30	17.45	106.17	17.43	47953.61	2.21	0.086	0.291	0.788
6th day	14:00	59.26	59.22	59.04	59.17	17.58	17.48	17.34	17.50	105.26	17.48	48057.23	2.19	0.077	0.293	0.697
8th day	20:00	59.37	59.25	59.29	59.30	17.54	17.80	17.65	17.64	104.58	17.66	48772.72	2.14	0.070	0.313	0.595

APPENDIX A.1. SUMMARY OF THE FREE SHRINK TESTS

Table A.1.2. Free Shrink Test Data for SW189

Date	Time	level1(mm)		crack (mm)	Average D	Height (mm)				weight	Average H	Volume	γ_d	w	e	S
		diameter 1	diameter 2	diameter3	(mm)	H ₁	H ₂	H ₃	H ₄	(g)	(mm)	(mm ³)	(g/mm ³)			
1st day	12:20	63.41	63.88		63.65	19.41	19.82	20.04	19.66	128.34	19.73	62776.95	2.04	0.2220	0.6677	0.9277
	12:50	63.18	63.5		63.34	19.18	19.67	19.75	19.60	127.74	19.55	61601.66	2.07	0.2163	0.6365	0.9481
	13:20	63.2	63.41		63.31	19.00	19.45	19.58	19.66	127.29	19.42	61132.29	2.08	0.2120	0.6240	0.9479
	13:50	63	63.09		63.05	19.02	19.33	19.35	19.39	126.89	19.27	60162.91	2.11	0.2082	0.5982	0.9709
	14:20	62.61	62.7		62.66	18.89	19.22	19.42	19.37	126.50	19.23	59274.42	2.13	0.2045	0.5746	0.9928
	15:21	62.45	62.88		62.67	18.45	19.13	19.16	19.26	125.65	19.00	58599.40	2.14	0.1964	0.5567	0.9842
	17:00	62.58	62.62		62.60	18.81	18.71	18.62	18.89	124.40	18.76	57731.54	2.15	0.1845	0.5337	0.9645
	18:00	62.43	62.62	62.48	62.51	18.72	18.73	18.64	19.04	123.78	18.78	57642.38	2.15	0.1786	0.5313	0.9378
	19:30	62.15	62.37	62.47	62.33	18.76	18.60	18.65	18.98	122.69	18.75	57204.10	2.14	0.1682	0.5196	0.9031
	21:00	62.13	62.3	61.65	62.03	18.72	18.60	18.54	18.99	121.75	18.71	56542.92	2.15	0.1593	0.5021	0.8850
23:50	62.13	62.3	61.19	61.87	18.54	18.52	18.54	18.98	120.19	18.65	56060.75	2.14	0.1444	0.4893	0.8234	
2nd day	9:15	62.13	62.25	61	61.79	18.71	18.57	18.44	19.10	119.86	18.71	56095.82	2.14	0.1413	0.4902	0.8040
	10:50	61.97	62.23	60.79	61.66	18.56	18.60	18.38	19.07	118.99	18.65	55703.25	2.14	0.1330	0.4798	0.7733
	13:15	62.01	62.11	60.52	61.55	18.63	18.46	18.38	19.15	117.95	18.66	55500.11	2.13	0.1231	0.4744	0.7238
	15:15	62.05	61.95	60.11	61.37	18.68	18.41	18.38	19.10	117.09	18.64	55144.97	2.12	0.1149	0.4649	0.6894
	18:30	61.95	62.03	59.49	61.16	18.56	18.41	18.38	19.10	116.11	18.61	54674.12	2.12	0.1056	0.4524	0.6509
3rd day	1:40	62.02	62.14	59.27	61.14	18.68	18.53	18.44	19.05	115.04	18.68	54833.80	2.10	0.0954	0.4567	0.5826
	11:00	62.06	61.93	59.52	61.17	18.77	18.54	18.48	19.05	114.88	18.71	54984.50	2.09	0.0938	0.4607	0.5683
	17:00	61.95	61.96	59.27	61.06	18.67	18.54	18.47	18.93	114.17	18.65	54618.55	2.09	0.0871	0.4510	0.5387
	22:00	61.91	61.99	59.11	61.00	18.66	18.52	18.39	18.93	113.88	18.63	54436.84	2.09	0.0843	0.4461	0.5273
4th day	13:50	61.85	61.97	59	60.94	18.75	18.54	18.64	18.89	113.84	18.71	54557.21	2.09	0.0839	0.4493	0.5212
	19:51	61.83	61.9	59.04	60.92	18.65	18.48	18.44	18.74	113.79	18.58	54155.69	2.10	0.0835	0.4387	0.5308
	23:00	61.81	61.97	59.16	60.98	18.16	18.37	18.26	18.71	113.76	18.38	53665.07	2.12	0.0832	0.4256	0.5452
5th day	9:30	61.78	62.1	59.03	60.97	18.28	18.36	18.26	18.67	113.76	18.39	53698.56	2.12	0.0832	0.4265	0.5441
6th day	14:00	61.79	62.1	62.09	61.99	18.49	18.33	18.21	18.57	113.25	18.40	55538.91	2.04	0.0783	0.4754	0.4596
8th day	20:00	61.96	61.86	61.87	61.90	18.60	18.52	18.23	18.59	112.83	18.49	55621.60	2.03	0.0743	0.4776	0.4342

APPENDIX A.1. SUMMARY OF THE FREE SHRINK TESTS

Table A.1.3. Free Shrink Test Data for Sporc

Date	Time	level (mm)		crack(mm)	Average D	Height (mm)				weight	Average H	Volume	γ_d	w	e	S
		diameter 1	diameter 2	diameter3	(mm)	H ₁	H ₂	H ₃	H ₄	(g)	(mm)	(mm ³)	(g/mm ³)			
1st day	12:20	63.54	63.54		63.54	19.4	19.35	19.36	19.44	123.69	19.39	61476.0	2.012	0.193	0.616	0.854
	12:50	63.36	63.51		63.435	19.13	19.22	19.18	19.16	123.04	19.17	60593.5	2.031	0.187	0.593	0.859
	13:20	63.36	63.2		63.28	19.06	19.1	19.08	19.07	122.64	19.08	59999.0	2.044	0.183	0.577	0.864
	13:50	63.02	63.93		63.475	19.01	19.11	18.99	18.98	122.24	19.02	60195.3	2.031	0.179	0.582	0.838
	14:20	62.6	62.98		62.79	18.85	18.86	18.91	18.96	121.83	18.90	58508.3	2.082	0.175	0.538	0.888
	15:21	62.36	62.69		62.525	18.51	18.48	18.67	18.94	120.9	18.65	57263.2	2.111	0.166	0.505	0.897
	17:00	62.27	61.56		61.915	18.47	18.28	18.56	18.47	119.81	18.45	55534.1	2.157	0.156	0.460	0.923
	18:00	61.95	61.31	62.48	61.63	18.48	18.51	18.53	18.52	118.92	18.51	55217.9	2.154	0.147	0.451	0.888
	19:30	61.65	61.18	62.47	61.415	18.11	18.27	18.25	18.43	117.94	18.27	54107.6	2.180	0.138	0.422	0.888
	21:00	61.44	60.83	61.65	61.135	18.16	18.25	18.27	18.33	116.98	18.25	53578.6	2.183	0.128	0.408	0.857
2nd day	23:50	61.21	60.53	61.19	60.87	18.16	18.22	18.22	18.18	115.5	18.20	52947.8	2.181	0.114	0.392	0.794
	9:15	61.22	60.52	61	60.87	18.08	18.15	18.1	18.16	115.31	18.12	52736.9	2.187	0.112	0.386	0.792
	10:50	61.14	60.45	60.79	60.795	18.06	18.12	18.12	18.13	114.27	18.11	52563.4	2.174	0.102	0.382	0.730
	13:15	61.09	60.47	60.52	60.78	18.09	18.19	18.06	18.13	113.08	18.12	52566.5	2.151	0.091	0.382	0.648
	15:15	61.07	60.4	60.11	60.735	18.02	18.21	18.06	18.14	111.84	18.11	52459.7	2.132	0.079	0.379	0.567
3rd day	18:30	61.06	60.36	59.49	60.71	18.04	18.14	18.11	18.13	110.32	18.11	52409.3	2.105	0.064	0.378	0.463
	1:40	61.07	60.35	59.27	60.71	18.04	18.19	18.11	18.15	108.45	18.12	52460.0	2.067	0.046	0.379	0.332
	11:00	61.16	60.38	59.52	60.77	18.22	18.35	18.3	18.3	108.25	18.29	53056.8	2.040	0.044	0.395	0.305
4th day	17:00	61.02	60.38	59.27	60.7	18.1	18.24	18.25	18.22	107.25	18.20	52674.2	2.036	0.035	0.385	0.245
	22:00	61.01	60.36	59.11	60.685	18.11	18.18	18.25	18.2	106.85	18.19	52597.6	2.031	0.031	0.383	0.219
	13:50	60.94	60.23	59	60.585	18.12	18.05	18.17	18.26	106.69	18.15	52323.4	2.039	0.029	0.375	0.212
	19:51	61.11	60.3	59.04	60.705	17.75	18.02	17.94	17.96	106.49	17.92	51858.0	2.053	0.027	0.363	0.204
5th day	23:00	60.88	60.29	59.16	60.585	17.73	18.01	17.96	17.96	106.44	17.92	51646.0	2.061	0.027	0.358	0.204
	9:30	60.86	60.33	59.03	60.595	17.79	18.08	17.94	17.96	106.4	17.94	51742.3	2.056	0.026	0.360	0.200
6th day	14:00	60.95	60.11		60.53	17.9	18	17.96	17.97	105.78	17.96	51674.6	2.047	0.020	0.358	0.155
8th day	20:00	60.97	60.42		60.695	17.98	18.22	18.01	17.88	105.35	18.02	52144.7	2.020	0.016	0.371	0.119

APPENDIX A.2. SUMMARY OF CALIBRATION CURVES FOR THE TRANSDUCERS

Table A.2.1. Calibration Curve for the Transducer TAMU 007 (Channel 0)

TAMU 007 (Channel 0)					
	displacement		output		
	(in)	(mm)	to	back	average
10	0	0	-0.84	-0.85	-0.0008
9	0.1	2.54	5.91	5.85	0.00588
8	0.2	5.08	12.67	12.6	0.01264
7	0.3	7.62	19.42	19.33	0.01938
6	0.4	10.16	26.17	26.06	0.02612
5	0.5	12.7	32.92	32.82	0.03287
4	0.6	15.24	39.67	39.57	0.03962
3	0.7	17.78	46.43	46.34	0.04639
2	0.8	20.32	53.16	53.08	0.05312
1	0.9	22.86	59.87	59.81	0.05984
0	1	25.4	66.58	66.58	0.06658

Calibration Curve of TAMU 007

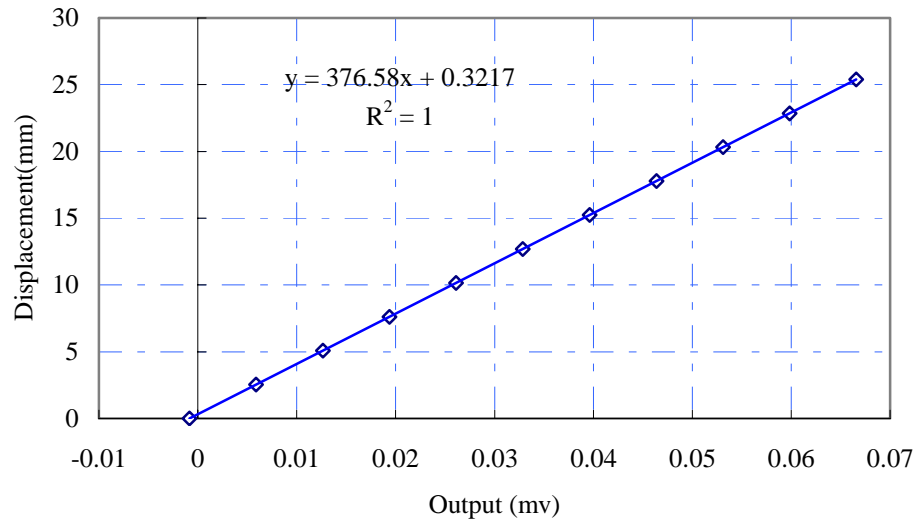


Figure A.2.1. Calibration Curve for the Transducer TAMU 007 (Channel 0)

APPENDIX A.2. SUMMARY OF CALIBRATION CURVES FOR THE TRANSDUCERS

Table A.2.2. Calibration Curve for the Transducer TAMU 003 (Channel 1)

TAMU 003 (Channel 1)					
	displacement		output		
	(in)	(mm)	to	back	average
10	0	0	0.26	0.26	0.00026
9	0.1	2.54	6.71	6.71	0.00671
8	0.2	5.08	13.16	13.13	0.01315
7	0.3	7.62	19.61	19.58	0.0196
6	0.4	10.16	26.07	26.04	0.02606
5	0.5	12.7	32.52	32.48	0.0325
4	0.6	15.24	38.97	38.92	0.03895
3	0.7	17.78	45.4	45.37	0.04539
2	0.8	20.32	51.85	51.82	0.05184
1	0.9	22.86	58.3	58.27	0.05829
0	1	25.4	64.77	64.77	0.06477

Calibration Curve of TAMU 003

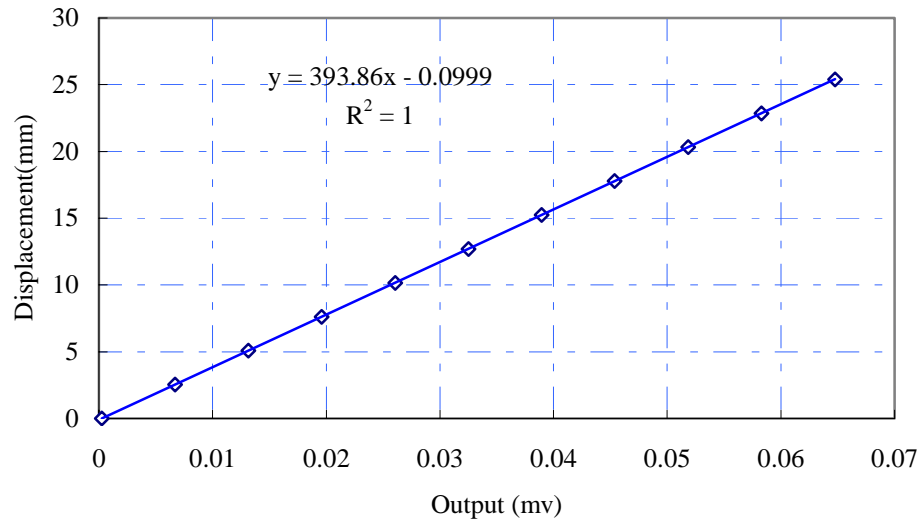


Figure A.2.2. Calibration Curve for the Transducer TAMU 003 (Channel 1)

APPENDIX A.2. SUMMARY OF CALIBRATION CURVES FOR THE TRANSDUCERS

Table A.2.3. Calibration Curve for the Transducer TAMU 003 (Channel 2)

TAMU 003					
	displacement		output		
	(in)	(mm)	to	back	average
10	0	0	-1.77	-1.75	-0.0018
9	0.1	2.54	4.43	4.43	0.00443
8	0.2	5.08	10.62	10.61	0.01062
7	0.3	7.62	16.76	16.73	0.01675
6	0.4	10.16	22.93	22.91	0.02292
5	0.5	12.7	29.18	29.15	0.02917
4	0.6	15.24	35.42	35.37	0.0354
3	0.7	17.78	41.64	41.6	0.04162
2	0.8	20.32	47.82	47.8	0.04781
1	0.9	22.86	54.05	54.03	0.05404
0	1	25.4	60.28	60.28	0.06028

Calibration Curve of TAMU 003

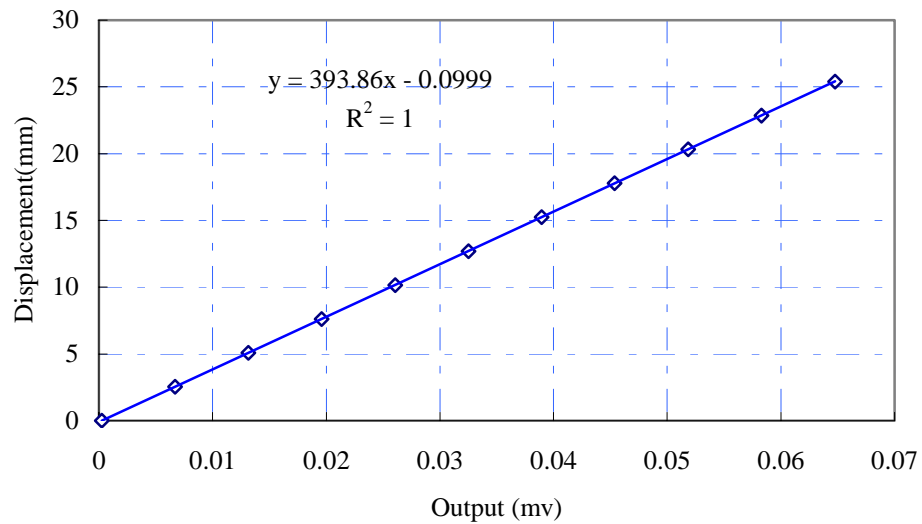


Figure A.2.3. Calibration Curve for the Transducer TAMU 003 (Channel 2)

APPENDIX A.3. SUMMARY OF THE SWELL-CONSOLIDATION TEST

Table A.3.1 Swell-Consolidation Test for SW145

	P	Output	Disp.	σ_v	σ_m	H	Δe	e	S	w
	(tsf)	(mv)	(mm)	(kPa)	(kPa)	(mm)				(%)
Swell Test	0	0.0275	10.67	0	0	19.2	0.0000	0.671	0.99	25.10
	0	0.0279	10.84	1	1.0	19.4	0.0153	0.686	1.00	25.89
Consoli- dation Test	0.125	0.0278	10.78	12.0	9.3	19.3	0.0095	0.680	1.00	25.67
	0.25	0.0275	10.69	23.9	18.6	19.2	0.0023	0.673	1.00	25.40
	0.5	0.0272	10.56	47.9	37.2	19.1	-0.0090	0.662	1.00	24.97
	1	0.0264	10.28	95.8	74.5	18.8	-0.0338	0.637	1.00	24.03
	2	0.0250	9.73	191.5	149.0	18.3	-0.0812	0.590	1.00	22.25
	4	0.0228	8.89	383.0	297.9	17.4	-0.1546	0.516	1.00	19.47
	8	0.0203	7.97	766.1	595.8	16.5	-0.2350	0.436	1.00	16.44
	16	0.0179	7.06	1532.2	1191.7	15.6	-0.3138	0.357	1.00	13.47
	32	0.0157	6.24	3064.3	2383.4	14.8	-0.3854	0.285	1.00	10.77

APPENDIX A.3. SUMMARY OF THE SWELL-CONSOLIDATION TEST

Table A.3.2 Swell-Consolidation Test for SW189

	P	Output	Disp.	σ_v	σ_m	H	Δe	e	S	w
	(psf)	(mv)	(mm)	(kPa)	(kPa)	(mm)				(%)
Swell Test	0	0.02623	10.23	0	0	19.20	0.00000	0.742	0.90	25.10
	0	0.02876	11.23	1	1	20.19	0.09029	0.833	1.00	29.84
Consoli- dation Test	0.125	0.02836	11.07	12.0	9.3	20.04	0.07617	0.819	1.00	29.34
	0.25	0.02814	10.98	23.9	18.6	19.95	0.06809	0.810	1.00	29.05
	0.5	0.02775	10.83	47.9	37.2	19.80	0.05419	0.797	1.00	28.55
	1	0.02709	10.57	95.8	74.5	19.54	0.03088	0.773	1.00	27.72
	2	0.02619	10.21	191.5	149.0	19.18	-0.00154	0.741	1.00	26.55
	4	0.02506	9.77	383.0	297.9	18.74	-0.04182	0.701	1.00	25.11
	8	0.02364	9.21	766.1	595.8	18.18	-0.09250	0.650	1.00	23.29
	16	0.0217	8.45	1532.2	1191.7	17.42	-0.16191	0.580	1.00	20.81
	32	0.01974	7.67	3064.3	2383.4	16.64	-0.23208	0.510	1.00	18.29

APPENDIX A.3. SUMMARY OF THE SWELL-CONSOLIDATION TEST

Table A.3.3. Swell-Consolidation Test for SW189

	P	Output	Disp.	σ_v	σ_m	H	Δe	e	S	w
	(psf)	(mv)	(mm)	(kPa)	(kPa)	(mm)				(%)
Swell Test	0	0.02803	12.22	0	0	25.40	0.00000	0.662	0.94	22.93
	0	0.03613	15.53	1	1.0	28.71	0.21696	0.879	1.00	32.27
Consoli- dation Test	0.125	0.0361	15.52	12.0	9.3	28.70	0.21613	0.879	1.00	32.24
	0.25	0.03532	15.20	23.9	18.6	28.39	0.19541	0.858	1.00	31.48
	0.5	0.03424	14.76	47.9	37.2	27.94	0.16634	0.829	1.00	30.41
	1	0.03233	13.98	95.8	74.5	27.16	0.11516	0.778	1.00	28.53
	2	0.02998	13.02	191.5	149.0	26.20	0.05228	0.715	1.00	26.23
	4	0.02817	12.27	383.0	297.9	25.46	0.00362	0.666	1.00	24.44
	8	0.02611	11.43	766.1	595.8	24.61	-0.05145	0.611	1.00	22.42
	16	0.02384	10.50	1532.2	1191.7	23.69	-0.11219	0.550	1.00	20.19
32	0.02105	9.36	3064.3	2383.4	22.54	-0.18711	0.475	1.00	17.44	

APPENDIX A.4. SUMMARY OF SUCTION TESTS

Table A.4.1. Summary of Suction Tests for SW145

Pressure Plate Test		Pressure Plate Test(wetted)		Summary	
Suction	Water Content	Suction	Water Content	Suction	w
(kPa)	(%)	(kPa)	(%)	(kPa)	(%)
17	28.04	42	28.50	17	28.04
160	25.59	1300	18.89	160	25.59
1100	24.18	42	26.78	1100	24.18
		1300	19.53	42	28.50
				1300	18.89
				42	26.78
				1300	19.53
				1303	18.89
				32776	11.01
				1303	19.67
				32776	11.09
				324	17.61
				1303	18.29
				3523	15.45
				7187	16.41
				19425	13.59
				32776	11.43
				324	19.36
				1303	16.96
				3523	16.46
				7187	15.44
				19425	13.80
				32776	10.75
				3523	21.37
				19425	12.02
				1	25.89
				1000000	0.00

1st Salt Concentration Test		1st Salt Concentration (wetted)	
Suction	Water Content	Suction	Water Content
(kPa)	(%)	(kPa)	(%)
1303	18.89	1303	19.67
32776	11.01	32776	11.09

2nd Salt Concentration Test		Imposed Points	
Suction	Water Content	Suction	Water Content
(kPa)	(%)	(kPa)	(%)
1303		Swell-consolidation test	
3523	21.37	1	25.89
19425	12.02	(Fredlund & Rahardjo)	
32776		1000000	0.00

3rd Salt Concentration Test		3rd Salt Concentration (wetted)	
Suction	Water Content	Suction	Water Content
(kPa)	(%)	(kPa)	(%)
324	17.61	324	19.36
1303	18.29	1303	16.96
3523	15.45	3523	16.46
7187	16.41	7187	15.44
19425	13.59	19425	13.80
32776	11.43	32776	10.75

APPENDIX A.4. SUMMARY OF SUCTION TESTS

Table A.4.2. Summary of Suction Tests for SPorc

Pressure Plate Test		Pressure Plate (wetted)		Summary	
Suction	Water Content	Suction	Water Content	Suction	w
(kPa)	(%)	(kPa)	(%)	(kPa)	(%)
17	24.93	42	29.39	17	24.93
160	24.50	1300	18.55	160	24.50
1100	19.99			1100	19.99
				42	29.39
				1300	18.55
1st Salt Concentration Test		1st Salt Concentration (wetted)		3523	18.82
Suction	Water Content	Suction	Water Content	19425	15.04
(kPa)	(%)	(kPa)	(%)	324	30.17
3523	18.82	324	30.17	7187	18.96
19425	15.04	7187	18.96	324	16.67
				1303	16.72
				3523	13.95
2nd Salt Concentration Test		Imposed Points		7187	14.37
Suction	Water Content	Suction	Water Content	19425	12.56
(kPa)	(%)	(kPa)	(%)	32776	6.30
324	16.67	Swell-consolidation test		1303	21.76
1303	16.72	1	32.27	3523	16.68
3523	13.95	(Fredlund & Rahardjo)		7187	15.71
7187	14.37	1000000	0.00	19425	9.99
19425	12.56			32776	6.88
32776	6.30			3523	14.59
				7187	13.74
				19425	9.70
3rd Salt Concentration Test		3rd Salt Concentration(wetted)		32776	6.49
Suction	Water Content	Suction	Water Content	1	32.27
(kPa)	(%)	(kPa)	(%)	1000000	0.00
1303	21.76				
3523	16.68	3523	14.59		
7187	15.71	7187	13.74		
19425	9.99	19425	9.70		
32776	6.88	32776	6.49		

APPENDIX B
SUMMARY OF MATERIAL PROPERTIES
FOR THREE SOILS

Appendix B.1.1. Summary of Material Properties for the Soil SW145

B.1.1.1. Consolidation Test: e - $\log(\sigma_v)$ Relationship

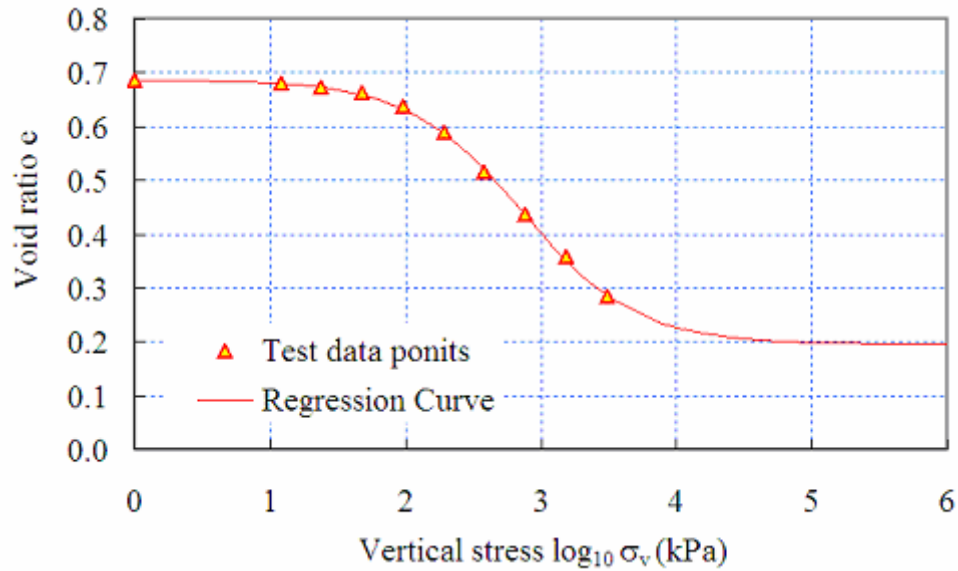


Figure B.1.1.1 Void Ratio vs. Vertical Mechanical Stress Curve for the Soil SW145

Mathematical expression

$$e = 0.1956125 + \frac{0.490945938}{1 + \exp\left(\frac{\log_{10}(\sigma_v) - 2.86157532}{0.421062101}\right)}$$

B.1.1.2. Consolidation Test: e - $\log(\sigma_m)$ Relationship

Mathematical expression

$$e = 0.195449 + \frac{0.49127602}{1 + \exp\left(\frac{\log_{10}(\sigma_m) - 2.75275012}{0.42147606}\right)}$$

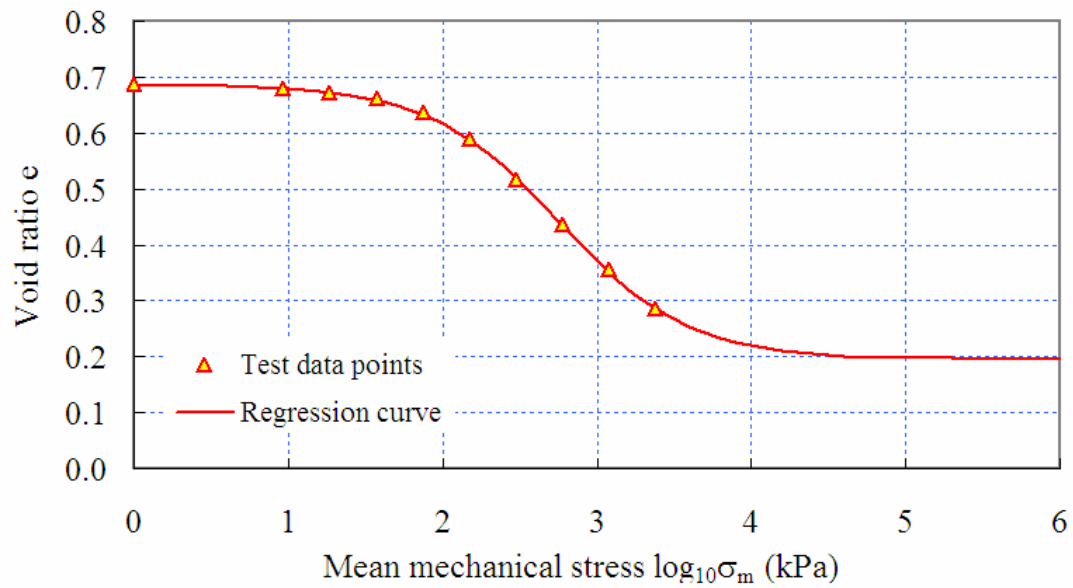


Figure B.1.1.2 Void Ratio vs. Mean Mechanical Stress Curve for the Soil SW145

B.1.1.3. Consolidation Test: w - $\log(\sigma_v)$ Relationship

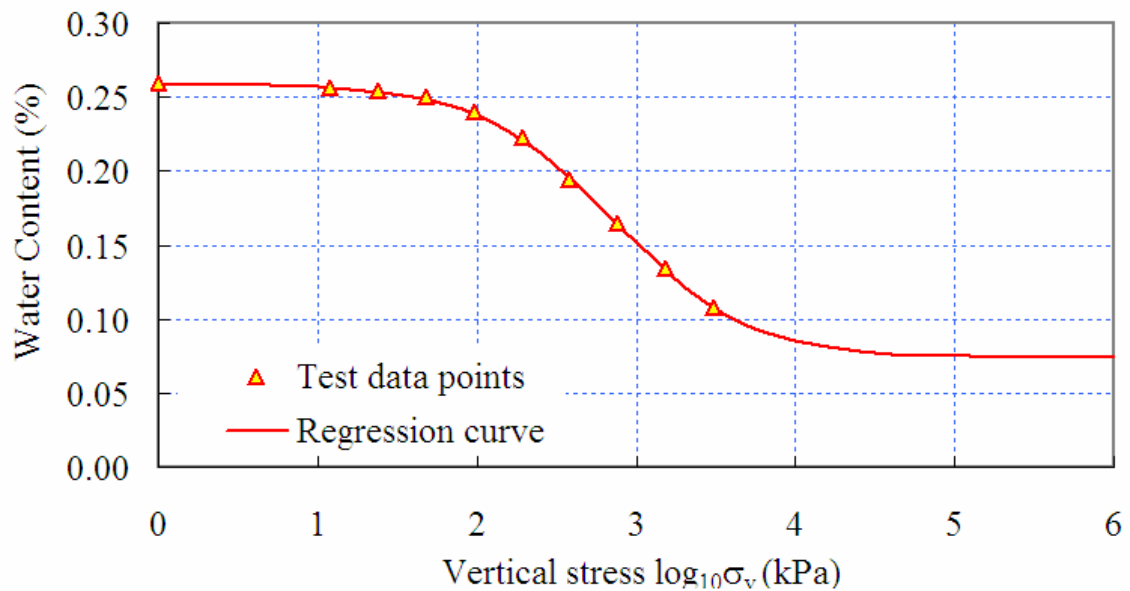


Figure B.1.1.3 Water Content vs. Vertical Mechanical Stress Curve for the Soil SW145

Mathematical expression

$$w = \frac{e}{G_s} = 0.07381605 + \frac{0.18526262}{1 + \exp\left(\frac{\log_{10}(\sigma_v) - 2.86157532}{0.42106210}\right)}$$

B.1.1.4. Consolidation Test: w - $\log(\sigma_m)$ Relationship

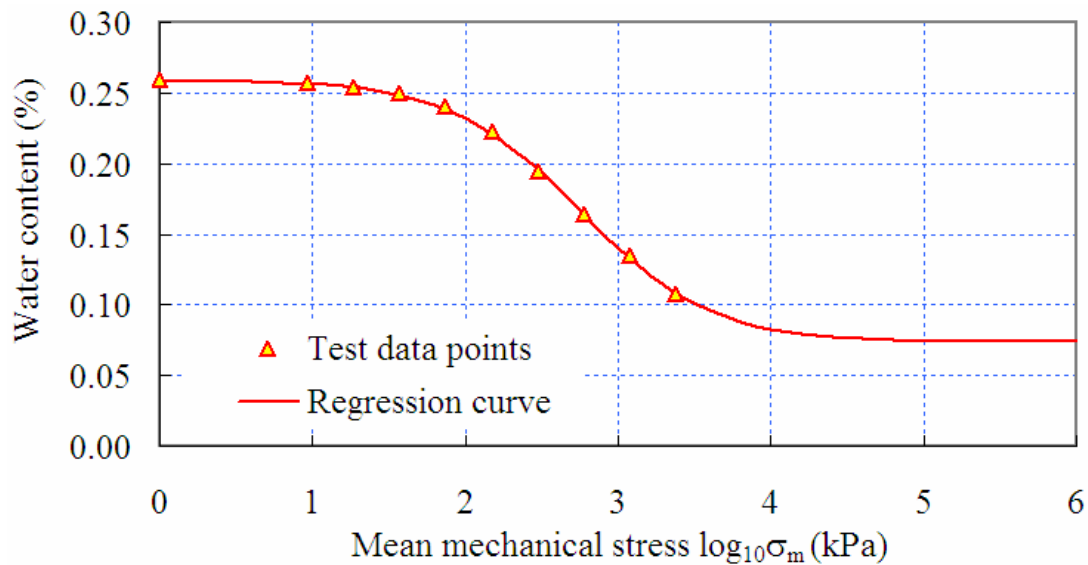


Figure B.1.1.4 Water Content vs. Mean Mechanical Stress Curve for the Soil SW145

Mathematical expression

$$w = \frac{e}{G_s} = 0.07375434 + \frac{0.18538718}{1 + \exp\left(\frac{\log_{10}(\sigma_m) - 2.75275012}{0.42147606}\right)}$$

B.1.1.5. Free Shrink test: e - w Relationship

Mathematical expression

$$S = -0.127572688 + \frac{1.128166863}{1 + \exp\left(-\frac{w - 0.052044763}{0.027400096}\right)} \quad (\text{For } w \geq 0.0944)$$

$$S = 8.4996w \quad (\text{For } w \leq 0.0944)$$

$$e = -0.3159323 + \frac{0.429355664}{1 + \exp\left(-\frac{w - 0.192599516}{0.036185098}\right)} \quad (\text{For } w \geq 0.0944)$$

$$e = 0.3120 \quad (\text{For } w \leq 0.0944)$$

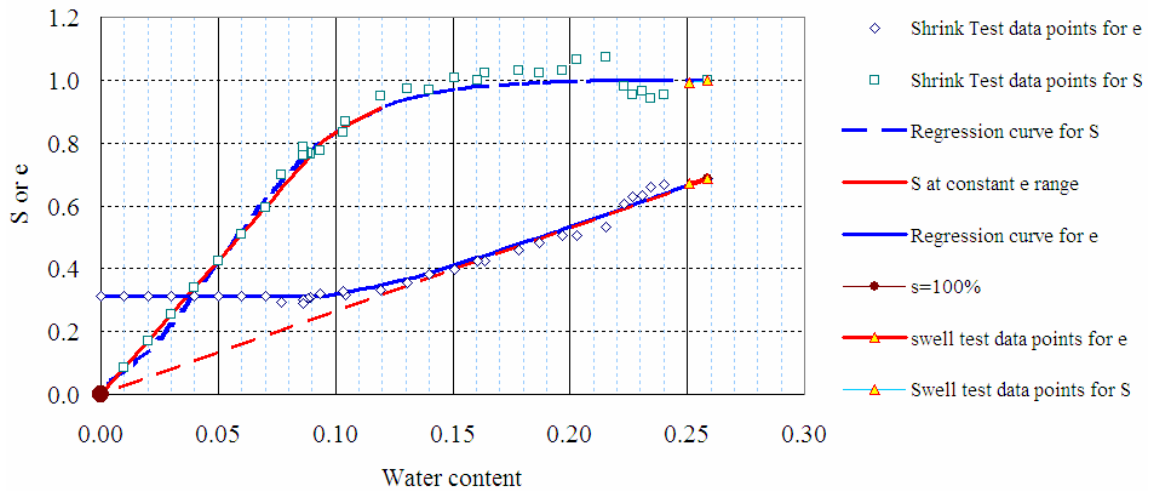


Figure B.1.1.5 Void Ratio and Degree of Saturation vs. Water Content Curve for the Soil SW145

B.1.1.6. Soil Water Characteristic Curve

Mathematical expression

$$w = -0.026264216 + \frac{0.285551272}{1 + \exp\left(\frac{\log_{10}(u_a - u_w) - 4.386436815}{0.671559558}\right)}$$

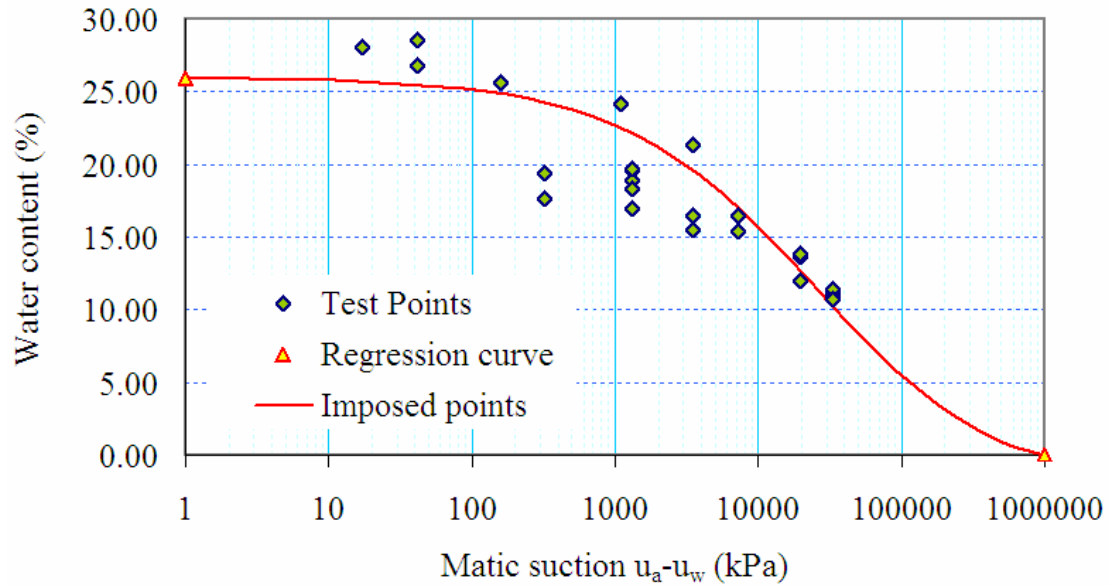


Figure B.1.1.6 Soil Water Characteristic Curve for the Soil SW145

B.1.1.7. Constructed e- Matric Suction: $e - \log_{10}(u_a - u_w)$ Relationship

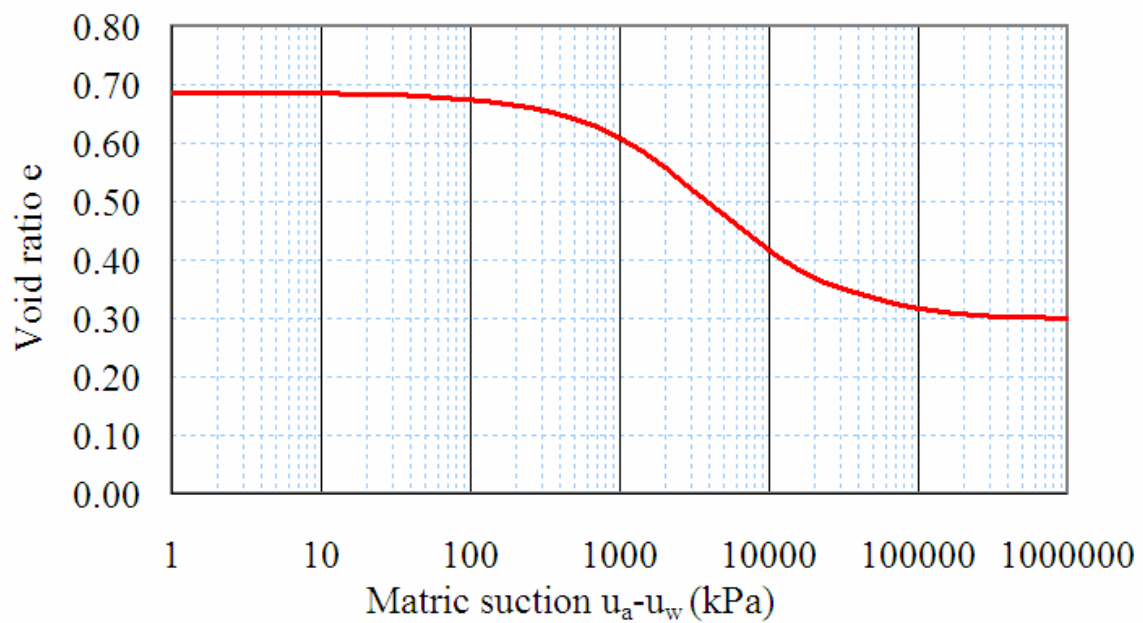


Figure B.1.1.7 Constructed e- Matric Suction: $e - \log_{10}(u_a - u_w)$ Relationship for the Soil SW145

$$e = 0.299088 + \frac{0.387060274}{1 + \exp\left(\frac{\log_{10}(u_a - u_w) - 3.624238826}{0.456383725}\right)}$$

B.1.1.8. Void Ratio Constitutive Surface:

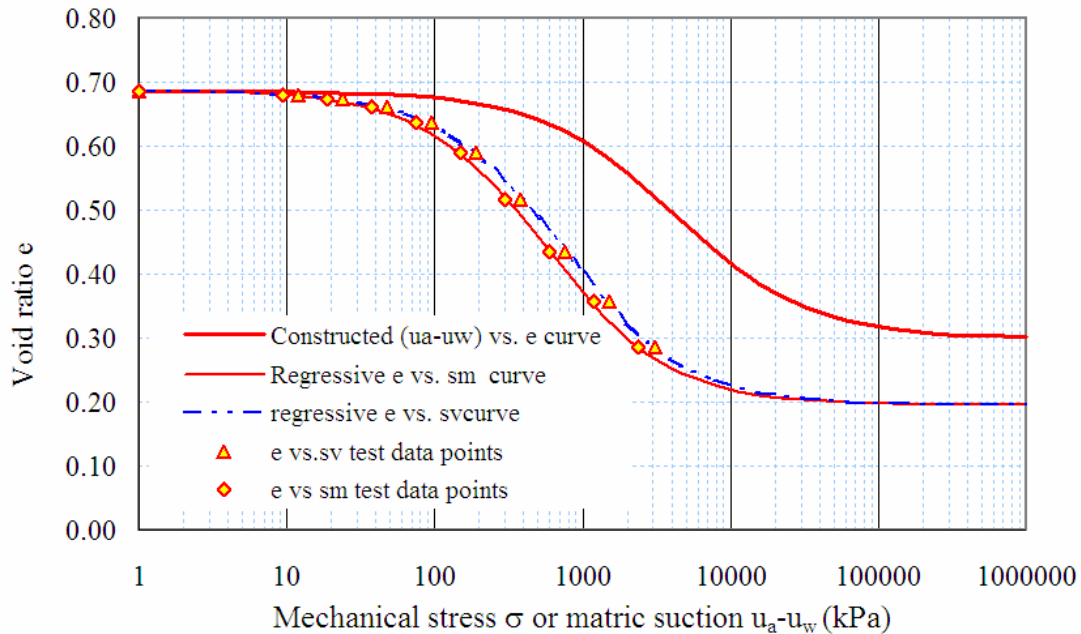


Figure B.1.1.8 Curves for Constructing the Void Ratio Constitutive Surface for the Soil SW145

B.1.1.8.1 Void Ratio e versus Vertical Mechanical Stress σ_v & Matric Suction ($u_a - u_w$) Surface

Boundary:

$u_a - u_w = 0$ (from 1-D consolidation test):

$$e = 0.1956125 + \frac{0.490945938}{1 + \exp\left(\frac{\log_{10}(\sigma_v) - 2.86157532}{0.421062101}\right)}$$

Therefore

$$\log_{10} \sigma_v = 0.421062101 \ln \left(\frac{0.490945938}{(e - 0.1956125)} - 1 \right) + 2.86157532$$

$\sigma_v = 0$ (from soil-water characteristic curve and free shrink test):

$$e = 0.299088 + \frac{0.387060274}{1 + \exp\left(\frac{\log_{10}(u_a - u_w) - 3.624238826}{0.456383725}\right)}$$

$$\log_{10}(u_a - u_w) = 0.456383725 \ln \left(\frac{0.387060274}{(e - 0.299088)} - 1 \right) + 3.624238826$$

B.1.1.8.2. e versus σ_v & $(u_a - u_w)$ Surface

(for 1 D consolidation theory for saturated-unsaturated soils)

linear assumption:

$$\frac{\sigma_v - u_a}{(\sigma_m - u_a)_{(u_a - u_w = 0)}} + \frac{u_a - u_w}{(u_a - u_w)_{(\sigma_m - u_a = 0)}} = 1$$

$$\frac{\sigma_v - u_a}{10^{\left(0.421062101 \ln \left(\frac{0.490945938}{(e - 0.1956125)} - 1 \right) + 2.86157532\right)}} + \frac{u_a - u_w}{10^{\left(0.456383725 \ln \left(\frac{0.387060274}{(e - 0.299088)} - 1 \right) + 3.624238826\right)}} = 1$$

B.1.1.8.3. Void ratio e versus Vertical Mechanical Stress σ_m & Matric Suction $(u_a - u_w)$ Surface (for 2 D or 3D consolidation theory for saturated-unsaturated soils)

Boundary:

$u_a - u_w = 0$ (from 1-D consolidation test):

$$e = 0.195449 + \frac{0.49127602}{1 + \exp\left(\frac{\log_{10}(\sigma_m) - 2.75275012}{0.42147606}\right)}$$

Therefore

$$\log_{10} \sigma_m = 0.42147606 \ln \left(\frac{0.49127602}{(e - 0.195449)} - 1 \right) + 2.75275012$$

$\sigma_m = 0$ (from soil-water characteristic curve and free shrink test):

$$e = 0.299088 + \frac{0.387060274}{1 + \exp \left(\frac{\log_{10}(u_a - u_w) - 3.624238826}{0.456383725} \right)}$$

$$\log_{10}(u_a - u_w) = 0.456383725 \ln \left(\frac{0.387060274}{(e - 0.299088)} - 1 \right) + 3.624238826$$

B.1.1.8.4. e versus σ_m & $(u_a - u_w)$ Surface

(for 2D or 3 D consolidation theory for saturated-unsaturated soils)

linear assumption:

$$\frac{\sigma_m - u_a}{(\sigma_m - u_a)_{(u_a - u_w = 0)}} + \frac{u_a - u_w}{(u_a - u_w)_{(\sigma_m - u_a = 0)}} = 1$$

$$\frac{\sigma_m - u_a}{10^{\left(0.42147606 \ln \left(\frac{0.49127602}{(e - 0.195449)} - 1 \right) + 2.75275012 \right)}} + \frac{u_a - u_w}{10^{\left(0.456383725 \ln \left(\frac{0.387060274}{(e - 0.299088)} - 1 \right) + 3.624238826 \right)}} = 1$$

B.1.1.9. Water Content Constitutive Surface

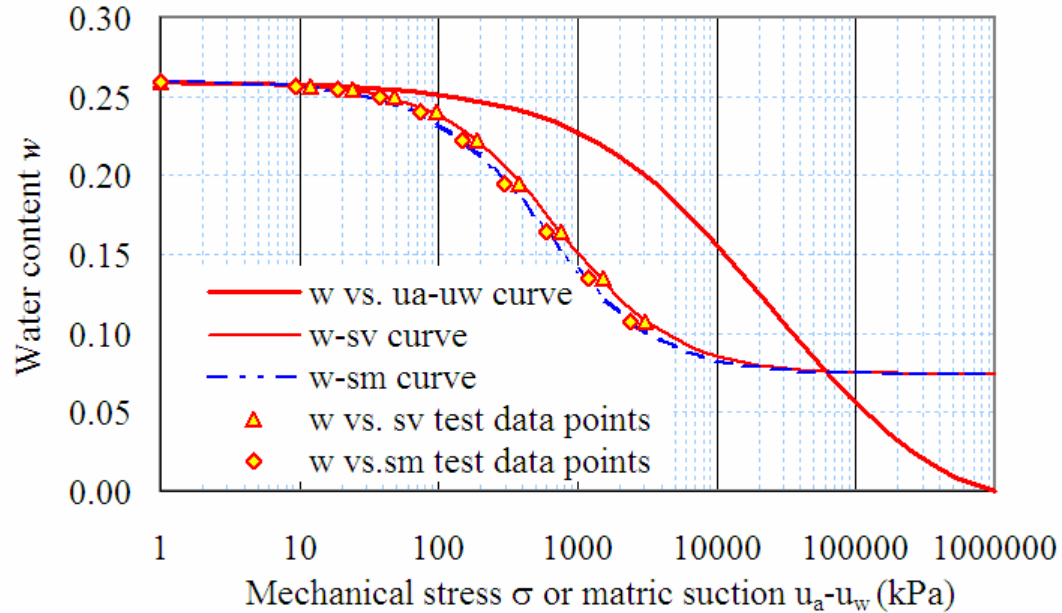


Figure B.1.1.9 Curves for Constructing the Water Content Constitutive Surface for the Soil SW145

B.1.1.9.1. Water Content w versus Vertical Mechanical Stress σ_v & Matric Suction ($u_a - u_w$) Surface

Boundary:

$u_a - u_w = 0$ (from 1-D consolidation test):

$$w = \frac{e}{G_s} = 0.07381605 + \frac{0.18526262}{1 + \exp\left(\frac{\log_{10}(\sigma_v) - 2.86157532}{0.421062101}\right)}$$

Therefore

$$\log_{10} \sigma_v = 0.421062101 \ln \left(\frac{0.18526262}{(w - 0.07381605)} - 1 \right) + 2.86157532$$

$\sigma_v = 0$ (from soil-water characteristic curve and free shrink test):

$$w = -0.026264216 + \frac{0.285551272}{1 + \exp\left(\frac{\log_{10}(u_a - u_w) - 4.386436815}{0.671559558}\right)}$$

$$\log_{10}(u_a - u_w) = 0.671559558 \ln\left(\frac{0.285551272}{(w + 0.026264216)} - 1\right) + 4.386436815$$

B.1.1.9.2. w versus σ_v & $(u_a - u_w)$ Surface

(for 1 D consolidation theory for saturated-unsaturated soils)

Linear assumption:

$$\frac{\sigma_v - u_a}{(\sigma_v - u_a)_{(u_a - u_w = 0)}} + \frac{u_a - u_w}{(u_a - u_w)_{(\sigma_v - u_a = 0)}} = 1$$

$$\frac{\sigma_v - u_a}{10^{\left(0.421062101 \ln\left(\frac{0.18526262}{(w - 0.07381605)} - 1\right) + 2.86157532\right)}} + \frac{u_a - u_w}{10^{\left(0.671559558 \ln\left(\frac{0.285551272}{(w + 0.026264216)} - 1\right) + 4.386436815\right)}} = 1$$

for $(\sigma_m - u_a) + (u_a - u_w) < 32637.8$ kPa

B.1.1.9.3. Degree of Saturation S versus Vertical Mechanical Stress σ_v & Matric Suction $(u_a - u_w)$ Surface

For $(\sigma_v - u_a) + (u_a - u_w) > 32637.8$ kPa

$$S = -0.024789788 + \frac{1.024790004}{1 + \exp\left(\frac{\log_{10}(u_a - u_w) - 4.979543423}{0.324013298}\right)}$$

B.1.1.9.4. Water Content w versus Mean Mechanical Stress σ_m & Matric Suction $(u_a - u_w)$ Surface

Boundary:

$u_a - u_w = 0$ (from 1-D consolidation test):

$$w = \frac{e}{G_s} = 0.07375434 + \frac{0.18538718}{1 + \exp\left(\frac{\log_{10}(\sigma_m) - 2.75275012}{0.42147606}\right)}$$

Therefore

$$\log_{10} \sigma_m = 0.42147606 \ln\left(\frac{0.18538718}{(w - 0.07375434)} - 1\right) + 2.75275012$$

$\sigma_m = 0$ (from soil-water characteristic curve and free shrink test):

$$w = -0.026264216 + \frac{0.285551272}{1 + \exp\left(\frac{\log_{10}(u_a - u_w) - 4.386436815}{0.671559558}\right)}$$

$$\log_{10}(u_a - u_w) = 0.671559558 \ln\left(\frac{0.285551272}{(w + 0.026264216)} - 1\right) + 4.386436815$$

B.1.1.9.5. w versus σ_m & $(u_a - u_w)$ Surface

(for 2 D or 3 D consolidation theory for saturated-unsaturated soils)

linear assumption:

$$\frac{\sigma_v - u_a}{(\sigma_m - u_a)_{(u_a - u_w = 0)}} + \frac{u_a - u_w}{(u_a - u_w)_{(\sigma_m - u_a = 0)}} = 1$$

$$\frac{\sigma_v - u_a}{10^{\left(0.42147606 \ln\left(\frac{0.18538718}{(w - 0.07375434)} - 1\right) + 2.75275012\right)}} + \frac{u_a - u_w}{10^{\left(0.671559558 \ln\left(\frac{0.285551272}{(w + 0.026264216)} - 1\right) + 4.386436815\right)}} = 1$$

for $(\sigma_m - u_a) + (u_a - u_w) < 32637.8$ kPa

B.1.1.9.6. Degree of saturation S versus mean mechanical stress σ_v & matric suction

$(u_a - u_w)$ surface

$$S = -0.024789788 + \frac{1.024790004}{1 + \exp\left(\frac{\log_{10}(u_a - u_w) - 4.979543423}{0.324013298}\right)}$$

For $(\sigma_m - u_a) + (u_a - u_w) > 32637.8$ kPa

B.1.1.10. Constitutive Surfaces and Material Parameters for the Soil SW145

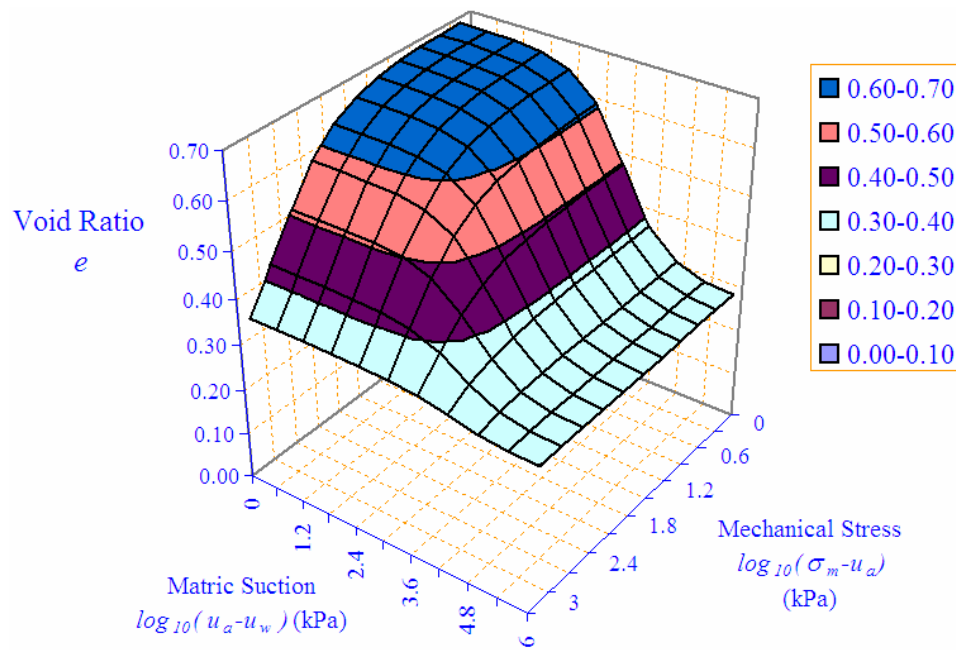


Figure B.1.1.10 Void Ratio Constitutive Surface for the Soil SW145

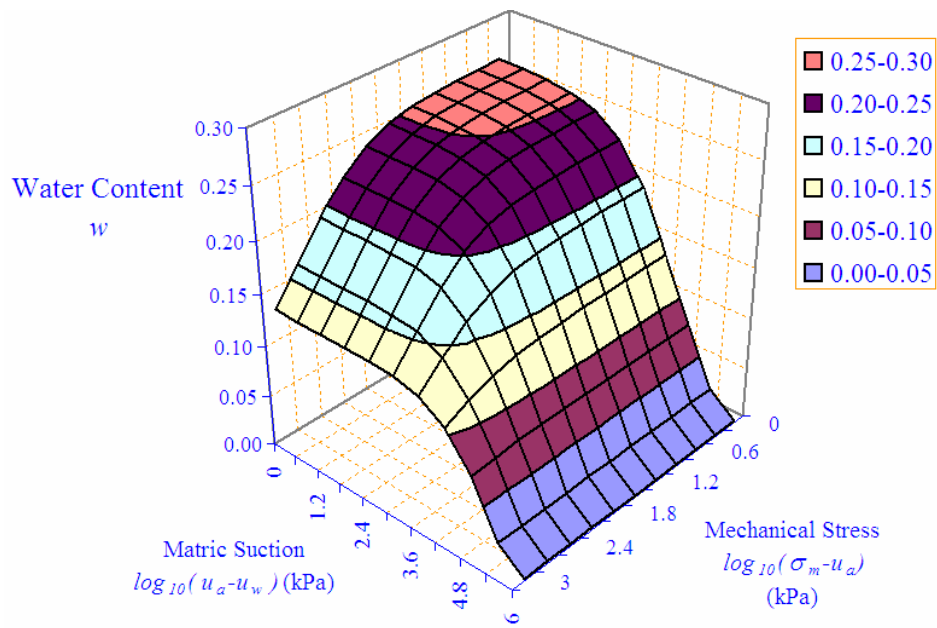


Figure B.1.1.12 Water Content Constitutive Surface for the Soil SW145

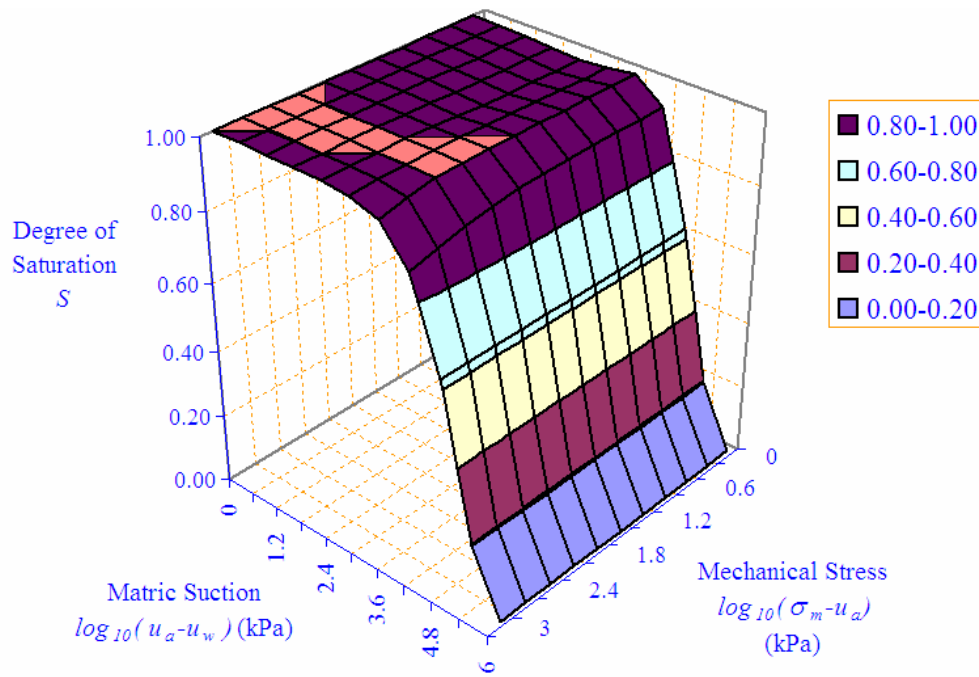


Figure B.1.1.13 Degree of Saturation Constitutive Surface for the Soil SW145

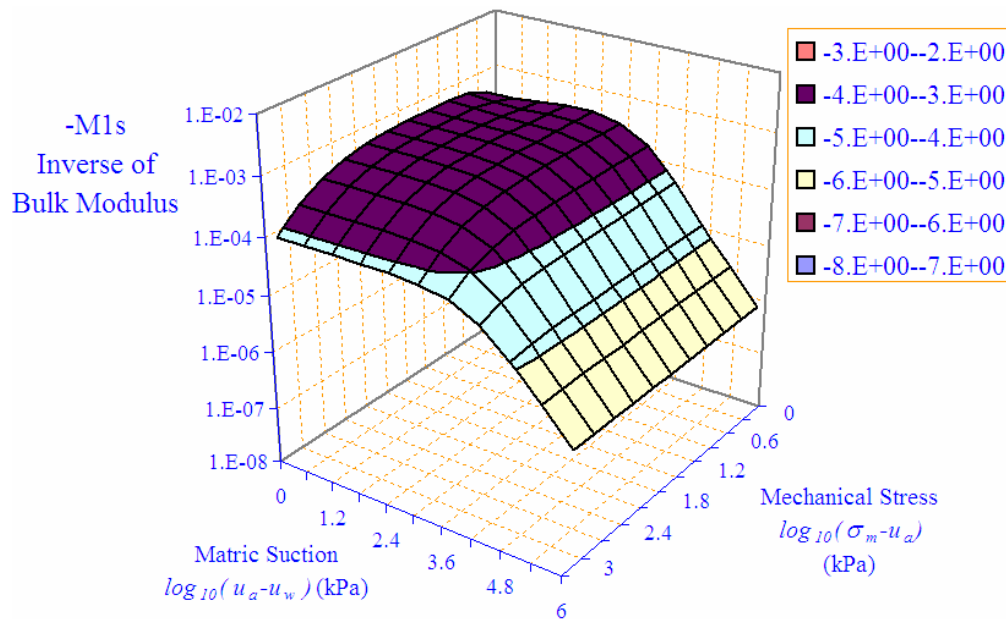


Figure B.1.1.14 Inverse of Bulk Modulus m_1^s Surface for the Soil SW145

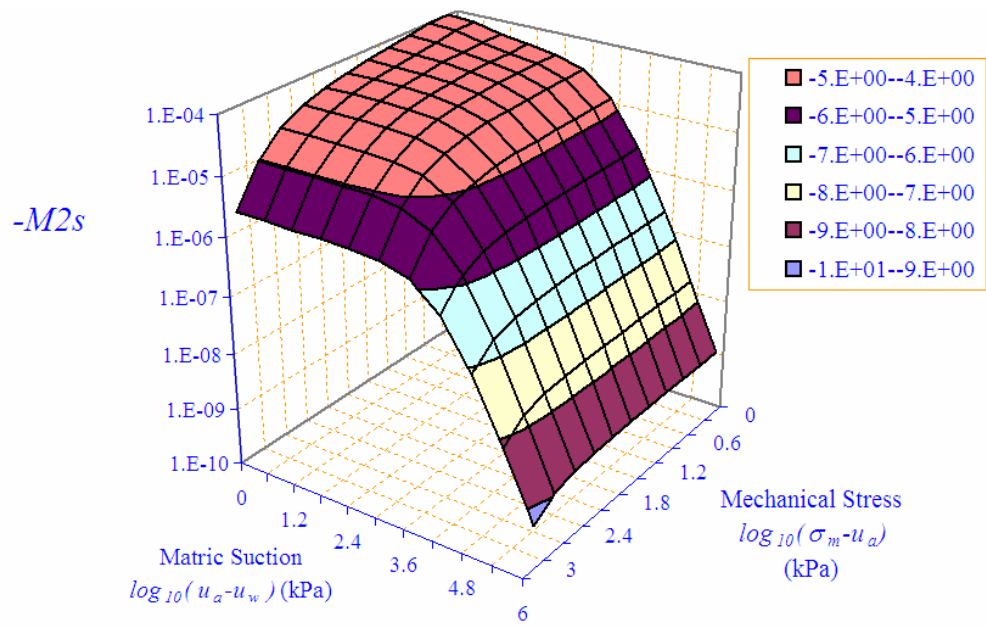


Figure B.1.1.15 m_2^s Surface for the Soil SW145

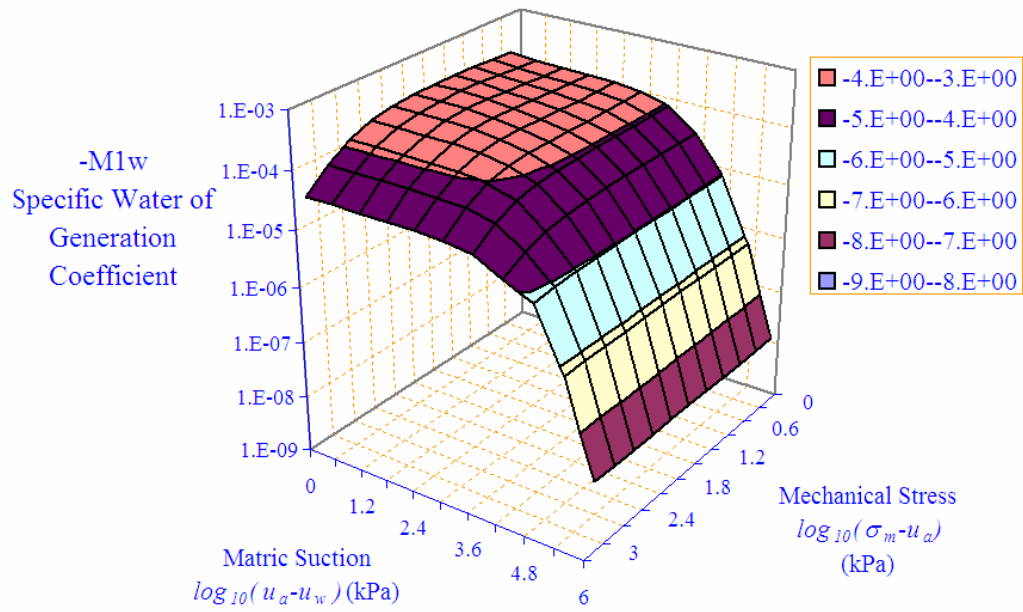


Figure B.1.1.16 m_1^w Surface for the Soil SW145

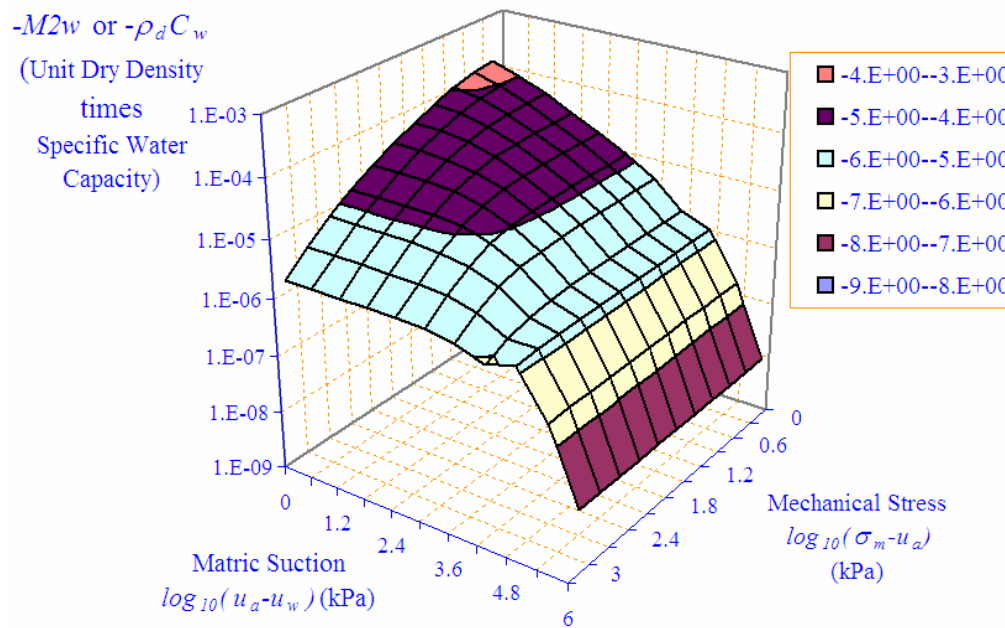


Figure B.1.1.17 m_2^w Surface for the Soil SW145

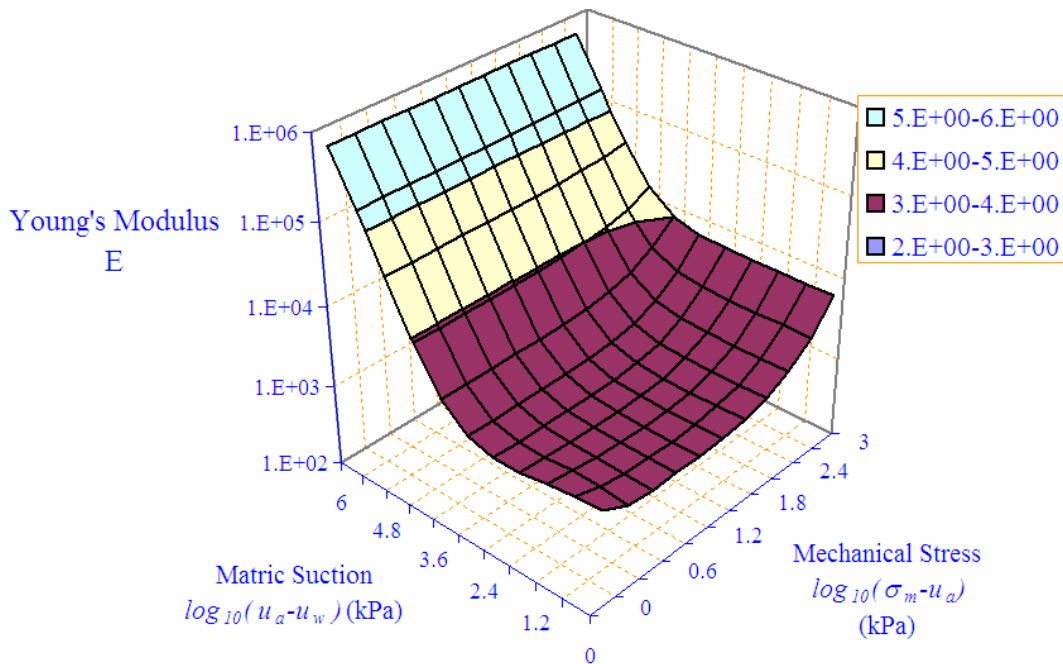


Figure B.1.1.18 Young's Modulus Surface for the Soil SW145

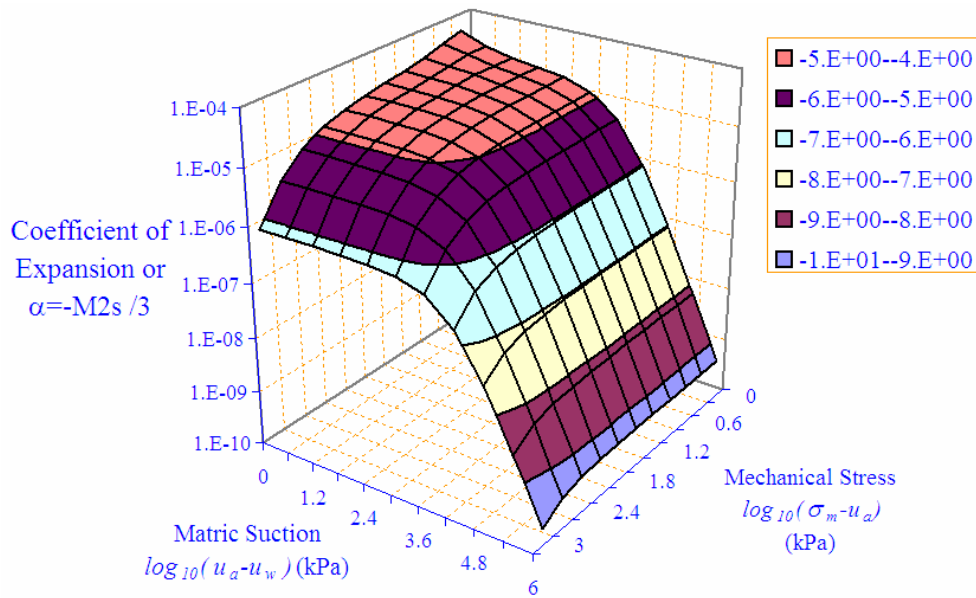


Figure B.1.1.19 Coefficient of Expansion Surface for the Soil SW145

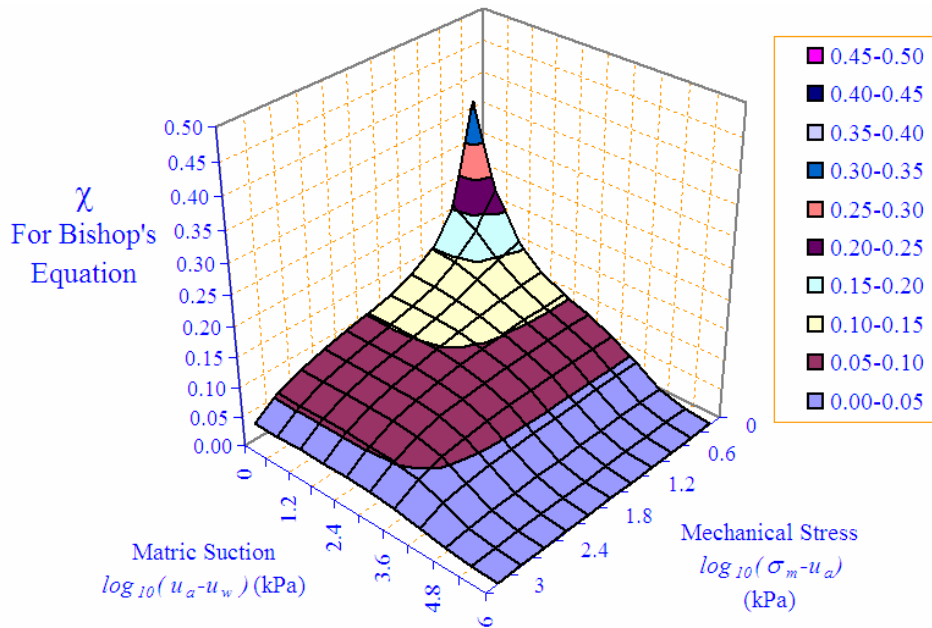


Figure B.1.1.20 χ Surface for the Soil SW145

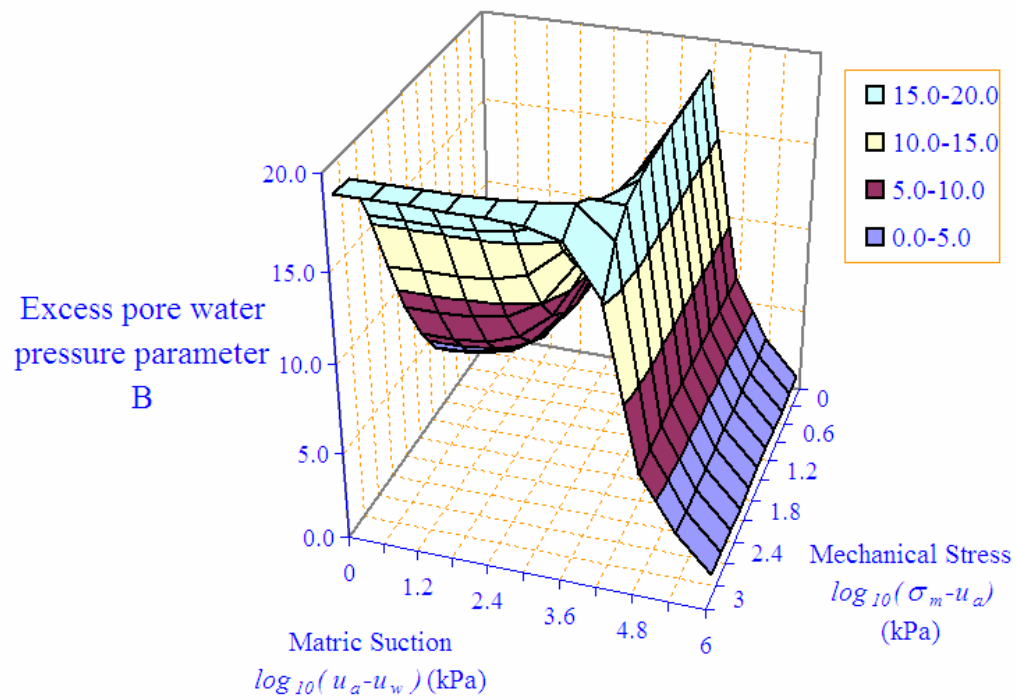


Figure B.1.1.21 Excess Pore Water Pressure Parameter Surface for the Soil SW145

Appendix B.1.2. Summary of Material Properties for the Soil SW189

B.1.2.1. Consolidation Test: e - $\log(\sigma_v)$ Relationship

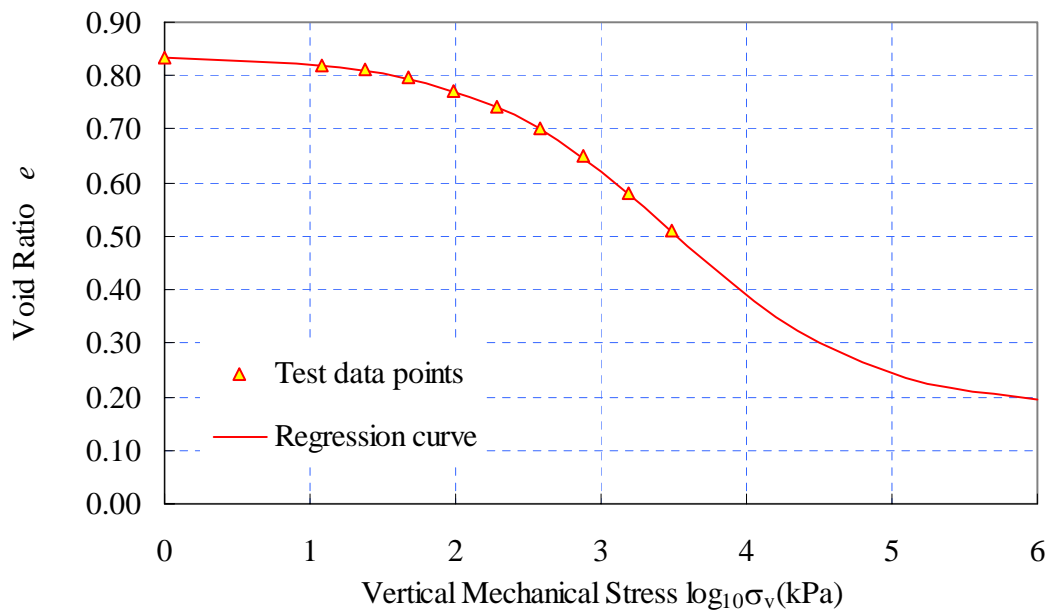


Figure B.1.2.1 Void Ratio vs. Vertical Mechanical Stress Curve for the Soil SW189

Mathematical expression

$$e = 0.1808890 + \frac{0.6554885}{1 + \exp\left(\frac{\log_{10}(\sigma_v) - 3.4899308}{0.6752219}\right)}$$

B.1.2.2. Consolidation Test: e - $\log(\sigma_m)$ Relationship

Mathematical expression

$$e = 0.1730660 + \frac{0.6641108}{1 + \exp\left(\frac{\log_{10}(\sigma_m) - 3.3957253}{0.6811336}\right)}$$

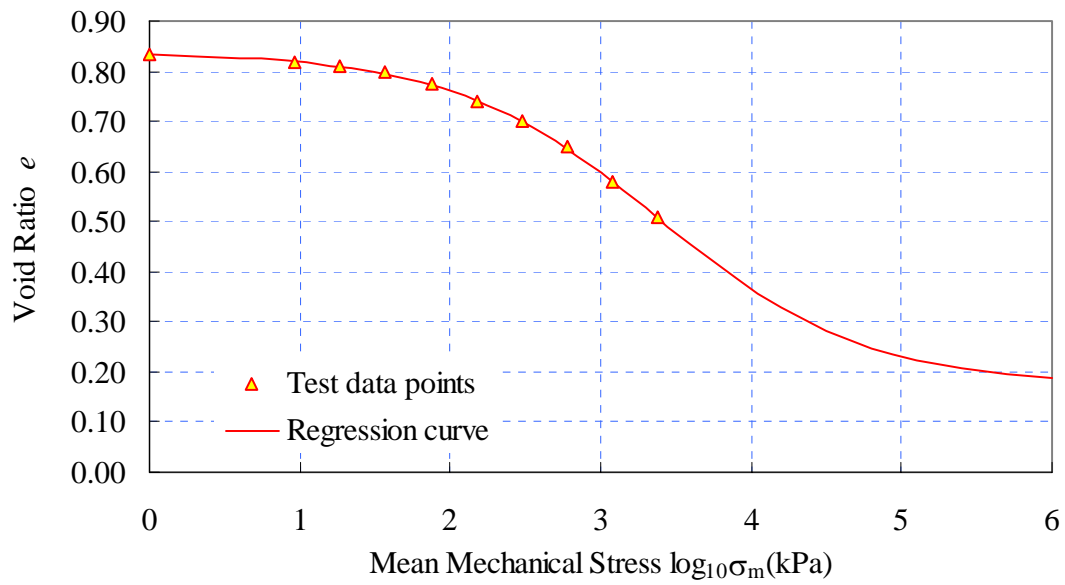


Figure B.1.2.2 Void Ratio vs. Mean Mechanical Stress Curve for the Soil SW189

B.1.2.3.. Consolidation Test: w - $\log(\sigma_v)$ Relationship

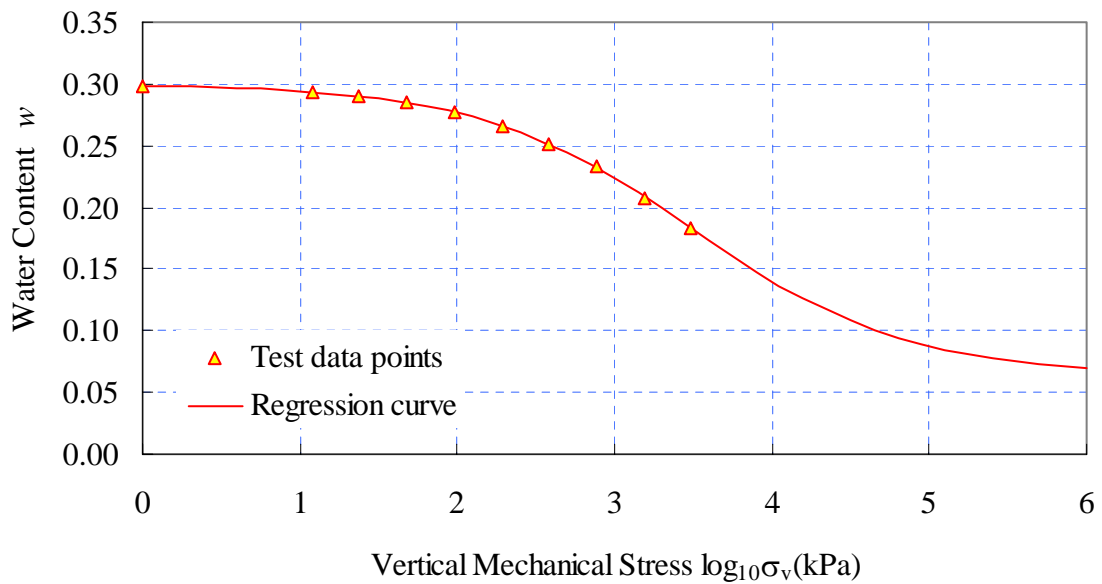


Figure B.1.2.3 Water Content vs. Vertical Mechanical Stress Curve for the Soil SW189

Mathematical expression

$$w = \frac{e}{G_s} = 0.0648348 + \frac{0.2349421}{1 + \exp\left(\frac{\log_{10}(\sigma_v) - 3.4899308}{0.6752219}\right)}$$

B.1.2.4.. Consolidation Test: w-log (σ_m) Relationship

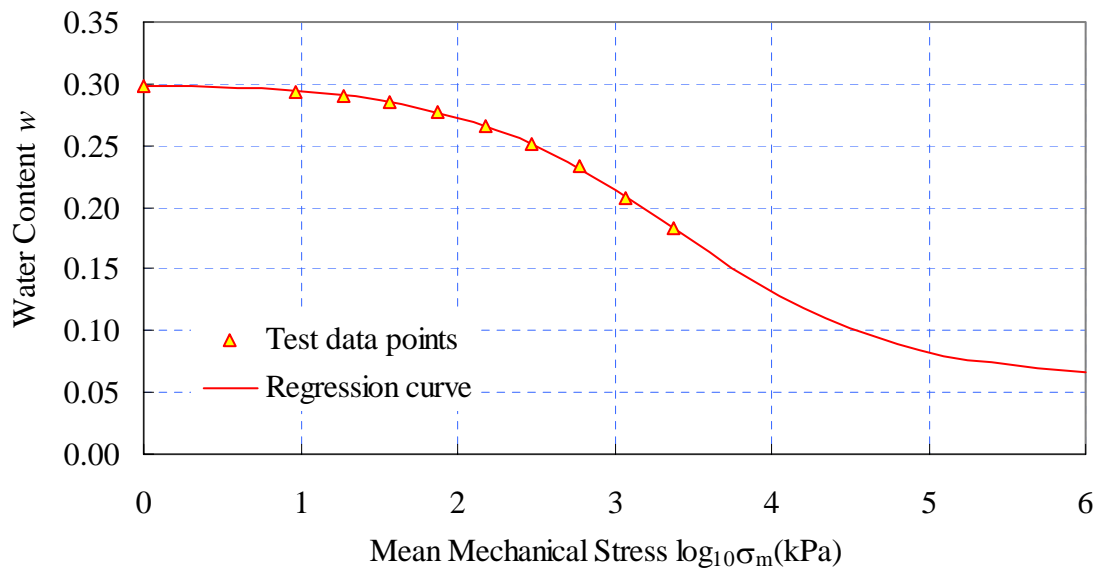


Figure B.1.2.4 Water Content vs. Mean Mechanical Stress Curve for the Soil SW189

Mathematical expression

$$w = \frac{e}{G_s} = 0.0620308 + \frac{0.2380325}{1 + \exp\left(\frac{\log_{10}(\sigma_m) - 3.3957253}{0.6811336}\right)}$$

B.1.2.5. Free Shrink test: e-w Relationship

$$S = \frac{wG_s}{e} = \frac{wG_s}{0.4445238 + \frac{0.434610371}{1 + \exp\left(-\frac{w - 0.226827085}{0.033741115}\right)}}$$

$$S = 5.909w \quad (\text{For } w \leq 0.0944)$$

$$e = 0.4445238 + \frac{0.434610371}{1 + \exp\left(-\frac{w - 0.226827085}{0.033741115}\right)} \quad (\text{For } w \geq 0.136)$$

$$e = 0.4721 \quad (\text{For } w \leq 0.136)$$

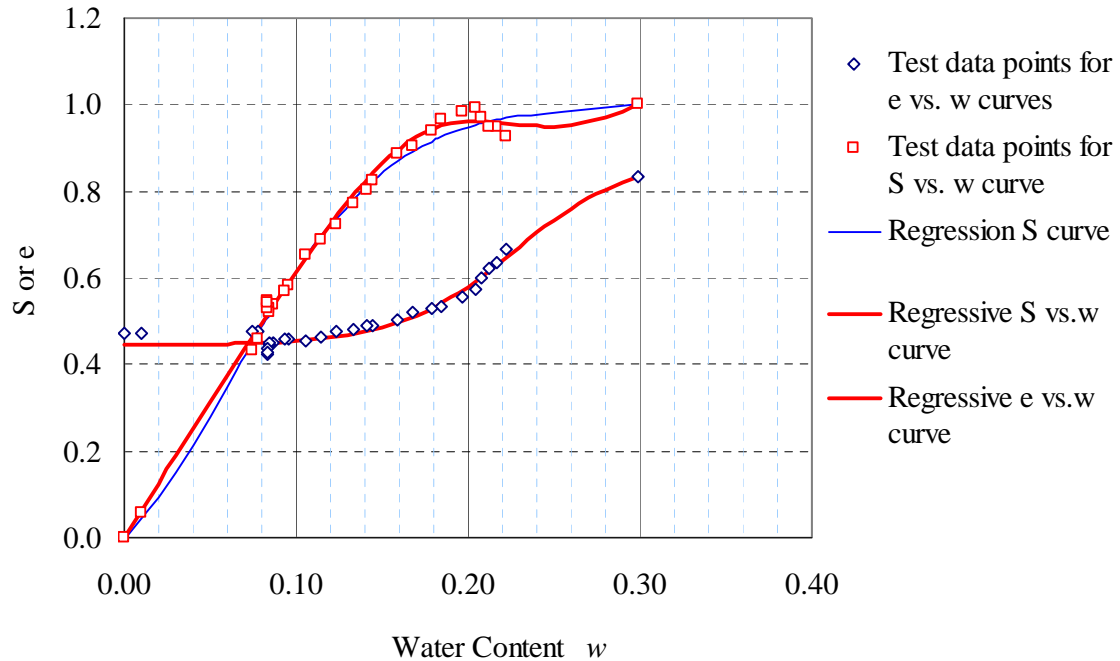


Figure B.1.2.5 Void Ratio and Degree of Saturation vs. Water Content Curve for the Soil SW189

B.1.2.6. Soil Water Characteristic Curve

$$w = -0.124213334 + \frac{0.437992975}{1 + \exp\left(\frac{\log_{10}(u_a - u_w) - 4.57346643}{1.378969054}\right)}$$

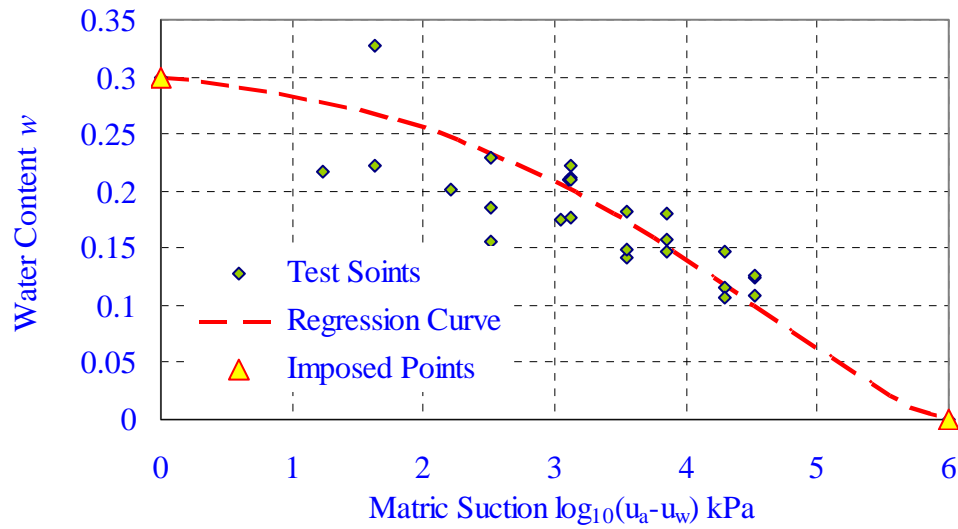


Figure B.1.2.6 Soil Water Characteristic Curve for the Soil SW189

B.1.2.7.. Constructed e- Matric Suction: e-log₁₀(u_a-u_w) Relationship

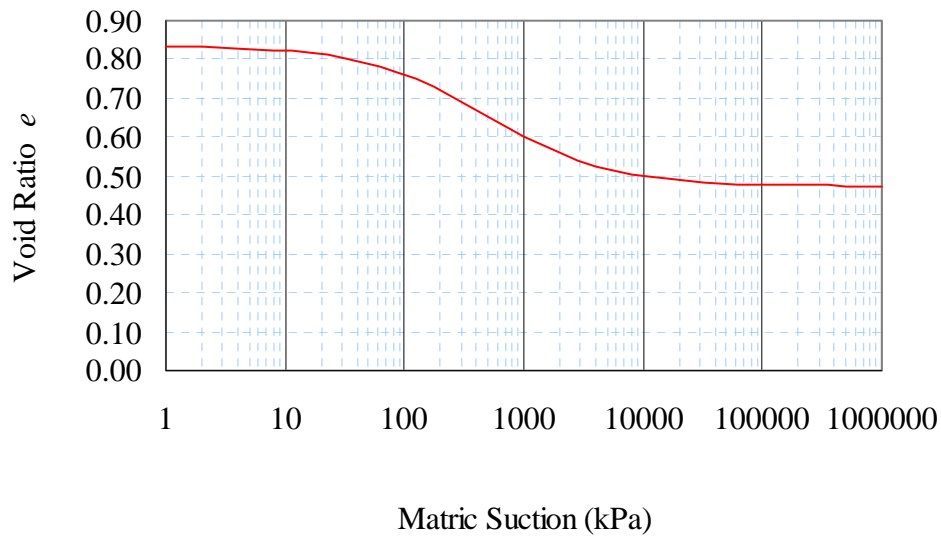


Figure B.1.2.7 Constructed e- Matric Suction: e-log₁₀(u_a-u_w) Relationship for the Soil SW189

$$e = 0.473999 + \frac{0.360413471}{1 + \exp\left(\frac{\log_{10}(u_a - u_w) - 2.701544106}{0.507278347}\right)}$$

B.1.2.8. Void Ratio Constitutive Surface:

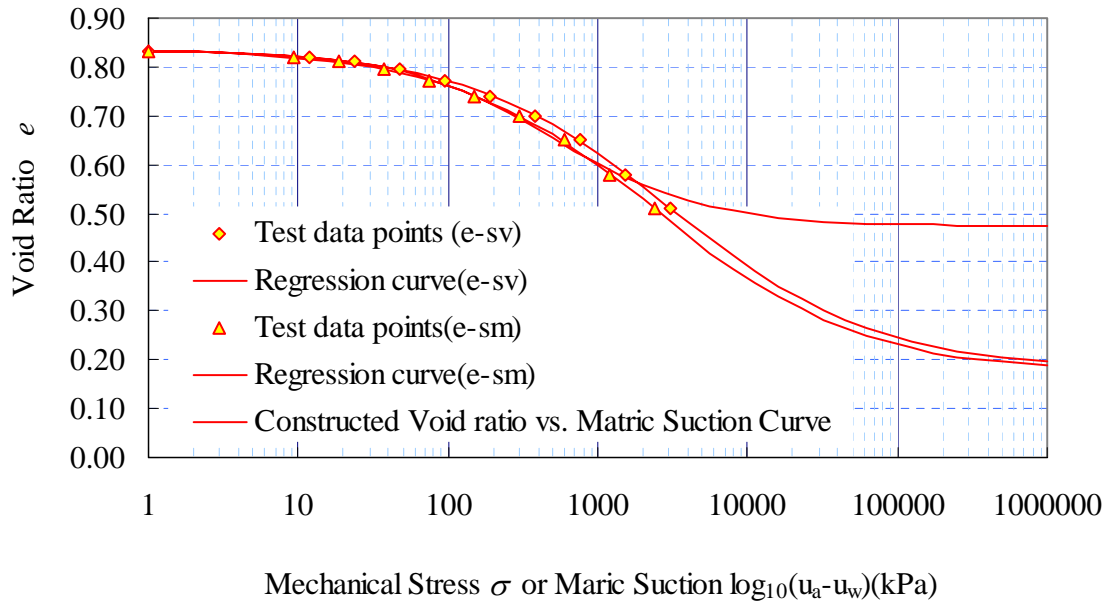


Figure B.1.2.8 Curves for Constructing the Void Ratio Constitutive Surface for the Soil SW189

B.1.2.8.1 Void Ratio e versus Vertical Mechanical Stress σ_v & Maric Suction ($u_a - u_w$) Surface

Boundary:

$u_a - u_w = 0$ (from 1-D consolidation test):

$$e = 0.1808890 + \frac{0.6554885}{1 + \exp\left(\frac{\log_{10}(\sigma_v) - 3.4899308}{0.6752219}\right)}$$

Therefore

$$\log_{10} \sigma_v = 0.6752219 \ln \left(\frac{0.6554885}{(e - 0.1808890)} - 1 \right) + 3.4899308$$

$\sigma_v = 0$ (from soil-water characteristic curve and free shrink test):

$$e = 0.473999 + \frac{0.360413471}{1 + \exp\left(\frac{\log_{10}(u_a - u_w) - 2.701544106}{0.507278347}\right)}$$

$$\log_{10}(u_a - u_w) = 0.507278347 \ln \left(\frac{0.360413471}{(e - 0.473999)} - 1 \right) + 2.701544106$$

B.1.2.8.2. e versus σ_v & $(u_a - u_w)$ Surface

(for 1 D consolidation theory for saturated-unsaturated soils)

linear assumption:

$$\frac{\sigma_v - u_a}{(\sigma_m - u_a)_{(u_a - u_w = 0)}} + \frac{u_a - u_w}{(u_a - u_w)_{(\sigma_m - u_a = 0)}} = 1$$

$$\frac{\sigma_v - u_a}{10^{\left(0.6752219 \ln \left(\frac{0.6554885}{(e - 0.1808890)} - 1 \right) + 3.4899308\right)}} + \frac{u_a - u_w}{10^{\left(0.507278347 \ln \left(\frac{0.360413471}{(e - 0.473999)} - 1 \right) + 2.701544106\right)}} = 1$$

B.1.2.8.3. Void ratio e versus Mean Mechanical Stress σ_m & Matric Suction $(u_a - u_w)$ Surface (for 2 D or 3D consolidation theory for saturated-unsaturated soils)

Boundary:

$u_a - u_w = 0$ (from 1-D consolidation test):

$$e = 0.1730660 + \frac{0.6641108}{1 + \exp\left(\frac{\log_{10}(\sigma_m) - 3.3957253}{0.6811336}\right)}$$

Therefore

$$\log_{10} \sigma_m = 0.6811336 \ln \left(\frac{0.6641108}{(e - 0.1730660)} - 1 \right) + 3.3957253$$

$\sigma_m = 0$ (from soil-water characteristic curve and free shrink test):

$$e = 0.473999 + \frac{0.360413471}{1 + \exp \left(\frac{\log_{10}(u_a - u_w) - 2.701544106}{0.507278347} \right)}$$

$$\log_{10}(u_a - u_w) = 0.507278347 \ln \left(\frac{0.360413471}{(e - 0.473999)} - 1 \right) + 2.701544106$$

B.1.2.8.4. e versus σ_m & $(u_a - u_w)$ Surface

(for 2D or 3 D consolidation theory for saturated-unsaturated soils)

linear assumption:

$$\frac{\sigma_m - u_a}{(\sigma_m - u_a)_{(u_a - u_w = 0)}} + \frac{u_a - u_w}{(u_a - u_w)_{(\sigma_m - u_a = 0)}} = 1$$

$$\frac{\sigma_m - u_a}{10^{\left(0.6811336 \ln \left(\frac{0.6641108}{(e - 0.1730660)} - 1 \right) + 3.3957253 \right)}} + \frac{u_a - u_w}{10^{\left(0.507278347 \ln \left(\frac{0.360413471}{(e - 0.473999)} - 1 \right) + 2.701544106 \right)}} = 1$$

B.1.2.9. Water Content Constitutive Surface

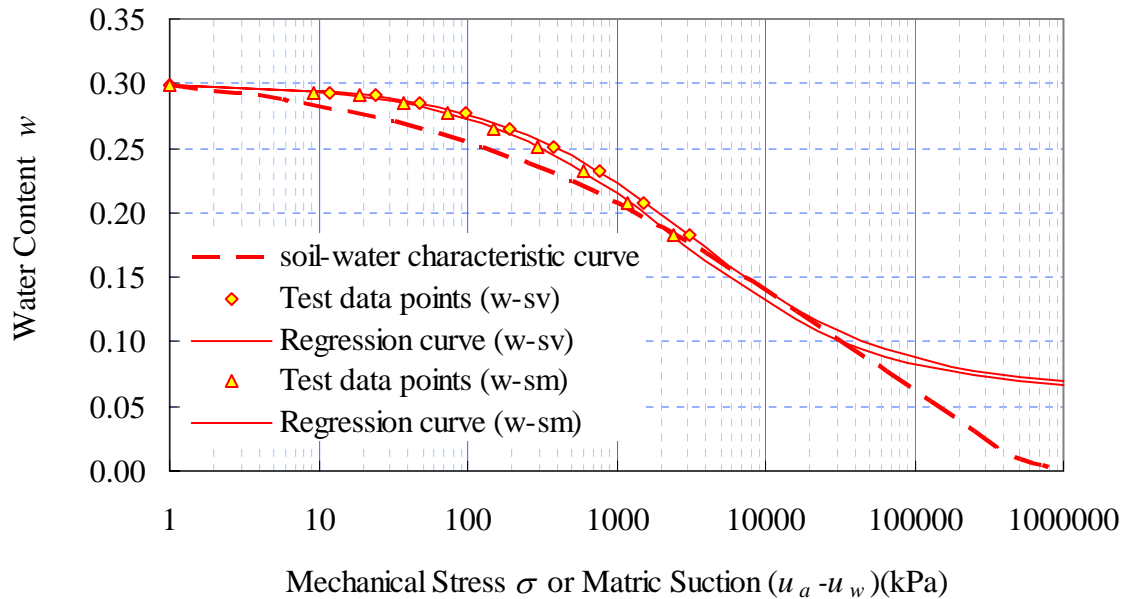


Figure B.1.2.9 Curves for Constructing the Water Content Constitutive Surface for the Soil SW189

B.1.2.9.1. Water Content w versus Vertical Mechanical Stress σ_v & Matric Suction $(u_a - u_w)$ Surface

Boundary:

$u_a - u_w = 0$ (from 1-D consolidation test):

$$w = \frac{e}{G_s} = 0.0648348 + \frac{0.2349421}{1 + \exp\left(\frac{\log_{10}(\sigma_v) - 3.4899308}{0.6752219}\right)}$$

Therefore

$$\log_{10} \sigma_v = 0.6752219 \ln \left(\frac{0.2349421}{(w - 0.0648348)} - 1 \right) + 3.4899308$$

$\sigma_v = 0$ (from soil-water characteristic curve):

$$w = -0.124213334 + \frac{0.437992975}{1 + \exp\left(\frac{\log_{10}(u_a - u_w) - 4.57346643}{1.378969054}\right)}$$

$$\log_{10}(u_a - u_w) = 1.378969054 \ln\left(\frac{0.437992975}{(w + 0.124213334)} - 1\right) + 4.57346643$$

B.1.2.9.2. w versus σ_v & $(u_a - u_w)$ Surface

(for 1 D consolidation theory for saturated-unsaturated soils)

Linear assumption:

$$\frac{\sigma_v - u_a}{(\sigma_v - u_a)_{(u_a - u_w)=0}} + \frac{u_a - u_w}{(u_a - u_w)_{(\sigma_v - u_a)=0}} = 1$$

$$\frac{\sigma_v - u_a}{10^{\left(0.6752219 \ln\left(\frac{0.2349421}{(w - 0.0648348)} - 1\right) + 3.4899308\right)}} + \frac{u_a - u_w}{10^{\left(1.378969054 \ln\left(\frac{0.437992975}{(w + 0.124213334)} - 1\right) + 4.57346643\right)}} = 1$$

for $(\sigma_m - u_a) + (u_a - u_w) < 20000 \text{ kPa}$

B.1.2.9.3. Degree of Saturation S versus Vertical Mechanical Stress σ_v & Matric Suction $(u_a - u_w)$ Surface

For $(\sigma_v - u_a) + (u_a - u_w) > 20000 \text{ kPa}$

$$S = 0.9684982 + \frac{1.0654200}{1 + \exp\left(\frac{\log_{10}(u_a - u_w) - 4.8246437}{0.5193185}\right)}$$

B.1.2.9.4. Water Content w versus Mean Mechanical Stress σ_m & Matric Suction $(u_a - u_w)$ Surface

Boundary:

$u_a - u_w = 0$ (from 1-D consolidation test):

$$w = \frac{e}{G_s} = 0.0620308 + \frac{0.2380325}{1 + \exp\left(\frac{\log_{10}(\sigma_m) - 3.3957253}{0.6811336}\right)}$$

Therefore

$$\log_{10} \sigma_m = 0.6811336 \ln\left(\frac{0.2380325}{(w - 0.0620308)} - 1\right) + 3.3957253$$

$\sigma_m = 0$ (from soil-water characteristic curve):

$$w = -0.124213334 + \frac{0.437992975}{1 + \exp\left(\frac{\log_{10}(u_a - u_w) - 4.57346643}{1.378969054}\right)}$$

$$\log_{10}(u_a - u_w) = 1.378969054 \ln\left(\frac{0.437992975}{(w + 0.124213334)} - 1\right) + 4.57346643$$

B.1.2.9.5. w versus σ_m & $(u_a - u_w)$ Surface

(for 2 D or 3 D consolidation theory for saturated-unsaturated soils)

linear assumption:

$$\frac{\sigma_v - u_a}{(\sigma_m - u_a)_{(u_a - u_w = 0)}} + \frac{u_a - u_w}{(u_a - u_w)_{(\sigma_m - u_a = 0)}} = 1$$

$$\frac{\sigma_m - u_a}{10^{\left(0.6811336 \ln\left(\frac{0.2380325}{(w - 0.0620308)} - 1\right) + 3.3957253\right)}} + \frac{u_a - u_w}{10^{\left(1.378969054 \ln\left(\frac{0.437992975}{(w + 0.124213334)} - 1\right) + 4.57346643\right)}} = 1$$

for $(\sigma_m - u_a) + (u_a - u_w) < 32637.8$

B.1.2.9.6. Degree of saturation S versus mean mechanical stress σ_v & matric suction

$(u_a - u_w)$ surface

For $(\sigma_m - u_a) + (u_a - u_w) > 32637.8$

$$S = 0.9684982 + \frac{1.0654200}{1 + \exp\left(\frac{\log_{10}(u_a - u_w) - 48246437}{0.5193185}\right)}$$

B.1.2.10. Constitutive Surfaces and Material Parameters for the Soil SW189

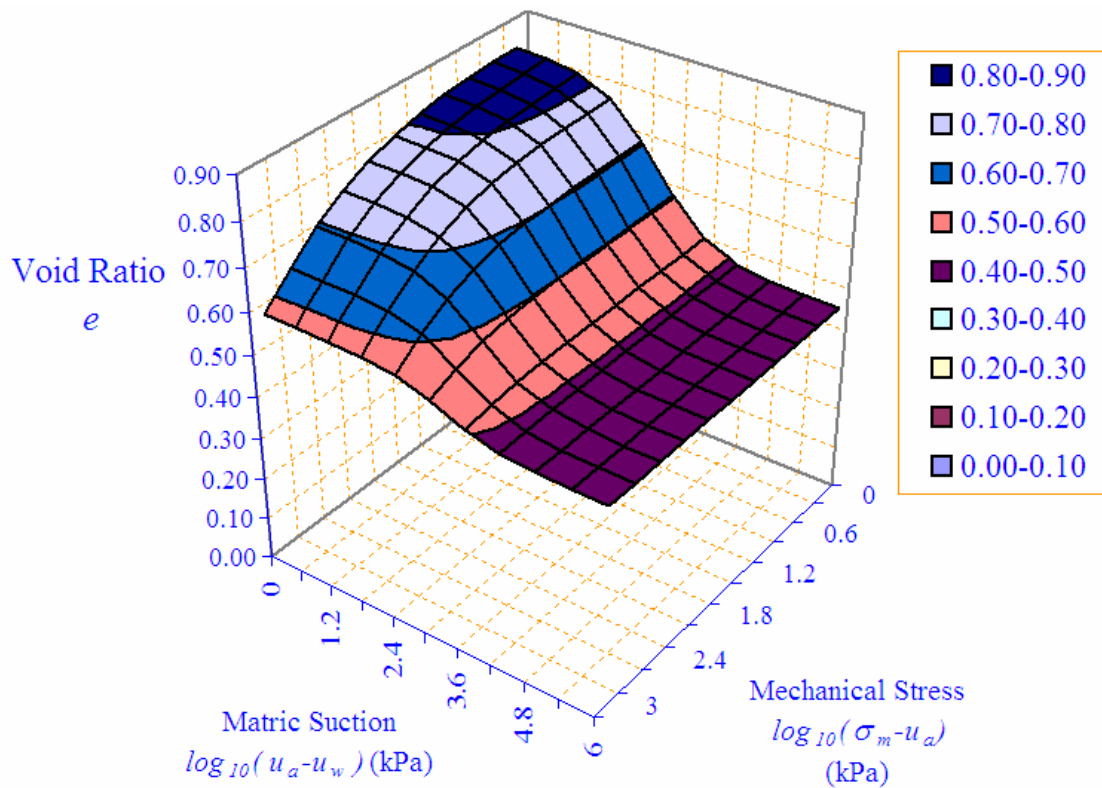


Figure B.1.2.10 Void Ratio Constitutive Surface for the Soil SW189

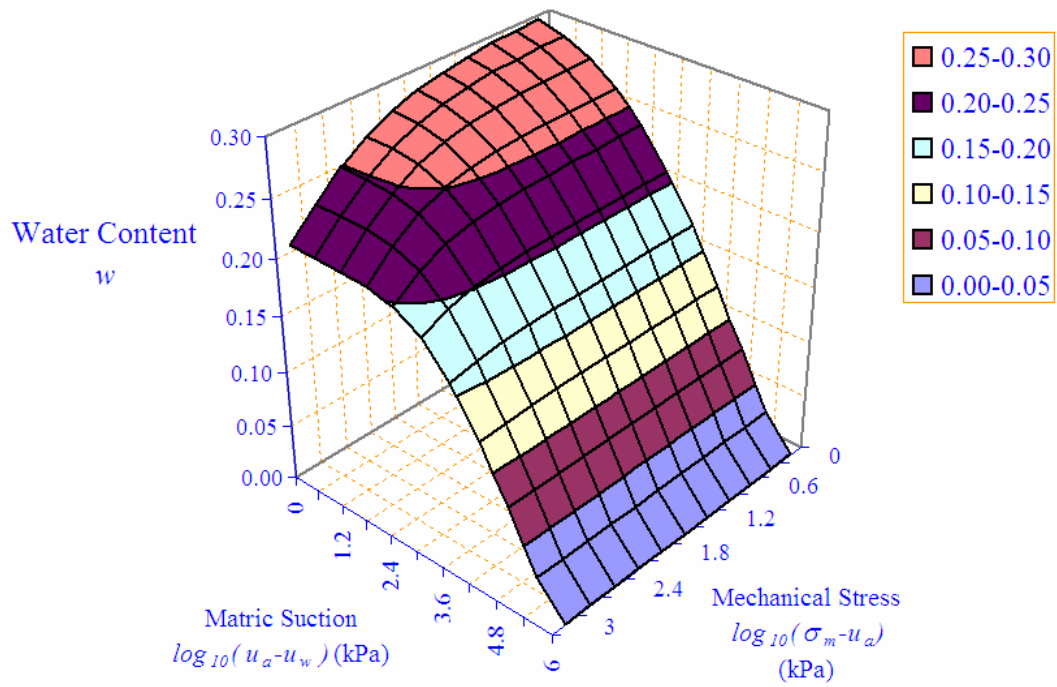


Figure B.1.2.12 Water Content Constitutive Surface for the Soil SW189

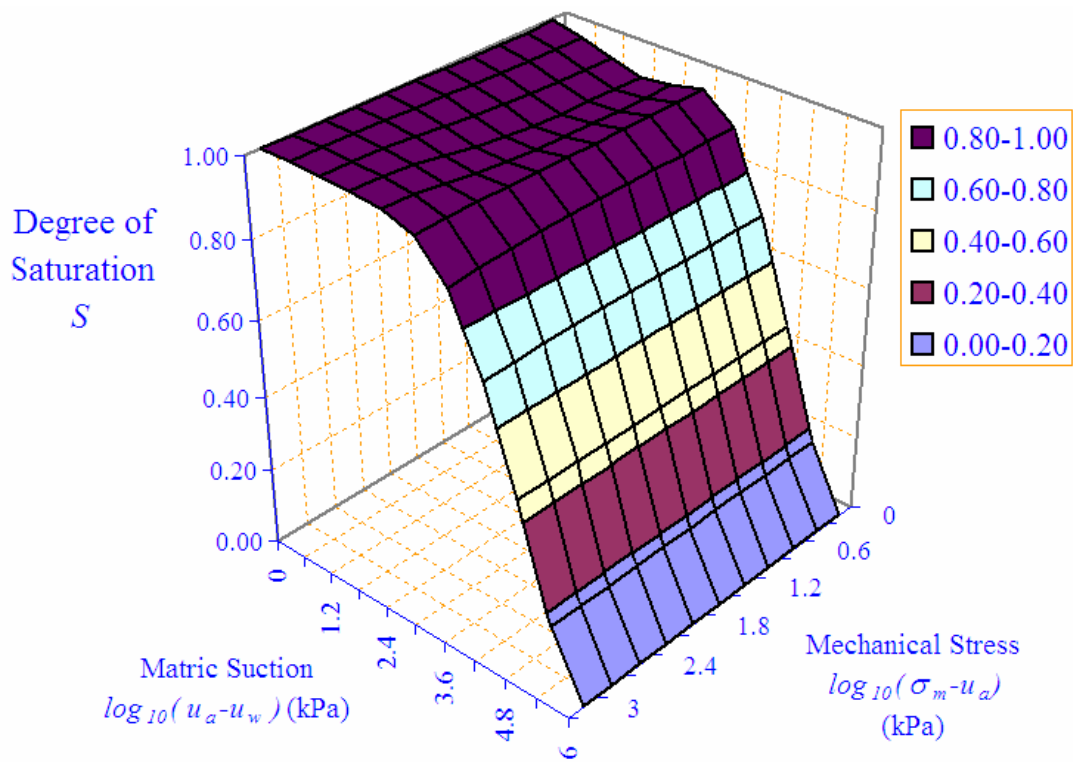


Figure B.1.2.13 Degree of Saturation Constitutive Surface for the Soil SW189

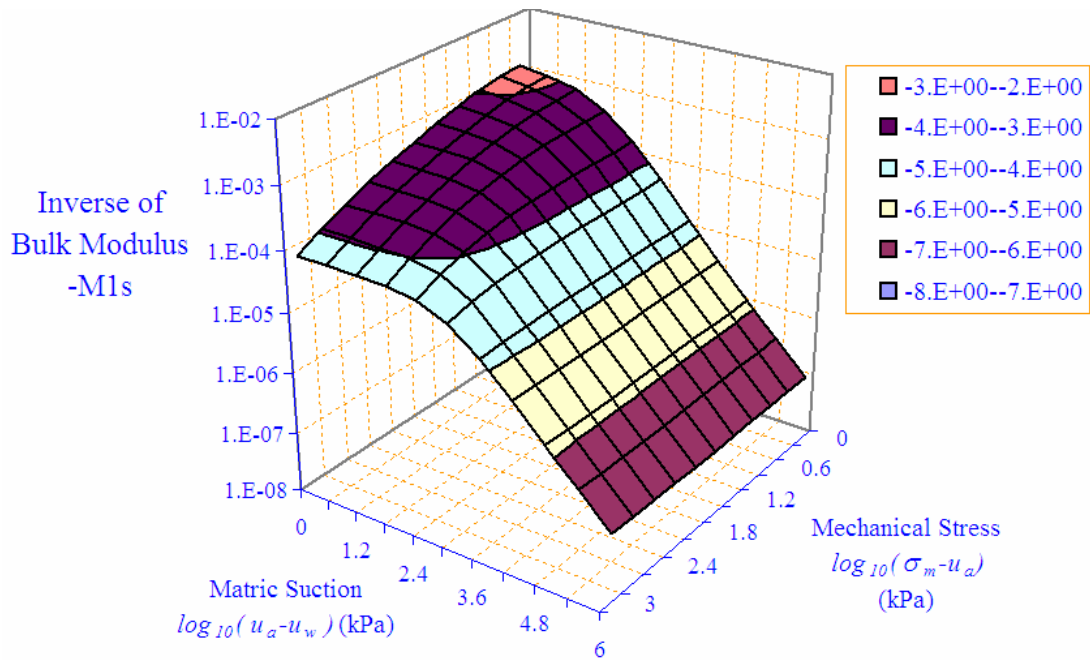


Figure B.1.2.14 Inverse of Bulk Modulus m_1^s Surface for the Soil SW189

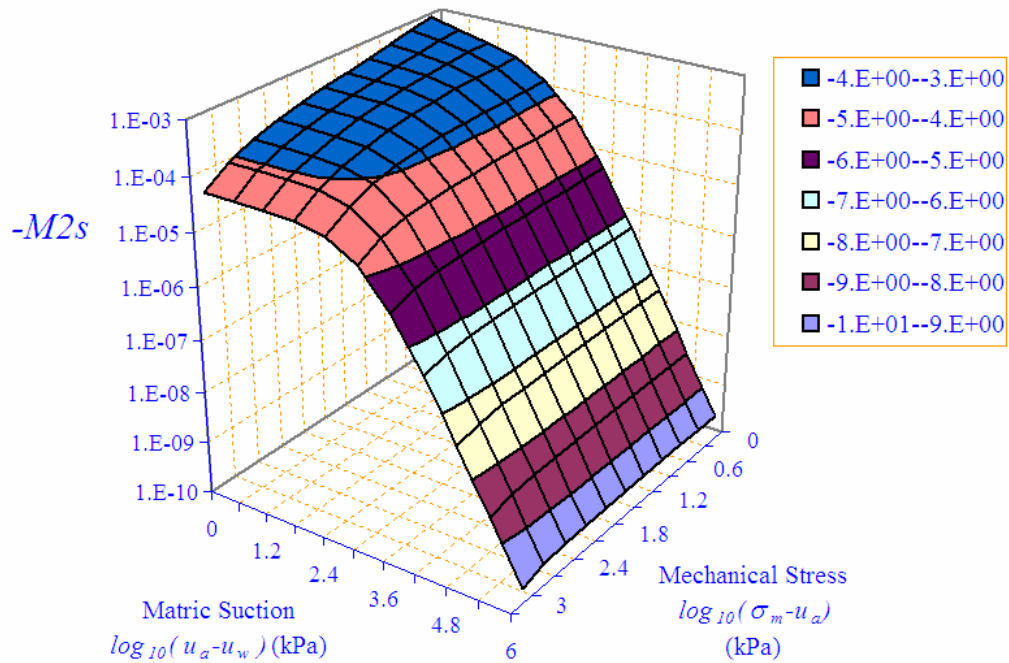


Figure B.1.2.15 m_2^s Surface for the Soil SW189

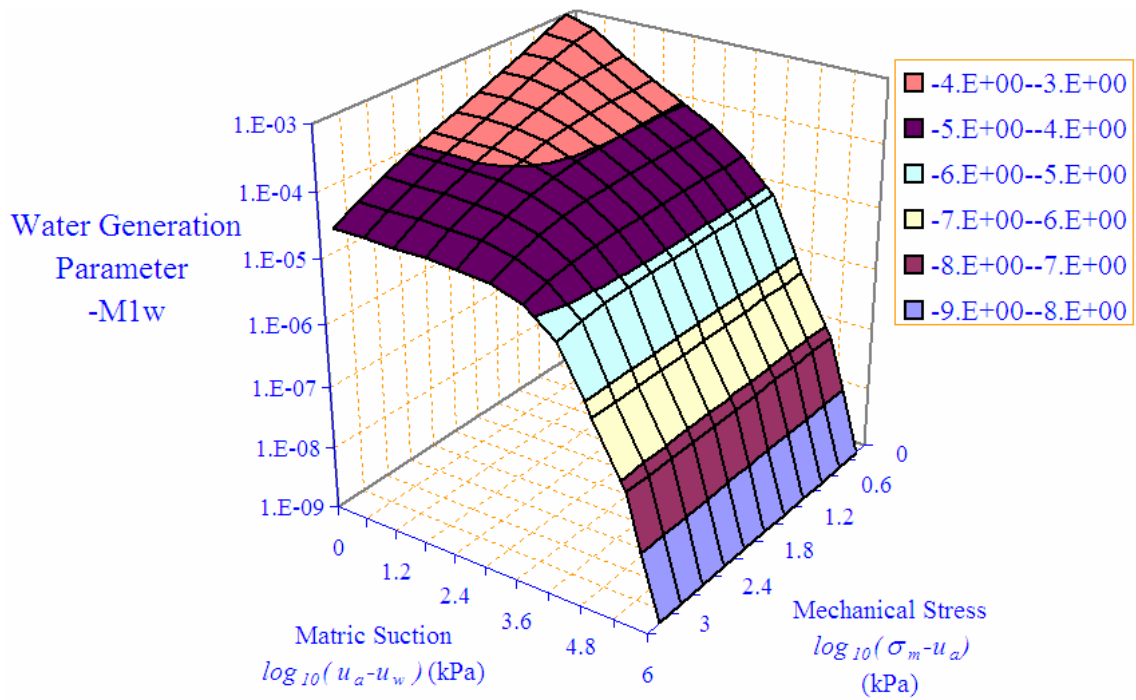


Figure B.1.2.16 m_1^w Surface for the Soil SW189

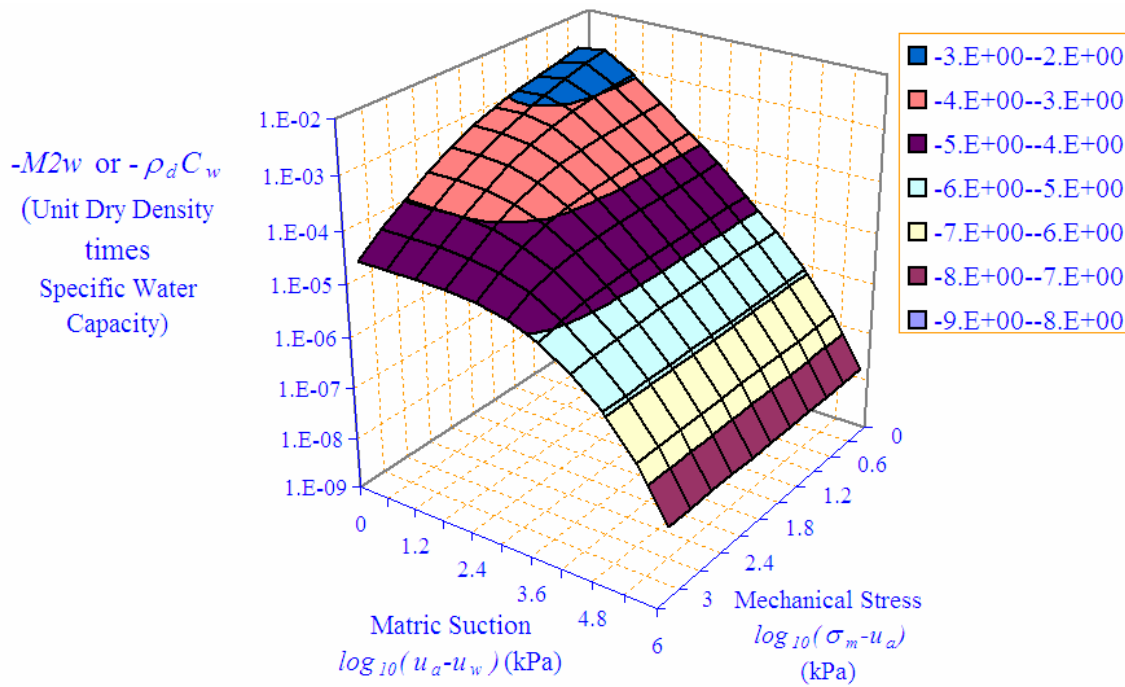


Figure B.1.2.17 m_2^w Surface for the Soil SW189

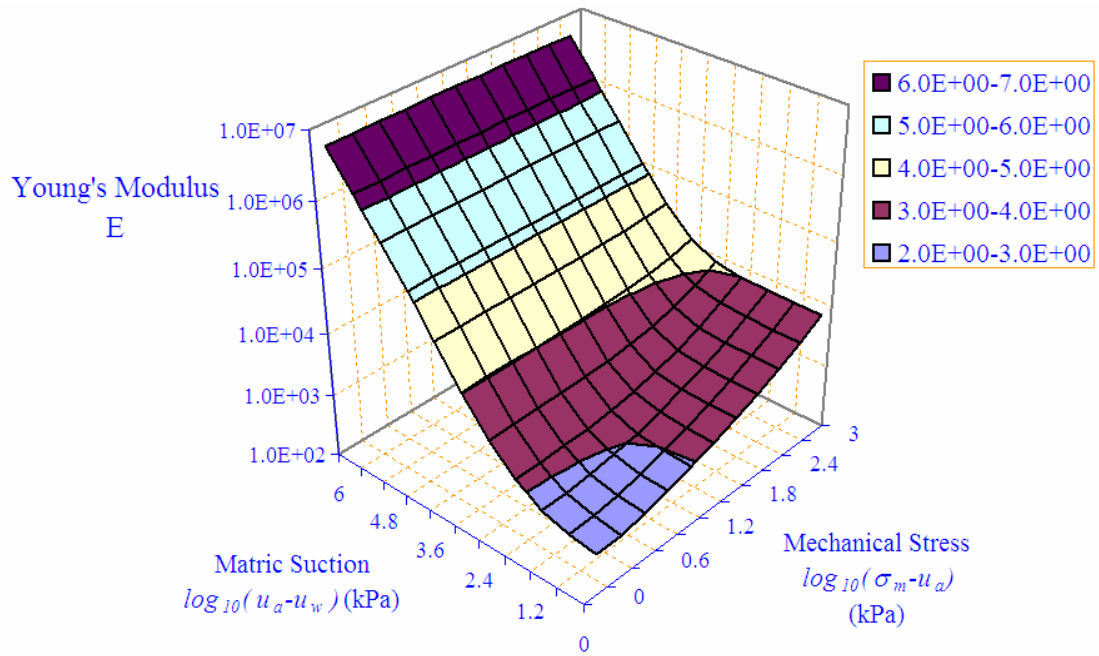


Figure B.1.2.18 Young's Modulus Surface for the Soil SW189

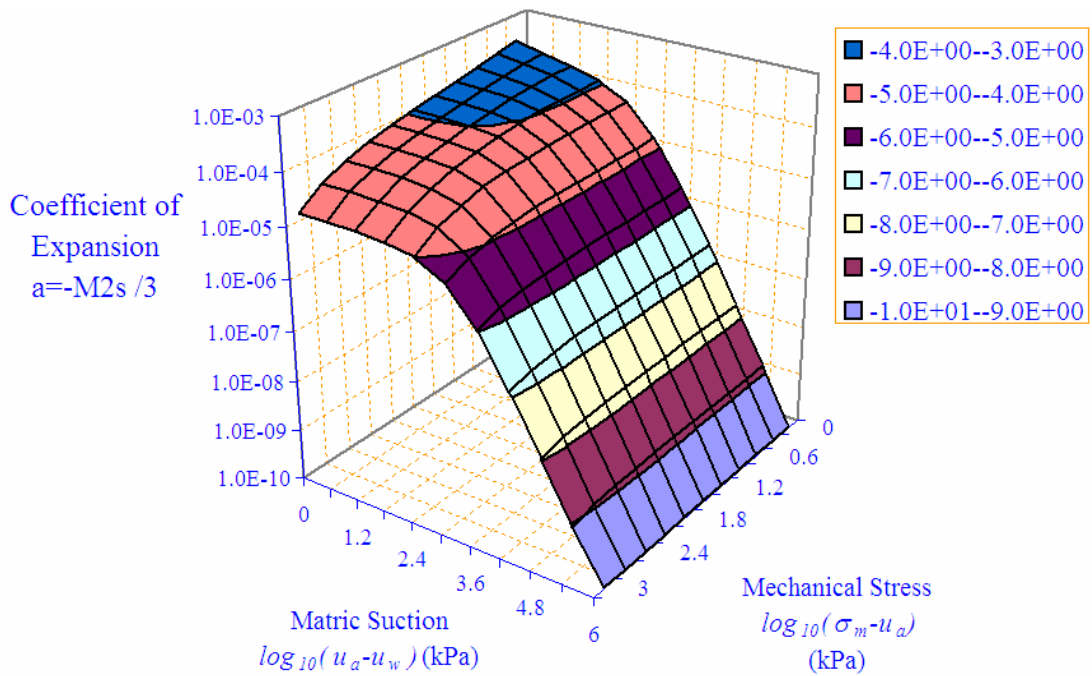


Figure B.1.2.19 Coefficient of Expansion Surface for the Soil SW189

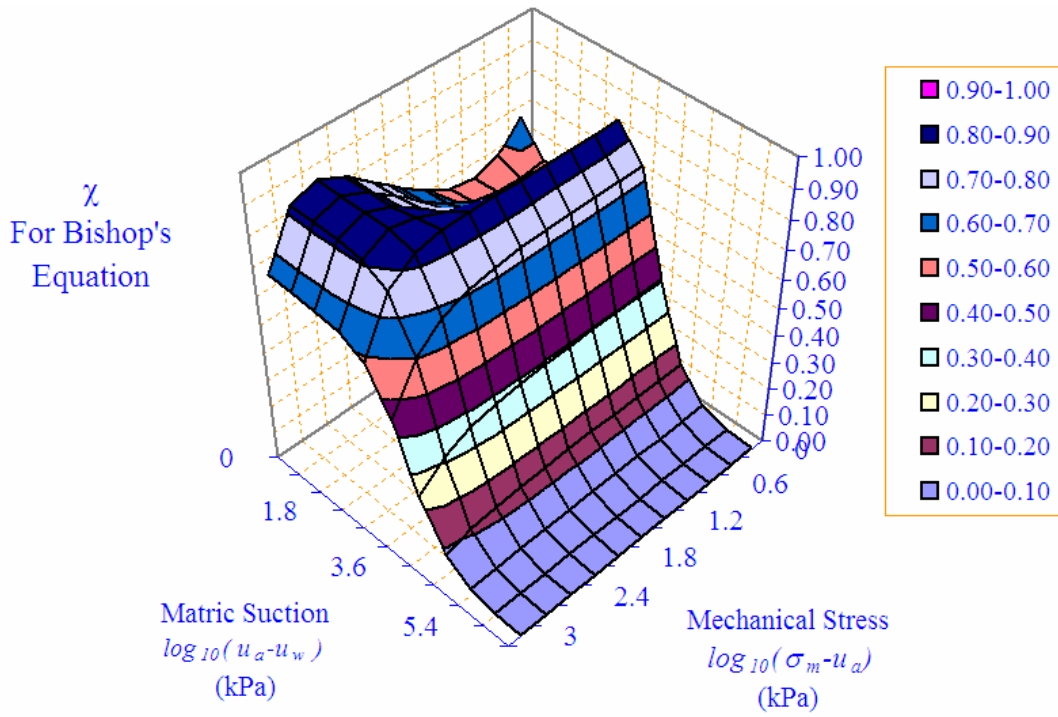


Figure B.1.2.20 χ Surface for the Soil SW189

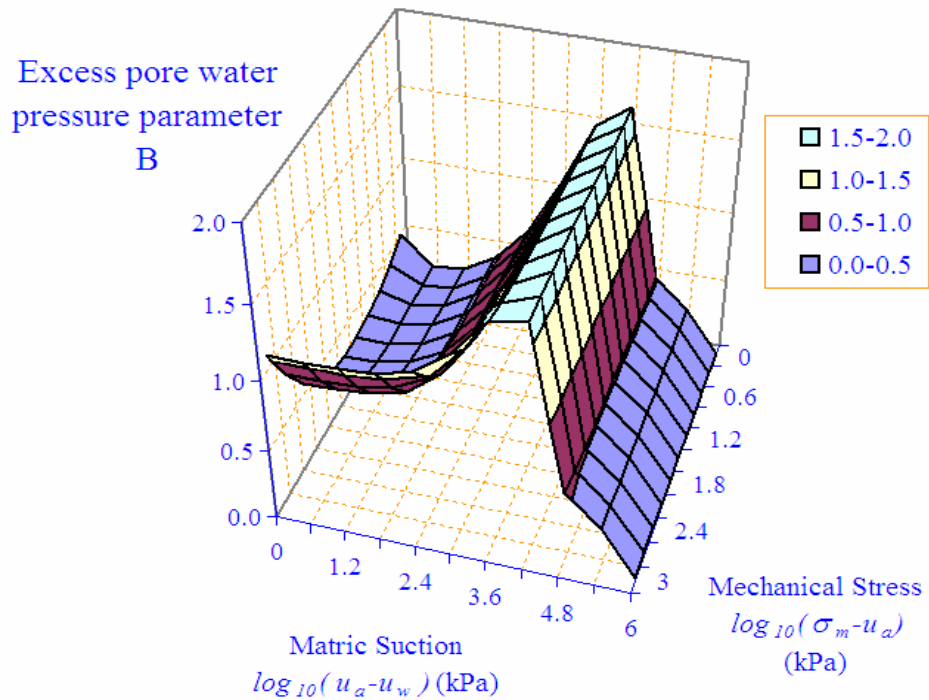


Figure B.1.2.21 Excess Pore Water Pressure Parameter Surface for the Soil SW189

Appendix B.1.3. Summary of Material Properties for the Soil SPORC

B.1.3.1. Consolidation Test: e - $\log(\sigma_v)$ Relationship

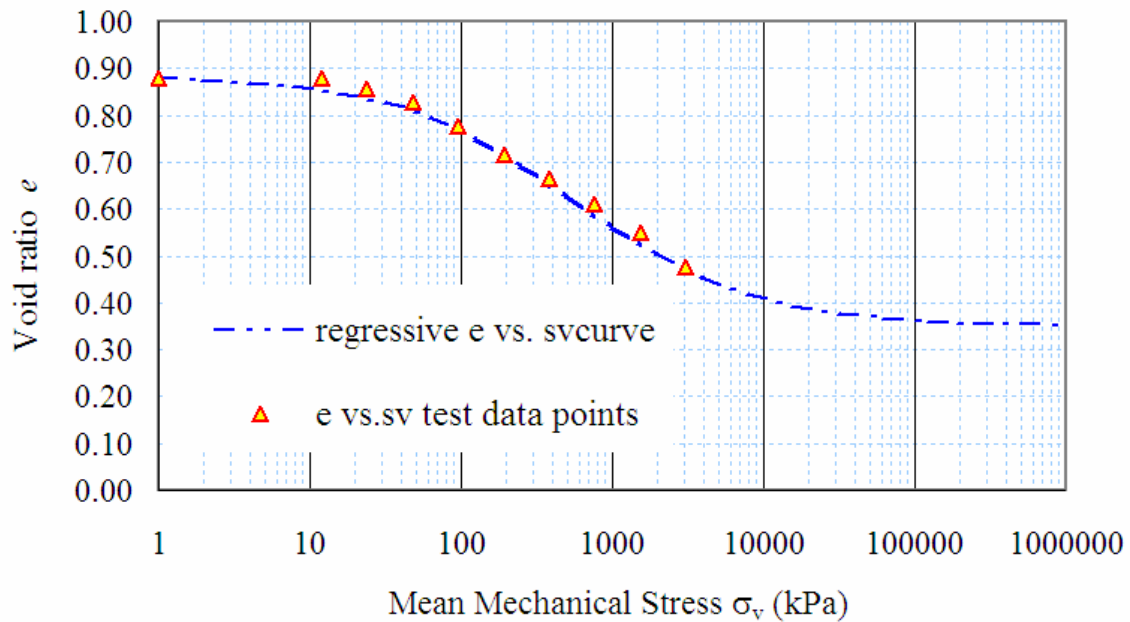


Figure B.1.3.1 Void Ratio vs. Vertical Mechanical Stress Curve for the Soil SPORC

Mathematical expression

$$e = 0.3497455 + \frac{0.5349465}{1 + \exp\left(\frac{\log_{10}(\sigma_v) - 2.7562152}{0.5994558}\right)}$$

B.1.3.2. Consolidation Test: e - $\log(\sigma_m)$ Relationship

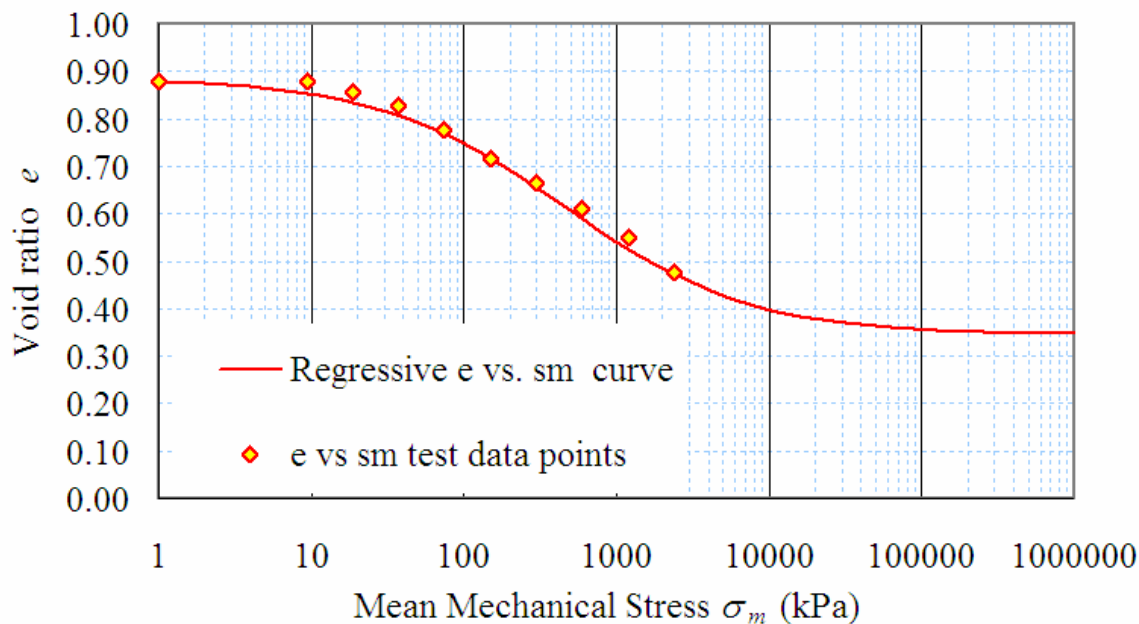


Figure B.1.3.2 Void Ratio vs. Mean Mechanical Stress Curve for the Soil SPORC

Mathematical expression

$$e = 0.3455563 + \frac{0.5405470}{1 + \exp\left(\frac{\log_{10}(\sigma_m) - 2.6544817}{0.6072872}\right)}$$

B.1.3.3.. Consolidation Test: w-log (σ_v) Relationship

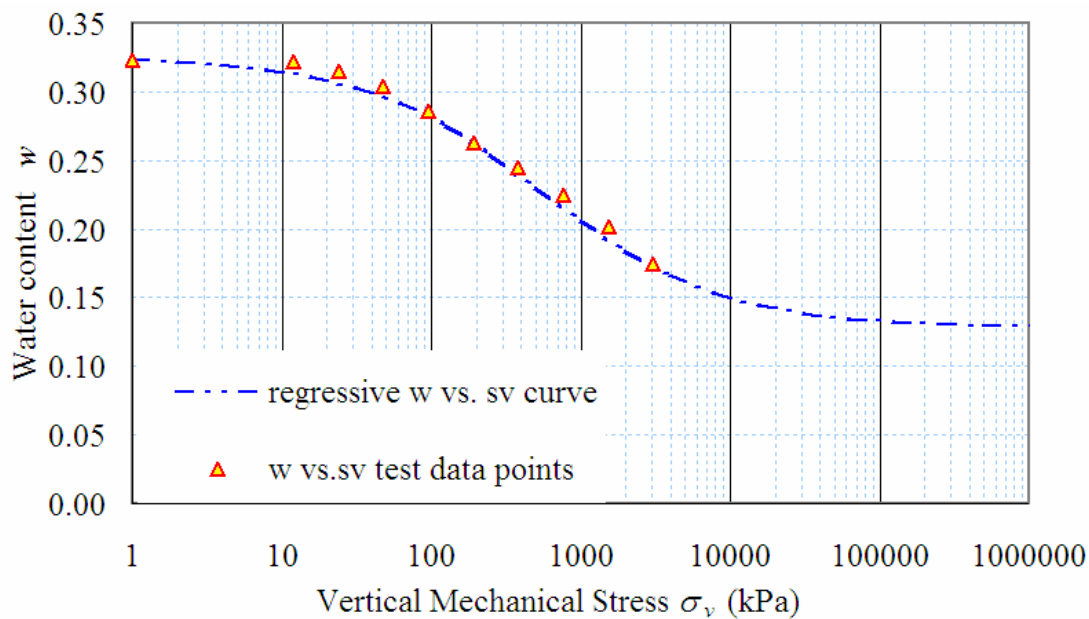


Figure B.1.3.3 Water Content vs. Vertical Mechanical Stress Curve for the Soil SPORC

Mathematical expression

$$w = \frac{e}{G_s} = 0.128346969 + \frac{0.196310655}{1 + \exp\left(\frac{\log_{10}(\sigma_v) - 2.756215212}{0.599455799}\right)}$$

B.1.3.4.. Consolidation Test: w-log (σ_m) Relationship

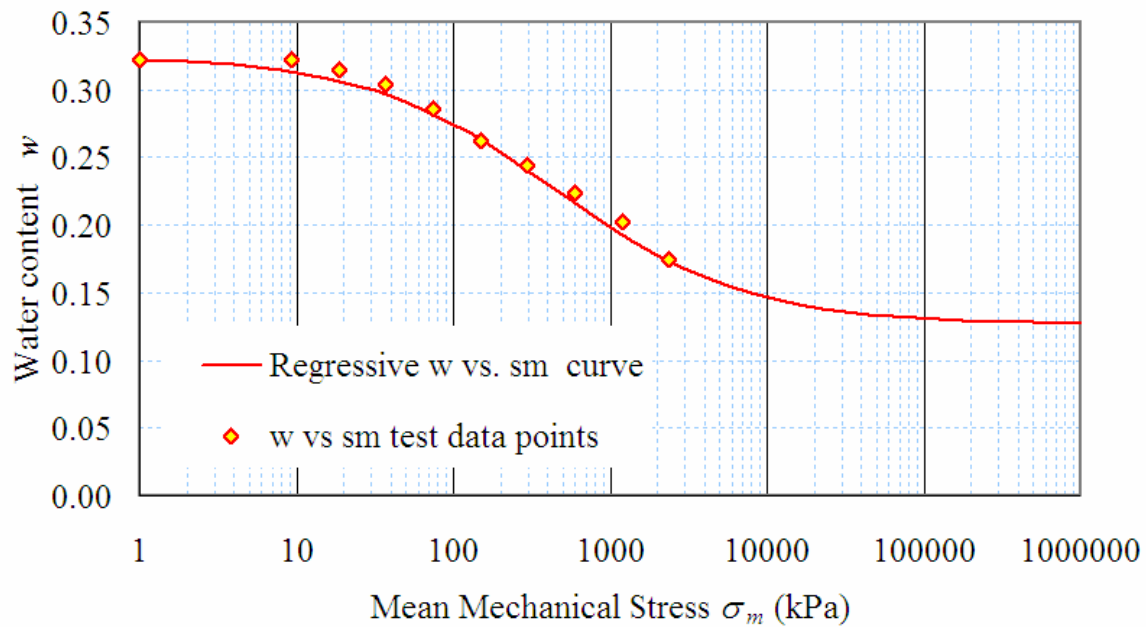


Figure B.1.3.4 Water Content vs. Mean Mechanical Stress Curve for the Soil SPORC

Mathematical expression

$$w = \frac{e}{G_s} = 0.128346969 + \frac{0.196310655}{1 + \exp\left(\frac{\log_{10}(\sigma_v) - 2.756215212}{0.599455799}\right)}$$

B.1.3.5. Free Shrink test: e-w Relationship

$$S = \frac{wG_s}{e} = \frac{wG_s}{0.371678 + \frac{0.511121147}{1 + e^{-\left(\frac{w-0.193148914}{0.025942151}\right)}}$$

$$S = 7.1469w \quad (\text{For } w \leq 0.0944)$$

$$e = 0.371678 + \frac{0.511121147}{1 + e^{-\left(\frac{w-0.193148914}{0.025942151}\right)}} \quad (\text{For } w \geq 0.0944)$$

$$e = 0.381284 \quad (\text{For } w \leq 0.0944)$$

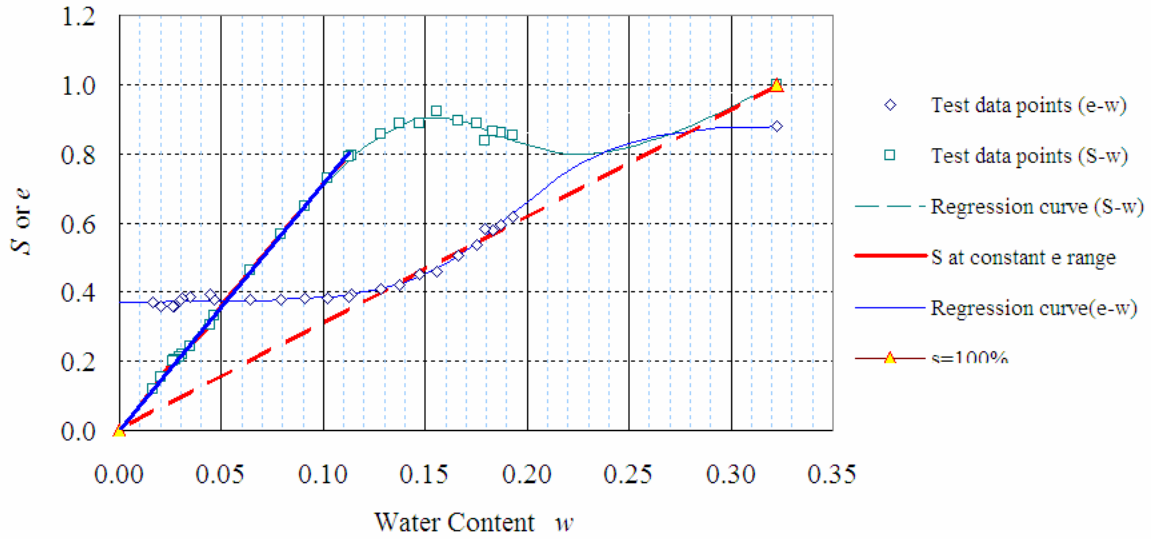


Figure B.1.3.5 Void Ratio and Degree of Saturation vs. Water Content Curve for the Soil SPORC

B.1.3.6. Soil Water Characteristic Curve

$$w = -0.03870051 + \frac{0.36657792}{1 + e^{\left(\frac{\log_{10}(u_a - u_w) - 3.88914394}{0.91603011}\right)}}$$

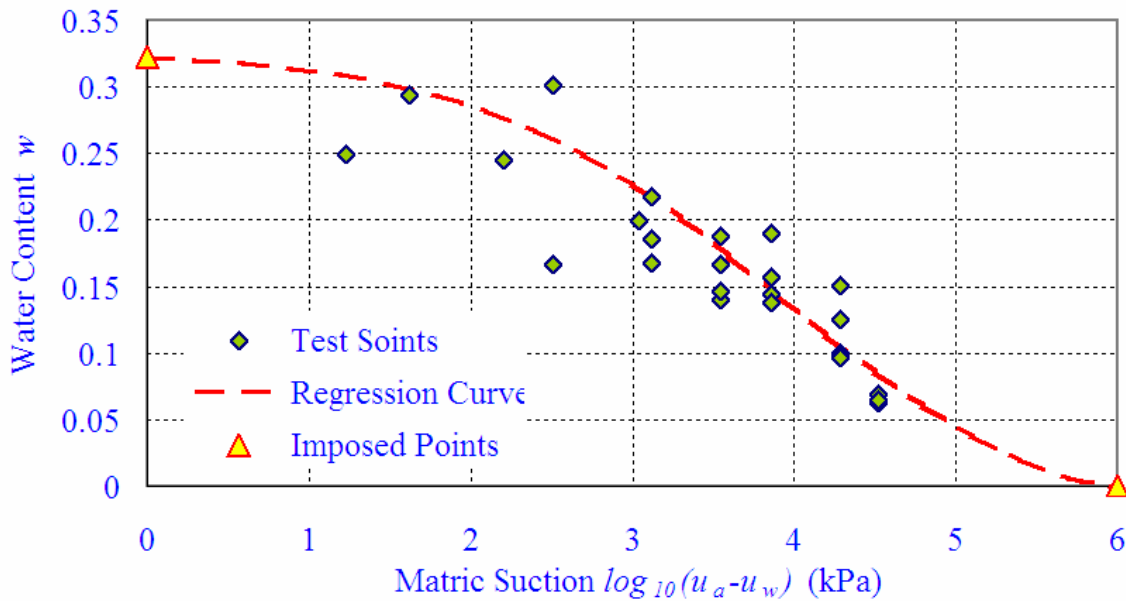


Figure B.1.3.6 Soil Water Characteristic Curve for the Soil SPORC

B.1.3.7.. Constructed e- Matric Suction: e-log₁₀(u_a-u_w) Relationship

$$e = 0.37167777 + \frac{0.51112115}{1 + e^{\frac{(\log_{10}(u_a - u_w) - 0.19314891)}{0.02594215}}}$$

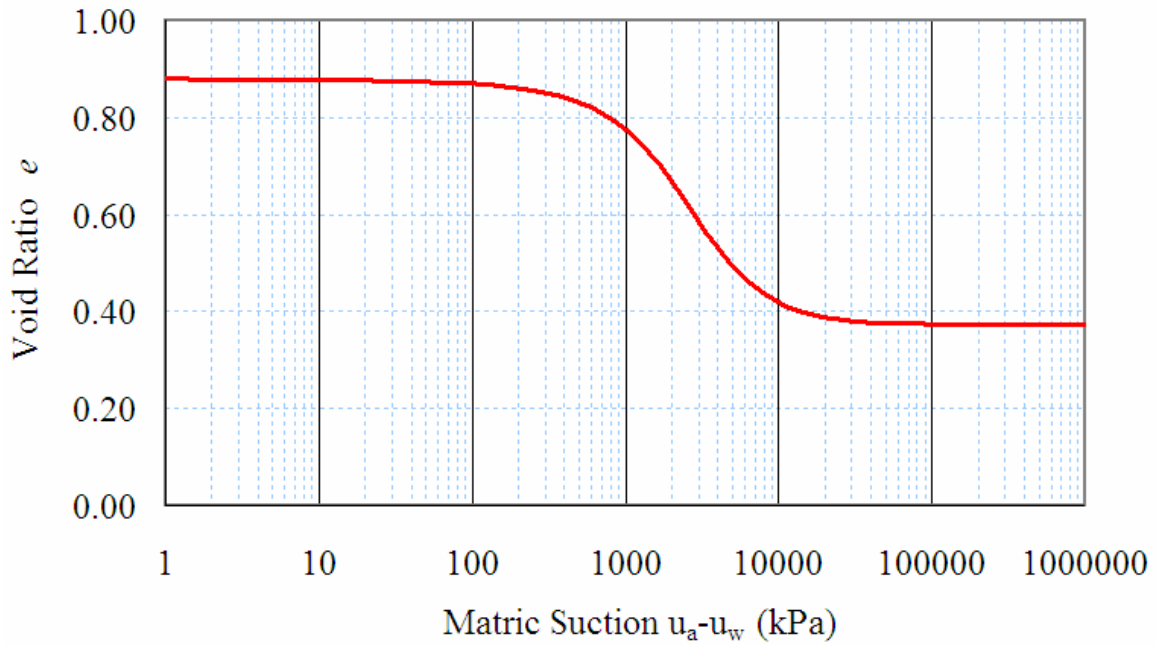


Figure B.1.3.7 Constructed e- Matric Suction: e-log₁₀(u_a-u_w) Relationship for the Soil SPORC

B.1.3.8. Void Ratio Constitutive Surface:

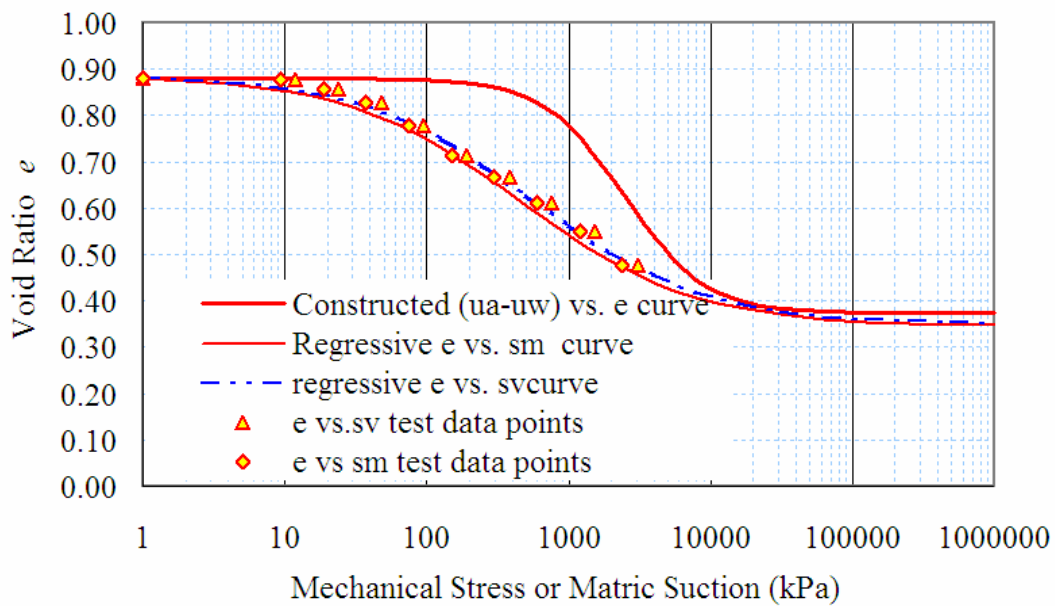


Figure B.1.3.8 Curves for Constructing the Void Ratio Constitutive Surface for the Soil SPORC

B.1.3.8.1 Void Ratio e versus Vertical Mechanical Stress σ_v & Matric Suction ($u_a - u_w$) Surface

Boundary:

$u_a - u_w = 0$ (from 1-D consolidation test):

$$e = 0.3497455 + \frac{0.5349465}{1 + e^{\left(\frac{\log_{10}(\sigma_v) - 2.7562152}{0.5994558}\right)}}$$

Therefore

$$\log_{10} \sigma_v = 0.5994558 \ln \left(\frac{0.5349465}{(e - 0.3497455)} - 1 \right) + 2.7562152$$

$\sigma_v = 0$ (from soil-water characteristic curve and free shrink test):

$$e = 0.37167777 + \frac{0.51112115}{1 + e^{\left(\frac{\log_{10}(u_a - u_w) - 0.19314891}{0.02594215}\right)}}$$

$$\log_{10} (u_a - u_w) = 0.02594215 \ln \left(\frac{0.51112115}{(e - 0.37167777)} - 1 \right) + 0.19314891$$

B.1.3.8.2. e versus σ_v & ($u_a - u_w$) Surface

(for 1 D consolidation theory for saturated-unsaturated soils)

linear assumption:

linear assumption:

$$\frac{\sigma_v - u_a}{(\sigma_m - u_a)_{(u_a - u_w = 0)}} + \frac{u_a - u_w}{(u_a - u_w)_{(\sigma_m - u_a = 0)}} = 1$$

$$\frac{\sigma_v - u_a}{10^{\left(0.5994558 \ln \left(\frac{0.5349465}{(e - 0.3497455)} - 1 \right) + 2.7562152 \right)}} + \frac{u_a - u_w}{10^{\left(0.02594215 \ln \left(\frac{0.51112115}{(e - 0.37167777)} - 1 \right) + 0.19314891 \right)}} = 1$$

B.1.3.8.3. Void ratio e versus Vertical Mechanical Stress σ_m & Matric Suction ($u_a - u_w$) Surface (for 2 D or 3D consolidation theory for saturated-unsaturated soils)

Boundary:

$u_a - u_w = 0$ (from 1-D consolidation test):

$$e = 0.3404224 + \frac{0.547578746}{1 + e^{\left(\frac{\log_{10}(\sigma_m) - 2.550588764}{0.617169246}\right)}}$$

Therefore

$$\log_{10} \sigma_m = 0.617169246 \ln \left(\frac{0.547578746}{(e - 0.3404224)} - 1 \right) + 2.550588764$$

$\sigma_v=0$ (from soil-water characteristic curve and free shrink test):

$$e = 0.37167777 + \frac{0.51112115}{1 + e^{\left(\frac{\log_{10}(u_a - u_w) - 0.19314891}{0.02594215} \right)}}$$

$$\log_{10} (u_a - u_w) = 0.02594215 \ln \left(\frac{0.51112115}{(e - 0.37167777)} - 1 \right) + 0.19314891$$

B.1.3.8.4. e versus σ_m & $(u_a - u_w)$ Surface

(for 2D or 3 D consolidation theory for saturated-unsaturated soils)

linear assumption:

$$\frac{\sigma_m - u_a}{(\sigma_m - u_a)_{(u_a - u_w = 0)}} + \frac{u_a - u_w}{(u_a - u_w)_{(\sigma_m - u_a = 0)}} = 1$$

$$\frac{\sigma_m - u_a}{10^{\left(0.617169246 \ln \left(\frac{0.547578746}{(e - 0.3404224)} - 1 \right) + 2.550588764 \right)}} + \frac{u_a - u_w}{10^{\left(0.02594215 \ln \left(\frac{0.51112115}{(e - 0.37167777)} - 1 \right) + 0.19314891 \right)}} = 1$$

B.1.3.9. Water Content Constitutive Surface

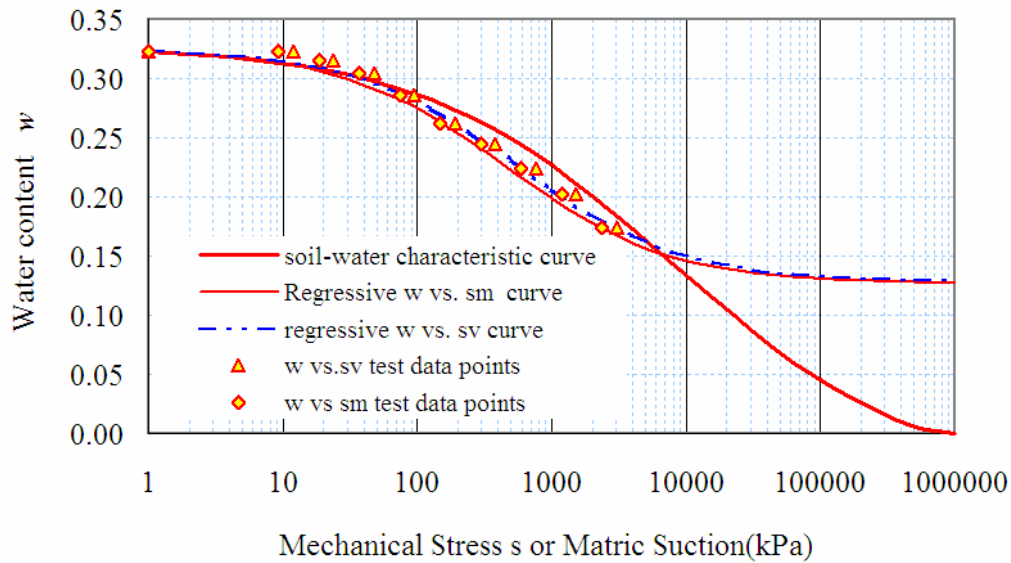


Figure B.1.3.9 Curves for Constructing the Water Content Constitutive Surface for the Soil SPORC

B.1.3.9.1. Water Content w versus Vertical Mechanical Stress σ_v & Matric Suction $(u_a - u_w)$ Surface

Boundary:

$u_a - u_w = 0$ (from 1-D consolidation test):

$$w = \frac{e}{G_s} = 0.128346969 + \frac{0.196310655}{1 + e^{\left(\frac{\log_{10}(\sigma_v) - 2.756215212}{0.599455799}\right)}}$$

Therefore

$$\log_{10} \sigma_v = 0.599455799 \ln \left(\frac{0.196310655}{(w - 0.128346969)} - 1 \right) + 2.756215212$$

$\sigma_v = 0$ (from soil-water characteristic curve and free shrink test):

$$w = -0.03870051 + \frac{0.36657792}{1 + e^{\left(\frac{\log_{10}(u_a - u_w) - 3.88914394}{0.91603011}\right)}}$$

$$\log_{10}(u_a - u_w) = 0.91603011 \ln \left(\frac{0.36657792}{(w + 0.03870051)} - 1 \right) + 3.88914394$$

B.1.3.9.2. w versus σ_v & $(u_a - u_w)$ Surface

(for 1 D consolidation theory for saturated-unsaturated soils)

linear assumption:

$$\frac{\sigma_v - u_a}{(\sigma_v - u_a)_{(u_a - u_w = 0)}} + \frac{u_a - u_w}{(u_a - u_w)_{(\sigma_v - u_a = 0)}} = 1$$

$$\frac{\sigma_v - u_a}{10^{\left(0.599455799 \ln \left(\frac{0.196310655}{(w - 0.128346969)} - 1 \right) + 2.756215212 \right)}} + \frac{u_a - u_w}{10^{\left(0.91603011 \ln \left(\frac{0.36657792}{(w + 0.03870051)} - 1 \right) + 3.88914394 \right)}} = 1$$

for $(\sigma_m - u_a) + (u_a - u_w) < 32637.8$

B.1.3.9.3. Degree of Saturation S versus Vertical Mechanical Stress σ_v & Matric Suction $(u_a - u_w)$ Surface

For $(\sigma_v - u_a) + (u_a - u_w) > 32637.8$

$$S = -0.024789788 + \frac{1.024790004}{1 + e^{\left(\frac{\log_{10}(u_a - u_w) - 4.979543423}{0.324013298}\right)}}$$

B.1.3.9.4. Water Content w versus Mean Mechanical Stress σ_m & Matric Suction $(u_a - u_w)$ Surface

$u_a - u_w = 0$ (from 1-D consolidation test):

$$w = \frac{e}{G_s} = 0.124925643 + \frac{0.200946329}{1 + e^{\left(\frac{\log_{10}(\sigma_m) - 2.550588764}{0.617169246}\right)}}$$

Therefore

$$\log_{10} \sigma_m = 0.617169246 \ln \left(\frac{0.200946329}{(w - 0.124925643)} - 1 \right) + 2.550588764$$

$\sigma_m = 0$ (from soil-water characteristic curve and free shrink test):

$$w = -0.03870051 + \frac{0.36657792}{1 + e^{\left(\frac{\log_{10}(u_a - u_w) - 3.88914394}{0.91603011}\right)}}$$

$$\log_{10}(u_a - u_w) = 0.91603011 \ln \left(\frac{0.36657792}{(w + 0.03870051)} - 1 \right) + 3.88914394$$

B.1.3.9.5. w versus σ_m & $(u_a - u_w)$ Surface

(for 2 D or 3 D consolidation theory for saturated-unsaturated soils)

linear assumption:

$$\frac{\sigma_v - u_a}{(\sigma_m - u_a)_{(u_a - u_w = 0)}} + \frac{u_a - u_w}{(u_a - u_w)_{(\sigma_m - u_a = 0)}} = 1$$

$$\frac{\sigma_m - u_a}{10^{\left(0.617169246 \ln \left(\frac{0.200946329}{(w - 0.124925643)} - 1 \right) + 2.550588764 \right)}} + \frac{u_a - u_w}{10^{\left(0.91603011 \ln \left(\frac{0.36657792}{(w + 0.03870051)} - 1 \right) + 3.88914394 \right)}} = 1$$

for $(\sigma_m - u_a) + (u_a - u_w) < 32637.8$

B.1.3.9.6. Degree of saturation S versus mean mechanical stress σ_v & matric suction $(u_a - u_w)$ surface

For $(\sigma_m - u_a) + (u_a - u_w) > 32637.8$

$$S = -0.024789788 + \frac{1.024790004}{1 + e^{\left(\frac{\log_{10}(u_a - u_w) - 4.979543423}{0.324013298}\right)}}$$

B.1.3.10. Constitutive Surfaces and Material Parameters for the Soil SPORC

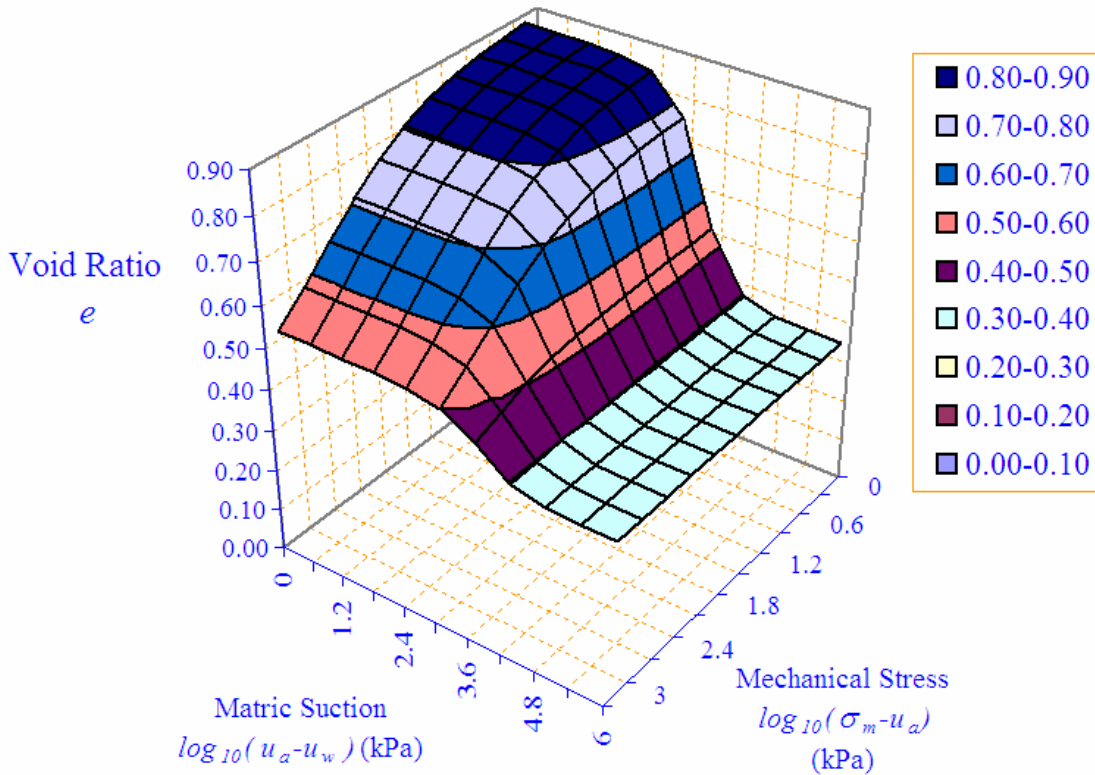


Figure B.1.3.10 Void Ratio Constitutive Surface for the Soil SPORC

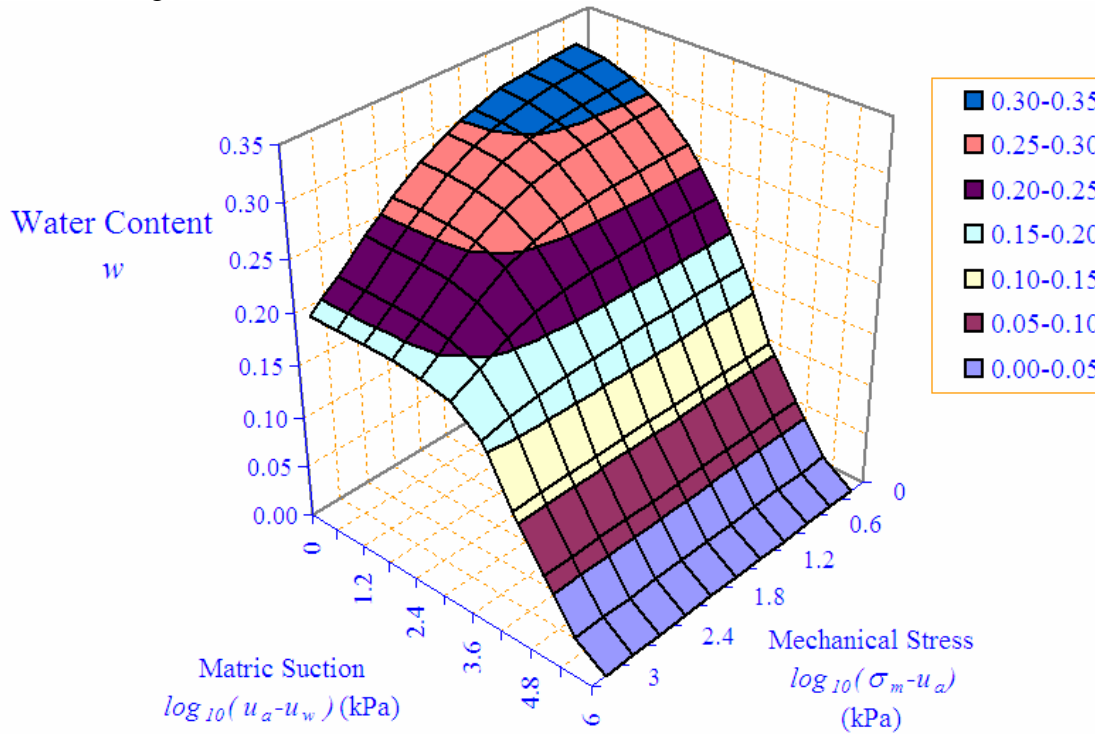


Figure B.1.3.12 Water Content Constitutive Surface for the Soil SPORC

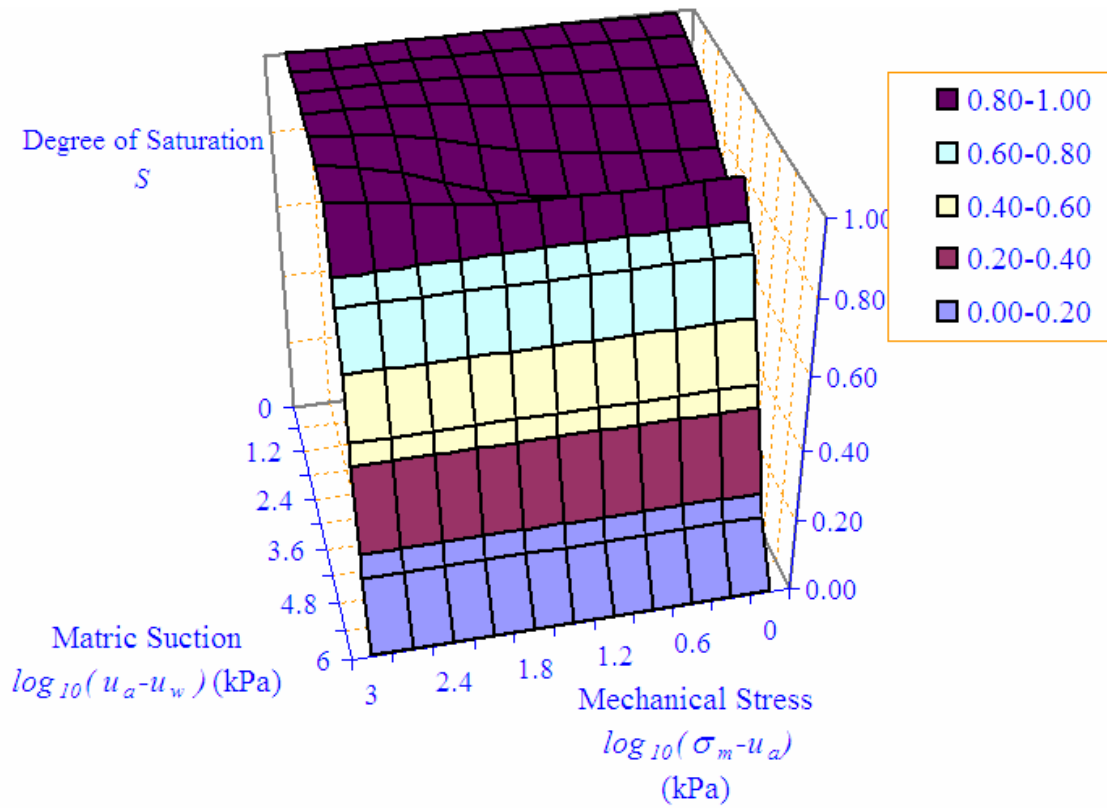


Figure B.1.3.13 Degree of Saturation Constitutive Surface for the Soil SPORC

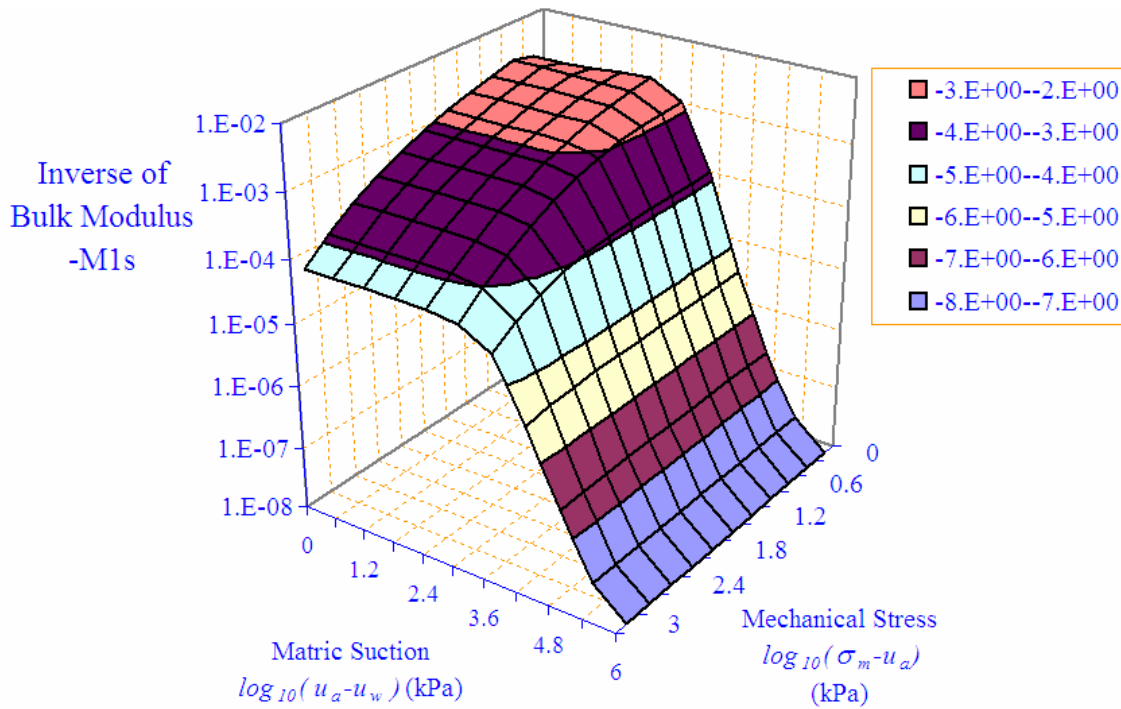
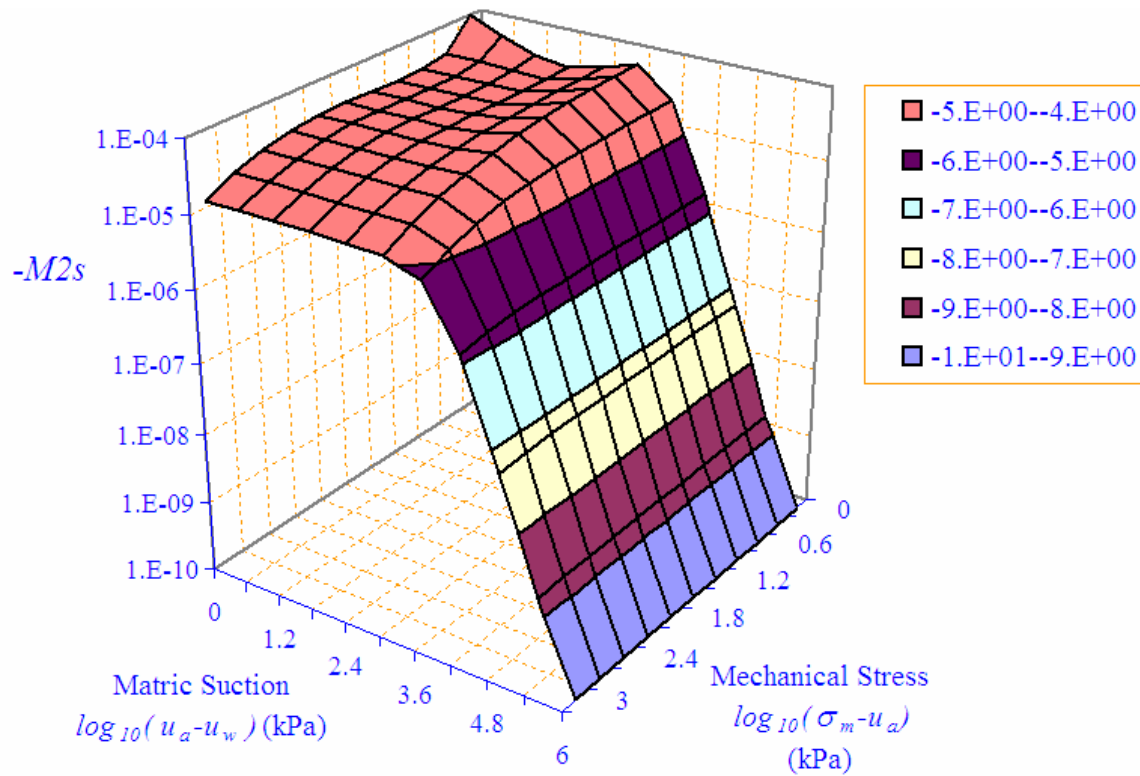
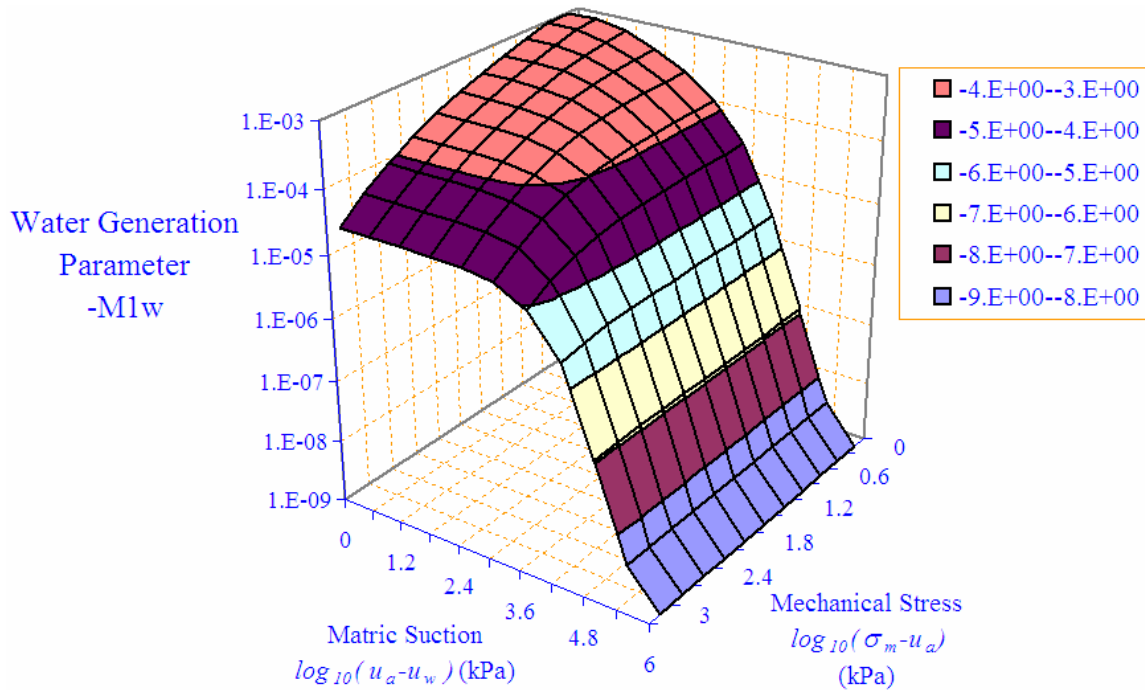


Figure B.1.3.14 Inverse of Bulk Modulus m_1^s Surface for the Soil SPORC

Figure B.1.3.15 m_2^s Surface for the Soil SPORCFigure B.1.3.16 m_1^w Surface for the Soil SPORC

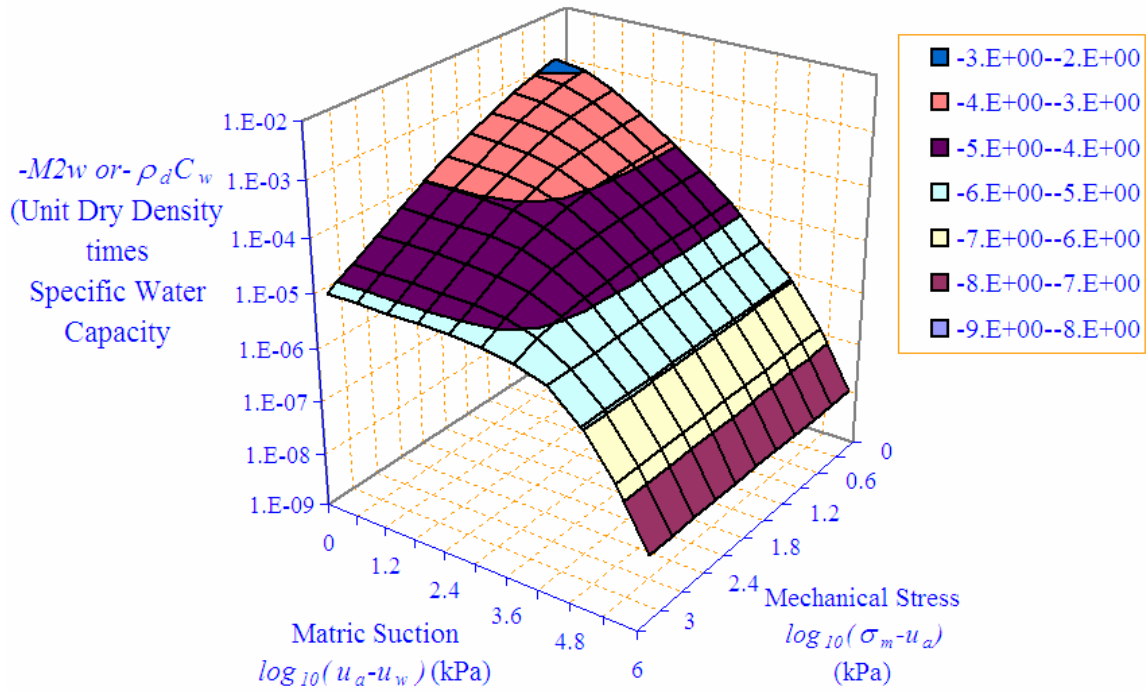


Figure B.1.3.17 m_2^w Surface for the Soil SPORC

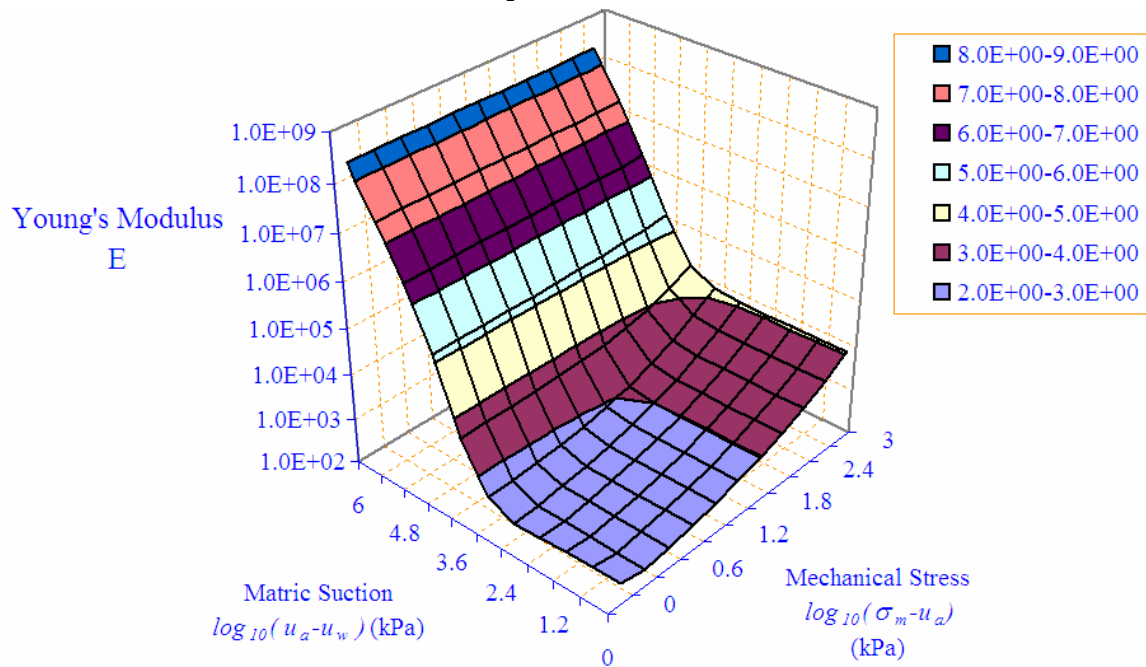


Figure B.1.3.18 Young's Modulus Surface for the Soil SPORC

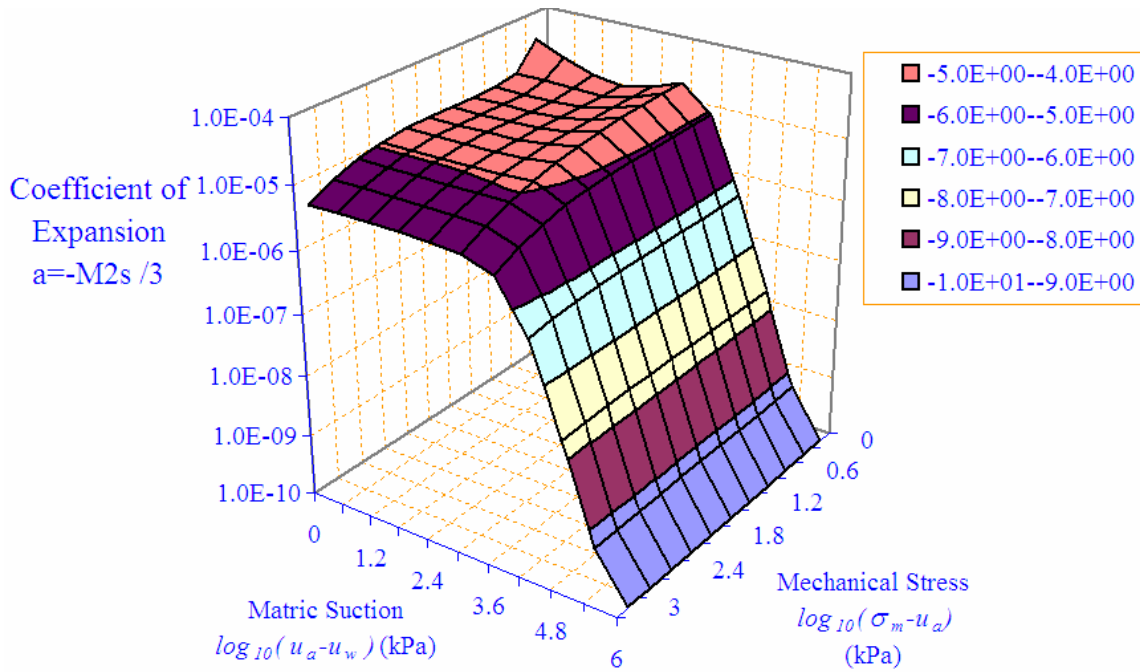


Figure B.1.3.19 Coefficient of Expansion Surface for the Soil SPORC

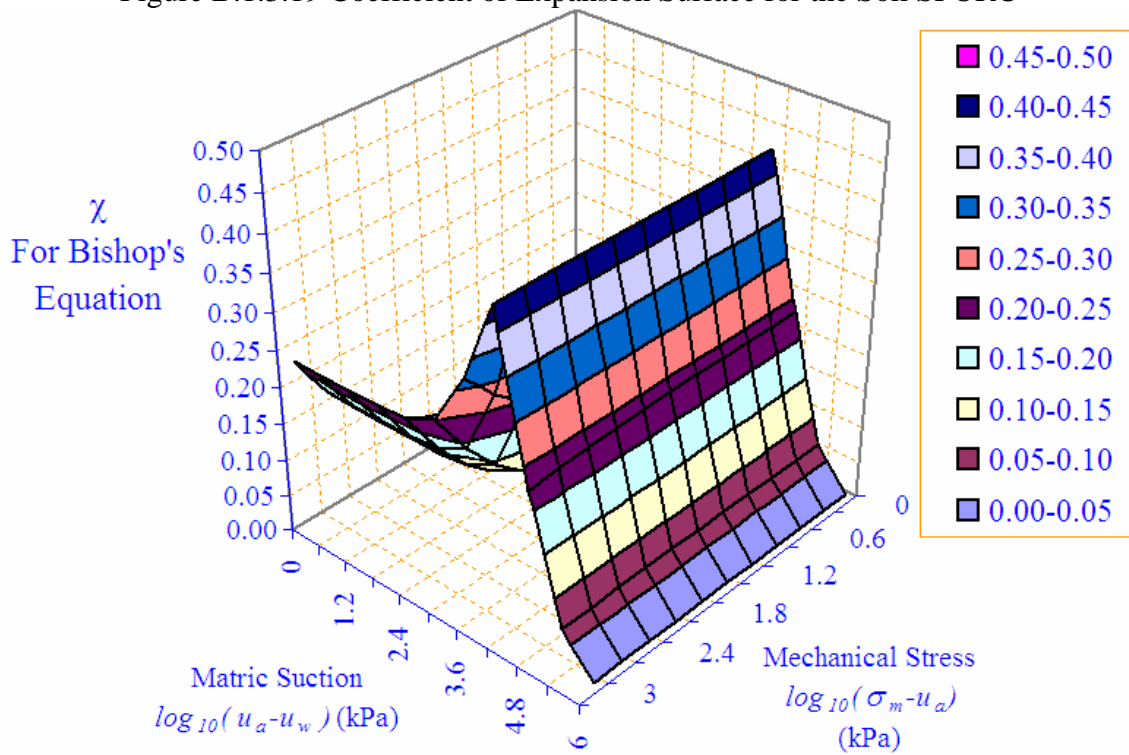


Figure B.1.3.20 χ Surface for the Soil SPORC

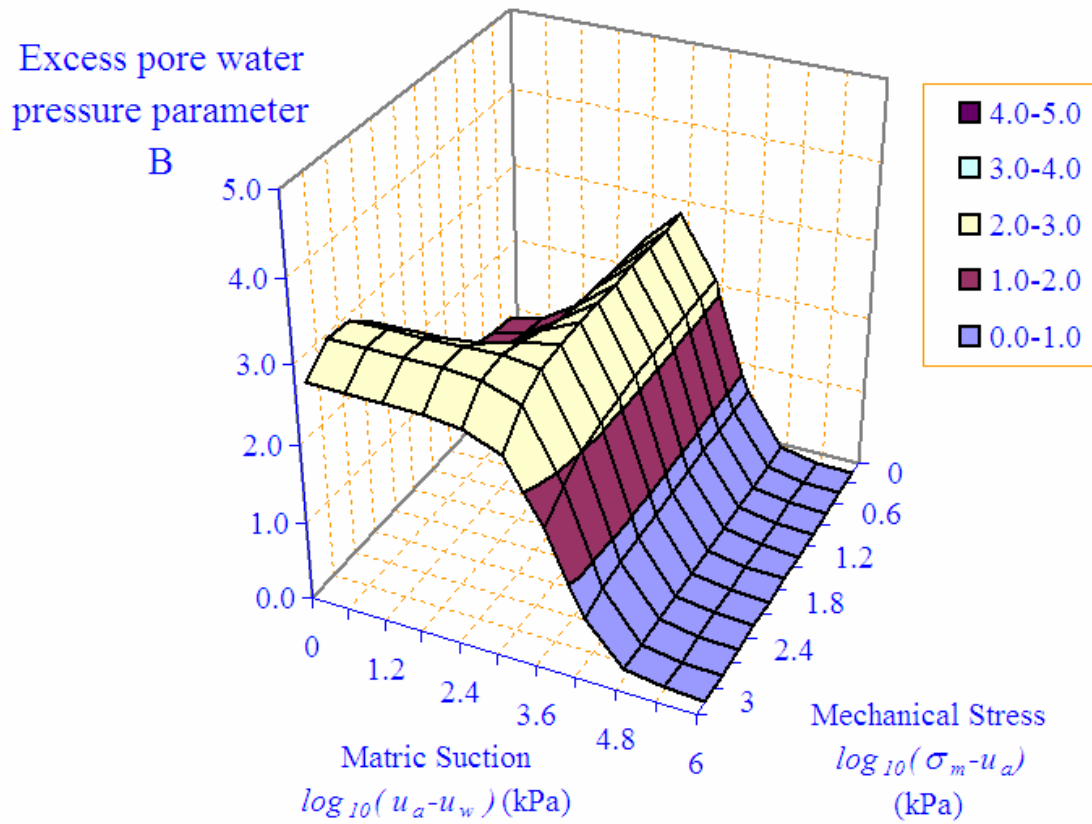


Figure B.1.3.21 Excess Pore Water Pressure Parameter Surface for the Soil SPORC

APPENDIX C

VERIFICATION OF BIOT'S CONSOLIDATION THEORY

AND DERIVATION OF SKEMPTON'S EQUATION

APPENDIX C.1. VERIFICATION OF BIOT'S CONSOLIDATION THEORY

Appendix C.1.1. Main Program

```

*Heading
** Verification Of Biot's Consolidation Theory**
** PARTS
**
*Part, name=Part-1
*End Part
**
** ASSEMBLY
**
*Assembly, name=Assembly
**
*Instance, name=Part-1-1, part=Part-1
*Node

Omitted

*Element, type=CAX4T

Omitted

** Region: (Section-1:Picked)
*Elset, elset=_I1, internal, generate
  1, 375, 1
** Section: Section-1
*Solid Section, elset=_I1, material=Material-1
1.,
*End Instance
*Nset, nset=allnodes, internal, instance=Part-1-1, generate
1, 416
*Elset, elset=allelements, internal, instance=Part-1-1, generate
1,375
*Nset, nset=out, internal, instance=Part-1-1, generate
13, 403, 26
*Elset, elset=out, internal, instance=Part-1-1, generate
13, 363, 25
*Nset, nset=_G4, internal, instance=Part-1-1, generate
26, 416, 26
*Elset, elset=_G4, internal, instance=Part-1-1, generate
25, 375, 25
*Nset, nset=_G5, internal, instance=Part-1-1, generate
1, 26, 1
*Elset, elset=_G5, internal, instance=Part-1-1, generate
1, 25, 1
*Nset, nset=_G6, internal, instance=Part-1-1, generate
391, 416, 1

```

```

*Elset, elset=_G6, internal, instance=Part-1-1, generate
 351, 375, 1
*Nset, nset=GSet-1, instance=Part-1-1, generate
 1, 26, 1
*Elset, elset=GSet-1, instance=Part-1-1, generate
 1, 25, 1
*Elset, elset=__G7_S3, internal, instance=Part-1-1, generate
 351, 375, 1
*Surface, type=ELEMENT, name=_G7, internal
__G7_S3, S3
*Elset, elset=__G8_S4, internal, instance=Part-1-1, generate
 1, 351, 25
*Surface, type=ELEMENT, name=_G8, internal
__G8_S4, S4
*End Assembly
**
** MATERIALS
**
*Material, name=Material-1
*Elastic
10000., 0.3
*USER MATERIAL,TYPE=THERMAL,constant=1,UNSYMM
*****Conductivity
****1e-09,
****Specific Heat
*****1e-06,
*Expansion
4e-5,
*Density
1.,
*USER DEFINED FIELD
*DEPVAR
6
*INITIAL CONDITIONS,TYPE=FIELD
*INITIAL CONDITIONS,TYPE=temperature
allnodes,0
** -----
**
** STEP: Step-1
**
*Step, name=Step-1
*Coupled Temperature-Displacement
1e-2,1
**
** BOUNDARY CONDITIONS
**
** Name: BC-1 Type: Symmetry/Antisymmetry/Encastre
*Boundary
_G4, YSYMM
** Name: BC-2 Type: Symmetry/Antisymmetry/Encastre
*Boundary
_G5, XSYMM
** Name: BC-3 Type: Temperature
*Boundary

```

```

_G6, 11, 11, 0
**
** LOADS
**
** Name: Load-1   Type: Pressure
*Dsload
_G7, P, 1000.
** Name: Load-2   Type: Pressure
*Dsload
_G8, P, 1000.
**
** OUTPUT REQUESTS
**
*Restart, write, frequency=1
**
** FIELD OUTPUT: F-Output-1
**
*Output, field, variable=PRESELECT
**
** HISTORY OUTPUT: H-Output-1
**
*Output, history, variable=PRESELECT
*Output, history
*node output, nset=out
NT11,
*El Print, freq=999999
*Node Print, freq=999999
*End Step
*Step, name=Step-2
*Coupled Temperature-Displacement
1,1e2
**
** BOUNDARY CONDITIONS
**
** Name: BC-1 Type: Symmetry/Antisymmetry/Encastre
*Boundary
_G4, YSYMM
** Name: BC-2 Type: Symmetry/Antisymmetry/Encastre
*Boundary
_G5, XSYMM
** Name: BC-3 Type: Temperature
*Boundary
_G6, 11, 11, 0
**
** LOADS
**
** Name: Load-1   Type: Pressure
*Dsload
_G7, P, 1000.
** Name: Load-2   Type: Pressure
*Dsload
_G8, P, 1000.
**
** OUTPUT REQUESTS

```

```

**
*Restart, write, frequency=1
**
** FIELD OUTPUT: F-Output-1
**
*Output, field, variable=PRESELECT
**
** HISTORY OUTPUT: H-Output-1
**
*Output, history, variable=PRESELECT
*Output, history
*node output, nset=out
NT11,
*El Print, freq=999999
*Node Print, freq=999999
*End Step
*Step, name=Step-3
*Coupled Temperature-Displacement
1e2,1e4
**
** BOUNDARY CONDITIONS
**
** Name: BC-1 Type: Symmetry/Antisymmetry/Encastre
*Boundary
_G4, YSYMM
** Name: BC-2 Type: Symmetry/Antisymmetry/Encastre
*Boundary
_G5, XSYMM
** Name: BC-3 Type: Temperature
*Boundary
_G6, 11, 11, 0
**
** LOADS
**
** Name: Load-1 Type: Pressure
*Dslload
_G7, P, 1000.
** Name: Load-2 Type: Pressure
*Dslload
_G8, P, 1000.
**
** OUTPUT REQUESTS
**
*Restart, write, frequency=1
**
** FIELD OUTPUT: F-Output-1
**
*Output, field, variable=PRESELECT
**
** HISTORY OUTPUT: H-Output-1
**
*Output, history, variable=PRESELECT
*Output, history
*node output, nset=out

```

```
NT11,
*El Print, freq=999999
*Node Print, freq=999999
*End Step
*Step, name=Step-4
*Coupled Temperature-Displacement
1e4,1e6
**
** BOUNDARY CONDITIONS
**
** Name: BC-1 Type: Symmetry/Antisymmetry/Encastre
*Boundary
_G4, YSYMM
** Name: BC-2 Type: Symmetry/Antisymmetry/Encastre
*Boundary
_G5, XSYMM
** Name: BC-3 Type: Temperature
*Boundary
_G6, 11, 11, 0
**
** LOADS
**
** Name: Load-1 Type: Pressure
*Dload
_G7, P, 1000.
** Name: Load-2 Type: Pressure
*Dload
_G8, P, 1000.
**
** OUTPUT REQUESTS
**
*Restart, write, frequency=1
**
** FIELD OUTPUT: F-Output-1
**
*Output, field, variable=PRESELECT
**
** HISTORY OUTPUT: H-Output-1
**
*Output, history, variable=PRESELECT
*Output, history
*node output, nset=out
NT11,
*El Print, freq=999999
*Node Print, freq=999999
*End Step
```

Appendix C.1.2. User Subroutines

C.1.2.1. User Subroutines USDFLD

```

subroutine
usdfld(field,statev,pnewdt,direct,t,celent,time,dtime,
  1 cmname,orname,nfield,nstatv,noel,npt,layer,kspt,kstep,kincl,
  2 ndi,nshr,coord,jmac,jmtyp,matlayo,laccfla)
c
  include 'aba_param.inc'
c
  character*80 cmname,orname
  character*8 flgray(15)
  dimension
field(nfield),statev(nstatv),direct(3,3),t(3,3),time(2),
  $ coord(*),jmac(*),jmtyp(*)
  dimension array(15),jarray(15)
c
c Get temperatures from previous increment
  call getvrm('TEMP',array,jarray,flgray,jrcd,
  $ jmac,jmtyp,matlayo,laccfla)
  temp = array(1)
  field(1) = temp
c
  WRITE(6,*)coord(3),ARRAY(1),TEMP,"temp"
  CALL GETVRM('S',ARRAY,JARRAY,FLGRAY,jrcd,
  $ jmac,jmtyp,matlayo,laccfla)
  S11 = ARRAY(1)
  S22 = ARRAY(2)
  S33 = ARRAY(3)
  S44 = ARRAY(4)
  S55 = ARRAY(5)
  S66 = ARRAY(6)
  SIGMAM =(S11+S22+S33)/3
C
  WRITE(6,*)s11,s22,s33,s44,s55,s66,SIGMAM,"SIGMAM "
C
C GET STRAINS FROM PREVIOUS INCREMENT
  CALL GETVRM('EE',ARRAY,JARRAY,FLGRAY,jrcd,
  $ jmac,jmtyp,matlayo,laccfla)
  E11 = ARRAY(1)
  E22 = ARRAY(2)
  E33 = ARRAY(3)
  E44 = ARRAY(4)
  E55 = ARRAY(5)
  E66 = ARRAY(6)
  CALL GETVRM('THE',ARRAY,JARRAY,FLGRAY,jrcd,
  $ jmac,jmtyp,matlayo,laccfla)
  THE11 = ARRAY(1)
  THE22 = ARRAY(2)
  THE33 = ARRAY(3)
  EPSILONV =E11+E22+E33+THE11+THE22+THE33
  DEEPSILONV=EPSILONV-STATEV(1)
  Dsigmam=sigmam-statev(3)
  STATEV(1)=EPSILONV

```

```

statev(2)=DEPSILONV
STATEV(3)=SIGMAM
STATEV(4)=DSIGMAM
C
RETURN
END

```

C.1.2.2. User Subroutines UMATHT

```

subroutine umatht(u,dudt,dudg,flux,dfdt,dfdg,statev,temp,
$ dtemp,dtemdx,time,dtime,predef,dpred,cmname,ntgrd,nstatv,
$ props,nprops,coords,pnewdt,noel,npt,layer,kspt,kstep,kinc)
C
include 'aba_param.inc'
C
character*80 cmname
C
dimension dudg(ntgrd),flux(ntgrd),dfdt(ntgrd),
$ dfdg(ntgrd,ntgrd),statev(nstatv),dtemdx(ntgrd),time(2),
$ predef(1),dpred(1),props(nprops),coords(3)
DSIGMAM=STATEV(4)
E1W=1.2e-4
cond =1.16e-8
specht =1.2e-4
dudt = specht
du= dudt*dtemp+E1W*DSIGMAM
u= u+du
C
C
C input flux = -[k]*{dtemdx}
C do i=1, ntgrd
C flux(i) = -cond*dtemdx(i)
C end do
C do i=1, ntgrd-1
C flux(i) = -cond*dtemdx(i)
C end do
C flux(ntgrd) = -cond*(dtemdx(ntgrd)+10)
C
Close(16)
return
end

```

Appendix C.2 Derivation of Skempton's Equation and its Problem

$$\Delta u = B \left[\Delta \sigma_3 + A (\Delta \sigma_1 - \Delta \sigma_3) \right]$$

$$\Delta u = \Delta u_{wn} + \Delta u_{wd}$$

$$\Delta \sigma' = \Delta \sigma_3 - \Delta u_w \quad (\text{Only for saturated soils, it is right})$$

$$\Delta V_c = -C_c V \Delta \sigma' = -C_c V (\Delta \sigma_3 - \Delta u_w)$$

$$\Delta V_v = -C_v n V \Delta u_w$$

$$\Delta V_c = \Delta V_v$$

$$-C_c V (\Delta \sigma_3 - \Delta u_w) = -C_v n V \Delta u_w$$

$$\frac{\Delta u_w}{\Delta \sigma_3} = B = \frac{1}{1 + \frac{n C_v}{C_c}}$$

For fully saturated soils (zero air voids), $\frac{C_v}{C_c}$ is considered to be approximately equal to zero thanks to the compressibility of water is negligible compared with that of the soil structure, consequently $B=1$.

If, in contrast, the soil is dry, then $\frac{C_v}{C_c}$ approaches infinity since the compressibility of air is far greater than that of the soil structure. Hence, for dry soils, $B=0$. For partially saturated soils, $0 < B < 1$.

From the above derivation, it can be seen that the effective stress principle for saturated soils was used. It is not right. A correct derivation should be as followings:

$$\Delta u = B \left[\Delta \sigma_3 + A (\Delta \sigma_1 - \Delta \sigma_3) \right]$$

$$\Delta u = \Delta u_{wn} + \Delta u_{wd}$$

$$\Delta \sigma' = \Delta \sigma_3 - \chi \Delta u_w \quad (\text{for unsaturated soils, Bishop's Equation should be used})$$

$$\Delta V_c = -C_c V \Delta \sigma' = -C_c V (\Delta \sigma_3 - \chi \Delta u_w)$$

$$\Delta V_v = -C_v n V \Delta u_w$$

$$\Delta V_c = \Delta V_v$$

$$-C_c V (\Delta \sigma_3 - \chi \Delta u_w) = -C_v n V \Delta u_w$$

$$\frac{\Delta u_w}{\Delta \sigma_3} = B = \frac{1}{\chi + \frac{n C_v}{C_c}}$$

For unsaturated expansive soils, $0 < \chi < 1$. For unsaturated collapsible soils, $\chi < 0$.

Under both conditions, it is possible that B has a value greater than 1.

APPENDIX D
VERIFICATION OF MOVEMENTS AT A SITE AT ARLINGTON, TEXAS
AND EQUILIBRIUM PROFILE

APPENDIX D.1.

VERIFICATION OF MOVEMENTS AT A SITE AT ARLINGTON, TEXAS

Appendix D.1.1. Main Program

```

*Heading
** Verification of Movements at a Site at Arlington, Texas**
** PARTS
**
*Heading
** Job name: G3 Model name: Model-1
**
** PARTS
**
*Part, name=Part-1
*End Part
*Part, name=Part-block
*End Part
**
** ASSEMBLY
**
*Assembly, name=Assembly
**
*Instance, name=Part-1-1, part=Part-1
*Node
  omitted
*Element, type=C3D8T
  omitted
** Region: (Section-soil:Picked)
*Elset, elset=_I1, internal, generate
1,90,1
101,190,1
201,290,1
301,390,1
401,490,1
501,590,1
601,690,1
701,790,1
801,890,1
901,990,1
495,496,1
595,596,1
*Elset, elset=_S1, internal, generate
91,100,1
191,200,1
291,300,1
391,400,1
491,494,1
497,500,1
591,594,1
597,600,1

```

```

691,700,1
791,800,1
891,900,1
991,1000,1
** Section: Section-soil
*Solid Section, elset=_I1, material=MAT1
*Solid Section, elset=_S1, material=Mat2
1.,
*End Instance
**
*Instance, name=Part-block-1, part=Part-block
0., 0., 4.
*Node
  omitted
*Element, type=C3D8T
omitted
** Region: (Section-block:Picked)
*Elset, elset=_I1, internal, generate
  1, 8, 1
** Section: Section-block
*Solid Section, elset=_I1, material=Material-block
1.,
*End Instance
*Nset, nset=_G12, internal, instance=Part-1-1, generate
  *Nset, nset=_G12, internal, instance=Part-1-1, generate
    1,89,11
122,210,11
243,331,11
364,452,11
485,573,11
606,694,11
727,815,11
848,936,11
969,1057,11
1090,1178,11
1211,1299,11
*Elset, elset=_G12, internal, instance=Part-1-1, generate
  1, 991, 10
*Nset, nset=_G13, internal, instance=Part-1-1, generate
  1, 99, 1
*Elset, elset=_G13, internal, instance=Part-1-1, generate
  1, 100, 1
*Nset, nset=_G14, internal, instance=Part-1-1, generate
11,99,11
132,220,11
253,341,11
374,462,11
495,583,11
616,704,11
737,825,11
858,946,11
979,1067,11
1100,1188,11
1221,1309,11

```

```

*Elset, elset=_G14, internal, instance=Part-1-1, generate
  10, 1000, 10
*Nset, nset=_G15, internal, instance=Part-1-1, generate
  1211, 1309, 1
*Elset, elset=_G15, internal, instance=Part-1-1, generate
  901, 1000, 1
*Nset, nset=_G16, internal, instance=Part-1-1
  1, 2, 3, 4, 5, 6, 7, 8, 9, 10, 11,
122, 123, 124, 125, 126
  127, 128, 129, 130, 131, 132, 243, 244, 245, 246, 247,
248, 249, 250, 251, 252
  253, 364, 365, 366, 367, 368, 369, 370, 371, 372, 373,
374, 485, 486, 487, 488
  489, 490, 491, 492, 493, 494, 495, 606, 607, 608, 609,
610, 611, 612, 613, 614
  615, 616, 727, 728, 729, 730, 731, 732, 733, 734, 735,
736, 737, 848, 849, 850
  851, 852, 853, 854, 855, 856, 857, 858, 969, 970, 971,
972, 973, 974, 975, 976
  977, 978, 979, 1090, 1091, 1092, 1093, 1094, 1095, 1096, 1097,
1098, 1099, 1100, 1211, 1212
  1213, 1214, 1215, 1216, 1217, 1218, 1219, 1220, 1221
*Elset, elset=_G16, internal, instance=Part-1-1
  1, 2, 3, 4, 5, 6, 7, 8, 9, 10, 101, 102, 103, 104,
105, 106
  107, 108, 109, 110, 201, 202, 203, 204, 205, 206, 207, 208, 209, 210,
301, 302
  303, 304, 305, 306, 307, 308, 309, 310, 401, 402, 403, 404, 405, 406,
407, 408
  409, 410, 501, 502, 503, 504, 505, 506, 507, 508, 509, 510, 601, 602,
603, 604
  605, 606, 607, 608, 609, 610, 701, 702, 703, 704, 705, 706, 707, 708,
709, 710
  801, 802, 803, 804, 805, 806, 807, 808, 809, 810, 901, 902, 903, 904,
905, 906
  907, 908, 909, 910
*Nset, nset=_G17, internal, instance=Part-block-1, generate
  1, 27, 1
*Elset, elset=_G17, internal, instance=Part-block-1, generate
  1, 8, 1
*Nset, nset=_G18, internal, instance=Part-1-1, generate
  1, 1331, 1
*Elset, elset=_G18, internal, instance=Part-1-1, generate
  1, 1000, 1
*Nset, nset=_G19, internal, instance=Part-1-1
  1, 2, 3, 4, 5, 6, 7, 8, 9, 10, 11,
122, 123, 124, 125, 126
  127, 128, 129, 130, 131, 132, 243, 244, 245, 246, 247,
248, 249, 250, 251, 252
  253, 364, 365, 366, 367, 368, 369, 370, 371, 372, 373,
374, 485, 486, 487, 488
  489, 490, 491, 492, 493, 494, 495, 606, 607, 608, 609,
610, 611, 612, 613, 614

```

615, 616, 727, 728, 729, 730, 731, 732, 733, 734, 735,
736, 737, 848, 849, 850
851, 852, 853, 854, 855, 856, 857, 858, 969, 970, 971,
972, 973, 974, 975, 976
977, 978, 979, 1090, 1091, 1092, 1093, 1094, 1095, 1096, 1097,
1098, 1099, 1100, 1211, 1212
1213, 1214, 1215, 1216, 1217, 1218, 1219, 1220, 1221
*Nset,nset=_G191,internal,instance=Part-1-1
12,13,14,15,16,17,18,19,20,21,22,
133,134,135,136,137,138,139,140,141,142,143,
254,255,256,257,258,259,260,261,262,263,264,
375,376,377,378,379,380,381,382,383,384,385,
496,497,498,499,500,501,502,503,504,505,506,
617,618,619,620,621,622,623,624,625,626,627,
738,739,740,741,742,743,744,745,746,747,748,
859,860,861,862,863,864,865,866,867,868,869,
980,981,982,983,984,985,986,987,988,989,990,
1101,1102,1103,1104,1105,1106,1107,1108,1109,1110,1111,
1222,1223,1224,1225,1226,1227,1228,1229,1230,1231,1232
*Nset,nset=_G192,internal,instance=Part-1-1
23,24,25,26,27,28,29,30,31,32,33,
144,145,146,147,148,149,150,151,152,153,154,
265,266,267,268,269,270,271,272,273,274,275,
386,387,388,389,390,391,392,393,394,395,396,
507,508,509,510,511,512,513,514,515,516,517,
628,629,630,631,632,633,634,635,636,637,638,
749,750,751,752,753,754,755,756,757,758,759,
870,871,872,873,874,875,876,877,878,879,880,
991,992,993,994,995,996,997,998,999,1000,1001,
1112,1113,1114,1115,1116,1117,1118,1119,1120,1121,1122,
1233,1234,1235,1236,1237,1238,1239,1240,1241,1242,1243
*Nset,nset=_G193,internal,instance=Part-1-1
34,35,36,37,38,39,40,41,42,43,44,
155,156,157,158,159,160,161,162,163,164,165,
276,277,278,279,280,281,282,283,284,285,286,
397,398,399,400,401,402,403,404,405,406,407,
518,519,520,521,522,523,524,525,526,527,528,
639,640,641,642,643,644,645,646,647,648,649,
760,761,762,763,764,765,766,767,768,769,770,
881,882,883,884,885,886,887,888,889,890,891,
1002,1003,1004,1005,1006,1007,1008,1009,1010,1011,1012,
1123,1124,1125,1126,1127,1128,1129,1130,1131,1132,1133,
1244,1245,1246,1247,1248,1249,1250,1251,1252,1253,1254
*Nset,nset=_G194,internal,instance=Part-1-1
45,46,47,48,49,50,51,52,53,54,55,
166,167,168,169,170,171,172,173,174,175,176,
287,288,289,290,291,292,293,294,295,296,297,
408,409,410,411,412,413,414,415,416,417,418,
529,530,531,532,533,534,535,536,537,538,539,
650,651,652,653,654,655,656,657,658,659,660,
771,772,773,774,775,776,777,778,779,780,781,
892,893,894,895,896,897,898,899,900,901,902,
1013,1014,1015,1016,1017,1018,1019,1020,1021,1022,1023,
1134,1135,1136,1137,1138,1139,1140,1141,1142,1143,1144,

1255,1256,1257,1258,1259,1260,1261,1262,1263,1264,1265
*Nset,nset=_G195,internal,instance=Part-1-1
56,57,58,59,60,61,62,63,64,65,66,
177,178,179,180,181,182,183,184,185,186,187,
298,299,300,301,302,303,304,305,306,307,308,
419,420,421,422,423,424,425,426,427,428,429,
540,541,542,543,544,545,546,547,548,549,550,
661,662,663,664,665,666,667,668,669,670,671,
782,783,784,785,786,787,788,789,790,791,792,
903,904,905,906,907,908,909,910,911,912,913,
1024,1025,1026,1027,1028,1029,1030,1031,1032,1033,1034,
1145,1146,1147,1148,1149,1150,1151,1152,1153,1154,1155,
1266,1267,1268,1269,1270,1271,1272,1273,1274,1275,1276
*Nset,nset=_G196,internal,instance=Part-1-1
67,68,69,70,71,72,73,74,75,76,77,
188,189,190,191,192,193,194,195,196,197,198,
309,310,311,312,313,314,315,316,317,318,319,
430,431,432,433,434,435,436,437,438,439,440,
551,552,553,554,555,556,557,558,559,560,561,
672,673,674,675,676,677,678,679,680,681,682,
793,794,795,796,797,798,799,800,801,802,803,
914,915,916,917,918,919,920,921,922,923,924,
1035,1036,1037,1038,1039,1040,1041,1042,1043,1044,1045,
1156,1157,1158,1159,1160,1161,1162,1163,1164,1165,1166,
1277,1278,1279,1280,1281,1282,1283,1284,1285,1286,1287
*Nset,nset=_G197,internal,instance=Part-1-1
78,79,80,81,82,83,84,85,86,87,88,
199,200,201,202,203,204,205,206,207,208,209,
320,321,322,323,324,325,326,327,328,329,330,
441,442,443,444,445,446,447,448,449,450,451,
562,563,564,565,566,567,568,569,570,571,572,
683,684,685,686,687,688,689,690,691,692,693,
804,805,806,807,808,809,810,811,812,813,814,
925,926,927,928,929,930,931,932,933,934,935,
1046,1047,1048,1049,1050,1051,1052,1053,1054,1055,1056,
1167,1168,1169,1170,1171,1172,1173,1174,1175,1176,1177,
1288,1289,1290,1291,1292,1293,1294,1295,1296,1297,1298
*Nset,nset=_G198,internal,instance=Part-1-1
89,90,91,92,93,94,95,96,97,98,99,
210,211,212,213,214,215,216,217,218,219,220,
331,332,333,334,335,336,337,338,339,340,341,
452,453,454,455,456,457,458,459,460,461,462,
573,574,575,576,577,578,579,580,581,582,583,
694,695,696,697,698,699,700,701,702,703,704,
815,816,817,818,819,820,821,822,823,824,825,
936,937,938,939,940,941,942,943,944,945,946,
1057,1058,1059,1060,1061,1062,1063,1064,1065,1066,1067,
1178,1179,1180,1181,1182,1183,1184,1185,1186,1187,1188,
1299,1300,1301,1302,1303,1304,1305,1306,1307,1308,1309
*Nset,nset=_G199,internal,instance=Part-1-1
100,101,102,103,104,105,106,107,108,109,110,
221,222,223,224,225,226,227,228,229,230,231,
342,343,344,345,346,347,348,349,350,351,352,
463,464,465,466,467,468,469,470,471,472,473,

```
584,585,586,587,588,589,590,591,592,593,594,
705,706,707,708,709,710,711,712,713,714,715,
826,827,828,829,830,831,832,833,834,835,836,
947,948,949,950,951,952,953,954,955,956,957,
1068,1069,1070,1071,1072,1073,1074,1075,1076,1077,1078,
1189,1190,1191,1192,1193,1194,1195,1196,1197,1198,1199,
1310,1311,1312,1313,1314,1315,1316,1317,1318,1319,1320
*Nset,nset=_G1910,internal,instance=Part-1-1
111,112,113,114,115,116,117,118,119,120,121,
232,233,234,235,236,237,238,239,240,241,242,
353,354,355,356,357,358,359,360,361,362,363,
474,475,476,477,478,479,480,481,482,483,484,
595,596,597,598,599,600,601,602,603,604,605,
716,717,718,719,720,721,722,723,724,725,726,
837,838,839,840,841,842,843,844,845,846,847,
958,959,960,961,962,963,964,965,966,967,968,
1079,1080,1081,1082,1083,1084,1085,1086,1087,1088,1089,
1200,1201,1202,1203,1204,1205,1206,1207,1208,1209,1210,
1321,1322,1323,1324,1325,1326,1327,1328,1329,1330,1331
*Nset,nset=_GOUT,internal,instance=Part-1-1
600,589,578,567,556,545,534,523,512,501,490,
*Elset, elset=_G19, internal, instance=Part-1-1
  1,  2,  3,  4,  5,  6,  7,  8,  9, 10, 101, 102, 103, 104,
105, 106
 107, 108, 109, 110, 201, 202, 203, 204, 205, 206, 207, 208, 209, 210,
301, 302
 303, 304, 305, 306, 307, 308, 309, 310, 401, 402, 403, 404, 405, 406,
407, 408
 409, 410, 501, 502, 503, 504, 505, 506, 507, 508, 509, 510, 601, 602,
603, 604
 605, 606, 607, 608, 609, 610, 701, 702, 703, 704, 705, 706, 707, 708,
709, 710
 801, 802, 803, 804, 805, 806, 807, 808, 809, 810, 901, 902, 903, 904,
905, 906
 907, 908, 909, 910
*Elset, elset=_GEOUT, internal, instance=Part-1-1
896,886,876,866,856,846,836,826,816,806
*Nset, nset=_G20, internal, instance=Part-1-1
 111, 112, 113, 114, 115, 116, 117, 118, 119, 120, 121,
232, 233, 234, 235, 236
 237, 238, 239, 240, 241, 242, 353, 354, 355, 356, 357,
358, 359, 360, 361, 362
 363, 474, 475, 476, 477, 478, 479, 480, 481, 482, 483,
484, 595, 596, 597, 598
 599, 600, 601, 602, 603, 604, 605, 716, 717, 718, 719,
720, 721, 722, 723, 724
 725, 726, 837, 838, 839, 840, 841, 842, 843, 844, 845,
846, 847, 958, 959, 960
 961, 962, 963, 964, 965, 966, 967, 968, 1079, 1080, 1081,
1082, 1083, 1084, 1085, 1086
 1087, 1088, 1089, 1200, 1201, 1202, 1203, 1204, 1205, 1206, 1207,
1208, 1209, 1210, 1321, 1322
 1323, 1324, 1325, 1326, 1327, 1328, 1329, 1330, 1331
*Elset, elset=_G20, internal, instance=Part-1-1
```

```

    91, 92, 93, 94, 95, 96, 97, 98, 99, 100, 191, 192, 193, 194,
195, 196
    197, 198, 199, 200, 291, 292, 293, 294, 295, 296, 297, 298, 299, 300,
391, 392
    393, 394, 395, 396, 397, 398, 399, 400, 491, 492, 493, 494, 495, 496,
497, 498
    499, 500, 591, 592, 593, 594, 595, 596, 597, 598, 599, 600, 691, 692,
693, 694
    695, 696, 697, 698, 699, 700, 791, 792, 793, 794, 795, 796, 797, 798,
799, 800
    891, 892, 893, 894, 895, 896, 897, 898, 899, 900, 991, 992, 993, 994,
995, 996
    997, 998, 999,1000
*Nset, nset=GS1, instance=Part-block-1
    7,9,25,27
*Nset, nset=GS3, instance=Part-block-1
    27,
*Elset, elset=_Surf-block_S3, internal, instance=Part-block-1
    1, 2, 5, 6
*Surface, type=ELEMENT, name=Surf-block
_Surf-block_S3, S3
*Elset, elset=_Surf-soil_S5, internal, instance=Part-1-1
    495, 496,595, 596,
*Surface, type=ELEMENT, name=Surf-soil
_Surf-soil_S5, S5
*End Assembly
**
** MATERIALS
**
*Material, name=Material-1
*Conductivity
    1e-03,
*Density
    2.4,
*Elastic
    4e+06,0.15
*Expansion
    1e-30,
*Specific Heat
    1e-05,
*Material, name=Material-3
*Density
    1.,
*Depvar
    8,
*User Defined Field
*User Material, constants=1, type=MECHANICAL
    0.4,
*User Material, constants=1, type=THERMAL
    1e-11,
**
*Expansion,user,type=ISO
** INTERACTION PROPERTIES
**

```

```

*Surface Interaction, name=IntProp-2
1.,
*Surface Behavior, pressure-overclosure=HARD
*Gap Conductance
  1e-30, 0.
  0., 0.2
** BOUNDARY CONDITIONS
**
** Name: BC-1n Type: Symmetry/Antisymmetry/Encastre
*Boundary
_G14, XSYMM
** Name: BC-1p Type: Symmetry/Antisymmetry/Encastre
*Boundary
_G12, XSYMM
** Name: BC-2n Type: Symmetry/Antisymmetry/Encastre
*Boundary
_G15, YSYMM
** Name: BC-2p Type: Symmetry/Antisymmetry/Encastre
*Boundary
_G13, YSYMM
** Name: BC-3n Type: Symmetry/Antisymmetry/Encastre
*Boundary
_G16, PINNED
**
** INTERACTIONS
**
** Interaction: Int-1
*Contact Pair, interaction=IntProp-1
Surf-soil, Surf-block
** -----
**
*initial condition, type=field
*initial condition, type=temperature
_G19,-10
_G191,-300
_G192,-4066
_G193,-1560
_G194,-424
_G195,-620
_G196,-240
_G197,-646
_G198,-761
_G199,-682
_G1910,-10000
***** STEP: Step-1
**
*Step, name=Step-1
*Coupled Temperature-Displacement,
1E-5,2E-5,,
**
** BOUNDARY CONDITIONS
**
** Name: BC-BottomT Type: Temperature
*Boundary

```

```

_G19, 11, 11, -10
** Name: BC-topT Type: Temperature
**
** LOADS
**
** Name: Load-bolckW   Type: Gravity
*Dload
_G17, GRAV, 10., 0., 0., -1.
** Name: Load-soilW   Type: Gravity
*Dload
_G18, GRAV, 10., 0., 0., -1.
**
** OUTPUT REQUESTS
** FIELD OUTPUT: F-Output-1
**
*Output, field, variable=PRESELECT, frequency=99999
**
** HISTORY OUTPUT: H-Output-1
**
*NODE PRINT,nset=_GOUT, f=1
nt11,
*NODE PRINT,nset=GS1, f=1
u,
*el print, ELSET=_GEOUT,f=1
FV2,
*el print, ELSET=_GEOUT,f=1
****s,
****ee,
****the,
FV,
*el print, ELSET=_GEOUT,f=1
FV3,
*End Step
*Step, name=Step1
*Coupled Temperature-Displacement
86400,8640000,,
*Boundary
_G19, 11, 11, -10
*Dload
_G17, GRAV, 10., 0., 0., -1.
** Name: Load-soilW   Type: Gravity
*Dload
_G18, GRAV, 10., 0., 0., -1.
**
** OUTPUT REQUESTS
*NODE PRINT,nset=_GOUT, f=1
nt11,
*****u
*NODE PRINT,nset=GS1, f=1
u
*End Step
*Step, name=Step2
*Coupled Temperature-Displacement
86400,8640000,,

```

```

*Boundary
_G19, 11, 11, -10
*Dload
_G17, GRAV, 10., 0., 0., -1.
** Name: Load-soilW   Type: Gravity
*Dload
_G18, GRAV, 10., 0., 0., -1.
**
** OUTPUT REQUESTS
*NODE PRINT,nset=_GOUT, f=1
nt11,
*****u
*NODE PRINT,nset=GS1, f=1
u
*End Step
*Step, name=Step3
*Coupled Temperature-Displacement
86400,8640000,,
*Boundary
_G19, 11, 11, -10
*Dload
_G17, GRAV, 10., 0., 0., -1.
** Name: Load-soilW   Type: Gravity
*Dload
_G18, GRAV, 10., 0., 0., -1.
**
** OUTPUT REQUESTS
*NODE PRINT,nset=_GOUT, f=1
nt11,
*****u
*NODE PRINT,nset=GS1, f=1
u
*End Step
*Step, name=Step4
*Coupled Temperature-Displacement
86400,8640000,,
*Boundary
_G19, 11, 11, -10
*Dload
_G17, GRAV, 10., 0., 0., -1.
** Name: Load-soilW   Type: Gravity
*Dload
_G18, GRAV, 10., 0., 0., -1.
**
** OUTPUT REQUESTS
*NODE PRINT,nset=_GOUT, f=1
nt11,
*****u
*NODE PRINT,nset=GS1, f=1
u
*End Step
*Step, name=Step5
*Coupled Temperature-Displacement
86400,8640000,,

```

```

*Boundary
_G19, 11, 11, -10
*Dload
_G17, GRAV, 10., 0., 0., -1.
** Name: Load-soilW   Type: Gravity
*Dload
_G18, GRAV, 10., 0., 0., -1.
**
** OUTPUT REQUESTS
*NODE PRINT,nset=_GOUT, f=1
nt11,
*****u
*NODE PRINT,nset=GS1, f=1
u
*End Step
*Step, name=Step6
*Coupled Temperature-Displacement
86400,8640000,,
*Boundary
_G19, 11, 11, -10
*Dload
_G17, GRAV, 10., 0., 0., -1.
** Name: Load-soilW   Type: Gravity
*Dload
_G18, GRAV, 10., 0., 0., -1.
**
** OUTPUT REQUESTS
*NODE PRINT,nset=_GOUT, f=1
nt11,
*****u
*NODE PRINT,nset=GS1, f=1
u
*End Step
*Step, name=Step7
*Coupled Temperature-Displacement
86400,8640000,,
*Boundary
_G19, 11, 11, -10
*Dload
_G17, GRAV, 10., 0., 0., -1.
** Name: Load-soilW   Type: Gravity
*Dload
_G18, GRAV, 10., 0., 0., -1.
**
** OUTPUT REQUESTS
*NODE PRINT,nset=_GOUT, f=1
nt11,
*****u
*NODE PRINT,nset=GS1, f=1
u
*End Step
*Step, name=Step8
*Coupled Temperature-Displacement
86400,8640000,,

```

```
*Boundary
_G19, 11, 11, -10
*Dload
_G17, GRAV, 10., 0., 0., -1.
** Name: Load-soilW   Type: Gravity
*Dload
_G18, GRAV, 10., 0., 0., -1.
**
** OUTPUT REQUESTS
*NODE PRINT,nset=_GOUT, f=1
nt11,
*****u
*NODE PRINT,nset=GS1, f=1
u
*End Step
```

Appendix D.1.2. User Subroutines

D.1.2.1. User Subroutines USDFLD

```

subroutine usdfld(field,statev,pnewdt,direct,t,celent,time,dtime,
  1 cmname,orname,nfield,nstatv,noel,npt,layer,kspt,kstep,kincl,
  2 ndi,nshr,coord,jmac,jmtyp,matlayo,laccfla)
c
  include 'aba_param.inc'
c
  character*80 cmname,orname
  character*8 flgray(15)
  dimension
field(nfield),statev(nstatv),direct(3,3),t(3,3),time(2),
  $coord(*),jmac(*),jmtyp(*)
  dimension array(15),jarray(15)

  open(unit=16,status='old',file='/home/x0z013a/house/ET.txt')
c
c Get temperatures from previous increment
  call getvrm('TEMP',array,jarray,flgray,jrcd,
  $ jmac,jmtyp,matlayo,laccfla)
  temp = array(1)
  tempT=temp
  field(1) = temp
c
  WRITE(6,*)coord(3),ARRAY(1),TEMP,"temp"
c
  CALL GETVRM('S',ARRAY,JARRAY,FLGRAY,jrcd,
  $ jmac,jmtyp,matlayo,laccfla)
  S11 = ARRAY(1)
  S22 = ARRAY(2)
  S33 = ARRAY(3)
  SIGMAM =(S11+S22+S33)/3
c
  if(noel.eq.600) then
c
  WRITE(6,*)cmname,noel,coord(3),temp,sigmam,"1. suction,
stress"
c
  else
c
  endif
C
  WRITE(6,*)coord(3),s33,"SIGMAM "
C
C GET STRAINS FROM PREVIOUS INCREMENT
  CALL GETVRM('EE',ARRAY,JARRAY,FLGRAY,jrcd,
  $ jmac,jmtyp,matlayo,laccfla)
  E11 = ARRAY(1)
  E22 = ARRAY(2)
  E33 = ARRAY(3)
  E44 = ARRAY(4)
  E55 = ARRAY(5)
  E66 = ARRAY(6)
  CALL GETVRM('THE',ARRAY,JARRAY,FLGRAY,jrcd,
  $ jmac,jmtyp,matlayo,laccfla)
  DSIGMAM=SIGMAM-STATEV(8)
  STATEV(8)=SIGMAM

```

```

STATEV(7)=DSIGMAM
IF(SIGMAM.GT.-1)SIGMAM=-1
UM=0.4
RD=0.517

IF(coord(3).gt.4.28221)THEN
Gs=2.65
c void ratio versus mean mechanical stress curve
a1=0.49127602
b1=-0.42147606
x1=2.75275012
y1=0.19544900
C void ratio versus matric suction curve
a2=0.387060
b2=-0.456384
x2=3.624239
y2=0.299088
C soil water characteristic curve
A3=0.285551272
B3=-0.671559558
X3=4.386436815
Y3=-0.026264216
C degree of saturation versus matric suction curve
A4=1.024790004
B4=-0.324013298
X4=4.979543423
Y4=-0.024789788
C4=32637
AKa=8.8874
AKb=-15.2329
*****
ELSE
Gs=2.79
c void ratio versus mean mechanical stress curve
a1=0.6641108
b1=-0.6811336
x1=3.3957253
y1=0.1730660
C void ratio versus matric suction curve
a2=0.360413471
b2=-0.507278347
x2=2.701544106
y2=0.473999
C soil water characteristic curve
A3=0.437992975
B3=-1.378969054
X3=4.57346643
Y3=-0.124213334
C degree of saturation versus matric suction curve
A4=1.065419979
B4=-0.519318546
X4=4.82464373
Y4=-0.096823436

```

```

C4=20000
AKa=9.5134
AKb=-17.5882
*****
ENDIF
a11=a1/Gs
y11=y1/Gs
emin=y2
C SATURATED SOILS
H=-TEMP
STS=-SIGMAM
IF(TEMP.GT.-1)THEN
ESIGMA=STS-H
IF(ESIGMA.LT.1)ESIGMA=1
BEP1=EXP(-(LOG10(ESIGMA)-X1)/B1)
E=Y1+A1/(1+BEP1)
S_SATURATION=1
WATER_CONTENT=E/Gs
EM1S=0.4343*A1*BEP1/((1+BEP1)*(1+BEP1)*ESIGMA*B1)/(1+E)
STATEV(1)=-1*3*(1-2*um)/Em1S
STATEV(2)=-1*Em1S/3
STATEV(3)=-EM1S
STATEV(4)=-EM1S
STATEV(5)=AK*E*E*E/(1+E)
ELSE
ALOGH=LOG10(H)
ALOGSTS=LOG10(STS)
EA=Y1+A1/(1+EXP(-(ALOGSTS-X1)/B1))
EB=emin
A1B1=A1*B1*2.302585093
A2B2=A2*B2*2.302585093
DO 301 k=1,10000
EYA1=EA-Y1
EYA2=EA-Y2
CA1=x1-b1*LOG(a1/EYA1-1)
CA2=x2-b2*LOG(a2/EYA2-1)
TCA1=10**CA1
TCA2=10**CA2
FA=STS/TCA1+H/TCA2-1
C*****
EP=EA+(EB-EA)/2
C*****
EYP1=EP-Y1
EYP2=EP-Y2
CP1=x1-b1*LOG(a1/EYP1-1)
CP2=x2-b2*LOG(a2/EYP2-1)
TCP1=10**CP1
TCP2=10**CP2
FP=STS/TCP1+H/TCP2-1
C*****
if(FP.eq.0.or.abs((EB-EA)/2).lt.1e-5)then
go to 302
elseif(FA*FP.gt.0) then
EA=EP

```

```

        FA=FP
        else
        EB=EP
        endif
301  continue
302  E=EP
C
    PART1=A1B1/(TCP1*EYP1*EYP1*(A1/EYP1-1))
    PART2=A2B2/(TCP2*EYP2*EYP2*(A2/EYP2-1))
    Em1S=1/((1+e)*(TCP1*(H*PART2+STS*PART1)))
    Em2S=1/((1+e)*(TCP2*(H*PART2+STS*PART1)))
C    WRITE(6,*)part1,part2,Em1s,Em2s,"Part1"
C*****WATER CONETNET CONSTITUTIVE SURFACE
    sum=H+STS
C    if(noel.eq.600) then
C    WRITE(6,*) sum, "sum"
C    else
C    endif
C    if(sum.lt.C4)then
    WA=Y3+A3/(1+EXP(-(ALOGH-X3)/B3))
    WB=0.1
    A11B1=A11*B1*2.302585093
    A3B3=A3*B3*2.302585093
    DO 311 k=1,10000
*****
    WYA1=WA-Y11
    WYA3=WA-Y3
    WCA1=x1-b1*LOG(a11/WYA1-1)
    WCA3=x3-b3*LOG(a3/WYA3-1)
    WTCA1=10**WCA1
    WTCA3=10**WCA3
    WFA=STS/WTCA1+H/WTCA3-1
C*****
    WP=WA+(WB-WA)/2
C*****
    WYP1=WP-Y11
    WYP3=WP-Y3
    WCP1=x1-b1*LOG(a11/WYP1-1)
    WCP3=x3-b3*LOG(a3/WYP3-1)
    WTCP1=10**WCP1
    WTCP3=10**WCP3
    WFP=STS/WTCP1+H/WTCP3-1
C*****
    if(WFP.eq.0.or.abs((WB-WA)/2).lt.1e-5)then
    go to 312
    elseif(WFA*WFP.gt.0) then
    WA=WP
    WFA=WFP
    else
    WB=WP
    endif
C
311  continue
312  WATER_CONTENT=WP

```

```

S_SATURATION=WATER_CONTENT*Gs/E
PART11=A11B1/(WTCP1*WYP1*WYP1*(A11/WYP1-1))
PART12=A3B3/(WTCP3*WYP3*WYP3*(A3/WYP3-1))
Em1W=1/(WTCP1*(H*PART12+STS*PART11))*(GS/(1+E))
Em2W=1/(WTCP3*(H*PART12+STS*PART11))*(GS/(1+E))
else
EXS=EXP(-(ALOGH-X4)/B4)
S_SATURATION=Y4+A4/(1+EXS)
WATER_CONTENT=S_SATURATION*E
DSDU=A4*EXS*0.4342944819/((1+EXS)**2*B4*H)
EM1W=S_SATURATION*EM1S
EM2W=S_SATURATION*EM2S+DSDU*E/(1+E)
END IF
C*****
C**YOUNG'S MODULOUS
STATEV(1)=-1*3*(1-2*um)/Em1S
c WRITE(6,*)STATEV(1),"E"
C**EXPANSION COEFFICIENT
STATEV(2)=-1*Em2S/3
C**MIW
if(time(2).lt.5e-5)then
STATEV(3)=0
else
STATEV(3)=-EM1W
endif
C**M2W
STATEV(4)=-EM2W
C**PERMEABILITY COEFFICIENT
S_K=10**(ES*AKA+AKB)
STATEV(5)=S_K*(S_saturation*E)**3/(1+e)
ENDIF
C*****
C** CURRENT VOLUMETRIC WATER CONTENT
VW=WATER_CONTENT*Gs/(1+E)
VWLP=0.245276282
VWFC=0.404919094
C
C*****
C
IF(coord(3).LE.(6-RD-TD))THEN
SINK=0.0
ELSE
* READ THE DATA FROM Weather FILE
Di=time(2)/86400
I=Int(Di)+1
DO 100 J=1,I
read(16,*)RainF,ETP
100 continue
AKC=0.6
p=0.5
TKS=(VW-VWLP)/((1-p)*(VWFC-VWLP))
C**CALCULATE WATER STRESS COEFFICIENT
IF(TKS.GT.1.0)THEN
AKS=1.0

```

```

ELSEIF(TKS.LT.0.0)then
    AKS=0.0
ELSE
    AKS=TKS
ENDIF
IF(coord(3).GT.(4-RD))THEN
    IF(ABS(COORD(1)).LE.1.AND.ABS(COORD(2)).LE.1)THEN
        SINK=0.0
    Else
C***CALCULATE NET WATER LOSS
        ANWL=AKs*AKc*ETP-RAINr
C***DETERMINE ACTUAL ETP
        IF(ANWL.GT.0.0)THEN
            if(ANWL.GT.RD*1000*(VW-VWLP))then
                SINK=(VW-VWLP)
            else
                SINK=ANWL/(RD*1000)
            endif
        ELSE
            STATEV(5)=AK*E*E*E/(1+E)
            if(ANWL.GT.RD*1000*(VW-VWFC))then
                SINK=ANWL/(RD*1000)
            else
                SINK=(VW-VWFC)
            endif
        ENDIF
    ENDIF
ENDIF

*****
STATEV(6)=SINK
RETURN
END

```

C
c
c

D.1.2.2. User Subroutines UMTHT

```

subroutine umatht(u,dudt,dudg,flux,dfdt,dfdg,statev,temp,
$ dtemp,dtemdx,time,dtime,predef,dpred,cmname,ntgrd,nstatv,
$ props,nprops,coords,pnewdt,noel,npt,layer,kspt,kstep,kinc)
c
include 'aba_param.inc'
c
character*80 cmname
c
dimension dudg(ntgrd),flux(ntgrd),dfdt(ntgrd),
$ dfdg(ntgrd,ntgrd),statev(nstatv),dtemdx(ntgrd),time(2),
$ predef(1),dpred(1),props(nprops),coords(3)
Sink=STATEV(6)/86400
DSIGMAM=STATEV(7)
EM1W=STATEV(3)*DSIGMAM
cond =statev(5)
specht =statev(4)

```

```

      if(noel.eq.600) then
        WRITE(6,*)DSIGMAM,EM1W,STATEV(3),STATEV(4),STATEV(5),STATEV(6)
      else
        endif
c
c          input specific heat
c
      dudt = specht
      du =(dudt*dtemp+Sink*dtime+EM1W)
      u = u+du
c
c          input flux = -[k]*{dtemdx}
c      do i=1, ntgrd
c          flux(i) = -cond*dtemdx(i)
c      end do
c      do i=1, ntgrd-1
c          flux(i) = -cond*dtemdx(i)
c      end do
c      flux(ntgrd) = -cond*(dtemdx(ntgrd)+10)
c
c          input isotropic conductivity
c
      do i=1, ntgrd
c          dfdg(i,i) = -cond
      end do
c
      Close(16)
      return
      end

```

```

c*****
*

```

D.1.2.3. User Subroutines UMAT

```

      SUBROUTINE UMAT(STRESS,STATEV,DDSDDE,SSE,SPD,SCD,
1 RPL,DDSDDT,DRPLDE,DRPLDT,STRAN,DSTRAN,
2 TIME,DTIME,TEMP,DTEMP,PREDEF,DPRED,MATERL,NDI,NSHR,NTENS,
3 NSTATV,PROPS,NPROPS,COORDS,DROT,PNEWDT,CELENT,
4 DFGRD0,DFGRD1,NOEL,NPT,KSLAY,KSPT,KSTEP,KINC)
c
      INCLUDE 'ABA_PARAM.INC'
c
      CHARACTER*80 MATERL
      DIMENSION STRESS(NTENS),STATEV(NSTATV),
1 DDSDDDE(NTENS,NTENS),DDSDDT(NTENS),DRPLDE(NTENS),
2 STRAN(NTENS),DSTRAN(NTENS),TIME(2),PREDEF(1),DPRED(1),
3 PROPS(NPROPS),COORDS(3),DROT(3,3),
4 DFGRD0(3,3),DFGRD1(3,3)
c
      DIMENSION EELAS(6),EPLAS(6),FLOW(6)

```

```

        DIMENSION ARRAY(15),JARRAY(15)
        PARAMETER (ONE=1.0D0,TWO=2.0D0,THREE=3.0D0,SIX=6.0D0, HALF
=0.5d0)
        DATA NEWTON,TOLER/40,1.D-6/
C
C
C -----
C      UMAT FOR ISOTROPIC ELASTICITY
C      CAN NOT BE USED FOR PLANE STRESS
C -----
C
        IF (NDI.NE.3) THEN
            WRITE(6,1)
1          FORMAT(/,30X,'***ERROR - THIS UMAT MAY ONLY BE USED FOR ',
1          'ELEMENTS WITH THREE DIRECT STRESS COMPONENTS')
            ENDIF
C
C      ELASTIC PROPERTIES
C
c
WRITE(6,*)STATEV(1),STATEV(2),STATEV(5),STATEV(7),STATEV(8),"umat**1"
        EMOD=statev(1)
        ENU=PROPS(1)
        IF(ENU.GT.0.4999.AND.ENU.LT.0.5001) ENU=0.499
        EBULK3=EMOD/(ONE-TWO*ENU)
        EG2=EMOD/(ONE+ENU)
        EG=EG2/TWO
        EG3=THREE*EG
        ELAM=(EBULK3-EG2)/THREE
C
C      ELASTIC STIFFNESS
C
C
        DO 20 K1=1,NTENS
            DO 10 K2=1,NTENS
                DDSDDE(K2,K1)=0.0
10          CONTINUE
20          CONTINUE
C
        DO 40 K1=1,NDI
            DO 30 K2=1,NDI
                DDSDDE(K2,K1)=ELAM
30          CONTINUE
                DDSDDE(K1,K1)=EG2+ELAM
40          CONTINUE
            DO 50 K1=NDI+1,NTENS
                DDSDDE(K1,K1)=EG
50          CONTINUE
C
C      CALCULATE STRESS FROM ELASTIC STRAINS
C
C
        DO 70 K1=1,NTENS
            DO 60 K2=1,NTENS
                STRESS(K2)=STRESS(K2)+DDSDDE(K2,K1)*DSTRAN(K1)

```

```

60     CONTINUE
70     CONTINUE

      RETURN
      END

```

D.1.2.4. User Subroutines UEXPAN

```

C*****
C          user subroutine uexpan
C
C          subroutine uexpan(expan,dexpandt,temp,time,dtime,predef,dpred,
$            statev,cmname,nstatv)
C
C          include 'aba_param.inc'
C
C          character*80 cmname
C
C          dimension expan(*),dexpandt(*),temp(2),time(2),predef(*),
$            dpred(*),statev(nstatv)
C
C          WRITE(6,*)STATEV(1),STATEV(2),STATEV(5),STATEV(7),STATEV(8),"uexpan"
              alpha =STATEV(2)
C
C          expan(1) = alpha*temp(2)
C
C          return
          end

```

APPENDIX D.2.

VERIFICATION OF EQUILIBRIUM PROFILE

Appendix D.2.1. Main Program

*Heading

***** VERIFICATION OF EQUILIBRIUM PROFILE*****

*Node

1,	5.,	5.,	0.
2,	0.,	5.,	0.
3,	-5.,	5.,	0.
4,	5.,	5.,	10.
5,	0.,	5.,	10.
6,	-5.,	5.,	10.
7,	5.,	5.,	20.
8,	0.,	5.,	20.
9,	-5.,	5.,	20.
10,	5.,	5.,	30.
11,	0.,	5.,	30.
12,	-5.,	5.,	30.
13,	5.,	5.,	40.
14,	0.,	5.,	40.
15,	-5.,	5.,	40.
16,	5.,	5.,	50.
17,	0.,	5.,	50.
18,	-5.,	5.,	50.
19,	5.,	5.,	60.
20,	0.,	5.,	60.
21,	-5.,	5.,	60.
22,	5.,	5.,	70.
23,	0.,	5.,	70.
24,	-5.,	5.,	70.
25,	5.,	5.,	80.
26,	0.,	5.,	80.
27,	-5.,	5.,	80.
28,	5.,	5.,	90.
29,	0.,	5.,	90.
30,	-5.,	5.,	90.
31,	5.,	5.,	100.
32,	0.,	5.,	100.
33,	-5.,	5.,	100.
34,	5.,	0.,	0.
35,	0.,	0.,	0.
36,	-5.,	0.,	0.
37,	5.,	0.,	10.
38,	0.,	0.,	10.
39,	-5.,	0.,	10.
40,	5.,	0.,	20.
41,	0.,	0.,	20.
42,	-5.,	0.,	20.
43,	5.,	0.,	30.

44,	0.,	0.,	30.
45,	-5.,	0.,	30.
46,	5.,	0.,	40.
47,	0.,	0.,	40.
48,	-5.,	0.,	40.
49,	5.,	0.,	50.
50,	0.,	0.,	50.
51,	-5.,	0.,	50.
52,	5.,	0.,	60.
53,	0.,	0.,	60.
54,	-5.,	0.,	60.
55,	5.,	0.,	70.
56,	0.,	0.,	70.
57,	-5.,	0.,	70.
58,	5.,	0.,	80.
59,	0.,	0.,	80.
60,	-5.,	0.,	80.
61,	5.,	0.,	90.
62,	0.,	0.,	90.
63,	-5.,	0.,	90.
64,	5.,	0.,	100.
65,	0.,	0.,	100.
66,	-5.,	0.,	100.
67,	5.,	-5.,	0.
68,	0.,	-5.,	0.
69,	-5.,	-5.,	0.
70,	5.,	-5.,	10.
71,	0.,	-5.,	10.
72,	-5.,	-5.,	10.
73,	5.,	-5.,	20.
74,	0.,	-5.,	20.
75,	-5.,	-5.,	20.
76,	5.,	-5.,	30.
77,	0.,	-5.,	30.
78,	-5.,	-5.,	30.
79,	5.,	-5.,	40.
80,	0.,	-5.,	40.
81,	-5.,	-5.,	40.
82,	5.,	-5.,	50.
83,	0.,	-5.,	50.
84,	-5.,	-5.,	50.
85,	5.,	-5.,	60.
86,	0.,	-5.,	60.
87,	-5.,	-5.,	60.
88,	5.,	-5.,	70.
89,	0.,	-5.,	70.
90,	-5.,	-5.,	70.
91,	5.,	-5.,	80.
92,	0.,	-5.,	80.
93,	-5.,	-5.,	80.
94,	5.,	-5.,	90.
95,	0.,	-5.,	90.
96,	-5.,	-5.,	90.
97,	5.,	-5.,	100.

```

          98,          0.,          -5.,          100.
          99,          -5.,          -5.,          100.
*Element, type=DC3D8
 1, 34, 35, 38, 37, 1, 2, 5, 4
 2, 35, 36, 39, 38, 2, 3, 6, 5
 3, 37, 38, 41, 40, 4, 5, 8, 7
 4, 38, 39, 42, 41, 5, 6, 9, 8
 5, 40, 41, 44, 43, 7, 8, 11, 10
 6, 41, 42, 45, 44, 8, 9, 12, 11
 7, 43, 44, 47, 46, 10, 11, 14, 13
 8, 44, 45, 48, 47, 11, 12, 15, 14
 9, 46, 47, 50, 49, 13, 14, 17, 16
10, 47, 48, 51, 50, 14, 15, 18, 17
11, 49, 50, 53, 52, 16, 17, 20, 19
12, 50, 51, 54, 53, 17, 18, 21, 20
13, 52, 53, 56, 55, 19, 20, 23, 22
14, 53, 54, 57, 56, 20, 21, 24, 23
15, 55, 56, 59, 58, 22, 23, 26, 25
16, 56, 57, 60, 59, 23, 24, 27, 26
17, 58, 59, 62, 61, 25, 26, 29, 28
18, 59, 60, 63, 62, 26, 27, 30, 29
19, 61, 62, 65, 64, 28, 29, 32, 31
20, 62, 63, 66, 65, 29, 30, 33, 32
21, 67, 68, 71, 70, 34, 35, 38, 37
22, 68, 69, 72, 71, 35, 36, 39, 38
23, 70, 71, 74, 73, 37, 38, 41, 40
24, 71, 72, 75, 74, 38, 39, 42, 41
25, 73, 74, 77, 76, 40, 41, 44, 43
26, 74, 75, 78, 77, 41, 42, 45, 44
27, 76, 77, 80, 79, 43, 44, 47, 46
28, 77, 78, 81, 80, 44, 45, 48, 47
29, 79, 80, 83, 82, 46, 47, 50, 49
30, 80, 81, 84, 83, 47, 48, 51, 50
31, 82, 83, 86, 85, 49, 50, 53, 52
32, 83, 84, 87, 86, 50, 51, 54, 53
33, 85, 86, 89, 88, 52, 53, 56, 55
34, 86, 87, 90, 89, 53, 54, 57, 56
35, 88, 89, 92, 91, 55, 56, 59, 58
36, 89, 90, 93, 92, 56, 57, 60, 59
37, 91, 92, 95, 94, 58, 59, 62, 61
38, 92, 93, 96, 95, 59, 60, 63, 62
39, 94, 95, 98, 97, 61, 62, 65, 64
40, 95, 96, 99, 98, 62, 63, 66, 65
*Elset, elset=_I1,generate
 1, 40, 1
** Section: Section-1
*Solid Section, elset=_I1, material=Material-1
*Nset, nset=_G4
 1, 2, 3, 34, 35, 36, 67, 68, 69
*Elset, elset=_G4
 19, 20, 39, 40
*Nset, nset=_G5
 31, 32, 33, 64, 65, 66, 97, 98, 99
*Elset, elset=_G5

```

```

19, 20, 39, 40
*Nset, nset=all, generate
  1, 99, 1
*Elset, elset=_G6, generate
  1, 40, 1
*Material, name=Material-1
*USER MATERIAL,TYPE=THERMAL,constant=2,UNSYMM
1e-9,1e-5
***Conductivity
***1e-9,
*Density
1,
*****Specific Heat
****1e-5,
** -----
**
** STEP: Step-1
**
*Step, name=Step-1, amplitude=RAMP
*Heat Transfer, steady state
1.0,
*Boundary
_G4, 11, 11, -0.01
*Dflux
_G6, BF, 0.
*Node Print,nset=all,freq=1
nt11,
*End Step

```

D.2.2. User Subroutines UMTHT

```

      subroutine umatht(u,dudt,dudg,flux,dfdt,dfdg,statev,temp,
      $      dtemp,dtemdx,time,dtime,predef,dpred,cmname,ntgrd,nstatv,
      $
props,nprops,coords,pnewdt,noel,npt,layer,kspt,kstep,kinc)
c
      include 'aba_param.inc'
c
      character*80 cmname
c
      dimension dudg(ntgrd),flux(ntgrd),dfdt(ntgrd),
      $      dfdg(ntgrd,ntgrd),statev(nstatv),dtemdx(ntgrd),time(2),
      $      predef(1),dpred(1),props(nprops),coords(3)
c
c
      COND=PROPS(1)
      SPECHT=PROPS(2)
c
      input specific heat

      dudt = specht
      du = dudt*dtemp+Sink*dtime+pw1*depsilon
      u = u+du
c

```

```
c           input flux = -[k]*{dtemdx}
do i=1, ntgrd-1
  flux(i) = -cond*dtemdx(i)
end do
flux(ntgrd) = -cond*(dtemdx(ntgrd)+10)
c
c           input isotropic conductivity
c
do i=1, ntgrd
  dfdg(i,i) = -cond
end do
return
end
```

APPENDIX E
NUMERICAL SIMULATION OF RESIDENTIAL BUILDINGS
ON EXPANSIVE SOILS

APPENDIX E
NUMERICAL SIMULATION OF RESIDENTIAL BUILDINGS
ON EXPANSIVE SOILS

Appendix E.1. Main Program

```

*Heading
** Job name: ff2 Model name: Model-1
*Preprint, echo=NO, model=NO, history=NO, contact=NO
**
** PARTS
**
*Part, name=Part-1
*End Part
*Part, name=Part-2
*End Part
**
** ASSEMBLY
**
*Assembly, name=Assembly
**
*Instance, name=Part-2-1, part=Part-2
           0.,           0.,           0.
*Node
NODE DEFINITIONS FOR SOIL DOMAIN
OMITTED
*Element, type=C3D8T
ELEMENT DEFINITIONS FOR SOIL DOMAIN
OMITTED
** Region: (Section-soil:Picked)
*Elset, elset=_G6, internal, generate
           1, 18432,           1
** Section: Section-soil
*Solid Section, elset=_G6, material=Material-3
1.,
*End Instance
**
*Instance, name=Part-1-2, part=Part-1
           0.,           0.,           6.
*Node
NODE DEFINITIONS FOR SLABS AND WALLS
OMITTED
*Element, type=S8RT
ELEMENT DEFINITIONS FOR SLABS AND WALLS
OMITTED
** Region: (Section-2:Picked)
*Elset, elset=_G22, internal, generate
           1, 640,           1
** Section: Section-2
*Shell Section, elset=_G22, material=Material-1
0.1, 3
** Region: (Section-1:Picked)

```

```

*Elset, elset=_G21, internal, generate
  641, 1408, 1
** Section: Section-1
*Shell Section, elset=_G21, material=Material-1
0.4, 3
*End Instance
DEFINITIONS OF NODE SETS, ELEMENT SETS AND SURFACE SETS
OMITEED
** MATERIALS
**
*Material, name=Material-1
*Conductivity
  1e-09,
*Density
  2.4,
*Elastic
  2e+07,0.
*Expansion
  1e-30,
*Specific Heat
  1e-05,
*Material, name=Material-3
*Density
  1.,
*Depvar
  8,
*User Defined Field
*User Material, constants=1, type=MECHANICAL
  0.4,
*User Material, constants=1, type=THERMAL
  1e-11,
**
*Expansion,user,type=ISO
** INTERACTION PROPERTIES
**
*Surface Interaction, name=IntProp-2
  1.,
*Friction, slip tolerance=0.005, exponential decay
  1, 0.3, 4.
*Surface Behavior, pressure-overclosure=HARD
*Gap Conductance
  1e-14, 0.
  0., 0.2
**
** BOUNDARY CONDITIONS
**
** Name: BC-4 Type: Symmetry/Antisymmetry/Encastre
*Boundary
_G43, XSYMM
** Name: BC-5 Type: Symmetry/Antisymmetry/Encastre
*Boundary
_G44, YSYMM
** Name: BC-6 Type: Symmetry/Antisymmetry/Encastre
*Boundary

```

```

_G45, XSYMM
** Name: BC-7 Type: Symmetry/Antisymmetry/Encastre
*Boundary
_G46, YSYMM
** Name: BC-8 Type: Symmetry/Antisymmetry/Encastre
*Boundary
_G47, PINNED
*initial condition, type=field
*initial condition, type=temperature
_G529, -300
**
**
** INTERACTIONS
**
** Interaction: Int-1
*Contact Pair,extension zone=0.2,interaction=IntProp-2, small sliding,
adjust=0.1, Hcrit=1.1
*****Contact Pair, interaction=IntProp-2, small sliding, adjust=0.2
_G528, _G527
** -----
**
** STEP: Step-1
**
*Step, name=Step-1, amplitude=RAMP, inc=1000
*Coupled Temperature-Displacement, steady state
**
** BOUNDARY CONDITIONS
**
** Name: BC-10 Type: Temperature
***Boundary
** Name: BC-9 Type: Temperature
*Boundary
_G239, 11, 11, -50.
**
** LOADS
**
** Name: Slab_weight Type: Gravity
*Dload
_G531, GRAV, 10.2, 0., 0., -1.
** Name: Wall_weight Type: Gravity
*Dload
_G530, GRAV, 10.0, 0., 0., -1.
** Name: soilweight Type: Gravity
*Dload
_G529, GRAV, 20., 0., 0., -1.
**
** OUTPUT REQUESTS
**
**
*Restart, write, frequency=1
**
** FIELD OUTPUT: F-Output-1
**
*Output, field, variable=PRESELECT

```

```

**
** HISTORY OUTPUT: H-Output-1
**
*Output, history, variable=PRESELECT
*EL PRINT, ELSET=_G531, Position=Centroidal
SE1, SE2, SM1, SM2
*Node Print, Nset=Soil_line
U3,
*Node Print, Nset=Shell_line
U3,
*End Step
*Step, name=Step1, amplitude=RAMP
*Coupled Temperature-Displacement
86400,8640000,,,
**
** BOUNDARY CONDITIONS
**
** Name: BC-10 Type: Temperature
***Boundary
** Name: BC-9 Type: Temperature
*Boundary
_G239, 11, 11, -50
**
** LOADS
**
** Name: Slab_weight Type: Gravity
*Dload
_G531, GRAV, 10.2, 0., 0., -1.
** Name: Wall_weight Type: Gravity
*Dload
_G530, GRAV, 10.0, 0., 0., -1.
** Name: soilweight Type: Gravity
*Dload
_G529, GRAV, 20., 0., 0., -1.
** OUTPUT REQUESTS
**
*Restart, write, frequency=1
**
** FIELD OUTPUT: F-Output-1
**
*Output, field, variable=PRESELECT
**
** HISTORY OUTPUT: H-Output-1
**
*Output, history, variable=PRESELECT
*EL PRINT, ELSET=_G531, Position=Centroidal
SE1, SE2, SM1, SM2
*Node Print, Nset=Soil_line
U3,
*Node Print, Nset=Shell_line
U3,
*End Step
*Step, name=Step2, amplitude=RAMP
*Coupled Temperature-Displacement

```

```

86400,8640000,,,
**
** BOUNDARY CONDITIONS
**
** Name: BC-10 Type: Temperature
****Boundary
** Name: BC-9 Type: Temperature
*Boundary
_G239, 11, 11, -50
**
** LOADS
**
** Name: Slab_weight   Type: Gravity
*Dload
_G531, GRAV, 10.2, 0., 0., -1.
** Name: Wall_weight   Type: Gravity
*Dload
_G530, GRAV, 10.0, 0., 0., -1.
** Name: soilweight   Type: Gravity
*Dload
_G529, GRAV, 20., 0., 0., -1.
** OUTPUT REQUESTS
**
*Restart, write, frequency=1
**
** FIELD OUTPUT: F-Output-1
**
*Output, field, variable=PRESELECT
**
** HISTORY OUTPUT: H-Output-1
**
*Output, history, variable=PRESELECT
*EL PRINT, ELSET=_G531, Position=Centroidal
SE1, SE2, SM1, SM2
*Node Print, Nset=Soil_line
U3,
*Node Print, Nset=Shell_line
U3,
*End Step
*Step, name=Step3, amplitude=RAMP
*Coupled Temperature-Displacement
86400,8640000,,,
**
** BOUNDARY CONDITIONS
**
** Name: BC-10 Type: Temperature
****Boundary
** Name: BC-9 Type: Temperature
*Boundary
_G239, 11, 11, -50
**
** LOADS
**
** Name: Slab_weight   Type: Gravity

```

```

*Dload
_G531, GRAV, 10.2, 0., 0., -1.
** Name: WALL_weight   Type: Gravity
*Dload
_G530, GRAV, 10.0, 0., 0., -1.
** Name: soilweight   Type: Gravity
*Dload
_G529, GRAV, 20., 0., 0., -1.
** OUTPUT REQUESTS
**
*Restart, write, frequency=1
**
** FIELD OUTPUT: F-Output-1
**
*Output, field, variable=PRESELECT
**
** HISTORY OUTPUT: H-Output-1
**
*Output, history, variable=PRESELECT
*EL PRINT, ELSET=_G531, Position=Centroidal
SE1, SE2, SM1, SM2
*Node Print, Nset=Soil_line
U3,
*Node Print, Nset=Shell_line
U3,
*End Step
*Step, name=Step4, amplitude=RAMP
*Coupled Temperature-Displacement
86400,8640000,,,
**
** BOUNDARY CONDITIONS
**
** Name: BC-10 Type: Temperature
***Boundary
** Name: BC-9 Type: Temperature
*Boundary
_G239, 11, 11, -50
**
** LOADS
**
** Name: Slab_weight   Type: Gravity
*Dload
_G531, GRAV, 10.2, 0., 0., -1.
** Name: WALL_weight   Type: Gravity
*Dload
_G530, GRAV, 10.0, 0., 0., -1.
** Name: soilweight   Type: Gravity
*Dload
_G529, GRAV, 20., 0., 0., -1.
** OUTPUT REQUESTS
**
*Restart, write, frequency=1
**
** FIELD OUTPUT: F-Output-1

```

```

**
*Output, field, variable=PRESELECT
**
** HISTORY OUTPUT: H-Output-1
**
*Output, history, variable=PRESELECT
*EL PRINT, ELSET=_G531, Position=Centroidal
SE1, SE2, SM1, SM2
*Node Print, Nset=Soil_line
U3,
*Node Print, Nset=Shell_line
U3,
*End Step
*Step, name=Step5, amplitude=RAMP
*Coupled Temperature-Displacement
86400,8640000,,,
**
** BOUNDARY CONDITIONS
**
** Name: BC-10 Type: Temperature
***Boundary
** Name: BC-9 Type: Temperature
*Boundary
_G239, 11, 11, -50
**
** LOADS
**
** Name: Slab_weight Type: Gravity
*Dload
_G531, GRAV, 10.2, 0., 0., -1.
** Name: Wall_weight Type: Gravity
*Dload
_G530, GRAV, 10.0, 0., 0., -1.
** Name: soilweight Type: Gravity
*Dload
_G529, GRAV, 20., 0., 0., -1.
** OUTPUT REQUESTS
**
*Restart, write, frequency=1
**
** FIELD OUTPUT: F-Output-1
**
*Output, field, variable=PRESELECT
**
** HISTORY OUTPUT: H-Output-1
**
*Output, history, variable=PRESELECT
*EL PRINT, ELSET=_G531, Position=Centroidal
SE1, SE2, SM1, SM2
*Node Print, Nset=Soil_line
U3,
*Node Print, Nset=Shell_line
U3,
*End Step

```

```

*Step, name=Step6, amplitude=RAMP
*Coupled Temperature-Displacement
86400,8640000,,,
**
** BOUNDARY CONDITIONS
**
** Name: BC-10 Type: Temperature
***Boundary
** Name: BC-9 Type: Temperature
*Boundary
_G239, 11, 11, -50
**
** LOADS
**
** Name: Slab_weight   Type: Gravity
*Dload
_G531, GRAV, 10.2, 0., 0., -1.
** Name: WALL_weight   Type: Gravity
*Dload
_G530, GRAV, 10.0, 0., 0., -1.
** Name: soilweight   Type: Gravity
*Dload
_G529, GRAV, 20., 0., 0., -1.
** OUTPUT REQUESTS
**
*Restart, write, frequency=1
**
** FIELD OUTPUT: F-Output-1
**
*Output, field, variable=PRESELECT
**
** HISTORY OUTPUT: H-Output-1
**
*Output, history, variable=PRESELECT
*EL PRINT, ELSET=_G531, Position=Centroidal
SE1, SE2, SM1, SM2
*Node Print, Nset=Soil_line
U3,
*Node Print, Nset=Shell_line
U3,
*End Step
*Step, name=Step7, amplitude=RAMP
*Coupled Temperature-Displacement
86400,8640000,,,
**
** BOUNDARY CONDITIONS
**
** Name: BC-10 Type: Temperature
***Boundary
** Name: BC-9 Type: Temperature
*Boundary
_G239, 11, 11, -50
**
** LOADS

```

```

**
** Name: Slab_weight   Type: Gravity
*Dload
_G531, GRAV, 10.2, 0., 0., -1.
** Name: Wall_weight   Type: Gravity
*Dload
_G530, GRAV, 10.0, 0., 0., -1.
** Name: soilweight   Type: Gravity
*Dload
_G529, GRAV, 20., 0., 0., -1.
** OUTPUT REQUESTS
**
*Restart, write, frequency=1
**
** FIELD OUTPUT: F-Output-1
**
*Output, field, variable=PRESELECT
**
** HISTORY OUTPUT: H-Output-1
**
*Output, history, variable=PRESELECT
*EL PRINT, ELSET=_G531, Position=Centroidal
SE1, SE2, SM1, SM2
*Node Print, Nset=Soil_line
U3,
*Node Print, Nset=Shell_line
U3,
*End Step
*Step, name=Step8, amplitude=RAMP
*Coupled Temperature-Displacement
86400,8640000,,,
**
** BOUNDARY CONDITIONS
**
** Name: BC-10 Type: Temperature
***Boundary
** Name: BC-9 Type: Temperature
*Boundary
_G239, 11, 11, -50
**
** LOADS
**
** Name: Slab_weight   Type: Gravity
*Dload
_G531, GRAV, 10.2, 0., 0., -1.
** Name: Wall_weight   Type: Gravity
*Dload
_G530, GRAV, 10.0, 0., 0., -1.
** Name: soilweight   Type: Gravity
*Dload
_G529, GRAV, 20., 0., 0., -1.
** OUTPUT REQUESTS
**
*Restart, write, frequency=1

```

```
**  
** FIELD OUTPUT: F-Output-1  
**  
*Output, field, variable=PRESELECT  
**  
** HISTORY OUTPUT: H-Output-1  
**  
*Output, history, variable=PRESELECT  
*EL PRINT, ELSET=_G531, Position=Centroidal  
SE1, SE2, SM1, SM2  
*Node Print, Nset=Soil_line  
U3,  
*Node Print, Nset=Shell_line  
U3,  
*End Step
```

Appendix E.2. User Subroutines

E.2.1. User Subroutines USDFLD

```

subroutine usdfld(field,statev,pnewdt,direct,t,celent,time,dtime,
  1 cmname,orname,nfield,nstatv,noel,npt,layer,kspt,kstep,kinc,
  2 ndi,nshr,coord,jmac,jmtyp,matlayo,laccfla)
c
  include 'aba_param.inc'
c
  character*80 cmname,orname
  character*8 flgray(15)
  dimension
field(nfield),statev(nstatv),direct(3,3),t(3,3),time(2),
  $coord(*),jmac(*),jmtyp(*)
  dimension array(15),jarray(15)

  open(unit=16,status='old',file='/home/x0z013a/house/ET.txt')
c
c Get temperatures from previous increment
  call getvrm('TEMP',array,jarray,flgray,jrcd,
  $ jmac, jmtyp, matlayo, laccfla)
  temp = array(1)
  tempT=temp
  field(1) = temp
c
  WRITE(6,*)coord(3),ARRAY(1),TEMP,"temp"
c
  CALL GETVRM('S',ARRAY,JARRAY,FLGRAY,jrcd,
  $ jmac, jmtyp, matlayo, laccfla)
  S11 = ARRAY(1)
  S22 = ARRAY(2)
  S33 = ARRAY(3)
  SIGMAM =(S11+S22+S33)/3
C
C GET STRAINS FROM PREVIOUS INCREMENT
  CALL GETVRM('EE',ARRAY,JARRAY,FLGRAY,jrcd,
  $ jmac, jmtyp, matlayo, laccfla)
  E11 = ARRAY(1)
  E22 = ARRAY(2)
  E33 = ARRAY(3)
  E44 = ARRAY(4)
  E55 = ARRAY(5)
  E66 = ARRAY(6)
  CALL GETVRM('THE',ARRAY,JARRAY,FLGRAY,jrcd,
  $ jmac, jmtyp, matlayo, laccfla)
  DSIGMAM=SIGMAM-STATEV(8)
  STATEV(8)=SIGMAM
  STATEV(7)=DSIGMAM
  IF(SIGMAM.GT.-1)SIGMAM=-1
C
  WRITE(6,*)SIGMAM, temp,"templ"
  UM=0.4
  RD=0.345
  TD=0.368

```

```

        IF(coord(3).gt.4.28221)THEN
          Gs=2.65
        C void ratio versus mean mechanical stress curve
          a1=0.49127602
          b1=-0.42147606
          x1=2.75275012
          y1=0.19544900
        C void ratio versus matric suction curve
          a2=0.387060
          b2=-0.456384
          x2=3.624239
          y2=0.299088
        C soil water characteristic curve
          A3=0.285551272
          B3=-0.671559558
          X3=4.386436815
          Y3=-0.026264216
        C degree of saturation versus matric suction curve
          A4=1.024790004
          B4=-0.324013298
          X4=4.979543423
          Y4=-0.024789788
          C4=32637
          AKa=8.8874
          AKb=-15.2329
        *****
          ELSE
          Gs=2.79
        C void ratio versus mean mechanical stress curve
          a1=0.6641108
          b1=-0.6811336
          x1=3.3957253
          y1=0.1730660
        C void ratio versus matric suction curve
          a2=0.360413471
          b2=-0.507278347
          x2=2.701544106
          y2=0.473999
        C soil water characteristic curve
          A3=0.437992975
          B3=-1.378969054
          X3=4.57346643
          Y3=-0.124213334
        C degree of saturation versus matric suction curve
          A4=1.065419979
          B4=-0.519318546
          X4=4.82464373
          Y4=-0.096823436
          C4=20000
          AKa=9.5134
          AKb=-17.5882
        *****
          ENDIF
          a11=a1/Gs

```

```

y11=y1/Gs
emin=y2
C SATURATED SOILS
H=-TEMP
STS=-SIGMAM
IF(TEMP.GT.-1)THEN
ESIGMA=STS-H
IF(ESIGMA.LT.1)ESIGMA=1
BEP1=EXP(-(LOG10(ESIGMA)-X1)/B1)
E=Y1+A1/(1+BEP1)
S_SATURATION=1
WATER_CONTENT=E/Gs
EM1S=0.4343*A1*BEP1/((1+BEP1)*(1+BEP1)*ESIGMA*B1)/(1+E)
STATEV(1)=-1*3*(1-2*um)/Em1S
STATEV(2)=-1*Em1S/3
STATEV(3)=-EM1S
STATEV(4)=-EM1S
STATEV(5)=AK*E*E*E/(1+E)
ELSE
ALOGH=LOG10(H)
ALOGSTS=LOG10(STS)
EA=Y1+A1/(1+EXP(-(ALOGSTS-X1)/B1))
EB=emin
A1B1=A1*B1*2.302585093
A2B2=A2*B2*2.302585093
DO 301 k=1,10000
EYA1=EA-Y1
EYA2=EA-Y2
CA1=x1-b1*LOG(a1/EYA1-1)
CA2=x2-b2*LOG(a2/EYA2-1)
TCA1=10**CA1
TCA2=10**CA2
FA=STS/TCA1+H/TCA2-1
C*****
EP=EA+(EB-EA)/2
C*****
EYP1=EP-Y1
EYP2=EP-Y2
CP1=x1-b1*LOG(a1/EYP1-1)
CP2=x2-b2*LOG(a2/EYP2-1)
TCP1=10**CP1
TCP2=10**CP2
FP=STS/TCP1+H/TCP2-1
C*****
if(FP.eq.0.or.abs((EB-EA)/2).lt.1e-5)then
go to 302
elseif(FA*FP.gt.0) then
EA=EP
FA=FP
else
EB=EP
endif
301 continue
302 E=EP

```

```

c      WRITE(6,*)e,"eA1B1"
PART1=A1B1/(TCP1*EYP1*EYP1*(A1/EYP1-1))
PART2=A2B2/(TCP2*EYP2*EYP2*(A2/EYP2-1))
Em1S=1/((1+e)*(TCP1*(H*PART2+STS*PART1)))
Em2S=1/((1+e)*(TCP2*(H*PART2+STS*PART1)))
c      WRITE(6,*)part1,part2,Em1s,Em2s,"Part1"
c*****WATER CONETNET CONSTITUTIVE SURFACE
      sum=H+STS
      if(sum.lt.C4)then
      WA=Y3+A3/(1+EXP(-(ALOGH-X3)/B3))
      WB=0.1
      A11B1=A11*B1*2.302585093
      A3B3=A3*B3*2.302585093
      DO 311 k=1,10000
*****
      WYA1=WA-Y11
      WYA3=WA-Y3
      WCA1=x1-b1*LOG(a11/WYA1-1)
      WCA3=x3-b3*LOG(a3/WYA3-1)
      WTCA1=10**WCA1
      WTCA3=10**WCA3
      WFA=STS/WTCA1+H/WTCA3-1
c*****
      WP=WA+(WB-WA)/2
c*****
      WYP1=WP-Y11
      WYP3=WP-Y3
      WCP1=x1-b1*LOG(a11/WYP1-1)
      WCP3=x3-b3*LOG(a3/WYP3-1)
      WTCP1=10**WCP1
      WTCP3=10**WCP3
      WFP=STS/WTCP1+H/WTCP3-1
c*****
      if(WFP.eq.0.or.abs((WB-WA)/2).lt.1e-5)then
      go to 312
      elseif(WFA*WFP.gt.0) then
      WA=WP
      WFA=WFP
      else
      WB=WP
      endif
c
311  continue
312  WATER_CONTENT=WP
      S_SATURATION=WATER_CONTENT*Gs/E
      PART11=A11B1/(WTCP1*WYP1*WYP1*(A11/WYP1-1))
      PART12=A3B3/(WTCP3*WYP3*WYP3*(A3/WYP3-1))
      Em1W=1/(WTCP1*(H*PART12+STS*PART11))*(GS/(1+E))
      Em2W=1/(WTCP3*(H*PART12+STS*PART11))*(GS/(1+E))
      else
      EXS=EXP(-(ALOGH-X4)/B4)
      S_SATURATION=Y4+A4/(1+EXS)
      WATER_CONTENT=S_SATURATION*E
      DSDU=A4*EXS*0.4342944819/((1+EXS)**2*B4*H)

```

```

      EM1W=S_SATURATION*EM1S
      EM2W=S_SATURATION*EM2S+DSDU*E/(1+E)
      END IF
C*****
C**YOUNG'S MODULOUS
      STATEV(1)=-1*3*(1-2*um)/Em1S
C**EXPANSION COEFFICIENT
      STATEV(2)=-1*Em2S/3
C**MIW
      if(time(2).lt.5e-5)then
      STATEV(3)=0
      else
      STATEV(3)=-EM1W
      endif
C**M2W
      STATEV(4)=-EM2W
C**PERMEABILITY COEFFICIENT
      S_K=10**(ES*AKA+AKB)
      STATEV(5)=S_K*(S_saturation*E)**3/(1+e)
      ENDIF
C*****
C** CURRENT VOLUMETRIC WATER CONTENT
      VW=WATER_CONTENT*Gs/(1+E)
      VWLP=0.245276282
      VWFC=0.404919094

C
C*****
C** GET THE MAXIMUM WATER CONTENT AT THE MECHANICAL STRESS LEVEL
C
C
WRITE(6,*)STATEV(1),STATEV(2),STATEV(3),STATEV(4),STATEV(5),"****1257"
C*****
C
      IF(coord(3).LE.(6-RD-TD))THEN
      SINK=0.0
      ELSE
*   READ THE DATA FROM Weather FILE
      Di=time(2)/86400
      I=Int(Di)+1
      DO 100 J=1,I
      read(16,*)RainF,ETP
100  continue
      AKC=0.6
      p=0.5
      TKS=(VW-VWLP)/((1-p)*(VWFC-VWLP))
C***CALCULATE WATER STRESS COEFFICIENT
      IF(TKS.GT.1.0)THEN
      AKS=1.0
      ELSEIF(TKS.LT.0.0)then
      AKS=0.0
      ELSE
      AKS=TKS
      ENDIF
      IF(coord(3).GT.(6-RD))THEN

```

```

                IF (ABS(COORD(1)) .LE. 7.5 .AND. COORD(2) .LE. 7.5 .AND.
$COORD(2) .GE. 0.0) THEN
                    SINK=0.0
                ELSEIF (COORD(1) .LE. 7.5 .AND. COORD(1) .GE. 0.0 .AND.
$COORD(2) .LE. 0.0 .AND. COORD(2) .GE. -7.5) THEN
                    SINK=0.0
                Else
C***CALCULATE NET WATER LOSS
                    ANWL=AKs*AKc*ETP-RAINP
C***DETERMINE ACTUAL ETP
                    IF (ANWL.GT.0.0) THEN
                        if (ANWL.GT.RD*1000*(VW-VWLP)) then
                            SINK=(VW-VWLP)
                        else
                            SINK=ANWL/(RD*1000)
                        endif
                    ELSE
                        STATEV(5)=AK*E*E*E/(1+E)
                        if (ANWL.GT.RD*1000*(VW-VWFC)) then
                            SINK=ANWL/(RD*1000)
                        else
                            SINK=(VW-VWFC)
                        endif
                    ENDIF
                ENDIF
            ELSE
                IF ((COORD(1)) .LE. -7 .AND. (COORD(1)) .GE. -13 .AND.
$(COORD(2)) .LE. 3 .AND. (COORD(2)) .GE. -3) THEN
                    ANWL=AKs*0.3*ETP
C***DETERMINE ACTUAL ETP
                    IF (ANWL.GT.0.0) THEN
                        if (ANWL.GT.TD*1000*(VW-VWLP)) then
                            SINK=(VW-VWLP)
                        else
                            SINK=ANWL/(TD*1000)
                        endif
                    ELSE
                        if (ANWL.GT.TD*1000*(VW-VWFC)) then
                            SINK=ANWL/(TD*1000)
                        else
                            SINK=(VW-VWFC)
                        endif
                    ENDIF
                ELSE
                    SINK=0.0
                ENDIF
            ENDIF
        ENDIF
    *****
    STATEV(6)=SINK
    RETURN
    END
C
c

```

E.2.2. User Subroutines UMTHT

```

c
      subroutine umatht(u,dudt,dudg,flux,dfdt,dfdg,statev,temp,
$      dtemp,dtemdx,time,dtime,predef,dpred,cmname,ntgrd,nstatv,
$      props,nprops,coords,pnewdt,noel,npt,layer,kspt,kstep,kinc)
c
      include 'aba_param.inc'
c
      character*80 cmname
c
      dimension dudg(ntgrd),flux(ntgrd),dfdt(ntgrd),
$      dfdg(ntgrd,ntgrd),statev(nstatv),dtemdx(ntgrd),time(2),
$      predef(1),dpred(1),props(nprops),coords(3)
      Sink=STATEV(6)/86400
      DSIGMAM=STATEV(7)
      EM1W=STATEV(3)*DSIGMAM
      cond =statev(5)
      specht =statev(4)
c
      input specific heat
c
      dudt = specht
      du =(dudt*dtemp+Sink*dtime+EM1W)
      u = u+du
c
c
      input flux = -[k]*{dtemdx}
c
      do i=1, ntgrd-1
          flux(i) = -cond*dtemdx(i)
      end do
      flux(ntgrd) = -cond*(dtemdx(ntgrd)+10)
c
c
      input isotropic conductivity
c
      do i=1, ntgrd
          dfdg(i,i) = -cond
      end do
c
      Close(16)
      return
      end

```

E.2.3. User Subroutines UMAT

```

c*****
c
      user subroutine uexpan
c
      subroutine uexpan(expan,dexpandt,temp,time,dtime,predef,dpred,
$      statev,cmname,nstatv)
c
      include 'aba_param.inc'

```

```

C
    character*80 cmname
C
    dimension expan(*),dexpandt(*),temp(2),time(2),predef(*),
$      dpred(*),statev(nstatv)
C
WRITE(6,*)STATEV(1),STATEV(2),STATEV(5),STATEV(7),STATEV(8),"uexpan"
    alpha =STATEV(2)
C
    expan(1) = alpha*temp(2)
C
    return
    end
C*****

```

D.2.4. User Subroutines UEXPAN

```

    SUBROUTINE UMAT(STRESS,STATEV,DDSDDE,SSE,SPD,SCD,
1  RPL,DDSDDT,DRPLDE,DRPLDT,STRAN,DSTRAN,
2  TIME,DTIME,TEMP,DTEMP,PREDEF,DPRED,MATERL,NDI,NSHR,NTENS,
3  NSTATV,PROPS,NPROPS,COORDS,DROT,PNEWDT,CELENT,
4  DFGRD0,DFGRD1,NOEL,NPT,KSLAY,KSPT,KSTEP,KINC)
C
    INCLUDE 'ABA_PARAM.INC'
C
    CHARACTER*80 MATERL
    DIMENSION STRESS(NTENS),STATEV(NSTATV),
1  DDSDE(NTENS,NTENS),DDSDDT(NTENS),DRPLDE(NTENS),
2  STRAN(NTENS),DSTRAN(NTENS),TIME(2),PREDEF(1),DPRED(1),
3  PROPS(NPROPS),COORDS(3),DROT(3,3),
4  DFGRD0(3,3),DFGRD1(3,3)
C
    DIMENSION EELAS(6),EPLAS(6),FLOW(6)
    DIMENSION ARRAY(15),JARRAY(15)
    PARAMETER (ONE=1.0D0,TWO=2.0D0,THREE=3.0D0,SIX=6.0D0, HALF
=0.5d0)
    DATA NEWTON,TOLER/40,1.D-6/
C
C
C -----
C    UMAT FOR ISOTROPIC ELASTICITY
C    CAN NOT BE USED FOR PLANE STRESS
C -----
C
    IF (NDI.NE.3) THEN
        WRITE(6,1)
1      FORMAT(//,30X,'***ERROR - THIS UMAT MAY ONLY BE USED FOR ',
1          'ELEMENTS WITH THREE DIRECT STRESS COMPONENTS')

```

```

        ENDIF
C
C   ELASTIC PROPERTIES
C
c
WRITE(6,*)STATEV(1),STATEV(2),STATEV(5),STATEV(7),STATEV(8),"umat**1"
      EMOD=statev(1)
      ENU=PROPS(1)
      IF(ENU.GT.0.4999.AND.ENU.LT.0.5001) ENU=0.499
      EBULK3=EMOD/(ONE-TWO*ENU)
      EG2=EMOD/(ONE+ENU)
      EG=EG2/TWO
      EG3=THREE*EG
      ELAM=(EBULK3-EG2)/THREE
C
C   ELASTIC STIFFNESS
C
      DO 20 K1=1,NTENS
        DO 10 K2=1,NTENS
          DDSDE(K2,K1)=0.0
10      CONTINUE
20      CONTINUE
C
      DO 40 K1=1,NDI
        DO 30 K2=1,NDI
          DDSDE(K2,K1)=ELAM
30      CONTINUE
          DDSDE(K1,K1)=EG2+ELAM
40      CONTINUE
      DO 50 K1=NDI+1,NTENS
        DDSDE(K1,K1)=EG
50      CONTINUE
C
C   CALCULATE STRESS FROM ELASTIC STRAINS
C
      DO 70 K1=1,NTENS
        DO 60 K2=1,NTENS
          STRESS(K2)=STRESS(K2)+DDSDE(K2,K1)*DSTRAN(K1)
60      CONTINUE
70      CONTINUE

      RETURN
      END

```

VITA

Xiong Zhang received his B.S. degree in the Department of Geotechnical Engineering at Tongji University, Shanghai, China in 1992 and his M.S. degree in geotechnical engineering at the China Institute of Water Resources & Hydropower Research (IWHR), Beijing, China in 1995. After graduation, he worked as a geotechnical engineer in the same institute for five years.

In 2000, he started his Ph.D. studies in the Department of Civil Engineering at Texas A&M University under the supervision of Dr. Jean-Louis Briaud. He worked as a research and teaching assistant in the Civil Engineering Department and received his degree in August 2004.

Xiong is a citizen of P.R. China. His permanent mailing address is:

Department of Geotechnical Engineering,

China Institute of Water Resources and Hydropower Research,

Beijing 100044, P.R. China.